Head Office: Università degli Studi di Padova

Department of Cultural Heritage: Archaeology and History of Art, Cinema and Music

Ph.D. course in History, Criticism and Conservation of Cultural Heritage

ARCHAEOMETRIC STUDY OF EGYPTIAN VITREOUS MATERIALS FROM TEBTYNIS: INTEGRATION OF ANALYTICAL AND ARCHAEOLOGICAL DATA

Coordinator: Prof. Andrea Tomezzoli

Supervisor: Prof. Gianmario Molin

Co-Supervisors: Prof. Ivana Angelini, Prof. Paola Zanovello

Ph.D. student: Cinzia Bettineschi

Ignoscetis mihi quod dixero:
ego malo mihi vitrea

Petronius
(Satyricon, 50.3)

CONTENTS

MATERIALS & METHODS

RESULTS AND DISCUSSION

ABBREVIATIONS

ÆGYPTVM	Ancient Egyptian Production Technology of Vitreous Materials
Approx.	approximately
BSE	Backscattered Electrons
Ca. (or c.)	circa
CLSM (or LSCM)	Confocal Laser Scanning Microscopy
EDS (or EDX)	Energy Dispersive System
EPMA	Electron Probe Microanalysis
FOSS	Free and Open Source Software
GIS	Geographical Information System
HMG	High Magnesium Glasses
Inv.	Inventory
IVSLA	Istituto Veneto di Scienze, Lettere ed Arti
LA-ICP-MS	Laser Ablation Inductively Coupled Plasma Mass Spectrometry
LBA	Late Bronze Age
LMG	Low Magnesium Glass
MAI	Italian Archaeological Mission in Egypt
MFI	Multi-Focal Imaging
MSA	Museum of Archaeological Sciences and Art
Nr. (or nn.)	Number
LMHK	Low Magnesium High Potassium
OBIA	Object-Based Image Analysis
OM	Optical Microscopy

PCA	Principal Component Analysis
PS	Proprietary Software
RBDMS	Relational Database Management System
SEM	Scanning Electron Microscopy
Sic	*sic erat scriptum*
SD	Standard Deviation
SE	Secondary Electrons
SM	Stereoscopic Microscopy
Unipd	University of Padova
XRD	X-Ray Diffraction
XRF	X-Ray Fluorescence

ABSTRACT

While substantial works were carried out on the analytical characterization of the glasses of the Late Bronze Age and the Roman period, Ptolemaic glass is still far from understood. The present research aims at contributing to fill this gap thanks to a multidisciplinary approach focused on the workshop of Tebtynis (Fayum oasis, Egypt), which was excavated by Carlo Anti in the early 1930s.

This project offers a critical interpretation of Anti's archival documents, in association with the functional and archaeometric investigation of the artifacts which were found in the workshop and that are now preserved at the Egyptian Museum of Turin (Italy). The objects comprise both tools (such as molds, trays, weights) and finished, semi-finished and waste fragments of glass, mainly related to the production of monochrome and polychrome inlays used for the decoration of the liturgical furniture.

After a preliminary study of the whole collection (ca. 800 fragments > 2mm), a representative selection of 70 objects comprising 144 different types of glass was sampled for in-depth archeometric investigations.

The research required the combined use of a wide range of analytical techniques and methods for data processing: stereoscopic and optical microscopy (SM and OM), confocal laser scanning microscopy (CLSM), scanning electron microscopy equipped with energy dispersive system (SEM-EDS), electron probe micro analysis (EPMA), micro-Raman spectroscopy (μ-Raman), multi-focal imaging (MFI), object-based image analysis (OBIA) and principal component analysis (PCA).

The results help to shed new light on Ptolemaic glass-working, constituting the biggest, coherent dataset of this phase analyzed to date. In particular, it was possible to reconstruct the technologies employed for the production of the different classes of glass inlays, investigating the *chaîne opératoire* and the production markers, also from a micro-textural point of view. A specific interest was also devoted to the identification of

the coloring processes and to the characterization of the raw materials, in terms of provenance of the sand source and type of the fluxing agent.

The type and quantity of the unreacted relics of the batch, and especially the heavy mineral fraction, suggests an Egyptian production of the base glass, which is well suited for a traditional craft such as that of glass inlays. Moreover, the analytical data show that the Tebtynis collection is mainly constituted by Low Magnesium Glasses (LMG), in accordance with the classic recipes of Graeco-Roman glass. A small amount of High Magnesium Glasses (HMG) was also found, especially (but not exclusively) connected with the dull red samples, together with intermediate compositions which were interpreted as natron-based glasses modified during the coloring processes. Soda-lime-lead and leaded glasses are present in all color classes, but the highest PbO levels are always associated to sealing-wax red, yellowish-orange and yellow samples.

Ionic coloring agents are Cu^{2+} for light blue and turquoise glasses, Co^{2+} (sometimes associated to Cu^{2+}) for dark blue glasses, Fe^{2+} mixed with Fe^{3+} for transparent green and aqua glasses. The dataset comprises both Mn-decolored and Sb-decolored glasses.

The main opacifiers identified in the white, blue, green and yellow glasses are Ca- Na- and Pb-antimoniates, sometimes in solid solution. Both *in situ* and *ex situ* technologies were identified, with frequent (but not systematic) associations to specific color-classes. Opaque red glasses were either obtained with nano-sized metallic copper drops (Cu^0) or synthetic cuprite (Cu_2O). Nano-crystals of cuprous oxides are also responsible for the opaque brown and yellowish-orange colors.

A comparison with the analyses performed on the earlier, coeval and later glasses showed that the basic recipes and the technological choices for glass-coloring employed during the Ptolemaic period share important links with the Roman production, but also highlighted the great deal of experimentation which is typical of transitional phases.

RIASSUNTO

Nonostante un gran numero di lavori abbiano riguardato la caratterizzazione analitica di vetri datati alla tarda età del Bronzo e all'epoca romana, il vetro Tolemaico è ancora poco noto. La ricerca qui presentata intende contribuire a colmare questo vuoto, grazie allo studio multidisciplinare dell'officina di Tebtynis (oasi del Fayum, Egitto), che è stata rinvenuta da Carlo Anti nei primi anni trenta del '900.

Questo lavoro offre innanzitutto una revisione critica della documentazione d'archivio, indagata in associazione con lo studio funzionale e archeomentrico dei reperti rinvenuti all'interno dell'officina, che sono ora in gran parte conservati presso il Museo Egizio di Torino (Italia). Gli oggetti indagati comprendono attrezzi (come stampi, vassoi, pesi) e una nutrita serie di prodotti finiti, semi-finiti e scarti in vetro, essenzialmente legati alla produzione di intarsi monocromi e policromi usati per la decorazione del mobilio liturgico templare.

Dopo un primo censimento e studio dell'intera collezione (circa 800 frammenti > 2mm), è stato selezionato un campione rappresentativo costituito da 70 reperti comprendenti 144 diversi tipi di vetro, che sono stati selezionati per essere sottoposti a ulteriori approfondimenti analitici.

La ricerca ha richiesto l'impiego combinato di una vasta gamma di strumentazioni analitiche e di metodi per il processamento dei dati: microscopio stereoscopico e ottico (SM e OM), microscopio confocale laser a scansione (CLSM), microscopio elettronico a scansione accoppiato a microsonda a dispersione di energia (SEM-EDS), microsonda elettronica (EPMA), spettroscopia micro-Raman (μ-Raman), imaging multi-focale (MFI), analisi d'immagine object-based (OBIA) e analisi delle componenti principali (PCA).

I risultati contribuiscono a gettare nuova luce sulla lavorazione del vetro in epoca Tolemaica e costituiscono il più numeroso set di dati di questa fase analizzato fino ad

oggi. In particolare, è stato possibile ricostruire le tecnologie impiegate per le diverse classi di intarsi in vetro, analizzando la *chaîne opératoire* e gli indicatori di lavorazione, anche da un punto di vista micro-tessiturale. Un approfondimento specifico è stato poi dedicato alla comprensione dei processi di colorazione e alla caratterizzazione delle materie prime, in termini di provenienza delle sabbie e di tipologia di fondenti impiegati.

Il tipo e la quantità di residui minerali derivanti dalle sabbie usate per la miscela vetrificabile, e in particolare i minerali pesanti, suggeriscono una produzione Egiziana del vetro base, che ben si accorda con un artigianato di antica tradizione locale come quello degli intarsi in vetro. Inoltre, i dati analitici mostrano che i reperti da Tebtynis sono perlopiù costituiti vetri LMG (Low Magnesium Glasses), in accordo con le ricette classicamente associate al vetro Romano. Sono stati, inoltre, identificati un piccolo nucleo di vetri HMG (High Magnesium Glasses), principalmente composto da vetri di colore rosso scuro (ma non solo), e altre composizioni intermedie, che sono state interpretate come vetri al natron la cui ricetta è stata modificata durante i processi di colorazione. Vetri sodico-calcico-piombici e piombici sono presenti in tutti i colori, ma i maggiori tenori di PbO sono sempre associati ai vetri rossi, giallo-arancione e gialli.

Tra i coloranti ionici si segnalano l'impiego di Cu^{2+} nei vetri azzurri e turchesi, Co^{2+} (talvolta associato a Cu^{2+}) per i campioni blu scuro, un mix di Fe^{2+} e Fe^{3+} ne vetri verdi trasparenti e in quelli non intenzionalmente colorati. Sono inoltre presenti sia campioni decolorati con manganese che con antimonio. I principali opacizzanti nei vetri bianchi, blu, verdi e gialli sono gli antimoniati di calcio, sodio e piombo. Sono testimoniate sia la precipitazione *in situ* che l'aggiunta *ex situ* degli opacizzanti, spesso (ma non sempre) ciascuna associata a specifiche classi cromatiche. I rossi opachi sono dovuti alla presenza di gocce nanometriche di rame metallico (Cu^0) oppure di dendriti di cuprite. Nano-cristalli di Cu_2O sono anche responsabili del colore e dell'opacità nei campioni giallo-arancioni e in quello marrone.

La comparazione dei risultati ottenuti con le analisi effettuate su campioni più antichi, coevi e successivi ha dimostrato che le ricette del vetro base e le tecnologie di colorazione impiegate durante il periodo Tolemaico condividono importanti similitudini con la produzione romana, ma ha anche evidenziato una massiccia propensione alla sperimentazione, che è tipica delle fasi di transizione.

1. Introduction

Archaeological glass has long been considered as a privileged mean to explore multiple aspects of the past societies, from ideology and belief to economy, trade and consumption, from social structure to technological evolution and organization of the production, from use and functionality of the artifacts to waste management and recycle.

Nowadays, it is generally accepted that Egypt had a central role in the early history of glass, not necessarily because the material itself first originated there[1], but because Egypt is the only place where a good number of glass workshops ranging from the II millennium BC to the I millennium AD were discovered and excavated (Keller, 1983; Schlick-Nolte, Leirke 2002; Nicholson, 2007; Pusch, Rehren, 2007). In this sense, Shortland and Eremin (2006) noted that "the study of Egyptian glass represents the most important window on the origins of man-made glass". However, while the contexts and the artifacts of the Late Bronze Age (i.e. the Egyptian New Kingdom) were investigated in detail by various authors, our knowledge on the glass dated between the Late and the Ptolemaic periods is generally limited to stylistic and typo-chronological studies, with very few analyzed samples able to provide a reference framework for the technology and the recipes used in those phases (Bimson, Freestone, 1988; Brill, 1999; Nenna, Gratuze, 2009). Nevertheless, the Ptolemaic period[2] is a transitional moment of crucial importance in the evolution of glass-making, as it set the basis for the so-called "revolution" of glass blowing, which took place around the last quarter of the I century BC (on this subject see among others Grose, 1977; Barag, 1985; De Carolis, 2006; Stern, 2008).

[1] The actual data for the first production of glass seem to point towards the Near East (see e.g. Peltenburg, 1992; Lilyquist, Brill, 1993; Shortland, 2000; Tite, Shortland, 2003), but the question is still open to some debate (Shortland *et alii*, 2017).

[2] When referring to the chronology of Graeco-Roman Egypt, the following terms will be used during this work: Hellenistic Egypt corresponds to the period starting from the conquest of Alexander the Great until the Actium battle (332-31 BC); the Ptolemaic period corresponds to the Ptolemaic dynasty, from the reign of Ptolemy I Soter to the death of Cleopatra VII (305-30 BC); the Roman or Imperial phase conventionally corresponds to the period ranging from the conversion of Egypt into a Roman province until the closure of the Philae temple (30 BC-538 AD). Hellenistic Egypt and Ptolemaic period will be sometimes used as synonyms, despite the slight chronological shift.

This project will thus focus on the archaeometric and archaeological study of a collection of more than 800 fragments of monochrome and polychrome glasses discovered by the Italian Archaeological Mission in Egypt (MAI) in the inlay workshop of Tebtynis (Fayum oasis) in 1931 and currently preserved at the Egyptian Museum of Turin (Italy). The Tebtynis workshop stands as a landmark in vitreous materials studies, not only because it yielded a huge quantity of semi-finished and finished products, but mostly because it preserved the tools, the kiln and the room furniture which were used for glass-making. Even though all the archaeological documentation regarding the location of the workshop and the planimetry of the structures was never published at the end of the excavations, the site is widely cited in the literature among the few Hellenistic glass-working centers known in the Mediterranean basin. Recently, the revision and census of the archives of Carlo Anti, director of the MAI and of the Tebtynis excavations, offered the chance to obtain first-hand data about the discovery of the workshop and its materials (Deotto, 2015). The critical review of the archival data will constitute the first original part of this dissertation, after a general introduction of the site.

A crucial goal of the project is to understand the role of the Tebtynis workshop in the context of Graeco-Roman Egypt, thanks to a comparative discussion of its relationship with the other coeval glass-working centers, especially those with material traces of craft areas located within the temples. This preliminary overview of the literature, associated with the new data deriving from the analysis of the archaeological evidences from Tebtynis (both structures and materials), will contribute to offer a possible interpretation on the role and meaning of the glass-working facilities in the Ptolemaic sanctuaries, including their ritual and economic framework.

The discovery of craft areas of archaeological significance raises issues related not only to the study of the materials and the structures identified, but also (and especially) connected to contextualize the production processes in the trajectory of the technological evolution and to understand the skills, the knowledge and the practices used in the ancient world. For this reason, this research employed a multimethodological and interdisciplinary approach which was developed with the following aims in mind:

- Localization and contextualization of the Tebtynis inlay workshop, its tools and vitreous materials in the context of Ptolemaic Egypt and at a broader, Mediterranean level;
- Understanding of the socio-economical values connected to the production of objects inlaid with glass in the Ptolemaic temples;
- Identification of the type of activities carried out in the site in terms of inlaid objects production;
- Study and classification of the vitreous materials on the basis of their typology (inlay, rod, lump etc.) and material characteristics (color, hue, opacity, homogeneity, texture);
- Investigation of the *chaîne opératoire* and the production markers (bubble orientation, flux lines, tool marks etc.);
- Identification of raw materials, glass-forming and coloring/ decoloring/ opacifying technologies, furnace conditions (times, temperatures, redox conditions);
- Reconstruction of the provenance of the raw and semi-finished materials (mineralizations, ores, sand source etc.), of the trade routes and of the distribution of the final products.

After a first screening of all the Tebtynis glasses in the Turin Museum, 70 objects in monochrome, stratified and complex mosaic glass for a total of 144 different glasses were chosen for in depth archaeometric analyses. The samples were investigated using a multi-methodological protocol aimed at offering a complete characterization of the glasses from the textural, mineralogical and chemical point of view.

The results offered the chance to obtain a clearer picture on the production and the secondary processing (coloring/ decoloring/ opacifying/ forming) of glass in Hellenistic Egypt and contributed to better contextualize the workshop discovered in Tebtynis in its ritual, socio-economic and technological framework, by combining the archival, archaeological, textural and chemico-mineralogical data collected during this research.

The tables with a brief description of the samples and a list of the analytical protocol employed case by case can be found in the appendix, together with the chemical data and a summary on the results of the image-analysis.

2. Tebtynis

2.1 Archaeological context and early excavations

The ancient village of Tebtynis lays at the south-eastern edge of the Fayum oasis, in an area currently known as *kôm* Umm el-Breigât (fig. 2.1). According to the interpretation of Gallazzi (1992), the modern name literally means "mother of the towers" and is likely to be related with the rugged landscape of ruins, which characterized the area before the beginning of the archaeological excavations (fig. 2.2).

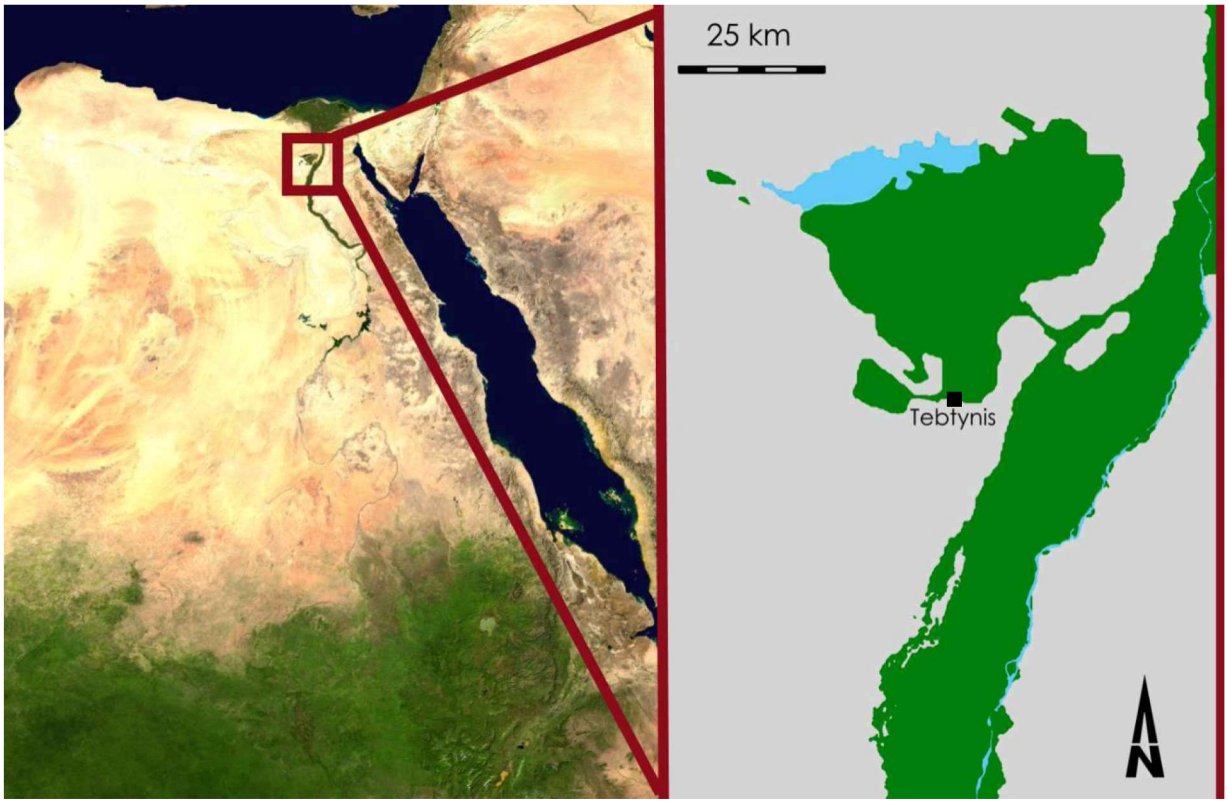

Fig. 2.1 – Localiziation of the archaeological site of Tebtynis (Fayum, Egypt).

The site was first occupied during the Middle Kingdom (late Dynasty XII, approximately 1800 BC), as testified by some of the burials discovered in the cemeteries around the village (Gallazzi, 2001), and survived until the XI century AD, when it was abandoned due to the gradual desertification of the area. At that point the village moved

north, towards the oasis, near the Bahr el Gharaq[1], where Tutun (the direct heir of Tebtynis) is located.

Fig. 2.2 - Kôm Umm el-Breigât in 1929, before Anti's excavations (from Gallazzi ,1992).

Most of the structures and artifacts discovered in the site date back to the Graeco-Roman age, the period of maximum topographic and demographic expansion of the village. Tebtynis, however, retained a discreet relevance in Coptic, Byzantine and Arabic times, when it became seat of various administrative offices. In particular, from the V century AD and until the Arab conquer, it turned into a regional capital and was re-named Theodosiopolis (Pensabene, 1995).

After the abandonment, the village was covered by the sands of the desert. The extension of the resulting mound is huge, between three hundred thousand and five hundred thousand square meters. A vast necropolis is located at the foot of the *kôm* and preserves both human and sacred animals remains (mostly crocodiles, as presented in Grenfell, Hunt, 1902).

[1] The Bahr el Gharaq is an artificial canalization in the lower Fayum oasis.

Investigations were undertaken for the first time by Bernard Grenfell and Arthur Hunt at the turn of the nineteenth century. The two researchers worked there for four months between 1899 and 1900 and recovered nearly five hundred papyri[2] in the central and southern area of the *kôm* (O'Connell, 2007). They also discovered the *temenos* of the temple of the crocodile god Sobek, locally worshipped as Soknebtynis (meaning "Sobek, Lord of Tebtynis").

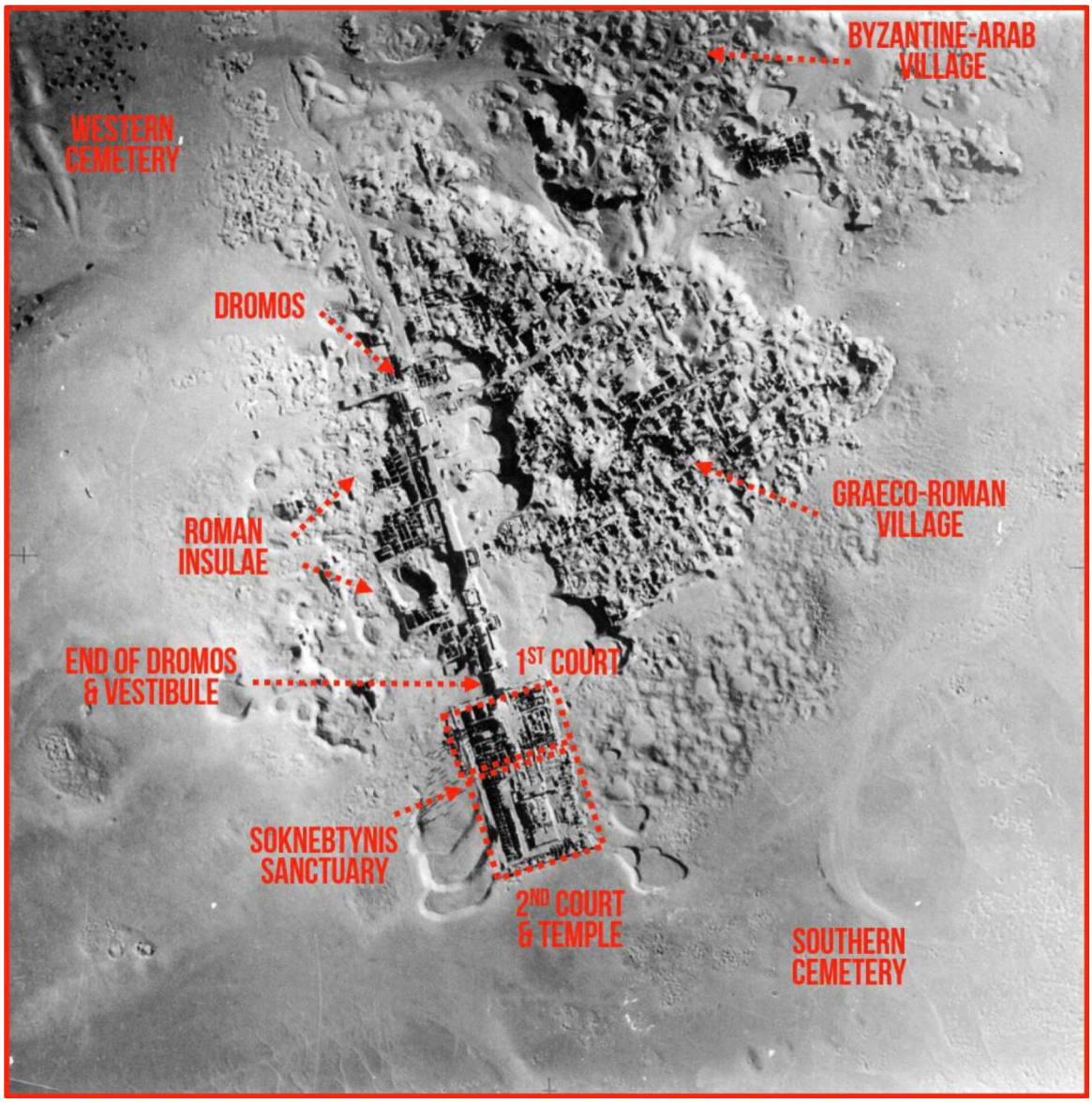

Fig. 2.3 – Aerial photomosaic of the 1936 flight over Tebtynis (courtesy of the Trent University, Canada) with the most relevant archaeological structures of the site.

[2] As well as numerous other archaeological materials currently preserved at the Phoebe A. Hearst Museum of Anthropology at the University of Berkeley. Please refer to the online catalogue of the Museum: https://webapps.cspace.berkeley.edu/pahma/search/search/ (visited in October 2017).

These findings quickly increased the fame of Tebtynis and in 1902 Otto Rubensohn organized an expedition aimed to expand the papyrological collection of the archaeological museum in Berlin. The campaign was not as fruitful as expected and after two weeks of excavation Rubensohn decided to abandon the site. However, the interest shown by the European scholars attracted the attention of the local peasants, the so-called *fellahin*, who saw the *kôm* as a source of artifacts to resale, but also as a quarry of *sebâkh*[3], thus increasing the progressive destruction of the archaeological record.

Since the beginning of the XX century and for the next thirty years the activities of *sebâkhin* and looters continued to be feverish, leading to the destruction of various areas of the settlement and its necropolises. From time to time, the *gafir*[4] sent groups of findings to the Cairo Museum (Rondot, 2004), but they were just the crumbs of an extensive patrimony that ended up destroyed or enriched private and public collections in Europe and the United States of America.

The lootings continued even following the return of the Western scholars. In 1929, Evaristo Breccia (at that time Director of the Graeco-Roman Museum of Alexandria) reached Tebtynis looking for papyri on behalf of the Papyrological Institute of Florence. Because of the scarcity of funding, he undertook surveys to identify the areas which were less plundered by the *sebâkhin*. He dug only a small group of houses near the temple of Soknebtynis and some burials, but recovered only very limited inscribed fragments (Breccia 1932).

2.1 Carlo Anti in Tebtynis

It was during a visit to Evaristo Breccia that Carlo Anti, director of the Italian Archaeological Mission in Egypt and Professor of Classical Archaeology at the University of Padova, set foot for the first time in Tebtynis (Gallazzi, 1992). The difficulties of the excavation emerge both from the words of Breccia, who defines the site as "un infame inferno di coccodrilli"[5], and from those of Anti (1930) who describes it as

[3] Sebâkh is constituted by decomposed organic material, highly fertilizing (Bailey, 1999).
[4] The *gafir* is a native watchman in charge to safeguard the local antiquities (Davoli, 2008).
[5] Translated by the author from the original Italian text: "*an infamous hell of crocodiles*".

"*una distesa caotica di mura, di frane di mattoni, di cumuli di sabbia e detriti, di fosse grandi e piccole fra le quali in un primo momento sembrava impossibile poter ritrovare i lineamenti della città*"[6].

Yet, Anti soon realized the potential of the *kôm*, as testified in the archival records at the Istituto Veneto di Scienze, Lettere ed Arti (IVSLA)[7]: "*Durante i lavori del Breccia ebbi occasione di visitare Tebtunis e di convincermi – in pieno accordo con il Breccia stesso – come il kôm di Tebtunis fosse uno dei rarissimi nel Faium nel quale era ancora possibile condurre ricerche archeologiche con speranza di qualche successo*"[8] (Deotto 2015). He asked, therefore, to the leaders of the Papyrological Institute of Florence to renew the permission for excavation, with the offer to intervene personally and to cover part of the mission costs (Bastianini, Deotto, 2014).

Carlo Anti's researches in Tebtynis took place in the years from 1930 to 1936. However, Anti was physically present on the site only during the first three of the seven campaigns. Following his election as Chancellor of the University of Padova in 1932, he entrusted his collaborator Gilbert Bagnani[9] with the field operations. The works provided for the first time an overview of the topography of the site[10], bringing to light the temple of Soknebtynis, long lost after the surveys of Grenfell and Hunt. The Italian mission also investigated the residential contexts of Graeco-Roman, Byzantine and Arabic times, the Coptic churches and the vast necropolises around the village.

Anti has never published a comprehensive edition of the excavations. However, a recent PhD thesis (Deotto, 2015) could finally catalogue, digitalize and study all the available documentation related to Carlo Anti's activities in Tebtynis, offering a

[6] Translated by the author from the original Italian text: "*a chaotic expanse of walls, collapsed bricks, sand heaps and debris, large and small pits, among which, at first, it was impossible to find the outline of the town*".

[7] The archival documentation of Anti's excavation in Tebtynis was the subject of a recenty discussed PhD thesis by Giulia Deotto (Deotto, 2015).

[8] Translated from the original Italian text: "*During the work of Breccia, I had the opportunity to visit Tebtunis and I was convinced – in full agreement with Breccia himself – that Tebtunis kôm was one of the rarest in the Faium where there is still a chance to conduct archaeological researches with the hope of some success*" (IVSLA, Anti's fund, envelope 6, dossier III, n. 3).

[9] Bagnani's archives are currently preserved at the Library of the Art Gallery of Ontario (AGO) and at the Trent University. Both are under study by Ian Begg (see e.g. Begg 1998a, 1998b, 2002; Zanovello *et alii* 2014-2015).

[10] From Anti, 1931: "*Lo scavo, condotto con scopo e metodi topografici, ha permesso il rilievo di ogni più piccolo indizio*" (translation by the author from the original Italian text: "*The excavation, led with topographic purpose and methods, allowed us to detect even the smallest clue*").

systematic synthesis of his researches in Egypt. As it will be seen, such private archival records have been of fundamental importance for the contextualization of the findings analyzed during this thesis.

2.2 Tebtynis after Anti: University of Milan and IFAO

Since 1936 and for over fifty years, the *kôm* remained at thrall of *sebâkhin* and antiquities hunters. It was only in 1988 that the excavations resumed, thanks to a joint mission of the French Institute of Oriental Archaeology (IFAO) and the University of Milan, with the direction of Claudio Gallazzi and Gisèle Hadji-Minaglou (fig. 2.4).

The earliest investigations of the Franco-Italian mission focused on the north-eastern side the Ptolemaic sanctuary of Soknebtynis, where they identified a chapel dedicated to Isis-Thermouthis (main phase I century BC – I century AD) and a small group of houses along the *dromos* of *Tefresudj[ty]* (Gallazzi, Hadji-Minaglou, 2000). Gallazzi (2010) translates this epithet as "colui il cui risveglio è propizio"[11] and thus refers the mention to either Osiris or Min. Further south, the excavations located a Hellenistic enclosure just at the edge of the village. Following the indications on a series of Greek papyri recovered in the area, the structure was interpreted as a station of the desert police, the so-called *eremophylakes* (Gallazzi, 1995). Later, the works moved within the main temple and its *dromos*, where Rondot (2004) carried out various surveys in order to identify the structures investigated during the Anti-Bagnani campaigns. In the western side of the village the researches unearthed a public bath, a thermal building and a *thesaurus* (warehouse) of Ptolemaic age, along with a small number of Roman houses (Gallazzi, 1997; Hadji-Minaglou, 2009).

From 2005 to 2008, the investigation shifted in the north-western area of the kôm, which has returned materials and structures dating back to the Byzantine era, mainly from the IV to VII century AD (Gallazzi, 2010). After that, the excavations returned in the Graeco-Roman part of the town, near the temple of Soknebtynis and discovered various houses, workshops and a cereal storehouse covering a time span from the III century BC until the III century AD (Gallazzi, 2015).

[11] Translation of the author from the original Italian text: "he, whose awakening is propitious".

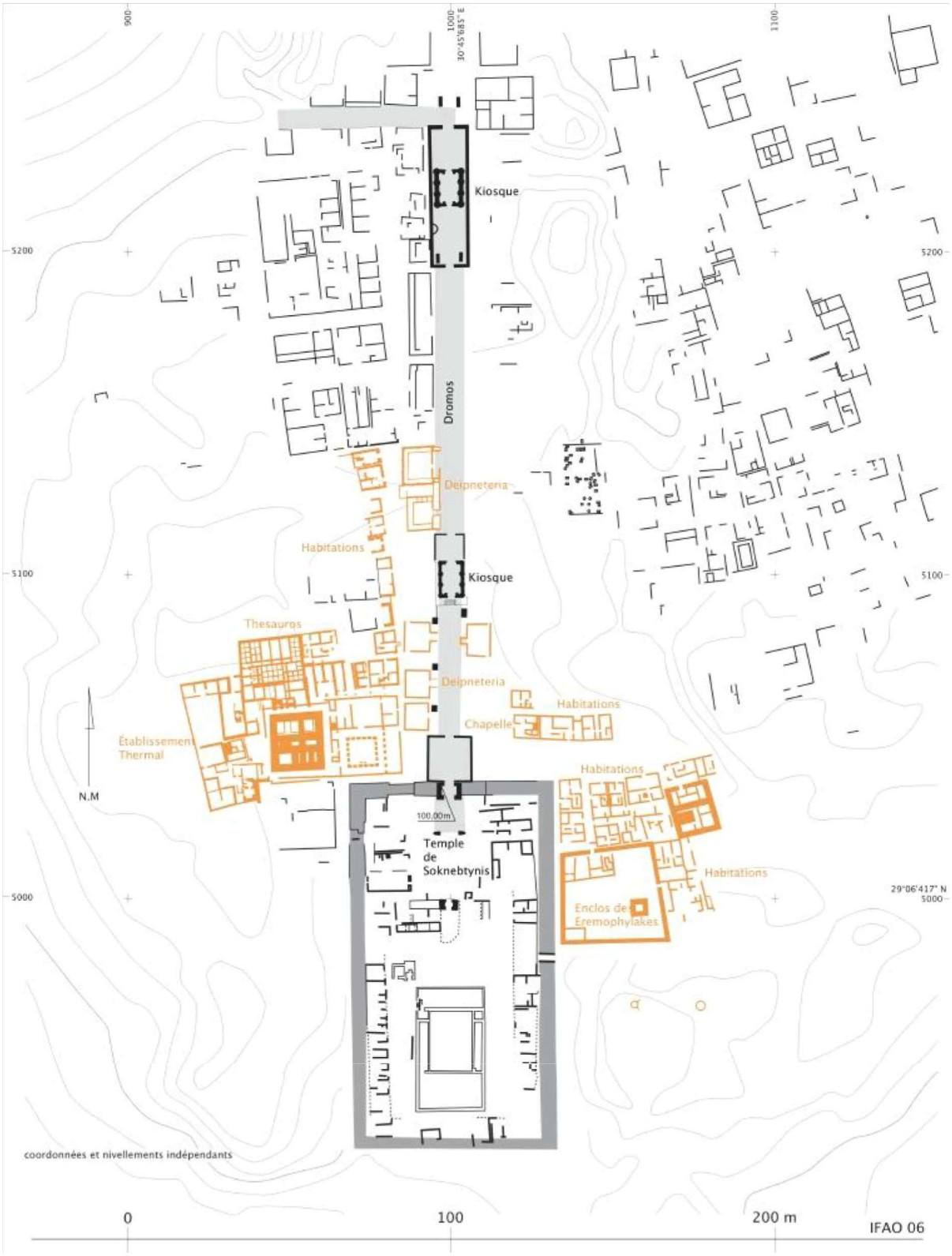

Fig. 2.4 – The topographic plan of the site according to the investigations of the Franco-Italian Mission (Rondot, 2004). In grey: Anti's and Bagnani's excavations (it should be noted that the inner part of the temple lacks important details and shows only what could still be identified on the ground during the recent surveys); in orange: excavations 1988-2006.

2.3 The University of Padova and Anti's heritage

Over the past few years, the University of Padova has been committed in a massive effort in order to assess, classify and study the heritage related to the excavations carried out by Carlo Anti and his team in the site of Tebtynis during the years 1930-1936. In addition to the "historical archives" project (Zanovello, Menegazzi, 2012; Deotto, 2015), numerous other multidisciplinary studies have been investigating the context and the material culture from the site. In particular:

1) Project EgittoVeneto[12]. Born in 2008 from the collaboration between the University of Padova and the Ca' Foscari University of Venice, the project has catalogued more than two thousand Egyptian and Egyptianizing artifacts preserved in twenty-eight different museums of the Veneto region (Zanovello, Ciampini, 2012), including those form Tebtynis.

2) The study of Anti's activities in Egypt led to the discovery of a Pan flute consisting in a series of reeds, tied with a thin rope and coated with animal glue in the Archaeological Museum of the University (MSA). The provenance of the instrument from Tebtynis is still uncertain, although it was found in Egypt during the period of Anti and Bagnani's excavations. Deeper investigations were launched as part of the project "Archaeology and Virtual Acoustics: a Pan flute from Ancient Egypt"[13] in collaboration with the Center for Computational Sonology of the University: starting from a 3D model of the artifact, the team implemented a virtual reconstruction of the flute and its sound (Avanzini *et alii,* 2015).

3) The project "Horus: visions from above of the archaeological space"[14] aimed to reconstruct the off-site landscape of Tebtynis using remote sensing technologies, in collaboration with the Center of Spatial Studies and Activities of the University. The Franco's general plan and the historic aerial photographs were digitalized,

[12] Financed by the Veneto Region and later chosen and funded by the Fondazione Cassa di Risparmio di Padova e Rovigo as "Progetto di Eccellenza" (PIs: Paola Zanovello, Emanuele Marcello Ciampini). In this context, I collaborated for the study of the vitreous materials and for the organization of the temporary exhibition "Egitto in Veneto".

[13] The project was funded by the University of Padova as PRAT "Progetto di Ricerca di Ateneo" (PI: Paola Zanovello). I collaborated to the archaeometric characterization of the coating of the pipes.

[14] Financed in the framework of the most innovative researches proposed by students (PIs: Giulia Deotto, Paola Zanovello), year 2015. I was part of the coordination team.

georeferenced in GIS environment, analyzed and compared with recent 8-bands multispectral satellite images WorldView2 (Deotto *et alii* (b), forthcoming). A follow-up project "Horus 2.0: new frontiers of predictive archaeology, from remote sensing to ground truth"[15] was funded in early 2017 and is focusing on the three-dimensional reconstruction of the site as it appeared in the early 1930s.

4) The study of the papyri from Tebtynis preserved in Padova started in 2010 with the "Papyri Patavinae"[16] project (Lunelli, 2014; Soldati, 2014). At present, the Department of Cultural Heritage is also engaged in another papyrological research: "Culture, society, public and private life of the multiethnic societies of the Egyptian *chora*: which is the legacy of Graeco-Roman Egypt for Western culture?"[17]. In addition to the study of the inscribed documentation, the project is also filming a documentary to communicate the results to a wider public.

5) The first archaeometric analysis on Egyptian vitreous materials from Tebtynis focused on a group of faience ornaments of the MSA (Bettineschi, 2013; Molin, Bettineschi, Angelini, 2013; Angelini *et alii,* 2014). Recently, ArExGlass (Archaeometry and Experimental Archaeology for Pre-Roman Glassworking) project was selected in the framework of most innovative researches proposed by students and funded by the University of Padova[18]. The project aims to investigate the composition, properties and technology of pre-Roman glass through a multidisciplinary approach, by integrating archaeometric investigations, experimental archaeology and innovative approaches used in researches on industrial glass.

This PhD thesis is, therefore, part of a larger group of activities promoted by the University of Padova for the study and promotion of its Egyptological heritage.

[15] Funded in the framework of the strategic departmental projects (SID) by the Department of Cultural Heritage of the University of Padova (PI: Armando De Guio). I am collaborating to the 3D reconstructions, both from the technical and archaeological point of view.

[16] Funded among the "Progetti di Eccellenza" by the Fondazione Cassa di Risparmio di Padova e Rovigo (PI: Aldo Lunelli).

[17] Funded by the University of Padova as "Progetto di Ricerca di Ateneo" (PI: Silvia Strassi). I am collaborating on the technical aspects of the production technologies employed in Graeco-Roman Egypt.

[18] I am the proposer and principal investigator from the student side, while Ivana Angelini is the reference professor.

2.4 Topographic overview of the village

The topography of the site will be discussed using data from four sets of documents and the related bibliography:

a) plans and drawings by Fausto Franco, Anti's field architect, which are preserved in the archives of the MSA and the IVSLA (Gallazzi, 1992; Carpinelli *et alii*, 2017; Meleri, 2017a-b; Menegazzi, 2017);

b) two sets of aerial photographs recorded by the Egyptian Air Force in 1934 and 1936 upon request of Gilbert Bagnani (Bagnani, 1935; Gallazzi, 1989; Brenningmeyer, Begg, 2006; Deotto *et alii,* 2017b);

c) plans of the Franco-Italian mission, published in Tebtynis I-II-IV and in the IFAO papers (Gallazzi, Hadji-Minaglou, 2000; Rondot, 2004; Hadji-Minaglou, 2007; Litinas, 2008).

d) panchromatic and multispectral 8-bands satellite images WorldView 2 acquired in October 2015, covering an area of 5x5 km^2 around the site (Burigana, 2017; Deotto *et alii* (b), forthcoming).

Considering the chronology of the structures, the site can broadly be divided into three main sectors: the central, eastern and southern area of the *kôm* dating back to the Graeco-Roman age, the northern one, of Arabic date, and the western part, occupied during the Byzantine and Arab period (fig. 2.3).

The Soknebtynis temple is located on the south-western edge of the site; heading north, the great processional way (*dromos*) constitute the main axis of the Graeco-Roman urban road network and determines the orientation of the residential quarters. The *dromos* ends in an enclosed kiosk decorated with a pair of lions. Perpendicularly, a second road continues westward to the desert. On the east side, there is a roman *fullonica*, i.e. a workshop for the processing of wool. Going south, the eastern and western sides of *dromos* host a series of Graeco-Roman quarters: among them stands the so-called *insula* of the papyri, widely known because of the exceptional discovery of a vast number of inscribed fragments in the spring of 1934. Various roman banquet

halls (*deipneteria*), probably related to religious ceremonies, are also located along the *dromos*. After the second kiosk, further domestic environments can be found.

Just in front of the temple there's an open vestibule, probably built by Ptolemy XII Neos Dionysos or Augustus, which was decorated with reliefs depicting the annual procession of the mummified crocodile Soknebtynis. A further *dromos* extends eastward just before the access to the main sanctuary, possibly leading to another temple dedicated to Osiris or Min. The shrine of Isis-Thermouthis is located at the crossroad between the two streets. South, the desert police station and a huge refuse dump where thousands of archaeological objects and written texts have been found since 1994: among them hieratic, demotic and greek papyri, *ostraka* and *tituli picti*.

Besides the vestibule, rises the complex of the Soknebtynis sanctuary, built by Ptolemy I over an existing pre-Ptolemaic temple. Two limestone pillars give access to the first courtyard: inside, various buildings hosting production activities (e.g. bread ovens, various kilns, a mint) and another roman *deipneterion*. The second courtyard contains the temple of the crocodile god himself, which is surrounded by warehouses and priests' houses. The necropolises of the village extend to the south and west of the *kôm*.

Before the beginning of this project, the Tebtynis glass-workshop was generically referred to the Soknebtynis sanctuary with no further specifications. A detailed discussion on this subject will be provided in the next chapter.

3. New data on the inlay workshop discovery

The present chapter is intended to offer a critical review on the discovery of the Tebtynis inlay workshop, as recently emerged from the archival documents related to the excavations of Carlo Anti. Over the years, many authors have reported the existence of an "enamel workshop" in Tebtynis, following the short reports published by Anti at the end of every field season (Anti, 1931a-b; 1931-1932). However, after the conclusion of the Italian campaigns, most of the structures unearthed within the sanctuary and the village were damaged or covered by the sand and have never been re-excavated ever since (Rondot, 2004).

During her PhD, Deotto (2015) recovered a series extracts from Anti's archive specifically related the discovery of the "enamel workshop". Starting from those data, the research presented here first aimed at verifying Anti's hypothesis, which had never been questioned before[1]. The confirm of the reliability of his interpretations was obtained thanks to a detailed scrutiny of the archival data and a first examination of the materials discovered in the craft area (now at the Egyptian Museum, Turin – Italy). After these preliminary steps, the project focused on the functional interpretation of the structures, the spaces and the material record, proposing new thoughts on the production processes and on the significance of the Tebtynis workshop, also in comparison with what is known from other coeval contexts.

3.1 Interpretation of the archival sources

The analysis of Anti's and Bagnani's archives provided an extraordinary opportunity to locate numerous structures and findings inside and outside the *temenos* of the Soknebtynis' temple, whose exact position had been completely lost over time (Deotto 2015)[2]. Anti cited the so-called *laboratorio di smalti* (enamel workshop) various times

[1] See the section "to be or not to be (a workshop), that is the question" in Bettineschi *et alii*, forthcoming.

[2] The following paragraphs resume and analyze the archival data published in Begg, 1998; Zanovello, Deotto, 2013; Deotto *et alii*, 2017a; Bettineschi *et alii*, forthcoming. For Anti's and Bagnani's archives the collaboration with Giulia Deotto and Ian Begg is greatly acknowledged.

in his preliminary papers (Anti, 1931a; Anti, 1931b; Anti, 1931-1932) as one of the major art finds in 1931, yet he never gave an accurate location of the discovery. The only sporadic reference occurs in a letter from Anti to Pierre Jouguet (1932), published on the annual reports of the *Académie des Inscriptions et Belles-Lettres*:

"*I^er^ s. ap. J.-C. – Dans la première cour on fait place à un plus grand nombre d'idiotai*[3]*: […] une autre [maison] est employée pour l'atelier des fabricants d'émaux colorés."*[4]

As a result of the surveys in the early 2000s, Rondot (2004) cautiously suggested that the workshop might be identified with either structure 20 D or 21 A on Franco's general plan (fig. 3.1). It should be noted, however, that both buildings are located in the second courtyard and that 21A was discovered only in 1932[5].

From its discovery onwards, the Tebtynis "enamel workshop" was cited by various scholars as one of the few Ptolemaic examples of glass (or glaze/ faience) working facilities (se e.g. Valz, 1992; Stern, Schlick-Nolte, 1994; Nenna, 1998; Auth, 1999; Nenna, Picon, Vichy, 2000; Mahnke, 2008; Henderson, 2013; Connor, 2014; Larson, 2016), yet all authors generically referred the structure to the *temenos* of the Soknebtynis' temple. Bianchi (1998) mentioned the presence of a faience workshop in Tebtynis, citing a papyrus fragment discovered in the site. The bibliographic references proposed by the author (that is: Bernand, 1981), however, did not provide a clue to ascertain the existence of the text and its specific content. The indication seems, more probably, the result of a translation error: in fact, the cited pages refer to the "enamel" workshop in the sanctuary of Tebtynis, but only as one of the structures identified during Anti's excavation, without any quote to a related papyrus fragment. There is, indeed, reference to a "glassworker" in one I century AD papyrus from Tebtynis published by Grenfell and Hunt (1907, p. 56-58, nr. 278). Yet, unfortunately, the text is a simple acrostic bearing a list of professions (such as, among others, tablet-maker,

[3] In ancient Greek, the term *idiotai* refers to private citizens or, sometimes, simple workers and artisans.

[4] Translated by the author from the original French text in Jouguet (1932): "*I c. AD – Within the first courtyard the number of idiotai grows: […] another [house] is employed for the colored enamel workshop*".

[5] This emerges quite clearly both from Franco's plan of 1931 excavations and from Deotto's reconstruction of the various campaigns.

engraver or goldsmith) in alphabetical order without any evident connection with the site itself.

After almost eighty years of speculations, the definite answer about the effective location of the workshop recently come from Anti's diaries and notes. However, it should be remarked that the available archival data show certain limitations: the documentation does not always clearly distinguish the phases or functions of the different areas, the photographs do not offer an overview of the inner rooms of the workshop and specific finding locations are given only for a few particularly significant materials. Finally, the temple has not been excavated systematically since 1936 and most of the structures have now been lost (at the hands of *sebâkhin* or antiquities hunters) or were buried again under the sand (Rondot, 2004).

Moreover, the terminology used in the early 1930s does not fully correspond with the modern vocabulary and can thus create bias and misunderstandings. A detailed list of the various interpretations given in the literature from the 1980s to date for the term "*smalti*" (enamels) used by Carlo Anti in his preliminary papers can be found in Deotto *et alii* (2017a). From a terminological point of view, this work will generally conform to the discussion proposed by Lucas and Harris back in 1962; these authors formalized a distinction between definitions based on functional parameters (e.g. inlays) *vs* definitions related to the material characterization (e.g. glass):

"Glass inlay is often called enamel, paste, or pâte de verre. It is certainly not enamel, which, although a vitreous material, is employed in the powdered state[6] *and fused into position by heat, whereas the ancient Egyptian material was always cut, or mould, and cemented into position. The terms paste and pâte de verre are unsatisfactory, because meaningless, and they are often used very loosely and sometimes are even intended to be non-committal. […] It is suggested, therefore, that the terms paste and pâte de verre should be discarded and that the material used should always be called for what it is, namely, glass."*

[6] Enamel is commonly defined from a combined functional and compositional point of view as an opaque (but sometimes translucent or transparent) glass characterized by a low melting point and often strongly colored, which is applied for decorative purposes to the surface of different types of materials, especially metals and metal alloys, not necessarily in the powdered form (Bayley, 2015).

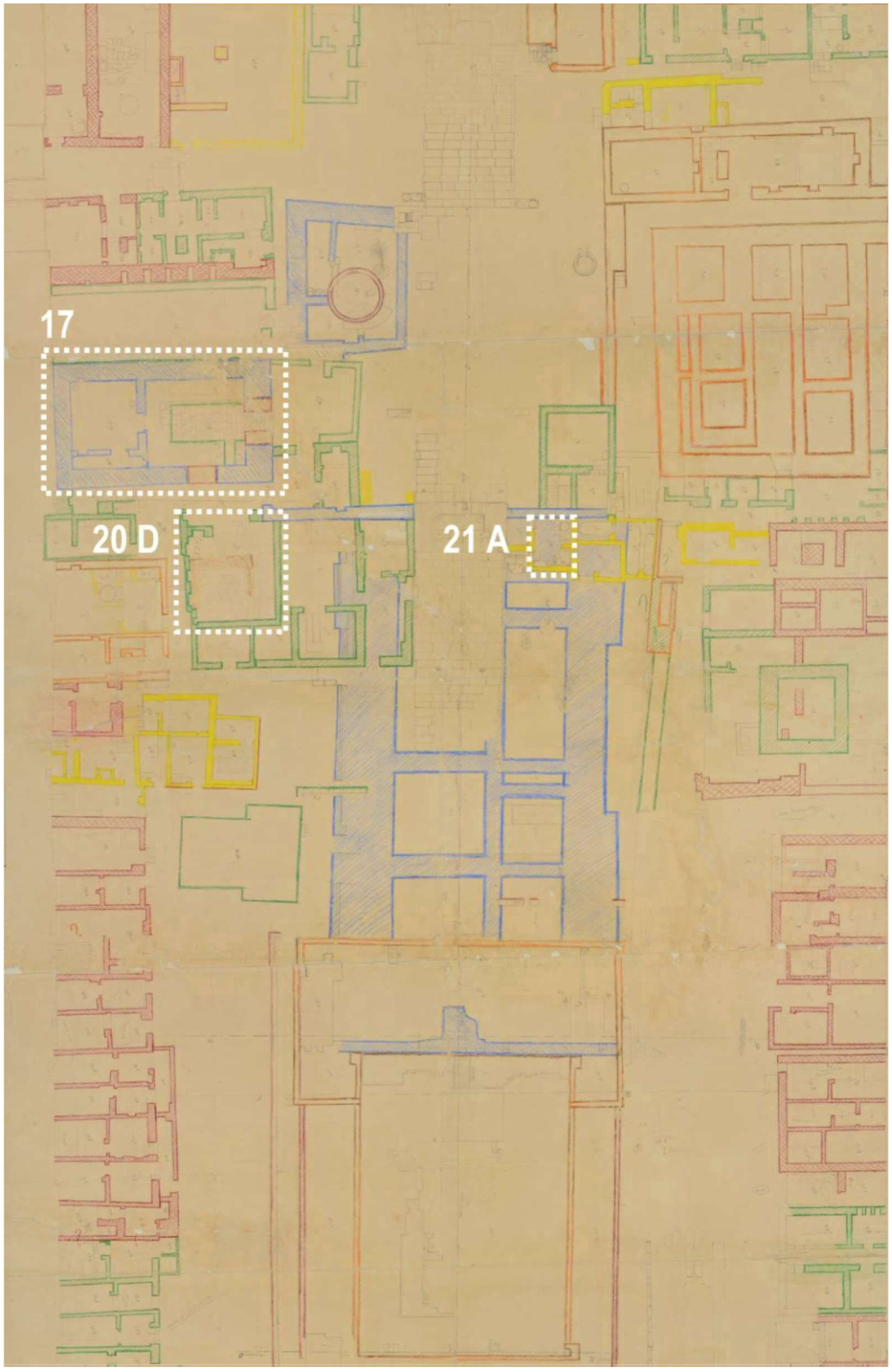

Fig. 3.1 – Detail of Fausto Franco's general plan of the temple (North-Up display). Colors indicate the chronological phases: blue is pre-Ptolmaic, orange early-Ptolemaic, red middle-Ptolemaic, green Roman, yellow Byzantine and Arab; for further data on the map and the digitalization project please refer to Carpinelli et alii, 2017; Menegazzi, 2017). MSA, Anti's archive.

The opportunity to link the archival papers with the collection of findings from Tebtynis preserved in the Egyptian Museum in Turin was indeed crucial to solve the issue. The extracts from Anti's and Bagnani's documentation dealing with the Tebtynis inlay workshop will be reported and discussed in the following paragraphs, giving a first critical review of their interpretation at the light of the most recent archaeological discoveries.

3.1.1 *Anti's documents*

During the campaigns in Tebtynis, Anti kept a detailed documentation of his works. Unfortunately, first his academic position as a Rector of the University of Padova and later the upheavals of World War II prevented him from publishing a revised synthesis of the excavations. However, he preserved a huge quantity of papers, sketches, photographs, maps, videos and notes in his personal archive. After Anti's death, the archive was split in various parts among his family, friends and different public institutes (Menegazzi, Urbani, forthcoming). Currently, the material regarding Tebtynis is divided between the Museum of Archaeological Sciences and Art (MSA) of the University of Padova and the Istituto Veneto di Scienze, Lettere ed Arti (IVSLA) in Venice.

The archival documents report that the workshop was found on February the 27 of 1931 (fig. 3.2). At first, it was simply labelled as "*la terza casa a sud della porta ovest*"[7] (Deotto *et alii,* 2017a). Subsequently, the building was identified as number 17 on Franco's general plan. Anti describes the stratigraphy of the various rooms; for 17 D he states:

"*Nello strato superiore si trovano i mattoni crollati dall'alto e resti della copertura senza oggetti. Nello strato di m. 0.50 sopra il pavimento, chiuso da un battuto antico entro terriccio fine con un po' di ωλέναι si raccolgono elementi di figure di smalto e forme*

[7] Translation from the author of the original Italian text: "*the third house to the south of the west gate*".

da fondere, che fanno pensare ad un laboratorio. Questo erano tutti in uno strato di terriccio finissimo alla superficie."[8]

(IVSLA, Anti's archive, envelope 7, dossier 1, n. 1).

Leaning against the western wall, Anti also recovered a counter made up of a few rows of bricks. Its chronology is not specified and yet, if coeval to the workshop, it could possibly refer to a working surface used during the production processes.

Soon after, the excavations unearthed room 17 E, which yielded various objects described as enamels, molds and a bronze pestle. But the most significant finding in that room is "*un fornello fornito di lunghissima canna e quindi ad alto tiraggio*" (Zanovello, Deotto, 2013).

Fig. 3.2 – Building 17, front view. MSA, Anti's Archive.

[8] From the original Italian text in Deotto *et alii* (2017a): "*In the upper layer, we found remains of bricks collapsed from the ceiling without objects. In the layer 0.50 m above the ground, closed by an ancient earthen floor with a little ωλέναι, we gathered elements of enamel figures and molds, which suggest a laboratory. All those materials came from a layer with fine soil surface*".

Fig. 3.3 – The kiln of the deipneterion, detail of the fire chamber. MSA, Anti's Archive.

The "*fornello*" (kiln) was described and partly illustrated in figure 3.3, but never indicated in the plan of the building. However, the reasoned comparison between the textual and planimetric sources suggest that the furnace can be identified with good confidence in the tripartite structure located in the south-eastern wall of room 17 E on Franco's plan (fig. 3.4a). The term "canna" in Italian is rather ambiguous, as it may refer to a cane, a blowpipe, a bellow or a chimney. Considering the reference to the high draught ("*alto tiraggio*") and the peculiar niche embedded in the wall of the kiln it is safe to assume that Anti is referring to a chimney. Therefore, the text can be translated as follows: "*a kiln with a long chimney and thus with high draught*". The identification of the kiln offered the chance to determine its shape and size, which are important pyro-technological indicators; the structure is quadrangular and its foundations (calculated inside the firing chamber) measure approximately 65x70 cm, while the chimney

embedded in the wall is 32x21 cm[9]. The exact height is not known, but judging from historical photographs of building 17, it was probably preserved until around 1.2-1.5 meters. There are no images of the kiln itself, just a close detail of the stoke hole, which is irregularly shaped (fig. 3.3). On the upper left side of the opening there are two circular hollows in the wall, possibly related to a small shelf or a sort of hangers. The overall size of the structure bears a certain resemblance with the glass-blowing furnaces represented on the I century AD oil lamps discovered in Italy and Dalmatia (Lazar, 2006), even if the elements for an effective comparison are lacking (fig. 3.4b).

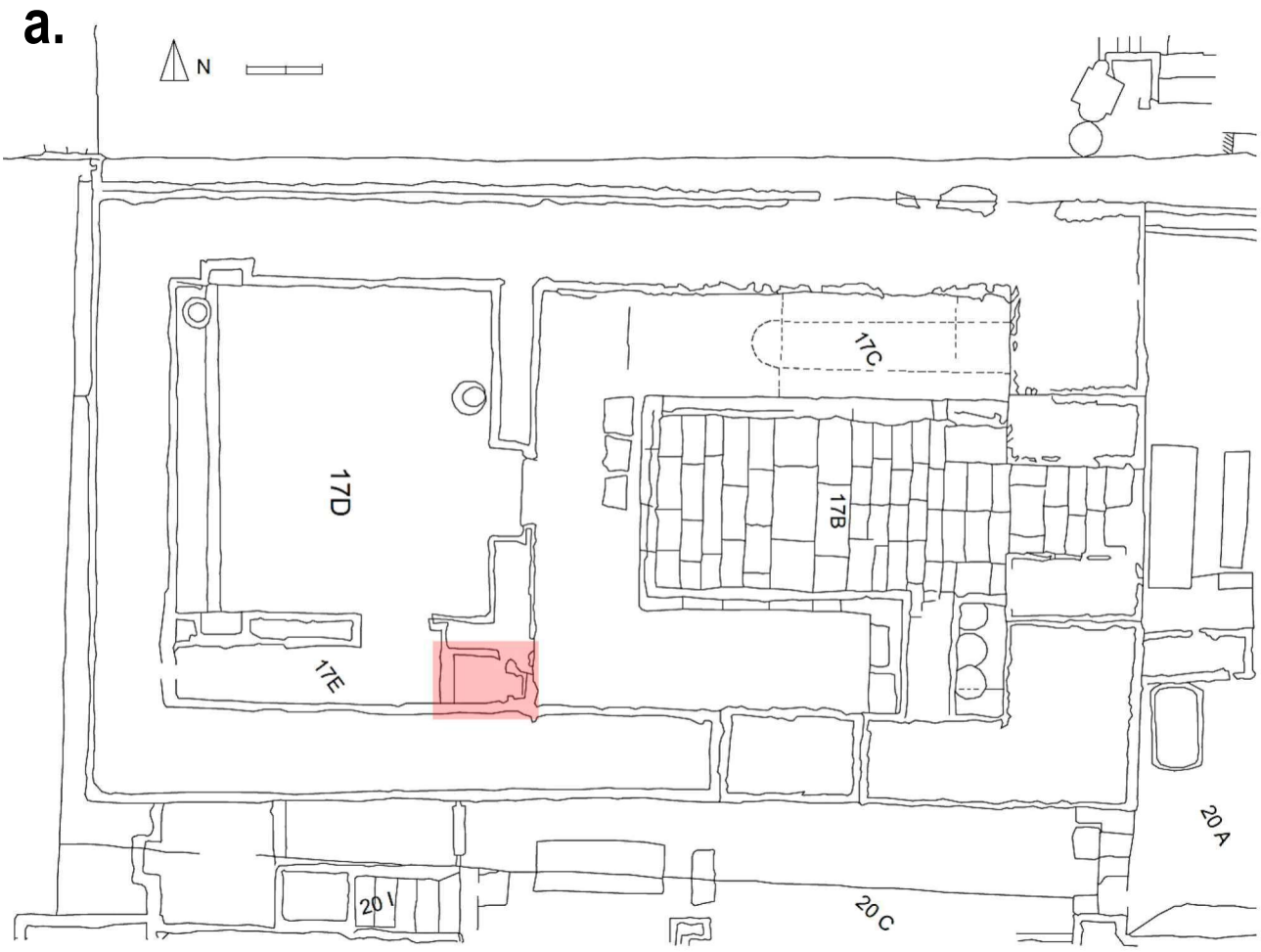

[9] The measures were calculated starting from the georeferenced version of Franco's map produced in the framework of the "Horus" project. The Bachelor thesis of Andrea Meleri (2017) have recently demonstrated that the distances extrapolated from the GIS are subject to an error in the order of 2-4% and can thus be considered very reliable.

Fig. 3.4 – a) detail of building 17 of the general plan (North-Up). The kiln is highlighted in red. Tracing by G. Deotto. MSA, Anti's Archive; b) picture and drawing of the oil lamp from Spodnje Škofi je near Koper with glass-blowing scene (Lazar, 2006).

Room 17 B was furnished with a series of benches, a stone floor and a small cellar. Because of its peculiar configuration, it was soon interpreted as a roman *deipneterion*, Anti yet notes that:

"*La sistemazione a δειπνετήριον è evidentemente posteriore. […] ai piedi del muro S, carboni e cenere. La parete è anche annerita.*"[10]

(IVSLA, Anti's archive, envelope 7, dossier 1, n. 1).

[10] Translated from the original Italian text in Deotto *et alii*, 2017a: "*The transformation in δειπνετήριον is clearly later. […] at the foot of the southern wall, coals and ashes. The wall is also blackened.*"

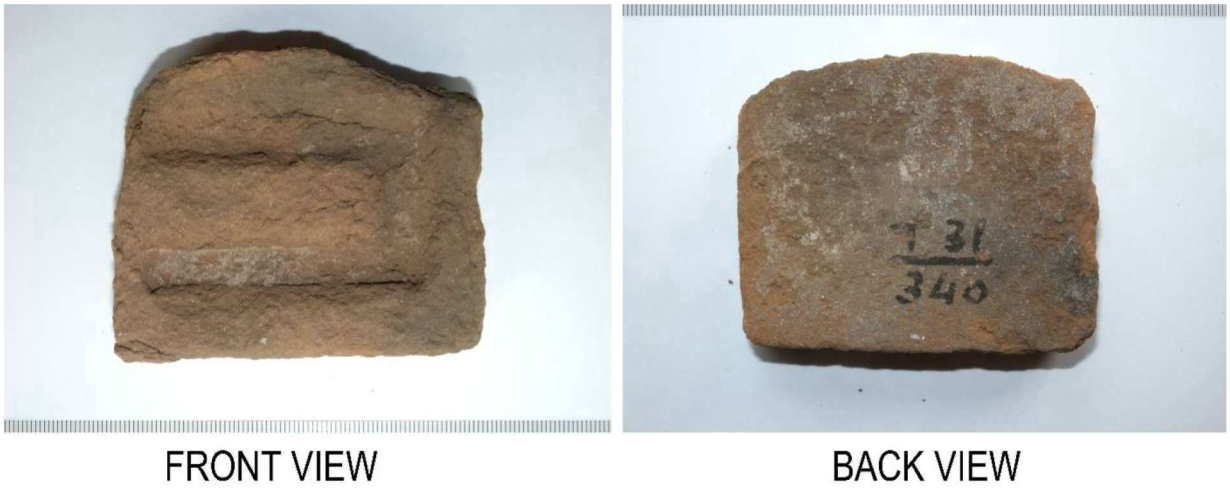

Fig. 3.5 – Mold inv. S. 19268: note the field inventory code on the backside. EMT, Tebtynis collection.

The presence of ashes and coal, and the soot on the wall seem again a clue of the functional transformation that turned the building from a manufacturing laboratory to a ceremonial hall. The reasons beyond this choice are still far from understood. It is, however, possible that roman religious practices (such as those associated with the *deipneteria*) played an important role in the renewal of the temple after the conquest.

Anti described the artifacts discovered in the workshop in two lists, one written in Egypt at the end of the 1931 campaign for the *partage* (cfr. section 3.1.2) and the other prepared in view of a first exhibition planned after their arrival in Italy (Bettineschi *et alii*, forthcoming). The majority of the finds were given inventory numbers directly on the field; their codes are also reported in black or red ink on the objects themselves or on the boxes which contained them (see e.g. fig. 3.5). For example, mold inv. S. 19268 (actual number in the Egyptian Museum collections), bears the code T31 340, where T stands for Tebtynis, 31 indicates the year of the discovery and 340 is the field inventory number, which finds direct reference in the artifact listings and in the annotated photographs preserved in the archive (fig. 3.6).

"*Materiali di un laboratorio di smalti. / Vennero tutti raccolti all'interno del peribolo sotto il pavimento rialzato di un locale che in epoca romana era stato trasformato in deipneterion, cioè in sala per banchetti rituali dei sacerdoti. Che si tratti di un vero e proprio laboratorio è provato dalla presenza di attrezzi, forme, materia grezza e dal fatto*

che in un piccolo ambiente vicino esisteva un fornello fornito di lunghissima canna e quindi ad alto tiraggio. Esso documenta che entro il santuario accanto agli edifici di culto vivevano oltre i sacerdoti quanti erano utili o interessati alla vita del santuario, operai e artisti di ogni genere. / nn. d'inv. 340-349. Forme in terra refrattaria o in calcare per elementi a smalto figurati (gambe, corna, corona, geroglifici, etc.) / nn. d'inv. Crogiuoli piatti in terra refrattaria per la fusione della pasta vitrea. / n. d'inv. 352 Frammento di modello in gesso rappresentante il disco solare alato. Serviva per preparare gli elementi a smalto necessari a decorare analogo motivo in legno. / n. d'inv. 362. Frammento di modello in gesso in forma di cornice a gola, d'uso uguale al precedente. / nn. 355 e 356. Spatola e pestello in bronzo per la macinatura e la mesticazione delle polveri. / nn. 358 e 359. Due pesi in basalto / nn. [sic.] Elementi a smalto figurati da servire per l'intarsio di mobili. / nn. [sic.] Elementi a smalto decorati da servire per l'intarsio di mobili / nn. [sic.] Campionario della materia prima (vetro filato di vari colori), usata per la preparazione degli smalti a mosaico. / n. 363. Tavoletta in legno intarsiata a smalto, esempio dei lavori che si eseguivano nel laboratorio. M. 0,21x0,125. In alto il disco solare alato (cfr. il modello n. 352) e sotto una striscia di stelle bianche in campo azzurro (cfr. il n. [sic.] tra gli elementi decorativi). / Sotto il Faraone seguito dalla Regina, adora Harpocrates e la dea Hathor. / n. d'inv. 425. Thoeris…"[11]

(IVSLA, Anti's archive, folder n. 6, dossier n. III, n. 4).

[11] Translated from the original Italian text from Bettineschi *et al.,* forthcoming: "*Materials from an enamel workshop. / They were all gathered inside the peribolos, under the raised floor of a room that in Roman times had been transformed into a deipneterion, that is, the ritual banquet hall for the priests. Whether it is a real workshop, it is proven by the presence of tools, molds, raw materials and by the fact that in a small room nearby there was a kiln provided with a long chimney and thus with high draft. It documents that the sanctuary, just beside the sacred buildings, hosted beyond the priests all those people who were useful or interested in the life of the sanctuary, workers and artists of all kinds. / nn. inv. 340-349. Refractory or limestone molds for figured enamel elements (legs, horns, crowns, hieroglyphs, etc.) / nn. inv.* [sic] *Flat crucibles in refractory fireclay for the fusion of the glass paste. / n. inv. 352. Fragment of a plaster model representing the winged solar disc. It was used to prepare the enamel elements needed to decorate a similar wooden motif. / n. inv. 362. Fragment of plaster model in the shape of Egyptian gorge, of the same use as the previous one. / nn. 355 and 356. Bronze spatula and pestle for grinding and mixing the powders. / nn. 358 and 359. Two basalt weights / nn. [sic] Figured enamel elements to be used for the inlay of furniture. / nn. [sic] Decorated enamel elements to be used for the inlay of furniture / nn. [sic] Sample of raw materials (glass of various colors), used for the preparation of the mosaic enamels. / n. 363. Wooden tablet inlaid with enamels, an example of the work carried out in the workshop. M. 0.21x0.125. At top the winged disk (see model n. 352) and below a strip of white stars on a blue background (see n. [sic] among the decorative elements). Below the Pharaoh followed by the Queen, worships Harpocrates and the goddess Hathor. / n. inv. 425. Thoeris...*"

This method was developed to simplify the identification of the pieces and, yet, Bagnani's words highlight the difficulties in recognizing the boxes and the objects after their arrival in Italy.

"*10/06/32 / 6 via Pompeo Magno/ Caro Professore, / Grazie della sua lettera e dell'assegno che ho ricevuto oggi come pure in questi giorni ho ricevuto l'Engelbach e le fotografie, compresa quella di Petesuchos. / So, di capitelli, ne sono riuscito a trovare solo 6 ma ci riguarderò. Il guaio è che tra spedizionieri, dogane, musei e altri impicci quelle benedette casse hanno tanti numeri che sembrano delle tavole Pitagoriche! E di conseguenza non si possono identificare sulla sua lista. In ogni modo quando esporrò gli oggetti del laboratorio farò una revisione di tutto quanto. Avverto che le casse sono in condizioni abbastanza pietose: si sfasciano da sé…*"[12]

(IVSLA, Anti's archive, folder 9, n. 53).

Despite the problems encountered by Bagnani, this method is an essential tool which can be used nowadays on the objects preserved at the Egyptian Museum of Turin (and eventually in The Cairo Museum) to identify the materials discovered during Anti's campaigns and to contextualize them according to their spatial and chronological provenance (see e.g. tab. 3.1 for the production tools).

3.1.2 *Bagnani's letters*

During his first season in 1931 excavating at Tebtynis with Carlo Anti, Gilbert Bagnani wrote letters every week to his wife, Stewart Bagnani, and to his mother, Florence Dewar Bagnani, both living in Rome.

[12] Translated from the original Italian text from Bettineschi *et al.*, forthcoming: "*10/06/32/ 6, Pompeo Magno street/ Dear professor,/ Thank you for your letter and check that I received today, as well as I received the Engelbach and the photographs, including that of Petesuchos, in these days. / I know of the capitals, I managed to find only 6 of them, but I will try again. The trouble is that among freight forwarders, customs, museums, and other things, those blessed boxes have so many numbers that they look like Pythagorean tables! As a result, one cannot identify anything on your list. Anyway, when I will display the objects of the workshop I will review everything. I know that the boxes are in pretty pensive conditions: they are falling apart by themselves...*"

Fig. 3.5 – Annotated photograph of the tools discovered within the glass workshop. Up left, note mold inv. S. 19268 of fig. 3.5. IVSLA, Anti's Archive.

Stewart's letters are preserved in the archives at Trent University, Peterborough, Ontario, and Florence's letters are in the archives of the Art Gallery of Ontario (AGO) in Toronto[13]. Most of Bagnani's correspondence is in English: he was raised bilingually speaking respectively to his mother (born Canadian, she later moved to Scotland and finally Italy) and father (from Pisa, Italy). Bagnani constantly updates his wife and his mother on the evolution of the dig. When talking about the artifacts discovered in the glass workshop he soon highlights the exceptionality of the find and expresses his aesthetic appreciation and scientific enthusiasm.

"The stuff is perfectly lovely. All Ptolemaic glass pastes for inlays, the men red the women a heavenly blue, and the [clothes] all the most wonderful colours. Some of the prettiest stuff I have seen for long time. Of course the worst of it is that most of it is going to be nabbed by the Museum which is not rich in pieces of that kind."

(Wednesday 4 March 1931 to Florence Bagnani, at the AGO)

The Museum confiscation Bagnani is referring to is the so-called *partage*, a system by which excavated artifacts were divided between Egypt and the international archaeological missions during the early XX century. The law was enacted in 1924 following the exceptional discovery of the Tutankhamen tomb and stated that all Egyptian antiquities were owned by the local government which, however, could agree to return those which were not necessary for implementing national collections to the foreign excavation teams (Stevenson, 2014). As for the Tebtynis inlays, Rondot (2004) recognized some of the finds present on the 1931 pictures at the MSA in the storage depots of the Cairo Museum (fig. 3.6a). However, contrary to Bagnani's prediction, most of the framed and unframed glass inlays were allowed to be sent to Rome, and are now preserved in Turin.

In 1931, Bagnani spent most of his time away from the dig getting supplies, keeping contacts with the local authorities, visiting sites, Museums and meeting other

[13] For permission to cite the following extracts, I am indebted with professor Ian Begg, who is currently studying the Bagnani's archives in Canada, and to the Archivists Jodi Aoki and Larry Pfaff.

archaeologists. This is the reason why he was not present on the day of the discovery of the inlay workshop. However, he was in Tebtynis when the temple library was found:

"The funny part is that all the workmen say that I am the lucky one. They knew I had come back on Saturday to remain till the end of the season and they say that when I came back then the papyri began to come. They forget that the pastes came when I was away, but then they do not realize their value. They think that we are out only for papyri, and anything else seems worthless to their eyes."

(Wednesday 11 March 1931 to Stewart Bagnani, at Trent University)

It is interesting to notice and compare the perception of the workers with the one of the scholar. Bagnani is deeply aware that the discovery of the "pastes" can be considered as much important as that of the library, yet the local workers – who had been used to dealing with papyrologists, such as Evaristo Breccia (or Rubensohn, Grenfell and Hunt before him) – could not understand their relevance.

Over the years, Bagnani kept on reporting the discovery of inlaid objects in his letters.

"This is the last week of the dig, and the funny part is that we have started finding a certain number of quite interesting things: a very nice piece of wood with a seated god on it in gilt and glass inlay, and three pieces of limestone with drawings on them, also a certain number of papyri, but not in very good condition."

(Monday 4 April 1932 to Florence Bagnani, at the AGO)

However, the most significant data related to the inlay workshop come from a letter to his wife of the early March 1931, where Bagnani lists the artifacts found within building 17. Not only does he give an account of the tools and inlaid objects unearthed there, but also proposes some preliminary hypotheses about the function of the structure and the materials, which are well worth considering.

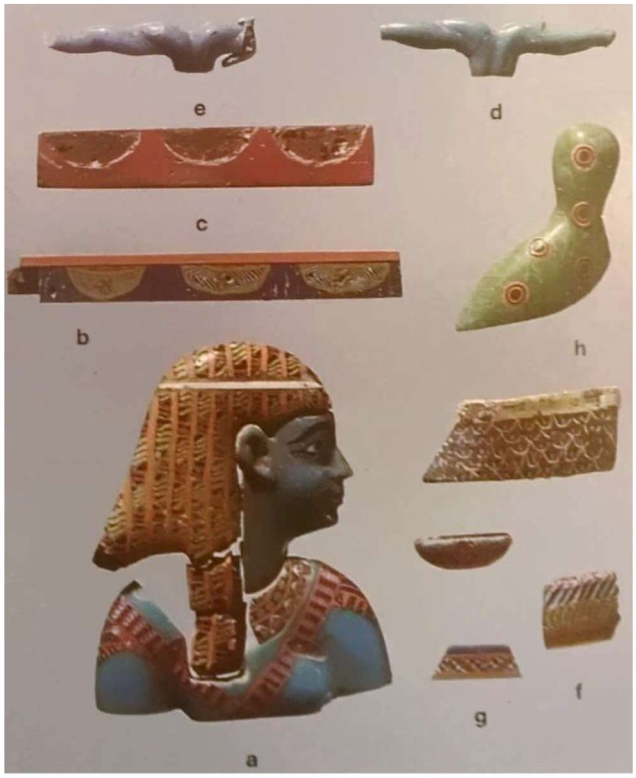

Fig. 3.6 – Glass inlays from Tebtynis, now in the Cairo Museum (from Rondot, 2004).

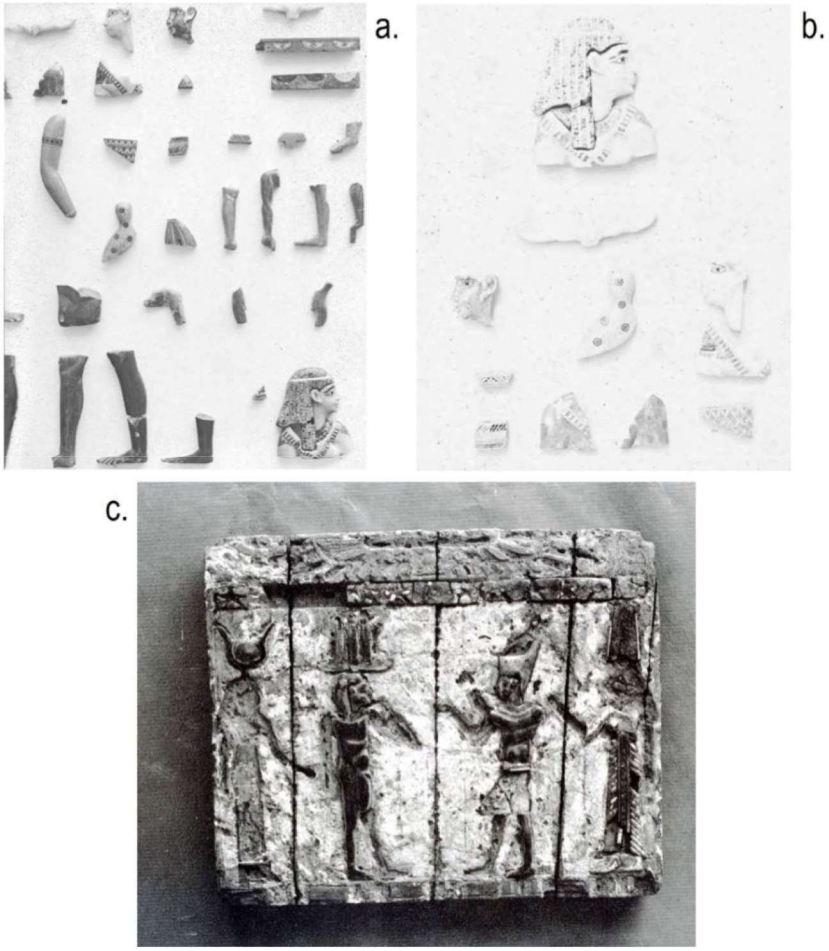

Fig. 3.7 – 1931 pictures of the glass inlays (a-b) and inlaid objects (c) discovered within the workshop. MSA, Anti's archive.

We then went back to the camp and Anti took [Director-General Pierre] Lacau[14] down to see the stuff in the storeroom. In one of the houses he had found a picture with its frame, unfortunately not in a good state of preservation, but always [sic] a piece of the greatest importance. Then in his tent he showed part of a really big find. Evidently the pilgrims of that day instead of getting oleographs and such like things, bought at the temple little sacred pictures done on stuccoed wooden tablets with the figures inlayed [sic] in coloured glass pastes. We have one of these pictures fairly complete and a number of fragments of pastes of the others, some perfectly lovely. The place where we found them must have been the dump of the shop that manufactures them since we have found a number of the fire-clay molds, chisels, stones for the drills, lumps of pitch and molten glass, and a whole lot of other things."

(Wednesday 4 March 1931 to Stewart Bagnani, at Trent University)

In February – March 1933, the Italian royal family paid a state visit to Egypt. The usual tourists' itinerary was altered so that the Italian excavations at Tebtynis in the Fayum could be included in their visit on March 6. Moreover, while touring the Cairo Museum, they were to be shown one of the glass inlay heads (fig. 3.6a). This is the same head of which Gilbert's wife Stewart painted a watercolor after her arrival in Egypt in 1932. Again, this highlights the huge interest and consideration reserved for the inlays unearthed within the sanctuary, two years after their discovery.

"On Monday [20] I was at the Museum at 8 & went round with Lacau & Engelbach[15] fixing up all the details of the programme [for the upcoming royal tour that week]. They had got their little glass paste head that we found & put it in a place of honour on a black background, very attractive, very decent thing to do."

[14] Pierre Lacau (25 November 1873 – 26 March 1963) was a French Egyptologist and philologist. From 1914 to 1936 he served as general director of the *Service des antiquités de l'Égypte*, currently merged into the Ministry of State for Antiquities (Vandier, 1970). In this role, he was in charge of overseeing the archaeological excavations and ensuring the conservation, protection and regulation of all Egyptian antiquities.

[15] Reginald Engelbach (July 9, 1888 – February 26, 1946) was an English Egyptologist and engineer. He assisted Flinders Petrie in various excavations and created the first Register of the Antiquities of the Cairo Museum (Dawson, Uphill, 1995).

(Friday 24 February 1933 to Florence Bagnani, at the AGO)

3.2 Tools for the craftsmen

The tools and equipment employed by the ancient glassworkers which was recovered in the archaeological record and correctly identified is, unfortunately, relatively small. Stern (2002) published a comprehensive study on the glassblower tools used from Roman to modern times, focusing on the type and evolution of jacks and shears. At present, there are no systematic data available on the instruments associated to Ptolemaic inlay production, except for mold examples.

As for Tebtynis, some of the tools discovered by the Italian Archaeological Mission in 1931 within the workshop are registered in an historical picture reproduced in figure 3.5 (first published in its original form without handwritten numbers in Zanovello, Deotto, 2013). Most of those artifacts have now been identified within the Turin collections thanks to the field inventories and notes preserved in Anti's archives, as noted in the previous sections (fig. 3.11).

Excluding the vitreous materials, so far it was possible to recognize in the Turin collections the following objects unearthed in the workshop (tab. 3.1):

- *Various molds and trays*

To date, not all the molds listed and photographed by Anti were effectively identified in the Turin collections. It is possible that at least some of the missing pieces are located at the Cairo Museum following the *partage*, such as the mold with ram horns T31 342 identified in the *Journal d'Entré*[16] as JE 55958 (Deotto, 2015). However, other artifacts (such as T31 344 and 346, among others) must be still laying in Turin depots, after their reference to Tebtynis got lost or forgotten[17].

[16] The *Journal d'Entré* is one of the three different types of handwritten register books of the Cairo Egyptian Museum. It was recently digitalized thanks to a combined project of the Supreme Council of Antiquity and the American Research Center in Egypt (see Kamrin, 2015).

[17] Giulia Deotto is currently working on a project for the identification of the Tebtynis materials in the depots of Turin. Her work will possibly help to retrace the missing artifacts in the near future.

Among the numerous fragments which were described as molds in the digital catalogue of the Museum, three cannot be associated with pyro-technological processes involving high temperatures and should more probably be interpreted as models or decorative elements. For example, S. 19309 still bears traces of red painting on the upper side and red, ochre-like, traces on the inside (tab. 3.1). The same applies to S. 19278 and, possibly, to S. 19276 even if this last piece has no color residues.

As for the effective molds suitable for firing, only S. 19268 has inner residues which possibly refer to traces of a powdered detaching agent (fig. 3.8). All other pieces show no specific marker associated to inlay production. A number of similar, coeval objects (fig. 3.9) was discovered in Gumaiyima (Petrie, Griffith, 1888; Cooney, 1976), Tanis (Nenna, 2011), Karnak (Fazzini, 2008) and Dyonisias (Schwartz, Wild, 1969), while others coming from private and public collections have unknown provenance (Nenna, 2011). Grose (1989) also published a positive, master mold in limestone with two profile faces coming from the Cairo antiquity market and now in the Ishiguro collection in Tokyo.

Fig. 3.8 – Whitish residues within mold inv. S. 19309.

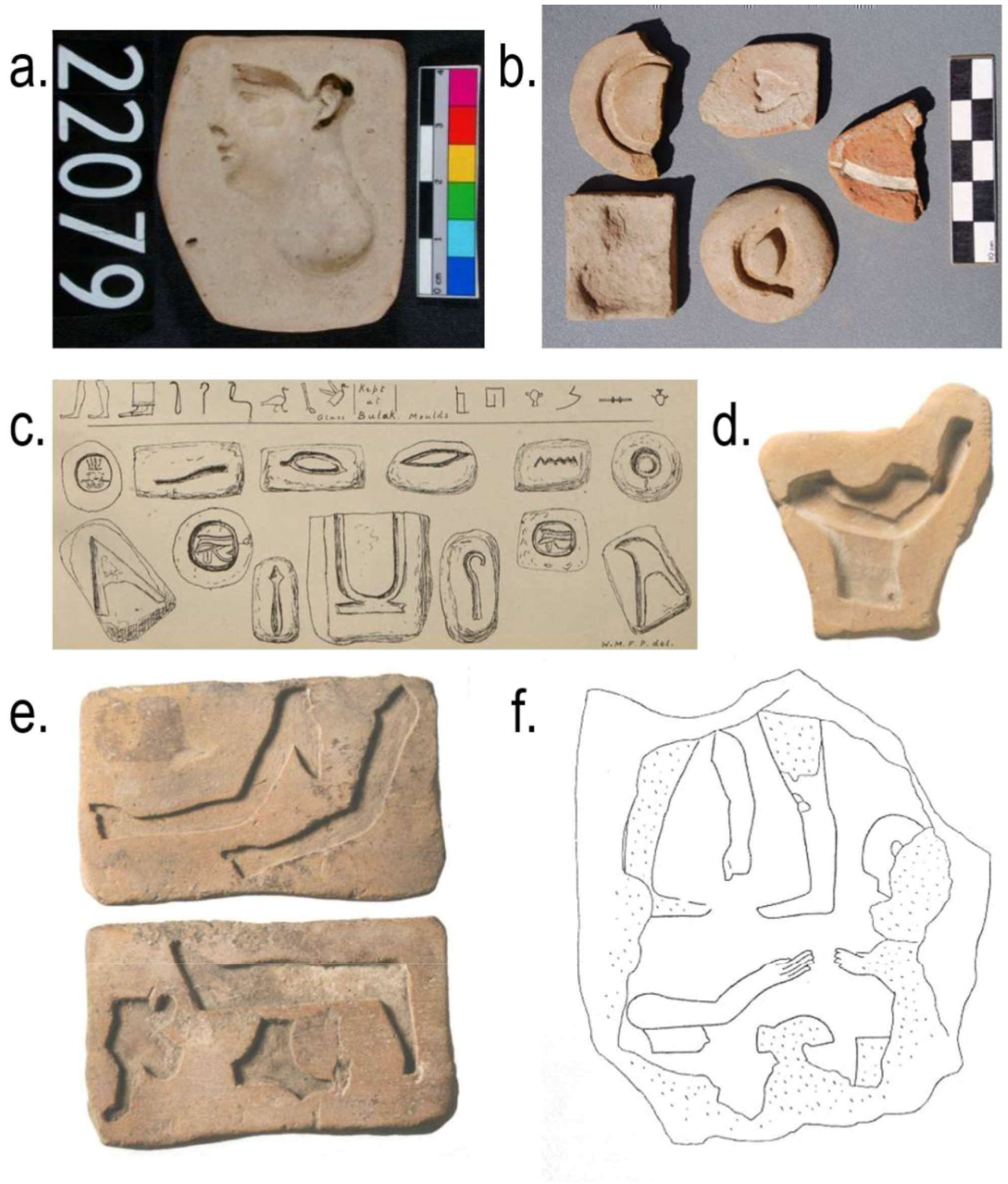

Fig. 3.9 – Inlay molds from Graeco-Roman Egypt: a) head-shaped from Gumaiyima inv. 22079 (Petrie Museum, UCL); b) various shapes, from Karnak (Fazzini, 2008); c) various shapes from Gumaiyima (Petrie, Griffith, 1888, plate XVIII); d) torso-shaped from Tanis, Louvre inv. E 16029 (Nenna, 2011); e) double-side mold with elements of the human body, Louvre inv. E 3225, unknown provenance (Nenna, 2011); f) limestone mold with elements of the human body from Dyonisias (Shwartz, Wild, 1969, fig. 53).

On the contrary, it was not possible to trace any significant archaeological comparison among published molds related to glass-working for inv. S. 19269 and S. 19921 (fig. 3.10). According to our interpretation, these tools were employed as trays for assembling stratified or mosaic glass canes from pre-fabricated bars. In particular, after being used for staking up the bars cold, they must have been introduced in the kiln for sintering the various glass elements. This would explain the traces of burning (and the rare charcoal residues) which characterize their bottom surface, but also the upper part and the edges.

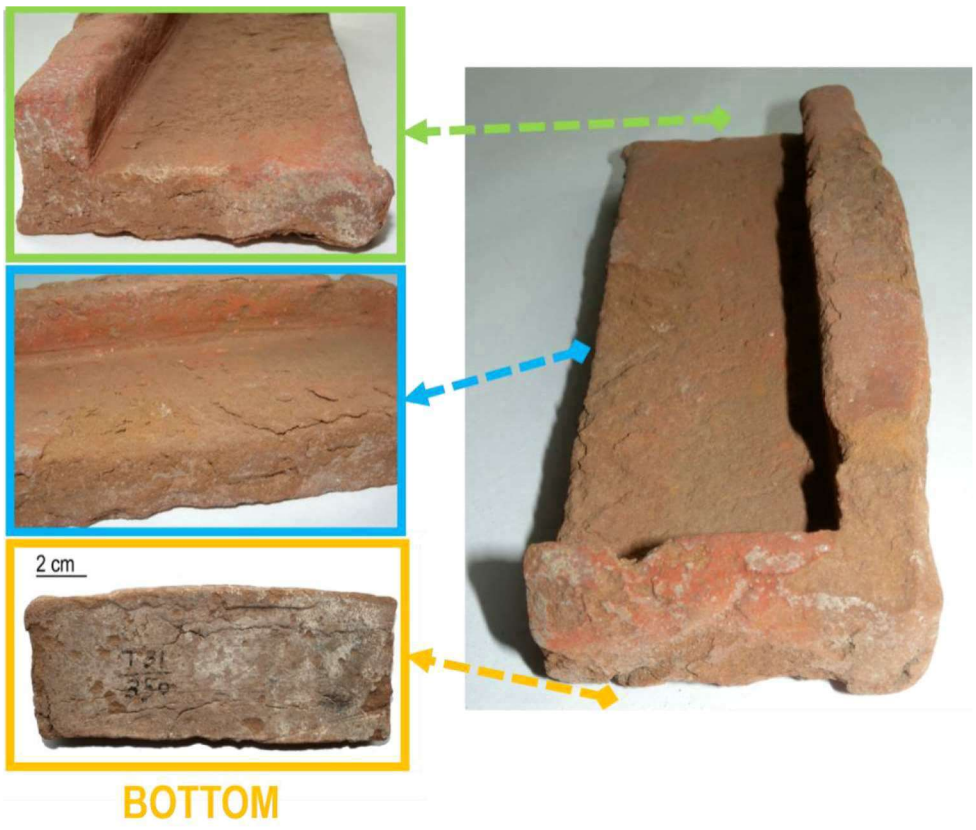

Fig. 3.10 – Tray in fireclay inv. S. 19269. Details of the firing marks (left, from top to bottom): side view, front view, bottom view.

- *A tablet in calcareous alabaster with traces of grinding*

Considering the soft stone used, it is hard to interpret the kind of material which was powdered. However, glass can be certainly ruled out for its hardness on the Mohs scale. Possible candidates may be certain types of pigments or other relatively soft materials (see fig. 3.11b).

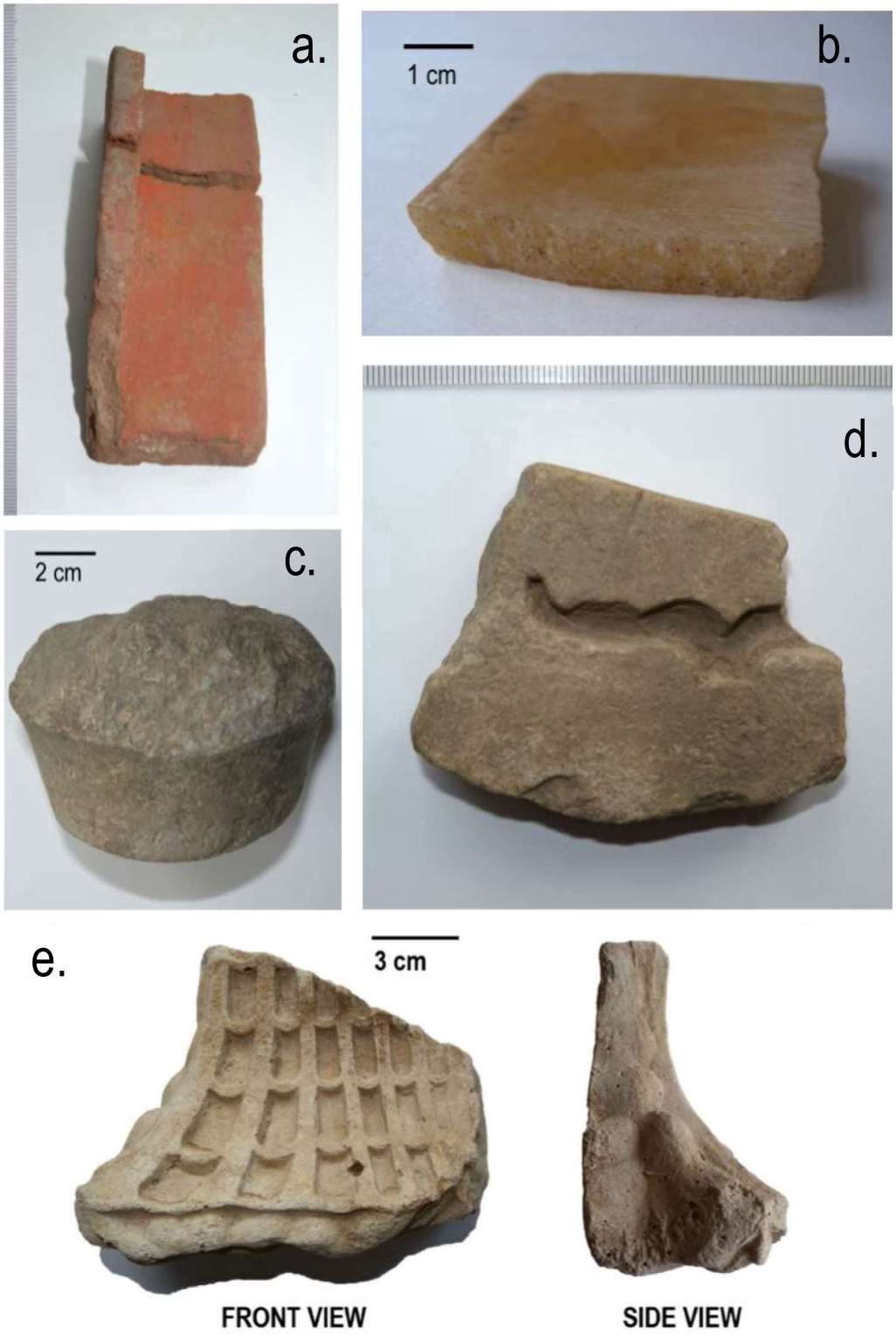

Fig. 3.11 – Selection of the tools recovered in the collection of the Egyptian Museum: a) tray in fireclay, possibly related to the assembling of mosaic canes (inv. S. 19921); b) alabaster table with traces of grinding (S. 18716); c) big, domed stone weight (S. 19272); d) stone mold in form of corkscrew ram horns, part of Hemhem crown (S. 19275); e) Gorge-shaped plaster fragment, possibly referring to a stucco model for wooden furniture or an architectural decoration (S. 18566).

Fig. 3.12: Relief of a sacred procession discovered in Dyonisias by the University of Siena (from Archeo 374, April 2016). Probably to be filled with (glass?) inlays.

- *Two domed weights in hard stone*

Between the two, only the smallest is complete and returned a weight of approximately 46 grams. The comparison to the Egyptian and Hellenistic weight systems concluded that our piece is compatible with the weight of five *qedets*, or a half *deben* (being a *deben* ca. 91-95 grams during the Late Period). The typological classification (Petrie, 1926) further strengthens its Egyptian origin and thus supports the hypothesis of an indigenous tradition for inlay manufacture (fig. 3.11c).

- *Two plaster fragments*

Inv. S. 18566 is in shape of Egyptian gorge (fig. 3.11e), while S. 19220 represents the wings of a solar disk (see tab. 3.1). Considering their composition, which is not suitable for firing, and the concave shape of the gorge-shaped fragment, none of them can be interpreted as a mold, as previously suggested (Nenna, 2015a). Our hypothesis is that we are dealing with stucco models for wooden furniture, as originally proposed by Anti, or with architectural decorations. It should be stressed that the glass inlays within S. 19220 do not appear to be present in the 1931 picture, so they are probably a later

insertion. This is further strengthened by the fact that Nenna (2015a) published a picture of the same object – probably shot in the early 2000s – where the inlays are placed in different spots.

There are no significant archaeological comparisons from Ptolemaic times, except for a hollow relief recently discovered in Dyonisias (fig. 3.12). The object came to light during the excavations of the University of Siena (Italy) and was only published in a preliminary paper (Archeo 374, April 2016) without further specifications. Historical excavations in the same site, also report the presence of "*toutes sortes d'ornements en plâtre modelé*" – that can be translated as "every kind of ornament in modeled plaster" – within one of the houses near the public baths (Schwartz, Wild, 1950). It is, indeed, interesting to note that Dyonisias is – perhaps not coincidentally – one of the few Egyptian sites with traces of a secondary glass workshop, as it will be better discussed in chapter 4. Plaster models with god figures were also discovered in Gumaiyima (Petrie, Griffith, 1888), but there are no published images currently available (cfr. chapter 4), so it is not possible to evaluate an eventual correlation with the Tebtynis examples.

- *A lump of organic binder*

No historical picture shows the lump of brown, solid and amorphous material inv. S. 19201 (tab 3.1). However, this is most probably one of the objects Bagnani is referring to when talking about the "*lumps of pitch"* discovered in the workshop. The point is also strengthened by the fact that a huge number of spare inlays and all inlaid objects still preserve a layer of a similar substance, used as a binder.

Similar traces were also found adhering to *sectilia* panels, architectural decorations, wooden furniture or inlay fragments in various Graeco-Roman sites in Egypt (see e.g. Harden, 1936; Petrie, Griffith, 1888). Archaeometric investigations on Tebtynis samples are planned for the near future, however it is already possible to propose some preliminary speculation on their composition on the basis of the analyses performed on a set of eleven specimens discovered in Antinoopolis, a Late Antique glass-working center in Middle Egypt (Silvano, Ribechini, 2014). Essentially, all samples revealed the presence of organic material, frequently mixed with a high proportion of calcite,

probably added to grant better working consistency and dryness to the final adhesives. Gas-chromatographic data, allowed Ribechini and colleagues (2009) to identify the main organic sources as pine pitch and beeswax, with eventual traces of brassica oil. Of course, these results cannot be directly applied to the case of Tebtynis; nevertheless, OM observations highly suggest a generic characterization as organic compound.

In addition to the artifacts listed in table 3.1, the archival documents and the historical pictures indicate the discovery of at least a bronze chisel, a metal rod, stones for the drills, a big mortar and a pestle. These elements appear well suitable for a glass-working area, yet the impossibility to conduct direct observations on the pieces prevents from going into the details of their role in the production processes. Hopefully, the ongoing census of the Tebtynis collection at the Egyptian Museum of Turin will soon offer the chance to identify and study also these missing objects.

Image	Historical image	Anti's field inventory	Museum inventory	Material (macroscopic observations)	Typology
	n.d.	n.d.	S. 19201	organic	lump of adhesive, fragmented ir joinable peces
		T31 340	S. 19268	fireclay	mold with white residues on the inside. Possibly traces of a powdered detaching agent or glass residues
		T31 343	S. 19275	stone	mold in form of corkscrew ram horns part of Hemhem crown, fragmentary
		T31 345	S. 19277	fireclay	double-sided mold, fragmentary
		T31 347	S. 19309	fireclay	model/ architectural element never exposed to fire or to high temperatures, with traces of red painting on the upper side and red, ochre-like, traces on the inside. Fragmentary
		T31 348	S. 19278	organogenic limestone	model/ architectural element never exposed to fire or to high temperatures: it bears red, ochre-like, traces on the inside. Fragmentary
		T31 350	S. 19269	fireclay	tray or mold, possibly used for assembling mosaic canes
		T31 351	S. 19921	fireclay	tray or mold, possibly used for assembling mosaic canes, fragmented in two joinable pieces
	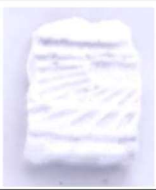	T31 352	S. 19220	gypsum or plaster	fragment of winged solar disk

	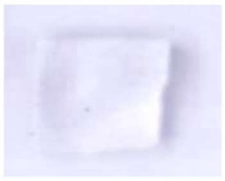	T31 353	S. 18716	calcareous alabaster	tablet with traces of grinding
		T31 358	S. 19272	stone	weight, broken (709 g)
		T31 360	S. 19276	stone	model/ architectural element/ tool never exposed to fire or to high temperatures. Fragmentary
		T31 362	S. 18566	gypsum or plaster	Egyptian gorge-shaped model or architectural element, fragmentary
		T31 359	S. 18914	stone	wieght (46 g)

Tab. 3.1 – Table listing all non-vitreous artifacts discovered in the workshop of Tebtynis and identified in the Turin collection to date. The table shows the modern picture of the objects (column 1) associated with its historical counterpart (column 2), the field inventory code given by Anti (column 3) and Turin's inventory number. Moreover, the pieces are briefly described according to their material composition, as emerged by OM observations (column 4), and typology (column 5).

3.3 The chronology of the workshop

According to Anti, structure 17 lives 3 main phases: the implant of the building is pre-Ptolemaic, but no clear function is known for this first phase; during Ptolemaic times, room 17 D and 17 E (and partially 17 B) were involved in the "laboratorio di smalti" (enamel workshop). Finally, in Roman times (before the first half of the I century AD), the building was restored and 17 B was transformed into a banquet hall for religious ceremonies (*deipneterion*). According to stratigraphic evidence, the activity of the workshop seems, thus, dated to a wide time-span, ranging at least from the Middle Ptolemaic phase until the early Roman era.

Moreover, in his unpublished paper presented at the 18th International Congress of Orientalists, Anti mentions the existence of "*frammenti di mobili intarsiati a smalto, ora nel commercio antiquario del Cairo, ma trovati alcuni anni fa tra le rovine del santuario [di Tebtynis], portano la cartuccia di Tolomeo Evergete*."[18]

Nenna has repeatedly suggested that the glass workshop in Tebtynis is a temporary installation connected to the building of the temple at the very beginning of the Ptolemaic period (Nenna, Picon, Vichy, 2000; Nenna, 2015a) on the basis of the stylistic analysis of the figured inlays.

The existence of glass inlays with the name of Ptolemy III (246-221 BC) provides an important chronological indication, given that the great temple of Sobek was built under the reign of Ptolemy I (305-282 BC). If Nenna is correct in associating the workshop with the production of sacred furniture during the implant phase of the temple, there is a narrow chronological range, between 305 and 221 BC, when the structure was certainly in use.

However, considering the stratigraphic data and Anti's interpretation, it seems that the manufactural area is obliterated by a Roman *deipneterion* only as late as the early-middle I century AD. Therefore, it would be logical to infer that the artifacts discovered by the Italian mission do also date to the last period of activity of the workshop.

[18] Translation of the author from the original Italian text: *"fragments of furniture inlaid with enamel, now in The Cairo antiquity market, but found some years ago in the ruins of the [Tebtynis] sanctuary, carry the cartouche of Ptolemy Euergetes."*

The archaeological study points in two different directions, that cannot be better clarified without further radiocarbon investigations:

1) the Tebtynis glass workshop is a temporary installation, active for less than one century, and Anti failed to recognize the functional conversion which must have taken place somewhere between the Middle/ Late Ptolemaic phase;

2) the workshop is a long-lasting productive structure within the economy of the temple and the artifacts discovered there, although dating to the early Roman period, are heir of the Ptolemaic tradition as not to be distinguishable from a stylistic point of view from their early Ptolemaic counterparts.

4. ÆGYPTVM database: presentation and discussion of the data

Databases, i.e. systematic assemblages of data, have always been part of the archaeological research, even before the advent of computerized technologies. However, it was only during the early 1970s that the increased diffusion of electronic computing devices offered the chance for an exponential growth in the use of quantitative methods in archaeology (Labrador, 1996). In the same period, Codd (1970) introduced the concept of relational model, which laid the foundations for most of the following applications.

Over the years, databases spread widely in the archaeological and archaeometric fields supported by continuous hardware developments and by the opportunities granted by the world wide web. Nowadays, they constitute integral parts of the methods and strategies for the study of the ancient world. However, very few published databases show a real integration between archaeological data (i.e. typological, stratigraphic, topographic, stylistic analyses) and archaeometric *corpora*, especially in the field of glass studies[1]. In this sense, the project *Immensa Aequora* offered a methodological reference point, since it constitutes an organic archaeologic and archaeometric data bank related to ceramics produced in central and southern Italy (Olocese *et alii,* 2013).

ÆGYPTVM (acronym of Ancient Egyptian Production Technology of Vitreous Materials) was conceived as an open-source database aimed to include all published (and partly unpublished) information about Ptolemaic glass-related centers, raw, semi-finished and waste materials and their analytical composition, where available. The most important earlier and later contexts (from the New Kingdom to the Late Antiquity) are also considered for analytical reference. It goes without saying that an hopefully low yet undetermined number of data may have been inadvertently neglected, for example in the case of publications with local distribution or in languages other than English, French, Italian and partly German.

In general terms, this database was developed to guarantee ease of management and of data exchange. These aspects reflect the increasing necessity to process large amounts of different (but related) data and to achieve a rapid updating, consulting and

[1] On the contrary, databases with pure archaeologic or archaeometric aims are actually quite frequent. On the archaeometric side, see for example the FP7-funded project ARCHGLASS (Degryse, 2014) or the ongoing works of Elisabetta Gliozzo (2016) and Cloe Duckworth (2016).

manipulation time. Moreover, ÆGYPTVM was designed to offer an open platform, freely accessible, to be used for researches which may lay outside the scope of this specific PhD project.

4.1 Analysis, design and implementation

Designing ÆGYPTVM involved, as a first step, deciding the types of relevant information to be collected and examined, the most suitable attributes and their relationships. A preliminary assessment of the quality/ quantity/ typology of available data and a trade-off study aimed at minimizing potential errors during data entry while maximizing analytical flexibility was the starting point for planning the architecture of the database. A second, fundamental choice was the selection of the type of Relational Database Management System (RDBMS), between free and open source (FOSS) or proprietary software (PS). The first category includes programs such as Apache OpenOffice Base, LibreOffice Base, SQLite, MySQL, PostgreSQL and the like. Proprietary software is generally licensed at a charge and prevents the end user from modifying, sharing, redistributing and studying their source code. This category comprises some of the most common DBMSs such as Microsoft Access, Oracle and FileMaker.

The best option to guarantee an open data exchange appeared the use of a free software. However, all solutions that required exclusive SQL (Structured Query Language) programming with no graphic interface were excluded, in order to speed-up the process of database design for entry-level users. Ultimately, we opted for LibreOffice Base, which guarantees extensive data exportability (the final product is compatible with other widely-used PS o FOSS such as Microsoft Access, Oracle, OpenOffice Base etc.), constant updating and a relatively simple, but reliable structure.

The ÆGYPTVM Entity-Relationship Diagram (ERD) consists of four basic tables (fig. 4.1): 1) archaeological site; 2) artifact; 3) archaeometric analysis; 4) bibliography. Moreover, there are three associative (or junction) tables to link the bibliography table with the other main tables and a set of utility tables (or *thesauri*) that contain the information included in the so-called combined fields.

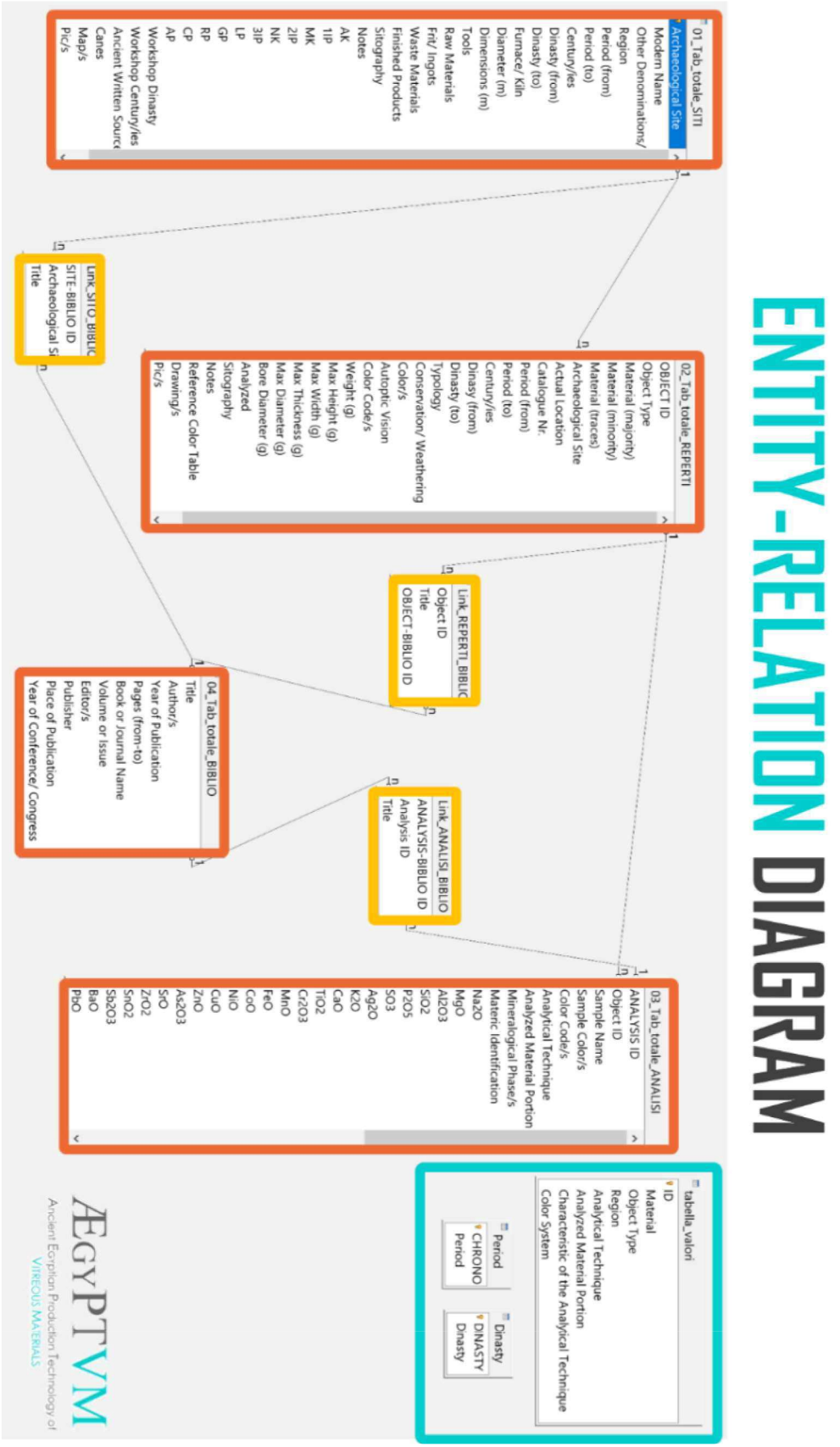

Fig. 4.1 – Entity-Relation diagram of the ÆGYPTVM database. The border colors should be read as follows: orange, the four basic tables; yellow, the three junction tables; light blue, the thesauri.

Each basic table is linked to the others through a pattern of relationships with cardinality one-to-many (1:n), i.e. any element in the parent table can match infinite elements in the secondary table, but not vice-versa.

In the ÆGYPTVM structure, the parent table is constituted by 01_Tab_totale_SITI, whose textual primary key is the site name (Archaeological Site). This field is linked by a 1:n relationship with the same attribute field within the secondary table 02_Tab_totale_REPERTI. Thus, in the secondary table it is only possible to choose (from a drop-down menu) those archaeological sites that already exist in the parent table.

The same cardinality one-to-many links 02_Tab_totale_REPERTI with 03_Tab_totale_ANALISI, by using the primary key and the external key called Object ID, that is an auto-incremental numeric field that constitutes the unique identifier of each record in the parent table. On the contrary, 04_Tab_totale_BIBLIO is linked to the three previous tables through a many-to-many (n:n) cardinality, since each paper can deal with numerous sites/ finds /analyses and each site/ find/ analysis may have several related publications. To avoid problems arising from complex relationships, it was therefore necessary to simplify the structure of the database and transform n:n into 1:n relationships. To do this, the methodology applied in this work was the use of junction tables (Link_SITO_BIBLIO, Link_REPERTI_BIBLIO and Link_ANALISI_BIBLIO), that could connect two 1:n type relationships.

4.1.1 *Input Masks*

ÆGYPTVM comprises three input masks. In particular:

1) Archaeological site (fig. 4.2)

01_Tab_totale_SITI contains indications that enable the geographic and chronological contextualization of the site, but mainly focuses on the production markers, on the structure and the dating of the local vitreous material workshop. Where possible, data entry is supported by pre-compiled drop-down menus to minimize typing errors while populating the database (such as in the case of *region*, *period* and *dynasty*).

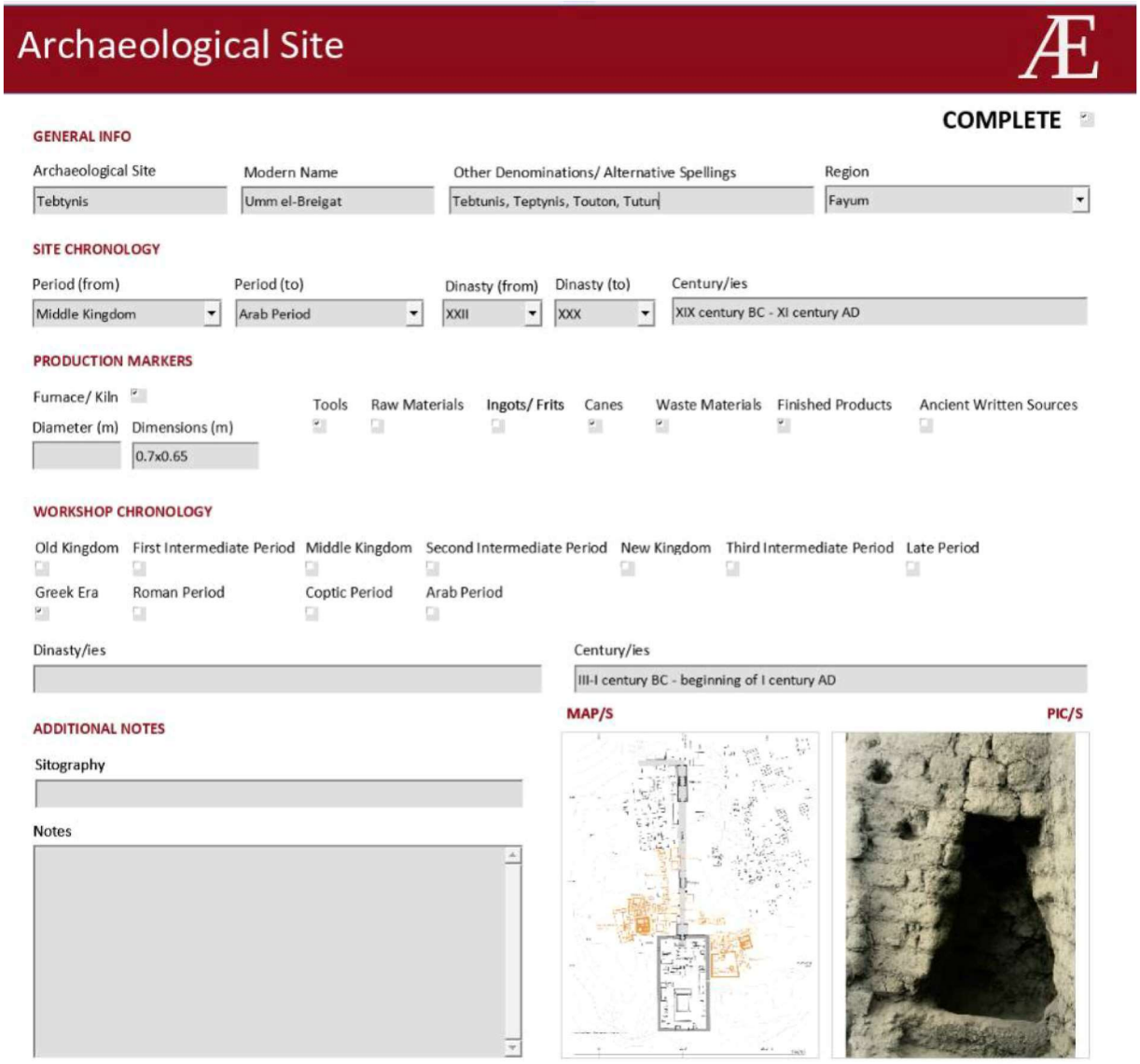

Fig. 4.2 – Input mask "archaeological site".

This mask is divided into various sections; first the general info, comprising name of the archaeological site, modern name, other denominations or alternative spellings and regional contextualization (Upper/ Lower/ Middle Egypt, Fayum, Eastern/ Western Desert/ Nubia). The second section is dedicated to the chronology of the site, which can be expresses with various degrees of detail: period (from Old Kingdom to Arab era), dynasty and century/ centuries. In the "production markers" section, checkboxes are used to indicate the existence of: kiln or furnace (with metric dimensions), tools, raw materials, ingots/ frits, canes, waste materials, finished products and ancient written sources which testify a local glass manufacture. The chronology of the workshop is also

registered with checkboxes, for an easier searching procedure; however, dynasties and centuries can be further specified in dedicated cells.

There is also a space for sitography and eventual notes of relevant data which do not fit in the predefined model of the datasheet. To avoid slow processing times, no more than two low resolution images can be uploaded per entry.

2) Archaeological remains and related analysis (fig. 4.3)

The input mask "Archaeological Remains and related Analysis" combines within the same graphical interface 02_Tab_totale_REPERTI and 03_Tab_totale_ANALISI.

Each object is first described in general terms thanks to pre-compiled drop-down menus, considering its type (e.g. bead, droplet, vessel, shabti, ingot etc.) and material composition (glass, faience, stone etc.), distinguishing the main, minor and trace constituents. Provenance, actual location and inventory number are also considered.

The chronology section is structured following the same principles of the one in "Archaeological Site". Moreover, the mask gives account of the specific typology, the weathering conditions, the dimensions (in mm) and the color/s of the considered artifact.

There is also the possibility to use checkboxes for indicating whether the object was examined autoptically and/ or analyzed. For images and notes, the same rules already mentioned shall apply.

Analyses are collected in a specific sub-mask, which includes name and color of the sample, typology (e.g. SEM-EDS, EPMA, XRF, LA-ICP-MS etc.) and characteristics of the analytic technique (bulk, point, area, surface etc.) used and the analyzed material portion (glass, glaze, interaction layer etc.). The eventual normalization at 100% of the data can be specified with a checkbox.

Results comprise both the mineralogic identification of the sample or its inclusions and a series of cells for registering chemical data (calculated in weight %) on a selection of elements typically found in vitreous materials. A maximum of two SEM images, diffractograms or spectra per entry can be uploaded as low-resolution images. Again, great attention was paid to the creation of combined fields to facilitate, speed up and standardize the compilation of the records.

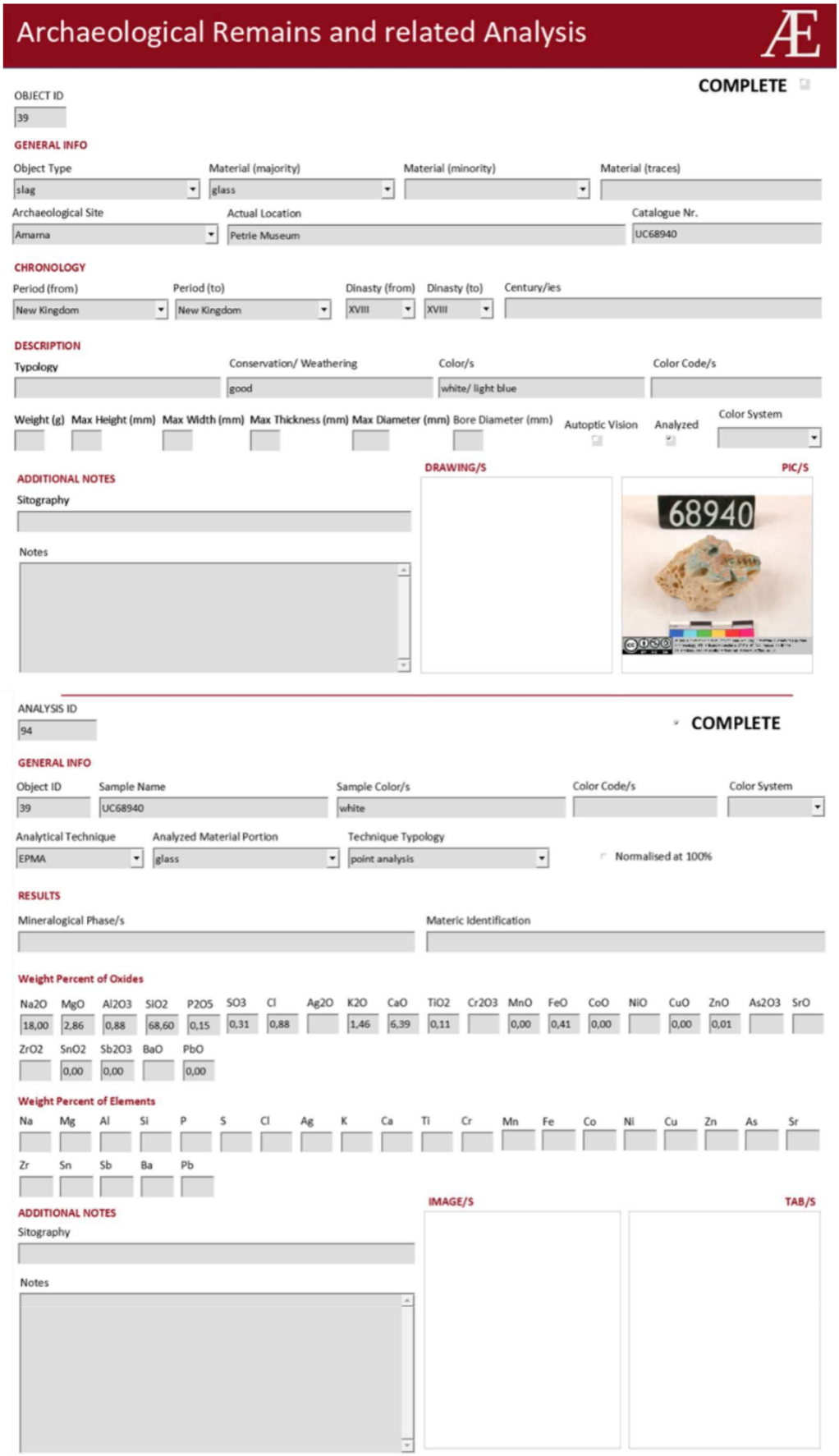

Fig. 4.3 – Input mask "archaeological remains and related analysis".

3) Bibliography (fig. 4.4)

04_Tab_totale_BIBLIO and the related mask "Bibliography" are designed to include all the bibliographic details for identifying a publication, whether a journal paper or a monograph.

Moreover, the mask comprises three junction tables that can be used to relate each bibliographic entry with a potentially unlimited number of archaeological sites, finds or analyses already registered in their respective tables.

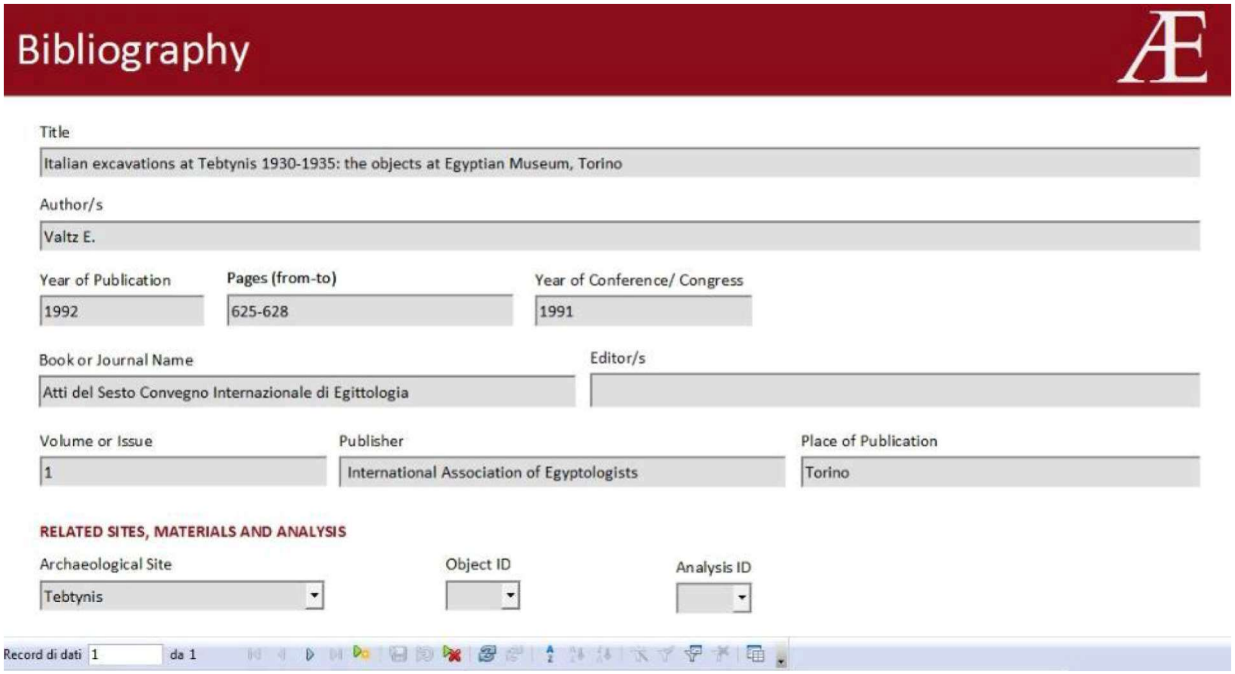

Fig. 4.4 – The input mask "bibliography".

4.2 Glass manufacture in Ptolemaic and Roman Egypt

4.2.1 *Rethinking the paradigm of glass-working vs glass-making*

No introduction on the history of glass is complete without a former premise on the distinction between glass-making and glass-working (see e.g. Shortland, 2012; Rasmussen, 2012; Henderson, 2013; Antonaras, 2013; Moretti, Hreglich, 2013; just to name a few). These definitions have led to distinguish primary workshops, for glass-making, and secondary workshops, for glass-working (Nenna, Picon, Vichy, 2000), thus creating a sort of ranking where glass production centers are frequently stressed with

major emphasis in the glass-related literature with respect to those devoted to the forming of the finished products. Stern (2004) has efficiently summed up the main points of the matter:

"*In antiquity, glassmaking and glassworking were two separate crafts; this has been the case from the very beginning in the second millennium B.C.E. and remained customary throughout antiquity into the Middle Age. The division into primary workshops for making the material and secondary workshops for working and shaping the glass had important consequences for the structure of the Roman glass industry. It is generally accepted that few primary workshops existed in the centuries prior to the introduction of commercial glassblowing in the early Augustan period*."

However, it is becoming more and more clear that this strict separation does not fully correspond to the complexity of the real-life data coming from archaeological excavations. In fact, the debate on the organization of the ancient glass industry has often forgotten to reflect on the substantial role of glass-coloring in the overall process for the manufacture of glass. In fact, the coloring/ decoloring/ opacifying of glass is not only a matter of aesthetic taste or cultural significance, but mostly a technological problem. As it will be better discussed in the following chapters, certain colors or hues require well-calibrated quantities of raw materials, but also specific times, temperatures and redox conditions during firing. One might even say that obtaining certain colors can be even harder than producing the raw glass itself. Thus, trying to highlight when coloring took place in the course of the production processes is a question of huge relevance in the study of ancient glass.

The evidences of Amarna (Nicholson, 2007) and Quantir/ Piramesse (Push, Rehren, 2007) demonstrate that at the dawn of glass history, during the Egyptian New Kingdom (Late Bronze Age), glass was produced in relatively small batches and colored within the primary workshops. On the other hand, Roman glass was generally made in huge tank furnaces without any intentional coloring agent (Nenna, 2015b). Pliny (Nat. Hist. 36.193) wrote that "*ex massis rursus funditur in officinis tingiturque*" (in the workshops

[glass] is melted again from the chunks and colored), implying that by his time glass-coloring usually took place in secondary workshops.

As for the Hellenistic period, the problem is still open; finds from Rhodes comprise ingots and chunks of naturally colored glass as well as pigments, lead and crucibles with glass coating, possibly indicating that glass was colored there; but while Triantafyllidis (2000) suggests the possibility of interpreting the site as a primary production center, Henderson (2013) seems more inclined to explain the evidences in terms of a secondary workshop. Judging from the published data, Henderson's caution seems better justified.

For the sake of comparability with the previous literature, this thesis will use the terms glass-making and glass-working in the sense which was reported above. However, whenever possible, the following terms will be also used to offer a univocal definition of the different kinds of workshops known in the ancient world:

1) glass-manufacture will be used in a generic sense, for example when it will not be possible to distinguish the effective role of the investigated workshop from the available data;

2) glass-forming will designate those workshops where glass was shaped into objects, but definitely not intentionally colored;

3) glass-coloring will indicate those primary or secondary workshops with archaeological evidence of the voluntary manipulation of the optical properties of glass thus comprising the processes of coloring, decoloring and opacifying.

4.2.2 *Review of the material evidences for glass-working*

The central role of Greco-Roman Egypt in the evolution and spread of glass-related technological innovations throughout the Mediterranean has long been suggested on the basis of several literary and material evidences. Numerous Greek and Latin authors such as Cicero[2] (BC 106-43), Strabo[3] (64 BC – 24 AD), Pliny[4] (23-79 AD) and Flavius Vopiscus[5] (IV century AD) cite an Egyptian, and especially Alexandrian, provenance of

[2] Cicero, Pro Rabirio Postumo, 14.40
[3] Strabo, Geography, 16.2.25 and 16.756
[4] Pliny, Naturalis Historia, 5.75, 36.65-66 and 66.193
[5] Historia Augusta, Vopisc.Aurel.45; Vopisc.Saturn.8, 10

some of the glass sold in the Roman market. Moreover, the Price Edit of Diocletian (issued in 301 AD) lists the cost of six varieties of glasses, among which the Alexandrian type is the most expensive. Stern (2004) has, however, noted that those geographical specifications should not be taken literally, as they refer to a general distinction between naturally colored (Judean) or intentionally decolored (Alexandrian) glass.

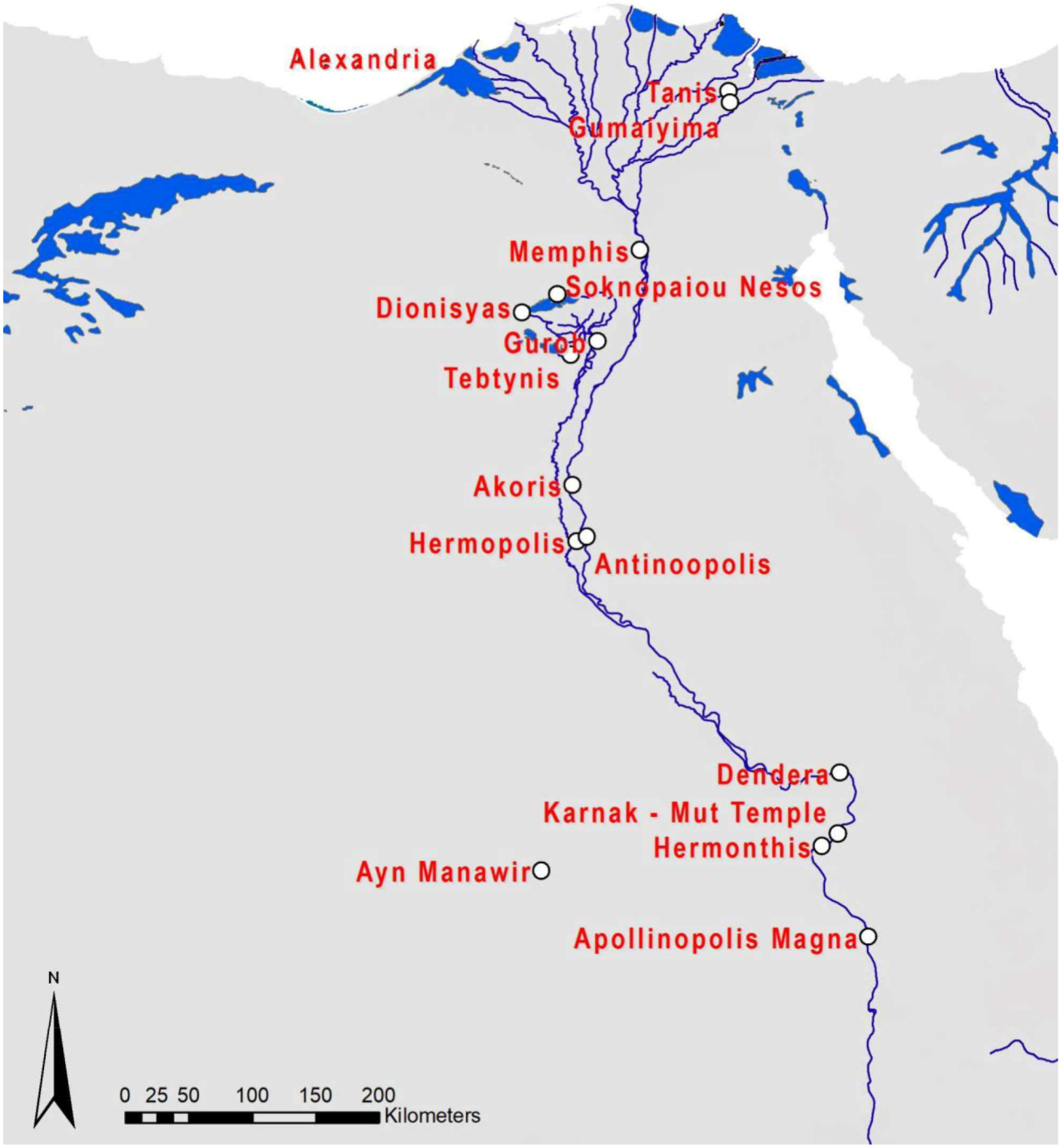

Map. 4.1 – Georeferenced map of the glass-working sites cited throughout the text (GIS project developed by the author starting from the database entries).

On the other hand, papyrological data are very scarce and concentrated towards the final centuries of the Roman rule, especially the late III and IV century AD; Melaerts (2007) observed that the term "glass-worker" appears in one papyrus from Asyut (P.Sijp. 17), three from Oxyrynchos (P.Oxy. LIV 3742.3, P.Oxy. XLV 3565.5 and perhaps P.Oxy. XLVIII 3428.14), one from Koptos (P.Got. 7.4) and possibly one from Thebes (O.Ont.Mus. 7.7), one from Hermopolis (P.Ross.Geor. V 60.21) and a few others of unknown provenance.

The material evidence of glass workshops in Graeco-Roman Egypt is also rather limited. Nevertheless, the creation of ÆGYPTVM offered the occasion of a general review of the literature. From a methodological point of view, we considered the presence and combination of the following elements as clues of a possible local manufacture:

a) fixed pyro-technological installations;

b) instruments and tools;

c) production evidences (e.g. semi-finished objects, droplets, cullets and process wastes);

d) raw materials;

e) traces in the stratification;

f) concentration of finished products.

It must, however, be considered that not all manufacture evidences have the same value and meaning for interpretative purposes, both qualitatively and quantitatively. In fact, a few wastes and droplets may be sufficient to identify a craft area, while, for example, the presence of glass ingots may not, since they could be placed in the foundation deposits of the temples[6] or even traded over long distances[7].

[6] Such as the dark blue and opaque green ingots from Osiris' temple in Canopus (Bailey, 1984; Bimson, Freestone, 1988) with the names of Ptolemy III and Queen Berenice. Three lumps of red glass do also come from an unspecified location in Memphis and were roughly dated between the VII and the V century BC (Arkell, 1950). Another occurrence was discovered within an undetermined tomb in Thebes: it is a disc-shaped, gold-foil ingot in greenish transparent glass recovered in 1824 by Ippolito Rossellini and now preserved at the Pigorini National Museum of Prehistory and Ethnography of Rome (Italy). Cappozzo (2006) proposed a New Kingdom chronology, yet the overall shape and the gold layer are clear indicators of a later dating, probably to the Graeco-Roman period.

[7] This is known as early as the Bronze Age, during the Egyptian New Kingdom. See, for example, the discovery of Uluburun shipwreck, which was carrying ca. 175 ingots of colored glass as mentioned in Bass, 1986. Only three shipwrecks of the Hellenistic period carried raw glass: the Sanguinaire A, sunken during the III century BC near Corsica, which contained approximately 550 kg of glass chunks (Alfonsi, Gandolfo, 1997), the Lequin 2 of the early II century BC and the Jaumegarde (I century BC), both discovered in the southern coast of France (Foy, Nenna, 2001).

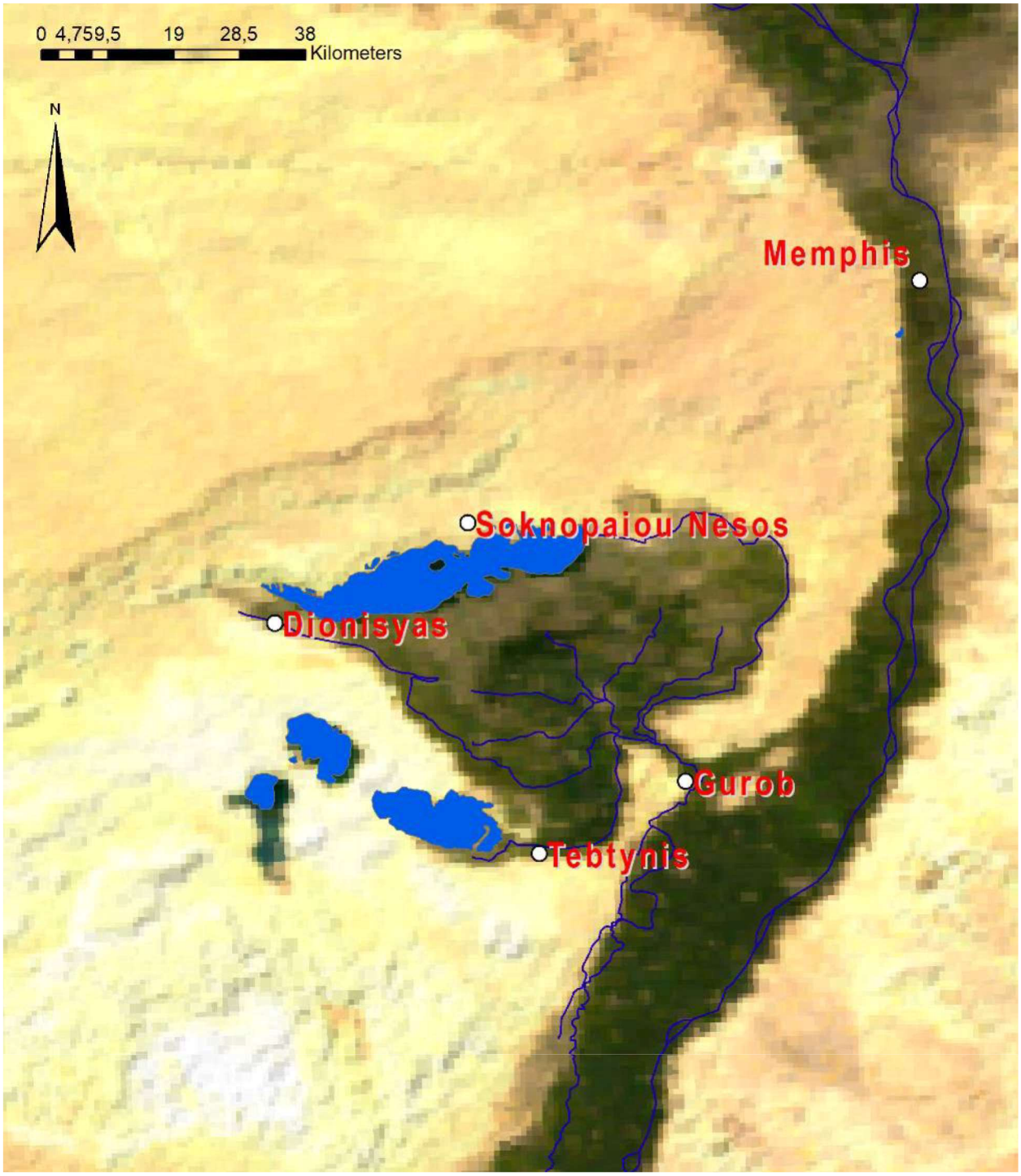

Map. 4.2 – Location of the glass-working sites cited in the text on a georeferenced map of Middle Egypt, with detail of the Fayum oasis (GIS project developed by the author starting from the database entries).

Since in most cases the dating of these craft areas has a wide chronological range, the archaeological contexts will be listed and discussed following an alphabetical order (see tab. 4.1 and map 4.1-4.2 for a summary of the main data and the geographic location

of the sites). The sites that will prove of comparative relevance with Tebtynis will also be highlighted with one, two or a maximum of three asterisks, according to their significance (* = low; ** = medium; *** = high). When no specific link or relation will be detected from the available data, no asterisk will be used.

ALEXANDRIA

Alexandria as often been credited as one of the most important glass-working centers in Hellenistic times, mainly on the basis of literary evidences. Nenna, Picon and Vichy (2000) cite the archaeological discovery of a life-sized chryselephantine figure of Isis or Serapis found in association with a set of polychrome glass inlays to suggest the presence of a workshop active between the reign of Ptolemy IV at the end of the third century BC in the production of glass canes and bars for inlaying sacred statues[8]. Similarly, Henderson (2013) cites the existence of a Ptolemaic glass workshop in Alexandria, but gives no further specification, nor any bibliographic reference.

The only well-dated archaeological documentation of glass-working in Alexandria comes from the excavations in *kôm* el-Dikka directed by the Polish Centre of Mediterranean Archaeology in collaboration with the Supreme Council of Antiquities (Majcherek, 1992; 1999; 2007).

Kucharczyk (2005) described the discovery of three "circular structures made of red bricks, obviously furnaces" two under the floor of auditorium G and another within auditorium R (fig. 4.5); in particular, she noted that there are no traces of the superstructures, yet one of them preserved the residues of a green glass layer adhering to its inner walls. The investigations clearly showed that this workshop is nevertheless of a much later dating, between the Late Roman and Early Byzantine period.

In the same site, but along Street R4, the Polish excavation team also unearthed a Late Antique glass workshop for bead production with its own small furnace (Rodziewicz, 1984). The area also yielded segmenting molds in hard stone, twisted beads and many examples of finished objects.

[8] However, Rodzievicz (1991) when discussing the statue and its context of discovery tends to prefer a Roman dating, because of the association with other well datable I-IV century AD objects.

Fig. 4.5 – Alexandria, kôm el-Dikka. Auditorium G with remains of two circular glass furnaces in mudbricks (from Majcherek, 2007).

AKORIS

Akoris, the modern Tihna el-Gebel, is an archaeological site located in Upper Egypt, on the west bank of the Nile. The history of the site begins during the Old Kingdom, as demonstrated by the famous rock-cut tombs, and goes way down at least until the Coptic period, with an important Graeco-Roman phase. The context was excavated several times since its mention in the *Description de l'Égypte*; from 1981 onwards, the investigations are conducted by a Japanese team (Paleological Association of Japan, 1995).

In this case, the identification as a possible glass-working center is very uncertain and relies only on the generic reference to "some glass crucibles […] found in Akoris". No context or picture is given for their discovery in the related publication, but the

authors suggest a possible relation with the "cloudy vessels" discovered in huge quantities in the site and dated to the VI or early VII century AD (Chikira, 1995). Even so, glass inlays of earlier dating were also found in the site, such as the human torso in brown glass with green necklace (fig. 4.6a) unearthed within chapel A (Kawanishi, Myamoto, 1995).

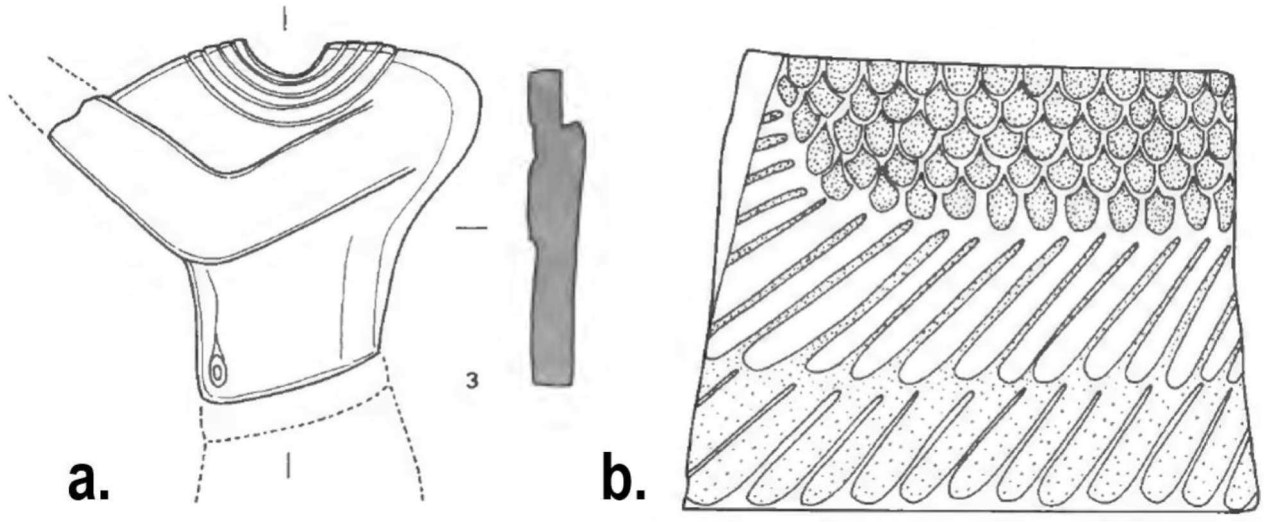

Fig. 4.6 – Glass inlays from Akoris (from Kawanishi, Myamoto, 1995): a) inlay of a male torso in brown glass with green necklace; b) fragment of wing-shaped inlay in dark blue and green glass.

ANTINOOPOLIS*

Antinoopolis was founded in 130 AD by Emperor Hadrian on the Eastern bank of the Nile, not far from the place where Antinous lost his life. The excavations are currently in progress thanks to a mission of the Papyrological Institute "Girolamo Vitelli" of Florence, Italy, that is digging the northern necropolis and the southern quarter of the town (Pintaudi, 2008). Silvano (2015) published evidences of both secondary and primary production dating to the Late Antique/ Early Byzantine phase.

Three small, round kilns were found near the banks of the river (fig. 4.7a). Their internal surfaces were coated with a thick layer of lime and showed no traces of vitrification, however, significant quantities of chunks in light to dark green glass were discovered in the surrounding area (fig. 4.7b). Thus, the author suggests that "the

artisans probably melted the raw glass chunks in these three small furnaces and worked the hot glass to make vessels and other objects" (Silvano, 2015).

Primary production was proposed based on the discovery of a bigger furnace in the city center (fig. 4.7c) in association to Islamic glazed pottery, which constitutes an important chronological reference. The dump of the workshop returned a huge number of raw glass fragments and furnace debris, frequently coated with opaque and translucent layers of glass. The analytical investigations, performed by SEM-EDS, showed that the opaque phase is way richer in CaO, which was interpreted as a clue that those fragments represent "an intermediate phase of the vetrification process: a raw glass with non-completely homogenised fractions".

Summing up, only the secondary workshop seems to be related to the (Late) Roman period, while the primary furnace is most probably associated to the Islamic phase. This last chronology suggested a possible connection to the glass-making site of Hermopolis Magna, which lays just on the other side of the Nile river (Bimson, Freestone, 1991).

Fig. 4.7 – Antinoopolis (from left to right): a) small kiln near the river; b) raw glass, furnace debris and wasters; c) primary furnace of Islamic dating (from Silvano, 2015).

APOLLINOPOLIS MAGNA*

Apollinopolis Magna is the Greek name of the village, located on the west bank of the Nile just north of Aswan, which corresponds to the modern city of Edfu. The site was excavated by different international missions since 1921, but it was during the Franco-Polish campaigns directed by Kazimierz Michałowski and colleagues (1950) that the remains of a possible glass workshop emerged in the North sector of the town.

The "atelier de verrier" was discovered within room 132 during the excavations of a I century AD barrack. This has important implications for the chronology of the workshop, as the military headquarter must have already been dismissed by the time

when the area was re-used for craft activities. Michałowski (*et alii*, 1950) suggests that the functional change can be attributed to the end of the II century AD, as demonstrated by an *ostrakon* dated to the reign of Commodus (180-192 AD).

Room 132 hosted a small enclosure with a single range of bricks, a kiln and a possible fireclay basin. The area returned many fragments of mosaic glass rods, mostly in red and blue glass, with tiny decorations in transversal section. Unfortunately, no pictures of the context or the objects are available in the original publications.

'AYN MANAWIR**

'Ain Manawir was a small agricultural community in the oasis of Kharga (Libyan desert), not far from Dush. The site was occupied since the early V century BC throughout the Persian period. It was frequented only in a very narrow time-span, until the beginning of the IV century BC, and thus its materials constitute an important chronological reference. In 1976 the IFAO took over the excavations and is now working on building an archaeological map of the entire oasis (Wuttmann *et alii*, 1996).

Nenna (*et alii*, 2000) lists 'Ain Manawir among the three temporary templar workshops of the early Hellenistic period in Egypt, with Tebtynis and Gumaiyima. While describing the glass and faience objects discovered in the site, she divides the fragments from 'Ain Manawir in two groups, according to their provenance (Nenna, 1997). The first set was discovered within a jar buried in room O1 of the building next to the temple (red in fig. 4.8) and comprised inlays that were interpreted as remains of dismissed *naoi* (sacred shrines).

A similar situation also applies, for example, to the Dendera cache (Cooney, 1976), where fragments of a votive pectoral and a *naos* were found in two jars discovered in the animal catacombs (Auth, 2012) and to the scattered pieces of *naos* emerged in Tell el-Herr (Valbelle, Marchi 2012).

The second group was found dispersed on the floor of the hypostyle hall (yellow in fig. 4.8) and included various kinds of manufacturing wastes.

Fig. 4.8 – 'Ain Manawir: left, the plan of the temple, in red room O1 and in yellow the hypostyle hall were the inlays were found; right, selection of the glass inlays discovered in the site (modified from Wuttmann et alii, 1996).

Among them, shapeless mixtures of several layers of colored glass, two twisted glass plates and glass bars stretched and pinched at one end. The kiln has not been identified, but the discovery of these elements clearly suggests a connection between sacred spaces and glass-working as early as the middle V century BC.

DENDERA***

Dendera, also known with the Greek name Tentyris, was an important religious and administrative center located on the western side of the Nile river. The site was occupied since Predynastic times, but the most important archaeological remains are those related to the Graeco-Roman phase (Cauville, 1999).

During a census of the vitreous materials in the depots of the Egyptian Museum in Cairo, Boschetti (2017) identified a series of finished and semi-finished glass objects which point towards the effective identification of a new inlay workshop. The materials

all related to historical excavations of the early XX century and were dated with a certain caution to the I century BC – I century AD. The data are still preliminary and yet they seem to testify a direct connection with the other facilities for inlay production discovered within the Graeco-Roman temples in Egypt.

DYONISIAS**

Dyonisias is the name of a Graeco-Roman village located on the western edge of the Faiyum oasis, at the south-western corner of the lake Moeris. In the mid-20th century, the site was excavated by a Franco-Swiss team (Schwartz, Wild, 1950; Schwartz, 1969); in 2009 the works were resumed by a mission of the University of Siena (Papi *et alii*, 2012).

The workshop was discovered by chance back in 1948, while surveying the site after the working hours. The production area was identified thanks to the presence of "big, round stone tables, with channels for casting", waste materials and various chunks of green raw glass (Schwartz, Wild, 1950). Moreover, remains of vessels with traces of vitrification were also found.

It doesn't seem easy to precise the chronology of the structures in the long history of the site, that still retained a fairly important role in Late Antiquity. However, the discovery in 1950 of a mold for the production of figured glass inlays (Schwartz, 1969), which has already been cited in the previous chapter (fig. 3.9f), points towards a Ptolemaic/ Early Roman dating. The object was not recovered in the context of the workshop, but a functional connection seems reasonable. However, considering the lack of archaeological data, it is possible that what we are seeing is the evidence of two glass workshops flourished in different periods.

GUMAIYIMA***

Gumaiyima, also known as Gemaiyemi, is a small mound not far from Tanis, in Lower Egypt. It was excavated by Petrie and Griffith (1888), who found remains of Graeco-Roman mud-brick houses and two limestone enclosures, one of which interpreted as the *temenos* wall. Unfortunately, the structures were in most cases preserved only in foundation. Despite the desolating situation, Griffith wrote that "a find occurred in the

first hours, and made me stay and work out the piece thoroughly": it is the discovery of a depot with numerous chips of colored inlays (fig. 4.9) and a wooden panel inlaid in glass representing a flying hawk, now preserved at the British Museum.

The area also yielded numerous tools, models and semi-finished objects which refer to various artisanal activities that must have taken place within the sanctuary (fig. 4.10): among them, glass and metal plaques, chisels, knifes, nails, pieces of "trial works" in limestone and bronze slags. There were also numerous plaster fragments representing incomplete or entire figures of various gods, such as Osiris, Isis, Harpocrates and Khem that were interpreted as models, but no images are available.

In Griffith's words "the remains of glass-working area are of considerable interest". They included a number of terracotta and limestone molds, waste glass, figured inlays, hieroglyphs and border ornaments (probably simple bars) in deep blue, light blue, green, orange, red, brown, dark green, sealing-wax red and black glass. The molds mainly refer to animal or human body parts (hawk's beak, Bes face) or hieroglyphs. The excavations recovered various cartouche fragments, and the related signs – although none is uniquely linked with the name of a Pharaoh – were attributed to the Ptolemaic dynasty. The chronology of the recovered pottery also agrees with an early Ptolemaic dating.

According to the authors after "the first Persian invasion the enclosure was taken up by artistic workers, who covered the ruins with fresh buildings, now almost entirely washed away. Here, they seem to have flourished into the Ptolemaic period, when their trade was suddenly put to a stop by panic. The artisans buried their unfinished work and some of their less portable stocks in trade before taking flight, but never returned to claim them".

Cooney (1976), later followed by Nenna (*et alii*, 2000), suggested that the workshop of Gumaiyima is a minor, temporary installation devoted to renovating or restoring the sacred furnishing of the temple. This would also explain the short life of the artisanal production. Moreover, he proposed a different chronology for the inlays which, in his opinion, must be dated "during the climax of the mosaic glass industry or *c.* I century BC to I century AD, assuming that all glass is about the same date". On the other hand, Nenna is convinced of a III century BC date for the inlay production in the site.

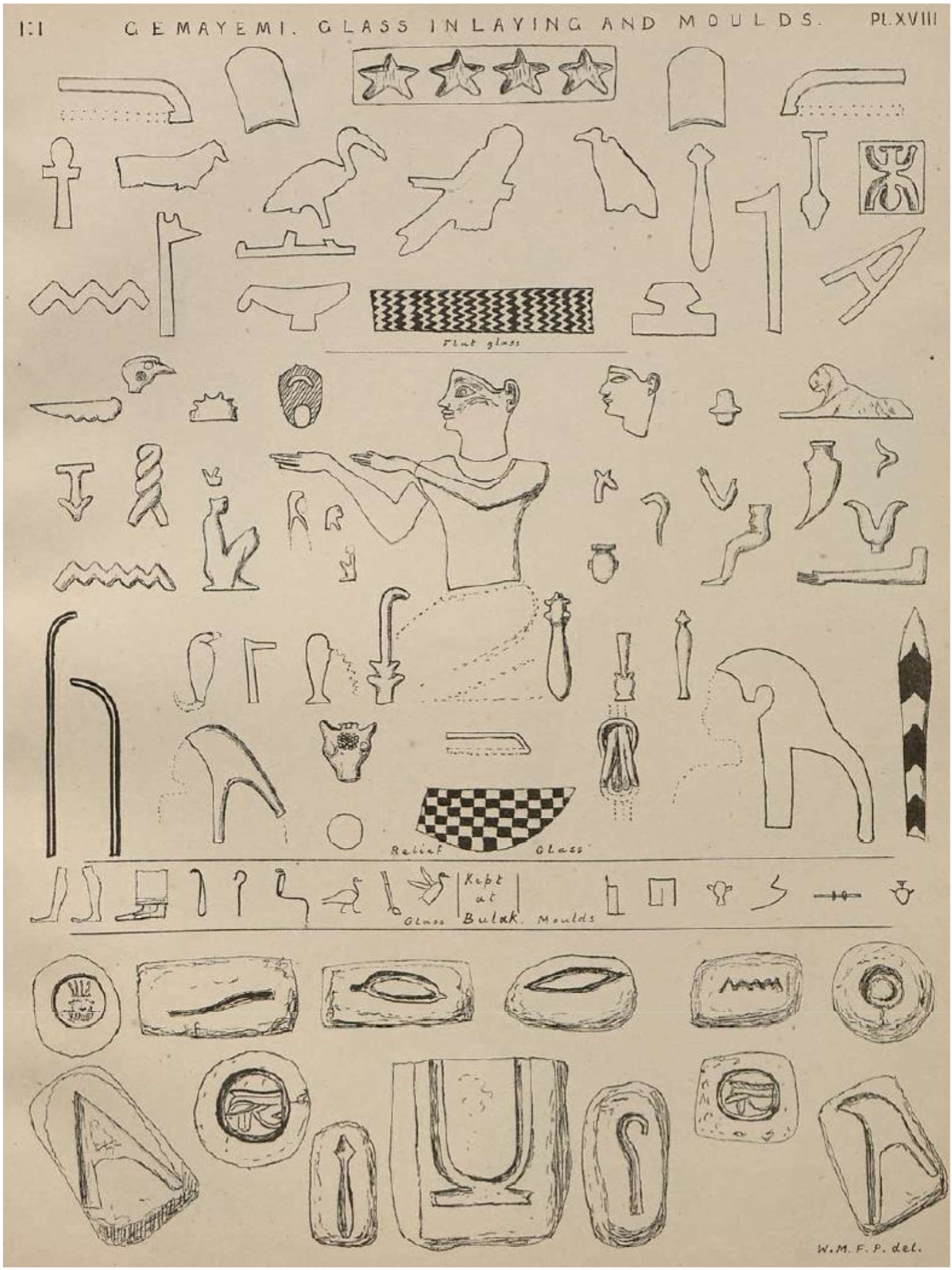

Fig. 4.9 – Gumaiyima, selection of the inlays and molds from Petrie, Griffith (1988).

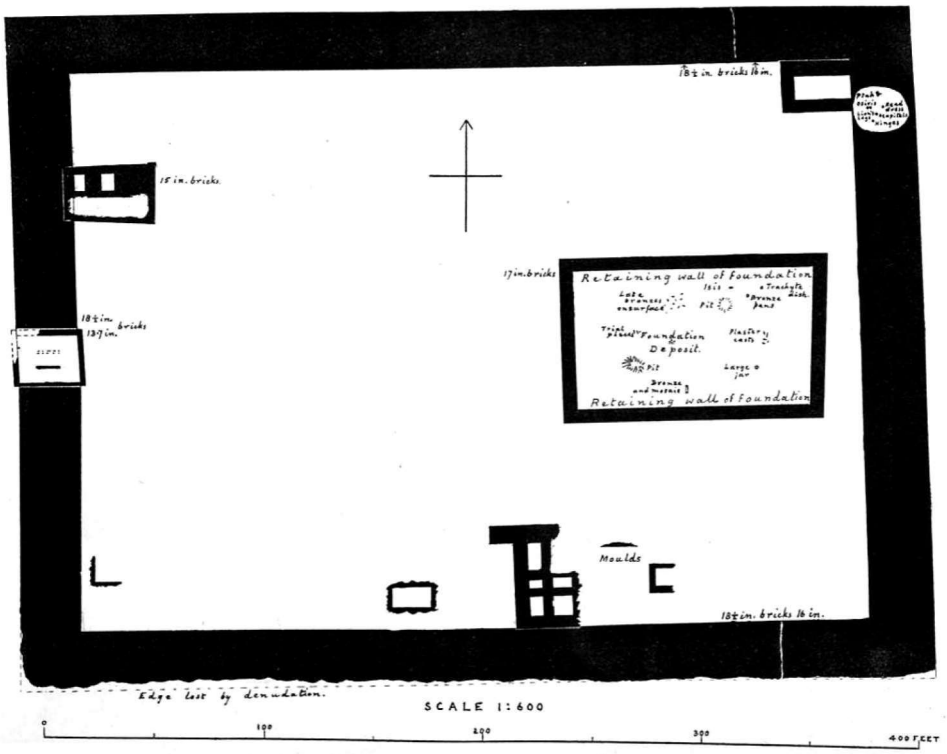

Fig. 4.10 – Gumaiyima, plan of the temple and its temenos, with the localization of the major archaeological finds (from Petrie, Griffith, 1888).

Recent excavations at the site allowed identification of a craft area with more than forty ovens, which were interpreted as firing structures for pottery and vitreous materials that the author also associates to the inlays discovered by Griffith (Ashmawy Ali, 2006). The kilns – with diameter ranging from 50 cm to 3 m – lay over the public baths of Ptolemaic and Early Roman times. It would seem very unlikely that these kilns were used to produce the sacred inlays discovered in the temple, considering that the chronology proposed for the glass pieces never exceeds the I century AD. Ashmawy Ali's hypothesis should thus be dismissed. However, the implant of pyro-technological structures over pre-existing public buildings is quite common in Late Roman Egypt and these ovens may be probably interpreted in that sense.

GUROB

The archaeological site of Gurob is located in the south-eastern side of the Fayum depression; it comprises a New Kingdom settlement, with the famous royal harem, currently excavated by a joint team of the University of Liverpool, University of

Copenhagen and University College London (Shaw, 2013), but also various pre-dynastic, early dynastic, Old Kingdom and New Kingdom cemeteries. Petrie (1890; 1891) also discovered a Ptolemaic necropolis on a small *kôm* north of the main town.

Brunton and Engelbach (1927) mentioned the discovery of "glass factories and lime-kilns" on the top of a small enclosure near the fort. Unfortunately, they were not able to understand the stratigraphic relationship with the surrounding structures, hence the dating remained problematic. Nicholson (2007) has suggested that "it may be contemporary to Amarna, or possibly have predated both Amarna and Malkata only to resume on a more limited scale later". In general terms, he seems confident of a New Kingdom chronology. On the contrary, Nenna and colleagues (2000) cite the same bibliographic reference to include Gurob among the possible Roman glass-working centers.

Recent excavations have tried to shed some light on the actual function and dating of the structures. A magnetometric survey identified two circular depressions possibly associated to pyro-technological activities in the area cited by Brunton and Engelbach. The subsequent field check allowed Hodgkinson (2012) to identify numerous fragments of vitrified mudbricks and various stone tools. The excavation showed two circular kilns with diameter ranging from 2 to 3 meters (fig. 4.11); one also had its inner walls coated in dark-green and black slags.

The overall interpretation was that the area had been most likely intended for pottery production, but multi-functionality was also speculated for the thickness of the walls the one of the kilns, which could have reached higher temperatures suitable for glass-making. The diagnostic sherds discovered within the kilns point towards a New Kingdom chronology, especially from the second half of dynasty XVIII until the first half of dynasty XIX, as previously suggested by Nicholson. For what is known to date, Nenna's hypothesis of a Roman chronology for Gurob glass-working can be ruled out.

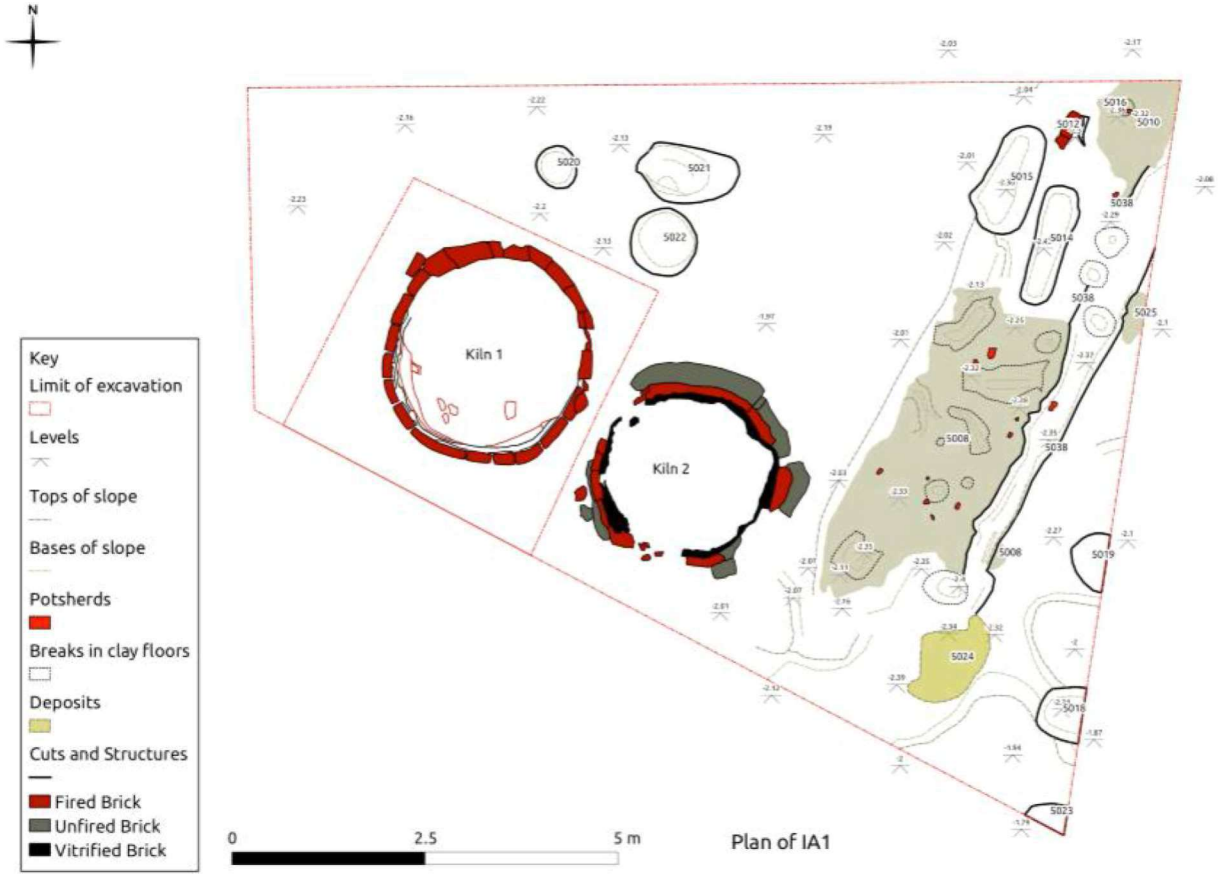

Fig. 4.11 – Gurob, the two kilns excavated near the fort (from Hodgkinson, 2012).

HERMONTHIS

Hermonthis, originally cited by Strabo (Geography, 17.1.47), is an archaeological site in Upper Egypt, few kilometers south of Thebes. It is also known as Armant or Ermant. The earliest systematic investigations date back to the 1930s and were followed by sporadic interventions of the Supreme Council of Antiquities during the years 1980-1990. Since 2002-2003, the IFAO took over the investigations with specific interest in the architectural, topographic and epigraphic analysis of the main temple of Montu (Thiers, Volokhine, 2005).

Harden (1940) highlights the discovery of numerous fragments of vitreous materials, mostly dating 250-450 AD. Among them, one inlay fragment and four "cylindrical objects" with circular or rectangular borings[9], in opaque red, dark blue and black glass.

[9] From the description, they seem consistent with the drums of glass (but also faience and Egyptian blue) which were used to decorate the columns of the small Graeco-Roman *naoi* discovered throughout Egypt, such as those in the Metropolitan Museum of Art inv. 21.2.2.

Significantly, he also mentions two vessel-glass wasters badly twisted by heat (one of them also bearing jack-marks), a scrap of green frit and various crucible fragments. Therefore, he concludes that it is "reasonably certain that glass was made at Armant". It should, however, be noted that the published evidences point towards a local glass-working, rather than glass-making facility.

KARNAK, PRECINCT OF MUT***

Karnak was the most important religious center dedicated to the divine triad of Mut, Amen and Khonsu. Epigraphic and archaeological evidences indicate that Mut's temple was founded between dynasty XVII and dynasty XVIII and continued to be renewed and frequented until the early Roman period. Between the II and IV century AD, private houses were progressively built within the precinct and the temples testifying a cease of its cultic significance (Fazzini, 1999). The history of the excavations is very long and comprises, among others, Briton Margaret Benson and Janet Gourlay, Maurice Pillet, the IFAO, the Brooklyn Museum of Art and, most recently, the Johns Hopkins University (Bryan, 2008).

The 2008 excavations brought to light the remains of a pyro-technological installation dating back to the Ptolemaic period in the area between the first pylon of Mut's temple and the so-called temple A (Fazzini, 2008). The kiln is preserved only in its foundations, after a functional transformation of the area dated to Roman times (I-II century AD); the firing chamber has a quadrangular structure, with inner compartments (fig. 4.12a-b) that seem to delimit a sort of chimney comparable to the one of Tebtynis. The dimensions are also similar, less than (or around) one meter each side.

Ashes, coal, baked bricks and fragments of burnt clay with one metal slag and various glass wastes were also found in the area (fig. 4.12c). Furthermore, the investigations have discovered a jar containing traces of blue pigment and five terracotta molds of the type known for the production of inlays. Fazzini (2009) concludes that "it may have been an oven or kiln used for smelting copper or for producing faience or glass".

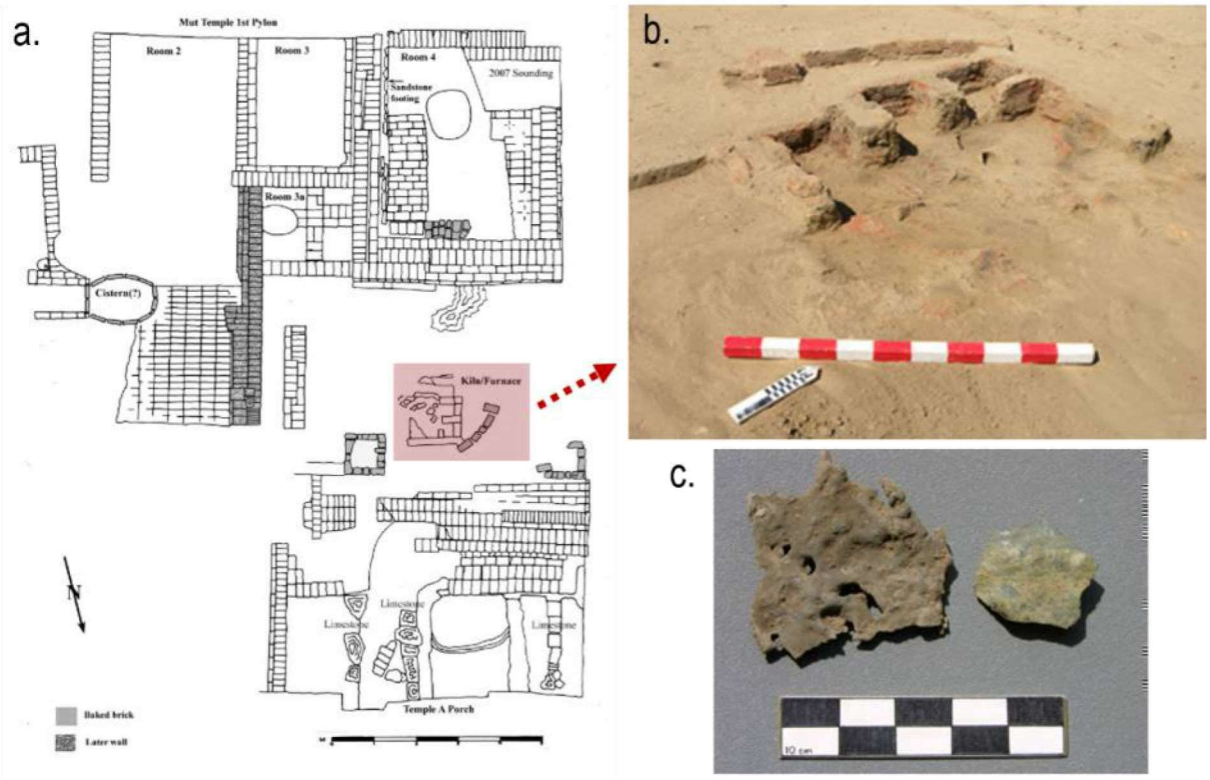

Fig. 4.12 – Karnak, precinct of Mut: a) plan of the area between the first pylon of Mut's temple and the so-called temple A, the kiln is highlighted in red; b) view of the foundations of the kiln; c) example of metal and glass scraps (from Fazzini, 2008).

MEMPHIS

Located in the heart of the country just at the mouth of the Nile Delta, Memphis is probably the most important center throughout Egyptian history. All the main explorers and archaeologists of the XIX and early XX century, such as Belzoni, Caviglia, Champollion, Lepsius, Mariette and Petrie, visited or conducted digs at the site.

Thompson (1988) suggested Memphis as a possible Ptolemaic glass-working center following the notes on the kilns discovered by Petrie (1911). Her idea was that the site must have been self-sufficient in terms of craft production. Petrie's accounts, as well as the excavations directed by Nicholson at *kôm* Hellul (2013), however, made reasonably clear that the kilns were intended for a different kind of vitreous material: faience. Moreover, the recent investigations showed that the main phase of activity of the workshop can attributed to the Roman period, rather than the Greek era.

The only semi-finished glass elements recovered in the site are three red lumps from an unspecified location (Arkell, 1957), which – as previously stated – cannot account alone for a local manufacture.

SOKNOPAIOU NESOS***

Soknopaiou Nesos was a Graeco-Roman village on the northern edge of the Fayum oasis. Founded during the III century BC, it was abandoned by the second half of the III century AD (Capasso, Davoli 2012). As most of the Graeco-Roman villages in the Fayum, the earliest explorations are related to the search of papyri, with very little interest for their topographic contextualization. Later, in 1931-32 the site was excavated by a mission of the University of Michigan. From 2001, Soknopaiou Nesos is the heart of a pluriannual project directed by the University of Lecce (Italy).

During the excavations in the temple, the Italian mission discovered a concentration of evidence for manufacture, such as semi-finished products and glass wastes, and fragments of inlaid wooden furniture within layers dating back to the Late Antiquity in the first courtyard of the *temenos* (and specifically within room E, fig. 4.13). However, the chronology of the inlays and wooden fragments refers to the III century BC; Cervi (2012) has therefore speculated that such furnishings were stored for a long time after disposal because of their religious significance or that room E was originally intended as a warehouse and spare inlays were kept there for maintenance after the closure of the workshop that had produced them.

The typology of the wooden objects and of the glass inlays relates very well from those discovered in Tebtynis (cfr. § 5, fig. 5.8). Comparisons can be made among the feather motifs, the star patterns, various floral elements (in shape of lotus or rosette), the figured inlays with parts of the human body and the *ankh-was* hieroglyph combination, also in terms of dimensions and colors.

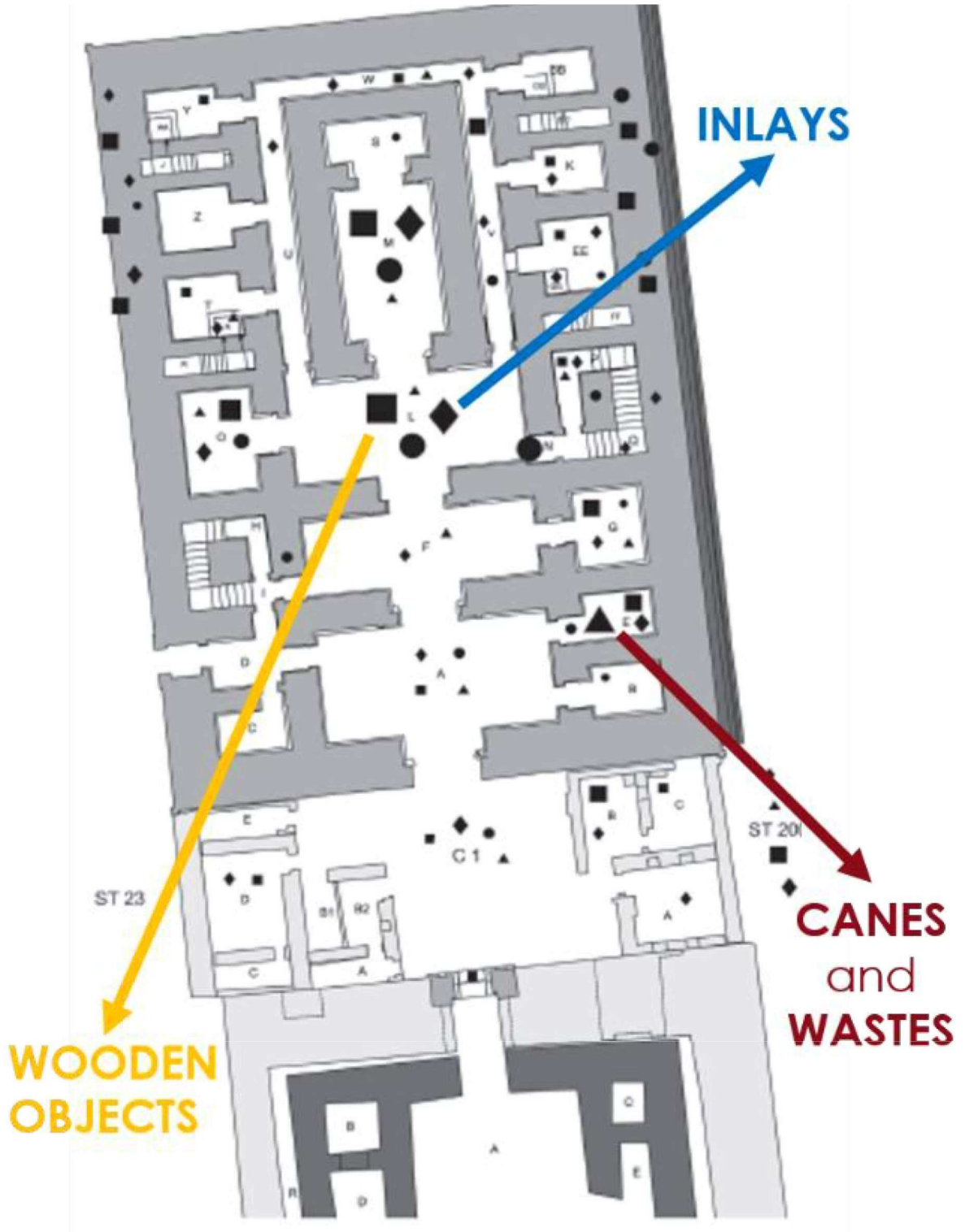

Fig. 4.13 – Soknopaiou Nesos, plan of the temple. Squares represent fragments of wooden furniture, diamonds correspond to spare glass inlays and triangles to canes, semi-finished inlays and process wastes (edited from Cervi, 2012). The dimension of the symbols is proportional to the quantity of fragments discovered in the area.

TANIS*

Tanis is an archaeological site located in the north-eastern Delta; the town lived its maximum splendor during the Third Intermediate and the Late Periods, but was occupied at least until the VI century AD when it was flooded by lake Manzala and abandoned (Brissaud, Zivie-Coche, 1998).

The only archaeological evidence of glass-making discovered in Tanis is the previously cited torso-shaped mold inv. E 16029 published by Nenna (2011) in the catalogue of the Louvre glasses and dated by the same author to the VI-III century BC (fig. 3.9d). It emerged during the excavations of Pierre Montet in the royal necropolis and arrived in France with the *partage* of 1938. Obviously, it is not possible to infer a potential production activity from one single object, however the proximity to Gumaiyima may suggest a correlation between the two sites during the Graeco-Roman era. This is further strengthened by the discovery of numerous glass rods, bars and slices of complex mosaic glass acquired in the 1885-1888 by the British Museum from the Egypt Exploration Fund excavations in the local cemetery (fig. 4.14), which range in chronology from the III century BC to the I-II century AD (Cooney, 1976).

Fig. 4.14 – Tanis, selection of the glass inlays discovered in the site (online catalogue of the British Museum inv. EA29092).

Archaeological Site	Location	Chronology of the glass workshop/s	Comparability with Tebtynis
Alexandria	Lower Egypt	Late Antiquity	/
Gumaiyima	Lower Egypt	Ptolemaic (until early Roman?) period	***
Tanis	Lower Egypt	Ptolemaic - Early Roman?	*
Memphis	Middle Egypt	no glass workshops identified to date	/
Dyonisias	Fayum Oasis	Graeco-Roman, possibly Ptolemaic era?	**
Gurob	Fayum Oasis	New Kingdom (XVIII-XIX dinasties)	/
Soknopaious Nesos	Fayum Oasis	Ptolemaic period	***
Ayn Manawir	Kharga Oasis	V - early IV century BC	**
Akoris	Upper Egypt	Late Antiquity - Coptic Period	/
Antinoopolis	Upper Egypt	Late Antiquity - Islamic Period	*
Apollinopolis Magna	Upper Egypt	after the end of the II century AD	*
Dendera	Upper Egypt	I century BC - I century AD	***
Hermonthis	Upper Egypt	probably Late Antiquity	/
Karnak, precinct of Mut	Upper Egypt	Ptolemaic (until early Roman?) period	***

Tab. 4.1 – Name, location, chronology and comparability with Tebtynis of the sites discussed in the text with possible archaeological evidences of glass-working during the Graeco-Roman era.

4.2.3 *Crafts in the temple*

The economic role of temples in Graeco-Roman Egypt has been stressed on various occasions. In fact, they constituted key points of the local administrative system and did not only cover religious functions. The main sanctuaries consisted in the temple building, home of the god, which contained his living effigy, and a series of connected *paraphernalia*. Warehouses, workshops and shrines inside the *temenos*, but also accommodations for the pilgrims, certain shops and workshops in the city and several hectares of cultivated land in the surrounding countryside were all part of the temple properties (Clarysse, 2010). The sanctuary of Tebtynis, for example, possessed a wealth of little more than 3000 acres in farmland between the II and I century BC (Crawford, 1971).

Among the economic activities of the temples, in addition to the revenues derived from agriculture and processing of vegetal resources (for the production of oil, bread and beer, linen, papyrus etc.), textual sources document breeding, the monopoly on specific transport routes or fishing spots, tax collection, prostitution and religious activities, including divination and medical practices, mummification, organization of funeral

ceremonies and daily rituals for the dead. Moreover, priests were sometimes asked to draft or translate private contracts for their ability to read and write (Connor, 2014).

From an archaeological point of view, production facilities and warehouses inside the temples are often poorly visible, because they were mainly built of mudbricks, and therefore are more exposed to post-depositional processes. Some interesting data, however, come from depictions decorating the walls of royal officials' tombs during the New Kingdom (Masquelier-Loorius, 2008). The burial of Neferrenpet (TT178) is particularly noteworthy in this regard, because it bears the representations of the workshops located within the temple of Amon in Karnak at the time of Ramesses II (fig. 4.15). On the northern wall of room B, several artisans are working on gilding a wooden statue, drilling stone beads, processing gold and producing metal (possibly bronze) vessels. The activities seem to be carried out within the same space, whose access is controlled by an armed guard. From the iconographical point of view, although craft scenes are relatively frequent in Egyptian funerary representations (either in clay models, paintings or reliefs), neither in this nor in the previous periods do we have representations of glass working or glass production[10].

In this context, the discovery of the Tebtynis inlay workshop within the first court of the temple is neither surprising, nor unique. Yet it opens a new window on the link between craft productions and sacred spaces in Ptolemaic times. Glass crafts within the temples are also attested for other Hellenistic workshops, even outside Egypt, such as the well-known case of Phydia's at Olympia (Schiering, 1991; 1999) or in the Sanctuary of Jupiter Ammon of Carthage (Gauckler, 1915; Seefried, 1982), which however is still open to some discussion.

As highlighted in the previous section, evidences for glass-working within the *temenoi* of Ptolemaic and Early Roman temples are common to various sites spread across Egypt. Among the most interesting Karnak, Gumaiyima, Dendera, Soknopaious Nesos and 'Ain Manawir. Only in the first site, however, the excavations were lucky enough to identify the effective location of the artisanal area. Nevertheless, all other

[10] For an overview of New Kingdom burials with craft scenes see Marini, 2014. The only representation possibly associated with the manufacture of vitreous materials is located in the tomb of Ibi (TT36, XXVIth dynasty) and refers to the modeling of faience as suggested in Nicholson, 1998.

cases show manufacture wastes, tools, finished and unfinished objects, frequently unearthed within the first court.

In fact, considering the location and the typology of the objects which were produced within the "glass" workshops in the temples, it is reasonable to infer that they probably manufactured both sacred furniture for the temple, such as statues and *naoi*, and devotional articles for the pilgrims. The production of divine statues, which acted as a physical form for the *ba* of the god, was perceived as a ritual act in itself. At the same level, sacred furniture allowed the gods to travel outside the holy space of the temple during the festivals by protecting their effigy within a restrained, sanctified space (Falk, 2015). It is no surprise that the production of these specific objects – which in Ancient Egyptian culture had little to do with artisanal activities, in the modern sense of the term, and much to do with ritual purity – took place within the *temenos*.

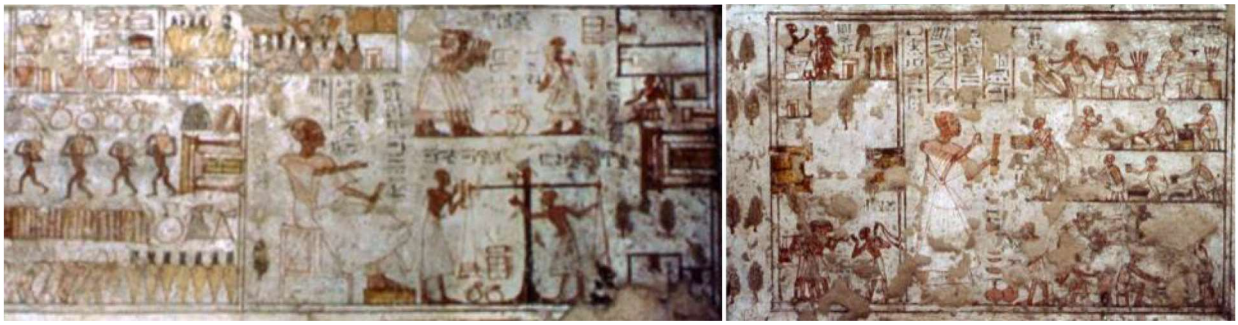

Fig. 4.15 – TT178, wall paintings in the tomb of Neferrenpet with the representations of the workshops and warehouses within the temple of Amon in Karnak at the time of Ramesses II (dynasty XIX).

Comment?
Vous n'avez pas de verres de couleur?
Des verres roses, rouges, bleus,
des vitres magiques,
des vitres de paradis?

Le Mauvais Vitrier

Charles Baudelaire
(1821-1867)

MATERIALS & METHODS

5. Overview of the collection

This chapter will present the results related to the census and the preliminary functional and material classification of the Tebtynis collection of vitreous materials at the Egyptian Museum of Turin, starting from a general distinction between finished glass inlays, production evidences (such as semi-finished products and wasters) and other types of vitreous materials (vessel sherds, beads etc.).

The creation of a complete index of the collection lays outside the scope of this project, which is rather intended to offer a background for the archaeological and archaeometric contextualization of the Tebtynis inlays in their chrono-cultural environment. The archaeological catalogue is currently in progress by Marie-Dominique Nenna of the *Centre d'études Alexandrines*, but there is no defined publication date yet.

This chapter will also offer a short introduction on the history of the collection and will discuss the early works on the vitreous materials considered during this project. Finally, it will present the issues related to the typo-chronological classification of this type of objects and the most relevant examples of coeval inlays and inlaid objects available in the literature for comparative purposes.

5.1 Short history of the collection

As already reported in chapter 3, many of the objects discovered by Carlo Anti in Tebtynis were sent to Italy after every field season as part of the *partage* agreement. In 1931, the shipment comprised 403 individually numbered artifacts, 1 box with Islamic glazed pottery recovered on the surface of the *kôm* and directed to the International Museum of Ceramics in Faenza and 14 boxes containing fragments of loose glass inlays, divided per color (Deotto, 2015). These latter were not counted, probably because they were too numerous.

The materials were originally sent to the National Roman Museum of the "Diocletian's Baths", where Gilbert Bagnani saw the boxes and attempted a first cross-check of the finds in view of a temporary exhibition (see §3), probably related to that "Mostra d'Arte Antica" held in the National Gallery of Modern Art in Valle Giulia in

April-June 1932[1]. After 1936, the objects slept unnoticed until 1972, when Silvio Curto, Superintendent at the Egyptian Museum of Turin, discovered the boxes in Rome. Understanding their value, he pledged to move them to Turin and, with the help of Gianfilippo Carettoni of the Roman Soprintendenza, he finally succeeded (Valtz, 1992).

Fig. 5.1 – The wooden tablet from Tebtynis inlaid with glass currently exposed at the Egyptian Museum of Turin (inv. S. 18155).

[1] The exhibition catalogue (Mostra d'Arte Antica, 1932) lists some of the objects from Tebtynis exposed in room VI, mentioning in particular the statues of a priest and a Pharaoh (that can certainly be associated with those discovered in the vestibule during the 1931 campaign, noted in Anti, 1931 and published in Rondot, 2004), and two Coptic capitals. However, ivi, in the general comment on Tebtynis excavations, glass and enamels are also cited.

In the same year, the inlaid wooden tablet inv. S. 18155 (fig. 5.1), was subject to non-invasive XRF (X-Ray Fluorescence) analysis in order to determine the main chemical components of the enamels (Cesareo *et alii*, 1972). These analyses cannot account for the complexity of the opaque glasses from Tebtynis for the specific analytical characteristics of the technique used[2], yet testify an early interest for the archaeometric investigation of these materials.

It was only in 1992 that Elisabetta Valtz conducted a preliminary survey of the Tebtynis collection in the depots of the Egyptian Museum, which was presented in occasion of the VI International Congress of Egyptology. In particular, she identified thirty-seven boxes related to the so-called "Tebtynis Sabauda" excavations.

During the 1990s and early 2000s, Nenna promoted a first archaeological study of the materials discovered in the inlay workshop, but never published a comprehensive study. However, she did mention the finds from Tebtynis in various works related to Hellenistic glass in Egypt and the Mediterranean (e.g. Nenna 1998; 1999; 2000; 2011; 2015; Nenna, Picon, Vichy 2000; Nenna, Gratuze, 2009).

5.2 Census and study of the Tebtynis collection of vitreous materials

The Egyptian Museum of Turin preserves more than 800 fragments of vitreous materials from Tebtynis, divided among more than 60 inventory numbers; this, however, is just a partial estimation, because it considers only fragments bigger than ca. 2 mm. The number of micro-chips, often in mosaic glass, is way higher. Each inventory number usually includes more than one single fragment and sometimes comprises eventual non-vitreous elements: that is, for example, the case of the *udjat* amulet in carnelian in inv. S. 18554/ 19 or the metal fragment in inv. S. 19200/01.

Nevertheless, the majority of the collection is constituted by finished, semi-finished and waste fragments of inlays in opaque and transparent glass, but a few beads (inv. S.

[2] The main limit of the technique is that X-Ray Fluorescence can only measure elements with a high atomic number (Z); moreover, it is a surface, bulk analysis which often does not offer enough control on the accuracy of the data, as glass may be subject to weathering etc.. Finally, data are always normalized at 100% (Calvo del Castillo, Strivay, 2012).

19200/05, /06), core-formed vessel shards (inv. S. 18553/01, /02, /03) and one handle in faience (inv. S. 19200/ 06) do also occur.

Over 99% of the Tebtynis vitreous materials in Turin is constituted by glass, for the most part finished and semi-finished inlays (fig. 5.2a): this suggests a rather uniform original context, such as that of the workshop, eventually complemented by its products discovered among the sanctuary and the town. On the contrary, the Tebtynis collection of beads and small objects preserved at the Museum of Archaeological Sciences and Art of the University of Padova, which was already partially investigated in the course of previous studies (Bettineschi, 2013; Molin, Bettineschi, Angelini, 2013; Angelini *et alii*, 2014), or the one at the Phoebe A. Hearst Museum of Anthropology in Berkeley include objects with a wide chronological range and very different material characterization, thus suggesting an heterogeneous provenance, coming probably from different parts of the village and the cemetery, as previously proposed in the cited works.

Turin inlays were classified into 3 main groups on the basis of their technological complexity (fig. 5.2b): a) monochromes; b) stratified; and c) figured in mosaic glass. In general terms, monochrome glasses can be divided in two main categories: simple bars/ rods and figurative elements representing clothes, furniture or parts of the human body. Among them, there are various examples of legs (e.g. inv. S. 18556/02, /03, /04, /05, /06, /07, /08, /11), arms (e.g. inv. S. 18556/09, /10), shoulders (e.g. inv. S. 18556/14, /15), faces (e.g. inv. S. 18556/01, /18), torsos (e.g. inv. S. 18556/17, /19), hands (e.g. S. 18556/21, /22), the base of a *usekh* collar (inv. S. 19200/ 06), possibly one knee fragment (inv. S. 18555/ 07) and some unidentified pieces.

Stratified glasses usually have from two up to seven layers of alternating colors, while mosaic canes and slices represent a huge variety of motifs, generally connected to the Egyptian iconography: rosettes and lotus flowers, *ankh-was* hieroglyphs, stars, arrangements of arcs in imitation of plumage, pattern of triangles or other geometric designs for the clothes or the decorative friezes.

Semi-manufactured pieces are sometimes hard to distinguish from the corresponding finished products. In fact, simple bars may be used both as such, for bordering figurative representations, or assembled to create stratified glass or mosaic representations.

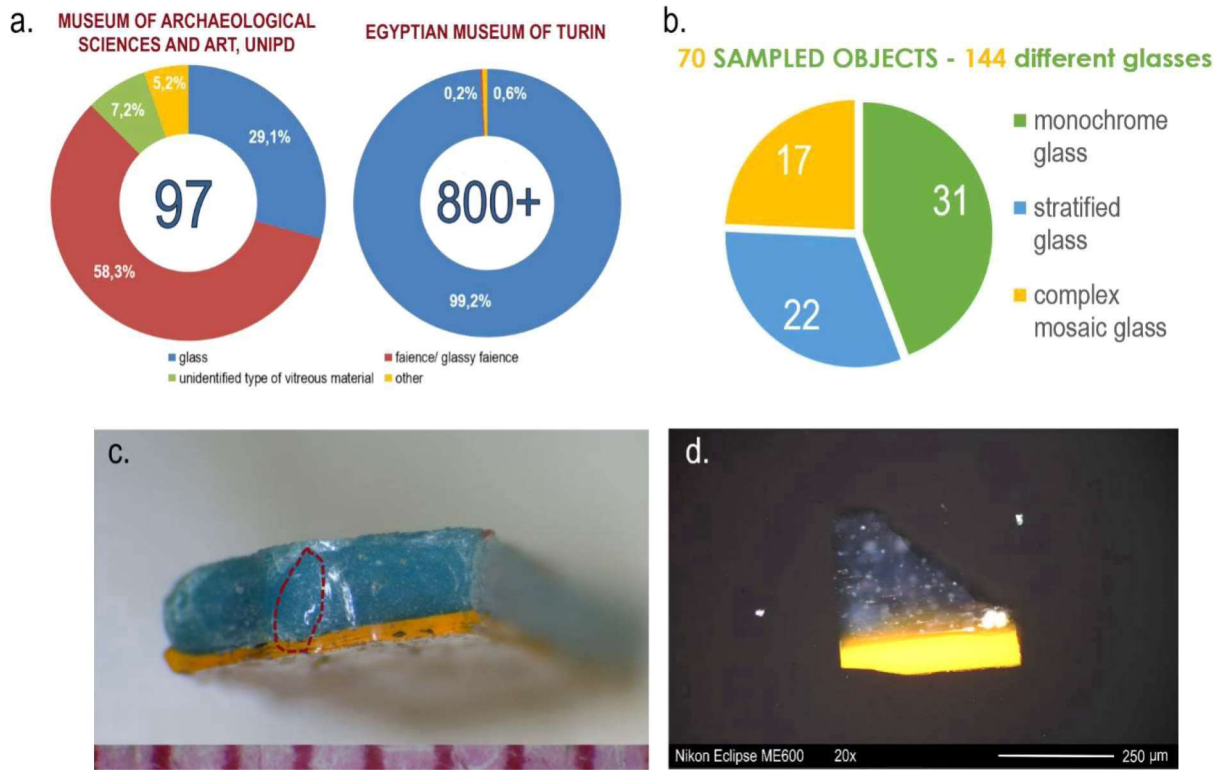

Fig. 5.2 – a) material characterization of the objects from Tebtynis in the collections of vitreous materials at the Museum of Archaeological Sciences and Art of the University of Padova (left) and the Egyptian Museum of Turin (right); b) number of sampled objects divided among monochrome, stratified and complex mosaic glasses; c) SM image of the sampled area in Ty-S-GA-005; d) OM image of sample Ty-S-GB-413, showing the average dimension of sampled chips.

The differentiation of the two occurrences is somewhat facilitated by the presence of traces of gold leaf or organic binders, which characterize finished inlays already mounted in place. Their absence, however, cannot account alone for a semi-finished status, as the adhesive or metal layer may have been lost during time. When no residues are present, sections of mosaic canes are generally ascribed to one category or the other mainly on the basis of an eventual presence of production markers, such as tool marks, or according to their dimensions, where longer or bigger segments tend to indicate semi-finished elements and thin slices finished products. Of course, this is a simplification with respect to the complexity of real world production processes and yet it is necessary to bring order to such a multifaceted matter. In some cases, the evidence of certain types of mosaic motifs in the finished objects, such as the wooden tablet inv. S. 18155, contributed to the interpretation of different pieces as semi-finished elements. This is,

for example, the case of various floral patterns which were identified, further miniaturized, in the armbands and collars of the human (and divine) figures of the collection.

The assemblage shows a wide range of colored, opaque glasses: from red, brown, orange and yellow to blue, light blue, green and white. Translucent and transparent glasses are also present, sometimes in the classic light green of non-intentionally colored glass. Preliminary OM (optical microscopy) observations allowed us to group the glasses in 7 main classes considering their color, hue, opacity, homogeneity and texture (see tables I-II in the appendix). These classes comprise: 1 type of opaque brown, 1 of opaque white, 2 types of transparent colorless glass (true colorless and aqua), 2 of opaque red (dull red and sealing-wax red), 2 of opaque yellow and yellowish-orange, 2 of green (transparent green and opaque turquoise) and 3 of blue (transparent and opaque dark blue, and opaque light blue). One additional violet-blue class was attributed to weathering processes, while all other small variations to possible differences in the quantity and quality of coloring, decoloring and opacifying agents.

5.3 Selection of the objects and sampling procedure

After a first OM observation of the whole collection, the sampling procedure was planned in collaboration with the Egyptian Museum and the local Soprintendenza following these basic principles:

1) absence of significant surface weathering or cracks, that might compromise the integrity of the objects during sampling and/or the results of the chemical analyses;

2) obtaining samples comprising all the various types of artifacts connected with the workshop activities (lumps, semi-finished pieces, finished inlays, production wastes etc.);

3) acquiring samples of all the classes of monochrome glasses preliminarily identified on the basis of their color, hue, opacity, homogeneity and texture (see § 5.2).

4) selecting samples representative of all polychrome color combinations in stratified and mosaic glasses.

A total of 70 objects, with 144 different glass types, were selected for in-depth archaeometric investigations.

Whenever possible, samples were collected from the millimetric fragments already present in many boxes. However, when specific colors or color associations were needed in order to guarantee the statistical significance of the data and the representativeness of the whole collection, micrometric glass chips measuring approximately 200-500 x 200-500 µm were detached from the artifacts using a surgical scalpel with very sharp blade in order to preserve the aesthetic and structural integrity of the objects (fig. 5.2c-d).

Despite the struggle to obtain a representative sampling of the whole collection, the selection process leads to a physiologic loss of information, which is further increased during the instrumental measures. The analytical choices must thus be carefully guided by the experience of the operator and his knowledge of the related literature to identify the highlights in each sample and avoid any unnecessary noise. The post-processing of the data, such as the statistical and the digital image analysis, together with the critical review of the literature presented in the discussion, can broaden out the information curve and lead to the creation of new historical reconstructions (fig. 5.3).

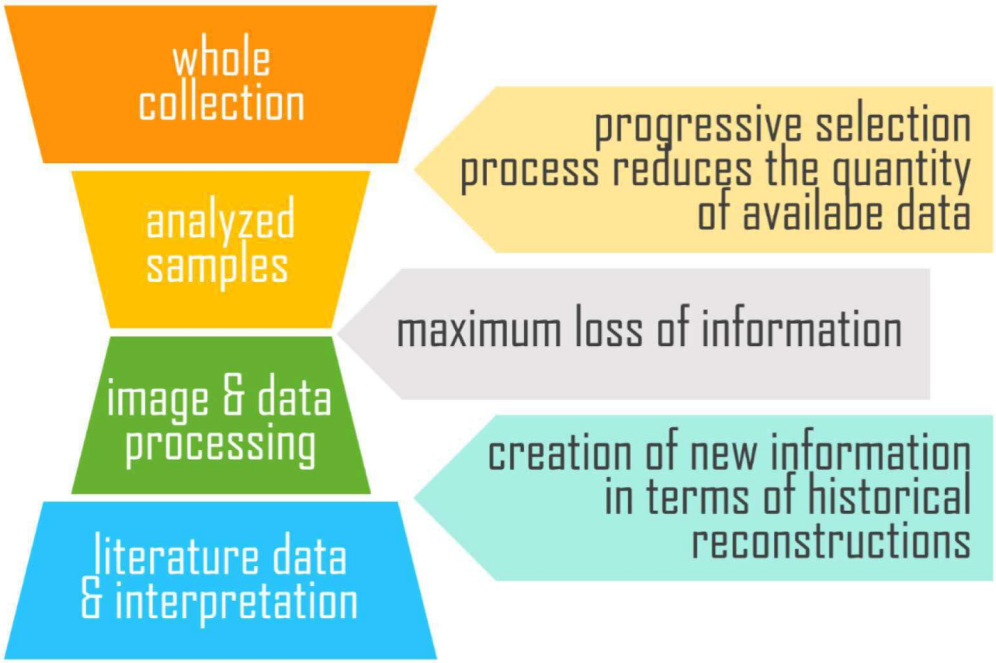

Fig. 5.3 – Diagram representing the progressive loss of information during the selection process and the analytical measures and the associated creation of new information (historical reconstructions) thanks to data processing and interpretation.

dBC

UNIVERSITÀ DEGLI STUDI DI PADOVA

DIPARTIMENTO DEI BENI CULTURALI:
ARCHEOLOGIA, STORIA DELL'ARTE,
DEL CINEMA E DELLA MUSICA

SCHEDA DI CAMPIONAMENTO

Sigla del Campione	Ty-S-BiR-507
Scopo del Campionamento	Indagini archeometriche
Analisi programmate	OM, SEM-EDS, EPMA, micro-Raman, micro-XRD
Identificazione della proprietà	
Numero di inventario	S. 18555/07
Materiale	Vetro
Tipologia	Frammento di sbarretta a strati bianco e rosso
Cronologia	Epoca greco-romana
Provenienza	Egitto, Tebtynis
Proprietà	Statale
Identificazione del campione	
Data del campionamento	21 giugno 2016
Responsabile del campionamento	Dr. Ivana Angelini (dBC, Università degli Studi di Padova)
Localizzazione campionamento/i	Da un'estremità già fratturata
Descrizione del campione	Il vetro si presenta in buono stato di conservazione
Fotografia del campione	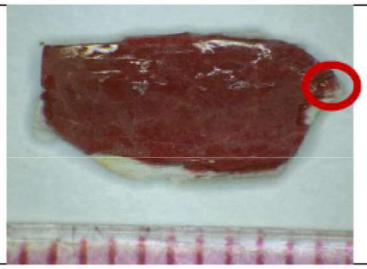
Metodo di campionamento	Distacco tramite bisturi dotato di apposita lama
Note	

Fig. 5.4 – Example of sampling data sheet UNI EN 16085: 2012 for the glass inlays from Tebtynis preserved at the Egyptian Museum of Turin.

Data sheets prepared according to the scheme of the standard requirements UNI EN 16085: 2012 "Conservation of Cultural property - Methodology for sampling from materials of cultural property. General rules"[3] were also realized and provided to the Museum. For every sample, they include: inventory number; sample code; property, provenance, typology and chronology of the object; responsible, date, aims, methods and localization of the sampling; expected analytical protocol; description and picture of the sample (fig. 5.4).

5.4 Tebtynis inlays in the context of Graeco-Roman Egypt

Glass inlays represent one of the highest points of pre-roman craftsmanship in Egypt. Just like artificial gemstones, their color and opacity reproduce the dark blue of lapis lazuli, the orange shades of carnelian, the deep red of jasper or the greenish tints of turquoise, whose magical powers were recognized in Ancient Egypt since Predynastic times (Aufrère, 1991; Duckworth, 2012; Bettineschi, 2016).

They were first produced during the New Kingdom, with few examples dating to the Late Period and a significant reprisal in Ptolemaic and Roman times, when new colors and techniques were introduced. Stylistic, typological and chronological studies were published since the late 1970s by Cooney (1976), Bianchi (1983a, 1983b), Nenna (among others: 1995; 2015), Grose (1989), Stern & Schlick-Nolte (1994). These last authors were the first to propose a coherent reconstruction of the production processes used to obtain both figured and non-figured inlays, which was followingly accepted among all other scholars (e.g. Auth, 1999; Nenna, 2006; 2011; Gasperini *et alii*, 2008).

Despite their relative frequency in Museum collections all over the world, the study of Egyptian glass inlays suffers from three main limitations:

[3] Italian National Unification, acronym UNI, represents Italian legislative activity at the International Standards Organization (ISO) and European Committee for Standardization (CEN). The standard 16085: 2012 provides criteria and procedures for sampling cultural heritage for scientific investigations. For more details see (visited October 2017): https://infostore.saiglobal.com/preview/is/en/2012/i.s.en16085-2012.pdf?sku=1566977.

1) most of the recovered inlays are scattered fragments, i.e. they lost any connection with the inlaid panel they belonged to. However, some authors (Cervi, 2012; Nenna, 2015; and MetMuseum inv. 21.2.2-related) were able to propose meaningful reconstructions for the arrangement of the inlays (fig. 5.5), when unitary groups were concerned (such as in the case of small shrines buried in the depots of the temples).

2) Very few spare inlays and inlaid objects come from well-dated, stratigraphic contexts. Most of them were excavated at the end of the XIX or beginning of the XX century and ended up in the antiquity market without any reference to their provenance. For this reason, the dating of these kind of objects generally relies on stylistic reasons and on the comparison with other specimens which, however, may not be securely dated as well.

3) Even when the inlays are found in context, their chronology may be problematic to interpret. In Ancient Egypt, ritual articles have always experienced a certain level of stylistic conservatism; moreover, these objects might have remained in use for a long time before being discarded and incorporated in the archaeological record. This is also clearly pictured by the Romano-Egyptian papyrological evidences, which testify very few changes to the temples' ritual treasures inventories (χειρισμοί) over time spans which exceed seventy years (Burkhalter, 1985). The only unequivocal reference to the exact period of production is the presence of royal cartouches, which are unfortunately very rare, especially in Ptolemaic times.

Despite the limits presented above, a general contextualization of the materials from Tebtynis will be offered hereinafter, summarizing the main data and directions of the recent literature in the field.

Bianchi (1983a) distinguished two main types of inlay techniques: in the Saitic/ Persian group, attributed to the Late Period, "the various inlays are each set into their own hollow, or cell, and rarely are the figures built up of contiguously set and abutting pieces". On the contrary, "inlays of the Sebennytic/ Ptolemaic type could be constructed in noncellular, contiguous fashion to produce complete figures".

Fig. 5.5 – Reconstruction of a plausible arrangement for the glass inlays inv. 21.2.2-related at the Metropolitan Museum of Arts, with the Pharaoh offering to Harpocrates and to a female deity (MetMuseum online catalogue: https://www.metmuseum.org/art/collection).

Gasperini, Paolucci & Tocci (2008) proposed the use of a different terminology for defining the same two technological variants. In particular, they suggested the French terms *cloisonné* and *champlevé*, which have a very long tradition in the field of jewelry production and metal (or ivory) enameling. According to these authors, the *cloisonné* would correspond to the Saitic/ Persian group characterized by small cells each containing one inlay, well separated from the others. However, the *cloisonné* involves the addition of a thin metal wire to create the various compartments (or *cloisons*); conversely, the hollows of the Ancient Egyptian inlaid objects were generally carved in wood, which is better consistent with the description of the c*hamplevé* technique. Altogether, it would seem better to reject this terminological proposal, as it tends to be misleading.

The oldest, surely dated example of *naos* inlaid with glass dates back to the XXVIth dynasty and is constituted by the *gates of the sky*[4] of a shrine (Louvre, inv. E605 N504) representing the Pharaoh Amasis (570-526 BC) in the act of offering to Sopdu, the falcon-headed god of the sky and of the Eastern borders of Egypt (fig. 5.6a). In this case, the vitreous materials constitute only the freezes, hieroglyphs and frames, while the human and divine figures are carved in wood and covered by gilded stucco. The number of glass colors is limited to dark blue, light blue and red. A shrine of the same Pharaoh was also discovered in Saqqara and is now preserved in the Royal Ontario Museum of Toronto (inv. 969.137.8). Another early shrine doorjamb at the Louvre Museum (inv. N 503), but without any inlay preserved in place (fig. 5.6b), bears the cartouche of a king that Yoyotte (1972) interpreted as Seheruibre Pedubast III (522-520 BC). The same author also attributed to Pedubast III a shrine fragment currently at the Archaeological Museum in Bologna (inv. KS 289), which represents a winged Isis with a Pharaoh holding the *neb* sign (fig. 5.6c). A recent study after the restoration of the fragment, however, interpreted the name as that of king Sehibra of dynasty XXIII (823–716 BC)[5]. Judging from the epigraphic and archaeological evidence, Yoyotte's hypothesis seems

[4] *Gates of the sky* is name given in Ancient Egypt to the doors of the tabernacle containing the living effigy if the god. These doors acted as a sort of magic access from the world of man to the divine realm and vice versa (Étienne, 2009).

[5] This last chronology is stated both in the Museum label and in the online catalogue of the collection (visited July 2017): http://www.museibologna.it/archeologicoen/percorsi/66287/id/75337/oggetto/74921/.

better justified. One last fragment of the same *naos* is now hosted at the Metropolitan Museum of Art (inv. 23.6.75a). The Isis' panel inv. 37.260E at the Brooklyn Museum, although anepigraphic, shows high similarities with the one of Bologna and can thus be attributed to the same period.

Fig. 5.6 – a) Naos of Amasis (Louvre, inv. E 605 N 504); b) doorjamb of Pedubast III naos (Louvre, inv. N 503); c) shrine fragment from Bologna (inv. KS 289) also attributed to Pedubast III; d) Darius I naos at the British Museum (inv. EA37496); e) naos of Nectanebo II at the Brooklyn Museum (inv. 37.258E); e) sarcophagus of Petosiris, Cairo Museum (inv. JE 46952). All images taken from the web[6].

[6] Museum webpages (a-e) and pinterest (f): a-b) www.louvre.fr/en/moteur-de-recherche-oeuvres; c) www.comune.bologna.it/museoarcheologico/; d) http://www.britishmuseum.org/research.aspx; e) https://www.brooklynmuseum.org/opencollection; f) https://www.pinterest.com/.

A third example is Darius I's (521-486 BC) *naos* at the British Museum (inv. EA37496). The scene represents Darius dressed as a Pharaoh, offering to the seated god Anubis and to Isis, behind him (fig. 5.6d). The object was discovered before 1828 and sold in the antiquity market without further references. For the first time, the figurative decoration is entirely made up of glass inlays in cellular fashion, as described by Bianchi for the Saitic/ Persian typology. The colors of the preserved inlays range from light blue to dark-blue and yellowish-orange. Another wooden shrine of the Achaemenid king exists in the Mallawi Antiquities Museum[7] and was found at Tuna el-Gebel (the cemetery of Hermopolis Magna), but has no inlaid decoration.

Remains of glass inlays of the middle V century BC were discovered in the temple of 'Ain Manawir. As already stated (cfr. §4), they seem to belong to more than one *naos*. Lacking the wooden boxes, is not possible to distinguish between contiguous or non-contiguous fashion. Nevertheless, the chronology of the site and the style of the heads seems to better fit in the Saitic/ Persian typology.

One last example of this group is the wooden shrine of Nectanebo II (359-341 BC) at the Brooklyn Museum (inv. 37.258E), which shows for the first time inlays in mosaic glass (fig. 5.6e), a technology which will become more and more frequent in the following years.

Unfortunately, inlays of the Sebennytic/ Ptolemaic group cannot claim an equally adequate coverage in terms of well-dated pieces. Some of the most interesting evidences are related to wooden or cartonnage sarcophagi, starting from the second half of the IV century BC. Among the best pieces, those of the brothers Petosiris (fig. 5.6f) and *Djedthotiuefankh* (fig. 5.7a) preserved respectively in Cairo (inv. JE 46952) and Turin (inv. 2241). In this case, the glass pieces are closely juxtaposed and fixed by means of an organic binder for the composition of complex hieroglyphs; mosaic glass is also frequently used. Bianchi (1983a) and Nenna (2011) also cite the so-called Gliddon mummy case of the Smithsonian (inv. A1415-0), but it was not possible to determine whether glass or paint was used in this specimen from the available pictures (fig. 5.7b).

[7] Or at least it was there before the looting and destructions of August 2013. For more details see (visited in October 2017): http://www.unesco.org/new/en/culture/themes/illicit-traffic-of-cultural-property/emergency-actions/egypt/warning-looting-of-the-malawi-national-museum/

Fig. 5.7 – a) detail of the sarcophagus of Djedthotiuefankh, Turin (inv. 2241); b) Gliddon mummy case of the Smithsonian (collections.si.edu), front and bottom view (inv. A1415-0); c) broad collar inv. 33.383 of the Brooklyn Museum (https://www.brooklynmuseum.org/opencollection), front view and detail of the inlaid decoration.

The museum catalogue reports an early label that says "Mummy *cartonnage* (section), wooden with linen cover, painted with hieroglyphs, naturalistic, Egyptian, late period?"[8]. The same authors (Bianchi, 1983b; Nenna, 2011; 2015) list various other examples of glass inlaid sarcophagi dating to the Greek and Roman period that cannot be reported as a whole for the sake of briefness. It is, however, worth citing the broad collar inv. 33.383 of the Brooklyn Museum (fig. 5.7c) possibly associated with the name of Ptolemy V, which shows another use for glass inlays, and the *naos* discovered in the sacred animal necropolis of North Saqqara attributed to as early as the VI-V century BC (Insley Green, 1987), where the figures of the Pharaoh worshipping Isis and Harpocrates are entirely made of glass (inv. JE 91103).

However, most of the glass inlays known for this phase are scattered fragments with very generic dating, such as those of the Per-Neb/ Groppi collection (1992a; 1992b; 2012), the Ernesto Wolf collection (Stern, Schlick-Nolte, 1994) and many others (just to name a few Riefstahl, 1968; Von Saldern *et alii*, 1974; Goldstein, 1979; Grose, 1989; Antonaras, 2013). Even the pieces which were recovered in context suffer from critical issues for their chronological identification. This is for example the case of the inlays from Gumaiyima (Cooney, 1972), excavated at the end of the XIX century (Petrie, Griffith, 1888) and ascribed to the beginning of the III century or to the Late Ptolemaic/ Early Imperial period according to the various scholars (see § 4, fig. 4.9). The glass elements comprise mosaic borders, drawn mosaic canes and slices, numerous hieroglyphs, inlays for gorge-shaped and winged-sun disks cornices, various geometric pieces and figurative elements for clothes, accessories, furniture and human/ divine representations. The most famous object is a wooden panel of a *naos* representing a gilded falcon.

The inlays from Bakchias (North-Eastern Fayum) published by Gasperini, Paolucci and Tocci (2008) were discovered within the first and second courtyards of templar structures A and C. The first temple was built in the II - early I century BC, while the second has been attributed to the Augustan era; however, the inlays were all dated with some caution to the early Ptolemaic period, because they were discovered in superficial

[8] See (visited October 2017): http://n2t.net/ark:/65665/33980500f-cc3a-4fb9-9cd1-81f2d1fd1393.

layers, at times strongly compromised by modern activities, and thus their chronology was proposed according to stylistic reasons by comparison with other sites and single uncontextualized objects. The iconographic themes have much in common with those found in Tebtynis, Gumaiyima and Soknopaiou Nesos (fig. 5.8). There are for example: sequences of stars (see inv. B96/92/433 and B97/163/508), that can be associated to friezes representing the night sky; *ank-was* hieroglyphs, that symbolize life and happiness and can be read as the blessing formula "hail, life, hail", common from the II millennium BC (Stern, Schlick-Nolte, 1994); wing elements; checkboard and zigzag patterns; monochrome hieroglyph signs and figurative elements (crown, clothes, legs, human bodies, faces etc.).

Fig. 5.8 – A selection of inlays representative of the most significant typological varieties in Bakchias (from Gasperini et alii, 2008).

The Soknopaiou Nesos fragments do also come from secondary fills, as already stated (see § 4), and cannot be used as a chronological reference. However, they offer the best comparison for many inlays and wooden fragments of Tebtynis at the Egyptian Museum from the stylistic, dimensional and chromatic point of view[9]. The objects from the two sanctuaries present slight variations on the same subjects, that are possibly related to the presence of two different local workshops, but they are certainly coeval (fig. 5.9).

[9] See e.g. Soknopaiou Nesos inv. ST07/ 423/ 1930 or ST07/ 424/ 1954 and Tebtynis inv. S. 18764; Soknopaiou Nesos inv. ST08/ 557/ 2469 or ST06/ 343/ 1405 and Tebtynis inv. S. 19569/1; Soknopaiou Nesos inv. ST09/ 636/ 2817 and Tebtynis inv. S. 18556/ 21; Soknopaiou Nesos inv. ST25/ 256/ 1727 or ST07/ 43/ 1940 and Tebtynis inv. S. 18554/06; Soknopaiou Nesos inv. ST06/ 356/ 1762 and Tebtynis inv. S. 18554/ 14 (later analyzed as sample Ty-P-R-414) and many others.

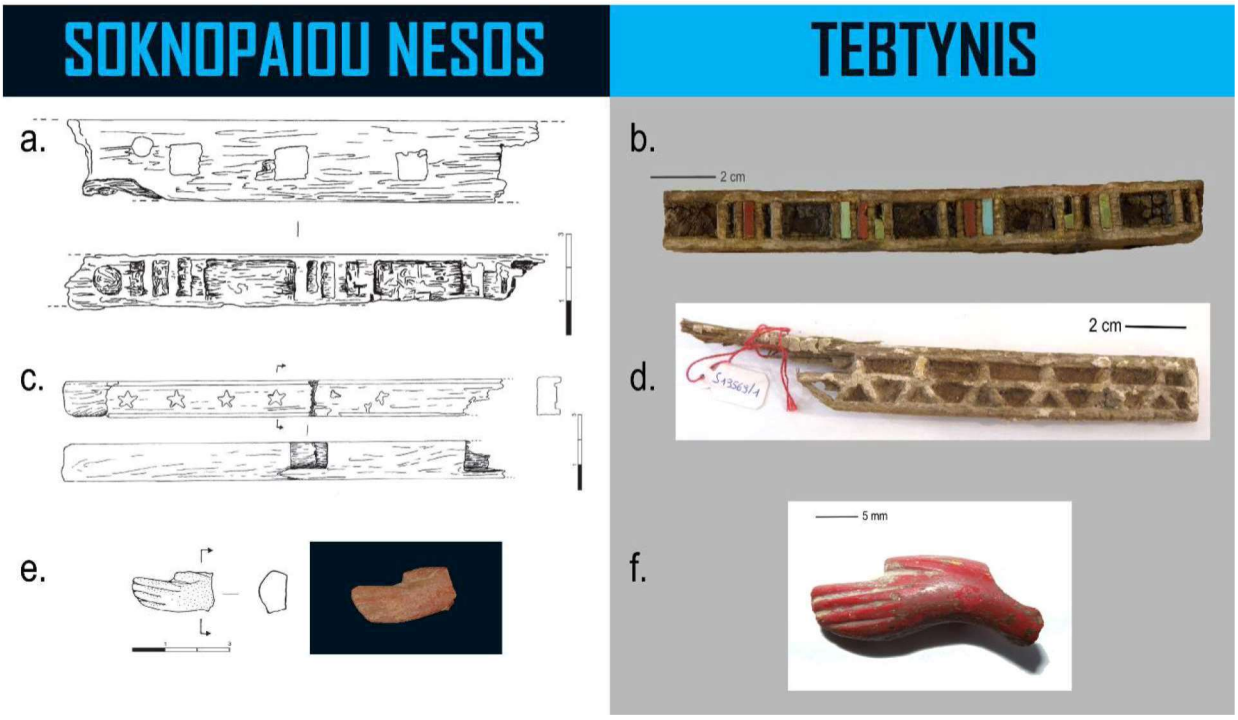

Fig. 5.9 – Comparison between some of the inlays and inlaid wooden fragments from Soknopaiou Nesos (left, from Gasperini et alii, 2008) and Tebtynis (right): a) Soknopaiou Nesos inv. ST07/ 423/ 1930; b) Tebtynis inv. S. 18764; c) Soknopaiou Nesos inv. ST06/ 343/ 1405; d) Tebtynis inv. S. 19569/1; e) Soknopaiou Nesos inv. ST07/ 43/ 1940; f) Tebtynis inv. S. 18554/06.

6. Analytical methods and data processing

In this work, a broad range of analytical techniques and software for data processing was used to investigate the production technologies, the texture and the chemico-mineralogical composition of the investigated glasses. Each analytical technique employed is unique yet complementary to the others with regards to the results that can be obtained; only their combined use can contribute to the cross-validation of the data and to the complete characterization of the samples, suitable for interpretative purposes. The analytical protocol was designed in view of the specific characteristics of the samples and in accordance with the aims of the project (fig. 6.1). After a first screening on the whole collection by SM, a statistically significant set of 144 glasses was accurately characterized by means of OM, CLSM, SEM-EDS and EPMA. Finally, μ-Raman was used for the identification of a selection of crystalline inclusions present in the different opaque color classes.

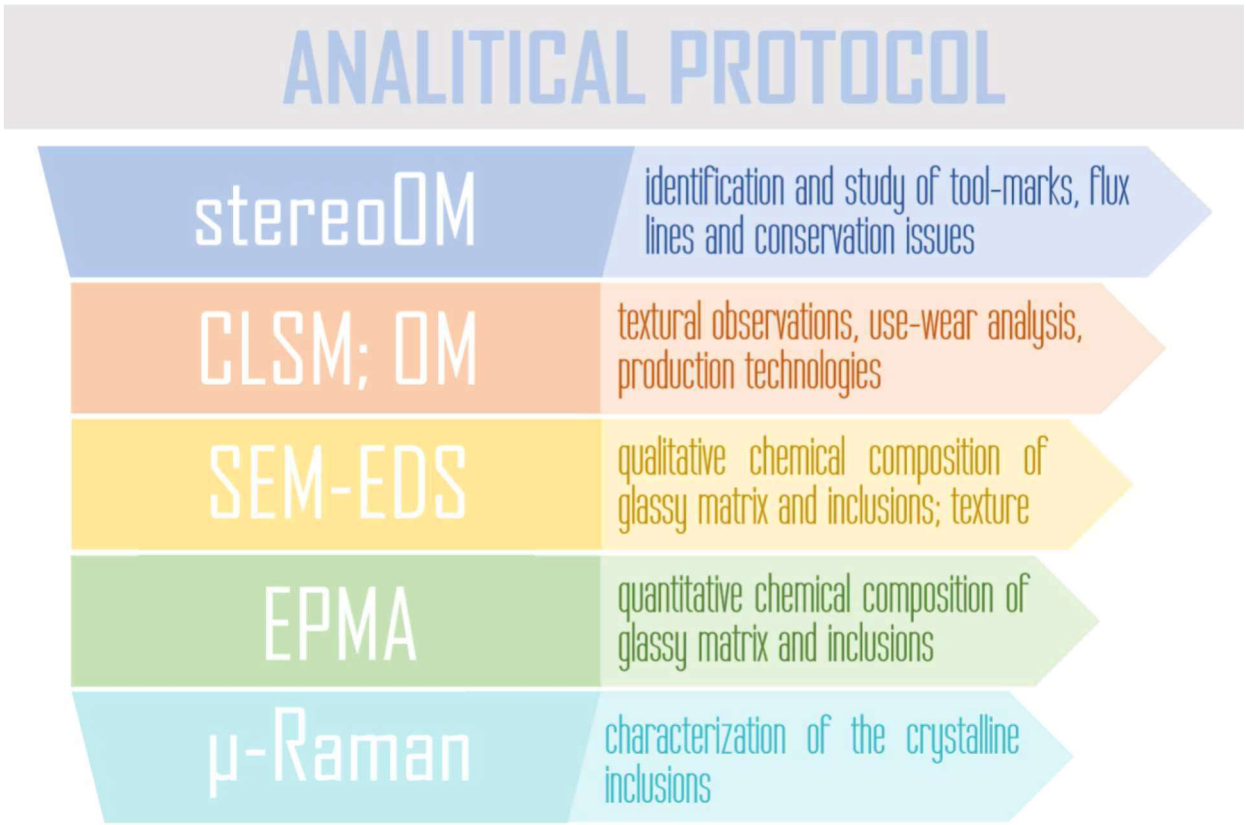

Fig. 6.1 – Workflow of the analytical protocol employed with short description of the most important applications of each analytical technique.

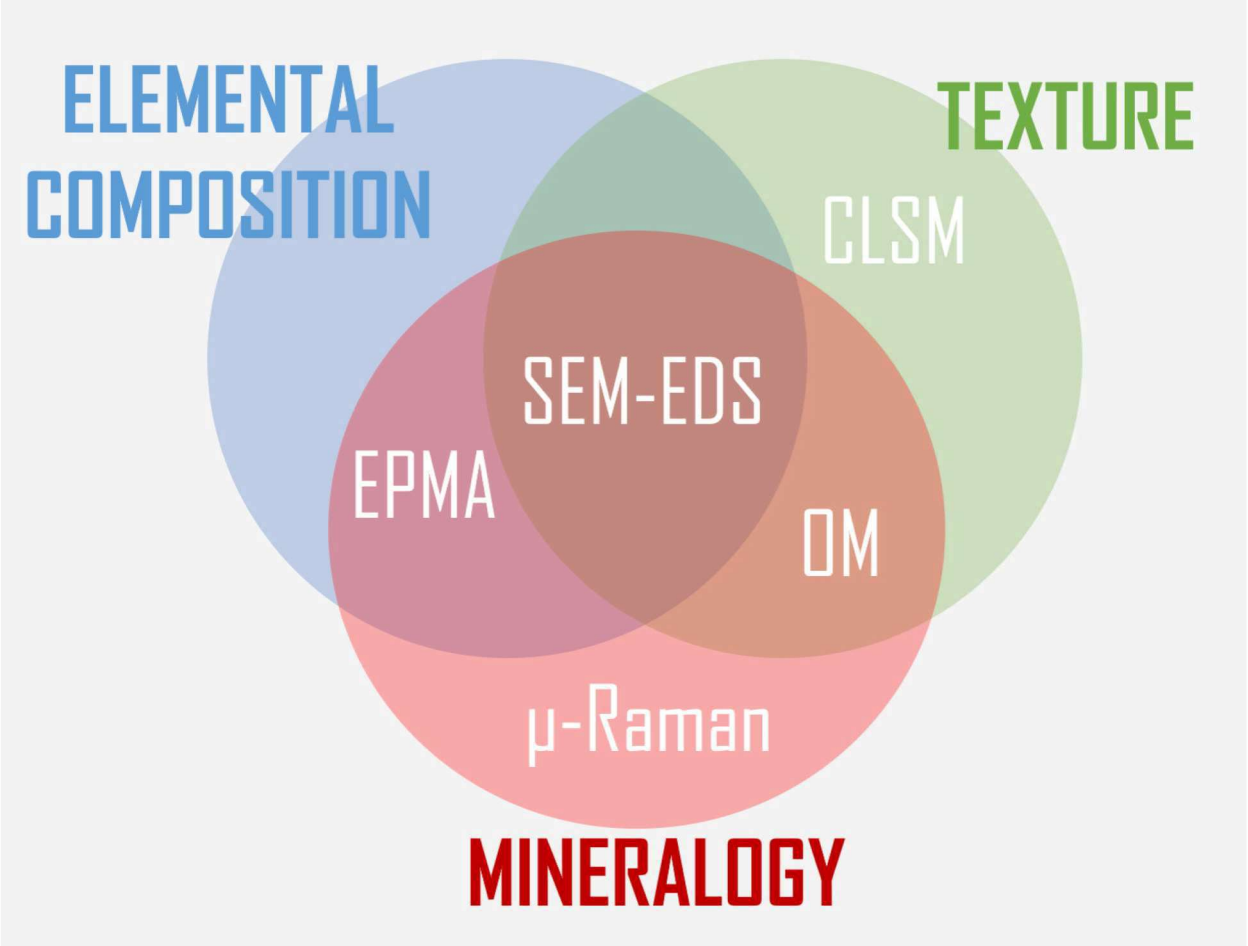

Fig. 6.2 – The analytical protocol: fields of overlapping of the multi-analytical approach used.

6.1 Optical microscopy (OM)

Preliminary morphological observations were carried out on the whole collection directly at the Egyptian Museum with a stereoscopic microscope (SM or stereoOM) Nikon SMZ 645 equipped with a digital camera Nikon Coolpix 6.1. This first screening contributed to: 1) evaluate the conservation state of the objects and the presence of eventual weathering layers or cracks that could compromise their integrity during sampling; 2) offer a general overview of the color, texture and homogeneity of the glasses; 3) investigate the production technologies, thanks to the presence of specific markers (flux lines, bubble orientation, tool marks etc.); 4) select the glasses to be sampled and direct the sampling procedure.

The most representative 70 artifacts were selected and sampled for in-depth archaeometric investigations. Detached chips (measuring ca. 200-600x200-600 μm) were mounted in epoxy resin, abraded with silicon carbide (800-4000 mesh) and polished with diamond and colloidal silica suspensions of decreasing grain size in the laboratories of the Department of Geoscience of the University of Padova to obtain polished cross sections.

Subsequently, they were observed with a high magnification (50x-1000x) polarizing optical microscope (OM) Nikon Eclipse ME600 operating in reflected light and crossed (XN), parallel (//N) or shifted nicols. Image sequences were acquired with a reflex camera Canon EOS 600D. OM investigations helped to evaluate the texture of the samples and, specifically, gave information about the mineral inclusions, laying the basis for the following SEM-EDS and μ-Raman analyses. For obvious reasons of synthesis, this thesis contains only the most relevant images.

6.2 Confocal Laser Scanning Microscopy (CLSM or LSCM)

Non-invasive, micro-topographic observations were performed using an Olympus LEXT OLS 4000 Confocal Laser Scanning Microscope of the Department of Geosciences (University of Padova) directly on the surfaces of the archaeological objects, before sample preparation. The confocal technology relies on a pinhole located just in front of the detection system, which excludes all out-of-focus light. Three-dimensional images are created from single-points by scanning and subsequent merging of the X-Y-Z data (Fabich, 2009).

Essentially, the CLSM can register sub-micrometric digital images and three-dimensional models, contributing to the study of production technologies, surface alteration and use-wear analysis. Optical plus digital magnification ranges from 108x to 17280x, granting a spatial resolution of 10 nm on Z axis (height) and 120 nm in the X-Y plan for very high-resolution metrology measurements. The incident laser light is fixed at 405 nm. Z resolution is dependent on the physical control of the Z-movement of the objective, while the X-Y resolution is inversely proportional to the wavelength of the

illuminating light: thus, as the wavelength decreases, the resolution of the system increases.

6.3 Scanning Electron Microscopy with Energy Dispersive System (SEM-EDS)

Prepared samples were coated with carbon film (thickness ca. 200 Å) and analyzed at the Department of Geoscience (University of Padova) with a scanning electron microscope (SEM) CamScan MX3000 equipped with EDAX energy dispersive system (EDS) for chemical and morphological characterization. Acquisitions included backscattered (BSE) and secondary electron (SE) images, as well as EDS spectra for elemental analyses. Two sets of operating conditions were used: 1) standard W filament, working distance 25 mm, beam current 50-60 nA, accelerating voltage 25 kV, 60-100 s counts per point analysis; 2) LaB_6 filament, working distance 25 mm, beam current 150-250 nA, accelerating voltage 20 kV, 60 s counts per point analysis. The detection limit can vary, but is generally in the order of 1%, except for light elements or elements with overlapping peaks.

SEM-EDS is a fundamental tool for the study of the glassy matrix and of the residual, newly formed and coloring/ opacifying phases. It should, however, be noted that sometimes the dimensions of the mineral inclusions or the chemical zoning to be determined can be very scarce. Considering the dimensions of the electronic beam, this sometimes implies a partial contamination of the point spot data with the surrounding glassy matrix. The results that will be presented throughout the work must thus be considered semi-quantitave or even qualitative, when areas or inclusions smaller than 4-5 μm are concerned.

Areal analyses were also performed to obtain data about the spatial composition of the samples, including glassy matrix and mineral phases. The 2D areal distribution was considered as representative of the tridimensional one; the obtained compositions can thus be compared to bulk analyses, such as the LA-ICP-MS (Laser Ablation Inductively Coupled Plasma Mass Spectrometry) or the XRF (X-Ray Fluorescence), sometimes used in the literature. In this case, table VII in the appendix reports the average of 3-5 measures in areas of ca. 50x75 μm to 150x300 μm, according to the dimensions of the

samples. By default, all the semi-quantitative analyses obtained are normalized at 100%.

A test for the morphological study of the nanometric inclusions was performed on sample Ty-M-G-504a by means of a Zeiss Sigma Field Emission SEM with an Oxford X-MAX EDS at the ICAMTE laboratory of the National Research Center (CNR) of Padova.

6.4 Electron Probe Micro Analysis (EPMA)

After SEM-EDS analyses, a total of 139 glasses (plus various chemical zoning) were investigated by EPMA to obtain chemical data with higher precision and accuracy. The instrument used is the JEOL 8200 Super Probe with 5 wavelength-dispersive spectrometers (WDS) at the Earth Sciences Department of the University of Milan. 18 elements were analyzed: Na, Mg, Al, Si, P, S, Cl, K, Ca, Ti, Mn, Fe, Sb, Co, Cu, As, Sn and Pb whose mineral standards and analyzing crystals can be found in table 6.1. Due to instrumental problems it was not possible to measure Ni and Zn as initially planned.

Corning glass standards A and B were analyzed before every daily session to evaluate the accuracy (values) and the precision in terms of reproducibility of the data (Standard Deviations). The reference composition of the Corning glass standards[1] is compared to the measured data with a probe diameter of respectively 5 μm and 10 μm (as a mean of 9-12 spot analyses) in table 6.2. Standard Deviation (SD) is always in the order of 0.01-0.09, except for Na_2O that shows values of ca. 0.2-0.3. The highest variability was found in silica, which reaches peaks of 0.78-0.96. However, the percentage error for SiO_2 is low, ca. 1-1.5% at 10 μm spot size and 3-4% for 5 μm spot size.

Working conditions were set at 15 kV accelerating voltage and 5 μA sample current; spot size was varied according to the textural characteristics of the samples: for transparent glasses, we opted for 3 to 5 measures with beam defocused at 10 μm to reduce alkali loss, which is a well-known problem in the field of natural and synthetic glass studies (see e.g. Nielsen, Sigurdsson, 1981). Opaque samples with homogeneously dispersed crystalline inclusions were investigated with 4-6 measures at 5 μm spot size,

[1] According to the recent revision of Adlington (2017) on Brill's (1999) compositional data.

in order to better distinguish the composition of the glassy matrix from the bulk composition of glass; 2 additional points at 10 μm spot size were used to evaluate the sodium volatilization rates.

Element	Standard type	Crystal
Si	grossular	TAP
Na	omphacite	TAP
Ca	grossular	PETH
K	K-feldspar 113	PETH
Mg	olivine 153	TAP
Al	grossular	TAP
P	apatite 139 or Y-phosphate	TAP
S	galena	PETJ
Cl	scapolite	PETJ
Ti	ilmenite 149	PETJ
Mn	rhodonite	LIFH
Fe	fayalite 143	LIFH
Co	metallic Co	LIFH
Cu	metallic Cu	LIFH
As	nikeline	TAP
Sn	metallic Sn	PETH
Sb	metallic Sb	PETH
Pb	galena	PETJ

Tab. 6.1 – List of the elements analyzed by EPMA, with related standards and analyzing WDS crystals.

Considering the high variability of the three major elements in the glassy matrix (Na_2O, SiO_2 and PbO, when present in high concentrations) observed between the 10 μm and 5 μm spot size measures, it was decided to standardize all opaque glass data by systematically combining the values of Na_2O, SiO_2 and PbO registered at 10 μm with all other elements registered at 5 μm. This procedure, on one hand grants a better accuracy in the evaluation of the Na_2O, significantly improving the problem of alkali loss, and on the other helps to minimize the overall contribution of crystalline inclusions dispersed in the vitreous phase, since they are generally related to minor and trace elements registered at 5 μm (and thus in a smaller volume). The reliability of the method is also proven by the high precision of the instrument as emerged from the analyses on

the Corning glass standards before each work session, which suggest a significant reproducibility of the data even in case of a lower number of acquisitions (tab. 6.2).

Mineral inclusions were analyzed with a 1 μm probe diameter, in order to reduce the contribution of the glassy matrix to the acquired data.

6.5 Micro-Raman Spectroscopy (μ-Raman)

The mineralogic characterization of the crystalline inclusions in the opaque glasses was carried out at the Department of Chemistry of the University of Padova with a DXR Thermo Scientific micro-Raman, using a single mode diode 532 nm green laser as excitation source. Non-destructive acquisitions were performed directly on the surfaces of the polished samples. Spot analyses were carried out with a 50 LWD (long working distance) objective, with a spectral resolution in the range of 2.7-4.2 cm^{-1} and a spatial resolution of 1.1 μm. The exposure time was set to 3 seconds, with 32 scan accumulations. The other experimental conditions were varied to reduce sample fluorescence effects and maximize the scattering efficiency. In particular: 1) for silicates and antimoniates, laser power of 5 mW and a filter with a 25 μm pinhole; 2) for metals, laser power of 6 mW and 50 μm pinhole aperture; 3) for metal oxides, laser power of 3 mW with a pinhole aperture of 25 μm and Raman shift range between 100-1500 cm^{-1}.

Spectra were treated and identified by means of Omnic 9 software (Thermo Scientific), associated with the RRUFF web-database (at: rruff.info/, see Down, 2006) and the published literature related to synthetic phases in ancient glasses (e.g. Rosi *et alii*, 2009; Gedzevičiūtė *et alii*, 2009; Basso *et alii*, 2013; Olmeda *et alii*, 2015).

6.6. Image and data processing

6.6.1 *Focus staking and image stitching*

SM and OM images were recorded at different focal planes and reconstructed using the focus staking software Helicon Focus 6, with bicubic interpolation and dust maps for improved reconstructions.

Corning A	10 µm spot size Measured Values MEAN	S.D.	Standard	Absolute error	5 µm spot size Measured Values MEAN	S.D.	Standard	Absolute error
Na_2O	**14.11**	**0.32**	14.30	0.19	**13.40**	**0.20**	14.30	0.90
MgO	**2.62**	**0.09**	2.66	0.04	**2.74**	**0.08**	2.66	0.08
Al_2O_3	**0.90**	**0.04**	1.00	0.10	**0.98**	**0.05**	1.00	0.02
SiO_2	**67.19**	**0.78**	66.56	0.63	**68.76**	**0.51**	66.56	2.20
SO_3	**0.12**	**0.04**	0.08	0.04	**0.13**	**0.03**	0.08	0.04
P_2O_5	**0.12**	**0.03**	0.14	0.02	**0.13**	**0.05**	0.14	0.01
Cl	**0.09**	**0.02**	0.09	0.00	**0.11**	**0.01**	0.09	0.02
K_2O	**2.90**	**0.01**	2.87	0.03	**2.91**	**0.02**	2.87	0.04
CaO	**4.99**	**0.05**	5.03	0.04	**5.10**	**0.04**	5.03	0.07
TiO_2	**0.83**	**0.06**	0.79	0.04	**0.85**	**0.04**	0.79	0.06
MnO	**0.91**	**0.09**	1.00	0.09	**0.95**	**0.06**	1.00	0.05
FeO	**0.98**	**0.11**	0.98	0.00	**1.01**	**0.04**	0.98	0.03
CoO	**0.17**	**0.04**	0.17	0.00	**0.20**	**0.05**	0.17	0.03
CuO	**1.21**	**0.10**	1.17	0.04	**1.29**	**0.04**	1.17	0.12
As_2O_5	**0.02**	**0.02**	0.00	0.02	**0.01**	**0.01**	0.00	0.01
SnO_2	**0.18**	**0.03**	0.19	0.01	**0.20**	**0.03**	0.19	0.01
Sb_2O_5	**1.84**	**0.06**	1.75	0.09	**1.92**	**0.04**	1.75	0.17
PbO	**0.05**	**0.05**	0.07	0.02	**0.04**	**0.05**	0.07	0.03
Total	**99.23**		98.86		**100.71**		98.86	

Corning B	10 µm spot size Measured Values MEAN	S.D.	Standard	Absolute error	5 µm spot size Measured Values MEAN	S.D.	Standard	Absolute error
Na_2O	**16.84**	**0.32**	17.00	0.16	**15.73**	**0.24**	17.00	1.27
MgO	**1.02**	**0.04**	1.03	0.01	**1.10**	**0.03**	1.03	0.07
Al_2O_3	**4.19**	**0.07**	4.36	0.17	**4.59**	**0.04**	4.36	0.23
SiO_2	**62.41**	**0.56**	61.55	0.86	**64.05**	**0.96**	61.55	2.50
SO_3	**0.92**	**0.05**	0.82	0.10	**0.90**	**0.13**	0.82	0.08
P_2O_5	**0.43**	**0.05**	0.49	0.06	**0.52**	**0.13**	0.49	0.03
Cl	**0.17**	**0.02**	0.16	0.01	**0.18**	**0.01**	0.16	0.02
K_2O	**1.03**	**0.02**	1.00	0.03	**1.05**	**0.02**	1.00	0.05
CaO	**8.63**	**0.04**	8.56	0.07	**8.93**	**0.07**	8.56	0.37
TiO_2	**0.11**	**0.03**	0.09	0.02	**0.10**	**0.03**	0.09	0.01
MnO	**0.24**	**0.01**	0.25	0.01	**0.21**	**0.03**	0.25	0.04
FeO	**0.30**	**0.04**	0.31	0.01	**0.33**	**0.04**	0.31	0.02
CoO	**0.03**	**0.03**	0.05	0.02	**0.04**	**0.03**	0.05	0.00
CuO	**2.82**	**0.11**	2.66	0.16	**2.96**	**0.06**	2.66	0.30
As_2O_5	**0.02**	**0.02**	0.00	0.02	**0.01**	**0.01**	0.00	0.01
SnO_2	**0.03**	**0.03**	0.02	0.00	**0.03**	**0.03**	0.02	0.01
Sb_2O_5	**0.48**	**0.04**	0.46	0.02	**0.50**	**0.04**	0.46	0.04
PbO	**0.39**	**0.10**	0.61	0.22	**0.45**	**0.11**	0.61	0.16
Total	**100.06**		99.42		**101.68**		99.42	

Tab. 6.2 – Published composition of Corning glass standards A and B (green columns) compared to the mean values calculated from an average of 9-12 point analyses measured with probe diameter of 10 µm and 5 µm. Standard Deviations (SD) and absolute errors are also reported.

Rendering methods were chosen based on a trial and error process according to the spectral and textural characteristics of each image set. Radius and smoothing parameters were adjusted for optimal results respectively between values of 8-22 and 3-7. Tridimensional rendering of the most significant surfaces was also achieved with the same software.

Image stitching was performed using FIJI (version 1.51g), an open source image processing package based on ImageJ (see https://imagej.nih.gov/ij/). SEM-BSE and SEM-SE maps, usually constituted by sequences of more than 40 images, were reconstructed using the "Grid/ Collection stitching" plugin in "filename defined" configuration for faster processing times (Preibisch *et alii*, 2009); on the contrary, SM and OM images – which never exceed 20 units – were stitched using the "MosaicJ" plugin, that offers a manual control on the overall procedure.

6.6.2 *Object-based Image Analysis (OBIA)*

Image analysis of OM and SEM images for archaeometic purposes have long been used in the specialized literature for the study of archaeological pottery, metals, vitreous materials and bones (see e.g. Whitbread, 1991; Goins, Reedy, 2000; Turner-Walker, Syversen 2002; Polla, Angelini, Artioli, 2006; Livingood, Cordell, 2008; Šelih, Van Elteren, 2011). However, even the most recent published works (Reedy, 2013; Eramo *et alii*, 2014; Dal Sasso *et alii*, 2014) essentially rely on a pixel-based approach. From the early 2000s, this method was gradually abandoned in the fields of remote-sensing and bio-medical applications, as it fails to detect textural changes and spatial relationships between the investigated entities, whether bubbles and inclusions within a glassy matrix or bomb craters in open field (Magnini, Bettineschi, De Guio, 2016). For this purpose, Object-Based Image Analysis (OBIA) was frequently proposed as the best alternative solution (Blaschke, Strobl, 2001; Yan *et alii*, 2006).

Image-objects are self-consistent regions created by aggregating proximal pixels according to their spatial, spectral and textural homogeneity, in contrast with the traditional "per-single-pixel" approach (Blaschke *et alii*, 2014). This implies a major shift in the protocol of image analysis, because object-based methods take into account

shape, pattern and spatial context, thus providing an improved basis for classification and interpretation. The workflow of an OBIA project can be broadly divided into 3 main stages:

1) partitioning of the image into primitive image-objects (segmentation). Segmentation is the basic step of OBIA. This process aims to divide the image in homogeneous groups of pixels, called image-objects (Haralik, Shapiro, 1985; Hay *et alii*, 1997). For this work, we chose the multiresolution algorithm included in eCognition Developer 9.1 (Trimble Navigation Ltd). Multiresolution segmentation is a region growing method: it starts from a single pixel, which is progressively combined to proximal ones according to criteria of minimized intra-object heterogeneity (Baatz, Shäpe, 2000; Benz *et alii*, 2004). Before segmenting the image, it is necessary to specify a set of parameters that influence the dimension (scale parameter), the shape and the compactness of the resulting image-objects. These values were adjusted case by case according to the characteristics of the various images and they will be specified in the discussion of the results when needed;

2) primitive image-objects usually do not correspond to geo-objects or real-world entities. However, every primitive image-object can be described with a huge set of information attributes (in OBIA language: features) which define its spectral properties, shape, size, texture, context and relations. These parameters can be used to direct the classification process, in order to identify meaningful real-world entities. Classification is, thus, a matter of mental models and experience. Literature data and the specific knowledge of the operator were the starting point to identify the most suitable object-features characterizing the various kinds of investigated elements;

3) post-classification analysis, such as statistical manipulation of the data, set the base for further segmentation/ classification cycles in order to fine-tune the results obtained.

A series of 64 SEM-BSE images were selected to represent the most significant color classes found in the Tebtynis collection. A minimum of 3 images per sample were processed, classified and quantitively analyzed in order to obtain indications on the number of the coloring and opacifying inclusions, their maximum and average

dimensions and on the ratio between the total volume of the glassy matrix and the volume of the crystalline inclusions, porosity excluded. Assuming a random distribution of the crystalline particles within the sample, this method provides an objective and reproducible estimation of the textural characteristics of the different glasses, offering new hints on the production technologies used and on the standardization of the manufacturing processes. The main results are summarized in the appendix (see table VI).

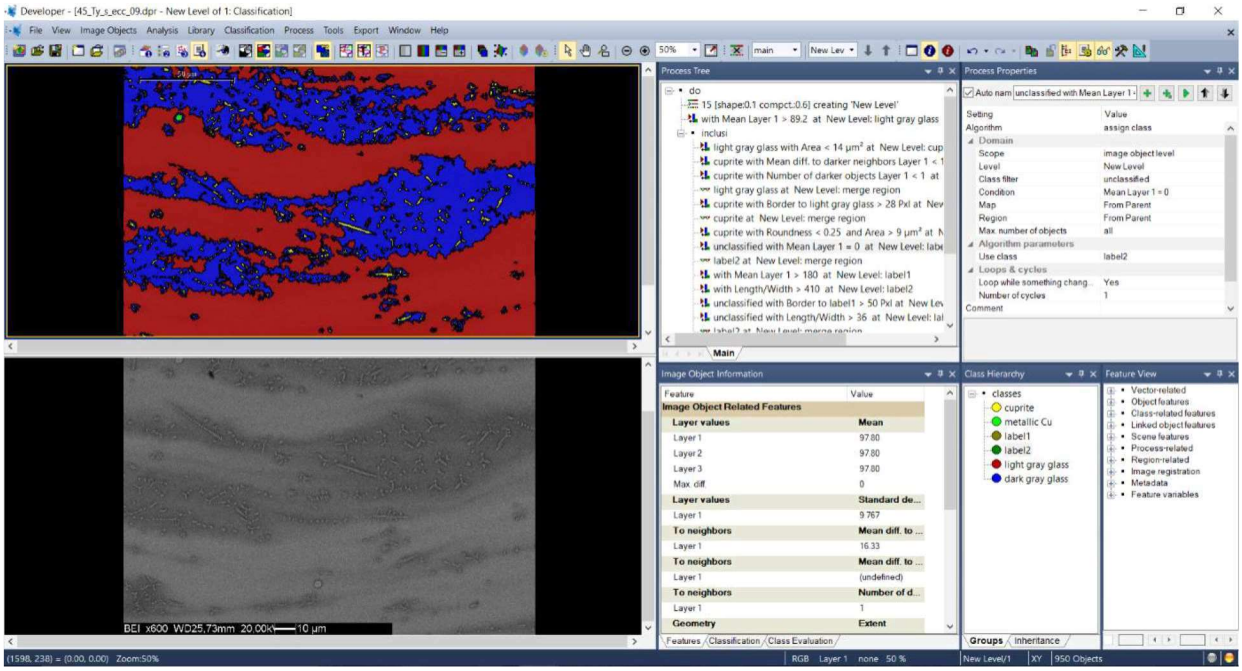

Fig. 6.3 – Workspace of an eCognition 9.1 project showing sample Ty-S-RV-418-R2.

6.6.3 *Principal Component Analysis (PCA)*

The Principal Component Analysis (PCA) is a statistical method of multivariate analysis that allows the user to extract – or summarize – the highest possible level of the total, meaningful variance of a dataset in a limited number of principal components, which can be visualized as a bi-dimensional or a three-dimensional (scatter)plot. In other words, the PCA reduces the dimensionality of a dataset, helping to identify groups and correlations (Wold *et alii*, 1987; Drennan, 2009). This method has been widely used

in archaeometry (Bieber *et alii*, 1976; Baxter, 1995; Blomster *et alii*, 2005; Panich, 2016), also in the field of glass studies (e.g. Cox & Gillies, 1986; Polikreti *et alii*, 2011).

Our dataset (in form of oxides wt%) was treated with R-Chemiometry, a software developed by the Group of Chemometrics of the Italian Chemical Society[2]. Data were always centered and scaled. The PCA was generally performed including all the elements of the dataset, except when specifically stated.

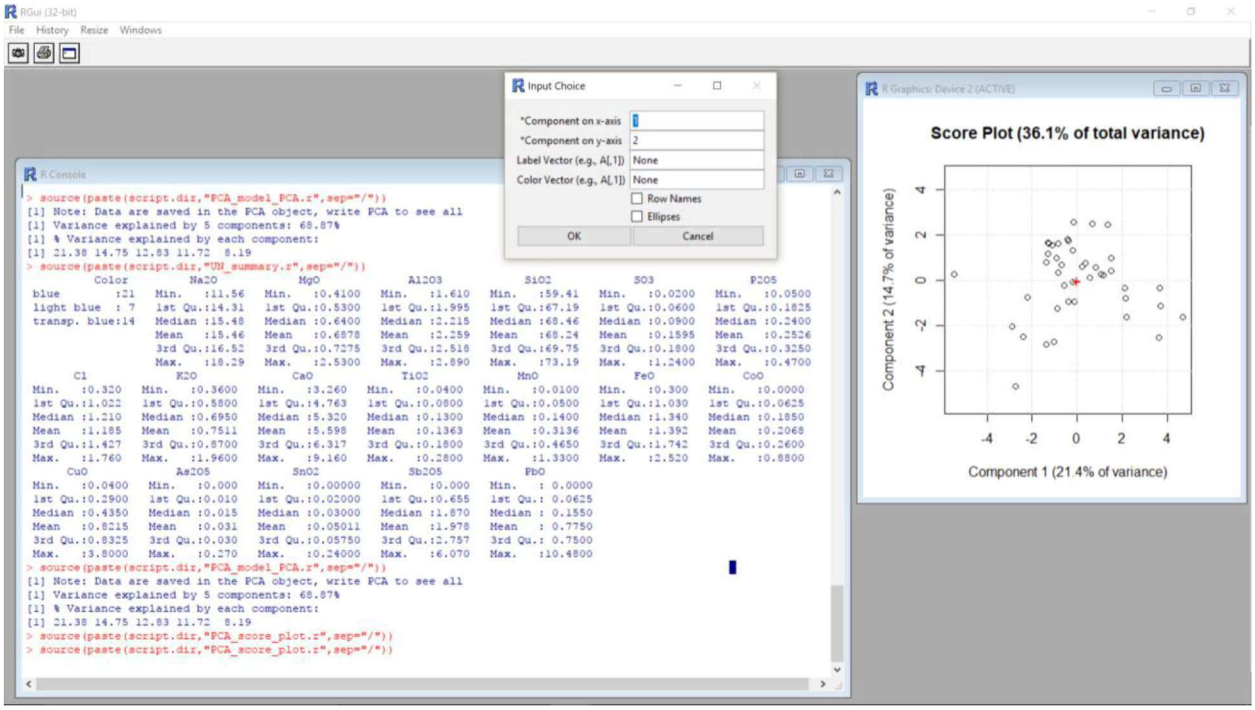

Fig. 6.4 – Workspace of the R-based software R-chemiometry for the statistical analysis of chemical data (univariate to multivariate).

[2] See (visited last time in October 2017): http://www.gruppochemiometria.it/index.php/software

Who, when he saw the first sand and ashes, by a casual intenseness of heat, melted into a metallic form, rugged with excrescences and crowded with impurities, who would have imagined that in this shapeless lump lay concealed so many conveniences of life, as would in time constitute a great part of the happiness of the world?

Samuel Johnson
(1750)

RESULTS AND DISCUSSION

7. Results

This chapter will present the results of the archaeometric investigations for what concerns the chemical, textural and mineralogical analysis and the image and data processing. The results will be organized in the following order: first, those related to the composition of the glassy matrix (silica source and flux composition) and followingly, those connected to glass coloring/ decoloring and opacifying processes.

7.1 Silica source

EPMA data (see table III in the appendix) show that all samples are silica and lead silica glasses with SiO_2 ranging from 38.87% to 73.19%. The use of sand as the main silica source in all the analyzed samples is testified by the high quantity of both Al_2O_3, ranging from 0.91% to 3.22% (average 2.21%,) and FeO, in the range of 0.24-2.70% (average 1.29%). FeO ≤ 0.4% is found especially in transparent, white and turquoise samples, suggesting that purified or purer sand was probably selected for this kind of glasses; in any case, the corresponding alumina is definitely high, from 1.81 to 2.39%, so the use of crushed quartzite or quartz-rich pebbles should be discarded.

Considering the plot FeO *vs* TiO_2, (fig. 7.1.1a), there is a clear positive trend that can be interpreted as a combined contribution from the heavy minerals typical of the Egyptian sands (Himly, 1951; Turner, 1956; El-Innawi, 1964; Samy, Abou El-Anwar, 2013; Ramadan, 2014). Moreover, the binary diagram TiO_2 *vs* Al_2O_3 highlights three well-defined compositional classes (fig. 7.1.1b), by associating the chemical composition of the glass to the mineralogy of the sands (Schibille *et alii*, 2016): the first, composed by 4 samples of various colors, has low alumina (0.91-1.02%) and low TiO_2 (0.05-0.12%), the second – comprising most of the samples – is characterized by Al_2O_3 in the order of 1.48%-3.06% and titanium between 0.02 and 0.31 wt%. The last one is restricted to a set of 4 red glasses and has very high TiO_2 (0.48-0.57%) and high Al_2O_3 (2.76-3.22%) values. All these data suggest multiple sand sources, with a preference from one specific area that seems associated with the majority of the analyzed samples.

From the textural point of view, SEM-EDS highlighted the presence of various crystalline inclusions related to unreacted relics of the original raw materials or impurities introduced during the glass-forming/ assembling in a sand-rich environment. In fact, silicates and Fe/ Fe-Ti/ Al oxides can be found within the glass, but are also frequent at the interface between layers of different colors thus suggesting in certain cases a possible sand contamination during the sintering process (fig. 7.1.2b). The mineralogical identification of the inclusions was possible by coupling EDS, EPMA and μ-Raman analyses.

The most common inclusion identified in the Tebtynis samples is quartz (μ-Raman data), which is present in all the main color classes – except colorless transparent glasses – in varying sizes (from a few μm up to 150 μm) and shapes, from rounded to angular.

Other widespread sand-related light minerals include epidotes, pyroxenes and feldspars (both alkali and plagioclase feldspars), such as the big oligoclase (EDS data: Na_2O = 8.3%, Al_2O_3 = 23.6%, SiO_2 = 63.3%; CaO = 4.8%) in Ty-P-FL-004-B (fig. 7.1.2f). It should be noted that potassium feldspars were also found in various samples (fig. 7.1.3c); this is consistent with the early suggestion from Parodi (1908), later followed by Turner (1956), that Egyptian glasses tend to contain higher potash than generally associated with the alkali flux.

Fe and especially Fe-Ti oxides (frequently in an ilmenite-type stoichiometry with traces of Mg or Mn) are also regularly present in all glass colors. Corundum was identified in six samples of dark blue, light blue, turquoise, yellowish-orange, dull red and sealing-wax red glass: the biggest occurrence (120÷150 μm with respect to an average of 10-20 μm) was found in Ty-S-TA-005-A and is characterized by inclusions of Ti-Fe/ Fe-oxides. The only zircon occurrence (EDS data: SiO_2 = 70.2%, Hf_2O_3 = 2.6%, ZrO_2 = 27.2%) was detected in the brown glass Ty-S-MR-502-M and shows rounded edges, related to a long weathering processes. A selection of the Raman spectra of the most common inclusions in the Tebtynis samples is presented in figures 7.1.3-.4-.5.

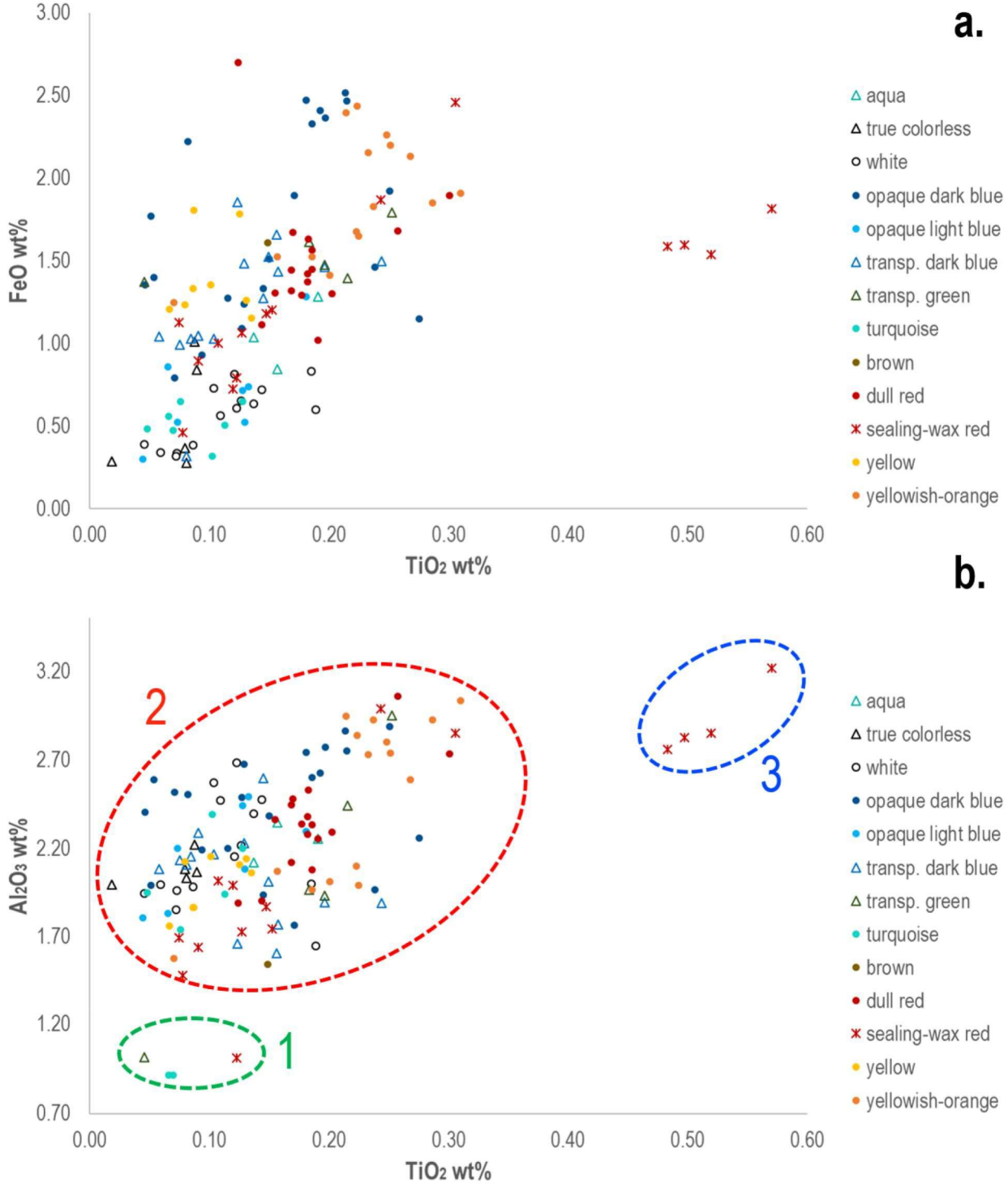

Fig. 7.1.1 – a-b) TiO_2 vs FeO and TiO_2 vs Al_2O_3 contents in the glass phase of the analyzed samples from Tebtynis. The three compositional groups in TiO_2 vs Al_2O_3 are highlighted with dotted lines (symbols: empty triangles = transparent glasses; colored dots and asterisks = opaque glasses; the color of the symbols is related to the color seen during macroscopic observations).

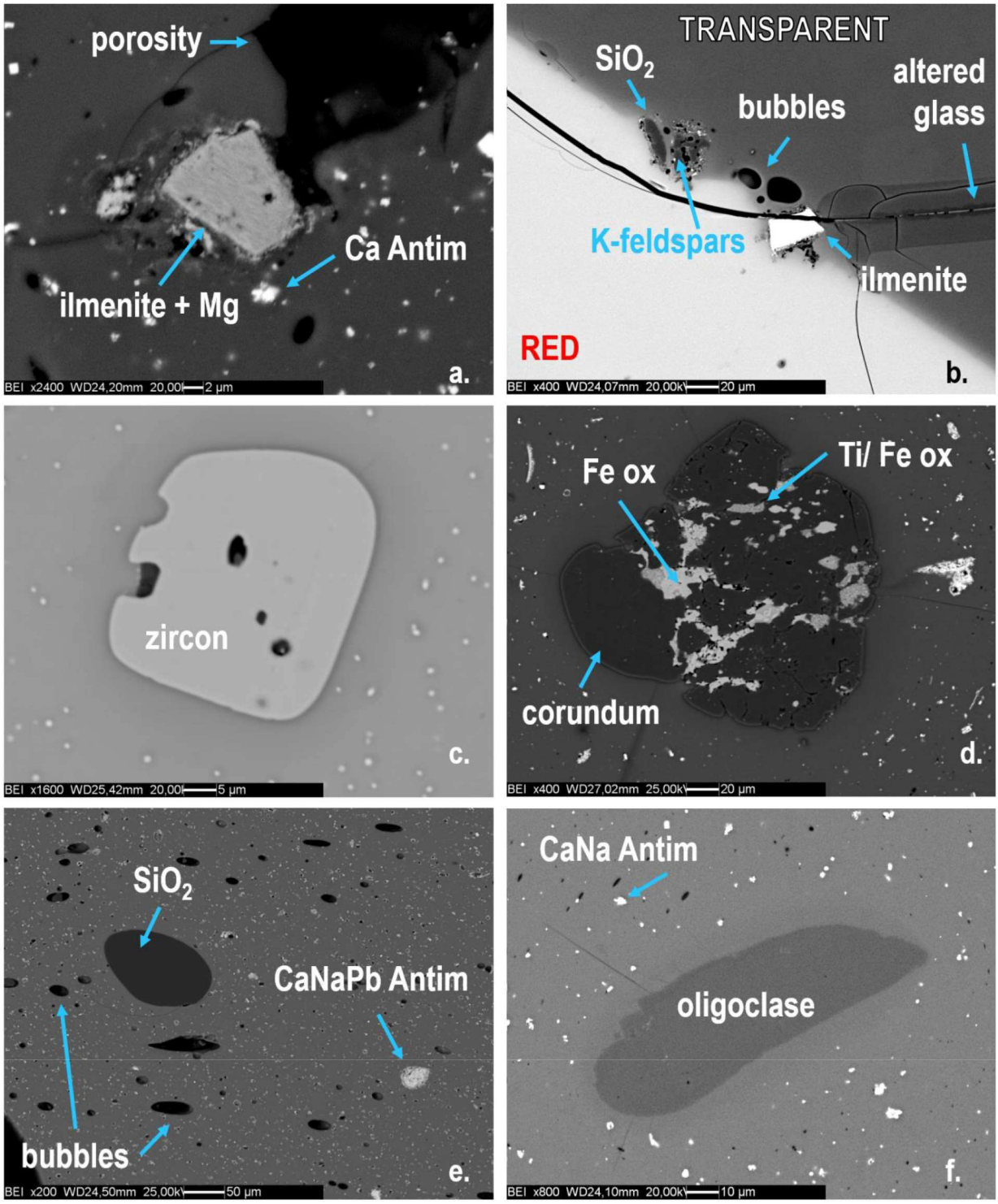

Fig. 7.1.2 – SEM-BSE images showing a selection of the sand-related inclusions found in Tebtynis samples: a) ilmenite inclusion in the white sample Ty-P-FL-004-Bi; b) ilmenite, SiO_2 and k-feldspar inclusions in the interface between red and transparent glass of sample Ty-S-TR-501; c) zircon in the brown sample Ty-S-MR-502; d) Corundum with Ti/ Fe-oxides inclusions in the light blue sample Ty-S-TA-005; e) big, rounded SiO_2 grain in sample Ty-M-A-006; f) K-feldspar with stoichiometry close to oligoclase (EDS data) in the dark blue sample Ty-P-FL-004-B.

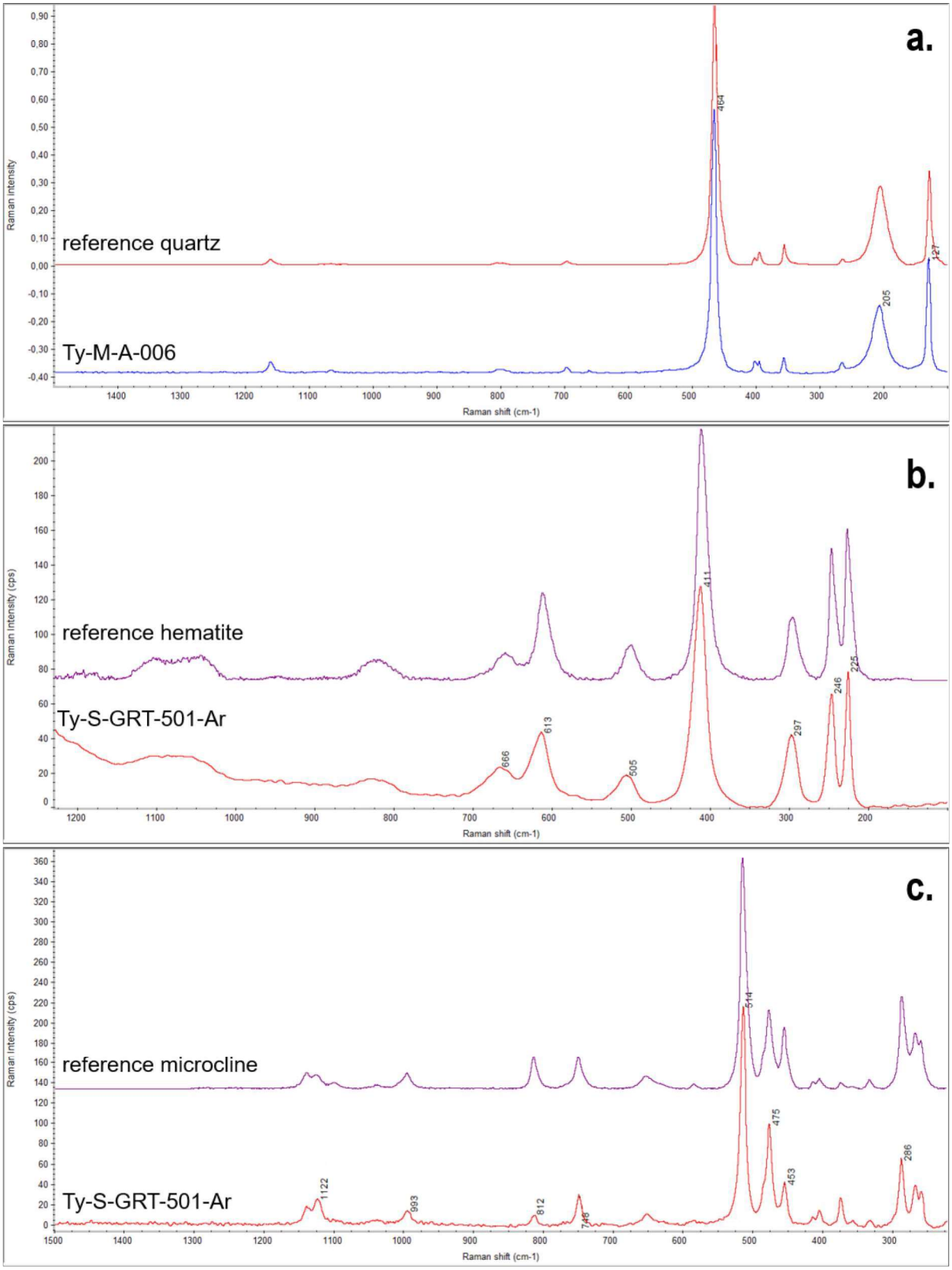

Fig. 7.1.3 – Raman spectra with standard reference spectra (RRUFF web-database) of: a) quartz crystal in the light blue sample Ty-M-A-006; b) hematite crystal in the yellowish-orange sample Ty-S-GRT-501-Ar; c) microcline crystal in the yellowish-orange sample Ty-S-GRT-501-Ar.

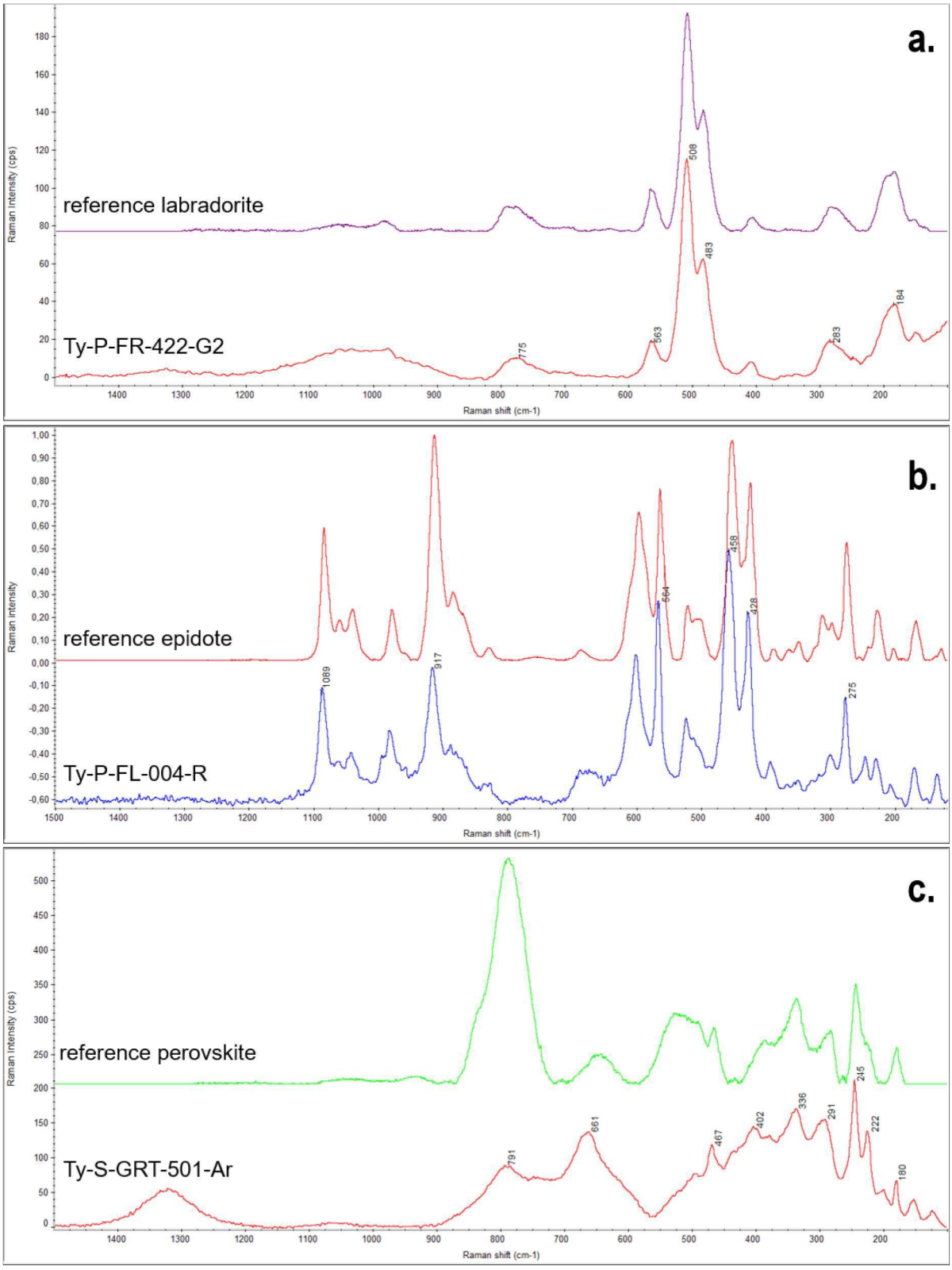

Fig. 7.1.4 – Raman spectra with standard reference spectra (RRUFF web-database) of: a) labradorite crystal in the yellow sample Ty-P-FR-422-G2; b) epidote crystal in the dull red sample Ty-P-FL-004-R; c) Ca-Ti oxide crystal (probably perovskite, as confirmed by EDS data) in the yellowish-orange sample Ty-S-GRT-501-Ar.

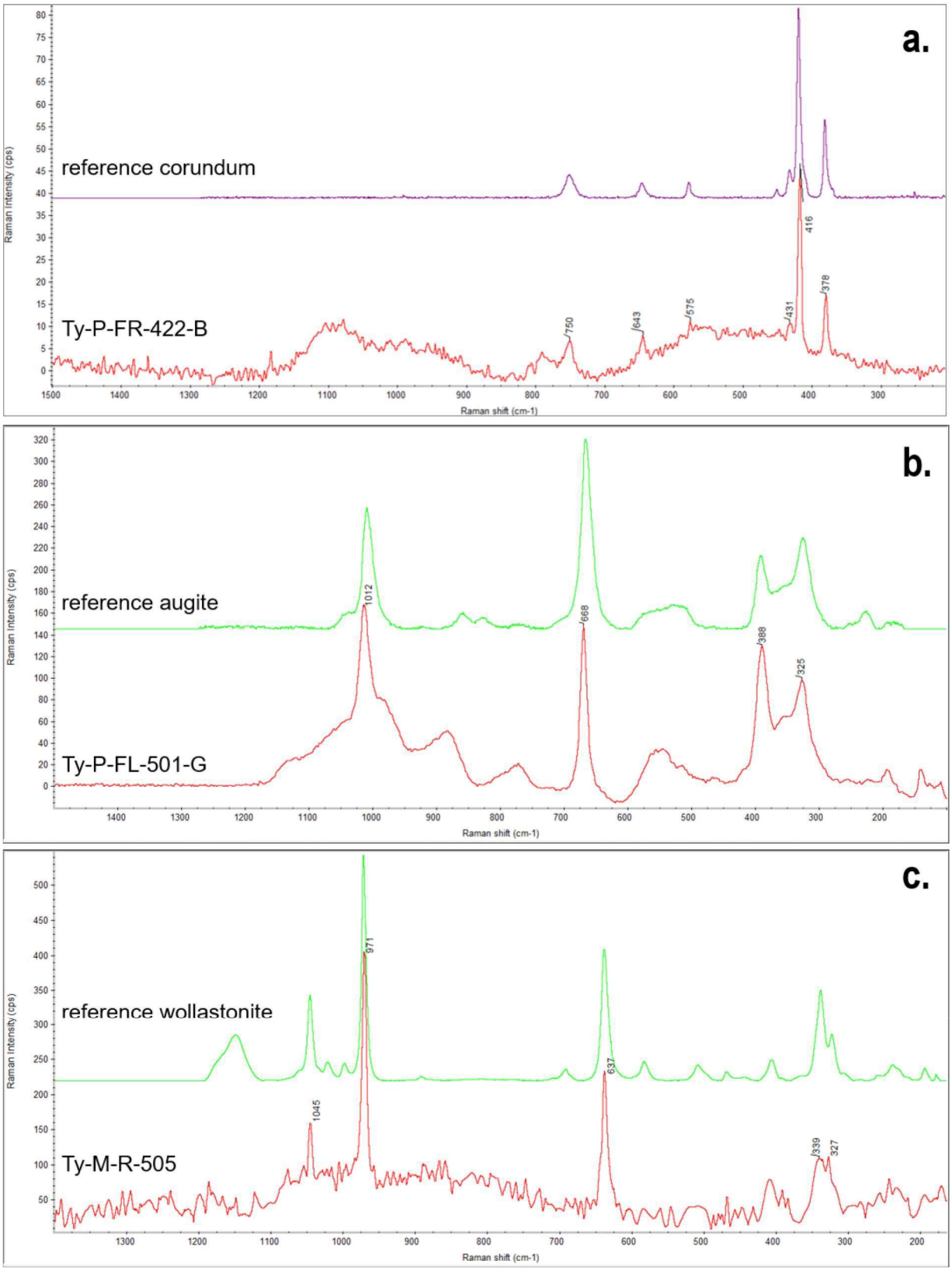

Fig. 7.1.5 – Raman spectra with standard reference spectra (RRUFF web-database) of: a) corundum crystal in the dark blue sample Ty-P-FR-422-B; b) augite crystal in the yellow sample Ty-FL-501-G; c) wollastonite crystal in the dull red sample Ty-M-R-505;

7.2 Flux composition

The alkali content is extremely variable: Na_2O ranges from 0.13% to 18.29%, K_2O from 0.29% to 3.00%, CaO from 0.73% to 9.99% and MgO from 0.20% to 5.15%. The low Na_2O values in seven samples (Ty-P-CR-421-Bi, Ty-S-BTW-004-W, Ty-S-GB-413-BT, Ty-P-R-419-G, Ty-P-A-402-G, Ty-M-G-504, Ty-Pn-B-001) can be attributed to a heavy (Na_2O from 0.13% to 1.07%) or moderate (Na_2O from 5.93% to 7.03%) weathering of the glass, as supported by SEM-BSE images. Lead, which can also act as a fluxing agent, is present in different concentrations, from as low as under detection limit to as high as 40.11 wt%.

In general terms, this wide compositional range shows that different glass recipes were used. The plot K_2O *vs* MgO, classically used to discriminate the type of alkali used, shows that most of the samples lay in the compositional range of the classic Low Magnesium Glasses (LMG), produced using natron as fluxing agent (Henderson, 1985; Shortland *et alii*, 2006; Jackson *et alii*, 2016). In fact, K_2O ranges from 0.24% to 1.20%, MgO from 0.24% to 1.48% and Na_2O from 8.41% to 18.29%, excluding altered samples. Minor elements, such as P, S and Cl do also agree with the values typical of this compositional class.

Part of the glasses from Tebtynis were instead produced with the typical recipe of High Magnesium Glasses (HMG), obtained using soda-rich plant ash as flux (Henderson 1988, 2000; Tite *et alii*, 2003). This second class presents higher levels of both K_2O (1.39-3.00%), MgO (2.30-4.61%) and comparable Na_2O (12.42-17.19%). Most of the HMG glasses are dull red, but a few transparent green, one transparent blue and two transparent aqua samples are also present.

The composition of various samples, especially yellowish-orange and (in minor extent) red, falls between plant ash and natron glass and is characterized by low K_2O, in the range 0.71% to 1.28%, MgO comprised between 1.56% and 2.06% and Na_2O from 13.59% to 17.19%. A uniform group of five white glasses (Ty-P-FR-422-Bi, Ty-S-BiBR-404-Bi, Ty-P-FL-004-Bi, Ty-S-BiBR-507-Bi, Ty-S-423a-Bi) clusters for its high MgO (4.98-5.16%) content, associated with a very low K_2O, in the order of 0.52-0.69%. Values

of major, minor and trace elements are so similar that they may have been produced with very similar raw materials proportions.

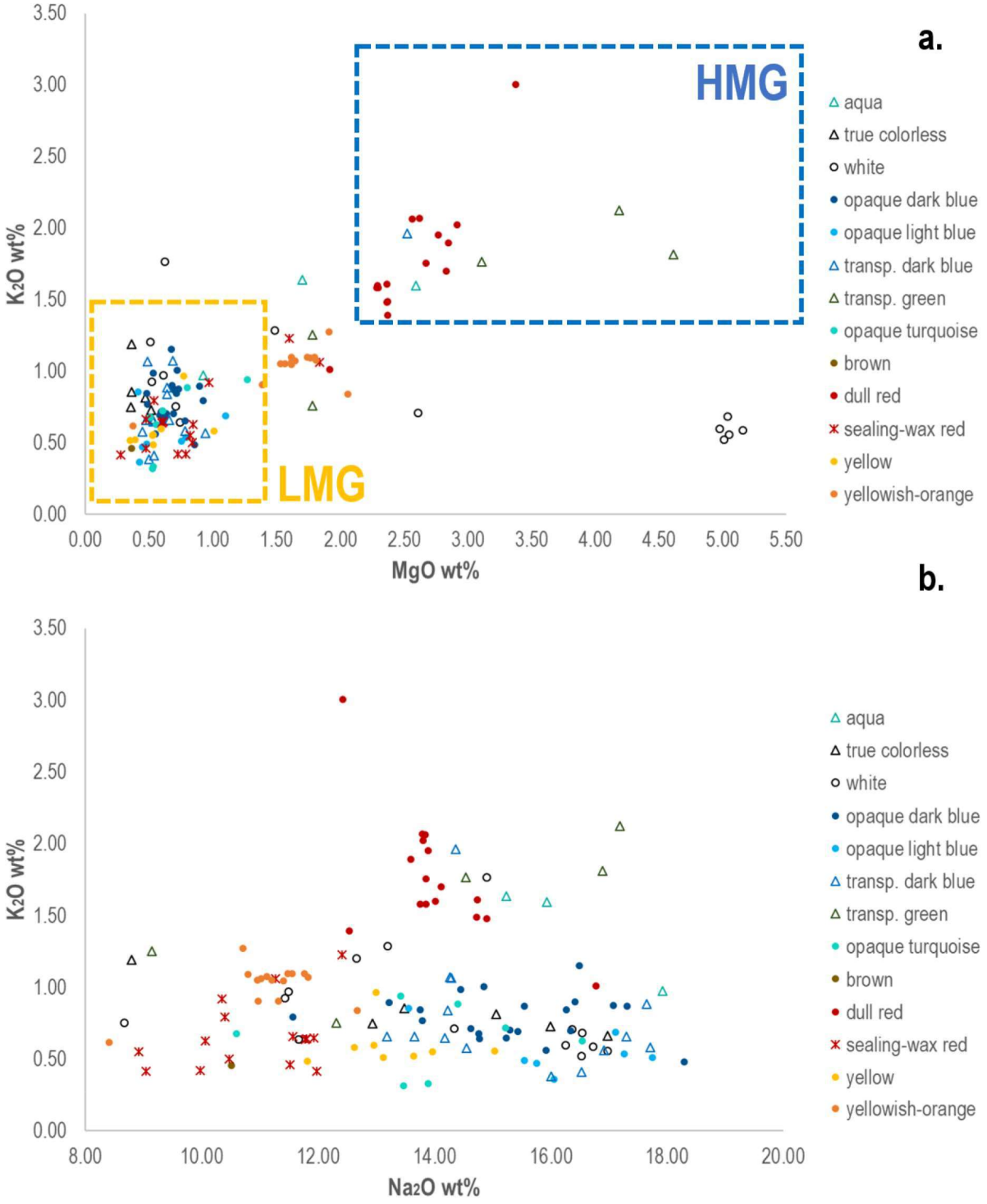

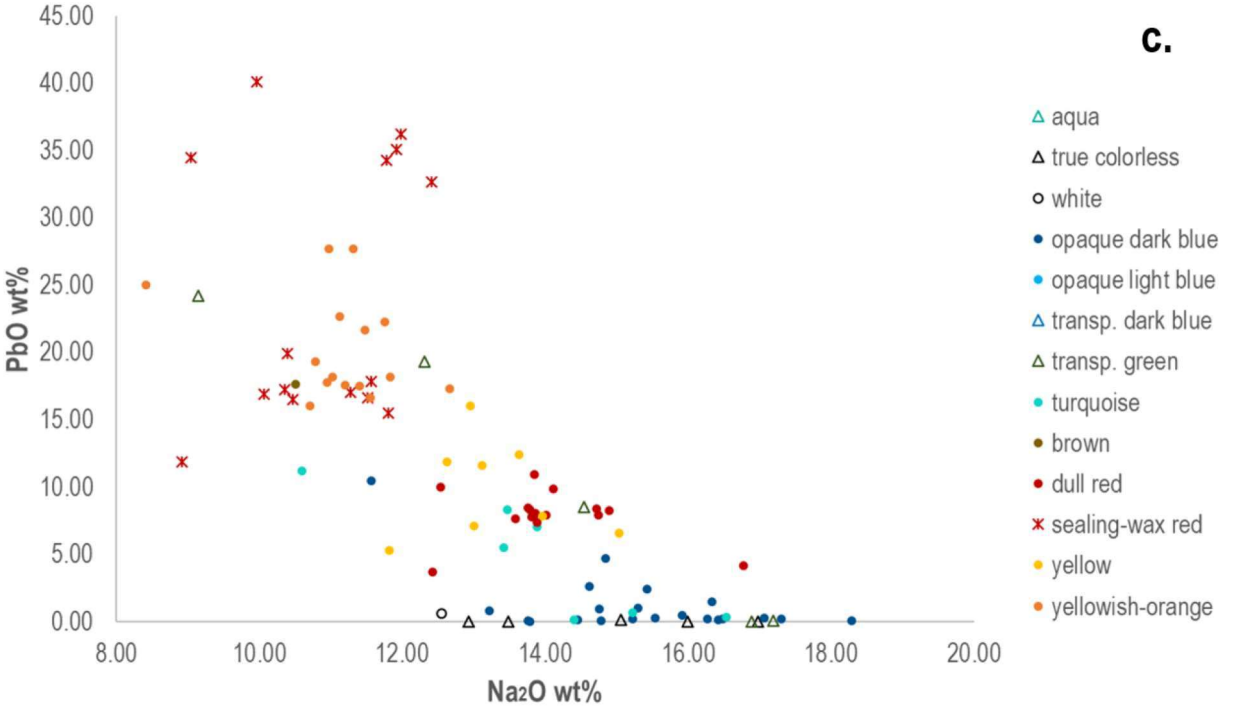

Fig. 7.2.1 – a-b) K_2O vs MgO and K_2O vs Na_2O contents of the glass phase in the analyzed samples from Tebtynis (excluding weathered glasses). Compositional fields of HMG and LMG glasses (dotted lines) refer to Henderson, 2013. c) Na_2O vs PbO content of the glass phase in the analyzed samples from Tebtynis (symbols: empty triangles = transparent glasses; colored dots and asterisks = opaque glasses; the colors of the symbols are related to the colors observed during macroscopic observations).

The K_2O/ Na_2O diagram shows that despite the increasing amounts of silica (anticorrelated with the lead content) there are only slight variations in the potash content of LMG glasses, which is probably related to the sand source. On the contrary, even with equal amounts of SiO_2, HMG glasses show higher K_2O contents, associated with the use of a plant ash flux.

Considering the lead oxide content, it is possible to identify three different compositional groups, according to the classification proposed by Vandini and colleagues (2006) for Byzantine glass. This classification, which is often employed even for samples of earlier dating, considers the ratio between PbO and the total value of Na_2O plus SiO_2 plus CaO. A ratio of less than 0.01 accounts for soda-lime glasses, between 0.01 and 0.1 for soda-lime-lead glasses and if higher than 0.1 for leaded-glasses. Following this method, the Tebtynis collection comprises: 55 soda-lime samples, 35 soda-lime-lead

samples and 50 leaded-glass samples. All Pb-based categories show at least one or more HMG samples, even if LMG glasses are far more common in the dataset. Lead oxide is, thus, not specifically related to one of the two main recipes used in the production of the considered glasses, but possibly a secondary addition related to the coloring process. Despite the lack of a systematic association between color and lead content, the Na_2O vs PbO plot clearly shows that blue and white samples tend to have low, or even absent, PbO, while all sealing-wax red, brown and yellowish-orange samples are characterized by very high content of PbO, between 15.50% and 44.11%, with one single outlier at 11.91%.

7.3. Coloring, decoloring and opacifying agents

7.3.1 *Colorless glasses*

Two color categories are included in this class: true colorless glasses (6) and naturally colored glasses (3), which were labeled as "aqua" according to the classification proposed by Brill (1988) for the Jalame fragments. Colorless samples from Tebtynis show very low values of intentionally added chromophores, such as CuO (from under detection limit to 0.22%), CoO (from under detection limit to 0.04%), while FeO is very variable ranging from 0.24% to 1.28%, but is systematically higher in aqua samples (0.84-1.28 wt %).

The K_2O *vs* MgO and the Sb_2O_5 *vs* MnO plots show two well defined compositional classes (fig. 7.1.2). In the HMG class, MnO ranges from 0.83% to 1.31%, with low Sb_2O_5 between 0.11% and 0.20%.

On the contrary, LMG glasses have higher Sb_2O_5 (0.51-0.81%) and much lower MnO, from under detection limit to 0.03%, except in the aqua sample, where it reaches values of 0.16% and should thus be more properly defined as Sb-Mn decolored, according to Gliozzo (2016).

From the textural point of view, all the samples are essentially homogeneous with rare bubbles up to 100 μm in size (fig. 7.3.3).

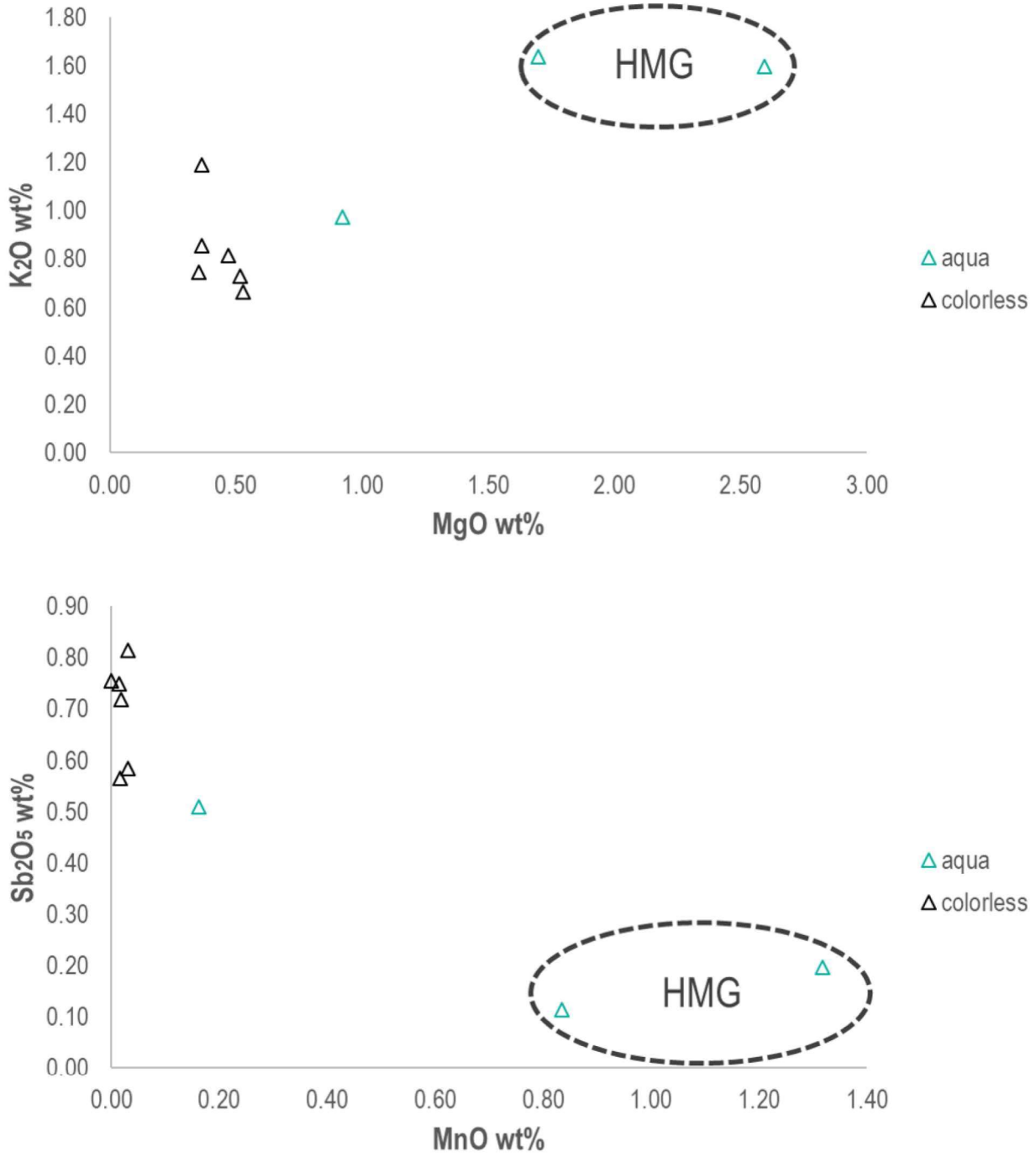

Fig. 7.3.2 – K_2O vs MgO and Sb_2O_5 vs MnO contents of the glass phase in the colorless samples from Tebtynis. Compositional fields of HMG glasses are highlighted with a dotted line (symbols: turquoise triangle: aqua glasses; black triangles = true colorless glasses).

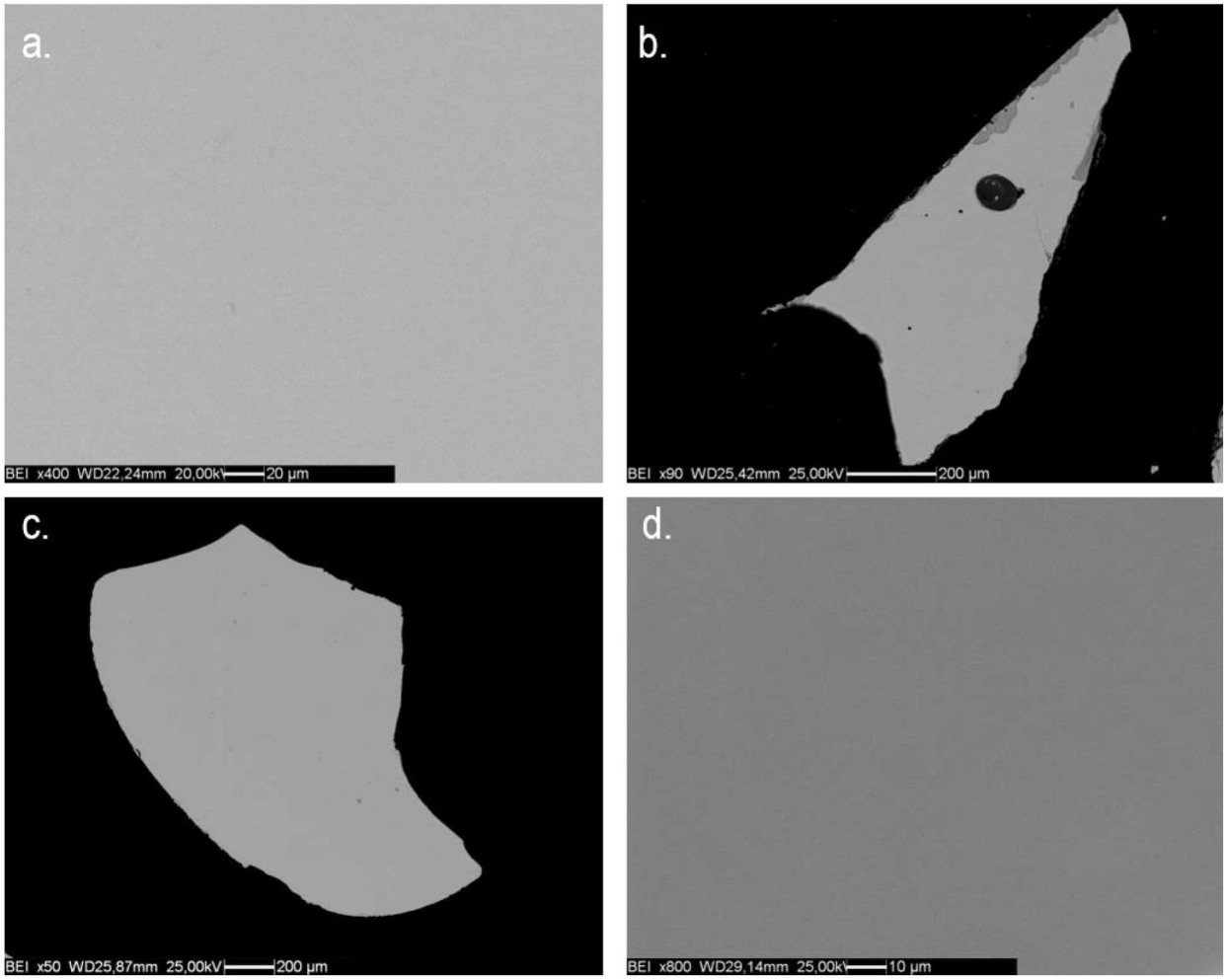

Fig. 7.3.3 – SEM-BSE images of the homogeneous texture in four colorless glasses from Tebtynis: a) Ty-M-T-503; b) Ty-M-T-503a; c) Ty-Pn-T-001; d) Ty-S-423a.

7.3.2 *White glasses*

In the Tebtynis collection, opaque white glass was only found in stratified and mosaic compositions and never on its own as main constituent of single inlays or bars. Out of the 14 analyzed samples, one comes from a figured inlay (Ty-I-BBi-613-Bi), 5 from stratified samples (Ty-S-423a-Bi, Ty-S-BBi-004-Bi, Ty-S-BiBR-404-Bi, Ty-S-BiBR-507-Bi, Ty-S-BiR-507-Bi, Ty-S-BTW-004-Bi) and all others (8) from complex mosaic glasses with different motives: two arches (Ty-P-A-418-Bi and Ty-P-A-419-Bi), two lotus flowers (Ty-P-FL-004-Bi and Ty-P-FL-501-Bi), one rosette (Ty-P-FR-422-Bi), one star (Ty-P-St-415-Bi) and one triangles pattern (Ty-P-T-417-Bi).

Considering the K_2O *vs* MgO content, two main groups appear quite clearly: the first is a uniform high MgO (from 4.98% to 5.16%), low K_2O (0.52%-0.60%) group (Ty-S-BiBR-404-Bi, Ty-P-FL-004-Bi, Ty-P-FR-422-Bi, Ty-S-423a-Bi, Ty-S-BiBR-507-Bi), already mentioned in the alkali source section (§ 7.2). Ty-P-A-418-Bi has lower values of MgO (2.61%) and slightly higher K_2O (0.70%); on the contrary, Ty-P-T-417-Bi has high K_2O (1.77%) and low MgO (0.62%). Their peculiar compositions will be better examined in the discussion of the data. All other samples are classic LMG glasses, with a sub-set (Ty-I-BBi-613-Bi, Ty-P-A-419-Bi and Ty-S-BTW-004-Bi) characterized by high lead (7.07-12.55 wt%) and proportionally higher levels of tin (0.13-0.21 wt%) and manganese (0.44-1.46 wt%) content with respect to the non-leaded LMG glasses.

As shown by the CaO *vs* Sb_2O_5 plot, all samples have significant levels of both CaO and Sb_2O_5, in the range of 3.48-7.98% and 2.86-6.65% respectively. These values are consistent with the textural and chemical analyses, which revealed a diffuse presence of Ca antimoniates dispersed in the glassy matrix as opacifying agents. Synthetic crystals of euhedral brizziite ($NaSbO_3$) were also found in the sample Ty-S-BiR-507, as confirmed by the μ-Raman spectra (fig. 7.3.6b). WDS data on the biggest crystal (fig. 7.3.5a) returned a Na_2O value of 18.5% with Sb_2O_5 at 82.66% (and traces of SnO_2 e As_2O_5), which is compatible with the microprobe analysis performed on the natural brizziite samples at the time of its discovery (Na_2O = 15.98%; Sb_2O_5 = 83.28%; see Olmi, Sabelli, 1994). Unfortunately, the glassy matrix of this sample is slightly weathered, and it is not possible to establish a connection with the exact original alkali composition to understand what favored the precipitation of this specific phase in contrast to the classic calcium antimoniate compounds, since CaO in the glassy matrix is sufficiently high (6.14%).

The stoichiometric range of the Ca antimoniates analyzed by WDS lays in the range of CaO from 13.59% to 23.96% and Sb_2O_5 from 48.79% to 82.90%; various inclusions show partial substitutions of Ca with Na. One exception is represented by a crystal in Ty-I-BBi-616-Bi that contains lead in the order of 2.82 wt%, partially substituting CaO. It should also be noted that all Na, Ca and Na-Ca antimoniates analyzed by EPMA contain varying amounts of SnO_2 (from 0.19% to 0.73%) and As_2O_5 (from 0.18% to 0.83%), significantly exceeding those registered in the relative glassy matrix.

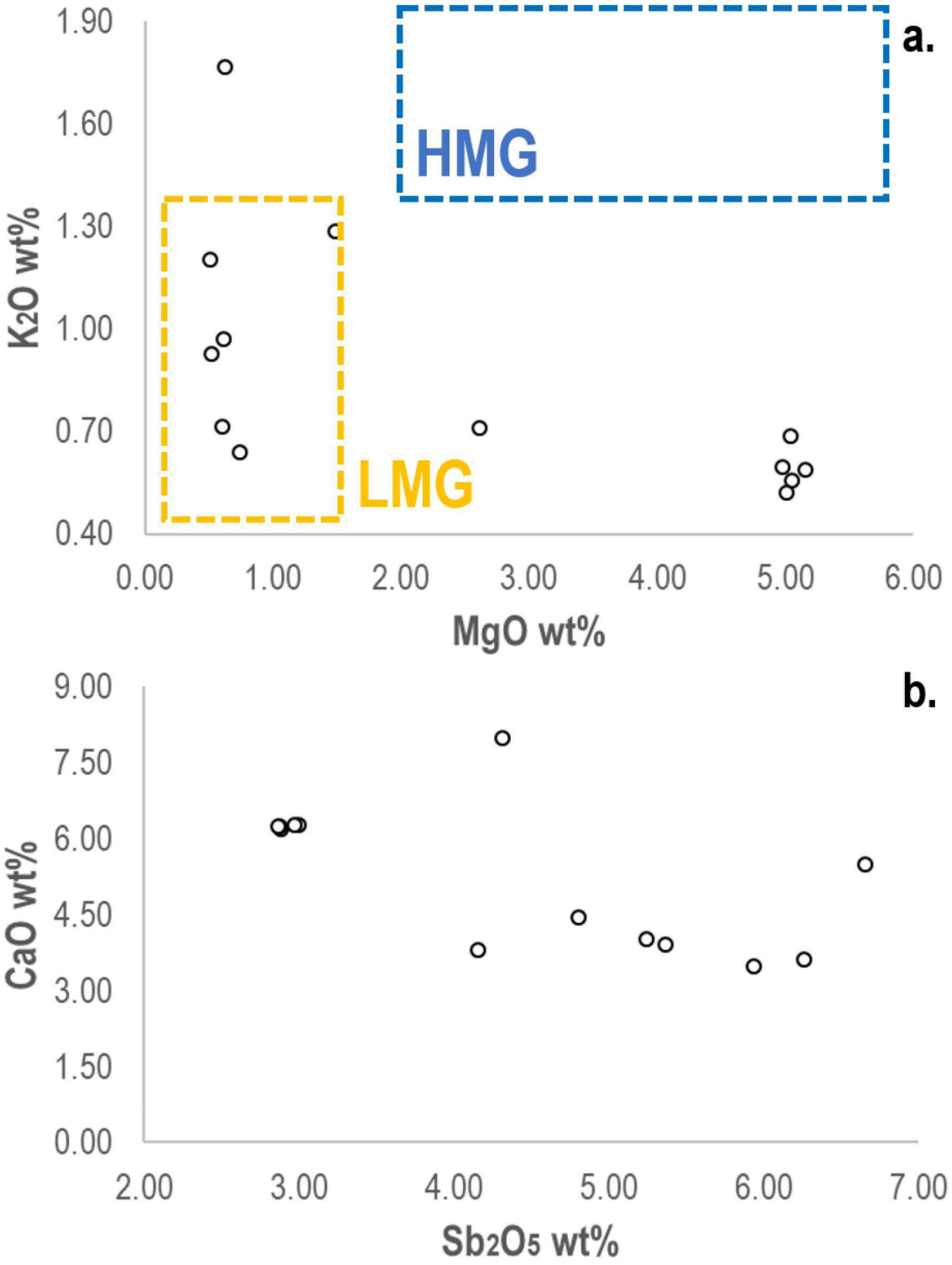

Fig. 7.3.4 – a-b) K_2O vs MgO and Sb_2O_5 vs CaO contents of the glass phase in the white samples from Tebtynis. Compositional fields of HMG and LMG glasses (dotted lines) refer to Henderson, 2013.

In the white samples, it was possible to recognize three main types of texture (fig. 7.3.5a-f): Ty-P-FL-501-Bi and Ty-P-A-419-Bi show a homogeneous dispersion of small hexagonal and rectangular crystals (size of 5 μm or less), often formed around bubbles (texture type I). Texture characterized by feathery- and rosary-shaped anhedral inclusions with very variable dimensions ranging from 100 μm to nanometric size is defined as texture type II. This kind of inclusions have often reacted edges partially dissolved into the glassy matrix and may also produce a sort of flour-like effect with thinly dispersed grains and uneven agglomerates. A mix of the previous two typologies, with partially dissolved rosary-shaped aggregates associated with rare euhedral crystals of micrometric size, alone or in small, isolated groups characterizes texture type III, as identified in Ty-S-BiR-507-Bi or Ty-P-CR-421-Bi.

Calcium antimoniates exist in two spatial configurations, corresponding to different stoichiometric formulae, $Ca_2Sb_2O_7$ (orthorhombic structure) and $CaSb_2O_6$ (hexagonal structure). Considering that the WDS analyses showed frequent substitution of Ca with Na (and rarely Pb, only in leaded glasses), it was possible to distinguish the two forms of antimoniates using the ratio between Sb_2O_5 and CaO + PbO + Na_2O in the crystalline inclusions. Looking at figure 7.3.8, the analyzed antimoniates can be divided in two well defined groups: the first is characterized by a ratio comprised between 4.97 and 6.02 and corresponds to the hexagonal form, while the second has values ranging from 2.46 to 2.98 and reflects the composition of the orthorhombic crystals, with double CaO + PbO + Na_2O content. This chemical-based distinction was also confirmed by the μ-Raman spectra of various sample inclusions of both typologies (figg. 7.3.6-7.3.7).

However, Raman data showed that $CaSb_2O_6$ and $Ca_2Sb_2O_7$ are not the only Ca-antimoniates present in the white glasses from Tebtynis: sample Ty-P-CR-421-Bi has both euhedral and rosary-shaped crystals totally similar to the classic morphologies and sizes of $CaSb_2O_6$ and $Ca_2Sb_2O_7$ phases, which returned the spectrum of the mineral romeite, i.e. $(Ca, Mn, Fe, Na)_2(Sb, Ti)_2O_6(OH, F, O)$. Moreover, an aggregate of brizziite and romeite was found in sample Ty-S-BiR-507-Bi, while an aggregate of romeite and $Ca_2Sb_2O_7$ was identified in sample Ty-P-FR-422-Bi (fig. 7.3.8c).

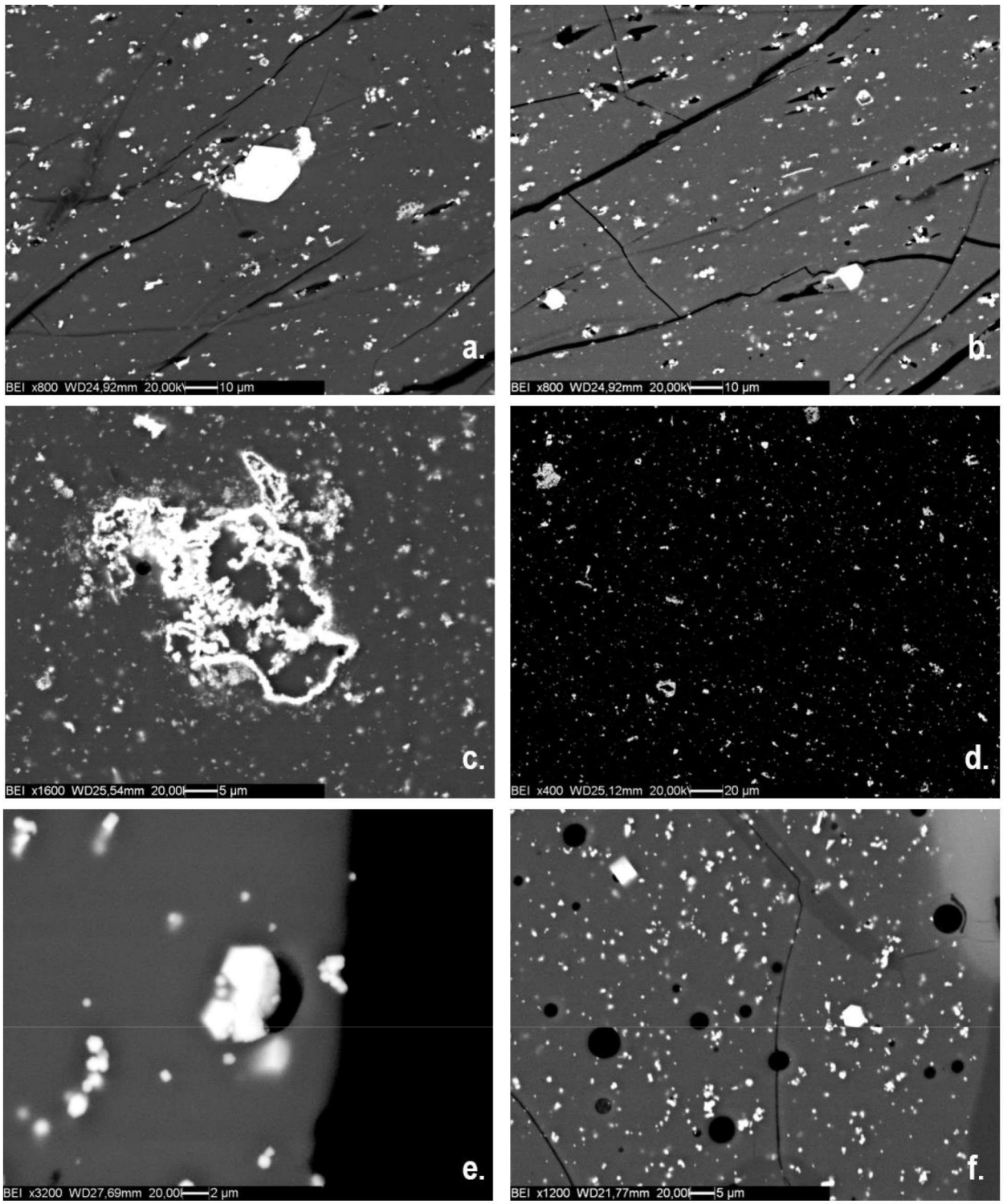

Fig. 7.3.5 – SEM-BSE images of the opacifying phases in some of the white glasses from Tebtynis: a-b) euhedral brizziite crystals in sample Ty-S-BiR-507-Bi; c-d) example of finely dispersed, anhedral Ca-antimoniates respectively found in samples Ty-P-A-418-Bi and Ty-S-BiBR-404-Bi; e-f) example of euhedral Ca-antimoniates respectively found in samples Ty-P-A-419-Bi and Ty-P-FL-501-Bi.

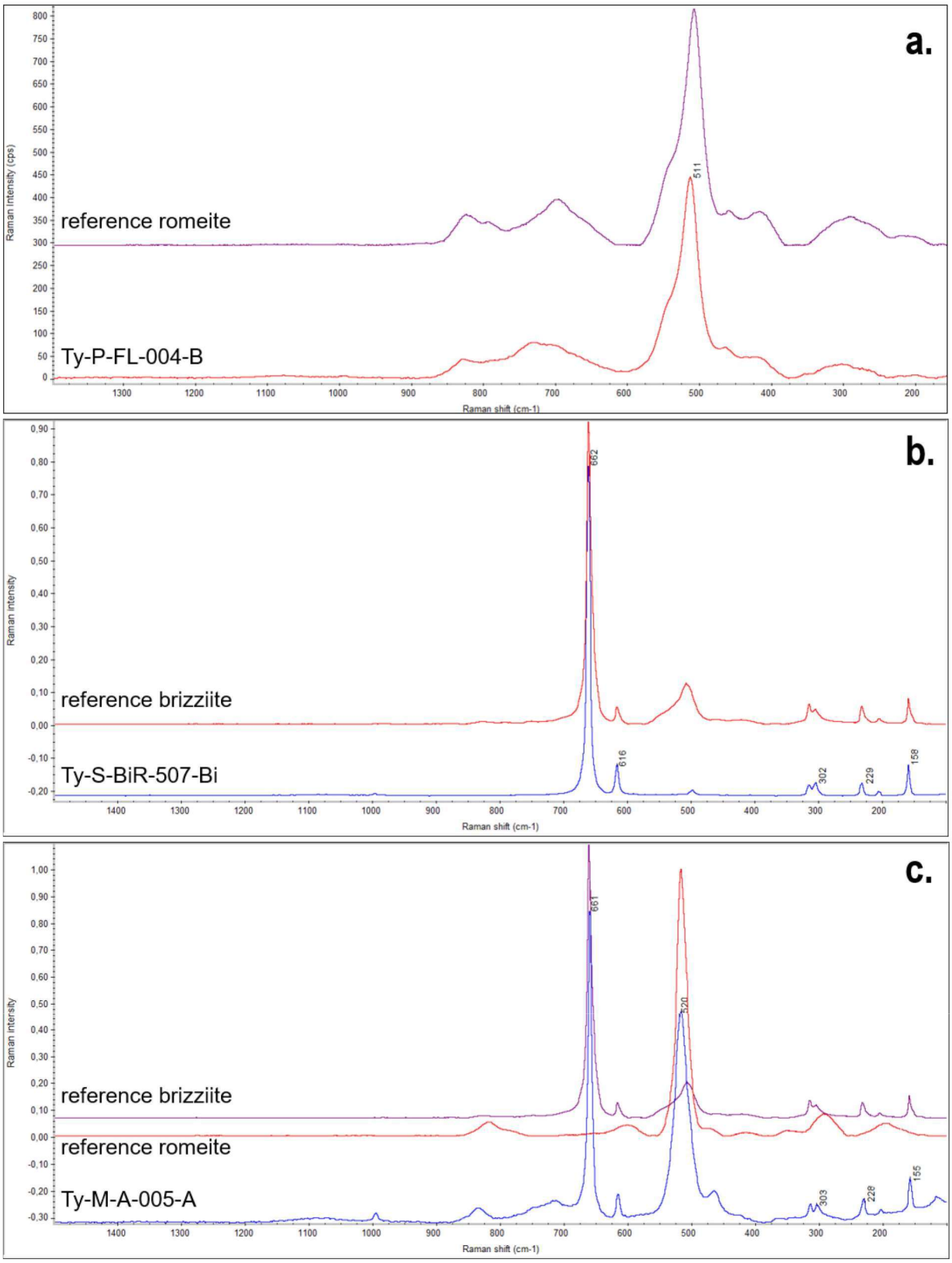

Fig. 7.3.6 – Raman spectra with standard reference spectra (RRUFF web-database) of: a) romeite crystal in the dark blue sample Ty-P-FL-004-B; b) brizziite crystal in the white sample Ty-S-BiR-507-Bi; c) a mix of romeite and briziite in the light blue sample Ty-M-A-005.

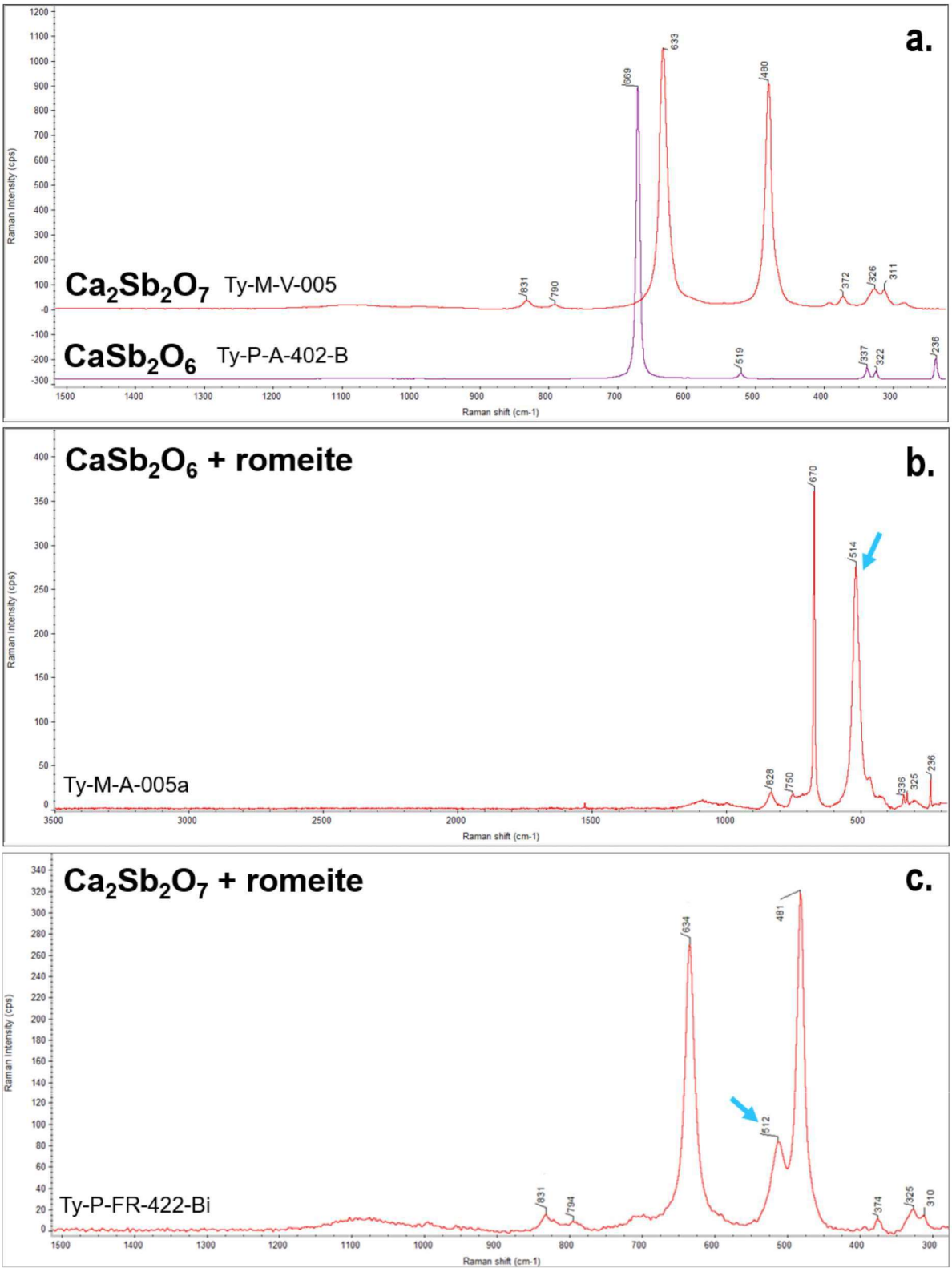

Fig. 7.3.7 – Raman spectra of Ca-Antimoniates: a) pure phases of $Ca_2Sb_2O_7$ (orthorhombic) in the turquoise sample Ty-M-V-005 and $CaSb_2O_6$ (hexagonal) in the dark blue sample Ty-P-A-402-B; b) mix of $CaSb_2O_6$ and romeite (see peak at ca. 512-514 cm^{-1}) in the light blue sample Ty-M-A-005a; c) mix of $Ca_2Sb_2O_7$ and romeite (see peak at ca. 512-514 cm^{-1}) in the white sample Ty-P-FR-422-Bi.

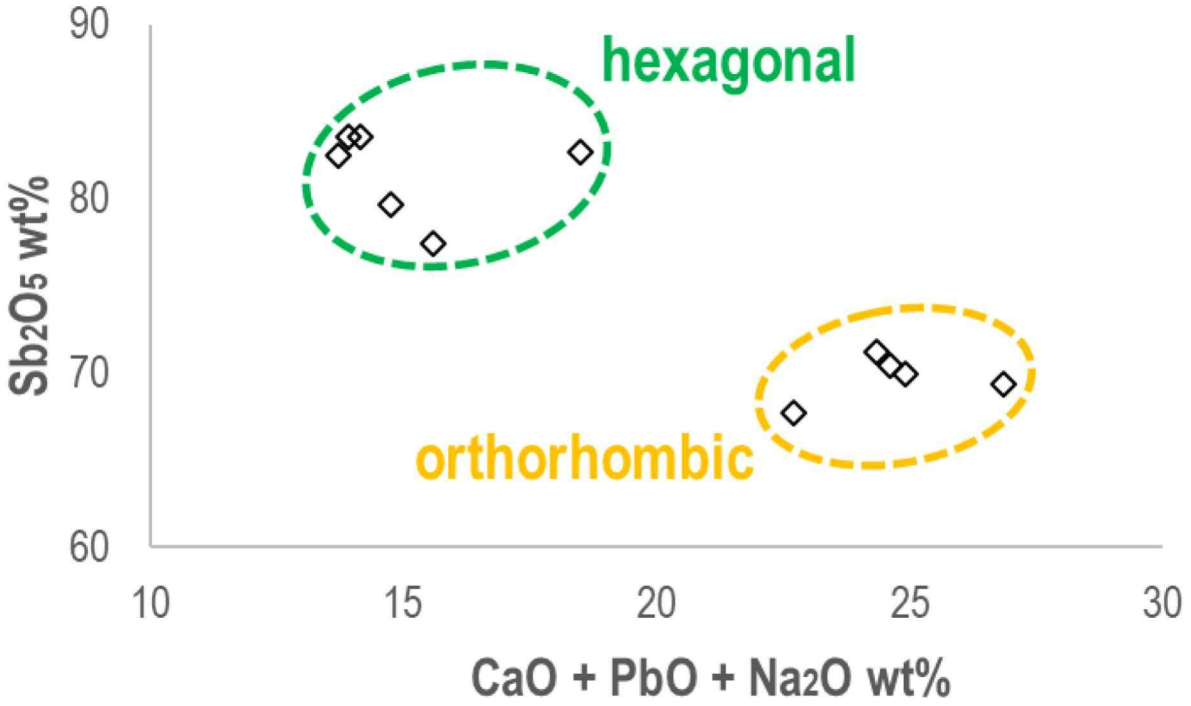

Fig. 7.3.8 – Biplot of Sb_2O_5 vs CaO + PbO + Na_2O ratio of the Ca- and Ca-Na antimoniate inclusions in the white glasses from Tebtynis, which was used to discriminate between the hexagonal and the orthorhombic forms using WDS chemical data.

7.3.3 *Blue glasses*

All analyzed blue samples, regardless of their shade and/ or opacity, are colored with cobalt, copper or a combination of the two chromophores. Observing the Sb_2O_5 *vs* CuO and the CuO *vs* CoO binary plots (fig. 7.3.9) of all the considered dark blue and light blue samples, three compositional groups can be clearly identified. Group 1 comprises 7 LMG glasses characterized by very low levels of CoO (from under detection limit to 0.04%), Sb_2O_5 between 1.15% and 1.99% and high amounts of copper (2.24-3.80 wt%). Group 1 perfectly corresponds to the opaque light blue class, as defined by macroscopic observations. The second group is represented by 10 LMG and 1 HMG (Cu)Co-colored glasses[1] (CoO between 0.04% and 0.55%), low CuO (from under detection limit to 0.90%) and Sb_2O_5 never exciding 0.88%. Group 2 matches fairly well with the "transparent dark

[1] The main chemical zonings of heterogeneous glasses were also characterized by WDS; this explains the discrepancy between the number of glasses of each group or color-class cited in the text and the total number of point analyses in the diagrams of the various color classes.

blue" color-class, except for sample Ty-P-A-419-BT which has significantly higher antimony levels (2.77 wt%) and was thus classified in the last sample-set. Group 3 is constituted by 22 LMG glasses that show Sb_2O_5 in the order of 1.73-6.07%, traces or low amounts of CuO (0.06 to 1.21%) and CoO ranging from 0.06% to 0.88%, but mainly around 0.2-0.4%. This group fits properly with the opaque dark blue class observed before sampling and can be interpreted as the (Cu)Co-colored group 2, with the addition of antimony-based opacifiers.

As for the texture, group 2 (plus sample Ty-P-A-419-BT) is characterized by no intentional opacifying agent. The only exception is Ty-P-A-419-BT itself, which presents very few, localized, micrometric and sub-micrometric calcium antimoniate inclusions (EDS data) possibly precipitated from the Ca-Sb rich glassy matrix (fig. 7.3.11e-f).

The sand-relics in transparent blue glasses comprise only one small crystal of iron and titanium oxide (EDS data), most probably ilmenite, in Ty-M-B-004 (fig. 7.3.11c). Bubbles, elongated or circular, are not very frequent and usually small, with exceptionally big occurrences reaching up to 100-120 μm in maximum diameter.

From the chemical point of view, the texture is generally very uniform, but Ty-S-BBi-004-BT shows a peculiar zoning in BSE which can be interpreted as the result of an imperfect mixing (fig. 7.3.11b): in fact, the glass shows three different gray levels that are associated with variable concentrations of CuO, CoO, FeO and MnO (WDS data). Dark gray glass has lower CuO (0.15%), CoO (0.10%) and MnO (0.73%) and higher FeO (1.85%). On the contrary, light gray glass has CuO at 0.90%, CoO at 0.55%, MnO at 1.33% and FeO at 1.44%. The intermediate gray level shows an average composition, probably related to a better mixing of the chromophores into the glass batch: CuO is 0.37%, CoO 0.26%, MnO 0.91% and FeO 1.66%.

Just as in the case of the white glasses, the micro-structure of opaque light blue and dark blue glasses is characterized by the presence of both Na and Ca antimoniates (sometimes in solid solution), with one single analyzed case of Pb-doped Ca antimoniate in Ty-M-B-002. By applying the same chemical ratio proposed above (§ 7.3.2), it was possible to establish that hexagonal $CaSb_2O_6$ and orthorhombic $Ca_2Sb_2O_7$ are both present in Tebtynis samples (fig. 7.3.10), as also seen from the μ-Raman data (fig. 7.3.7). irrespectively of the macroscopic color or the CuO/ CoO rate in the glassy matrix.

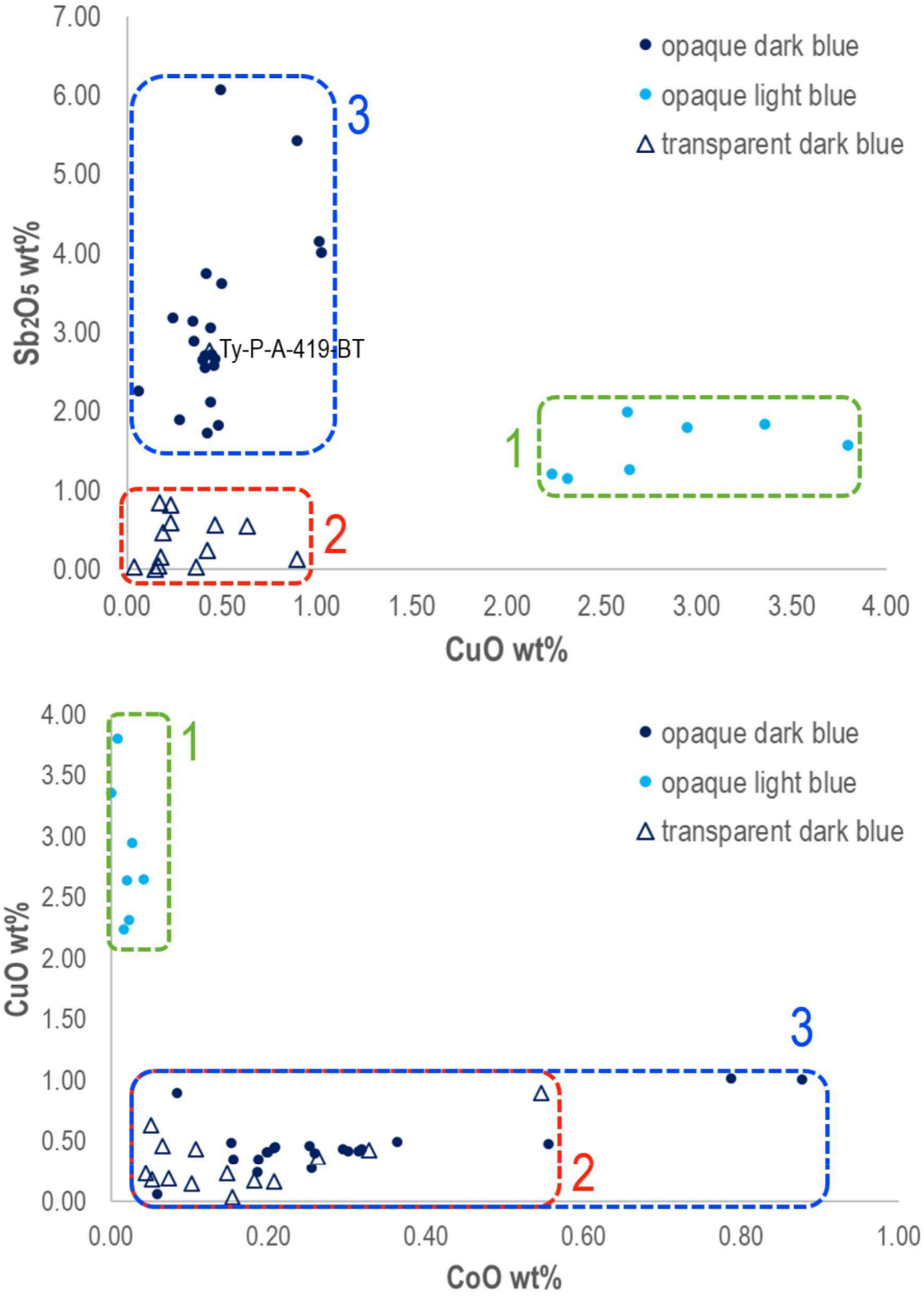

Fig. 7.3.9 – Sb_2O_5 vs CuO (up) and CuO vs CoO (down) binary plots of the glass phase in the Tebtynis blue samples. Dotted lines represent the three compositional groups identified (symbols: empty triangles = transparent glasses; colored dots = opaque glasses; the colors of the symbols are rlated to the colors observed during macroscopic observations).

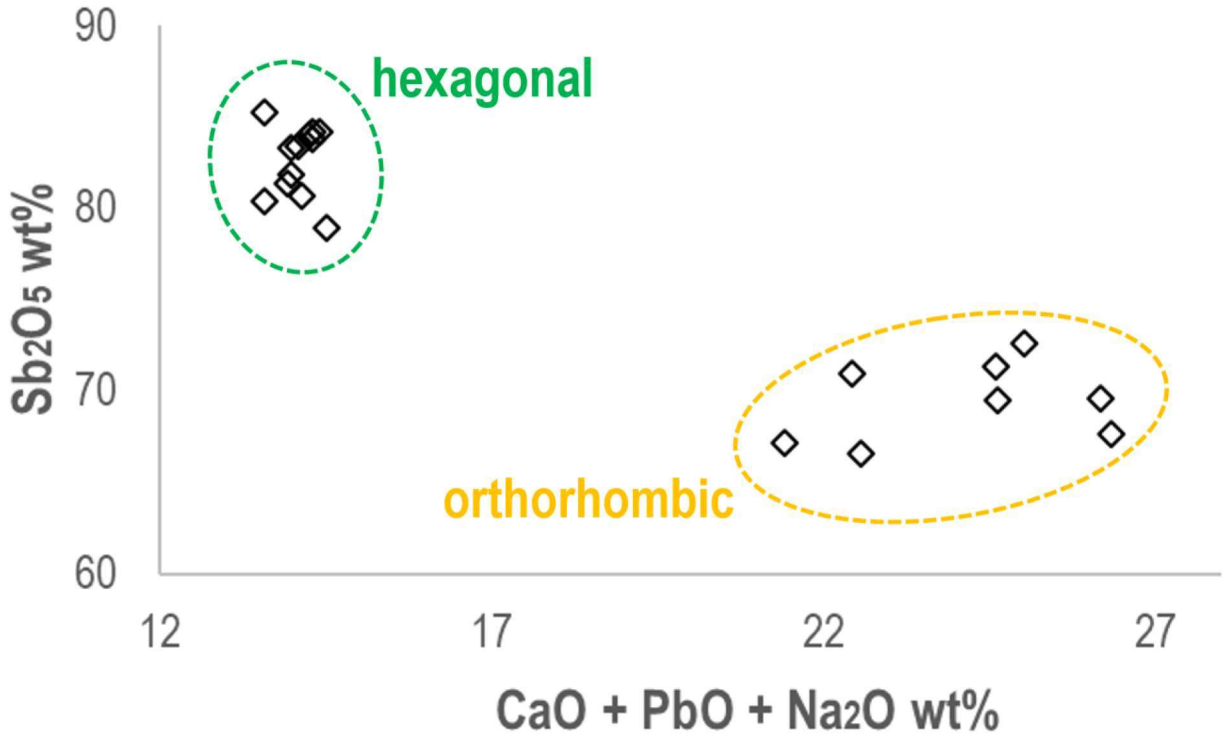

Fig. 7.3.10 – Biplot of Sb_2O_5 vs CaO + PbO + Na_2O ratio of the Ca- and Ca-Na antimoniate inclusions in the opaque blue glasses from Tebtynis, which was used to discriminate between the hexagonal and the orthorhombic forms using WDS chemical data.

One dark blue sample (Ty-S-GB-413-BO) was again found to be opacified using synthetic brizziite (Na_2O = 17.05%; Sb_2O_5 = 83.76%), as shown by WDS data. Romeite was found in light blue samples associated with brizziite (Ty-M-A-005) and $CaSb_2O_6$ (Ty-M-A-005 and Ty-M-A-005a), but also in one aggregate in the dark blue sample Ty-P-CR-421-B.

Considering the high number of samples in the two opaque classes, it was possible to identify the three different texture types seen in white glasses from Tebtynis (fig. 7.3.12a-f). Texture (I), showing small (1-5 μm), euhedral and well-separated crystals with low to medium density in the glassy matrix, is the most common occurrence, especially in dark blue glasses. Texture (II) is rare, being only doubtfully identified in sample Ty-VA-405-B; however, in this case the texture is characterized by a low number of anhedral feathery- and rosary-shaped aggregates of 50-70 μm in size unevenly distributed into an otherwise homogeneous glassy matrix, without any flour-like effect. Mixed texture (III) is quite common, both in light blue and dark blue glasses.

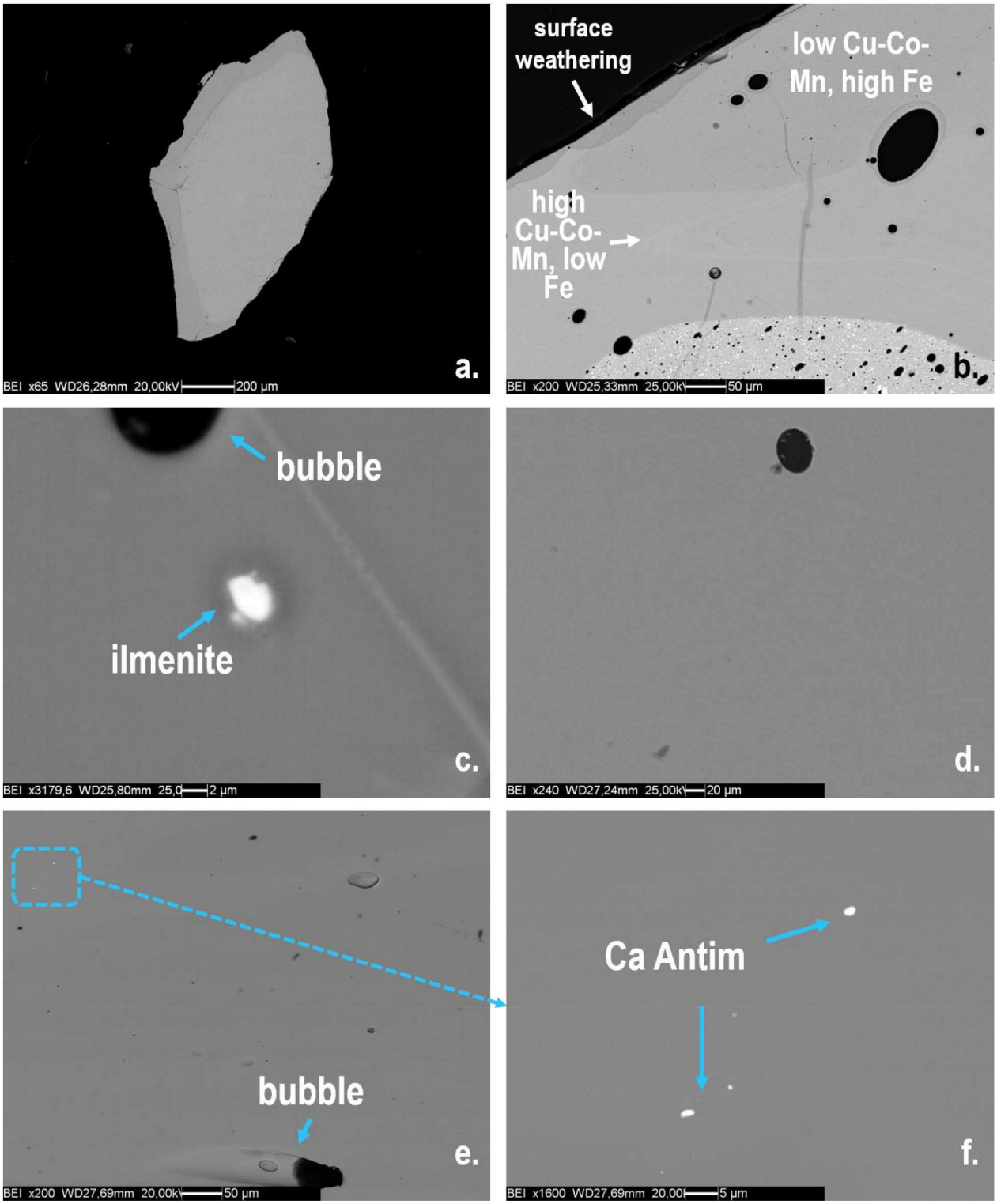

Fig. 7.3.11 – SEM-BSE images of the texture and inclusions in the transparent dark blue glasses from Tebtynis: a) cross section of sample Ty-I-BBi-613-BT; b) chemical zoning in sample Ty-S-BBi-004-BT; c) small Fe-Ti oxide inclusion (ilmenite) in sample Ty-M-B-004; d) homogeneous texture of sample Ty-Sb-B-003; e) sample Ty-P-A-419-BT; f) detail of the area in the dotted square of fig. d) with the rare Ca-antimoniate inclusions.

In addition to these typologies, sample Ty-P-V-423-BO showed a peculiar microstructure, defined as texture (IV), which is characterized by a small number of big (approx. 70÷100 μm), isolated, angular lumps showing euhedral (especially hexagonal) crystalline inclusions of Ca and Ca-Na antimoniates dispersed in a heterogeneous matrix (fig. 7.3.12g-h). The chemical composition of this matrix is reported in tab. 7.1 as a mean of 5 point analyses (EDS data); it shows high Sb_2O_3 (53.3%) and SiO_2 content (23%), CaO at 11.5% and Na_2O at 6.1%; moreover, it exhibit minor quantities of FeO (1.3%) and Al_2O_3 (1.4%). The origin and meaning of this peculiar texture will be presented in detail in the chapter of the discussion of the results.

Elem	Na_2O	MgO	Al_2O_3	SiO_2	P_2O_5	SO_3	Cl	K_2O	Sb_2O_3	CaO	FeO
wt %	6.1	0.7	1.4	23.0	0.7	0.8	0.6	0.7	53.3	11.5	1.3

Tab. 7.1 – EDS chemical composition as a mean of 5 point analyses of the heterogeneous matrix in the lumps of texture IV.

Considering the unreacted raw materials and the newly formed mineral phases, blue glasses show occasional relics of SiO_2, plagioclase (e.g. albite, oligoclase), ilmenite, Fe oxides and corundum, which were already discussed in the "silica source" section.

Moreover, samples Ty-S-TA-005-A and Ty-M-A-005 display a similar association of Ca-antimoniates precipitated over wollastonite aggregates measuring ca. 35-130 μm (fig. 7.3.13d). Ty-S-PA-408-B has also a peculiar inclusion characterized by a core of metallic Cu with external layers composed by a combination of Cu-S (intermediate layer) and Cu-Cl (outer layer) that can be associated to the raw materials for glass-coloring (fig. 7.3.13a-b).

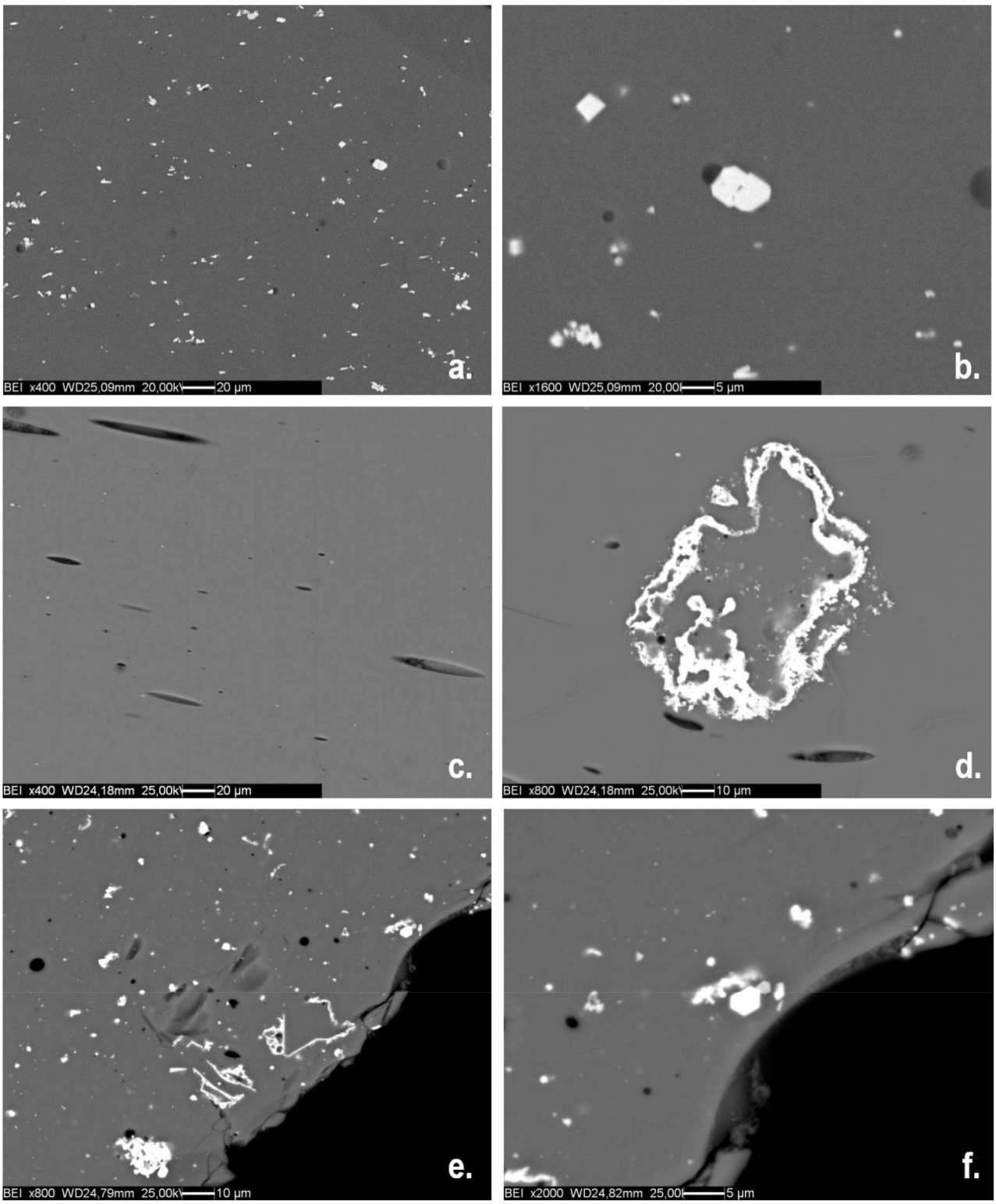

Figure 7.3.12 – SEM-BSE images of the four types of textures identified in the opaque blue class: a-b) texture (I) with small, euhedral crystals of sample Ty-I-B-616 (general view and detail); c-d) the only doubtful example of texture (II) with rosary-shaped inclusions in Ty-S-VA-405-B (general view and detail); e-f) mixed texture (III) with *both rosary-shaped aggregates and euhedral crystals in sample Ty-M-A-005 (general view and detail).*

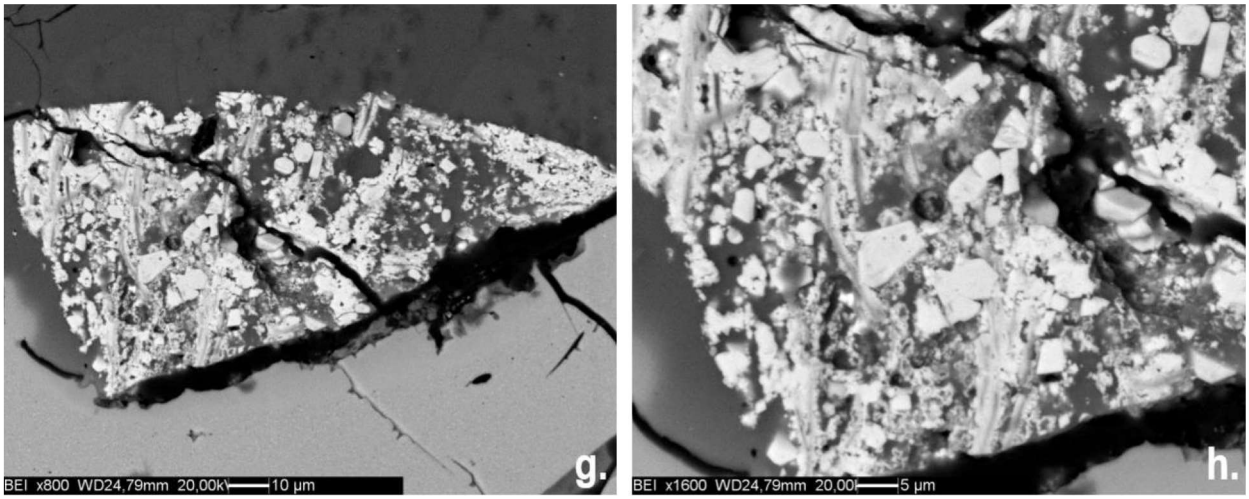

Fig. 7.3.12 – SEM-BSE images of the four types of textures identified in the opaque blue class: g-h) angular lump with euhedral crystalline inclusions dispersed in a heterogeneous matrix in sample Ty-P-V-423-B (general view and detail), typical of texture (IV).

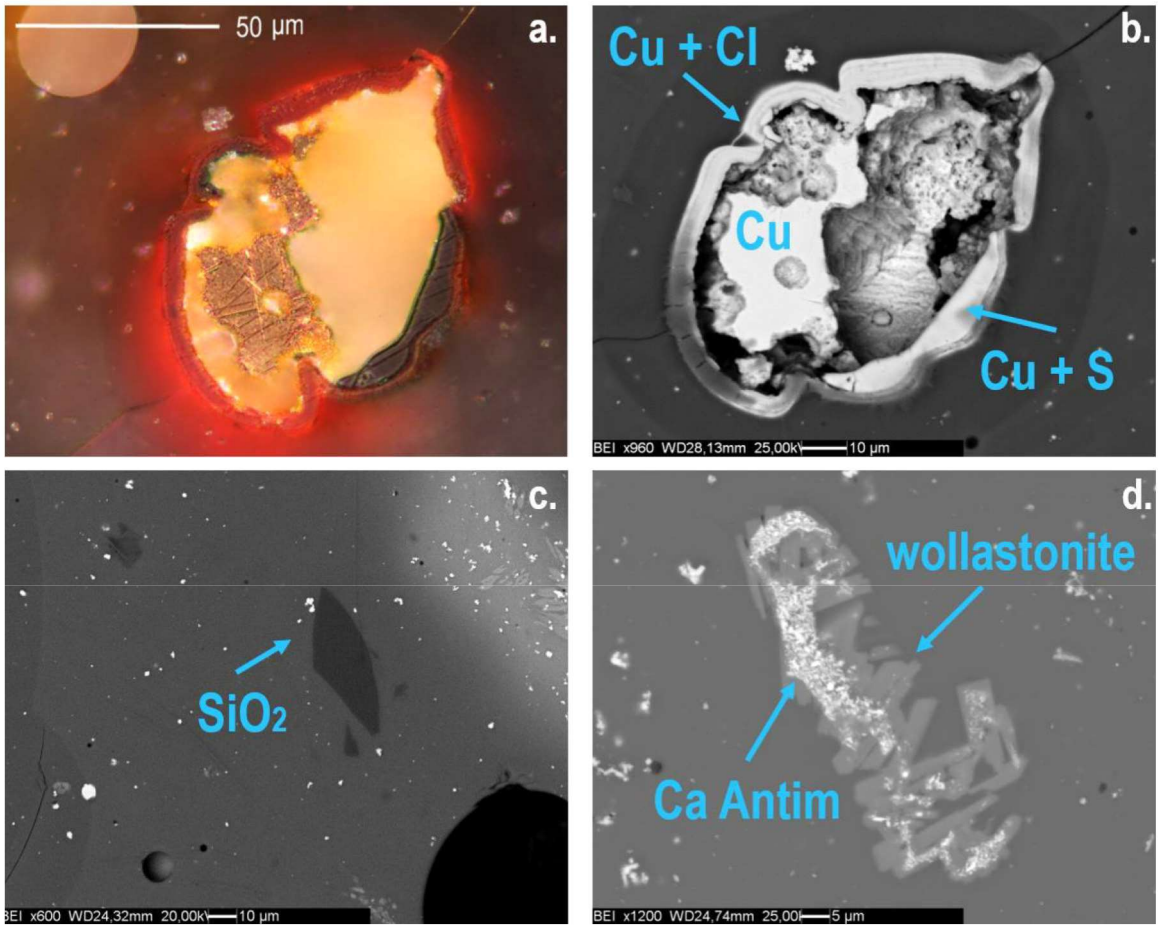

Fig. 7.3.13 – Micrographs of other types of inclusions identified in opaque blue glasses: a-b) OM in reflected light (crossed nicols) and SEM-BSE image of the zoned Cu inclusion in sample Ty-P-A-408-B; c) SiO_2 grain in sample Ty-P-FR-422-B; d) Ty-M-A-005, Ca antimoniate over wollastonite.

7.3.4 *Green glasses*

Green glasses can be divided into two main categories according to their color intensity and opacity: transparent green (5 samples) and opaque turquoise (7 samples). Transparent green glasses were mainly identified after sample preparation and OM study, since from a macroscopic point of view they often appeared as transparent, dark blue glasses, especially when sandwiched between two layers of deeply colored glass, e.g. in Ty-P-T-417. Just as in the case of white glasses, transparent greens were never found alone, but always in association with other colors to create stratified or mosaic patterns. Conversely, turquoise samples are found both alone in bars and inlays (Ty-M-A-006, Ty-M-V-005, Ty-M-V-005a, Ty-M-V-006, Ty-M-V-006a) and in polychrome compositions (Ty-S-RV-418-V and Ty-S-VA-405-V).

The chemical composition of this group is very heterogeneous. The plot CuO *vs* FeO (fig. 7.3.14) defines three different classes:

1) three transparent green glasses (Ty-P-R-423-VT, Ty-P-T-417-VT, Ty-S-BiBR-507-VT) show no other ionic chromophore in significant concentrations, except for FeO (ranging from 1.37% to 1.61%), which can thus be considered as their main coloring agent. Moreover, these glasses have high MgO (3.11%-4.19%), CaO (8.51%-9.99%), SO_3 (1.14%-1.74%) and K_2O (1.77%-2.12%) with respect to all other samples and can be thus interpreted as HMG glasses;

2) the two remaining transparent glasses (Ty-S-GRT-501-T and Ty-P-R-419-VT) are characterized by high amounts of copper (4.85-4.35 wt%) and lead (19.35-24.19 wt%). Considering their low potassium (0.76 wt% and 1.26 wt% respectively) and the average concentration of magnesium (MgO = 1.78%) they can most probably be interpreted as leaded-LMG glasses;

3) the last set well corresponds to the color-class of turquoise glasses, with very low FeO, in the order of 0.32% to 0.65%, and medium to high copper, ranging from 1.59 wt% to 5.48 wt%, with an average of 2.60 wt%. The greenish hue must thus be attributed to copper, with a limited iron contribution. This group can be distinguished from the others also for the significant levels of antimony between 2.13% and 5.22 wt%.

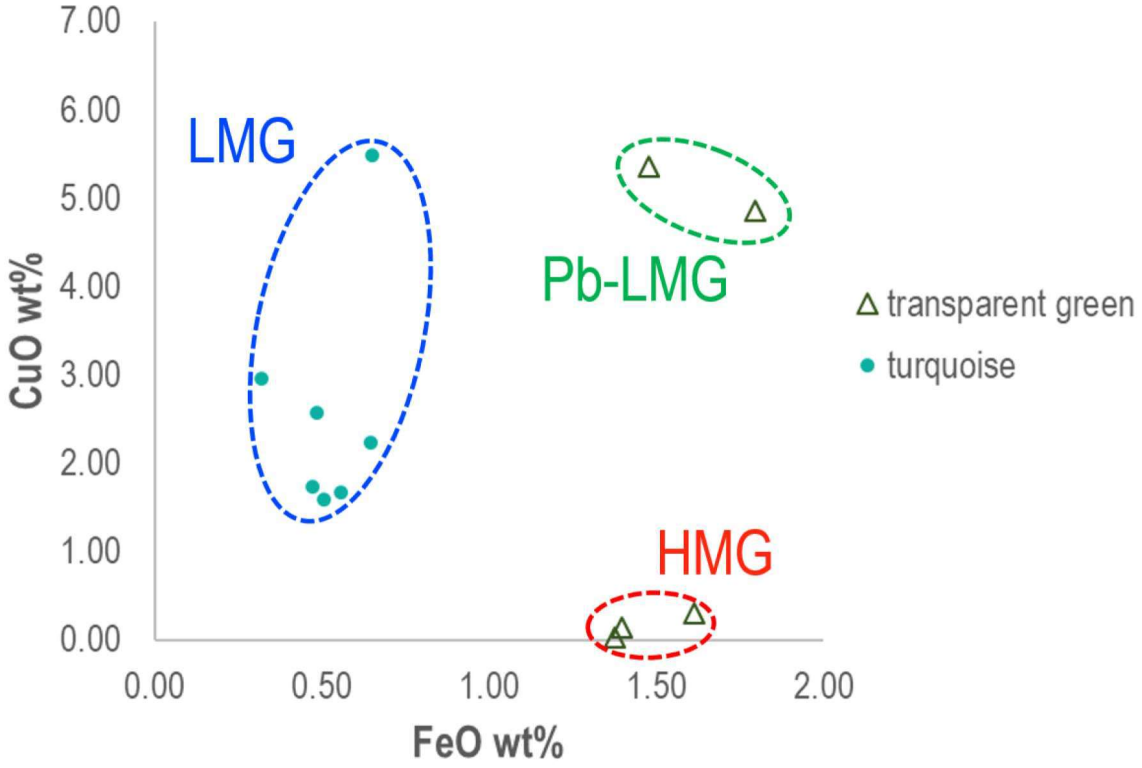

Fig. 7.3.14 – CuO vs FeO binary plot of the Tebtynis green samples. Dotted lines circumscribe the three compositional groups identified (symbols: empty triangles = transparent green glasses; colored dots = opaque turquoise glasses).

Lead is present in high concentrations in the glassy matrix of 4 turquoise samples (PbO 5.49%÷11.20%), while the remaining 3 turquoise glasses have only traces or minor contents of PbO (0.18%-0.69%).

As already noted, copper in turquoise samples is always associated with antimony and varying quantities of calcium (2.01 wt%-7.91 wt%), that are related to the presence of opacifiers dispersed in the glassy matrix. In fact, examination via SEM-EDS confirmed the presence of diffused inclusions of calcium antimoniates, often in solid solution with sodium (in Ty-M-V-006a and Ty-M-A-006) and small amounts of lead, reaching up to 3.6 wt%. The WDS and μ-Raman analyses performed on several crystalline inclusions (at least one for each sample, chosen among the largest available), confirmed the presence of pure Ca antimoniates (Ty-M-V-006, Ty-S-VA-405-V, Ty-S-RV-418-VO) in hexagonal ($CaSb_2O_6$) and orthorhombic ($Ca_2Sb_2O_7$) form. Moreover, they show that pure Ca antimoniates are sometimes associated to Ca-Pb (Ty-M-V-006a and

Ty-M-A-006) and Ca-Na-Pb antimoniates (Ty-M-V-005-4, Ty-M-V-005a); surprisingly, a few inclusions also contain SiO_2 in significant concentrations, ranging from 3.73%-6.94%. Considering the dimensions of the aggregates (≥ 5μm) and the chemical contrast in BSE, there is a low chance that these values can be exclusively due to a contamination from the glassy matrix; instead, they may possibly refer to an intermediate synthetic phase.

Considering the types of texture described for the white and blue glasses (see § 7.3.3, pp. 151-153), the turquoise samples show absence of texture type (I) and (IV), with a net dominance of texture (II) and, in minor measure, (III). All samples have a porosity from medium to high, with rounded and elongated bubbles; their size goes from sub-micrometric to very large (over 600 μm), such as in Ty-M-V-006a.

Relics of the minerals derived from the sand used are present in three of the seven samples belonging to the turquoise class (fig. 7.3.15), in particular: one big SiO_2 grain in Ty-M-A-006, one ilmenite with 2.2% MgO and 1.1% MnO in Ty-S-VA-405-A, one corundum and one plagioclase with stoichiometry close to anorthoclase (EDS data: Na_2O = 5.8%, Al_2O_3 = 19.6%, SiO_2 = 68.2%, K_2O = 6.4%) in Ty-M-V-006a.

Coming to the transparent green glasses, as expected the texture is generally homogeneous with limited or no porosity and no intentional opacifiers. However, three samples show peculiar inclusions, related to an incipient coloring process (fig. 7.3.16): Ty-S-BiBR-507-VT has a cluster of wollastonite crystals measuring ca. 250x100 μm and a 50 μm drop of chalcocite (Cu_2S, WDS data); OM images in reflected light and crossed nicols clearly show a red rim emanating from the copper sulfide inclusion. Ty-P-R-423-VT also has small copper sulfide drops of 1-2 μm diameter (probably chalcocite, EDS data), associated with one Cu-Fe and Pb sulfide (possibly chalcopyrite and galena, EDS data), and various Ca-P-Na silicates, that can be interpreted as devitrification products. Finally, Ty-P-R-419-VT is characterized by the nucleation of small dendritic crystals of cuprous oxide (synthetic cuprite) growing at the interface with a yellowish-orange glass and thus suggesting that this kind of composition could possibly have been used as the base glass for red and yellowish-orange glasses. This is further strengthened by the fact that red cuprite glasses show a transparent greenish glassy matrix at OM observations (see § 7.3.5).

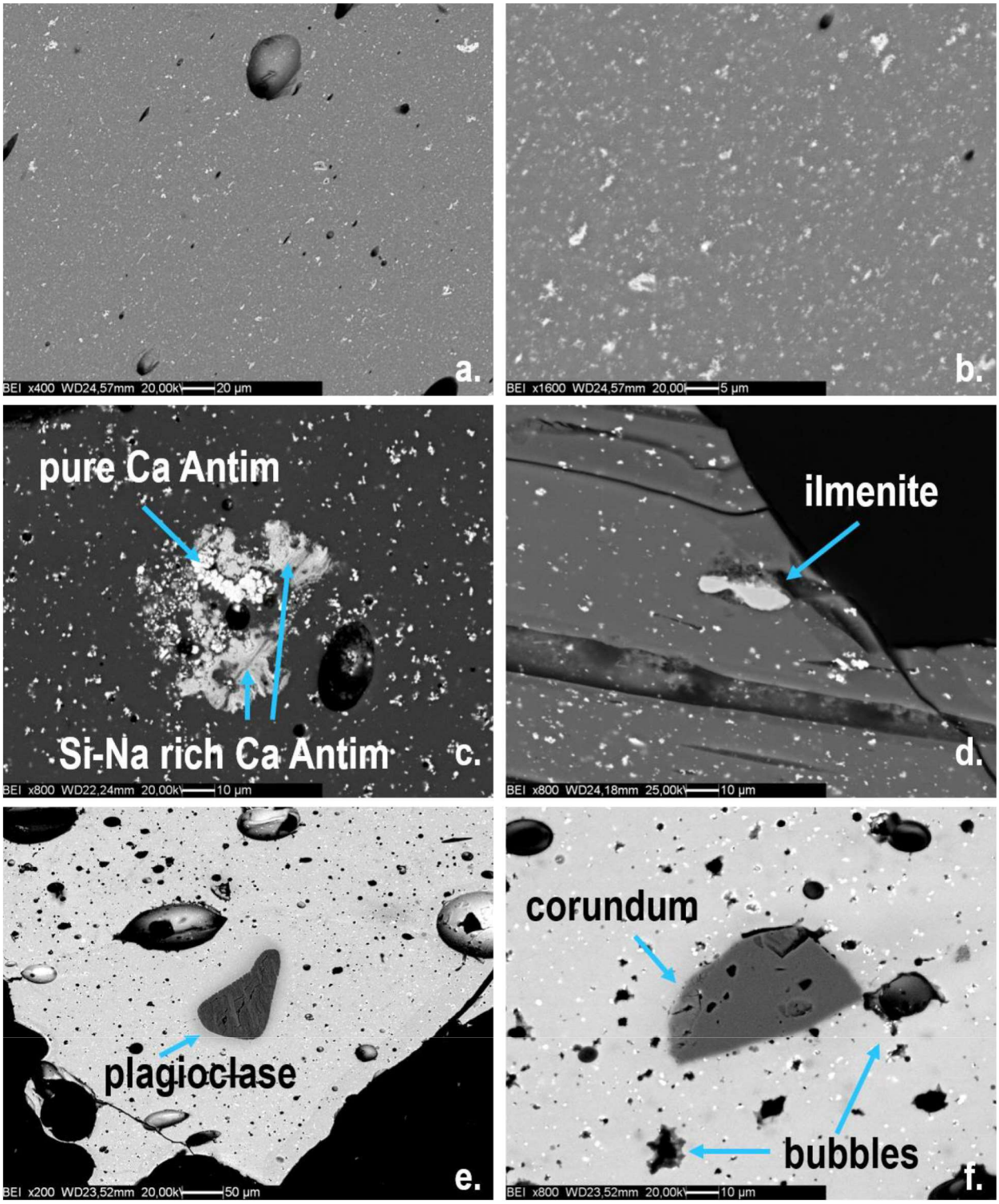

Fig. 7.3.15 – SEM-BSE images of the most texture and crystalline inclusions identified in the turquoise class of Tebtynis glasses: a-b) Ty-M-V-005, typical texture (II) in turquoise samples (general view and detail); c) antimoniate aggregate, zoned for the presence of Na/ Si in Ty-M-V-006; d) ilmenite inclusion containing Mn and Mg in sample Ty-S-VA-405-VO; e-f) plagioclase close to the composition of anorthoclase and corundum inclusions in sample Ty-M-V-006a.

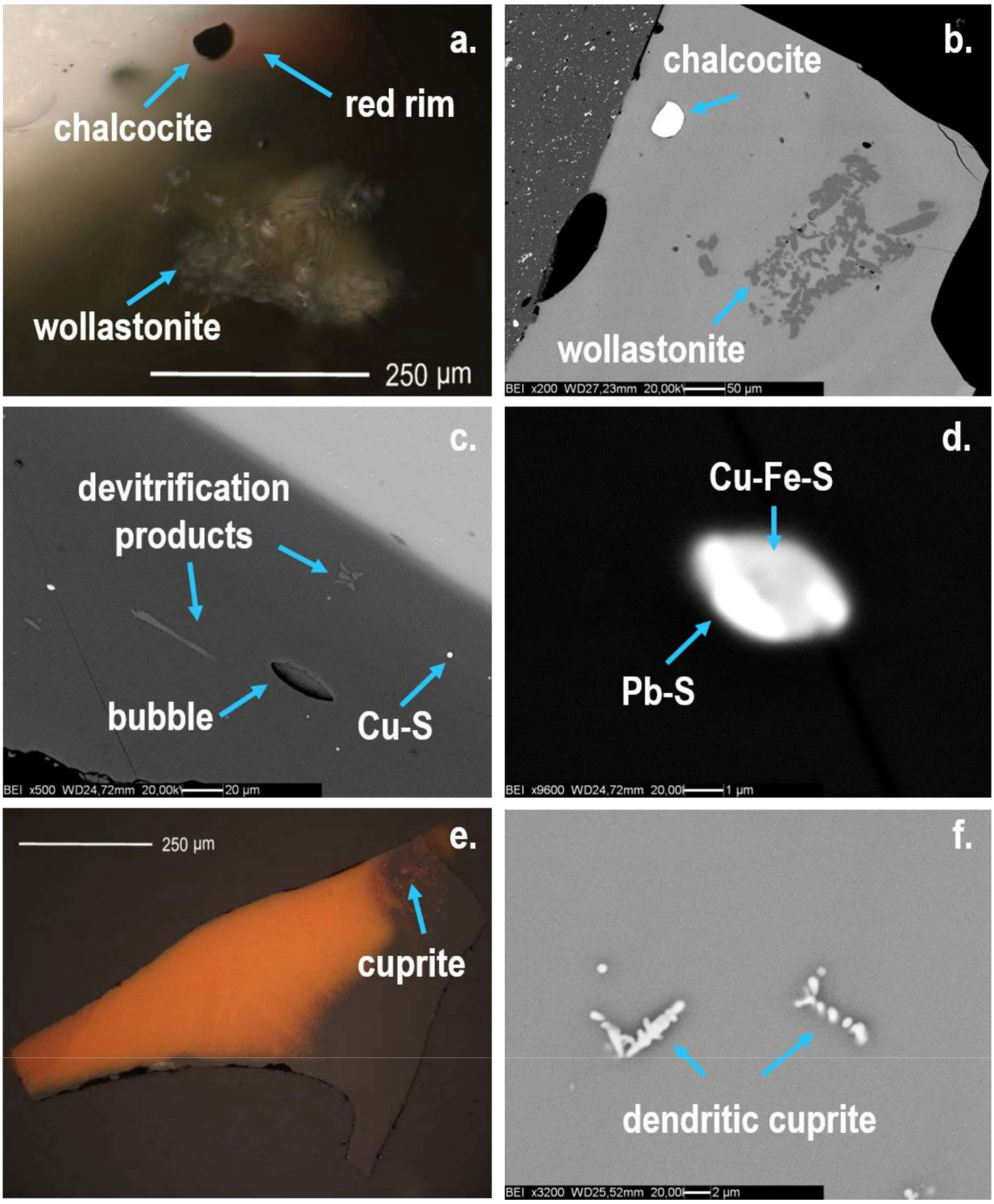

Fig. 7.3.16 – Inclusions identified in transparent green glasses from Tebtynis: a-b) OM image in reflected light and crossed nicols and SEM-BSE image of a wollastonite aggregate associated with a 50 µm chalcocite drop (WDS data) in sample Ty-S-BiBR-507-VT; c-d) sample Ty-P-R-423-VT, chalcocite, devitrification products and Cu-Fe and Pb sulfides dispersed in the glassy matrix; e-f) nucleation of dendritic cuprite crystals at the interface with a yellowish-orange glass in Ty-P-R-419-VT (OM in reflected light and shifted nicols and SEM-BSE images).

7.3.5 *Yellow, yellowish-orange, red and brown glasses*

The "yellow, yellowish-orange, red and brown" class counts the highest number of total samples with 54 analyzed glasses. In the whole collection, brown glass is represented only by a single occurrence in the bichrome bar Ty-S-MR-502; likewise, yellow glass was never found on its own but only in polychrome combinations, just like opaque white and transparent green glass. Red glasses (dull red and sealing-wax red), on the contrary, are commonly used for figured inlays (sometimes with gold traces) and for numerous types of monochrome bars, stratified glasses, and mosaic compositions. Yellowish-orange glasses were never seen figurative inlays, but are frequently found as bars and in polychrome pieces. All samples in this set are leaded glasses (from soda-lime-lead to heavily leaded compositions), comprising amounts of PbO in the order of 3.67%-40.11%. Considering the contents PbO *vs* CuO, one can observe an excellent correspondence between the colors defined through macroscopic examination and the chemical variability in the dataset (fig. 7.3.17).

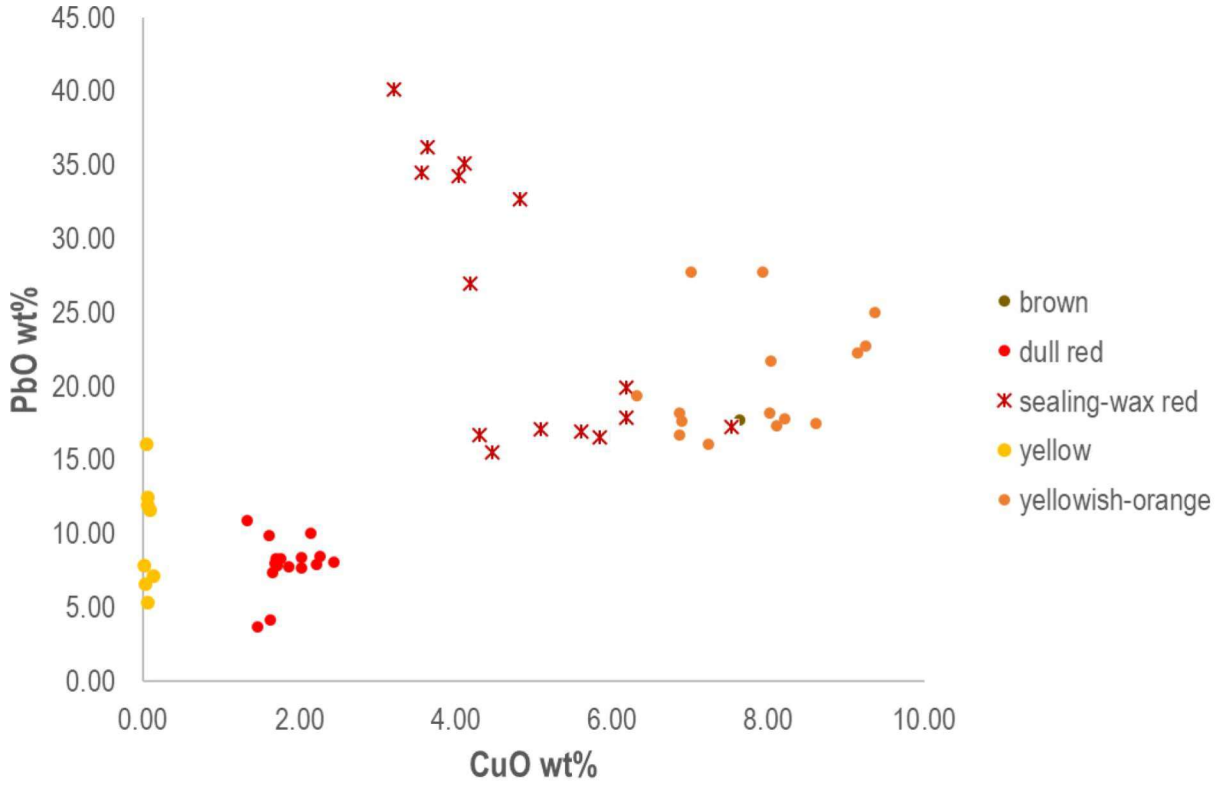

Fig. 7.3.17 – PbO vs CuO binary plot of the Tebtynis yellow, orange, red and brown samples.

YELLOW GLASSES

Yellow glasses are characterized by absence or very low CuO (0.01%-0.13%) and PbO ranging from 5.34% to 16.04%; moreover, they show high Sb_2O_5 content, which reaches values of 0.86%-4.15%. The alkali composition is consistent with LMG glasses, with magnesia ranging from 0.35% to 1.01% and potash from 0.49% to 0.96%.

The opacity and color of the yellow glasses is due to the presence of small, anhedral inclusions of lead and lead-tin antimoniates, as demonstrated by SEM-EDS (fig. 7.3.18), WDS and μ-Raman data (fig. 7.3.26). The dimensions of the aggregates vary widely from 20 μm to sub-micrometric size. Textural examinations also showed that many yellow glasses are characterized by diffuse chemical zonings with alternating stripes richer and poorer in lead, the latest bearing the highest concentration of antimoniate crystallites (fig. 7.3.18a).

However, three of the eight yellow samples show a homogeneous texture. In addition to lead antimoniates, Ty-P-A-402-G also includes numerous, rounded quartz grains with unreacted edges (μ-Raman data), reaching up to 50 μm (fig. 7.3.18c-d). Considering their very high number and their rather homogeneous distribution, in this specific case they can more probably be interpreted as intentional additives, rather than relics from the sand used.

Ty-P-FL-501-G revealed the presence of abundant, euhedral calcium antimoniate crystals ($CaSb_2O_6$), together with lead-tin antimoniates as determined by a combination of μ-Raman and WDS data (fig. 7.3.18b). The presence of hexagonal Ca antimoniates might have been voluntary, in order to obtain a clearer yellow, but is more probably related to the conversion from lead to calcium antimoniates that takes place during firing at more than 1000°C, as demonstrated by the experimental replicas of Molina (*et alii*, 2014). Other inclusions in this sample comprise one small crystal of iron oxide, possibly a relic of the sand used, and one newly formed cluster of pyroxene crystals.

It is interesting to observe that yellow glasses with different textures can be present even within the same inlay. For examples, Ty-FR-422-G1 is characterized by the absence of a banded-texture, in contrast with Ty-FR-422-G2, which was used for other parts of the same inlay.

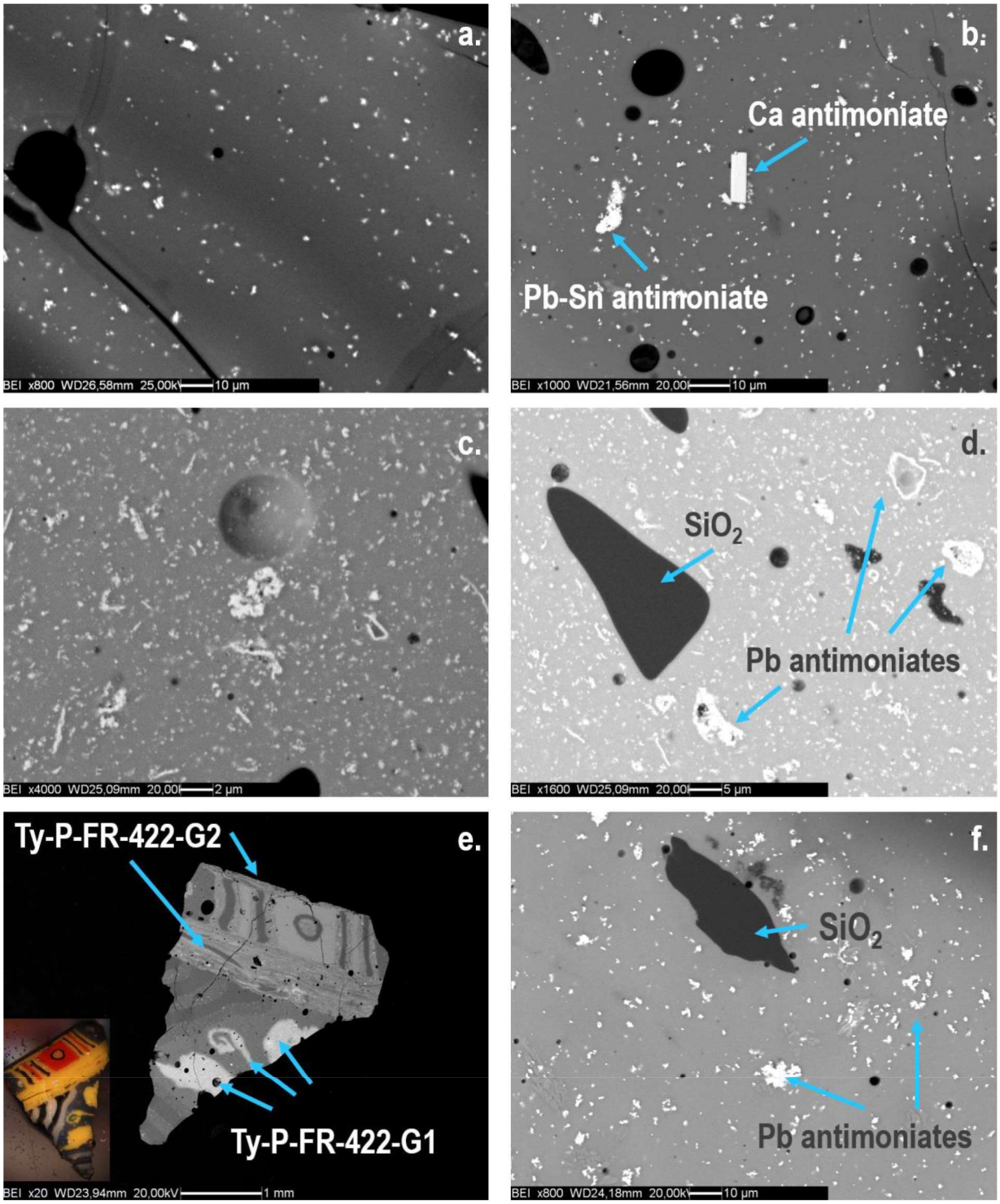

Fig. 7.3.18 – Texture and coloring/ opacifying agents identified in opaque yellow glasses from Tebtynis: a) Pb-banded texture of sample Ty-S-ARG-403-G; b) Ca and Pb-Sn antimoniates in sample Ty-P-FL-501-G; c-d) uniform texture with evenly dispersed Pb antimoniates and quartz inclusions in sample Ty-P-A-402-G; e) OM and BSE images of sample Ty-P-FR-422, with two different types of opaque yellow glass, one with homogeneous texture (details of the flower, petals and pistil) and the other with Pb-banded texture (simple bars); f) Pb antimoniates and quartz inclusion in sample Ty-P-FR-422-G1.

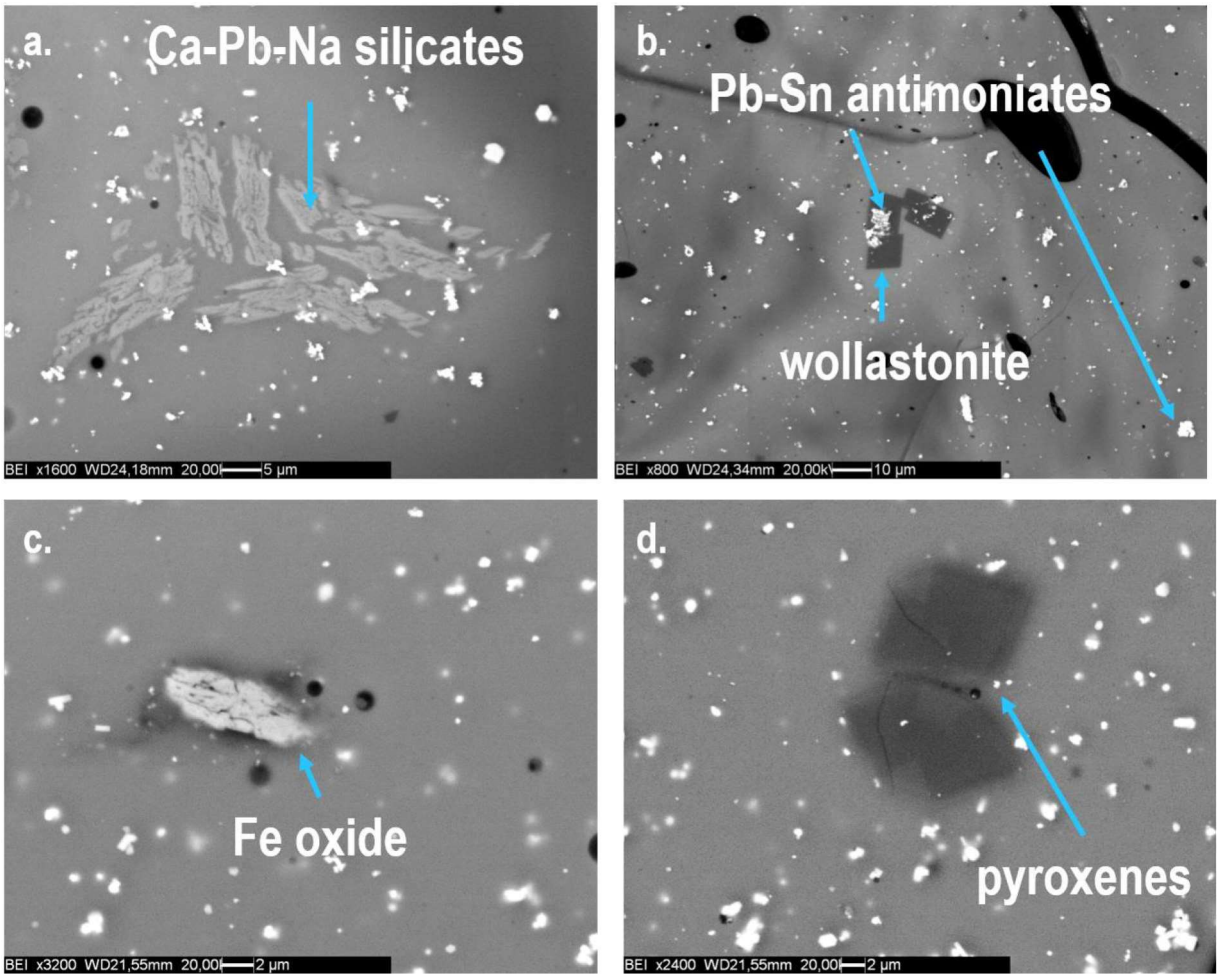

Fig. 7.3.19 – Newly formed and sand-related phases in the Tebtynis yellow glasses: a) Ca-Pb-Na silicates in sample Ty-FR-422-G1; b) Pb-Sn antimoniates over wollastonite in Ty-P-CR-421-G1; c-d) Iron oxide and pyroxene crystals in sample Ty-P-FL-501-G.

SEM-BSE observations showed in Ty-FR-422-G1 a very high number of Pb-Ca-Na silicates, with different stoichiometric ratios (EDS data), sometimes grown in bigger, radial aggregates reaching up to 40-50 µm (fig. 7.3.19a). Their composition is consistent with the combination of the main constituents of the glassy matrix and can be interpreted in terms of devitrification products. The sample also shows a couple of quartz crystals, which are rather common in yellow glasses, often as residues from the sand used.

Other inclusions found in yellow glasses comprise one crystal of iron oxide in Ty-P-FL-501-G and a cluster of newly formed euhedral pyroxenes in the same sample (fig. 7.3.19c-d).

Considering the WDS composition of the nine analyzed antimoniates in yellow glasses (see table V in the appendix), it is possible to distinguish two main types of pigments: lead antimoniates (3 occurrences), with PbO between 48.56% and 54.60%, Sb_2O_5 between 31.30% and 33.87% and FeO between 4.34% and 4.83% (in Ty-P-FR-422-G1, Ty-P-A-402-G and Ty-S-GA-411-G), and lead-tin antimoniates (6 occurrences) characterized by PbO ranging from 44.76 to 52.87%, Sb_2O_5 from 25.05% and 37.25%, SnO_2 from 1.71% to as high as 17.02% and FeO from 1.16% to 4.44%.

DULL RED GLASSES

Dull reds are again well separated from other samples, as they exhibit intermediate levels of both CuO and PbO, respectively 1.33%-2.45% and 1.92%-3.67%. Considering the alkali content, it is also clear that this class is notably different from the others also in terms of high MgO (1.10%-3.00%), K_2O (1.91%-3.38%), CaO (7.42%-9.13%) and SO_3 content (from 0.23% to peaks of 1.60% and an average of 0.99%), suggesting a plant-ash recipe for the base glass, as discussed in the related section (§ 7.2, p. 136).

Looking at OM and SEM-BSE images (fig. 7.3.20), dull red glasses are characterized by the diffuse presence of nano-sized particles homogeneously dispersed in the vitreous phase. Despite their very limited size, that prevent a specific chemical characterization by EDS or WDS, they were interpreted as metallic copper considering textural features and μ-Raman analyses (fig. 7.3.25). Instead, the biggest spheroidal inclusions (ca. 1÷5 μm) which are present in most samples were recognized as copper sulfides, especially chalcocite (Cu_2S), such as in Ty-P-A-418-R1 (WDS data: Cu 78.37% and S 18.47%).

Coming to the newly formed mineral phases (fig. 7.3.21), euhedral crystals of wollastonite are by far the most common occurrence, as they appear in most of the dull red glasses often in big aggregates ranging from 5 μm up to 100 μm. Moreover, sample Ty-P-FR-422-R shows large aggregates of Ca-Pb-Na silicates, that again can be interpreted as devitrification products.

Residual batch minerals are rather scarce: one pyroxene with stoichiometry close to esseneite ($CaFe^{3+}AlSiO_6$), but lower in FeO, was found in Ty-P-FR-422-R (EDS data: Al_2O_3 = 25.5%, SiO_2 = 39.5%, CaO = 24.0%, FeO = 11.0%), while one alkali felspar with a mix of albite (EDS data: Na_2O = 9.8%, Al_2O_3 = 19.5%, SiO_2 = 70.6%) and K-Na feldspar

(EDS data: Na_2O = 3.8%, Al_2O_3 = 17.9%, SiO_2 = 65.3%, K_2O = 13.0%) was identified in sample Ty-P-CR-421-R.

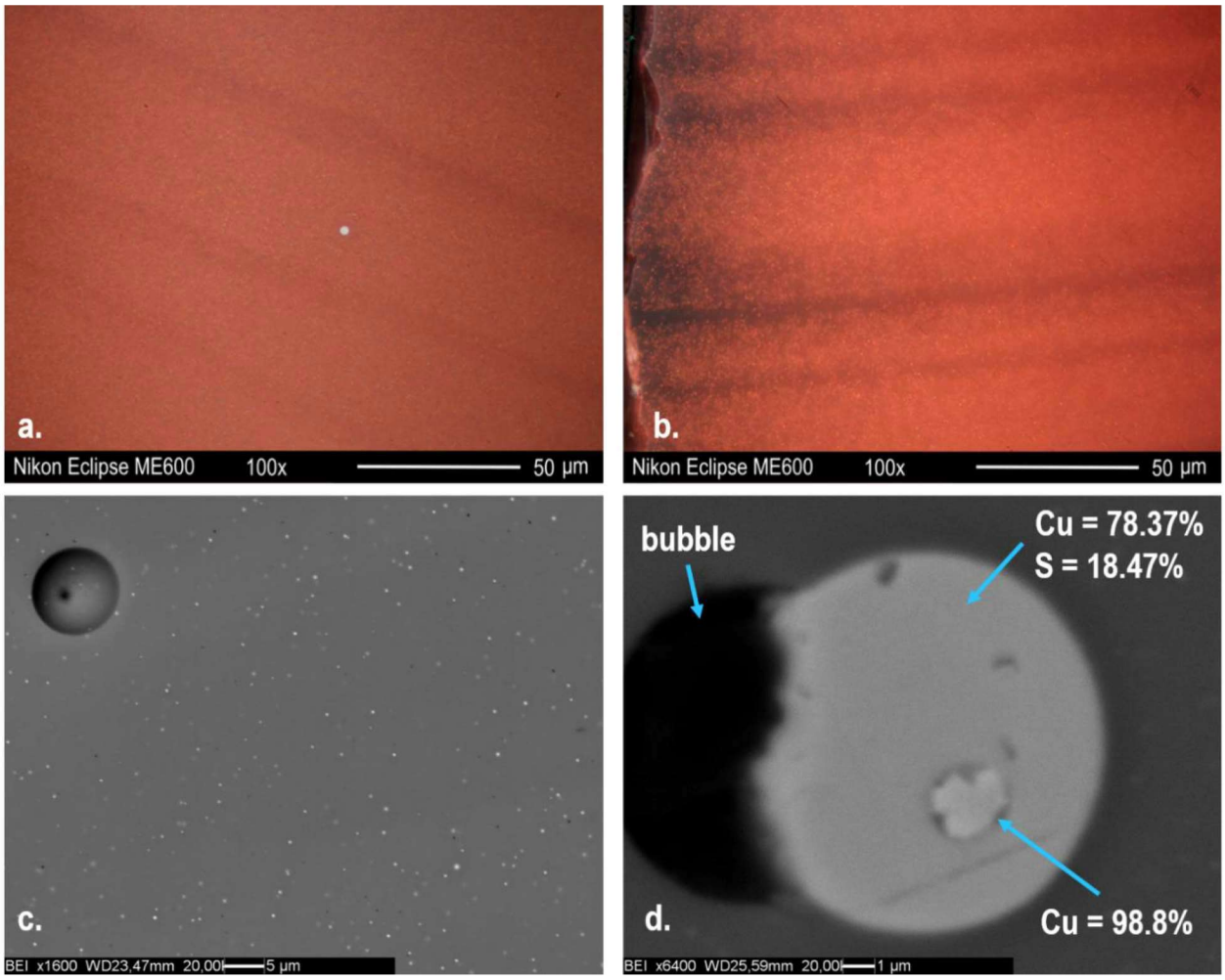

Fig. 7.3.20 – Texture and coloring/ opacifying agents in Tebtynis dull red glasses: a) OM image in reflected light and shifted nicols of the texture of sample Ty-M-R-501. The larger, central inclusion is a copper sulfide (EDS data); b) OM image in reflected light and shifted nicols of the texture of sample Ty-S-GRT-501-G (multi-focal image reconstructed with EliconFocus); c) SEM-BSE image of the texture of sample Ty-S-mix-006-R with nanometric metallic copper drops; d) SEM-BSE image of metallic copper (EDS data) surrounded by chalcocite (WDS data) in sample Ty-P-A-418-R.

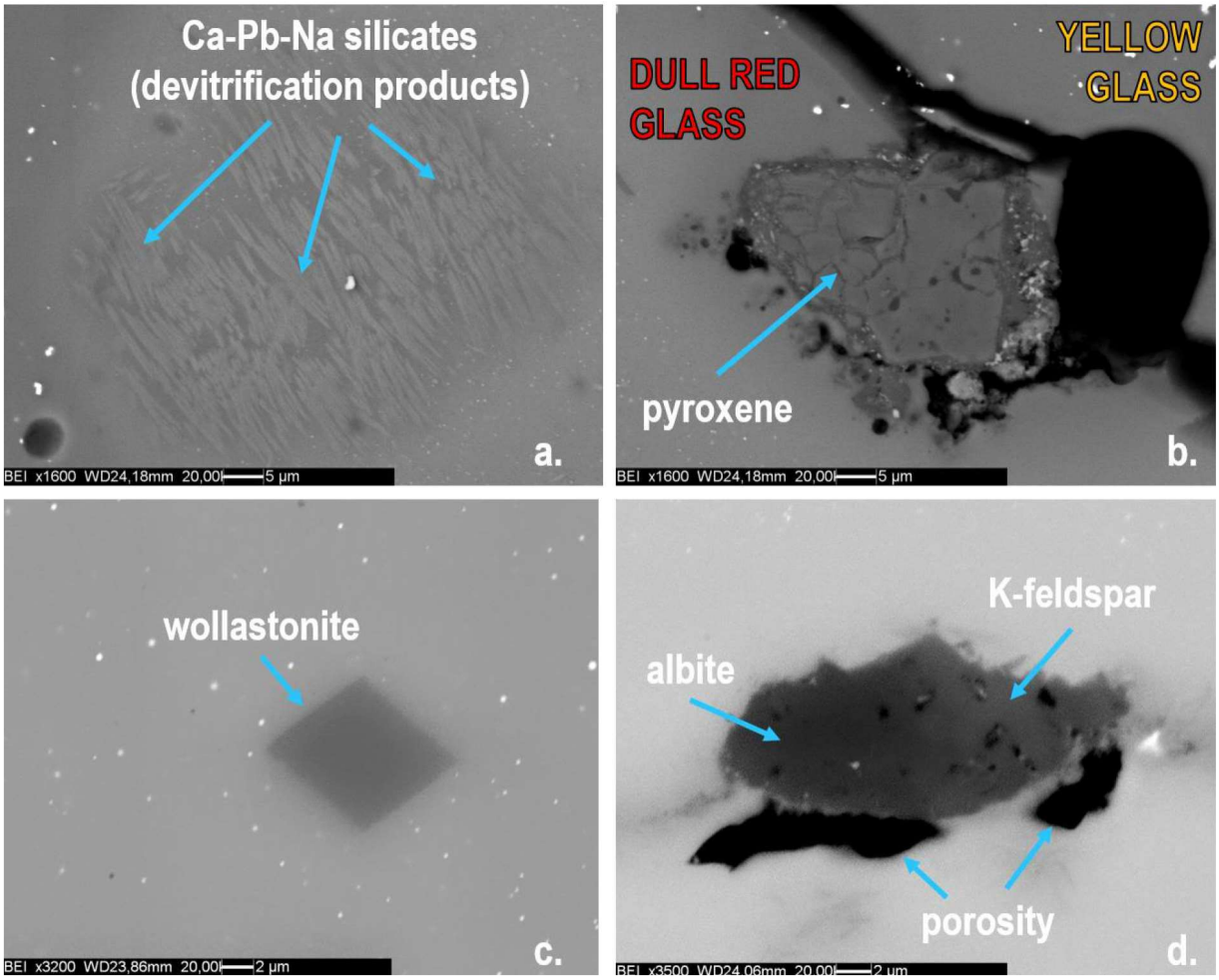

Fig. 7.3.21 – Newly formed and unmelted mineral phases in dull red glasses from tebtynis: a) Ca-Pb-Na silicates in sample Ty-P-FR-422-R; b) pyroxene inclusion at the interface between the dull red glass and the yellow glass in sample Ty-P-FR-422-R; c-d) wollastonite and alkali feldspar inclusions in sample Ty-P-CR-421-R.

YELLOWISH-ORANGE, BROWN AND SEALING-WAX RED GLASSES

From the compositional point of view, yellowish-orange, brown and sealing-wax red glasses form a continuous series, with a marked tendency towards higher PbO/ CuO levels in red glasses.

Sealing-wax red and brown glasses were certainly produced starting from a LMG base glass, given the values of MgO (average 0.8%) and K_2O (average 0.67%). Sealing-wax red glasses show the highest PbO (15.50%-40.11%) and CuO (3.21%-7.53%) concentrations; however, the CuO *vs* PbO plot clearly indicate that they can be further

divided in two sub-groups on the basis of the PbO content: the first has PbO in the range of 15-20%, while the second has PbO varying from ca. 25% to 40%. Antimony also shows wide variations: one sample set has medium to high (0.40 wt%-1.61 wt%) and one very low Sb_2O_5 contents (from under detection limit to 0.02%).

Considering its overall chemical composition, the brown glass Ty-S-MR-502-M stands in the lowest compositional range of sealing-wax reds, with PbO at 17.78% and CuO at 7.36%.

As already noted, the yellowish-orange samples exhibit an intermediate composition between HMG and LMG glasses, which will be better presented and contextualized in the discussion of the results (see § 8). Yellowish-orange samples have PbO from 16.06% to 27.73%, CuO between 6.31% and 9.36% and low – but always present – antimony (0.17-0.57 wt%), except for sample Ty-M-Ar-506 with Sb_2O_5 at 1.90%.

The major colorant in the yellowish-orange, sealing-wax red and brown series is cuprous oxide (Cu_2O) associated with a low number of metallic copper crystals (often with small copper sulfides segregations around the edges), as demonstrated by SEM-EDS and μ-Raman analyses (fig. 7.3.25). From the textural point of view, yellowish-orange glasses are characterized by cuprite crystals of ca. 100-250 nm with octahedral habitus, as emerged from FEG-SEM observations (fig. 7.3.22c-d). Brown glass Ty-S-MR-502-M has inclusions of a similar, nanometric size. Interestingly, euhedral crystals of calcium-lead antimoniate are associated to nano-particles of cuprite in Ty-M-Ar-506 (fig. 7.3.22a). This is consistent with the results of the chemical analyses, that highlighted Sb_2O_5 concentrations higher in this sample than for the typical yellowish-orange glasses in the Tebtynis collection. Ty-M-Ar-506 is also unique for the presence of a few, small "pockets" depauperated in lead (darker in BSE), with incipient nucleation and growth of dendritic cuprite crystals (≤ 5 μm), attesting an intermediate stage between classic yellowish-orange glasses and sealing-wax red glasses.

Sealing-wax reds show two different types of texture: samples with ca. PbO ≥ 30% have well-defined bands of chemical zoning with stripes richer and poorer in lead; low-lead areas contain most of the coloring agents, both cuprite dendrites (average size 1÷60 μm) and metallic copper inclusions (average size 2÷10 μm). It is to note that SEM-BSE allows to estimate the dimensions of the dendrites branches only in two dimensions,

while the real extension of the inclusions can be studied qualitatively only by OM observations. In fact, crystals are dispersed in a transparent, greenish glass: by performing a series of stacked image acquisitions (see § 6.6.1), it is possible to reconstruct the microstructure of the inclusions even inside the glassy matrix and obtain 3D images of the crystals (fig. 7.3.23).

On the contrary, sealing-wax red samples with PbO comprised between 15% and 20% have very homogeneous glassy matrix, smaller cuprite dendrites (up to 20 μm) and a lower number of slightly larger metallic copper inclusions (5-15 μm). In general terms, there is a clear trend in the dimensions of the crystallites: in low-lead sealing-wax red glasses they are smaller, with less developed branching and cruciform or radial morphologies (fig. 7.3.24a-b); on the contrary, in high-lead sealing-wax red glasses they show complex dendritic shapes and exhibit a bigger size (fig. 7.3.24c-d), especially considering their tri-dimensional development as seen in OM observations.

Samples with intermediate lead composition (25% ≤ PbO ≤ 30%), such as the yellowish orange sample Ty-M-Ar-506 or the sealing-wax red sample Ty-I-RAu-622, may sometimes exhibit evidence of zoning and incipient crystal growth.

Considering the newly formed phases in yellowish-orange glasses, wollastonite is the most frequent inclusion encountered, together with malayaite, i.e. $CaSnO(SiO_4)$, which was found in four out of fifteen samples (Ty-S-ArG-506-Ar, Ty-S-GA-005-Ar, Ty-P-A-408-Ar and Ty-S-GRT-501-Ar). Sand minerals are generally present within the bubbles or at the interface between glass layers of different colors and comprise quartz together with a wide number of Al, Fe and Fe-Ti oxides and various types of feldspars and pyroxenes. Cassiterite (SnO_2) was identified only in sample Ty-S-GA-005-Ar, and can be associated to a voluntary addition related to the coloring process.

A similar situation appears in sealing-wax red glasses, which however do not show any tin-bearing crystalline inclusion. This is consistent with the lower levels of SnO_2 in the glassy matrix, which has average values of 0.30% in sealing-wax red glasses and of 0.89% in yellowish-orange samples. Among the most peculiar crystals identified in the sealing-wax red class, it is to mention the only occurrence of a lead copper halide mineral, which was identified with good confidence by WDS data as chloroxiphite, i.e. $Pb_3CuO_2Cl_2(OH)_2$. The crystal lays on the external surface of sample Ty-M-R-502d (fig.

7-3-24e) and most likely derives from the alteration of lead and copper-rich minerals in an evaporitic environment.

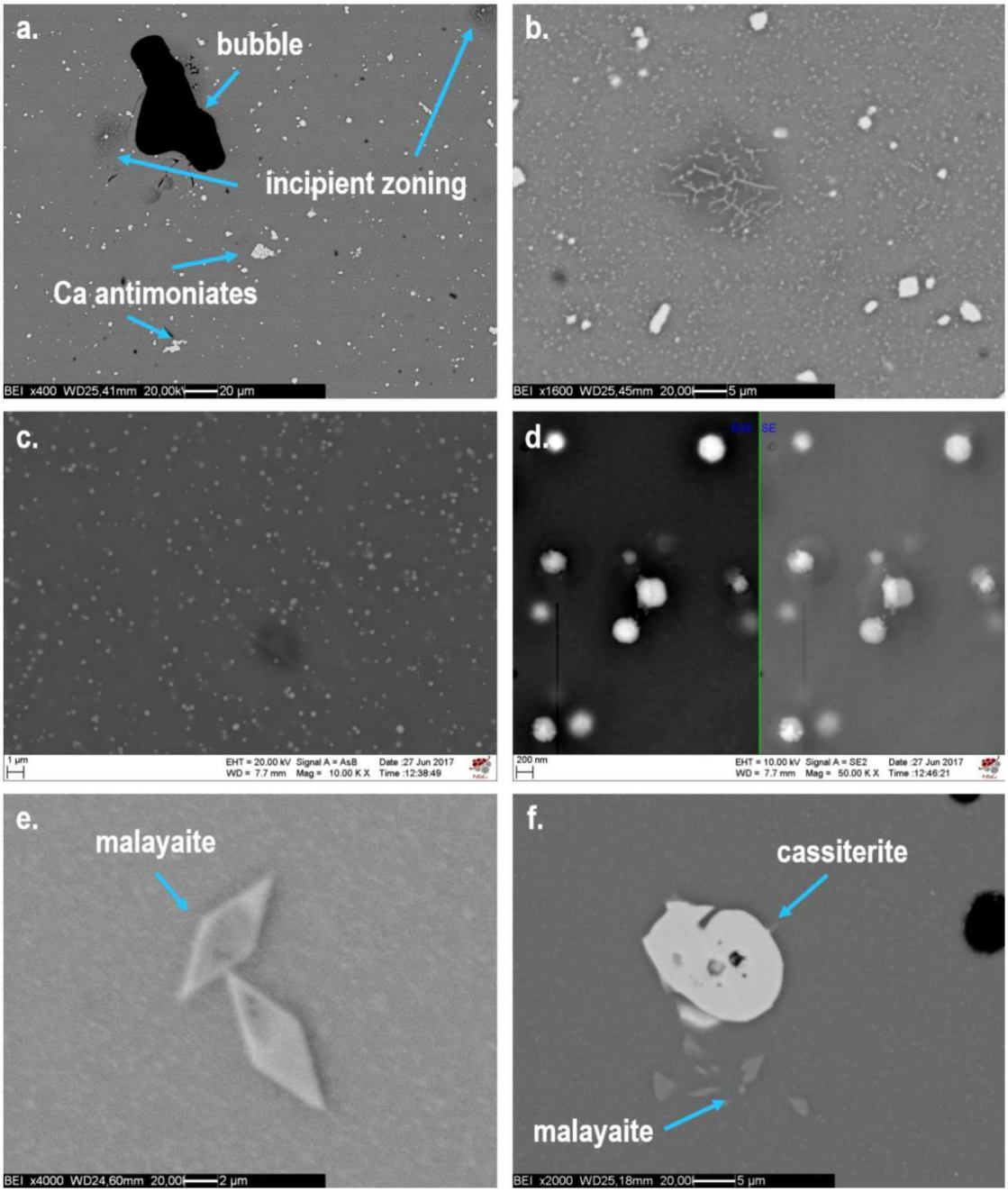

Fig. 7.3.22 – SEM-BSE images of the texture and inclusions identified in yellowish-orange glasses from Tebtynis: a-b) general view and detail of the texture in sample Ty-M-Ar-506 showing euhedral Ca-Pb antimoniates associated to nano-sized cuprite and areas with incipient crystal growth; c-d) general view and detail of the nanometric cuprite crystals in sample Ty-S-GB-413-Ar; e) euhedral malayaite crystals in sample Ty-S-ArG-506-G; f) cassiterite (WDS data) and malayaite (EDS data) inclusions in sample Ty-S-GA-005-Ar.

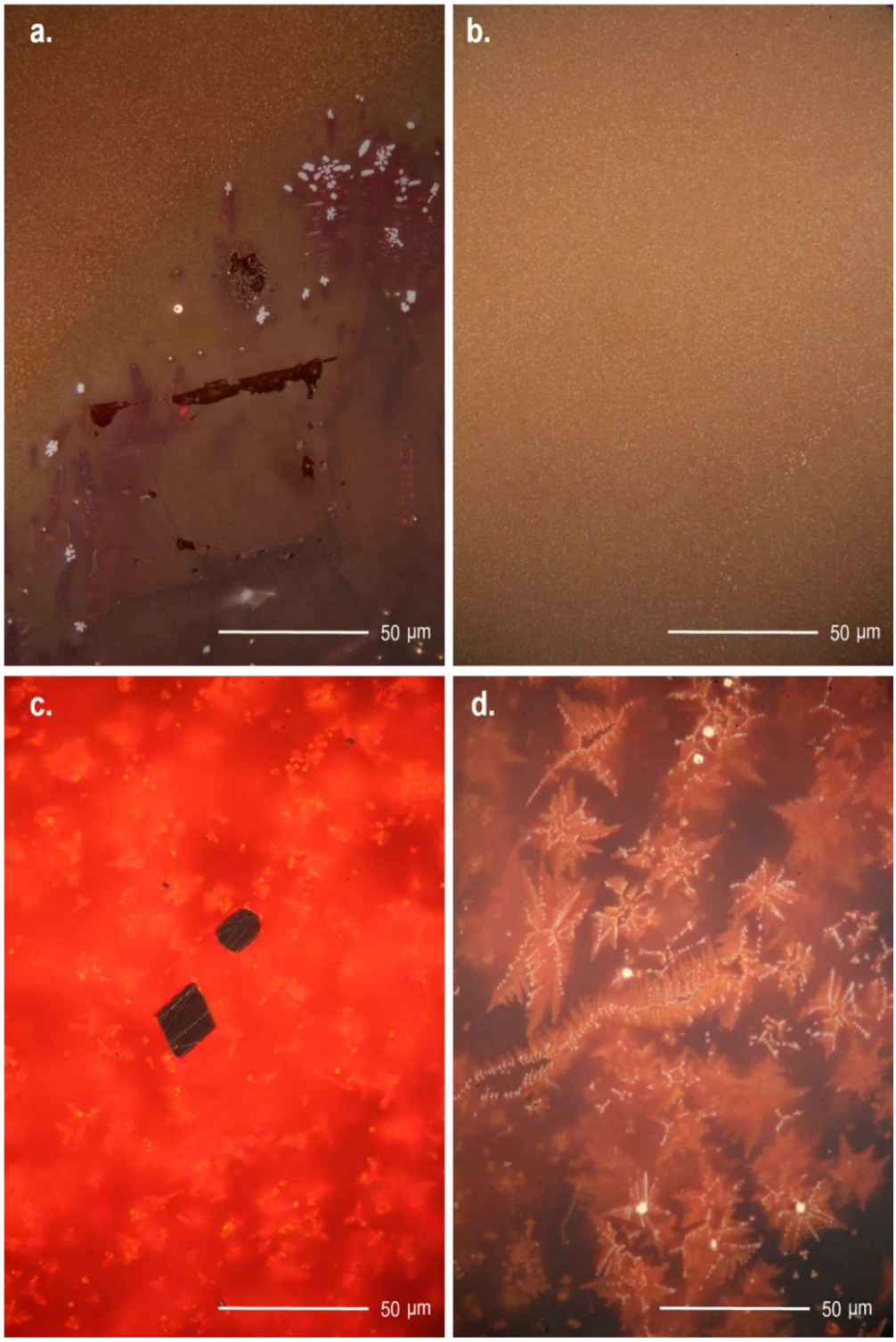

Fig. 7.3.23 – Multi-focal OM images in reflected light of cuprite-colored samples in the Tebtynis collection: a) interface between yellowish-orange and sealing-wax red glasses in sample Ty-S-GR-506 (shifted nicols): b) yellowish-orange sample Ty-S-GRT-501-Ar (shifted nicols); c) metallic copper (dark brown) and cuprite crystals in sample Ty-M-RAu-502a (crossed nicols); d) metallic copper and cuprite crystals in sample Ty-S-RV-418-R1 (shifted nicols).

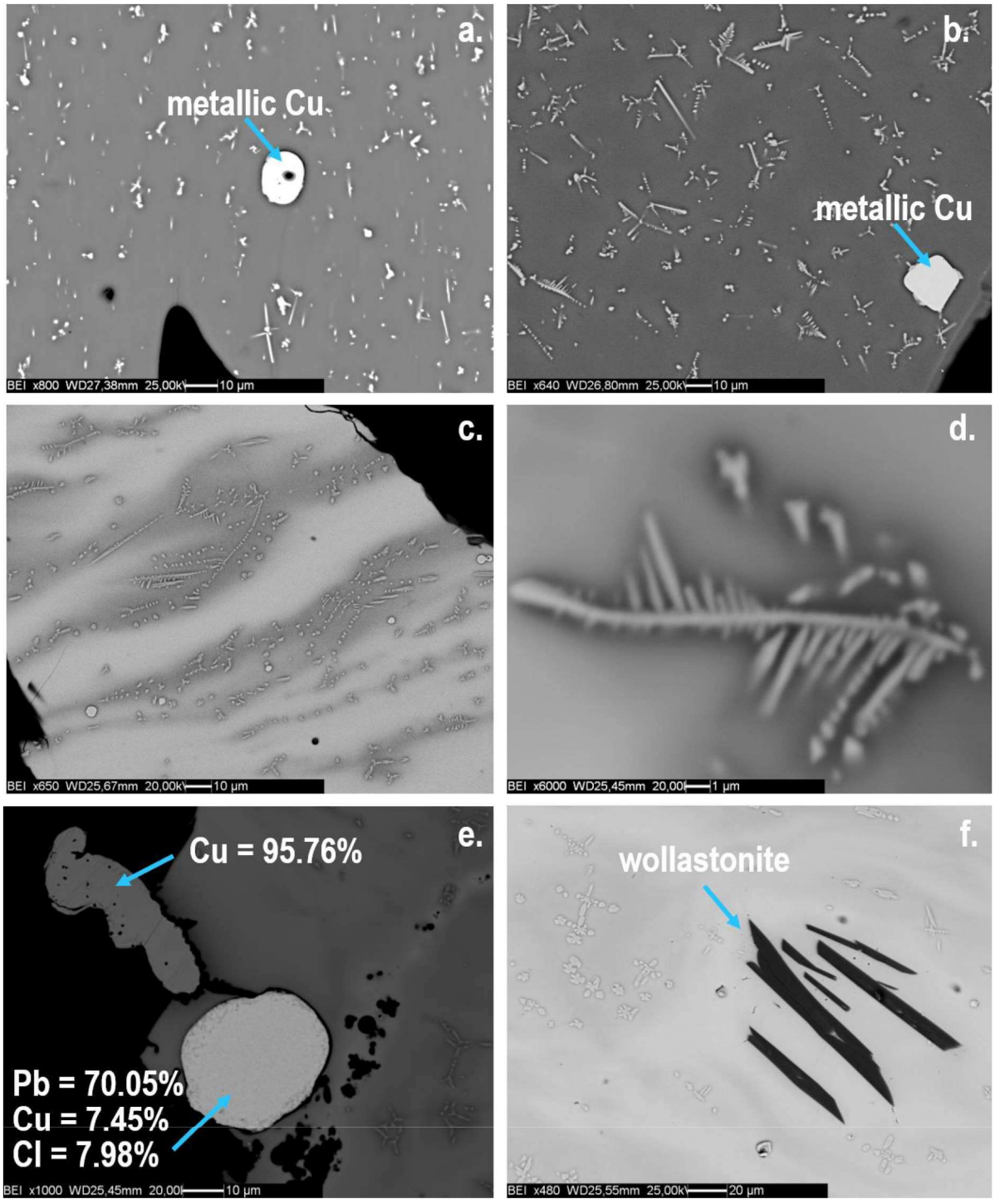

Fig. 7.3.24 – SEM-BSE mages of the texture and inclusions identified in sealing-wax red glasses from Tebtynis: a) texture of sample Ty-M-RAu-502b, with small cuprite crystallites and a drop of metallic copper; b) texture of sample Ty.M-R-507 with well-developed cuprite dendrites and a crystal of metallic copper; c) sample Ty-S-RV-418-R2 with banded texture, cuprite dendrites and a series of metallic copper drops; d) detail of a cuprite dendrite in the banded sample Ty-M-R-502d; e) inclusions of metallic copper and chloroxiphite (WDS data) in sample Ty-M-R-502d; f) wollastonite crystals in the banded sample Ty-M-RAu-502a.

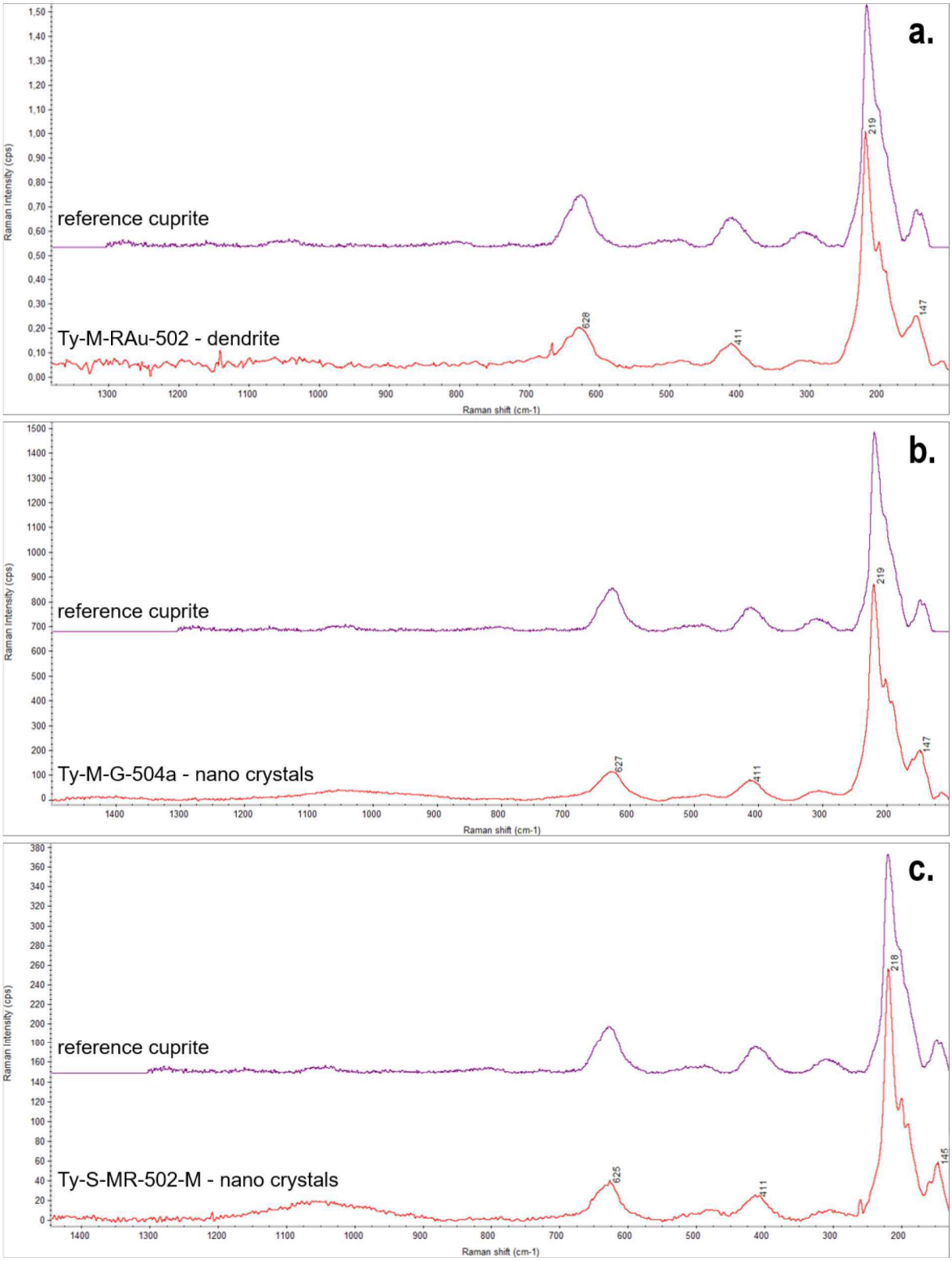

Fig. 7.3.25 – Raman spectra with standard reference spectra (RRUFF web-database) of: a) dendrite of cuprite in the sealing-wax red sample Ty-M-RAu-502; b) cuprite nano-crystals in the yellowish-orange sample Ty-M-G-504a; c) cuprite nano-crystals in the brown sample Ty-S-MR-502-M.

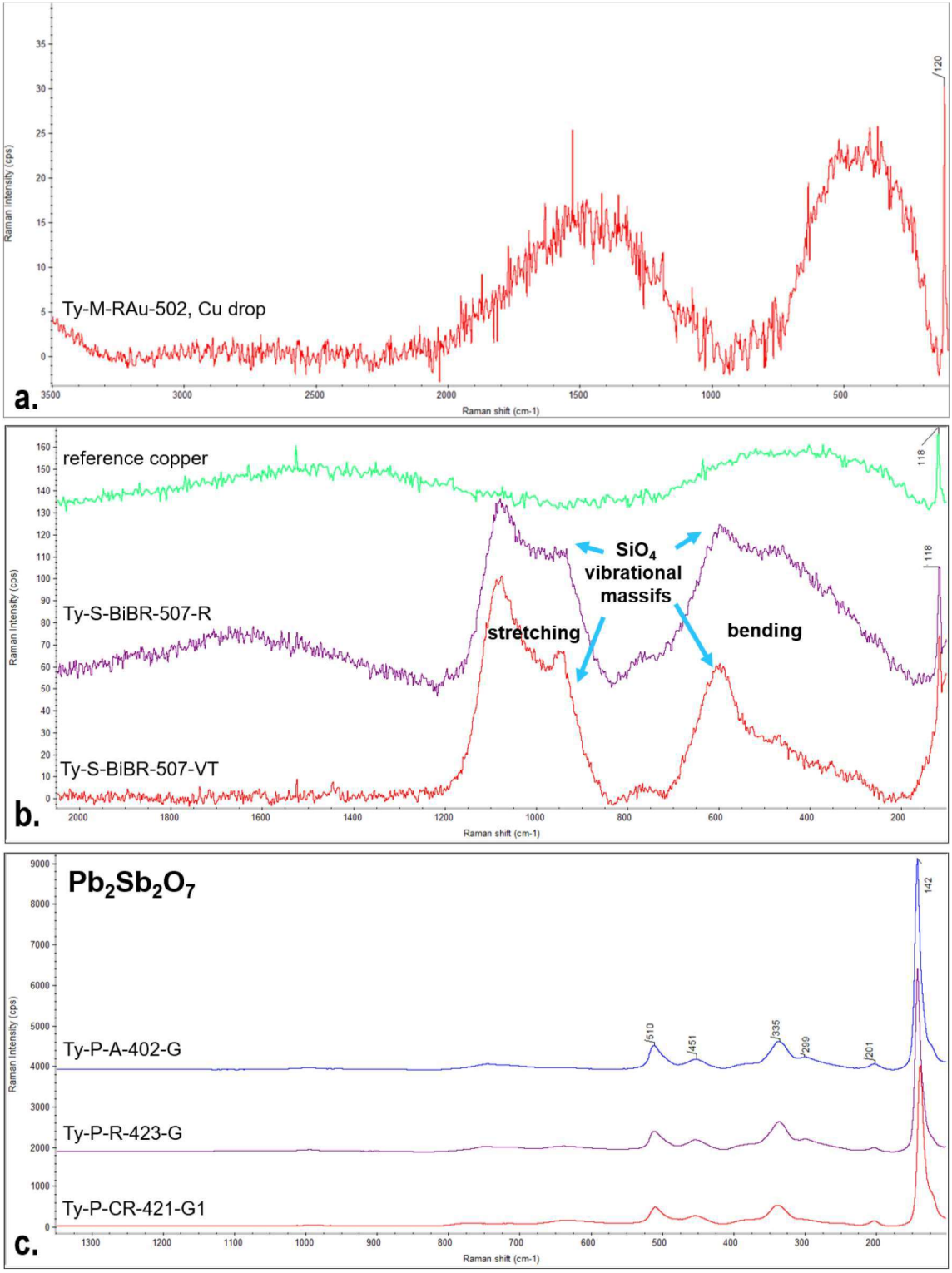

Fig. 7.3.26 – Raman spectra of: a) drop of pure metallic copper (Cu = 99.18 wt% WDS data) in the sealing-wax red sample Ty-M-RAu-502; b) glass phase of the transparent green and red glasses in sample Ty-S-BiBR-507, compared with a reference copper spectrum, note the difference in the vibrational massifs of the SiO_4 tetrahedra and the presence of the metallic copper peak (ca. 118-120 cm^{-1}); c) lead antimoniates in the yellow samples Ty-P-A-402-G, Ty-P-R-423-G and Ty-P-CR-421-G1.

8. Discussion

8.1 Outline of the literature and comparability of the results

The Hellenistic period stands as watershed in the technological evolution of glass, as it set the basis for the transformation of glass from a luxury product to a mass-produced commodity following the introduction and spread of glassblowing. It is thus natural to wonder if the birth of glassblowing can be associated to eventual changes in the composition of glass in the course of the III-I century BC. However, despite the key role of this phase, only the main points of Hellenistic recipes were investigated in detail and the glass of this period is usually regarded as a predecessor of its Roman counterpart, without specific chemical or technological markers.

Two of the major concerns, when analyzing the specialized literature, regard the frequent lack of an accurate chronological framework for the archaeological materials[1] and the low number of analyzed specimens in each dataset. The most comprehensive effort in this sense is the publication of Nenna and Gratuze (2009) on mosaic glass which considered ca. 110 samples coming from 9 archaeological sites spread around the Mediterranean. Among them, there are also 19 objects (with 33 different glasses) from the Tebtynis inlay workshop. Unfortunately, the paper does not provide the chemical data for each investigated sample and the results are only presented by means of binary plots focused on specific elements, thus preventing a possible comparison with the data acquired during this work, apart from a general, interpretative perspective.

Dussart & Velde (1990), Connolly *et alii* (2012), Rehren *et alii* (2015) and Reade & Privat (2016) analyzed glasses from various sites in Greece, Asia Minor and the Syro-Palestinian coast. A significant part of the available analyses is related to *unguentaria* and, in particular, to vessels Mediterranean Group I-II and III (according to the classification in Grose, 1989), which however partly lay outside the chronological framework of Hellenism: archaeometric data were published – among others – by Arletti *at alii* (2011), Gallo *et alii* (2014), Blomme *et alii* (2015) and Oikonomou *et alii* (2016). A

[1] The term "Graeco-Roman" is frequently used to define glasses (usually from private or public collections) with no excavation references and generically dated to the Classical Antiquity.

few mosaic *tesserae* from Italy and inlay fragments of unknown provenance, but generally dated to the same time span, were also investigated (Gedzevičiūtė *et alii*, 2009; Boschetti *et alii*, 2016). Analyses from Late Ptolemaic – Early Roman vessel glass discovered in Beyrut and other Mediterranean sites were also published by Thirion-Merle (2005).

As far as the Late Period and Ptolemaic glass is concerned, the number of investigated specimens is even more scarce. Caley (1962) summarized the previous literature in the field, starting from the early analyses of Mercantoni (Minutoli, 1836), Parodi (1908) and Jackson (Collie, 1918) which however show significant limitations: the number of elements sought after is very scarce, and sometimes couples of oxides are counted together, such as iron and aluminum or – even more problematic – sodium and potassium, preventing an understanding of the alkali source or the contribution of iron in the color of the sample. Moreover, early chemical data often lack important details about the considered samples, such as color, opacity, provenance or typology and cannot thus be used as comparative terms for the glasses analyzed during this project, if not in a very broad sense.

Lucas & Harris (1962) also report early data on Graeco-Roman glasses from Egypt, such as the slag from Mareotis published in de Cosson's work (1935) or the objects analyzed by Matson (1951).

However, in this context, the most important comparative samples are no doubt those considered by Bimson and Freestone (1988), who analyzed two ingots discovered in the foundation deposit of Osiris' temple in Canopus closely dated by royal names to the reign of Ptolomey III and Queen Berenice (ca. 246-221 BC). These objects are currently preserved at the British Museum and are constituted respectively by translucent dark blue glass (Department of Greek and Roman Antiquities, 1895 – 10-30 2) and opaque blue greenish glass (Department of Greek and Roman Antiquities, 1895 – 10-30 3). The chemical composition of the greenish ingot, with high-levels of lead (PbO 16.6%), is considered "almost unknown, except for a rather special group of opaque red glasses". However, the authors state that "so few analyses are available for the Hellenistic period that one cannot be certain whether this composition represents a typical opaque green or an aberrant opaque red".

Another fundamental dataset is constituted by the analyses published by Brill (1999), who investigated – among other samples – the various colors of the *udjat*-eye plaque in mosaic glass of the Corning Museum of Glass (inv. 59.1.96, nr. 663 in Goldstein, 1979) dated between the III-I century BC.

In recent years, the collection of mosaic glasses from the Martin von Wagner Museum in Würzburg was subject to an archaeological study, which allowed the authors to distinguish various groups in terms of chronological and possibly geographical provenance of the fragments, with some samples attributed to the Ptolemaic and Romano-Egyptian phases (Gedzevičiūtė, 2006). A selection of those objects was analyzed with μ-Raman and EPMA and constitutes the richest analytical reference for our archaeometric data, with ca. 51 investigated glasses of the same period, even without a certain geographical provenance (Gedzevičiūtė *et alii*, 2009). Another small dataset on Late Ptolemaic/ Early Roman vessel glass is included in the huge study on Bubastis published by Rosenow and Rehren (2014), which is however more focused on Roman production.

The comparability of the results is a major problem, when dealing with data acquired with different analytical techniques, given the differences in the detection limit, the accuracy and the precision. In general terms, data acquired with the same technique are more easily comparable, despite the possible differences related to the standards used, the analytical conditions (e.g. spot size for EPMA analyses) and the protocol for data calibration. The plots presented in this work consider EPMA results both obtained here and published in the literature; when comparing data from different analytical techniques (such as areal/ point-spot EDS or bulk LA-ICP-MS), the results will be discussed considering the specific differences related to the instrument and settings used.

8.2 Tebtynis glasses in context

8.2.1 *Base glass*

Just like today, in ancient times only sands with high levels of silica and low impurities were considered adequate for glassmaking, as to avoid the variations of color that could be caused by certain accessory minerals, such as iron oxides (Henderson, 2013). However, the presence of relics of the original batch may prove very useful to tentatively circumscribe the provenance of the sands used (Messiga, Riccardi, 2001).

Looking at Tebtynis samples, both chemical analyses and mineralogical characterization of the crystalline inclusions agree in suggesting that sand was the main silica source used for the production of the base glass. The sources of sand employed by the ancient Egyptian glassmakers are not readily known. Turner (1956) reviewed the analyses available to date and concluded that Egyptian sands show wide geographical differences, considering the contents of the main constituents (SiO_2, Al_2O_3, Fe_2O_3, CaO and minor MgO, K_2O). In particular, he pointed out that seashore sands near Alexandria and around the Red Sea are very calcareous (CaO up to 34%) and of high purity (Al_2O_3 + Fe_2O_3 = 0.70%), while those from the Fayoum oasis or from Hermopolis Magna, in Upper Egypt, are essentially pure silica sand, with SiO_2 around 95% and moderate Al_2O_3/ Fe_2O_3 contributions.

The high concentration and the linear correlation of iron and titanium, and the abundant ilmenite, iron oxides, corundum and zircon in Tebtynis samples imply the use of sands rich in heavy minerals, which are often associated to detrital sediments typical of costal sands (Deer, Howie, Zussman, 1992; Aerts *et alii*, 2002). Himly (1951) stated that the western Mediterranean coast of Egypt presents two different types of sands: calcareous (from the Libyan border to the beginning of the delta) and quartz-dominant, with frequent marine shells and abundant heavy minerals derived from Nile sediments transported from the Abyssinian plateau (from Alexandria to Rosetta). However, he notes that local differences are rather frequent: “in the middle part of the beach around Alexandria the calcium carbonate is represented by shell fragments. Near the mouth of the Nile River the shell fragments are not very common and quartz sands are

dominant". A few years later, El-Hinnawi (1964) published a mineralogical and geochemical survey on the gray and black sands of the Nile Delta, evidencing a significant concentration of heavy minerals, particularly ilmenite and magnetite, which were the major phases identified. Moreover, he found zircon, representing ca. 7% of the total heavy mineral fraction considered, garnet (2%), monazite (1%) and rutile (1%).

These last data are well consistent with the analyses of the Tebtynis glass samples, even if they cannot be used to demonstrate a direct connection with Mediterranean sands of the Nile Delta. In fact, heavy minerals are rather common throughout Egypt: for example, ilmenite, magnetite, rutile and zircon (among others) were found in desert sand dunes in Lower Egypt, between Dayrut and Minya, together with carbonates and feldspars such as orthoclase, microcline and sodic plagioclase (Takla, Arafa, 1975). Nevertheless, the light fraction of the considered sand is essentially composed by quartz (93%) and lacks significant quantities of Ca or Mg carbonates, that are fundamental as stabilizers for glassmaking. This problem could, however, be overcome by the deliberate addition of lime to the batch (Silvestri *et alii*, 2006).

What can be said with some certainty is that, given the peculiar association of heavy minerals in the Tebtynis samples, the base glass was definitely produced with Egyptian sands and was not acquired from the Syro-Palestinian coast, whose shoreline deposits show a very different chemico-mineralogical (and isotopic) signature, generally characterized by higher purity (Turner, 1956; Degryse, Henderson, Hodgins, 2009; Degryse, 2014). These considerations are also strengthened by the results of the trace element analyses by LA-ICP-MS published by Nenna and Gratuze (2009), that highlighted for a different set of samples from Tebtynis ZrO between ca. 60 and 130 ppm.

The high amount of feldspars (as already mentioned, especially alkali feldspars) and the rare pyroxenes observed in the Tebtynis glasses considered during this work does not help to better precise the provenance of the sand used; in any case, their relevant number must be considered in terms of a possible contribution to the overall composition of the glass: specifically, they may supply some extra potash and magnesia and thus alter the ratio classically used to distinguish the various alkali sources, as it will be discussed later.

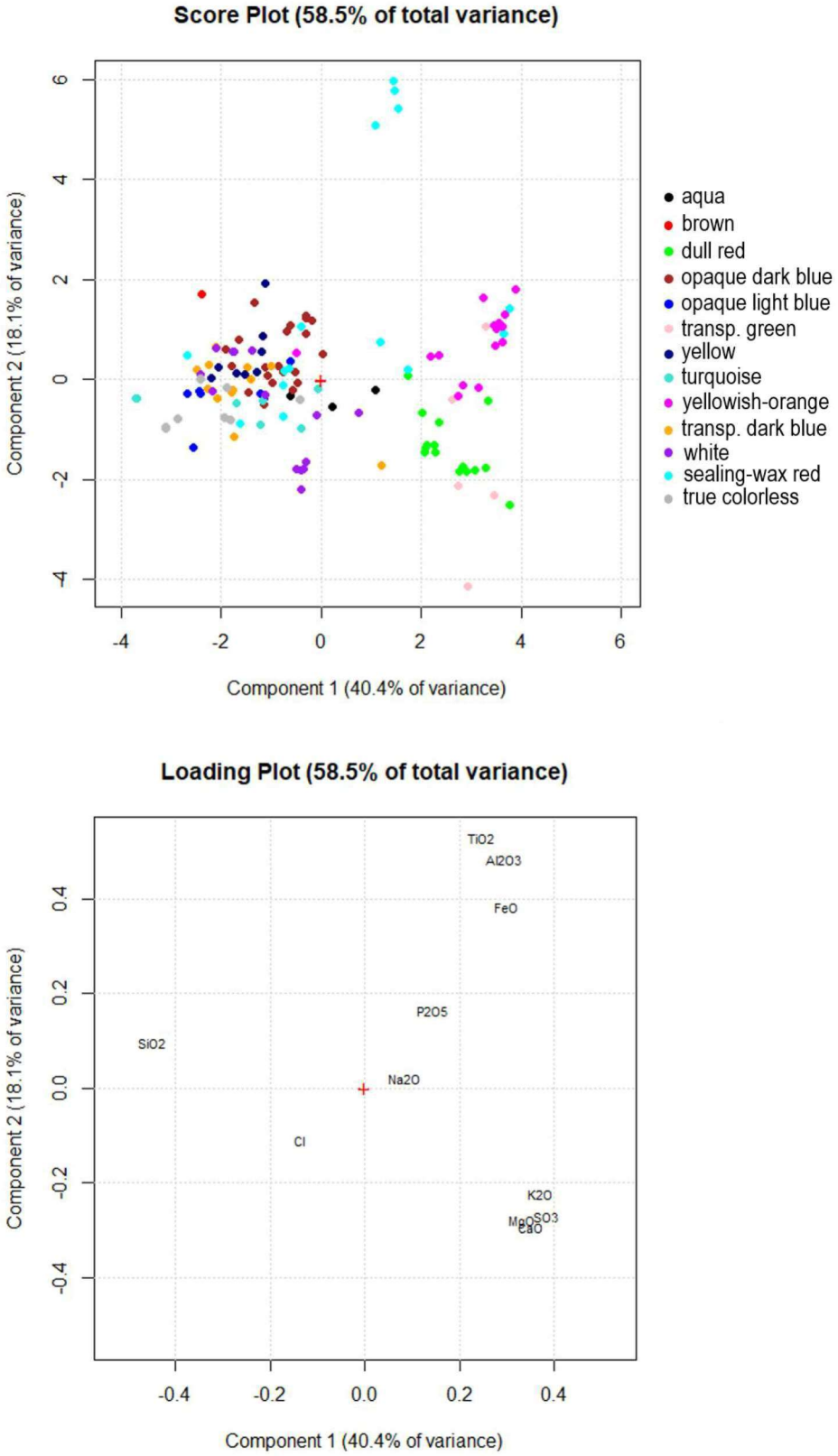

Fig. 8.2.1 – PCA score (up) and loading (down) plots of the reduced composition of the glassy matrix of the samples from Tebtynis, distinguished per color.

As previously noted, most part of the Tebtynis samples can be classified as natron glasses, with only a limited number of samples certainly associated with plant ash flux. However, several glasses, mainly opaque orange and white, showed an intermediate composition which could not be directly attributed to one class or the other. In order to try to better clarify the specific alkali source used for all the different groups identified, a reduced composition of glassy matrix was calculated[2] (see table IV in the appendix). This method is widely used in the literature (e.g. Brill, 1999; Rehren, 2000; Silvestri *et alii*, 2014) and helps to discriminate the contribution of the colorants, decolorants and opacifiers from the composition of the original glass batch.

The results of the PCA on the glass phase (reduced composition) confirm the presence of various groups (fig. 8.2.1a): most of the true colorless, brown, sealing-wax red, yellow, turquoise and blue glasses fall in a rather uniform group near the origin, which is consistent with natron glasses. The use of evaporitic salts as a fluxing agent for vitreous materials has a long tradition in Ancient Egypt, being first testified in the production of Predynastic glazed steatite (Tite, Shortland, Bouquillon, 2008). However, judging from the analyses of the Late Bronze Age (LBA) glasses, there is very limited evidence that natron might have been used at the dawn of the glass technology (e.g. Mass *et alii*, 2002; Shortland, Eremin, 2006). The low potash in a group of Co-colored glasses from the New Kingdom suggested the possibility of its use in association to cobaltiferous alums of the Western Desert (Shortland, Tite, 2000), but this evidence has been questioned in various occasions (Rehren, 2001; Tite, Shortland, 2003). The effective transition from plant ash to natron glass, seems to have started in the Third Intermediate Period, around the X century BC and was essentially accomplished in its main terms by the VIII century BC, both in Egypt and the Mediterranean (Sayre, Smith, 1961). However, it was during the Second Iron Age and throughout the Roman rule that natron became the standard flux for glass production, only to be replaced again by plant ashes around the VIII century AD (Henderson *et alii*, 2004; Fiori *et alii*, 2004; Gimeno *et alii*, 2008; Foster, Jackson, 2010; Jackson *et alii*, 2016).

[2] The oxides considered are those classically related to the silica source and alkali flux, in particular: Na_2O, MgO, Al_2O_3, SiO_2, SO_3, P_2O_5, Cl, K_2O, CaO, TiO_2 and FeO, which were followingly normalized to 100%.

According to the PCA, the anomalous group of five white glasses with very high MgO and low K_2O mentioned in section 7.2 appears as a separate sub-set of LMG glasses, possibly in excess of stabilizers. However, it is not possible to discard the possibility of the use of plant ashes particularly low in potash (Barkoudah, Henderson, 2006 and cited bibliography). Henderson (2013) has suggested the use of a mixture of natron and plant ash glass for a group of Early Medieval, white glasses from the Netherlands with unusually high MgO levels with respect to the K_2O content. Considering the very low levels of FeO and TiO_2 in all the Mg-rich Tebtynis samples, which suggest the use of pure/ purified sands, it would seem difficult that they were all produced using mixtures of glasses with different alkali sources but with equally pure sands. A combined contribution of the two alkali sources cannot be excluded, even if the Tebtynis samples seem more probably associated to an addition of stabilizers, possibly connected to the coloring process. A possible addition of talc aimed to obtain a higher opacity has been already suggested by Fiori (2014) for a Byzantine mosaic *tessera* with high Mg and very low K.

All dull red samples, together with three transparent green and one transparent blue glasses (plus, in minor measure, two aqua and one white glass) cluster in the score plot for their high levels of K_2O, SO_3, MgO and CaO, as shown in the loading plot. This composition is typical of the classic HMG glasses, produced using with soda-rich plant ash as flux, which is characteristic of all early Egyptian glasses. The *Salsola* and *Salicornia* spices, belonging to the *Chenopodiaceae* family, are some the most likely sources of soda employed by the ancient glassmakers: these plants, which grow in maritime and peri-desert environments, possess the ability to absorb alkaline salts from the soil and can thus be used to extract them by burning (Henderson, 2000; Tite *et alii*, 2006). The occurrence of HMG glasses in a Ptolemaic context is unexpected, but not unique. In fact, there are several examples of deeply colored glasses dated to the III BC – I AD and later, showing a chemical signature typical of plant ash glass (Henderson, 1996; Cosynis *at alii*, 2006). Nenna and Gratuze (2009) have also identified the use of a HMG recipe in various Hellenistic glasses around the Mediterranean, especially for red, green and amber samples. Henderson (1991), Santagostino Barbone (*et alii*, 2008) and Boschetti (*et alii*, 2016) published the results on the analyses of a series of dull red

enamels, *sectilia* panels and mosaic *tesserae* from the Roman period which show high levels of both potash and magnesia, pointing to a plant ash recipe. These data are consistent with the results on dull red glasses from Tebtynis and highlight a connection between dull red glasses and HMG-type composition. This can most likely be associated with the reducing conditions needed for the precipitation of copper in its metallic form (Cu^0), which could be eased by the presence of charcoal from plant ashes in the batch. However, considering the ritual prescriptions and the artisanal secrets connected to the ancient pyro-technologies (Oppenheim *et alii*, 1970), the long-lasting use of a traditional recipe may be another possible explanation.

Yellowish-orange glasses (together with a few sealing-wax red and transparent green samples) also stand out in the PCA as a uniform class, characterized by high levels of sand-related oxides (Al_2O_3, FeO and TiO_2) and significant amounts of MgO and K_2O, but not as high as to unambiguously imply a plant ash-type of flux. This peculiar composition is attested in various published cuprite-red and orange glasses of the Late Antiquity related to mosaic *tesserae* discovered in Italy and Turkey (Santagostino Barbone *et alii*, 2008; Schibille *et alii*, 2012; Silvestri *et alii*, 2014; Maltoni, Silvestri, 2016) and was generally interpreted as a secondary addition related to the coloring process, rather than a HMG-type of fluxing agent. In fact, Paynter's experimental data (2008) have clearly shown that fuel ashes may significantly contaminate the original composition of glass. Moreover, the K-rich Egyptian sands probably contribute in rising the average K_2O content of LMG glasses. The last compositional group that can be observed on the score plot is a set of four sealing-wax red glasses that are segregated for their very high content of Al_2O_3, FeO and TiO_2 and for the extremely low concentration of CaO, between 1.28% and 1.49%, and MgO, ranging from 0.72% and 0.84%. Interestingly, these glasses have the highest lead values of all the analyzed samples (over 30%); these aberrant values are possibly connected with the structural properties of lead, which can also act as a network modifier and thus stabilize the glass even in the case of very low lime amounts in the batch (Wang, Zhang, 1996).

Observing the K_2O *vs* MgO plot (fig. 8.2.2a), that is generally used to characterize the different compositional classes of ancient glass, Tebtynis samples perfectly fit in the context of the investigated Ptolemaic Egypt and Early Roman production. All considered

samples, despite their specific provenance and color, show similar variability in the range of K and Mg and provide interesting comparisons for specific compositional groups which were considered as anomalous, such as the high-Mg white glasses discussed above.

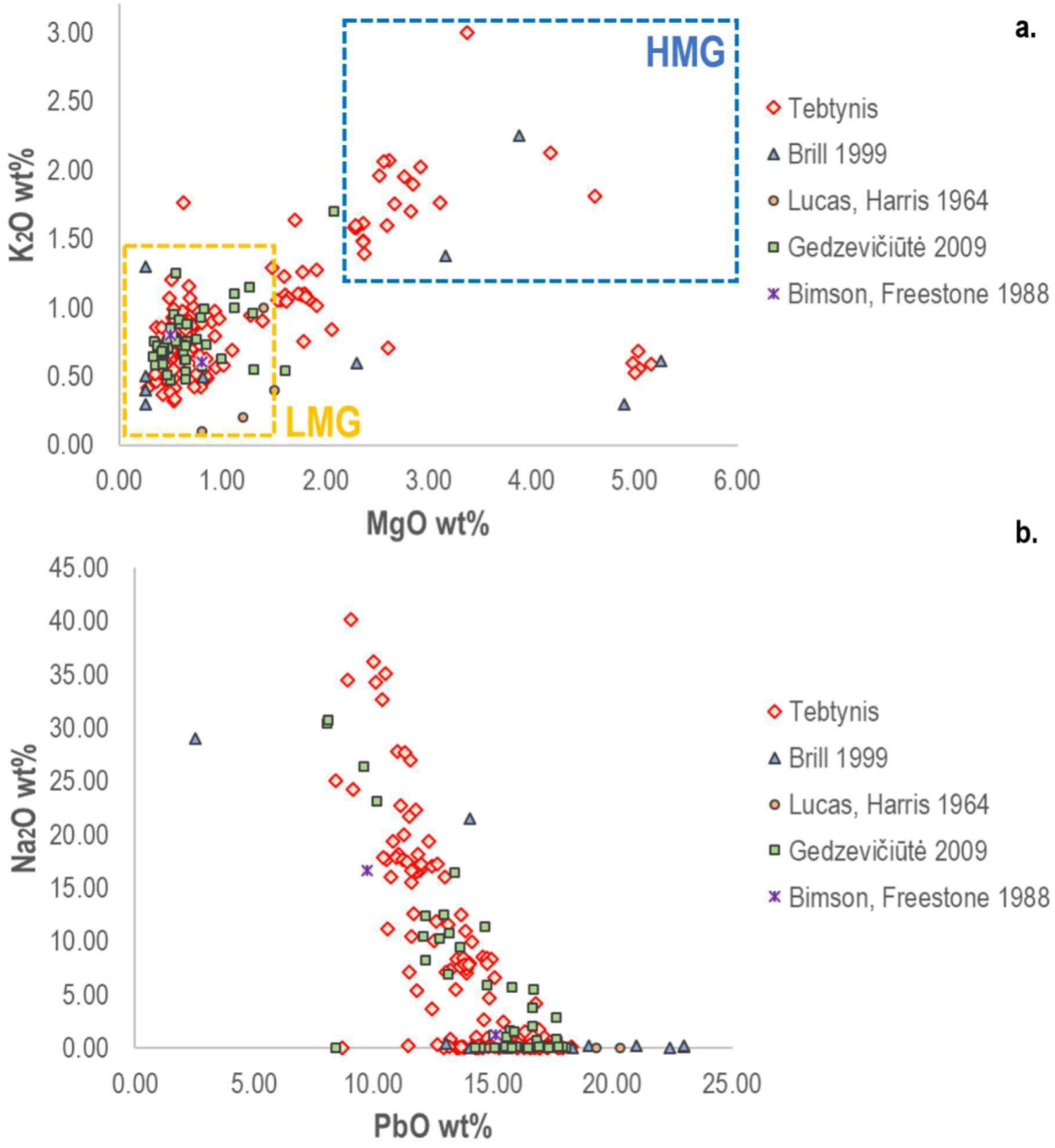

Fig. 8.2.2 – a-b) K_2O vs MgO and Na_2O vs PbO contents of the glass phase in the Ptolemaic glasses analyzed in this work (red diamonds) compared to a selection of the data published in the literature (asterisks = Bimson, Freestone, 1988; triangles = Brill, 1999; circles = Lucas & Harris, 1964; squares = Gedzevičiūtė et alii, 2009).

In fact, the analyses by Brill (1999) and Gedzevičiūtė (2009) comprise both sporadic samples with intermediate LMG-HMG composition and true HMG glasses. Moreover, the Na_2O *vs* PbO plot shows that during this phase there is a diffuse presence of leaded glasses, especially in opaque red, orange and yellow, but sometimes also in green and white samples (fig. 8.2.2b).

Considering the compositional variability of the glasses from Tebtynis, a more detailed discussion on the raw materials and the technological processes involved in the production and on the significance of the results in the trajectory of technological evolution of the glass industry (in relation to earlier and later case studies) will be presented case by case for each color-class.

8.2.2 *Coloring, decoloring and opacifying agents*

Most of the samples analyzed during this work comprise inlays in strongly colored glass. However, there is also a small proportion of colorless samples, which can be divided between non-intentionally colored, greenish glasses, labelled as aqua (3 samples) and true colorless glasses (6 samples).

The PCA (fig. 8.2.3) shows three well defined compositional groups: the first comprises two of the three aqua glasses. Considering the association with MgO, K_2O, P_2O_3 and MnO in the loading plot, these two samples stand out as Mn-decolored HMG glasses in contrast with all other samples.

The second and the third groups show the chemical signature of Sb-decolored LMG glasses with essentially no MnO (note that antimony and manganese are anticorrelated in the loading plot). However, they can be distinguished for peculiar differences especially in the contents of Na_2O (average in group 2 = 16.02% and in group 3 = 11.73%) and the FeO (on average 0.74% *vs* 0.27%, respectively).

The last aqua sample (Ty-Pn-T-001) is a LMG glass rather isolated in the score plot, due to the presence of both Sb and Mn and to the use of less purified sands with respect to the other LMG glasses of groups 2 and 3, considering the characteristic elements in the score plot, especially alumina.

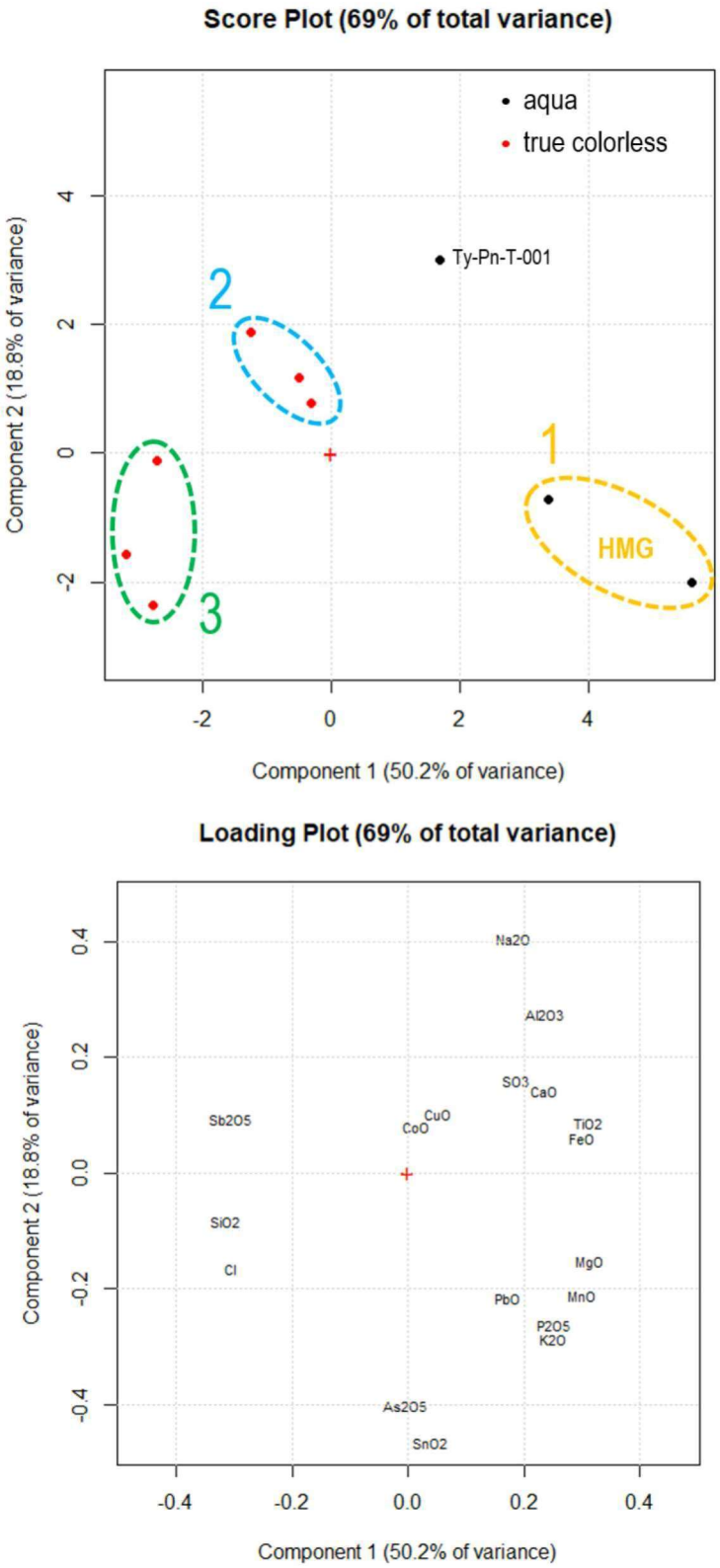

Fig. 8.2.3 – PCA score (up) and loading (down) plots of the colorless glasses from Tebtynis (all elements considered). The dotted line highlights the class of Mn-decolored, HMG glasses emerged by the statistical analysis (symbols: black dots = aqua glasses; red dots = colorless glasses).

Colorless glass is known from the LBA in Egypt and the Near East: from a compositional point of view, it was associated with very low levels of FeO and no deliberately added chromatophores. This is consistent with the use of very pure sands, or more probably – as demonstrated by the evidences of Quantir (Push, Rehren, 2007) and possibly Amarna (Nicholson, 2007) – of quartzite pebbles as silica source. The comprehensive review of Gliozzo (2016) on colorless glass and the data from previous analytical studies (among others: Sayre, 1963; Jackson, 2005; Paynter, 2006; Silvestri *et alii*, 2008; Foster, Jackson, 2010; Gliozzo *et alii*, 2015; Jackson, Paynter, 2015, Schibille *et alii*, 2016), pointed out significant trends in the popularity of the decoloring agents: antimony is usually found in pre-Hellenistic productions and is widespread during the Roman and Late Antique periods. Conversely, manganese is typical of the Hellenistic and Early Roman phases, but is also frequent in Imperial glasses and returns the main decolorant in Medieval times. The presence of both antimony and manganese in non-negligible concentrations, such as in Ty-Pn-T-001, a lump of twisted bars ready for reheating discovered in Tebtynis (Sb_2O_5 = 0.51%, MnO 0.16%), is generally considered as a marker of recycling, in perfect accordance with the functional attribution of the object (fig. 9.6a).

The results obtained on the colorless (and slightly colored) samples from Tebtynis were compared with those analyzed from the site of Bubastis (fig. 8.2.4), in the Eastern Nile Delta (Rosenow, Rehren, 2014). It should, however, be noted that the glass from Bubastis is related to Late Hellenistic and Roman vessels, with a chronological range from the I century BC to the III century AD (typological dating), and thus the considered samples are generally more recent than those from Tebtynis. Moreover, vessel glass, especially if blown, may have peculiar chemical features for improving its workability (especially in rheological terms). However, given the lack of coeval analytical data from Egypt, the glass from Bubastis offers the chance to evaluate the similarities and differences in the glass composition of two Graeco-Roman sites in Egypt.

Looking at the contents of K_2O *vs* MgO and Sb_2O_3 *vs* MnO, the picture is rather clear: in both sites, natron-type and plant ash-type recipes coexist, with LMG glasses significantly prevailing. HMG samples tend to have high levels of manganese (in the order of 0.5-1.5 wt%) and variable antimony content. The good correlation of the samples

from both sites, also in terms of major, minor and partly trace elements, may testify the existence of a long-lasting, but minor local tradition (Egyptian HMG glass) coexisting with the industrial-scale LMG production typical of the Graeco-Roman world.

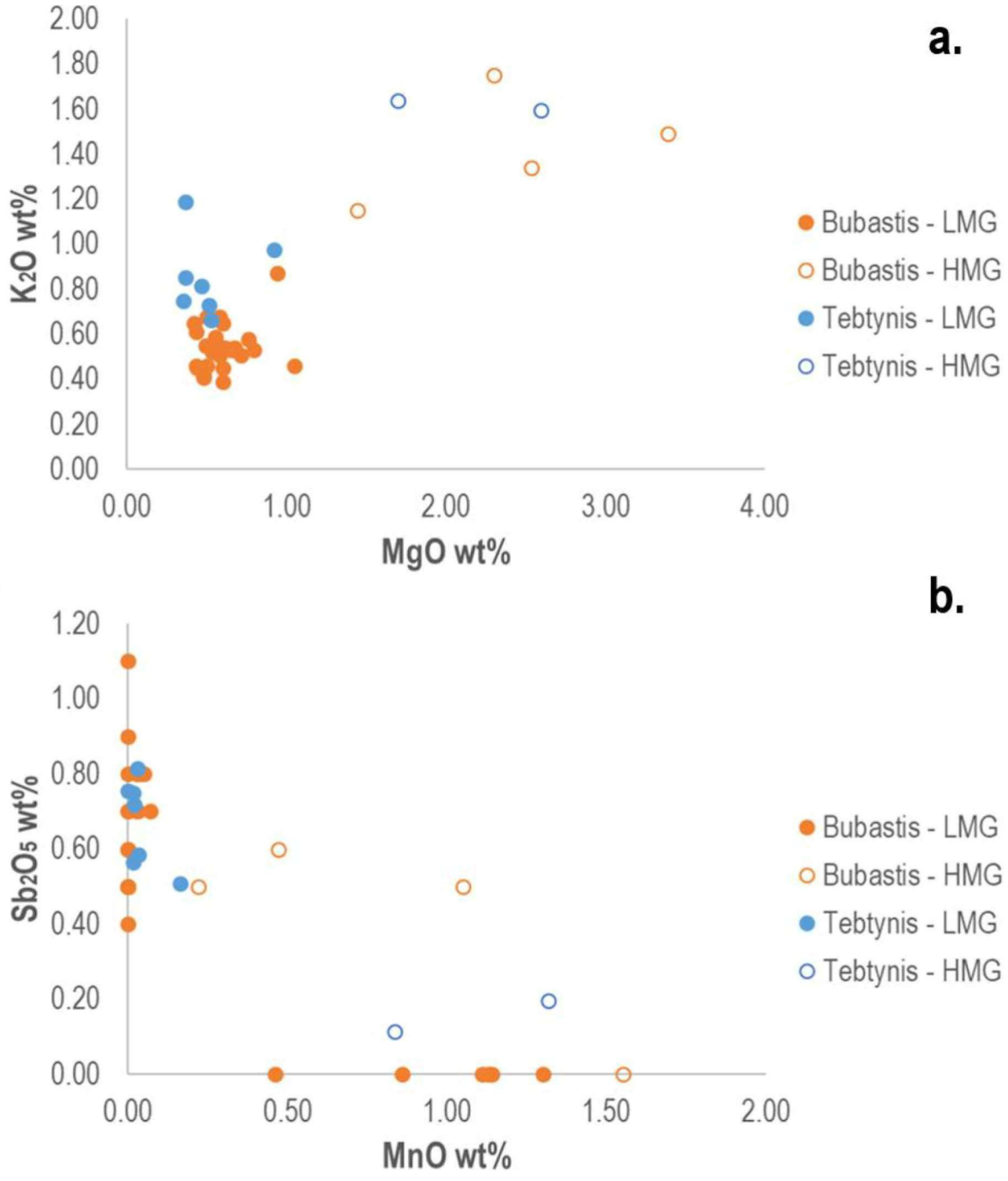

Fig. 8.2.4 – a-b) K_2O vs MgO and Sb_2O_5 vs MnO contents of the glass phase in the Tebtynis glasses (blue) compared with those of Bubastis samples published in Rosenow, Rehren, 2014 (orange). (symbols: colored dots = LMG glasses; empty circles = HMG glasses).

All the 14 white glasses analyzed in this work were sampled from polychrome objects in stratified and mosaic compositions. In the whole collection, there is no single example of white glass used on its own, for figured inlays or bars.

Again, the PCA proved to be an effective tool for the identification of compositional assemblages, as it highlighted very clearly three different classes (fig. 8.2.5):

1) classic LMG glasses, characterized by MgO and $K_2O \leq 1.5\%$, with one single example (Ty-P-T-417-Bi) of an intermediate K-rich composition ($K_2O = 1.77\%$, MgO = 0.62%), probably associated to the use of a sand particularly rich in K-feldspars, which are rather common the Tebtynis samples, or to a minor contamination of the fuel ashes;

2) soda-lime-lead and leaded LMG glasses, with PbO ranging from 7.07% to 12.55%;

3) Low-K (0.56%-0.60%) and Mg-rich glasses, having higher levels of soda and stabilizers, with MgO ranging from 4.98% to 5.16%, CaO from 6.19% to 6.25% and Na_2O from 16.26% to 16.98%, with respect to an average of MgO 0.56%, CaO 3.85% and Na_2O 13.33% in classic LMG glasses. In this group, antimony, titanium and iron are lower, an average of Sb_2O_5 2.92%, TiO_2 0.07% and FeO 0.35% in contrast with values of 5.29%, 0.14% and 0.63% respectively in the natron group.

The composition of Mg-rich glasses is similar to the one of the classic HMG glasses, but the very low potash may indicate a different recipe. The low levels of FeO seen in this class can be no doubt associated with the use of a very pure silica source. Hence, the very high levels and the correlation between the CaO and MgO concentrations (with an average Ca/ Mg elemental ratio of 1.4) and the lack of any association between K_2O/ MgO, may be the effect of a voluntary addition, deriving from a Ca- and Mg-rich source, such as dolomitic limestone (Matson, 1951; Henderson, 1985), which can be found in several outcrops in the Nile valley or in the Eastern and the Western deserts (Aston, Harrell, Shaw, 2000; Rapp, 2009; Sampsell, 2014).

Summing up, it is this argued that Mg-rich glasses probably constitute a sub-set of natron glasses produced by adding high quantities of CaO and MgO from a correlated source to pure/ purified sands.

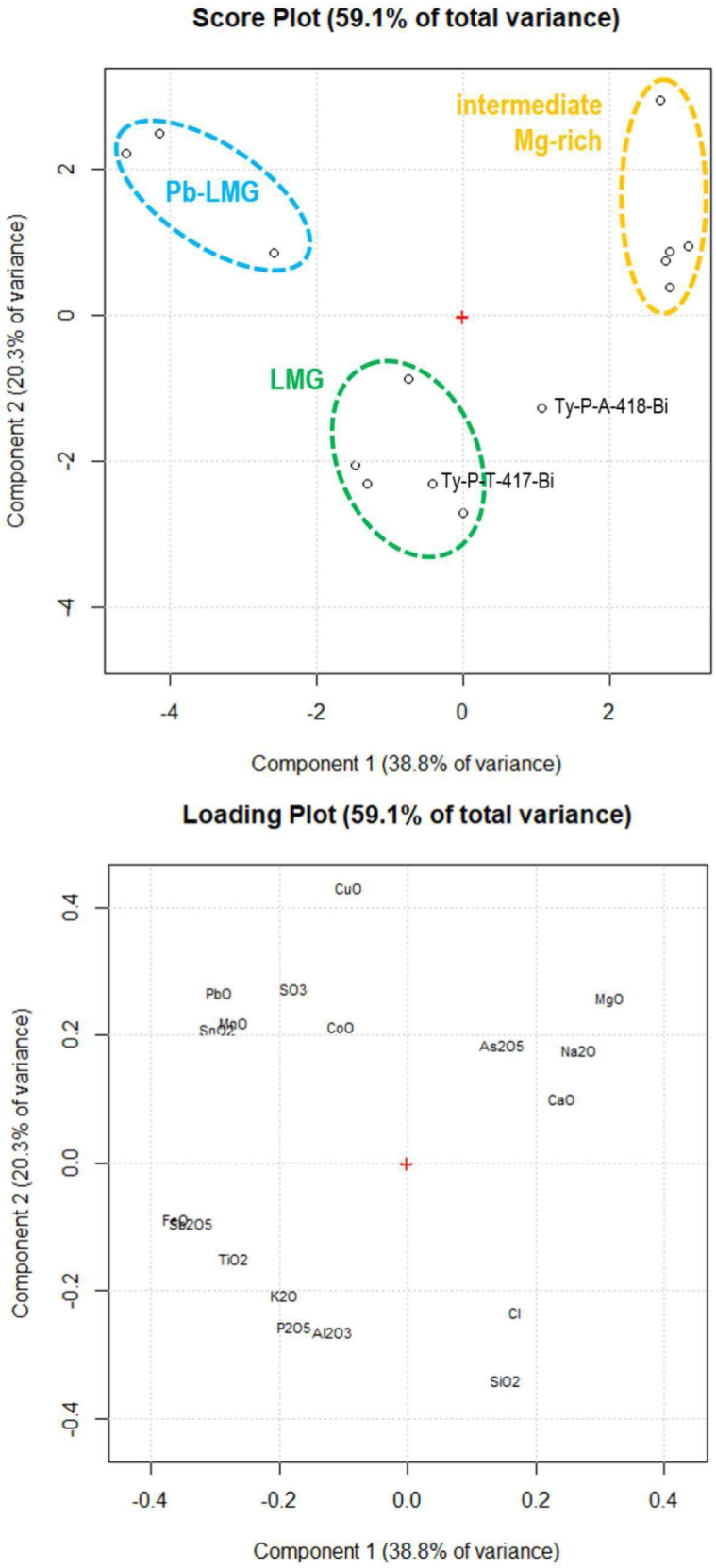

Fig. 8.2.5 – PCA score (up) and loading (down) plots of the glass phase of the white glasses from Tebtynis. Sample name were indicated only for outliers.

One analyzed sample (Ty-P-A-418-Bi) has an intermediate composition between LMG and Mg-rich glasses. However, judging from its overall composition, this sample fits relatively well in the latter group, even if the magnesia levels are slightly lower (2.61%) and lime is proportionally higher (7.89%) totaling ca. 11% CaO+MgO (as typical of this group), thus suggesting that the stabilizers were added using raw materials with different Ca/ Mg proportions.

White, opaque glass was used for trails and decorations of beads and vessels since the very beginning of the glass history in Egypt. Shortland and Eremin (2006) observed that these early compositions share a high similarity with those of colorless glasses, except for antimony, which is present in the vitreous phase in quantities around 1.5-2.5 wt%. In the Tebtynis samples, the content of Sb_2O_5 is always higher: from ca. 3% in Mg-rich glasses to an average of 5.5% in LMG and leaded-LMG glasses.

Antimony-based minerals are the main responsible of glass opacification in white, blue, green and yellow glasses since the LBA and are systematically substituted by tin-based opacifiers only in the IV century AD, despite some rare occurrences testified as early as the II-I century BC in continental Europe (Tite *et alii*, 2008). It is no surprise that all opaque white, blue and green/ turquoise glasses from Tebtynis are opacified using Ca, Na or a solid solution between Ca-Na or Ca-Na-Pb antimoniates, where Pb substitution occurs in soda-lime-lead or leaded glasses. Archaeometric analyses have demonstrated that Ca-antimoniates can be present in ancient glasses in two main synthetic phases (Shortland, 2002; Lahlil *et alii*, 2008): orthorhombic ($Ca_2Sb_2O_7$) and hexagonal ($CaSb_2O_6$). The WDS and μ-Raman analyses performed on a selection of antimoniate crystals in the opaque white, blue and turquoise glasses from Tebtynis showed that both forms are present in all color classes, sometimes even within the same sample. This has been observed various times in the literature and during experimental melts, since the hexagonal phase tends to develop at the expense of the orthorhombic one with increasing times/ temperatures during the heat treatment (Lahlil *et alii*, 2010b). In particular, the hexagonal modification starts to form at 927°C and becomes the major phase at 1094°C (Lahlil *et alii*, 2008).

One white, one turquoise and one dark blue sample from Tebtynis analyzed during this work are mainly opacified with euhedral crystals of synthetic brizziite ($NaSbO_3$),

while one light blue glass shows a mixture of brizziite and romeite (Ca, Mn, Fe, Na)$_2$(Sb, Ti)$_2$O$_6$(OH, F, O), as confirmed by the WDS data and the μ-Raman spectra. From the bibliographic research, only one other occurrence of brizziite has been identified to date in ancient glasses, specifically in one aquamarine mosaic *tessera* from the Paleo-Christian chapel of St. *Maria Mater Domini* in Vicenza (Silvestri *et alii*, 2015). In that case, the low amount of CaO (ca. 2%) was used to tentatively explain the precipitation of brizziite, rather than the classic Ca-antimoniates. This is true only for the turquoise glass from Tebtynis, which is characterized by CaO in the order of 2.03%. However, the two other samples show sufficient or even high concentrations of CaO (3.37% in the blue glass, 6.14% in the white glass), hence, a different explanation is needed. Experimental synthesis of $NaSbO_3$ with ilmenite-type structure (Ramìrez-Meneses *et alii*, 2007) have demonstrated that in specific conditions this phase can precipitate at temperatures in the range of ca. 700-900°C, that are lower than those needed for Ca-antimoniates. It may, thus, be argued that the samples containing brizziite were fired at lower temperatures, without reaching the thermal conditions for the precipitation of calcium antimoniates. Further experimental data on the *in situ* crystallization of brizziite in ancient glasses are however strongly required to clarify the matter.

The Raman signal of romeite was also frequently identified in the opaque glasses from Tebtynis. Romeite is a cubic natural mineral, belonging to the pyrochlore supergroup (Brugger *et alii*, 1997; Atencio *et alii*, 2010). Considering its chemical similarity with the classic Ca-antimoniates and the fact that it is usually a minor phase with concentrations < 1%, romeite was only identified in ancient glasses during a study on Roman mosaic *tesserae* of the II century AD performed using μ-Raman spectroscopy (Basso *et alii*, 2014), since other analytical techniques such as XRD or SEM-EDS may not be sufficient for its specific characterization (the very low content of romeite is not enough for a correct identification and quantification by XRD, as it is under the detection limit of the instrument).

Euhedral romeite was found in one single sample of a white glass[3] (crystal size ca. 2-3 μm), while in all other cases, euhedral crystals have spectra that can be attributed

[3] Suggesting that it is not an alteration phase linked to Ca-antimoniates weathering.

either to brizziite, $Ca_2Sb_2O_7$ or $CaSb_2O_6$. Conversely, anhedral aggregates (both compact and rosary-shaped) often show a mix of these various phases, as demonstrated by the frequent association of the peak at 512-514 cm^{-1} typical of romeite to the classic spectra of brizziite, $Ca_2Sb_2O_7$ or $CaSb_2O_6$ (fig. 7.3.6 and 7.3.7, pp. 148-149). It should be noted that the romeite identified in the ancient glass samples cannot be attributed to a deliberate addition of the natural mineral to the base glass. In fact, considering the shape, size and chemical variability of the inclusions (as emerged from EDS data), it should be considered a synthetic phase just as the other, better-known, Ca-antimoniates.

Looking at the SEM-BSE images of the Ca-Na antimoniate-opacified samples, four main types of texture can be recognized (fig. 7.3.11):

- texture (I) is characterized by the presence of small euhedral crystals (hexagonal or rectangular) with dimensions of 5 μm or less homogeneously, but not densely dispersed into the glass phase and often crystallized in small groups around the bubbles;
- texture (II) shows anhedral inclusions with feathery and rosary shape, lacking any evidence of crystal faces or preferential growth directions. Their size varies widely: bigger aggregates can reach up to 100 μm and often display reacted edges partially dissolved into the glassy matrix; however, the majority of the crystals is sub-micrometric with a dense distribution, which produces a sort of flour-like effect in the glassy matrix;
- texture (III) exhibits a hybrid microstructure, that combines rosary-shaped aggregates and rare euhedral crystals of micrometric size, alone or in small, segregated groups. In texture (III), feathery and rosary-shaped inclusions sometimes show preferential growth directions, with angles typical of the hexagonal system;
- texture (IV) was distinguished for the presence of a limited number of isolated, angular lumps with dimensions ranging from 70 to 100 μm, showing euhedral crystalline inclusions dispersed in a heterogeneous matrix.

Texture (II) and (III) are especially found in white, light blue and turquoise samples, while dark blue glasses can be mainly attributed to texture (I) and, in minor measure, (III). Texture (IV) was only identified in one single, dark blue sample.

These micro-textural differences reflect the use of various production technologies for the opacification of the glass. Hence, the presence of small crystallites showing well-defined euhedral morphologies, with a medium to low number of crystals per unit area typical of texture (I) implies *in situ* crystallization. It has been suggested that antimony was intentionally added to the melt in the form of stibnite (Sb_2S_3) or roasted stibnite, i.e. Sb_2O_3, Sb_2O_5 (Bimson, Freestone, 1983; Mass *et alii*, 1997), triggering the precipitation of calcium antimoniate crystals and subtracting lime from the glass phase. However, the average CaO contents in transparent and opaque dark blue glasses characterized by texture (I), are rather similar (5.28% and 5.40% respectively), possibly suggesting that for the production of the Tebtynis dark blue glasses, an extra supply of CaO was contextually provided. This would also seem strengthened by the tendency towards a rough correlation between calcium and antimony in the opaque dark blue samples (fig. 8.2.6a).

The lower values of Sb_2O_5 and the double contents of FeO and TiO_2 in the opaque dark blue glasses with respect to the opaque white samples clearly indicate that Co and Cu were not added to a white glass for coloring purposes. Similarly, the opaque glasses from Tebtynis are not the result of a mix between opaque white and transparent dark blue glass, as opaque dark blue samples contain on average higher CuO and CoO if compared to their transparent counterparts, thus implying that they were not diluted with white glass for opacification purposes.

The sub-micrometric, widespread crystals, sometimes aggregated in rosary- and feathery-shaped inclusions typical of texture (II) seem more consistent with the *ex situ* opacification process with calcium antimoniate nano-crystals that was proposed by Lahlil (*et alii*, 2010a) for LBA Egyptian glasses[4]. In fact, since $Ca_2Sb_2O_7$ progressively transforms into $CaSb_2O_6$ with higher temperatures/ longer firing times, it was proven

[4] This process implies the preliminary synthetization of Ca-antimoniates nano-crystals which are followingly added into a translucent glass.

that in the case of an *in situ* nucleation, when $Ca_2Sb_2O_7$ is the major phase, crystals cannot be of nanometric size. Nano-crystals of $Ca_2Sb_2O_7$ were observed in various white and turquoise samples through μ-Raman examination, suggesting that these glasses were probably produced with an *ex situ* process. However, a paper of Duckworth (*et alii*, 2012) has questioned this assumption after analyzing two rosary-shaped inclusions in two different samples of LBA turquoise and white glass, respectively. Time of Flight Secondary Ion Mass Spectrometry (ToF-SIMS) showed that the average composition of the micro-crystals is similar to that of the glassy matrix, this suggesting a direct precipitation from the melt. The problem should thus remain open until conclusive experimental data will be presented.

Mixed texture (III) shows clear evidence of *in situ* nucleation, considering the presence of both directions of preferential growth for the rosary-shaped inclusions and euhedral crystals. However, at the moment, it is not possible to determine if it is a primary crystallization directly from the glassy matrix or if the precipitation of the Ca-Na antimoniates is secondary and due to the presence of intentionally added opacifiers, partially dissolved and recrystallized into the glass phase.

Finally, texture (IV) can be attributed to the voluntary *ex situ* addition of lumps of crushed, pre-fritted opacifiers incorporated into the glassy matrix at relatively low temperatures. This evidence bears a certain similarity with the *corpo* process used to produce contemporary mosaic *tesserae* in Venice (Lahlil *et alii*, 2008). In this case, a vitreous phase very rich in *in situ* precipitated Ca-antimoniates is synthetized independently, ground and added to a transparent glass of the desired color. The quantity of the *corpo*, its size and distribution can be used to calibrate the opacity in the glass.

Summing up, the Tebtynis samples show that both *in situ* and *ex situ* techniques were in use at the same time in Ptolemaic Egypt and that general preferences for one process or the other can be broadly (but not systematically) seen between the different opaque color classes.

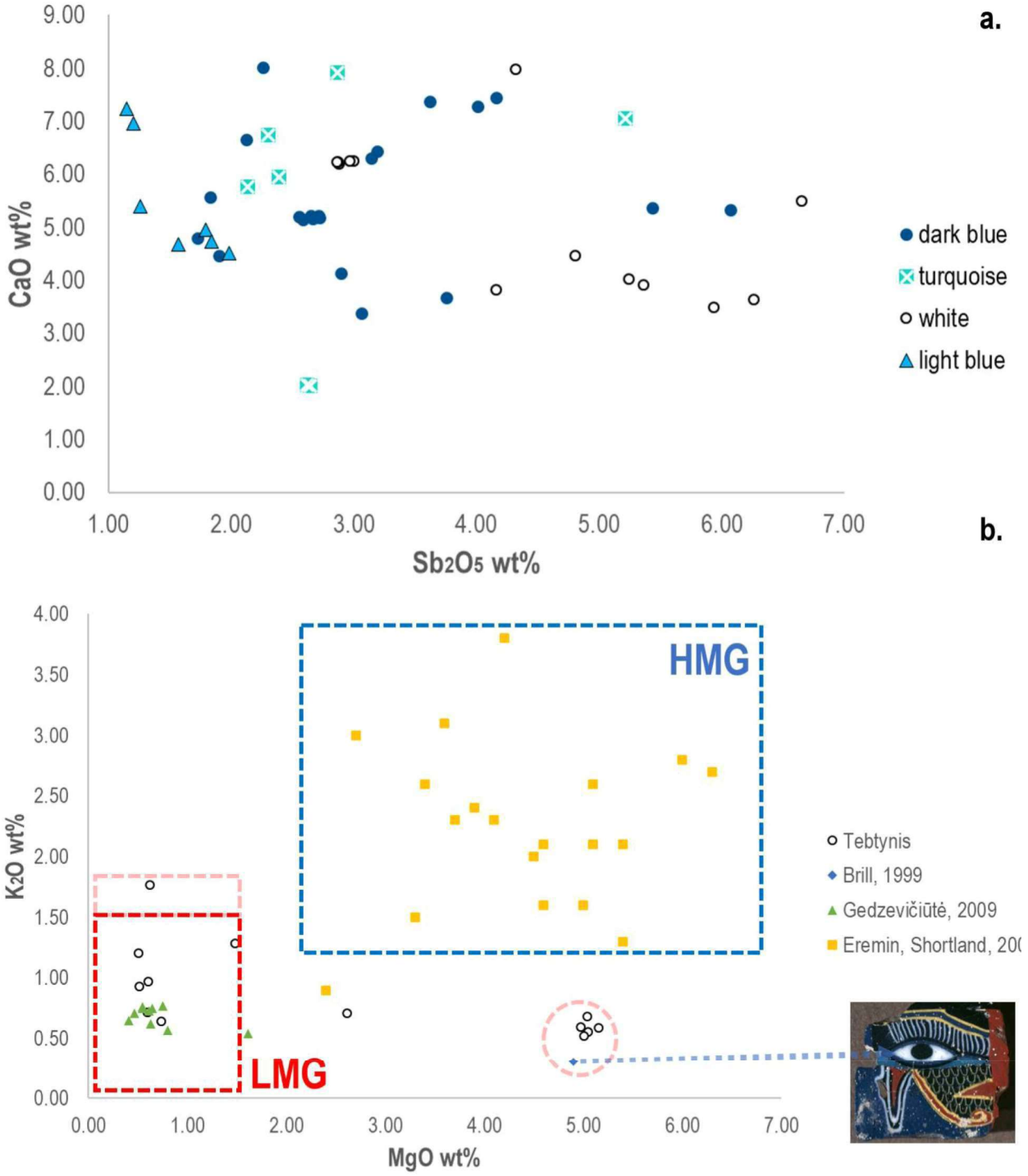

Fig. 8.2.6 – a) CaO vs Sb_2O_5 contents of the glass phase in the Tebtynis glasses opacified with Ca and Na antimoniates (symbols: the colors of the symbls are related to the macroscopic color of the samples); b) K_2O vs MgO contents of the glass phase in the Tebtynis white glasses (symbol: white dots) compared with a series of LBA white glasses published by Shortland and Eremin, 2006 (symbol: yellow squares) and with various coeval glasses analyzed by Brill, 1999 (blue diamonds) and Gedzevičiūtė et alii, 2009 (symbol: green triangles). Compositional classes from Henderson, 2013 are defined by dotted lines.

Looking at the white samples from Tebtynis in the context of earlier (LBA) and coeval Egyptian glasses (fig. 8.2.6b), it is possible to distinguish fairly well the various chronological productions on the basis of the alkali source. Moreover, it is interesting to note that no LBA plant ash glass is associated with the intermediate Mg-rich composition identified in five of the Tebtynis samples, while an *udjat*-eye mosaic plaque dated between the III and the I century BC (Goldstein, 1979) shows the same recipe (Brill, Moll, 1963; Brill, 1999), thus evidencing that this compositional signature can possibly be considered as a marker of a group of Ptolemaic glasses from Egypt. The presence of Mg-rich white glasses has also been noted by Nenna and Gratuze (2009), that found this peculiar composition in several of their Hellenistic samples discovered in various sites in Europe and Africa (Avenches and Augst in Switzerland and Heis, in Somaliland) and in some unprovenanced samples from the Gorga collection.

The PCA of the blue samples of the Tebtynis collection highlights three main compositional classes, well correlated with the macroscopic appearance of the glasses. Essentially, opaque light blue glasses have higher CuO and Sn_2O content, and lower FeO and TiO_2; opaque dark blue glasses show higher levels of CaO, Sb_2O_5 and PbO and share with transparent dark blue glasses a higher CoO content with respect to the light blue glasses. Transparent dark blue glasses have higher Na_2O and SiO_2 content and generally lower Sb_2O_5, with a few exceptions. In brief, the color of all blue glasses from Tebtynis is due to ionic colorants, i.e. copper (in light blue samples), cobalt or a combination of cobalt and copper (in transparent and opaque dark blue samples, with CuO always $\leq 0.72\%$). Opacity, when present, derives from the dispersion of Na and especially Ca-antimoniate inclusions in the glassy matrix, as discussed above.

Moreover, the PCA shows that two samples do not belong to the three groups previously described for blue glasses: one Co-colored, transparent HMG glass one heavily leaded-LMG sample, as shown by the associated elements in the loading plot. Additionally, the PCA confirms a partial overlapping of the opaque and transparent dark blue groups. As already suggested in the chapter 7.3, this indicates that opaque dark blue glasses were probably produced by adding opacifiers or inducing their precipitation into a (Cu)Co-colored transparent dark blue glass.

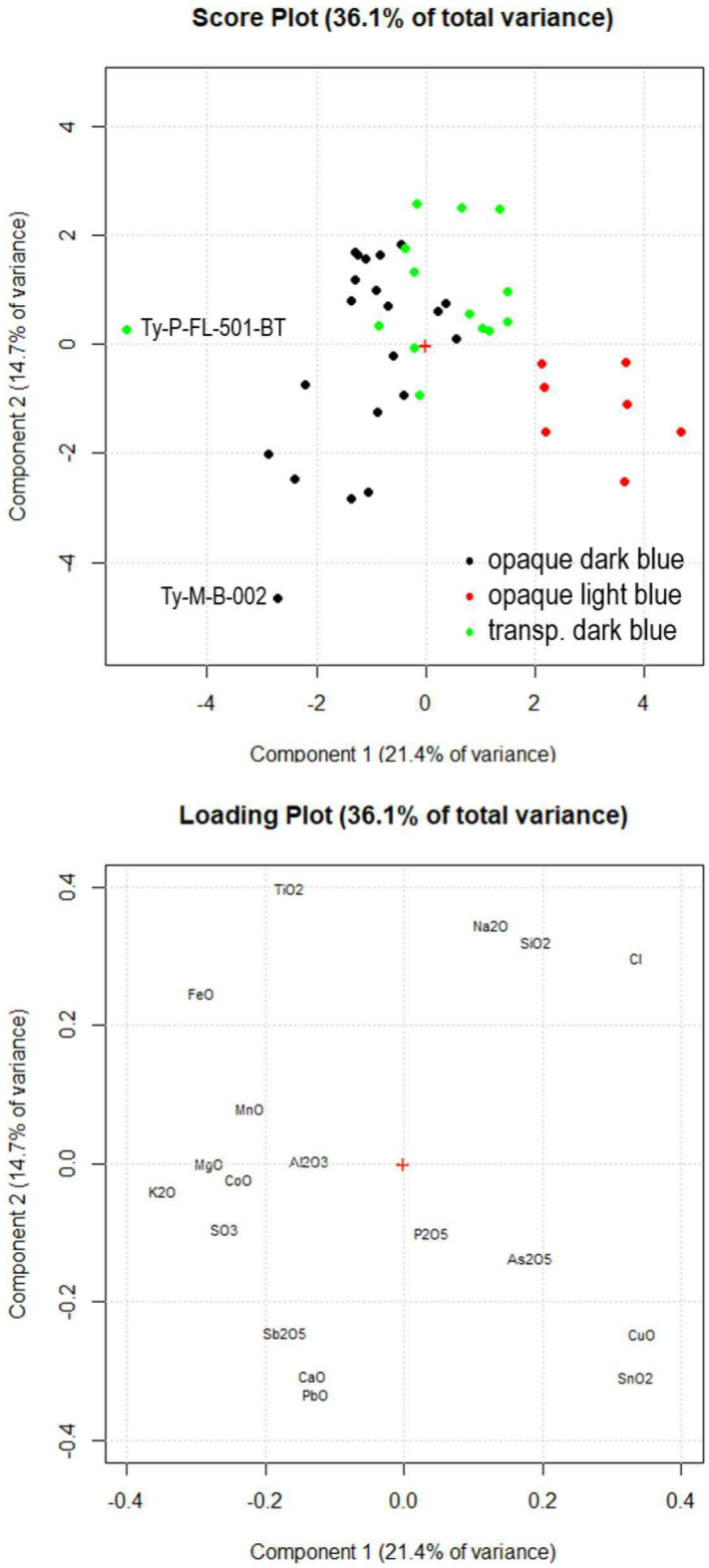

Fig. 8.2.7 – PCA score (up) and loading (down) plots of the blue samples from Tebtynis. Sample names are given only for the outliers, while all other glasses are only classified according to the macroscopic color-groups they belong to (symbols: black dots = opaque blue glasses; red dots = light blue glasses; green dots = transparent blue glasses).

Copper is the earliest and most common chromophore used for vitreous materials in glazed steatite, faience, glassy faience, Egyptian blue and green frits (Tite, Shortland, 2008) and, later, glass (Tite, 1987). Cu^{2+} can produce various shades of blue or green, according to its concentration, the association with other intentional or unintentional (de)colorants and opacifiers and the composition of the base glass. Starting from the LBA, traces of tin appear in Cu-colored glazes of faience objects (Kaczmarczyk, Hedges, 1983) sometimes with ratios Cu:Sn close to 10:1 by weight, suggesting that bronze started to be employed as copper-bearing raw material, in parallel with mineral sources.

Considering the Tebtynis samples, tin is essentially absent or very low (≤ 0.05%) in opaque and transparent dark blue glasses, while it is always present in the light blue glasses (Sn from 0.07% to 0.19%). The Cu:Sn ratio by weight shows a linear correlation in all light blue samples and in a few opaque dark blue glasses, ranging between 13 and 28 (fig. 8.2.8a). The lowest values are compatible with a low-Sn bronze alloy (Odgen, 2000), while in most cases, if scrap bronze was used, some extra copper must have been (intentionally or unintentionally) supplied from other sources. This hypothesis is strengthened by the identification of a huge copper chip (ca. 40 μm) in one of the opaque dark blue samples from Tebtynis (EDS data: Cu 98.5 wt%, Sn 0.3 wt%), which suggests that – at least in certain cases – pure copper was added as an independent coloring agent.

Cobalt is the strongest coloring agent used in antiquity, as it can impart a distinct blue color to the glass in concentrations of 0.05 wt% or even lower. However, noteworthy levels of copper have been reported in various Co-colored glasses of a wide chronological time span, which led to the hypothesis of a voluntary addition aimed to enhance the final color (Shortland, 2012). The earliest Co-colored glasses appeared in New Kingdom Egypt: various experimental and analytical studies have ascertained that the origin of the main mineral ore employed until the VII century BC (with a possible break caused by the political instability of the Third Intermediate Period) is the cobaltiferous alum from the Western oases of Egypt, as demonstrated by the presence in the glassy matrix of Co and related amounts of a series of paragenetic elements, especially Al, Ni, Zn, Mn and As (see e.g. Farnsworth, Ritchie, 1938; Bachmann *et alii*, 1980; Kaczmarczyk, Hedges, 1983; Rehren, 2001; Shortland *et alii*, 2006; Abe *et alii*, 2012; Smirnou, Rehren,

2013; Seccaroni, Haldi, 2016). Glasses produced using cobalt from Egyptian mineralizations have been identified throughout the Mediterranean and even in continental Europe starting from the LBA (Gratuze, Picon, 2005; Nikita, Henderson, 2006; Jackson, Nicholson, 2010; Varberg *et alii*, 2015).

According to Kaczmarczyk and Hedges (1983), during the Late Period and especially throughout the Ptolemaic and Roman era, Egyptian Co-colored faience glazes exhibit significantly lower values of MnO than in the previous phases. The authors associate this compositional change to a technological shift from the exploitation of the cobaltiferous ores of the Western desert to the discovery of different mines of Mn-free, Co-bearing sulphides and arsenides, which were tentatively suggested to be located in Iran (Kaczmarczyk, Hedges, 1983). Among the analyzed dark blue samples from Tebtynis, there is no evident correlation between CoO and Al_2O_3 and neither between CoO and MgO or Sb_2O_5 (for Sb_2O_5 only transparent samples were considered). There is, however, a discrete correlation between CoO and MnO in a group of dark blue glasses (mainly transparent), suggesting that the two elements might derive from the same source (fig. 8.2.8b). Unfortunately, due to instrumental problems, it was not possible to measure the NiO and ZnO contents in the Tebtynis glasses. Thus, at the moment, there is no chance to propose a specific provenance for the related cobaltiferous ore. What can be said with good confidence is that the ratio MnO/ CoO is very different from that of the coeval manganese-free faience glazes; this seems to suggest that minerals of the asbolane group might have been used as the cobalt source. However, no specific chemical markers linked to the provenance of the raw material could be identified to date.

Another possible explanation for the corelating values of cobalt and manganese can be traced in the (de)coloring properties of this element. In fact, in a Venetian recipe book of the XVI century AD it is explicitly noted that when blue glass has a purple tint, the color gets more deep and shiny (Seccaroni, Haldi, 2016). One transparent dark blue sample from Tebtynis has a peculiar zoning consisting in bands with varying amounts of CuO, CoO and MnO, anticorrelated the FeO values, which is the result of the uneven mixing of the coloring agents into the glassy matrix. This further proves the association between CoO, CuO and MnO (and the lack of a direct relation with Al_2O_3, As_2O_5, Sb_2O_5

and PbO), but again it does not give hints about the raw materials used. It is hoped that future research will help to shed light on this critical issue.

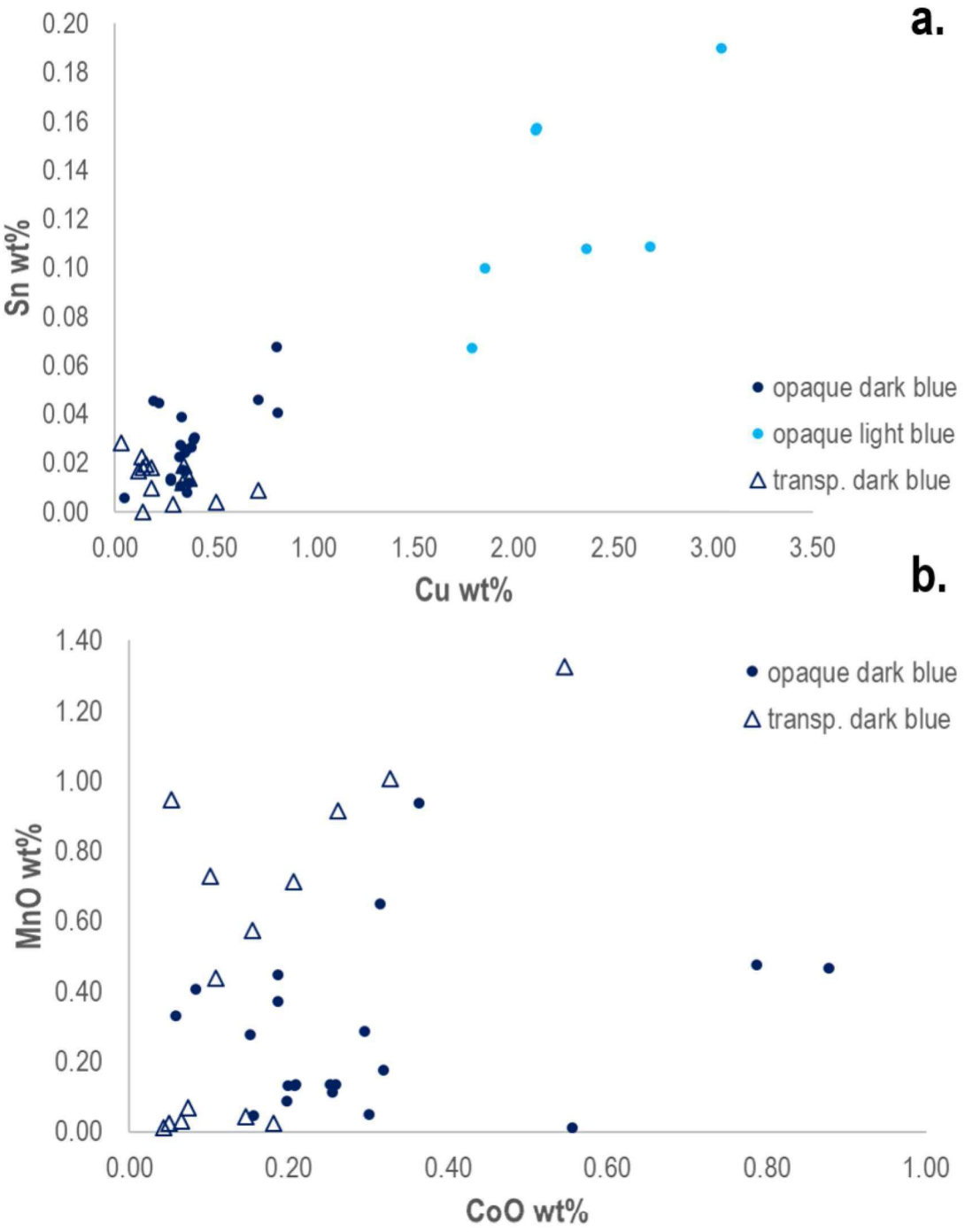

Fig. 8.2.8 – a) Sn vs Cu content in the glassy matrix of the blue samples from Tebtynis; b) MnO vs CoO in the gassy matrix of the (Cu)Co-colored dark blue glasses from Tebtynis (symbols: empty triangles = transparent glasses; colored dots = opaque glasses; the colors of the dots are related to the color of the samples).

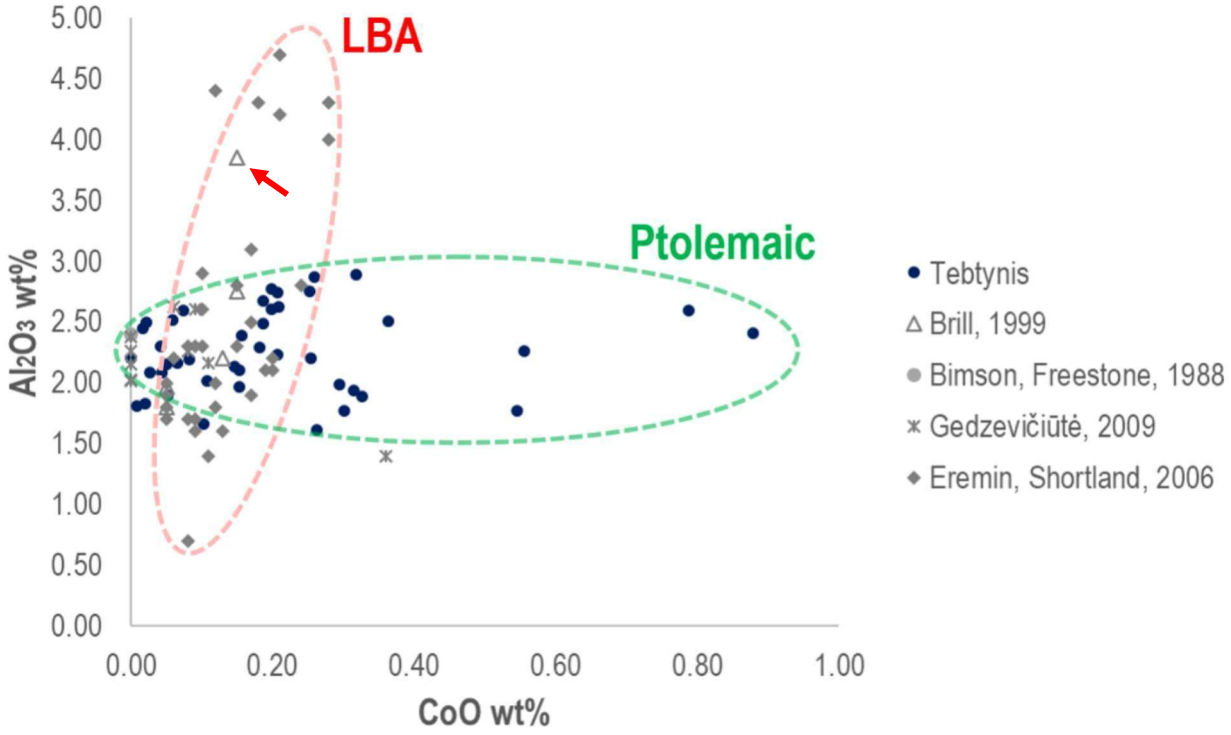

Fig. 8.2.9 – Al_2O_3 vs CoO content in the glassy matrix of the blue samples from Tebtynis (dark blue dots) and from other earlier and coeval sites considered in the literature, specifically: LBA glasses from Shortland, Eremin 2006 (gray diamonds) and Late Period and Ptolemaic glasses published by Brill, 1999 (gray triangles), Bimson and Freestone, 1988 (gray dots) and Gedzevičiūtė et alii, 2009 (gray asterisks). Chronological trends are defined by dotted lines.

Considering the Tebtynis (Cu)Co-colored samples in a diachronic perspective, the difference with LBA productions becomes apparent. The Al_2O_3 *vs* CoO plot highlights two well defined compositional trends (fig. 8.2.9): while in LBA glasses Al_2O_3 drastically increases with increasing CoO content, during the Ptolemaic period alumina is independent from cobalt and ranges in the variability of the sand-source, as shown by the analyzed specimen and other coeval samples. Moreover, the average amount of cobalt per sample seems to rise significantly moving towards the Roman period, which can perhaps be linked with a wider availability of the raw material.

The outlier sample from Brill (1999, cat. 3377, UC 25037) indicated by the red arrow in figure 8.2.9 is given in the volume as "late or of uncertain date", but considering its Al/ Co ratio, the high Mg and low K content, it can be more properly ascribed to the New Kingdom.

Green samples from Tebtynis can be essentially divided in two main categories on the basis of their textural and chromatic features: transparent green (5 samples) and opaque turquoise (7 samples). Looking at the PCA (fig. 8.2.10), turquoise glasses exhibit a good compositional consistency, having high Sb_2O_5, low FeO (0.19-0.87%) and moderate to high amounts of copper (1.58-5.48%), that reflect the recipe of Cu-colored and antimoniate-opacified LMG glasses. Transparent green samples are clustered in two groups, indicating that they were produced using different raw materials: three samples are characterized by high levels of CaO, K_2O, MgO and FeO, which are consistent with plant ash glass colored by a mixture of Fe^{2+} and Fe^{3+} ions (CuO is very low, from 0.02% to 0.3%, not sufficient for coloring). Conversely, two samples have significant concentrations of PbO, CuO, Al_2O_3 and SnO_2 and can be interpreted as leaded-LMG glasses colored with copper (4.85 wt% and 5.35 wt%) and iron (1.48 wt%-1.79 wt%).

As already noted, turquoise glasses are opacified by means of Ca-antimoniate inclusions, often characterized by anhedral habit and minor substitutions of Ca with Na and, more frequently, low amounts of Pb (when present, it usually accounts for the 2-4 wt%). This is consistent with what is reported in the literature on Ptolemaic (Bimson, Freestone, 1988) and Roman glass (Gedzevičiūtė *et alii*, 2009; Basso *et alii*, 2014; Silvestri *et alii*, 2014), even if examples of Pb-antimoniate (Gliozzo *et alii*, 2010; Basso *et alii*, 2014; Boschetti *et alii*, 2016) or cassiterite-opacified (Gedzevičiūtė *et alii*, 2009) green glasses were also reported, but mainly dated to the Late Antiquity. Lead antimoniate, in association with copper, is also known as the main colorant/ opacifier in the few analyzed LBA opaque green glasses from Egypt (Shortland, Eremin 2006), but has not been identified in the Tebtynis samples analyzed during this work.

Out of the three transparent green HMG glasses, one (Ty-S-BiBR-507-VT) is characterized by major levels of PbO (8.55%) and by the presence of a chalcocite drop (WDS data) with maximum diameter of ca. 50 μm. OM images in reflected light and crossed nicols show that the glassy matrix around the copper sulfide is gradually turning from transparent dark green to opaque red thanks to the presence of a number of nanometric crystalline inclusions. This is a clear evidence that an incipient coloring process is taking place within the sample.

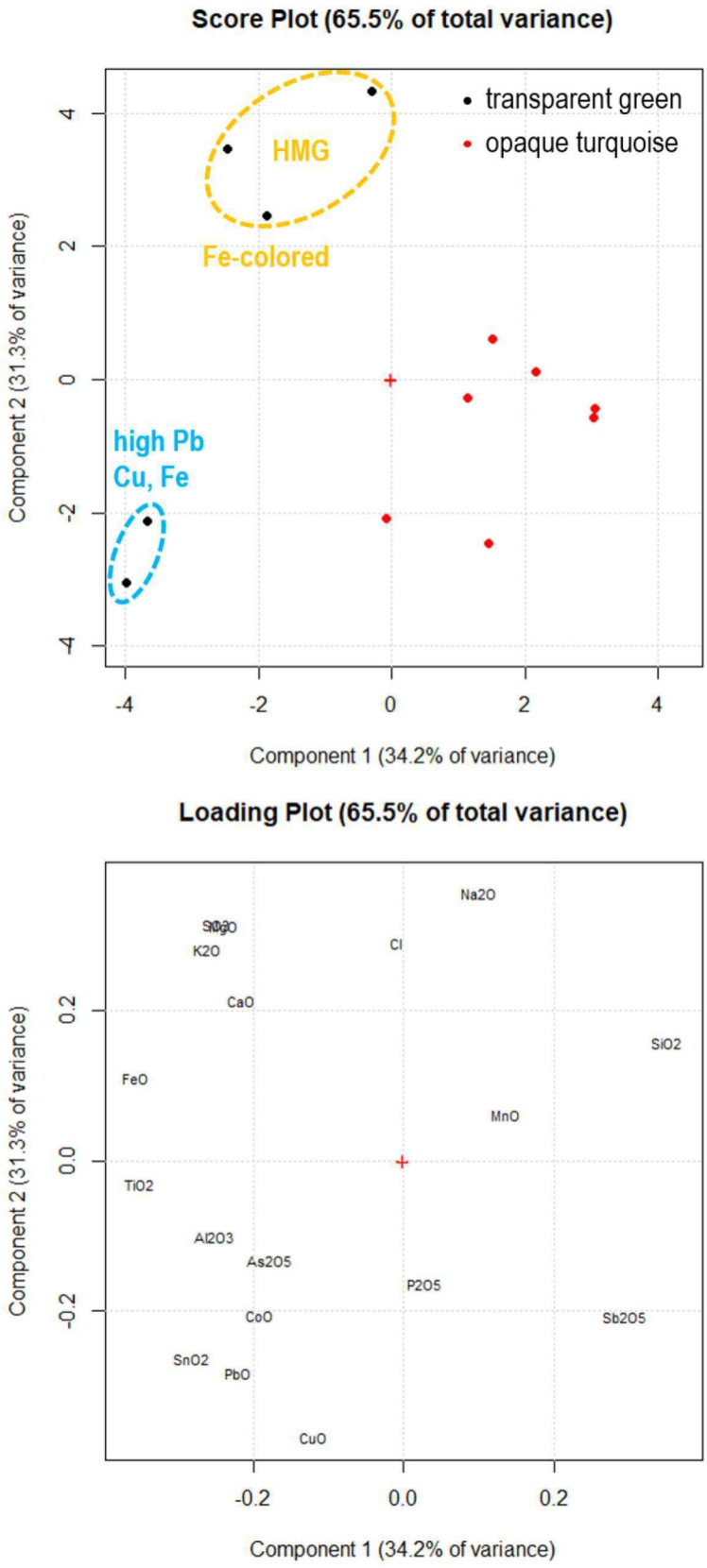

Fig. 8.2.10 – PCA score (up) and loading (down) plots of the green samples from Tebtynis. (symbols: black dots = transparent green glasses; red dots = opaque turquoise glasses).

The chemical composition of the base glass in Ty-S-BiBR-507-VT shows excellent similarities with the Tebtynis dull red glasses, both in terms of major, minor and trace elements. The only substantial difference lies in the concentration of copper (0.30% instead of an average 1.85%), which is due to an incomplete dissolution of the coloring agent, introduced in the form of chalcocite. In this specific case, the possible use of scrap bronze with relics of sulfides seems rather unlikely, considering the low amount of copper found in the glassy matrix. This can also explain why SO_3 is generally higher in dull red samples, even with respect to the classic plant ash glasses (average SO_3 is 0.94% in the Tebtynis samples and ca. 0.30% in LBA glasses). The intrinsic variability of the plant ashes may also cause significant fluctuations in the composition of the base glass (see e.g. Turner, 1956; Sanderson, Hunter, 1981; Jackson *et alii*, 2005; Tite *at alii*, 2006), but this seems not the case, considering the excellent uniformity of the mean compositions of the dull red glasses.

Similar considerations can be made for a second transparent green HMG sample, which again shows small drops of Cu sulfides, Cu-Fe sulfides and a small Pb-sulfide (ca. 1-2 μm or less), very low copper (0.13 wt%), and high sulfur (1.74 wt%). However, it differs from the previous sample because in this case PbO is also very low, in the order of 0.08%.

Considering the leaded-LMG samples, both seem correlated to the production of cuprite-colored glasses: this is particularly evident in one of them, which shows an incipient nucleation of small pseudo-dendritic crystallites at the interface with a yellowish-orange glass. In fact, looking at the sealing-wax red glasses from Tebtynis in OM, the dendrites appear dispersed in a clear, transparent and greenish glass phase, which is compatible with the composition of the two transparent green glasses considered.

It is not easy to understand if the nucleation and growth of the coloring and opacifing phases was intentionally stopped in order to obtain a transparent green glass for specific decorative needs. Of all the considered samples, there is only a couple of objects where transparent green glass has a specific role in the iconographic representation, such as in the patterns of triangles or lines in contrasting colors in Ty-P-T-417 and Ty-P-R-423-VT. It is probably not a case that these two glasses stand out as an autonomous class in

the K_2O *vs* MgO plot in figure 8.2.11a, while the remaining transparent green samples fit well in the compositional variability of dull red and yellowish-orange classes, respectively.

Summarizing, the transparent green HMG samples seem to have constituted the base glass for the production of dull red glasses, but were also used as an autonomous class for specific iconographic motifs. Conversely, the leaded-LMG transparent green glasses can be possibly interpreted as the result of an aborted or incomplete coloring aimed at the production of yellowish-orange or sealing-wax red glasses. This is especially plausible in view of the low amount and peculiar distribution of the green glass in the inlays and of the presence of intentionally added chromophores other than FeO.

Green samples from Tebtynis are rather heterogeneous. The two alkali sources used can be clearly distinguished even comparing them with earlier and coeval materials discovered in other Egyptian sites. In particular, the plot CaO *vs* MgO, shows that the three transparent HMG samples fall in the same group with the LBA plant ash glasses, while all other green samples of the Ptolemaic period are classic natron glasses.

The number of published archaeometric analyses related to pre-roman opaque greens is very scarce. Nevertheless, considering the PbO *vs* Sb_2O_5 content (fig. 8.2.12), the difference between the two chronological phases is very neat: New Kingdom glasses have low levels of both antimony and lead, despite being colored with a combination of copper and Pb-antimoniates. On the contrary, Ptolemaic glasses have Sb_2O_5 always over 1 wt% and variable amounts of lead, from absent to very high (sometimes over 10 wt%), which evidence the presence of two sub-group: one comprising high-Pb and the other low-Pb LMG turquoise glasses. All the Graeco-Roman samples considered in fig. 8.2.12 (including those from the literature) were opacified by means of Ca-antimoniates, with minor substitutions of Ca with Na and Pb (only in leaded glasses).

More analyses are still needed to better contextualize this heterogeneous class, but considering the Tebtynis glasses as a representative sample of Ptolemaic glass production, it is finally possible to address the question posed by Bimson and Freestone back in 1988. In fact, the ingot inscribed with the royal names of Ptolomey III and Queen

Berenice is surely not an aberrant red and, indeed, it can be included in the composite class of opaque green Ptolemaic glasses.

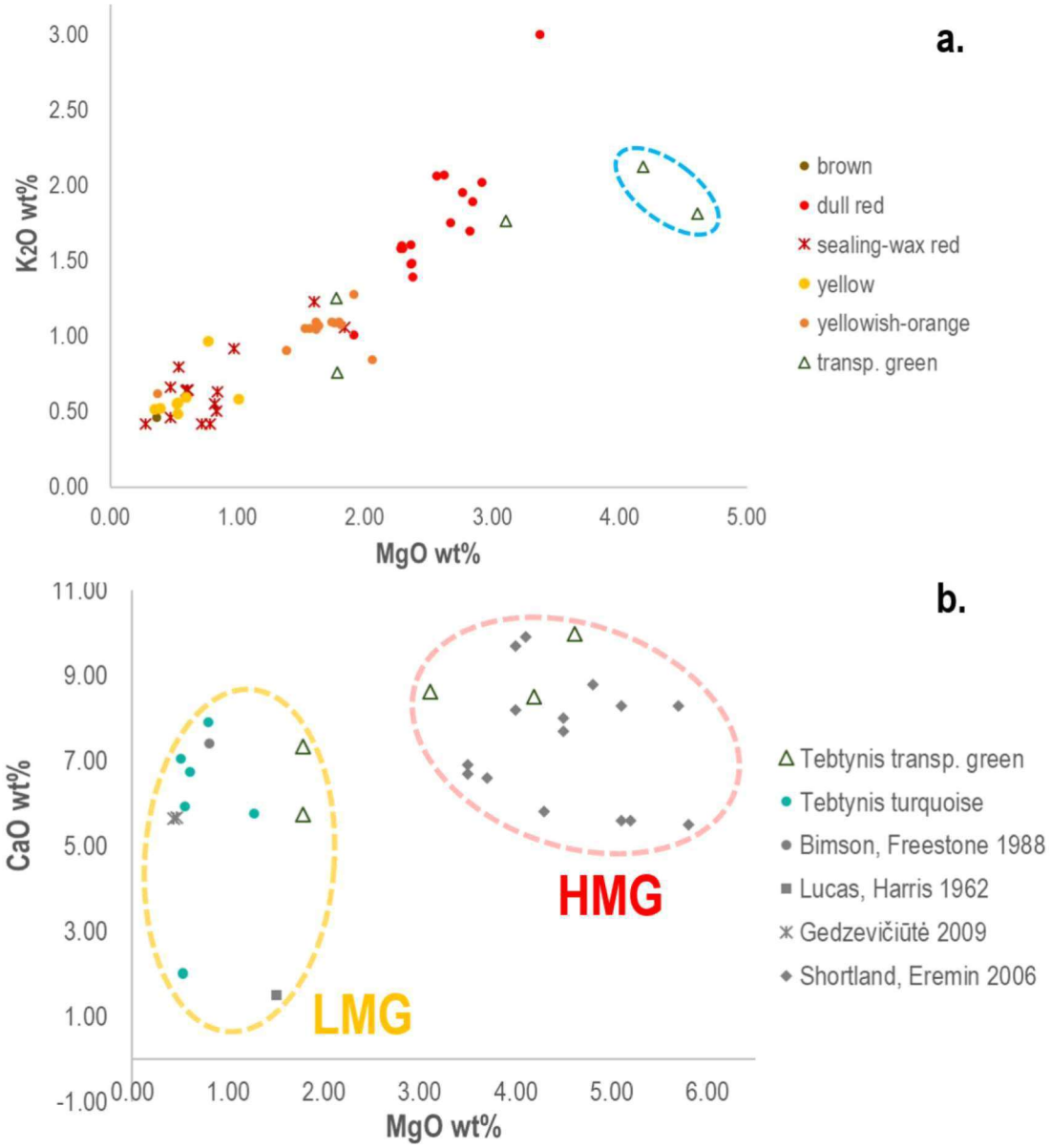

Fig. 8.2.11 – a) K_2O vs MgO content in the glassy matrix of the yellow, yellowish-orange, red and transparent green glasses from Tebtynis (symbols: empty triangles = transparent glasses; colored dots and asterisks = opaque glasses; the colors are related to the macroscopic color of the samples); b) CaO vs MgO content of the glassy matrix in the green glasses from Tebtynis (symbol: colored dots = opaque turquoise glasses; empty triangles = transparent green glasses) compared to a selection of green LBA glasses from Egypt analyzed by Shortland and Eremin, 2006 (symbol: gray diamonds) and to a set of Graeco-Roman green samples published by Bimson, Freestone, 1988 (symbol: gray dot), Lucas and Harris, 1962 (symbol: gray square) and Gedzevičiūtė et alii, 2009 (symbol: gray asterisks).

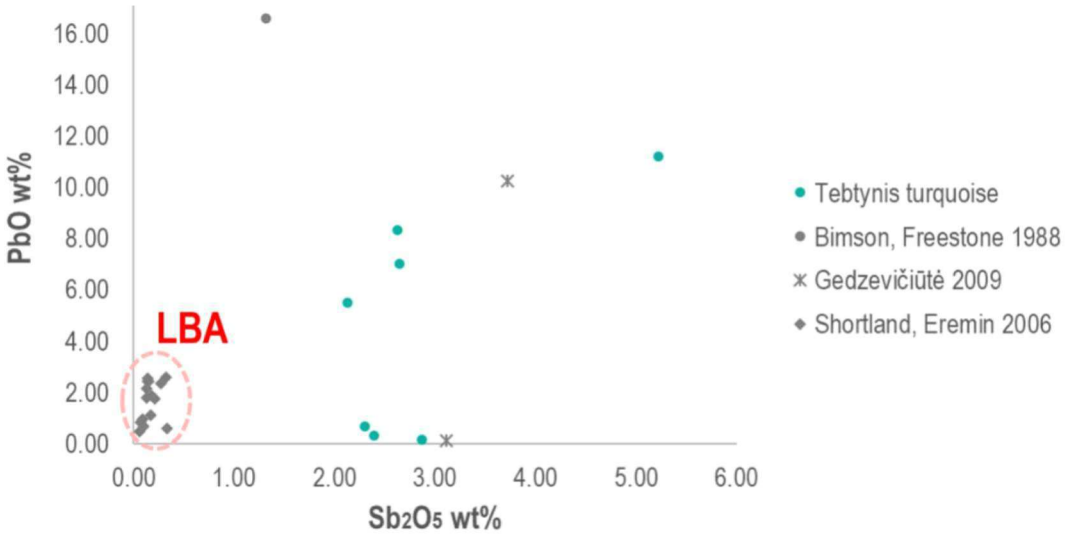

Fig. 8.2.12 – PbO vs Sb_2O_5 content of the glassy matrix in the opaque green, antimoniate-opacified glasses from Tebtynis (symbol: turquoise dots) compared to a selection of opaque green LBA glasses from Egypt analyzed by Shortland and Eremin, 2006 (symbol: gray diamonds) and to a set of Graeco-Roman samples published by Bimson, Freestone, 1988 (symbol: gray dot) and Gedzevičiūtė et alii, 2009 (symbol: gray asterisks).

The glasses of the Tebtynis collection show a wide range of colors varying from opaque yellow to red and brown, implying the use of different raw materials and a fully-developed awareness on the pyro-technological processes related to the coloring and opacification of glass. As already observed in the previous chapter, there is an effective correlation between the macroscopic appearance of the samples (in terms of hue, opacity, brightness) and the chemical, mineralogical and textural characteristics identified during the archaeometric investigations.

The PCA helps to summarize the main points of the matter: dull red glasses are characterized by significant concentrations of K_2O, MgO, CaO and SO_3, showing the classic HMG recipe that is typical of plant ash glasses. All other samples have a natron-based composition, with specific elemental concentrations linked to the coloring process employed. The yellowish-orange samples show significant levels of FeO and Al_2O_3, suggesting the use of particularly impure sands, and noteworthy levels of SnO_2; yellow glasses have the highest Sb_2O_5 and SiO_2 content in the dataset, associated with the medium to low PbO. Sealing-wax red glasses can be divided into four sub-sets on the

basis of the ratio PbO/ Sb_2O_5 and PbO/ CuO. Finally, the only opaque brown glass shares the main chemical trends of the sealing-wax red and yellowish-orange glasses.

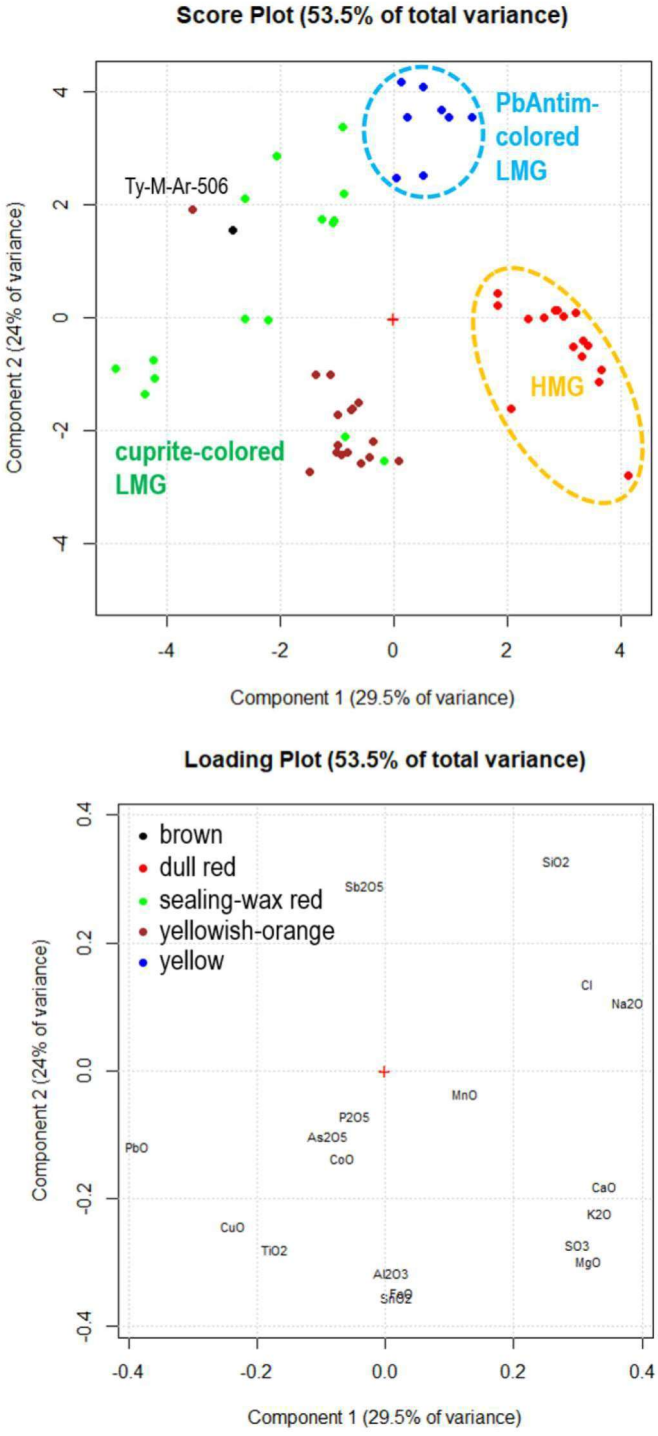

Fig. 8.2.13 – PCA score (up) and loading (down) plots of the yellow-orange-red and brown glasses from Tebtynis. Sample names are given only for the outliers, while all other samples are classified according to their macroscopic color-groups (symbols: black dot = brown glass; red dots = dull red glasses; green dots = sealing-wax red glass; orange dots = yellowish-orange glasses; blue dots = light yellow glasses).

From the textural and mineralogical point of view, these chemical differences correspond to the presence, size and distribution of three different coloring and opacifying agents: 1) lead- and lead-tin antimoniates in yellow glasses; 2) nano-drops of metallic copper in dull red glasses; and 3) cuprite associated to micrometric particles of metallic copper in brown, yellowish-orange and sealing-wax red glasses.

The color of the earliest yellow glasses found in Egypt and Near East is invariably due to lead-antimoniates in the form of anhydrous, synthetic bindheimite with formula $Pb_2Sb_2O_7$, sometimes labeled as Naples yellow (Brill, 1988; Mass *et alii*, 1998).

It has been reported that during the IV century AD this traditional recipe is abandoned in favor of lead-stannates (Tite *et alii*, 2008; Lahlil *et alii*, 2011). Verità (*et alii*, 2013), however, showed that the first examples of the use of tin-based yellow opacifiers can be traced back to the II century AD in a series of *sectilia* panels discovered in the villa of the Roman emperor Lucius Verus.

Lahlil (*et alii*, 2011) and later Molina (*et alii*, 2014) demonstrated that lead-antimoniates found in yellow glasses from the New Kingdom can include traces of iron and zinc, while those found in Roman glasses (scattered *tesserae* with no stratigraphic references) generically dated from II century BC and the V century AD usually contain small amounts of iron and moderate to high levels of tin. This evidence constitutes an important chronological indicator for distinguishing the two productions. Yet, the lack of analyzed samples dated from the Late Period to the Early Ptolemaic era cannot clarify when (and where) this transition first took place and the eventual correlations with the cultural, economic and social context.

The analyses of a selection of antimoniate inclusions in the yellow samples from Tebtynis show a significant correspondence with the Graeco-Roman production, considering both the presence of iron (FeO ranging from 1.16% to 4.44%) and tin, even in very high amounts (1.71%-6.13% with one crystal reaching 17.02 wt%), sufficient to account for lead-tin antimoniates. These mixed lead-tin compounds are rather common in Roman glasses and were identified by numerous authors especially in mosaic *tesserae* and *sectilia* panels throughout the Imperial phase and during the Late Antiquity (see e.g. Van Der Werf, 2009; Santagostino Barbone *et alii*, 2008; Verità *et alii*, 2013; Basso *et alii*, 2014).

The data acquired during this work confirm that the transition zinc/ tin in Pb-antimoniate inclusions within ancient glasses occurs in Egypt at least from the Late Ptolemaic Period or Early Roman period (and possibly even earlier, according to the specific dating of the workshop, as discussed in § 3.3), offering the chance to circumscribe the chronology for the introduction of this specific technique.

The Raman spectra of the antimoniate inclusions in the Tebtynis samples are in good accordance with the results proposed by Rosi (*et alii*, 2009), showing that the deformation of the pyrochlore structure in presence of tin causes the downfall of the peak at 510 cm^{-1}, which is the main band in unmodified lead antimoniates, the appearance of a shoulder at ca. 450 cm^{-1} and the shift of the band at 110 cm^{-1} to ca. 140 cm^{-1}.

Interestingly, one yellow sample (Ty-P-FL-501-G) shows the combined presence of Pb-antimoniates and Ca-antimoniates, where Ca-antimoniates are micrometric euhedral crystals in hexagonal form, compatible with an *in situ* crystallization. This evidence was never reported in the literature in ancient samples, but was identified during experimental melts by Molina *et alii* (2014). These authors state that lead-antimoniate particles are stable in glass at temperatures from approximately 900 to 1000°C, before converting to calcium antimoniate. Moreover, they suggest that the presence of tin and zinc improves the thermal stability of lead antimoniates up to ca. 1100°C (Dik *et alii*, 2005). However, the Pb-antimoniates in Ty-P-FL-501-G have the highest SnO_2 content encountered in all the analyzed inclusions in the Tebtynis yellow glasses, reaching the significant value of 17.02%. This implies that temperatures higher than 1100°C must have been occasionally surpassed in the production of this specific sample.

Considering the ratio PbO/ Sb_2O_5, the yellow glass phases of the samples from Tebtynis exhibit values between 5.8 and 18.7, which are way higher than the stoichiometric ratio of the Naples yellow pigment, 1.4. This means that yellow glasses were generally produced in excess of lead, an expedient possibly aimed at lowering the melting temperature and the viscosity of the glass and thus favor stirring and avoiding the color fading caused by the thermal instability of the lead antimoniates (Shortland, 2002). The only exception is again sample Ty-P-FL-501-G, whose ratio is closer to that

of the pigment, being 1.72 However, this effect may also be due to the conversion from lead to calcium antimoniate, as noted above.

The idea of an *ex situ* synthesis of the lead/ lead-tin antimoniates or the *anime* compound (a synthetic lead-antimony-silicate) has been widely accepted among all authors both for LBA and Roman glass production. Freestone and Stapleton (2015) reported that the reduced compositions of Roman yellow glasses usually show higher silica content with respect to that of the other color classes. This evidence has been intended as a clue of the use of *anime* as coloring and opacifying agent, in contrast with the addition of lead-antimoniates. Looking at the reduced CaO *vs* SiO_2 concentrations in figure 8.2.14a, it appears that yellow samples from Tebtynis do not show higher levels of silica with respect to the reduced composition of other colors of the same collection. However, the tendency towards higher SiO_2 contents in the loading plot of the PCA (fig. 8.2.13) may point in the same direction, for the majority of the samples.

From the textural point of view antimoniate-colored yellow glasses from Tebtynis can be distinguished in two main categories: five samples show peculiar lines of chemical zoning, defined by varying concentrations of PbO (as seen e.g. in Mass *et alii*, 2002; Shortland, 2002), while three samples have a very homogenous texture with uniform distribution of the Pb-antimoniate and Pb-Sn antimoniates (also identified by Verità *et alii*, 2013). It has been observed that zoned yellow glasses, especially common in LBA glass, can be associated to a higher viscosity of the glass melt, which complicates the even mixing of the pigment (Molina *et alii*, 2014).

Moreover, sample Ty-P-A-402-G is characterized by the presence of numerous big, rounded quartz particles. Given their number, their shape, size and distribution pattern they must be considered as an intentional addition, probably intended to improve the opacity as seen in other opaque blue or white glasses of different periods (e.g. Angelini *et alii*, 2010; Maltoni, Silvestri, 2016). From what is published to date, this is the first documented occurrence of such a texture in yellow glasses, that can perhaps be interpreted as one of the technical solutions tested by the Ptolemaic glassworkers that has never made it into the industrial-scale production of the Roman period.

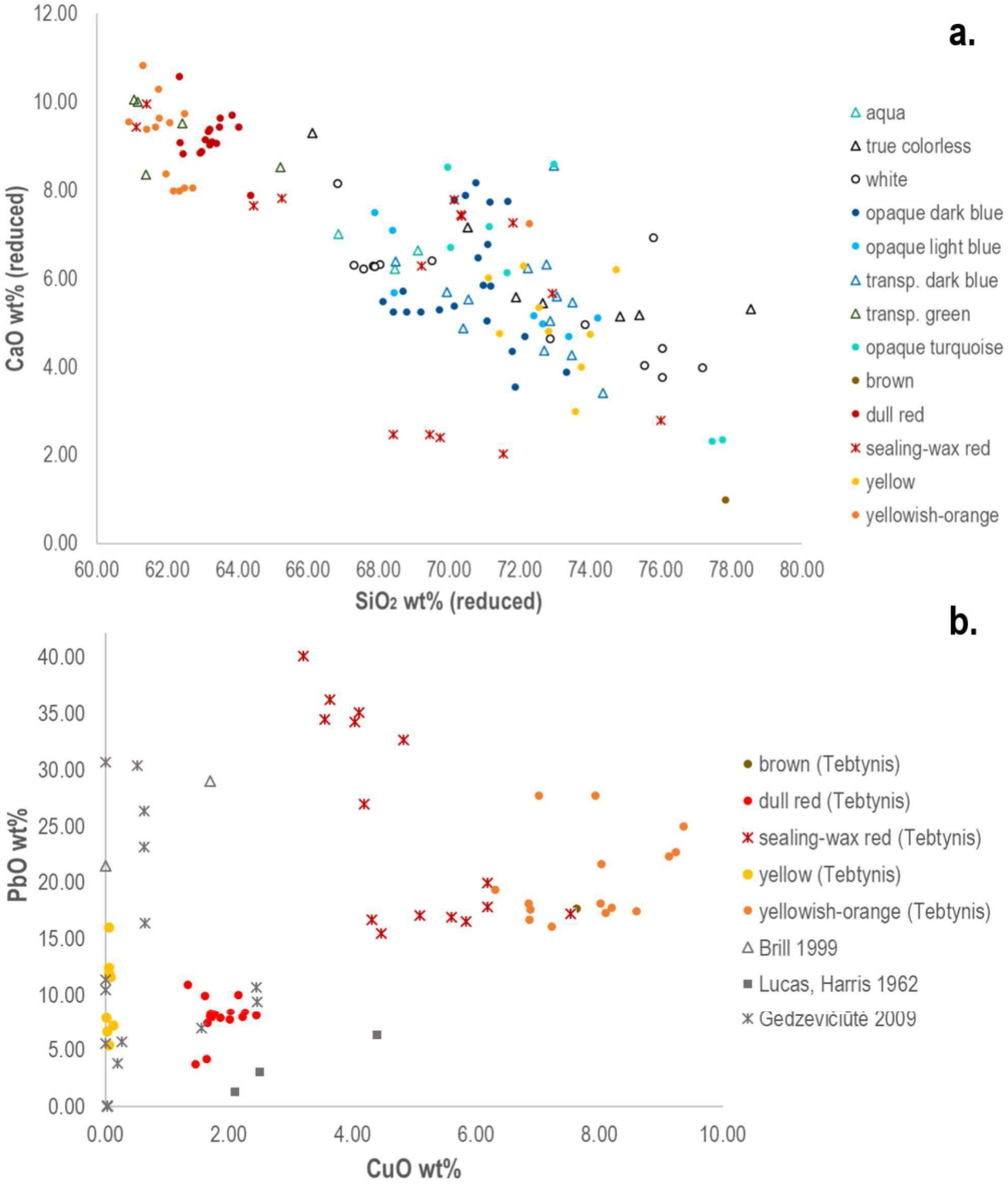

Fig. 8.2.14 – a) CaO vs SiO_2 reduced contents in the glassy matrix of the glasses from Tebtynis (the color of the symbols corresponds to the color observed from macroscopic examination); b) PbO vs CuO content of the brown, yellow and sealing-wax red glasses from Tebtynis (symbol: colored dots) compared to the coeval samples from Egypt analyzed by Brill, 1999 (symbol: gray triangles), Lucas and Harris, 1962 (symbol: gray squares) and Gedzevičiūtė et alii, 2009 (symbol: gray asterisks).

Red glasses have always attracted a huge attention from the researchers, as they testify the mastery achieved by the ancient glassworkers in the control of the raw materials and of the firing conditions (see e.g. Weyl, 1959; Ahmed, Ashour, 1981; Bimson, 1987; Cable, Smedley, 1987; Freestone, 1987; Brill, Cahill, 1988; Brun *et alii*, 1991; Welham *et alii*, 2000; Angelini *et alii*, 2004; Santagostino Barbone *et alii*, 2008; Barber *et alii*, 2009; Silvestri *et alii*, 2014; Fiori, 2015 just to name a few). Red glass was also highly valued in antiquity and is one of the main subjects of the most ancient surviving glass recipes (Oppenheim *et alii*, 1970).

Nowadays, all authors agree that copper, in different redox conditions, is responsible for the red color in most ancient glasses (except for gold ruby glasses); however, until the conclusive evidence presented by TEM analysis (Brun, 1991), considerable efforts were made to understand whether metallic copper (Cu^0) or cuprous oxide (synthetic cuprite, Cu_2O) nanoparticles were used as main coloring/ opacifying agent. It is now clear that the two forms have been contemporary in use during the Roman period, and even in earlier periods.

The first example of cuprite-colored glasses can be traced back to the New Kingdom Egypt: this technology was especially common in the site of Qantir/ Pi-Ramesse, as demonstrated by Push and Rehren (2007). The typical sealing-wax red is due to the intrinsic color of the cuprite crystals, which are dispersed in a transparent, greenish glassy matrix.

Nano-crystals of metallic copper were, instead, found in the glasses produced in the Final Bronze Age site of Frattesina, in Northern Italy, home of the so-called Low Magnesium High Potassium (LMHK) mixed alkali glasses (Angelini *et alii*, 2004). Nano-sized colloids of Cu^0 were also found in a glass rod from Amarna, Egypt, suggesting that both technologies were already in use during New Kingdom (Barber *et alii*, 2009). In this case, the dull red color can be attributed to the excitation of plasmon surface modes of copper nanoparticles, just like in the lustre decorations known from Medieval times (Borgia *et alii*, 2002).

The earliest cuprite-colored glasses can be distinguished from later productions as they usually contained very low or negligible amounts of lead. It is only in IX century

BC Iran that the role of lead in improving the formation of the red color is understood[5] (Brill, Cahill, 1988). This technology is thought to arrive in Egypt during VII-VI century BC (Bimson, 1987); it is probably not a case that the first yellowish-orange inlays appear in Egypt in the *naos* of Darius I, dated between the end of the VI – early V century BC (fig. 5.6d).

Cuprite colored orange and yellowish-orange glasses, have been generally treated as a sub-set of cuprite-colored red glasses. As a matter of fact, they were probably first synthetized as an accidental by-product of sealing-wax red glasses, but – at least in the Tebtynis samples – they show significant compositional differences with respect to red samples in terms of proportions of the main constituents, quantity of minor and trace elements and number of minerals related undissolved sand-relics, which are way higher with respect to the sealing-wax red glasses and all other color classes. Ahmed and Ashour (1981) demonstrated that the color of the yellowish-orange glasses derives from the dispersion of cubic/ octahedral cuprite-crystals of colloidal size. This is consistent with the μ-Raman results (fig. 7.3.25) on the Tebtynis glasses and with the FEG-SEM observations (fig. 7.3.22c-d), which highlighted the presence of octahedral crystals of cuprite with size in the order of 100-250 nm.

Among the yellowish-orange glasses, Ty-M-Ar-506 shows peculiar, noteworthy features. Specifically, the SEM-BSE images revealed the presence of both nano-sized cuprite and Ca-Pb antimoniates (WDS data) dispersed in the glassy matrix, associated to small pockets depauperated in lead, characterized by the incipient growth of dendritic cuprite-crystals. Calcium antimoniates were also noted in a sealing-wax red glass from Toprak Kale by Freestone (1987), who interpreted them as relics from the batch material. However, in the Tebtynis sample this seems not the case. In fact, Ca-Pb antimoniates are euhedral, thus suggesting a direct precipitation from the melt, possibly caused by an excess of antimony, which was found in an abundant set of the analyzed sealing-wax red glasses, as it will be discussed later. Small pockets with preferential dendritic growth were also observed by Ahmed and Ashour (1981) during

[5] As noted by Freestone (1987), there are four main advantages of introducing lead in red glasses: 1) increasing the potential cuprite precipitation; 2) reducing the melting temperatures; 3) reducing the phenomenon of devitrification; 4) increasing the refractive index and thus the brilliance of the glass.

their experimental tests and were associated to temperatures in the order of 1000°C. These data constitute an important technological indicator, as they offer new hints on the production of the yellowish-orange and sealing-wax red glasses and on the delicate equilibrium necessary for producing the desired colors.

Contrary to what was proposed by Nenna and Gratuze (2009), this work proved that not all red glasses from Tebtynis have a plant ash composition. Indeed, the HMG recipe is restricted to the Cu^0-colored dull red glasses, while all the cuprite-colored red samples range in the variability of LMG glasses. As already noted in the previous sections, yellowish-orange samples have higher K_2O and MgO contents with respect to the classic LMG recipe (threshold values of 1.5% for both alkali, according to Lilyquist, Brill, 1993), however, this difference seems to be due to the use of very impure sands rich in K and Mg-bearing minerals (as also observed by SEM-EDS) or to an intentional or unintentional pollution by the fuel ashes and the charcoal during the coloring process. This kind of contamination was only observed in two sealing-wax red glasses from Tebtynis, while all other samples show the usual chemical signature of natron glasses, in terms of potash and magnesia.

Considering the main compositional classes of the copper-colored red (both dull red and sealing-wax red), brown and yellowish-orange glasses proposed in the literature (e.g. Freestone *et alii*, 2003; Silvestri *et alii*, 2014; Fiori, 2015), the samples from Tebtynis can be distinguished in the following groups based on the CuO and PbO contents:

1) Low copper (CuO 1.46%÷2-45%), medium lead (PbO 3.67%÷10.92%), which is associated to metallic copper nano-particles;
2) Medium-copper (CuO 3.21%÷4.83%), very high-lead (PbO 32.68%÷40.11%), which is characteristic of cuprite-colored sealing-wax red glasses with zoned glassy matrix;
3) High-copper (CuO 4.04%÷6.19%), high-lead (PbO 15.50%÷19.93%), which is typical of cuprite-colored sealing-wax red glasses with no chemical zoning of the glassy matrix;

4) Very high copper (CuO 6.31%÷9.36%), high lead (PbO 16.26%÷27.73%), which is typical of cuprite-colored yellowish-orange glasses, but includes one sealing-glass red and one brown sample.

The only exception is a sealing-wax red sample (Ty-I-RAu-605) showing an intermediate composition with medium CuO (4.19%) and high PbO (26.93%).

These groups are in good agreement with the textural characteristics of the samples and the with compositional classes emerged from the PCA, which points out a series of other significant differences, especially related to minor and trace elements.

Looking at the micro-structure of the sealing-wax red glasses with medium CuO and very high PbO, they are characterized by bands of chemical zoning, with stripes richer (light gray in BSE) and poorer (dark gray in BSE) in lead. Inclusions of both dendritic cuprite and metallic copper are mostly concentrated in the darker areas (fig. 7.3.24c-d). On the contrary, high CuO - high PbO glasses have a uniform appearance, with well dispersed dendrites (fig. 7.3.24a-b).

It has been stated that the color of the cuprite crystallites is function of their size, which – in turn – depends on the firing times/ temperatures, the type of heat treatment and the composition of the base glass (Cable, Smedley, 1987; Welham *et alii*, 2000). This pattern is confirmed by the Tebtynis samples: in fact, the yellowish-orange samples are associated to colloidal-size cuprous oxide particles. The progressive increase of the crystal-size during the heat treatment leads to the development of the red dendrites: the biggest Cu_2O crystals can be found in the zoned, medium CuO - very high PbO glasses, where they reach dimensions up to 70 μm.

Antimony is rather frequent in a set of sealing-wax red glasses, yellowish orange and brown glasses from Tebtyins (up to 1.90 wt%). Brill and Cahill (1988) have suggested that antimony might have been added as an internal reducing agent and/ or as a decolorizer, in order to decrease the greenish tint of the base glass and thus improve the overall color intensity and the brilliance of the glass. Freestone (*et alii*, 2003) pointed out that not all opaque cuprite-red glasses show significant amounts of antimony and that the use of recycled glass may account for some of the analyzed occurrences. In the case of the Tebtynis glasses, the very high levels identified in at least some of the samples seem to speak in favor of an intentional, but non-systematic addition.

Tin is also frequently cited as an additive for facilitating the precipitation of the cuprous oxide (Shugar, 2000; Freestone *et alii*, 2003), so its frequency in the yellowish-orange glasses from Tebtynis is no surprise. The average values of Cu:Sn in this color class is 8-9, which is so close to the ratio of the classic bronze alloys produced in antiquity, to suggest that tin was added to the melt in the form of scrap bronze. A further proof of the presence of tin is the cassiterite inclusion (WDS data) identified in one yellowish-orange sample.

Yellowish-orange samples are also characterized by high FeO (up to 2.44%) and a considerable number of residual phases, especially hematite, as emerged from the μ-Raman investigations. Unfortunately, it is not possible to know if the FeO levels are only due to the use of a particularly impure sands or if iron was intentionally added as a reducing agent, as already proposed in other case studies from the literature (Silvestri *et alii*, 2014; Maltoni, Silvestri, 2016).

Figure 8.2.14b shows that lead-antimoniate yellow glasses are relatively common in the published sample-sets from Graeco-Roman Egypt. However, the plot also highlights the lack of analyzed yellowish-orange and sealing-wax red samples produced using cuprite as coloring and opacifying agent, except for those from Tebtynis considered during this work. This is certainly due to the low number of published analytical studies related to this period and geographical area. As already noted, yellowish-orange glasses appear in Egypt at least from the VI century BC and are already widespread by the second half of the IV century BC, as suggested by their abundant use in the sarcophagi of the *Petosiris* and *Djedthotiuefankh* brothers (see § 5.4). Thus, the lack of comparative data in that specific area of the plot shell not be considered in terms of absence from the archaeological record, but only as a bias created by the selection of samples analyzed to date.

9. Reconstructing the glass-working technologies in Tebtynis

One of the goals of this work is to understand the manufacture processes and the technological knowledge involved in the step-by-step production of glass inlays in Ptolemaic Egypt. In the following chapter, the analytical data on the vitreous materials will be complemented by the study of the production markers on the objects and by the interpretation of the role of the kiln, room furniture and tools identified during the excavations. This approach is devoted to better contextualize the findings and propose advanced hypotheses on the glass-working technologies employed by the craftsmen of Tebtynis.

The reconstruction of the different stages involved in the transformation from raw or semi-finished materials to finished objects will be based on those characteristics which can be scientifically measured and compared. It goes without saying that this perspective fails to identify all those traditional or ritual acts which do not cause any physically detectable change in the artifacts, such as spell casting or prayers to specific deities, that are however well known from ethnographic contexts or textual sources (Oppenheim *et al.*, 1970; Killick, 2004; Zakrzewski *et al.*, 2016).

9.1 Glass-forming methods

The preliminary SM survey of the glass inlays from Tebtynis allowed to identify two different modeling techniques: casting in open molds, reserved for figurative elements in monochrome glass (mainly heads, legs, arms, shoulders and *similia*), that will be defined throughout the text as "inlay/s type 1", and drawing, by heating and gradually stretching the glass, which is characteristic of bars and rods (also called "inlay/s type 2").

Both types were recognized by Stern & Schlick-Nolte (1994), who argued that inlays type 1 were probably made either from cold crushed glass or from pre-softened chunks[1] which were pressed into a mold.

[1] Referring to the so-called "chunk gathering" technique, as defined in Stern, 1993.

In the case of the Tebtynis inlays, SM, OM, LSCM and SEM-BSE observations suggest that powdered glass was never used in any of the investigated specimen. For example, the inlay Ty-I-RAu-605 shows flux lines and markers of uneven glass mixing (fig. 9.1a) that are not compatible with heating crushed glass within a mold. A similar, stratified, situation appears again in the inlay Ty-I-BBi-613, where two different kinds of blue (one transparent and one opaque) are separated by a white layer, which is exposed on backside of the object (fig. 9.1b). Bubble orientation observed in the arm-shaped inlay inv. 18556-04 by SM seems to point in the same direction.

The use of glasses of different colors which were not intended to be seen in molded inlays can perhaps be interpreted as an economical effort to save the most valued glass colors (for their ritual significance and/ or technological complexity, such as sealing-wax red) by substituting them in areas that were not to be seen; or, it might have been done to avoid wasting glass, thus finishing the color batches that were not enough to produce complete inlays.

On these bases, a plausible hypothesis is that inlays type 1 were produced by gathering glass chunks which were softened by heating, mixed and laid into open clay/ stone molds as represented in figure 9.2. The use of chunk gathering for both inlays type 1 and 2 is clearly testified by the texture of many analyzed samples. OM and SEM-BSE images allowed to identify relics of the original chunks, considering the presence of specific micro-structural markers such as flux lines, bubble orientation and/ or chemical zoning; moreover, the EDS and WDS analyses confirmed a slight compositional variation between the different chunks suggesting that the original glass cakes were highly heterogeneous or, more probably, that chunks from various batches were mixed together (fig. 9.3). The mixing of differently colored glass chunks might be interpreted as non-intentional or in terms of a technological choice aimed to variate the final color and create specific hues.

All our type 1 inlays have dull and opaque rear, suggesting that the final polishing was reserved for the main side. This is clearly shown by the circular, parallel lines or the cross-like patterns that can be seen on various objects of the Tebtynis collection, such as in the shoulder-shaped inlay inv. 18556-15 (not sampled) in figure 9.4.

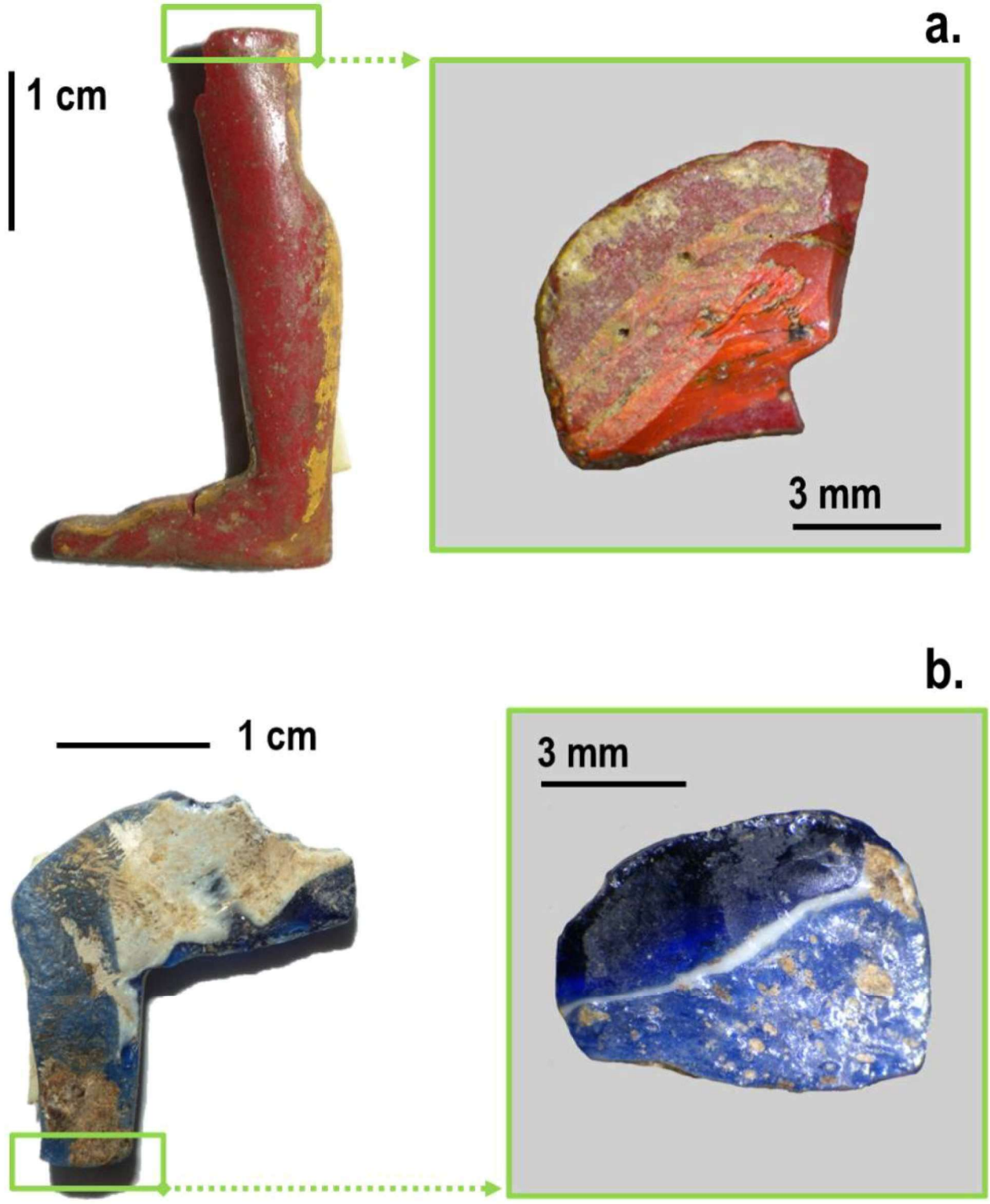

Fig. 9.1 – SM multi-focal images of the macroscopic evidences of glass mixing: a) inlay Ty-I-RAu-605 (inv. S. 18556/05), detail of the upper cross section showing traces of glass mixing and flux lines; b) inlay Ty-I-BBi-613 (inv. S. 18556/13): detail of the lower cross section showing layers of 3 different glasses.

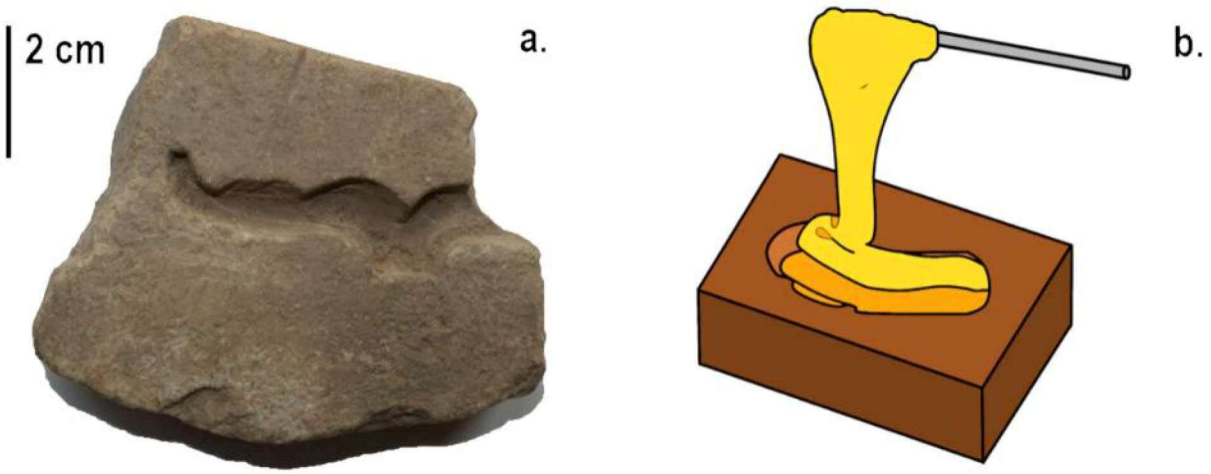

Fig. 9.2 – a) stone mold in form of corkscrew ram horns, part of Hemhem crown (inv. S. 19275); b) proposed reconstruction of the molding process for inlays type 1.

Most inlays preserve traces of both organic binders and decoration in gold leaf. After the preparation of the cross-sections, gold was still present only in a single analyzed sample, Ty-M-RAu-502. OM and SEM images highlighted that gold is not sandwiched between two layers of glass, as usual for beads and mosaic *tesserae* (Gratuze, 2013; Silvestri *et alii*, 2011), but is applied directly to the glass in the form of a gold foil approximately 5 μm thick. This kind of application could have been done when glass was still hot, as common in metal gilding, but was more probably applied cold using a binding agent, possibly similar to the one used within the wooden hollows. In fact, figure 9.5 clearly shows that the gold surface adhering to the glass is not perfectly flat, as expected in the case of hot working. Moreover, OM and SEM-SE/ BSE images show the presence of a thin, unidentified layer between the glass and the actual gold foil which can be interpreted as a binder, probably of organic origin.

Molded inlays were subsequently inserted in prefabricated wooden hollows side by side with other glass pieces and held in place with an organic adhesive. For complex compositions, such as those used in the clothes of the famous tablet inv. S. 18155 or in certain star-motives (such as Ty-P-StB-002), the single mosaic slices and bars were mounted on a monochrome plaque of glass, which served as the base to ensure a better fit of the overall composition into the frame. This technique is known as early as the V century BC and was used also for the divine figures of 'Ain Manawir (Nenna, 2015).

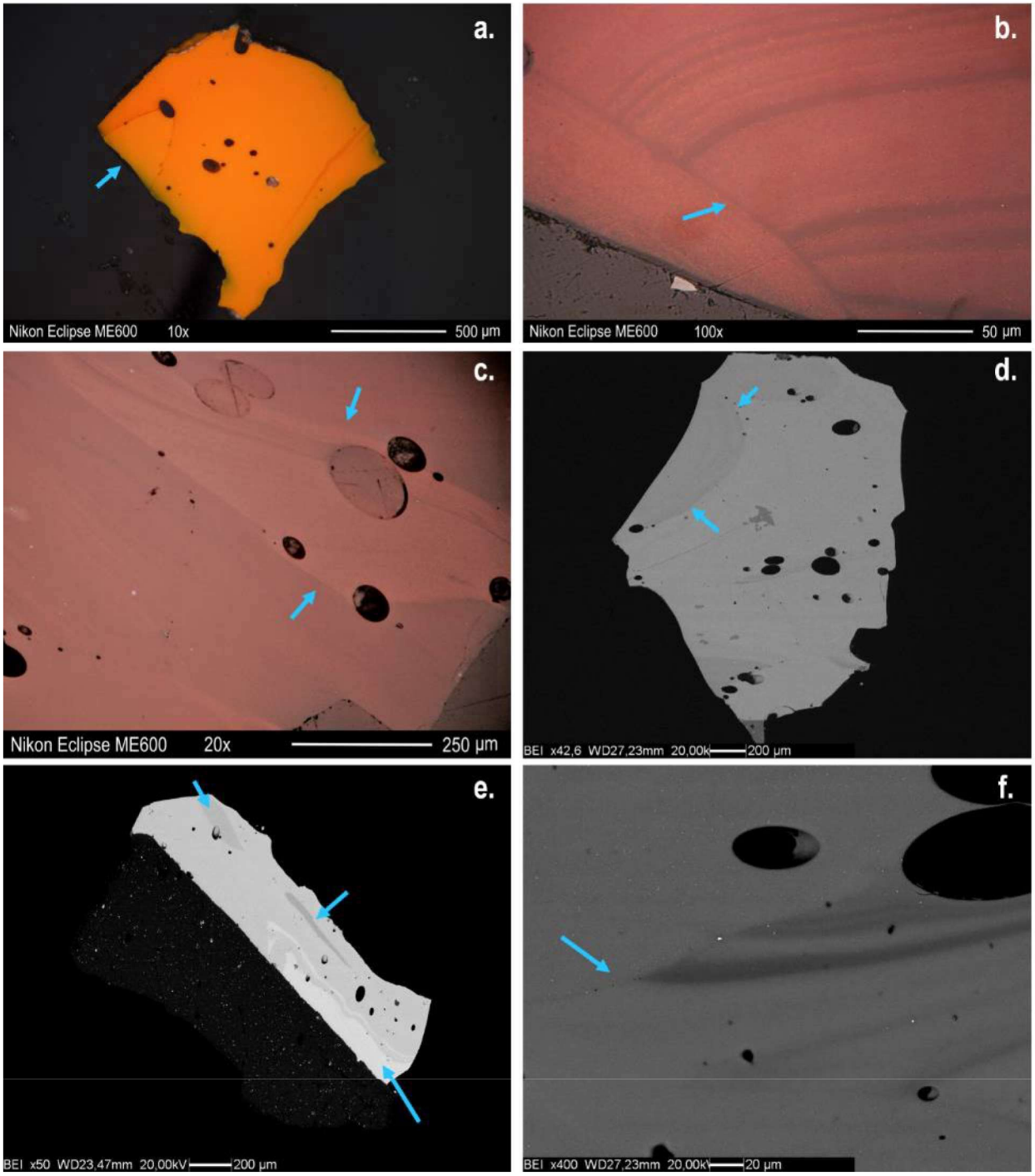

Fig. 9.3 – Microstructural evidences of chunk gathering in the glasses from Tebtynis: a) OM image in reflected light (crosses nicols) of the yellowish-orange sample Ty-M-Ar-506a; b) OM image in reflected light (shifted nicols) of the dull red sample Ty-M-R-505; c) OM image in reflected light (shifted nicols) of the dull red sample Ty-S-BiBR-507-R; d) SEM-BSE image of the section of the dull red sample Ty-S-BiBR-507-R; e) SEM-BSE image of the section of the yellowish-orange glass Ty-S-GA-005-Ar; f)) SEM-BSE image of a detail of the dull red sample Ty-S-BiBR-507-R.

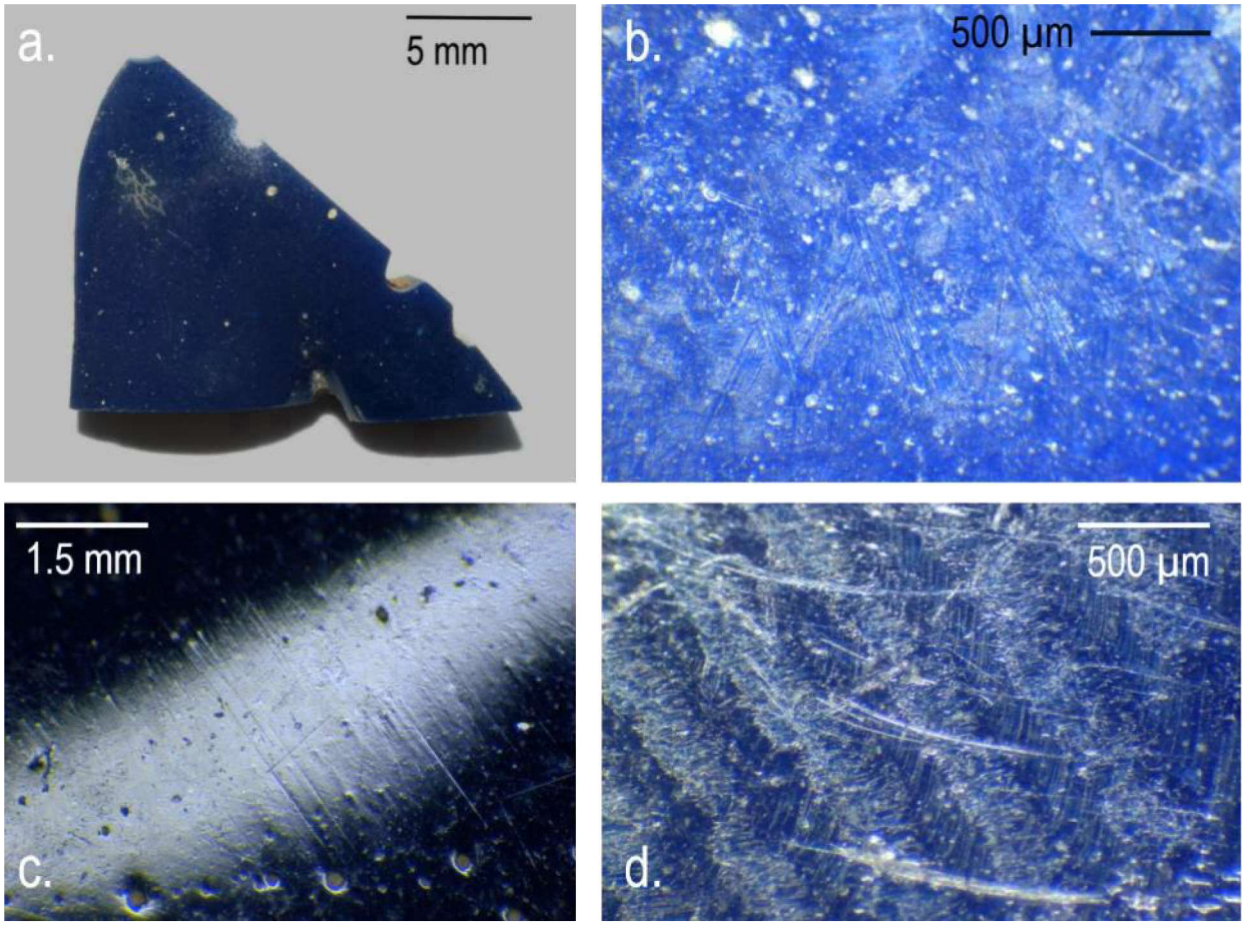

Fig. 9.4 – Polishing traces in the shoulder-shaped inlay inv. 18556-15 (not sampled): a) front view of the inlay; b-c-d) SM detail of the polished surface of the main side.

Inlays type 2 (bars and rods) were created by pulling and stretching the glass into a long thread while it was still hot. Pincer markers were found on many objects of the collection (such as Ty-M-A-005, Ty-S-BB-004 or Ty-M-R-501), because they constituted the terminal part of the bars, that could not be used for inlaying (fig. 9.6c).

However, after discarding, these wasters were probably stored for recycling. The practice of recycling is testified in Tebtynis by sample Ty-Pn-T-001, a mass of twisted bars ready for re-heating (fig. 9.6a).

Elongated bubbles and long, parallel flux lines are ubiquitously present in all inlays type 2 and can be considered as specific markers of this kind of glass-forming method (fig. 9.6b-d).

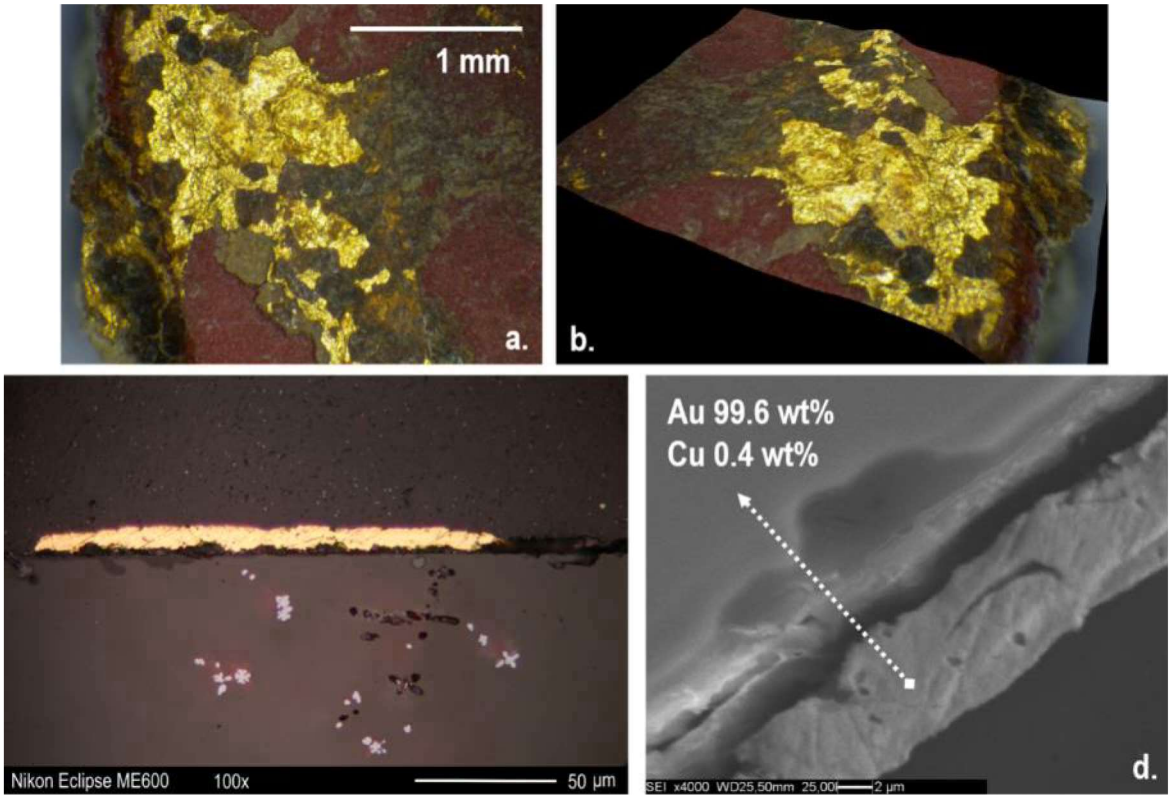

Fig. 9.5 – Gold foil on sample Ty-M-RAu-502: a) Non-invasive SM multifocal image of the inlay; b) Non-invasive SM-3D reconstruction of the inlay surface; c) OM multifocal image of the sampled section in reflected light and shifted nicols; d) SEM-SE image with results of the EDS analyses.

The technique of inlays type 2 is extremely similar to the one used for the production of the so-called "smalti filati" or glass threads, introduced for the first time in the Vatican restoration laboratories during XVI-XVII centuries AD and employed to create micro-mosaics (Grieco, 2008). A possible reconstruction of the manufacturing processes for inlays type 2 can thus be speculated thanks to an ethno-archaeological approach on this traditional craft (Fisher, 2008).

First, colored glass cakes are broken into chunks with a hammer and the chips are heated within a crucible in the kiln-mouth. Different glasses may be mixed at this stage to create specific colors. Softened glass is grabbed with a metal rod and mixed with a smaller tool to obtain a uniform mass. Glass is then drawn out with a pincer one or more times to form a flat, thin thread of the desired length. The thread is laid on the marver and removed from the metal rod with a sharp hit of the pincers.

Simple threads could then be used as such, for example in frames, as substrates or separators, or could be assembled and miniaturized. Rods could be assembled cold, using organic binders, or hot, to produce the classic mosaic glasses.

There are examples of both techniques in Tebtynis workshop. Various stratified or mosaic samples, such as Ty-S-BB-004, Ty-BBi-004, Ty-S-VA-405 or Ty-P-FL-404, show very sharp interface and no textural or chemical diffusion between the different glasses (fig. 9.7a and 9.12), leading to the assumption that they were assembled when both layers had partially or totally cooled, with further annealing and sintering stages. Bubbles and mineral inclusions probably related to traces of dirt on the worktop are also frequent along the contact line (fig. 9.7b), supporting the previous hypothesis.

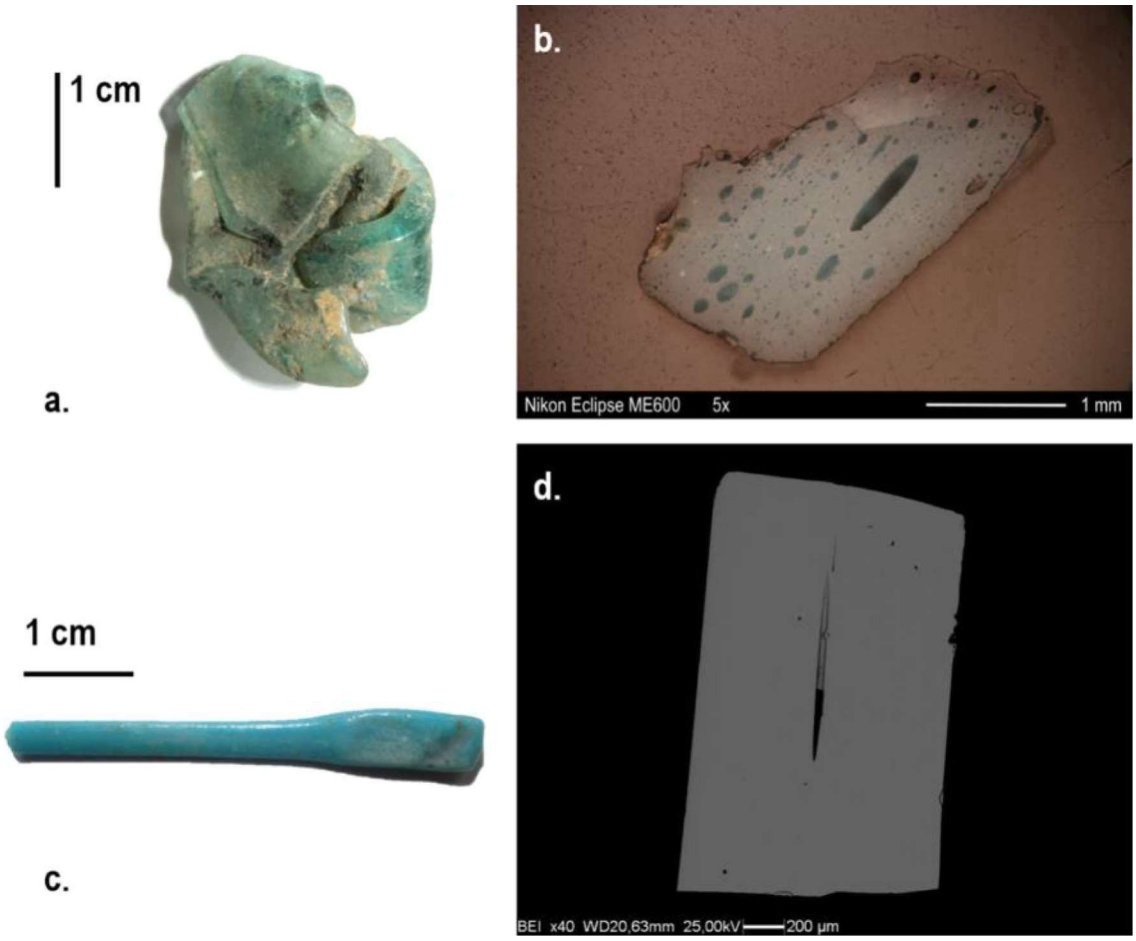

Fig. 9.6 – Technology of inlays type 2: a) mass of twisted bars in transparent aqua glass, sample Ty-Pn-T-001; b) OM image in shifted nicols of the turquoise sample Ty-M-V-006a, showing elongated bubbles; c) pincer mark on inlay Ty-M-A-005; d) SEM-BSE image of the yellowish-orange sample Ty-M-G-504a (inv. S. 18555/04), showing a long bubble.

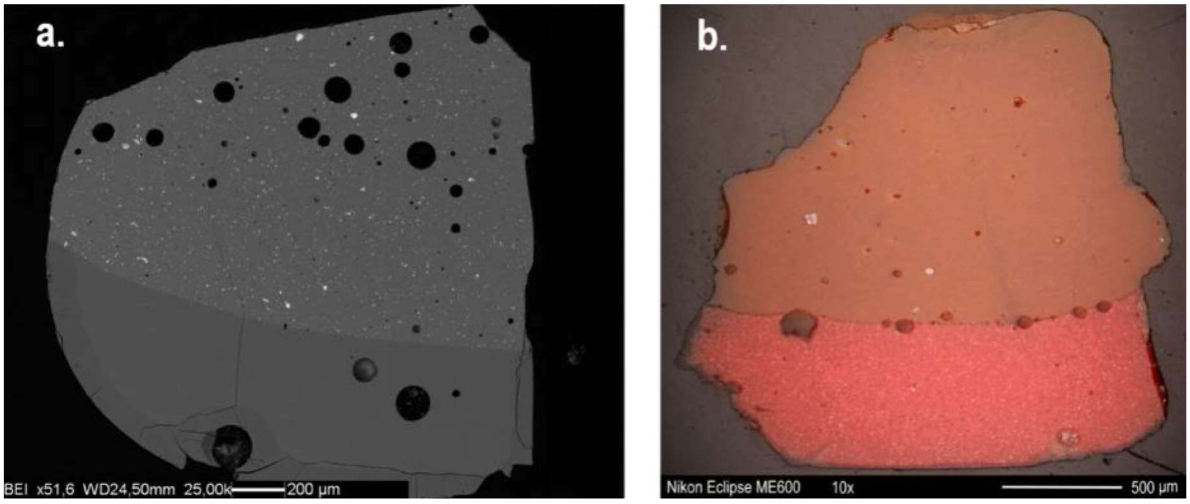

Fig. 9.7 – a) SEM-BSE image of sample Ty-S-BB-004 showing a sharp interface with no textural or chemical diffusion between the opaque dark blue and the transparent dark blue glasses; b) OM image in reflected light and shifted nicols of sample Ty-S-MR-502 showing a sharp interface and bubbles along the contact line of the brown and sealing-wax red glasses.

The sections and the mosaic slices were mostly separated from the canes cold. Following the experimental work published by Stern and Schlick-Nolte (1994), it is possible to exclude the use of a saw – which would have left a dull surface with thick, parallel lines – and clipping, as two opposed bulbs of percussions were never identified. The most common situation recognized on the slices and the bar sections from Tebtynis is that of a single point of percussion, with its related bulb and the typical conchoidal ripples which characterize pieces separated by striking or snapping (fig. 9.8). Striking might have been done with a heavy tool such as a chisel or a hammer, and could have been facilitated by a sharp metal anvil under the glass rod.

However, this last tool would have left a second, barely visible bulb on the opposite side of the primary percussion point, that was never seen in the considered samples. Snapping (or bending) was usually performed by hands or with a sharp hit after incising a preliminary notch on the glass with a blade. According to the experimentations, this method usually produces a homogeneous break, the bulb is less evident and there is a certain irregularity only in correspondence with the original score. Considering all these elements, striking would seem like the most probable option for Tebtynis pieces; however, in some cases post-depositional processes might have altered or erased the

production markers to such an extent that they cannot be correctly identified, thus other options should remain open.

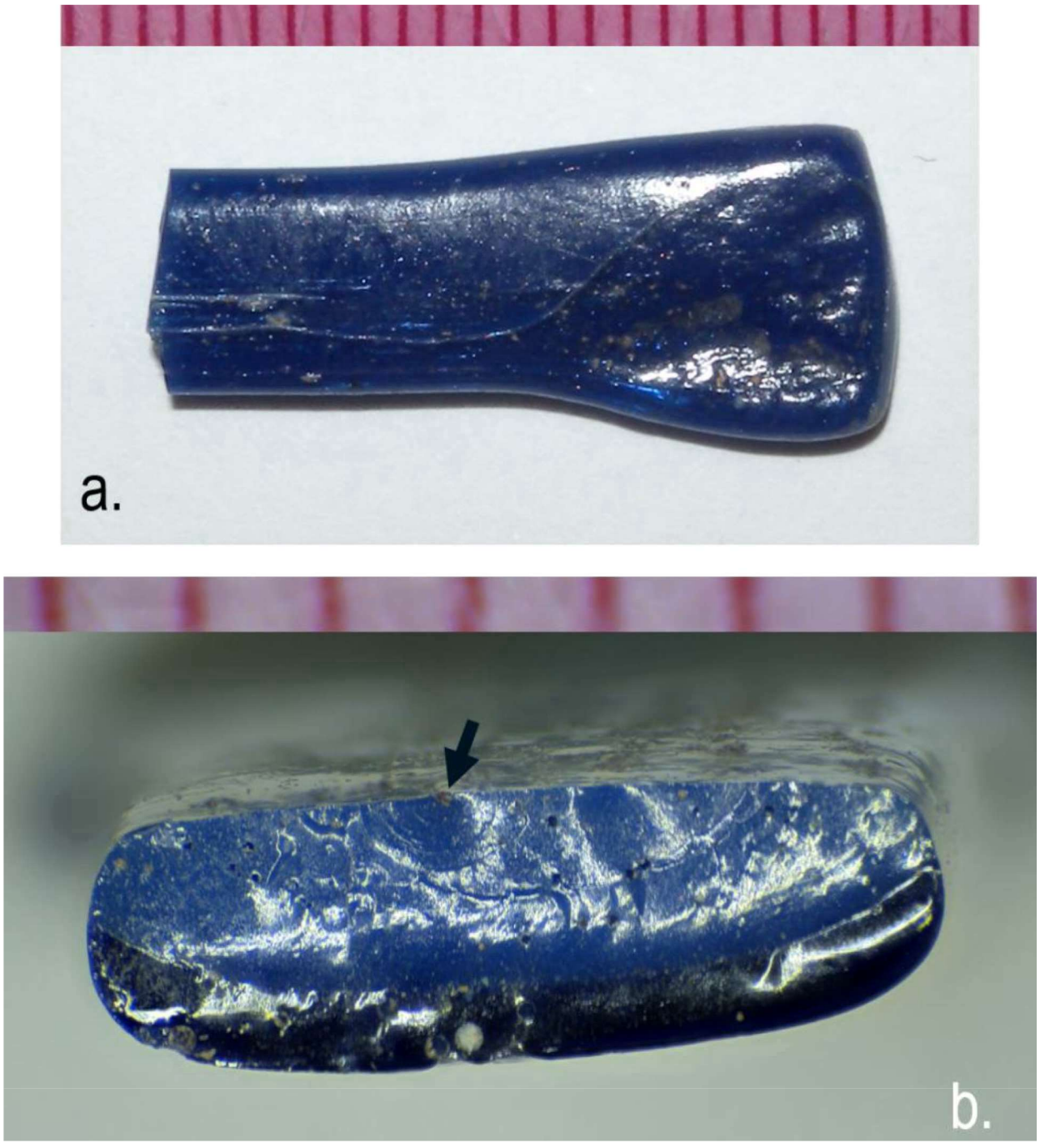

Fig. 9.8 – Sample Ty-S-BB-004: a) SM image of the inlay (type 2) with pincer mark; b) Multi-focal SM image of the percussion point (indicated by the arrow), with bulb and conchoidal ripples, typical of striking or snapping.

Moreover, the Turin collection offered the chance to investigate glass fragments pertaining to different stages of the mosaic glass production, allowing to propose possible reconstructions, such as those reported in figure 9.9, which shows (among other) the various stages for crating the tiny arches that constitute the shoulder-belts worn by the female figures represented in the inlays inv. S. 18556/17 and JE 55943 respectively in Turin and Cairo (figg. 3.6 and 3.7).

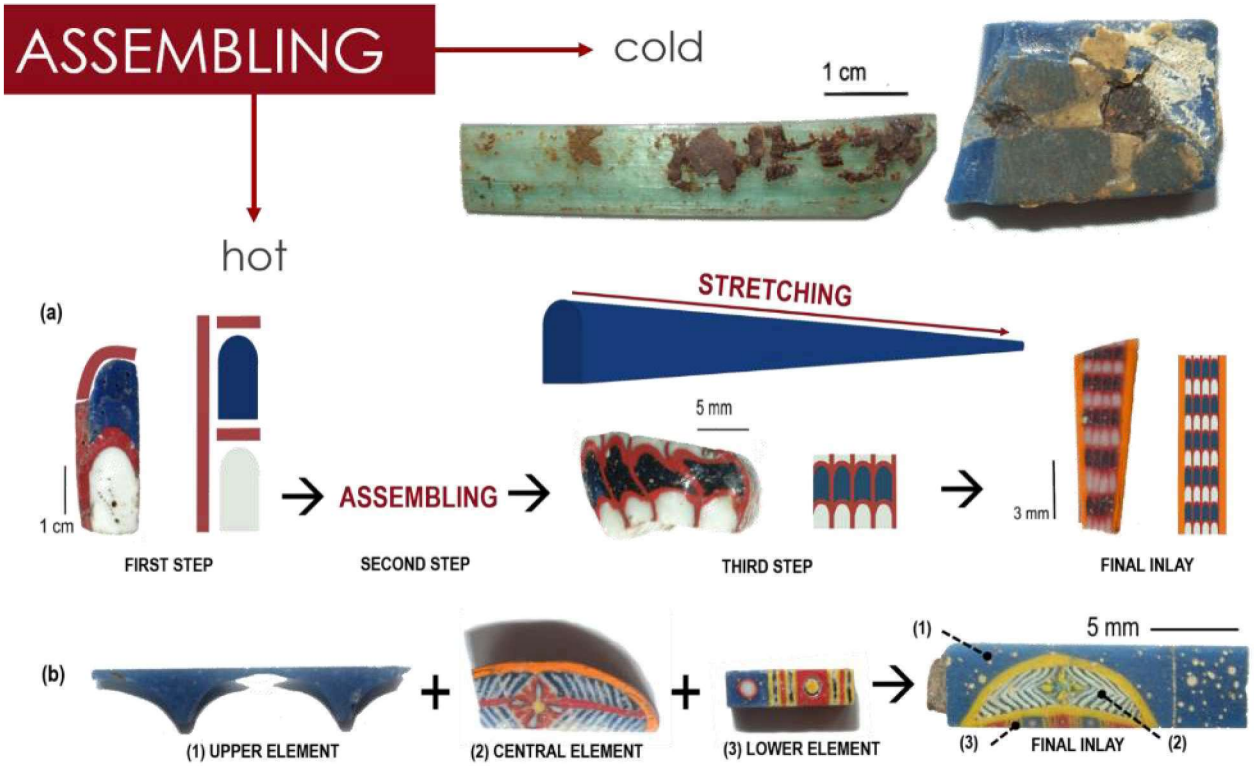

Fig. 9.9 – Hypothetic reconstruction of the two assembling methods used in Tebtynis, using inlays found in the workshop at different stages of the production process.

Judging from the flux lines and the orientation of the bubbles in Ty-P-A-418, it is possible to suggest that the base elements for the production of this pattern were three bars of red glass and two plaques, one blue and one white each approximately measuring 1.5 cm in high (fig. 9.10a). The interface between the red and the white layers of Ty-P-A-418 was also investigated with OM and SEM after sampling, and shows very little

chemical interaction between the two glasses, with diffuse porosity along the contact line (fig. 9.10c-d). This is coherent with a sintering of the various elements at relatively low temperatures and/ or in short times.

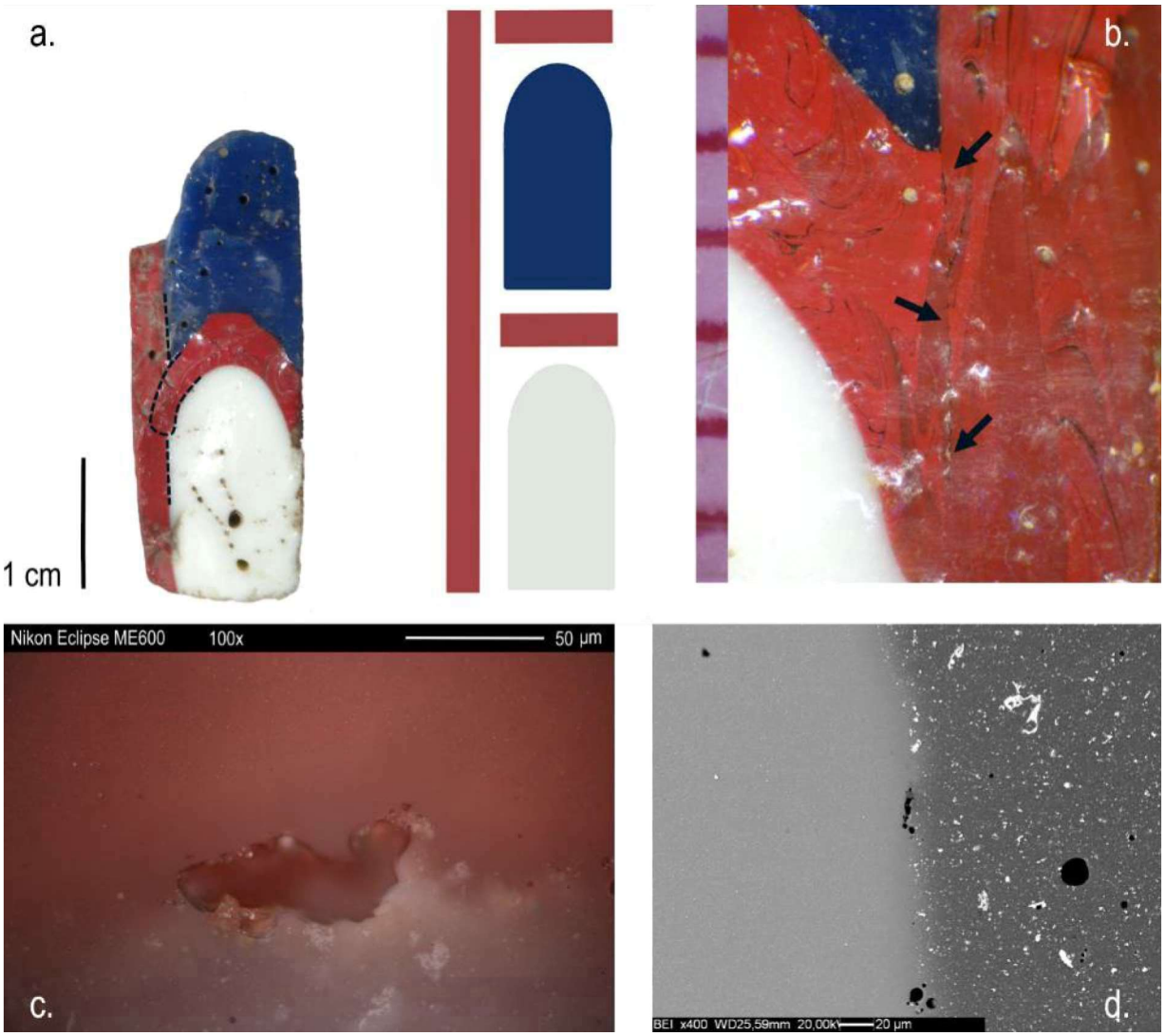

Fig. 9.10 – Production technology of sample Ty-P-A-418: a) SM image with the proposal of the five basic glass elements for the production of the semi-finished inlay; b) Non-invasive OM image on the actual inlay which shows the traces of the interface of the sintering process; c) OM image in reflected light and crossed nicols of the interface between white and dull red glass, showing an irregular bubble related to an imperfect sintering process (polished section); d) SEM-BSE image of the contact between white and dull red glass, showing very little chemical diffusion between the glasses and the presence of micrometric bubbles.

It is not possible to reconstruct whether this element was first drawn and then cut and assembled in groups of four or if it was first assembled with three similar pieces and later drawn to the dimensions of Ty-P-A-419, with each arch measuring ca. 5 mm in height (fig. 9.11). For sure, the first option seems more economic in terms of glass saving, since the quantity of glass originally used for Ty-P-A-418 could suffice for a very high number of millimetric-size arches intended as final products. After at least another stage of assembling and drawing, the arches were bordered with orange bars and reduced at 1 mm, hence ca. 1/15 of their original height.

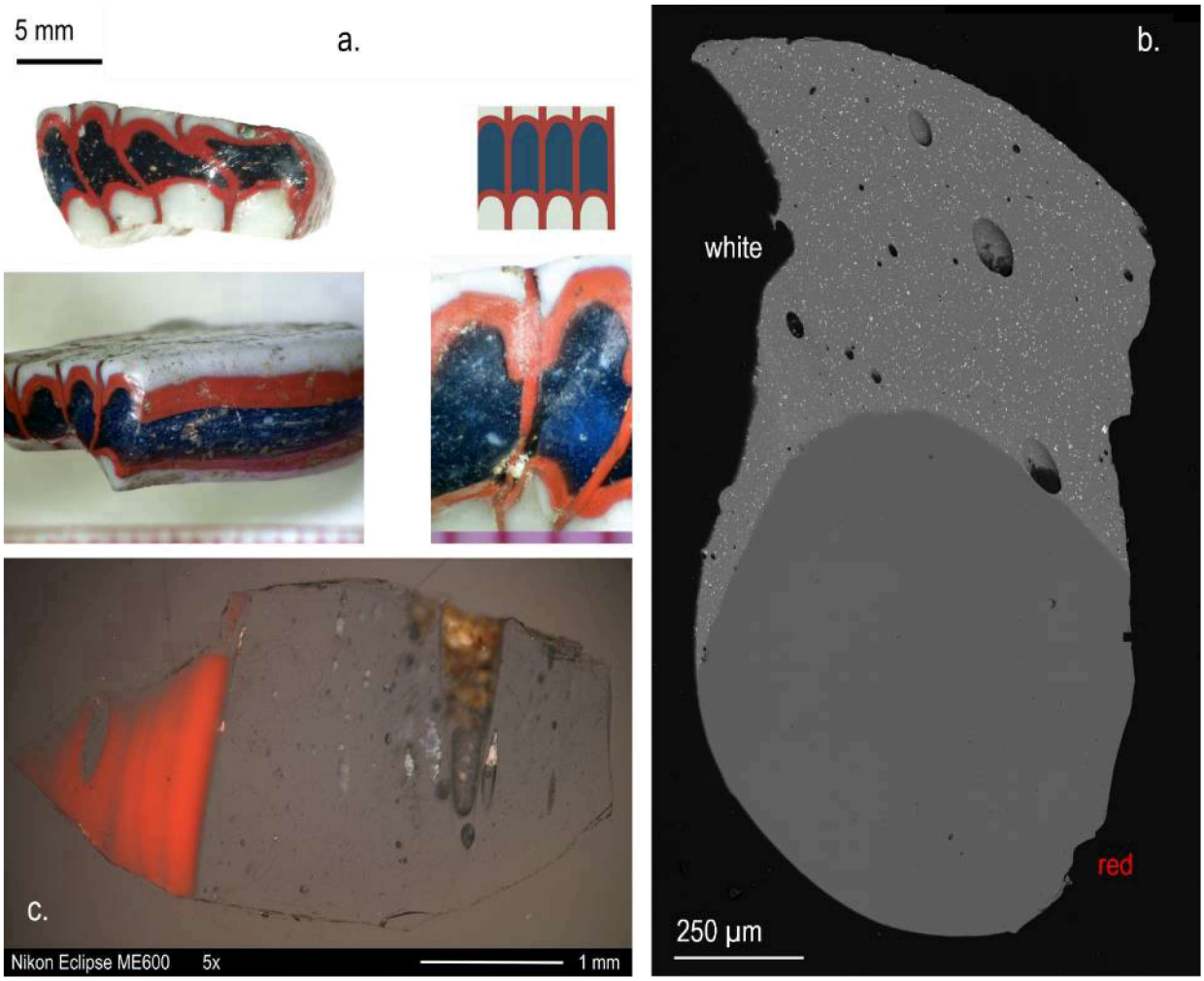

Fig. 9.11 – Production technology of sample Ty-P-A-419: a) SM images of the inlay (different views and detail of imperfect sintering) with the reconstructive proposal of the sequence of arches; b) SEM-EDS map of the fragment showing white and dull red glass; c) OM image in reflected light and crossed nicols of the second sample showing the interface between dark blue and dull red glass (polished section).

The sintering of the various glass rods for creating complex mosaic elements such as the sequence of arches described above implied the use of the kiln in room 17 D.

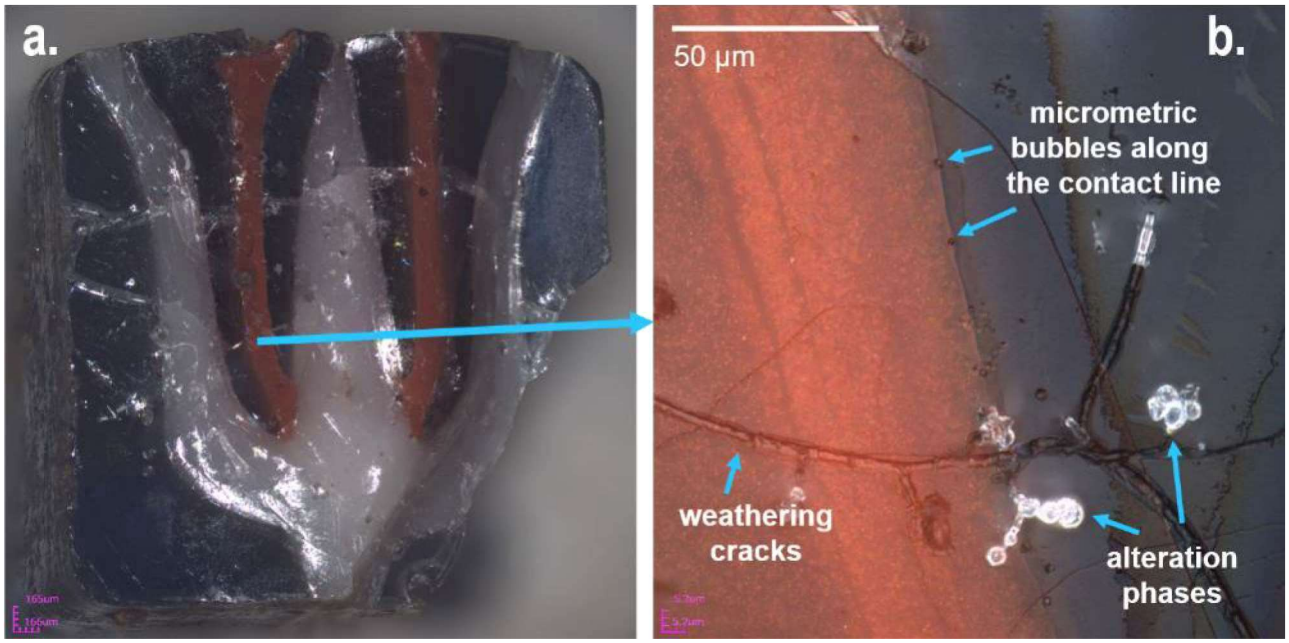

Fig. 9.12 – Non-invasive, high-resolution CLSM images of sample Ty-P-FL-404: a) optical, multifocal image textured over a digital elevation model of the surface of the mosaic bar; b) optical, multifocal image textured over a digital elevation model of a detail of the surface, showing the contact line between the dull red and the dark blue glasses with micrometric bubbles, weathering cracks and alteration phases.

According to the proposed reconstruction, the monochrome bars or the semi-finished polychrome inlays were placed in appropriate patterns on trays similar to those recovered in the workshop with inv. S. 19269 and S. 19921 (see § 3, tab. 3.1) and heated in the kiln. There is no clue about the presence of an annealing chamber, but for this operation the temperatures should have never exceeded 700-800 °C (or even less, according to the specific composition of the glass) in order to avoid the loss of detail caused by the incipient softening.

One further element to be considered is the relation between the composition of the glass and its working range in terms of viscosity in a specific time/ temperature interval (Stern, 1993). Observing the Tebtynis samples, there seem to be a direct connection between the average dimension of the opacifying crystals and the forming technique employed. In particular, it appears that sealing-wax red glass was never used for the

stretched bars and rods (inlays type 2); this can be tentatively explained by the significant size of the cuprite dendrites, which affects the viscosity, and thus the workability of the glass, especially when drawn.

However, the exploration of these aspects requires further in-depth investigations which are currently in progress in the framework of the project "ArExGlass: Archaeometry and Experimental Archaeology for Pre-Roman Glassworking", that will integrate statistical methods of predictive modeling on the base glass properties and experimental melts, both in controlled-environment and in a replicated furnace reconstructed on the basis of the archaeological evidences in order to shed light on this specific topic.

9.2 Glass coloring and furnace conditions

This research confirmed that primary production never took place in Tebtynis: the kiln is definitely to small (70 x 65 cm, plus chimney) if compared to the earlier and coeval productive structures (Nicholson, 2007; Nenna, 2015b and references cited in § 4.2.2) and the excavations found no trace of any raw materials or crucibles, which could account for a local production.

Conversely, the study of the Tebtynis collection in the Egyptian Museum and the revision of the archival data revealed the presence of numerous evidences of glass-forming, with a significant concentration of tools, semi-finished and waste materials discovered under the floor of a Roman *deipeneterion* within the first courtyard of Soknebtynis temple, in the rooms that have been interpreted as an inlay workshop.

Despite the lack of any direct evidence of glass-coloring, the archaeological study and the archaeometric investigations performed during this work revealed several clues that glass might have been colored and opacified within the secondary workshops – and specifically in Tebtynis – during the Ptolemaic period. The first indication comes from the precinct of Mut in Karnak, where the recent excavations have brought to light a bowl containing traces of an unidentified blue pigment in association with a few chunks of naturally colored glass, molds for inlay production, rare metal scraps and a pyro-technological structure very similar to the one discovered in Tebtynis (Fazzini, 2009).

From the archaeometric point of view, the following elements that emerged from the analyses of the Tebtynis samples performed during this work contribute to strengthen this working-hypothesis:

1) the base composition of the Tebtynis samples is rather homogeneous: glasses do not appear to be clustered according to their color, alkali source or lead concentration, which would instead suggest the contribution from different workshops for glass-production and glass-coloring (decoloring and opacifying) using different raw materials and technological solutions;

2) among the analyzed samples, there is a group of transparent green glasses with clear evidence of an incipient coloring process for the production of dull red and sealing-wax red glasses. This suggests a local manipulation of the optical properties of glass;

3) brown glass is used in none of the existent inlaid representations typical of Ptolemaic Egypt. In Tebtynis, this color class is represented by one single occurrence in a stratified sealing-wax red/ brown inlay (fig. 9.13). However, it is sure that brown glass was not intended to be seen, as the red side shows traces of gold foil, a treatment which was only reserved for the outer surface. Moreover, the chemical composition and the textural characterization of this brown glass showed significant similarities with the cuprite colored sealing-wax red and yellowish orange classes, thus suggesting that this hue represents and undesired accident in the coloration processes.

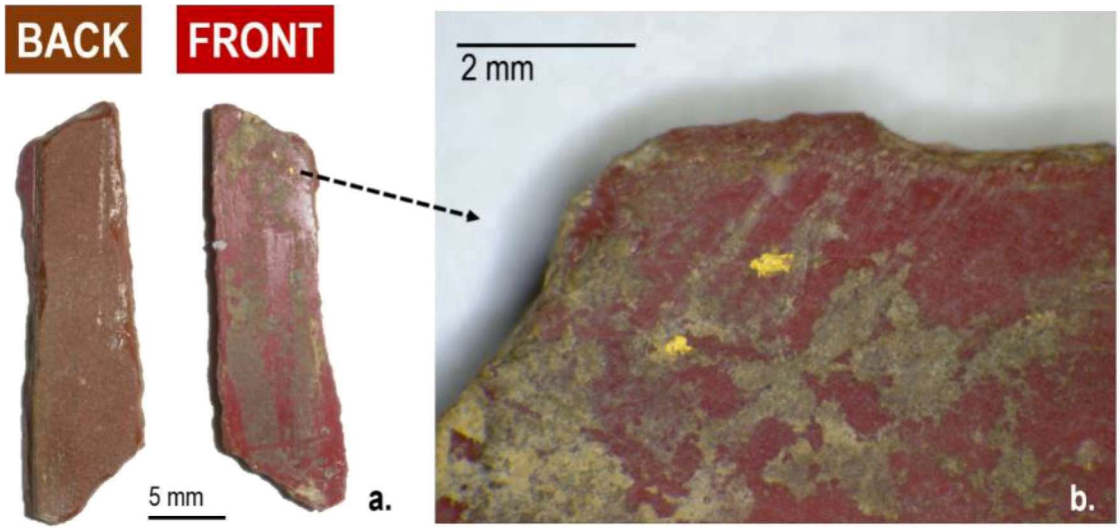

Fig. 9.13 – Inlay Ty-S-MR-502: a) front and back sides of the inlay; b) SM multi-focal image of the gold foil traces on the frontal sealing-wax red surface of the inlay.

Considering that this kind of faulty glass (in form of chunks, ingots or lumps) could not have been extensively traded (and especially not acquired by a templar workshop for the production of sacred goods), it seems more likely that the coloration process took place directly in Tebtynis and that imperfect batches were used for minor purposes, in order to save the proper colors for relevant iconographic subjects.

That errors may occur in the creation of yellow, yellowish-orange, sealing-wax red and dull red glasses is no novelty, judging from the results of the laboratory replications presented in the literature (e.g. Cable, Smedley, 1987; Welham *et alii*, 2000; Molina et alii, 2014). The cited works reveal that the production of these specific color-classes is subject more than others to very strict technological constraints and can, thus, offer hints about the times, temperatures and redox conditions of the heat treatment.

According to Freestone (1987), the cuprite identified in ancient glasses can derive from the use of a strongly reducing furnace atmosphere, from the use of internal reducing agents (such as lead, tin, antimony, iron or charcoal) or from the direct addition of cuprite to the glass melt and the maintaining the initial oxidation state. Freestone himself rises doubts about the feasibility of the first approach in ancient furnaces, as it requires high redox gradients and thigh control over the kiln. The presence of various types and concentrations of internal reducing agents in the Tebtynis glasses and the euhedral morphology of the cuprite crystals, strongly suggest an *in situ* precipitation facilitated by the presence of lead, tin, antimony, charcoal and ashes (only for the yellowish-orange class) and possibly iron, as already noted in the previous chapter.

It is, however, not possible to clarify if the nucleation of the Cu_2O crystallites occurred during cooling or when glass was annealed at temperatures slightly lower than the melting point (ca. between 475-900°C) as both heat treatments could be equally effective (Ahmed, Ashour, 1981). It was generally demonstrated that in leaded glasses cuprous oxide starts to crystallize in octahedral form at around 400°C and that glass maintains a yellow or yellowish-orange color until ca. 550-600°C; after that temperature limit, the small octahedral crystals start to develop a radiated form which grows into actual red dendrites at temperatures ranging from 650°C to 870°C (Ahmed, Ashour, 1981; Brill, Cahill, 1988). Welham *et alii* (2000) showed that the biggest dendrites, which are related

to a deeper and brighter red color, occur for short melting times and lower firing temperatures and that annealed glasses tend to produce a less intense sealing-wax red color with respect to those glasses which remain within in the furnace as it cools. They also pointed out that cooling the kiln after every coloring session is cost-intensive in terms of fuel, time and labor and that this may be one of the reasons why this kind of color is especially rare in the archaeological record.

Brill and Cahill (1988) also evidenced that when yellowish-orange glasses are re-heated (but not re-melted) they can develop a deep red color, as effect of the dendritic growth. This is probably what was happening to sample Ty-M-Ar-506, which shows pockets with incipient development of Cu_2O dendrites.

Antimoniate-colored and opacified glasses can also give important indications about the firing temperatures connected to the coloring processes. For example, Lahlil (*et alii*, 2008) showed that the two forms of Ca-antimoniates crystallize at different temperatures during *in situ* precipitation: in fact, the orthodromic modification ($Ca_2Sb_2O_7$) is typical of temperatures lower than 927°C, while the hexagonal form ($CaSb_2O_6$) develops at higher temperatures, starting from 927°C, and becomes the main phase at 1094°C. Since both cases are attested in the Tebtynis samples, it is possible to infer that the furnace conditions were rather variable in the production of opaque white, blue and green glasses.

As for Pb-antimoniate and Pb-Sn antimoniate-based opaque yellow glasses, the data presented in the discussion point towards the addition of a powdered anime for most of the Tebtynis glasses. This pre-fritted material must have been incorporated and stirred into the glass at relatively low temperatures, for preventing its complete dissolution into the glassy matrix (Lahill *et alii*, 2008). The same applies for Ca-animoniates added with an *ex situ* process to opaque glasses. Further data are related to the conversion from Pb to Ca-antimoniates, which has been observed in one yellow sample from Tebtynis and that has been experimentally determined to take place at temperatures over 1050°C.

The newly formed mineral phases can also offer interesting clues with regards to the furnace conditions. Wollastonite ($CaSiO_3$) is definitely the most frequent inclusion of this type in the whole collection, as it was identified in light blue, transparent green, yellow, dull red, sealing-wax red and yellowish-orange glasses.

Wollastonite is generally considered as indicator of high-temperatures. It should, however, be noted that the composition of the glass phase can substantially alter the temperatures presented in the phase diagrams in the literature, that are generally the result of experimental syntheses of wollastonite from a binary system of its component oxides (Deer, Howie, Zussman, 1978).

In the Tebtynis samples, wollastonite crystals were found both in large, euhedral morphology or in big, hollow occurrences. The first case can be interpreted in terms of thermally stable melts, with significant growth rates associated to low nucleation; conversely, Messiga (*et alii*, 2004) demonstrated that hollow or embayed crystals derive from the reabsorption of the wollastionite by a melt undersaturated of its constituents. This type was identified only in a set of cuprite-red and yellowish-orange samples (fig. 9.14).

Four yellowish-orange glasses are also characterized by the presence of euhedral malayaite crystals ($CaSnSiO_5$), which can be associated to the presence of high levels of tin in this color-class, as already discussed. Malayaite was also found in a series of Roman mosaic *tesserae* and was interpreted as an indicator of high-temperature (ca. 1200°C), in agreement with the values derived from the experimental study of the clinopyroxene inclusions in the same glass assemblage (Tonietto *et alii*, 2011). The only occurrence of a newly formed pyroxene cluster in Tebtynis glasses was found in a yellow glass and points towards the same interpretative direction.

Other common devitrification phases are represented by Ca-Na or Ca-Pb-Na silicates, constituted by a mixture of the main components of the glass phase. They are indices of high nucleation and slow growth rates and can thus be associated with fast cooling (Santagostino Barbone *et alii*, 2008). One transparent green sample also showed the unusual presence of Ca-P-Na silicates having the classic elongated or rayed morphologies typical of devitrite and similar secondary products. This peculiar

composition was also identified in the reaction phases occurred during the experimental melts of natron-based glasses in a Roman-type wood-fired furnace (Paynter, 2008).

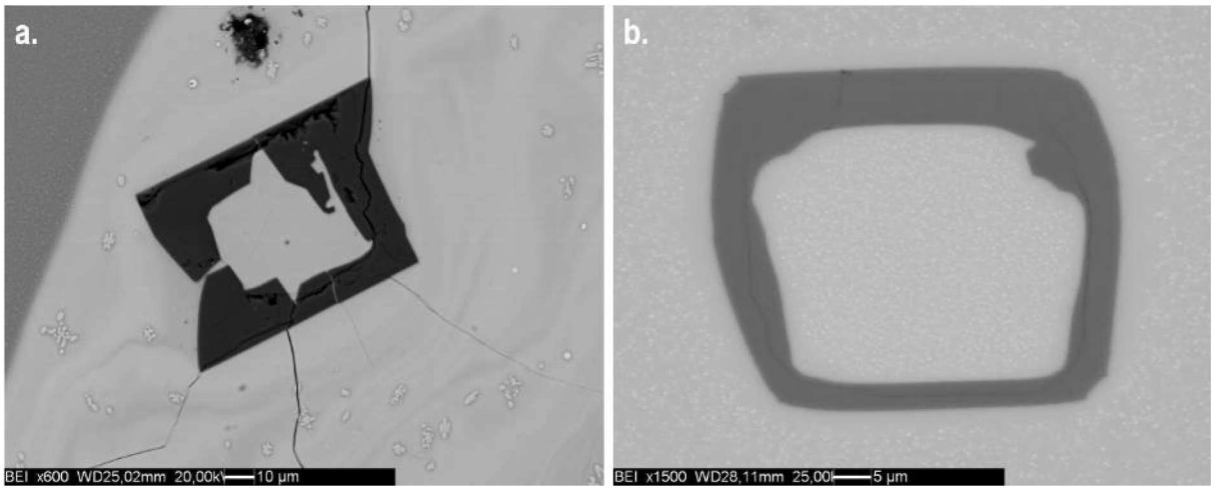

Fig. 9.14 – a) hollow wollastionite cystal in the sealing-wax red sample Ty-S-GR-506-R; b) hollow wollastionite cystal in the yellowish-orange sample Ty-P-A-408-Ar.

Clusters of acicular Ca-Pb-Na silicates were especially frequent in one sample of opaque yellow glass. Their presence reveals that the glass was held for a long time at relatively low temperatures, which is particularly significant in terms of production technologies of this color-class (Verità *et alii*, 2013). As already stated, Pb-antimoniates are unstable at high temperature, thus, it is necessary to introduce them in the melt below ca. 1000-1100°C to prevent the conversion to Ca-antimoniate and the consequential color loss. The high viscosity induced by these conditions accounts for the zoned appearance of some of the samples and the prolongated time needed for a proper mixing of the pigment into the glass can lead to the nucleation of the devitrification phases, as seen in the Tebtynis sample (fig. 7.3.18a).

The study of the mineralogic phases identified within the glasses of Tebtynis highlights the use of a wide range of technological solutions implying a strict control over the pyro-technological processes for the coloring and forming of glass, especially in terms of times, temperatures and redox conditions of the furnace, and in the proportions of the raw materials. In particular, some glasses show evidence of heat treatment at

high temperatures, up to ca. 1100-1200°C, while others have markers of low temperatures (450-600°C) and prolongated firing times. The atmosphere of the kiln also required extensive variations according to the specific color produced.

All things considered, the glasses from Tebtynis testify the mastery achieved by the Ptolemaic glassmakers in the coloring and forming of glass.

10. Concluding remarks and open questions

The artifacts from Tebtynis workshop carry important information about the technologies of production and manufacturing processes used under the Ptolemaic rule, offering a preliminary insight on the complexity of the Egyptian glass industry.

During this work, it was possible to identify the macroscopic and microscopic markers linked to the two main forming methods used in Tebtynis and to distinguish minor technological details, such as temperatures and step-by-step procedures for assembling stratified and mosaic glasses. Furthermore, some of the previously published tools were re-interpreted according to their shape and materic composition and better contextualized thanks to the critical review of the archival documents related to their discovery.

The economic and social significance of temples in Graeco-Roman Egypt is well known to specialists. The archaeological, textual and iconographic evidences show that sanctuaries hosted various facilities related to the production and processing of raw and semi-finished materials, from foods and vegetable resources to textiles and pyro-technological products (Clarysse 2010). However, the mudbrick structures of the workshops and warehouses within the temples are often poorly visible in the archaeological record and may be very hard to identify. The case of Tebtynis offered the unique chance to locate and analyze an important part of the annexes of the Soknebtynis sanctuary during the Hellenistic period, opening a new window on the link between craft productions and sacred spaces in Ptolemaic times.

The study of the Tebtynis inlays reveals that this specific typological class can be certainly attributed to a traditional Egyptian craft, both in terms of base glass production and secondary glass processing. Considering the mineralogical association of the heavy minerals in the sand, the provenance of the silica source – and consequently the production centers – can possibly be localized in the Nile Delta. This is consistent with what is known from the archaeological literature, as a series of tank furnaces generically dated to the Graeco-Roman period (III century BC – II century AD) was identified and excavated in the areas of Wadi Natrun and Mareotid, in the Western Delta (Nenna, 2015b). On the contrary, the secondary processing of glass, including

coloring/ opacifying and final forming into objects, seems to have taken place in the secondary workshops, at least in the case of Tebtynis. In Ancient Egypt each color had a specific meaning and was thus required for well-defined iconographic motifs (Duckworth, 2012; Bettineschi, 2016). The necessity of the local workshops to manage the types and quantities of each color required for the different decorative needs of the temples may be one of the reasons behind the segmentation of the glass-manufacture chain in Ptolemaic Egypt.

The analyses of the artifacts from Tebtynis have also highlighted the coexistence of glasses produced using two different alkali sources; while the classic LMG composition, typical of Roman glass, is clearly predominant, a few samples are consistent with the use of plant-ash as a flux (HMG). This recipe is especially typical (but not exclusive) of dull red glasses colored by metallic copper, and can probably be associated to the strongly reducing conditions which were needed for the manufacture of this specific color. Other intermediate compositions, such as the group of Mg-rich white glasses or the yellowish-orange samples were interpreted in terms of natron-based glasses which were subject to compositional changes occurred during the coloring process.

Lead can also decrease the melting point and thus act as a flux. In the Tebtynis collection, PbO is present in different concentrations, up to 40.11 wt%; soda-lime-lead and leaded-glasses are present in varying proportions in all color classes, but are always associated with sealing-wax red, dull red, yellow and yellowish-orange samples.

From the compositional point of view, the samples from Tebtynis are well integrated in the evolutionary trajectory leading to Roman glass. Looking at the coloring techniques, the site stands at the edge between two worlds, with ancient recipes coexisting with newer ones. This is the case of the lead-antimoniate yellow glass, heir of the LBA tradition, which can be found associated (at times even within the same inlay) with cuprite-based yellowish-orange glass, that represents a novelty of the mid I millennium BC which becomes increasingly common during the Roman period.

The same can be said for the combined used of *ex situ* and *in situ* precipitation of calcium antimoniates, where the first approach is especially typical of LBA Egyptian glasses, while the second seems to prevail in the Roman production.

The specific chronology of the Tebtynis workshop must still remain an open problem: while the typological studies have indicated an early dating (III century BC) on the basis of stylistic considerations (Nenna, 2015a and cited bibliography), the stratigraphic evidence presented in Anti's archival documents points towards a later date, at least for the final phase of the inlay production (I century BC – beginning of the I century AD). Judging from the overall composition of the samples, the Late Ptolemaic / Early Roman chronology would seem more fitting on the basis of the significant similarities with the Roman Imperial recipes. However, the very low number of artifacts securely dated to the Early and Central phases of the Ptolemaic period which were analyzed and reported in the literature is not sufficient to rule out the possibility of a III century BC chronology. Radiocarbon dating on the inlaid wooden fragments and of the organic binders adhering to the inlays has recently been proposed to clarify the matter.

Finally, the study of this collection highlighted that Tebtynis cannot be considered as a simple glass-working site, as previously assumed following the scarce notes published by Carlo Anti (1931) and revised by Rondot (2004). Instead, it was proven that the workshop in the temple of Soknebtynis represents the heart of a complex industry for the production of inlaid objects, functioning as a center for the acquisition and processing of several raw and semi-finished products including wood, plaster, organic binders and gold, in addition to glass (fig. 10.1). Considering its location and the typology of the objects which were produced there, the workshop probably manufactured both sacred furniture for the temple, such as statues and *naoi*, and devotional articles for the wealthy pilgrims. Ultimately, it contributed to the decorative and economic development of the Soknebtynis sanctuary.

Fig. 10.1 – Graphic representation of the various materials discovered in the Tebtynis workshop with their cross-craft interactions.

11. Acknowledgements

The Egyptian Museum of Turin, and in particular the Director dr. Christian Greco, is kindly thanked for giving us access to the collection of glasses from Tebtynis. A special thanks goes to dr. Alessia Fassone for devoting much of her time to assist us during our visits in Turin. Sampling was carried out with the supervision of the Soprintendenza Archeologica Belle Arti e Paesaggio per la Città metropolitana di Torino, represented by dr. Matilde Borla.

I am also grateful to the Museum of Archaeological Sciences and Art of the University of Padova, and especially to dr. Alessandra Menegazzi, for allowing me to use various unpublished pictures of the Anti's archive. Luisa Marcolin is heartfully thanked for her moral and technical support, especially in the design of the database. Dr. Giulia Deotto and dr. Ian Begg shared important unpublished data about the workshop discovery from Anti and Bagnani's archives and offered useful considerations about the documents; their collaboration surely helped to improve this thesis.

I also want to acknowledge the professors and the technicians that provided the opportunity to access the laboratories and contributed to the conclusion the work in due time: prof. Gilberto Artioli kindly allowed to transport the SM to Turin and to work on the LSCM, prof. Fabrizio Nestola facilitated the access to the μ-Raman at the Department of Chemistry, prof. Richard Spiess and prof. Stefano Poli accommodated our last-minute reservations for the SEM-EDS and EPMA analyses, respectively.

Leonardo Tauro offered technical assistance in the preparation of the samples and in the first SEM-EDS configuration. EPMA analyses were performed at the laboratories of the Department of Earth Sciences of the University of Milan with the support of Andrea Risplendente, whose efforts are sincerely appreciated.

I am greatly indebted to prof. Caroline Jackson and prof. Maria Pia Riccardi for their time and effort in reading and reviewing the first draft of this thesis. Their constructive comments have helped to improve the text.

I would also like to express my sincere gratitude to my PhD advisors, prof. Gianmario Molin, Ivana Angelini and Paola Zanovello for their help, their teachings and their patience. Ivana Angelini was always there for me, from an academic and personal point of view, showing me what kind of scientist and person I want to become. I couldn't have asked for a better guide. I received invaluable suggestions from Gianmario Molin, who provided insightful discussions about the project and offered precious advices to improve the final work. Paola Zanovello believed in this PhD research from the very beginning and always found a way to encourage me and my independent thinking. For all of this I'll be forever grateful.

I owe a lot to prof. Armando De Guio, one of the smartest and most enthusiastic people I know, for his trust and for involving me in many different projects. Dr. Alessandra Menegazzi of the MSA encouraged me to follow my aspirations, during my work at the Museum. If I'm here, it's also thanks to her.

Finally, thanks to all my colleagues both at the Department of Geosciences and the Department of Cultural Heritage, who shared the ups and downs of the last four years. A special mention is due to Laura Burigana, Flora Arena, Giulia Deotto, Luca Toninello, and to all the students of the Horus, Stempa and ArExGlass projects for the laughs and the fun and the hard work. Let's keep going!

Luigi Magnini contributed to this thesis in more than one way, from guidance for object-based image analysis to comfort food, from GIS to dishwashing. Thanks for being there for me in the last 14 years.

There are no words enough to express my gratitude for my family: my mom, my dad and my brother. Thanks to their constant love and support I'm here where I want to be, doing what I love the most.

I don't know where the journey will take me, but I did enjoy this ride.

REFERENCES

Abe, Y., Harimoto, R., Kikugawa, T., Yazawa, K., Nishisaka, A., Kawai, N., Sakuji, Y. and Nakai, I. (2012) Transition in the use of cobalt-blue colorant in the New Kingdom of Egypt. *Journal of Archaeological Science*, 39, pp. 1793-1808.

Adlington, L.W., (2017). The Corning Archaeological Reference Glasses: New Values for "Old" Compositions. *Papers from the Institute of Archaeology*, 27(1), pp. 1-8. DOI: http://doi.org/10.5334/pia-515

Aerts, A., Velde, B., Janssens, K., Dijkman, W., (2003) Change in silica sources in Roman and post-Roman glass. *Spectrochimica Acta*, part B 58, pp. 659-667.

Ahmed, A. and Ashour, G.M. (1981) Effect of heat treatment on the crystallisation of cuprous oxide in glass. *Glass Technology*, 22, pp. 24-33.

Alfonsi, H., and Gandolfo, P. (1997) L'épave Sanguinaires A. *Cahiers d'Archéologie Subaquatique,* 13, pp. 35-74.

Angelini, I., Artioli, G., Bellintani, P., Diella, V., Gemmi, M., Polla, A. and Rossi, A. (2004) Chemical Analyses of Bronze Age Glasses from Frattesina di Rovigo, Northern Italy. *Journal of Archaeological Science,* 31, pp. 1175-84.

Angelini, I., Bettineschi, C., Menegazzi, A., Molin, G. and Zanovello, P. (2014) Tra scienze e archeologia: le indagini archeometriche degli ornamenti da Tebtynis nell'ambito delle ricerche sulle collezioni egizie del Museo di Scienze Archeologiche e d'Arte (Università di Padova). *Museologia Scientifica Memorie*: *Proceedings of the XXI*

ANMS Congress: La ricerca nei musei scientifici. Padova, November 9-11, 2011. Padova, pp. 104-108.

Anti, C. (1930) Gli scavi della Missione Archeologica Italiana a Tebtunis (Fajum). *Aegyptus*, 2-4 (1929-1930), pp. 295-296.

Anti, C. (1931a) Gli scavi della Missione Archeologica italiana a Umm el Breighât (Tebtunis). *Aegyptus*, XI, pp. 389-391.

Anti, C. (1931b) Gli scavi della Missione Archeologica italana a Umm el Breighât (Tebtunis). *Bollettino dell'Associazione internazionale di Studi mediterranei*, II, pp. 23-24.

Anti, C. (1931-1932) Archeologia d'oltremare IV, Campagna 1931. *Atti del R. Istituto Veneto di Scienze Lettere ed Arti*, Tomo XCI, 2 (1931-1932), p. 1171 ss.

Antonaras, A. (2013) *Fire and Sand: Ancient Glass in the Princeton University Art Museum*. Princeton: Princeton University Art Museum ed.

Archeo 374 (2016), *Dyonisias: città dei segreti*, pp. 34-47.

Arkell, A.J. (1957) Ancient Red Glass at University College, London. *Journal of Egyptian Archaeology*, 43: 110.

Arletti, R., Dalconi, M.C., Quartieri, S., Triscari, M. and Vezzalini, G. (2006) Roman coloured and opaque glass: a chemical and spectroscopic study. *Applied Physics*, A 83, pp. 239-245.

Arletti, R., Rivi, L., Ferrari, D. and Vezzalini, G. (2011) The Mediterranean Group II: analyses of vessels from Etruscan contexts in northern Italy. *Journal of Archaeological Science*, 38, pp. 2094-2100.

Artioli, G., Angelini, I. and Polla, A. (2008) Crystals and phase transitions in protohistoric glass materials. *Phase Transitions*, 81(2-3), pp. 233-252.

Ashmawy Ali, A. (2006) Tell Gemaiyemi "Gomaimah" more than 100 years after Griffith's excavations. *Timelines: studies in honour of Manfred Bietak*, vol. I, *Orientalia Lovaniensia Analecta*, 145, Peeters: Leuven, pp. 55-64.

Aston, B.A.G., Harrell J. and Shaw I. (2000) Stone. *Ancient Egyptian materials and technology*, in Nicholson, P.T. and Shaw, I. (ed.), Cambridge: Cambridge University Press. pp. 5-77.

Atencio, D., Andrade, M.B., Christy, A.G., Gieré, R. and Kartashov, P.M. (2010) The pyrochlore supergroup of minerals: nomenclature. *Canadian Mineralogist*, 48, pp. 673-698.

Aufrère, S.H. (1991) *L'univers mineral dans la pensée Egyptienne.* Vol. 2. The Cairo: IFAO.

Aufrère, S.H. (2001) The Egyptian temple: substitute for the mineral universe, in Davies, W.V. (ed.), *Colour and Painting in Ancient Egypt*. London: The British Museum Press pp. 158-163.

Auth, S.H. (1999) Mosaic Glass Mask Plaques and the Ancient Theater. *Journal of Glass Studies*, 41, pp. 51-72.

Auth, S.H. (2012) The Denderah Cache of Glass Inlays: a possible votive pectoral, *Annales du 18e Congrès de l'Association Internationale pour l'Histoire du Verre*. Thessaloniki, 2009. Thessaloniki: Association Internationale pour l'Histoire du Verre, pp. 109-113.

Avanzini, F., Canazza, S., De Poli, G., Fantozzi, C., Pretto, N., Rodà, A., Angelini, I., Bettineschi, C., Deotto, G., Faresin, E., Menegazzi, A., Molin, G., Salemi, G. and Zanovello, P. (2015) Archaeology and Virtual Acoustics. A pan flute from ancient Egypt, *Proceedings of the SMC - Sound & Music Computing Conference*. Ireland, July 26 - August 1, 2015, Maynooth University.

Baatz, M., Hoffmann, C. and Willhauck, G. (2008) Progressing from Object-based to Object-oriented Image Analysis, in Blaschke, T., Lang, S. and Hay, G. (ed.), *Object-based image analysis. Spatial concepts for knowledge-driven Remote Sensing applications*. Springer: Berlin.

Bachmann, H.G., Everts, H. and Hope, C.A. (1980) Cobalt blue pigment on XVIII Dynasty Egyptian pottery. *Mitteilungen des Dutschen Archaologischen Instituts Abteilung Kairo*, 36, pp. 33-37.

Bagnani, G. (1935) Gli scavi di Tebtunis. *Bollettino di Antichità*, vol. VIII, pp. 376-387.

Bailey, D.M. (1984) Glass Plaques from a Foundation Deposit at Canopus, Egypt. *Antiquaries Journal*, 64, pp. 389-393.

Bailey, D.M. (1999) Sebakh, Sherds and Survey. *The Journal of Egyptian Archaeology*, 85, pp. 211-218.

Barag, D. (1985) *Catalogue of Western Asiatic Glass in the British Museum*. London: Trustees of the British Museum.

Barber, D. and Freestone, I.C. (1990) An investigation of the origin of the colour of the Lycurgus Cup by analytical transmission electron microscopy. *Archaeometry*, 32, pp. 33-45.

Barber, D.J., Freestone, I.C. and Moulding, K.M. (2009) Ancient copper red glasses: investigation and analysis by microbeam techniques. *From Mine to Microscope. Advance in the Study of Ancient Technology*, Oxbow Books, Oxford, pp. 115-127.

Barkoudah, Y. and Henderson, J. (2006) 'Plant ashes from Syria and the Manufacture of Ancient Glass: Ethnographic and Scientific Aspects. *Journal of Glass Studies*, 48, pp. 297-321.

Barnes, I.L., Brill, R.H., Deal, E.C. and Piercy, J. (1986) Lead isotope studies of the finds from the Serc¸e Limani shipwreck, *Proceedings of the 24th International Archaeometry Symposium*. Washington, D.C.: Smithsonian Institution Press, pp. 1-12.

Bass, G.F., Frey, D.A. and Pulak, C. (1984) A Late Bronze Age shipwreck at Kas, Turkey. *The International Journal of Nautical Archaeology*, 13, pp.271-279.

Bass, G.F. (1986) A Bronze Age Shipwreck at Ulu Burun (Kaş): 1984 Season. *American Journal of Archaeology*, 90, pp. 269-296.

Basso, E., Invernizzi, C., Malagodi, M., La Russa M.F., Bersanie D. and Lottici P.P. (2014) Characterization of colorants and opacifiers in roman glass mosaic tesserae through spectroscopic and spectrometric techniques. *Journal of Raman Spettroscopy*, 45, pp. 238-245.

Bastianini, G. and Deotto, G. (2014) Carlo Anti e Vitelli, *Ricerche Egittologiche in Italia: atti del convegno Nazionale*. Venezia, September 14-15, 2012. Venezia University Press: Venice, pp. 51-60.

Baxter, M.J. (1995) Standardization and transformation in principal component analysis, with applications to archaeometry. *Applied Statistics*, 44, pp. 513-527.

Baxter, M.J., Cool, H.E.M., Heyworth, M.P. and Jackson, C.M. (1995) Compositional variability in colourless Roman vessel glass. *Archaeometry*, 37, pp. 129-141.

Baxter, M.J., Cool, H.E.M. and Jackson, C.M. (2005) Further studies in the compositional variability of colourless Romano-British vessel glass. *Archaeometry*,47, pp. 45-68.

Bayley, J. (2015) Roman enamels and enameling, in Bayley, J., Freestone, I. and Jackson, C. (ed.) *Glass of the Roman World*. Oxbow books, pp. 179-189.

Begg, D.J.I. (1998a) The Canadian Tebtunis Connection at Trent University. *Echos du Monde Classique*, XLII, pp. 385-405.

Begg, D.J.I. (1998b) "It was Wonderful, Our Return in the Darkness with... the Baskets of Papyri!": Papyrus Finds at Tebtunis from the Bagnani Archives, 1931-1936. *Bulletin of the American Society of Papyrologists*, XXXV, pp. 185-210.

Begg, D.J.I. (2002) Greece 1921-1924 in the Bagnani Archives. *Scripta Mediterranea*, XXIII, pp. 55-81.

Beltsios, K.G., Oikonomou, A., Zacharias, N. and Triantafyllidis, P. (2012) Characterisation and provenance of archaeological glass artifacts from Mainland and Aegean Greece, in Liritsis, Y. and Stevenson, C.M. (ed.), *The dating and provenance of natural and manufactured glasses*. Albuquerque: University of New Mexico Press, pp. 166-84.

Benz, U.C., Hofmann, P., Willhauck, G., Lingenfelder, I. and Heynen, M. (2004) Multi-resolution, object-oriented fuzzy analysis of remote sensing data for GIS-ready information. *ISPRS Journal of Photogrammetry and Remote Sensing,* 58, pp. 239-258.

Beretta, M. (ed.) (2004) When glass matters: studies in the history of science and art from Graeco-Roman antiquity to early modern era. Firenze: Leo S. Olschki.

Bernand, É. (1981) Recueil des inscriptions grecques du Fayoum. III. La «méris» de Polémôn, in Bibliothèque d'Étude, 80, Il Cairo.

Bettineschi, C. (2013) *Ornamenti egizi da Tebtynis del Museo di Scienze Archeologiche e d'Arte: proposte di valorizzazione tra archeologia e archeometria*, Unpublished post-graduate dissertation, University of Padova.

Bettineschi, C., (2016) Tra natura e cultura: materiali vetrosi e minerali nell'Egitto pre-romano, *Bollettino del Gruppo di Mineralogia e Paleontologia Euganea*, 71, pp. 28-34.

Bettineschi C., Deotto, G., Begg, D.J.I., Angelini I., Molin, G. and Zanovello P. (Forthcoming) Crafts in the temple: the Ptolemaic inlay workshop in Soknebtynis sanctuary. *Quaderni del Museo del Papiro, Proceedings of the XVI Convegno di Egittologia e Papirologia*. Siracusa: Museo del Papiro Corrado Basile.

Bianchi, R.S., Schlick-Nolte B., Bernheimer, G.M. and Barag D. (2002) *Reflections on Ancient Glass from the Borowski Collection.* Bible Lands Museum Jerusalem. Mainz: Philip von Zabern.

Bianchi, R.S. (1983a) Those ubiquitous glass inlays from pharaonic Egypt: suggestions about their functions and dates. *Journal of Glass Studies*, 25, pp. 29-35.

Bianchi, R.S. (1983b) Those ubiquitous glass inlays. Part 2. *Bulletin of the Egyptological Seminar*, 5, pp. 9-29.

Bianchi, R.S. (1998) Symbols and meanings, in Friedman, F.D. (ed.), *Gifts of the Nile: ancient Egyptian faience*. London: Thames and Hudson, pp. 22-32.

Bieber, A. M., Brooks, D. W., Harbottle, G. and Sayre, E. V. (1976) Application of multivariate techniques to analytical data on Aegean ceramics. *Archaeometry* ,18, pp. 59-74.

Bimson, M. (1987) Opaque Red Glass: a review of the previous studies. *Early vitreous materials*, British Museum Occasional Paper, 56, British Museum, London, pp. 165-171.

Bimson, M. and Freestone, I.C. (1983) An analytical study of the relationship between the Portland vase and other Roman cameo glasses. *Journal of Glass Studies*, 25, pp. 55-65.

Bimson, M. and Freestone, I.C. (1988) Some Egyptian glasses dated by royal inscriptions. *Journal of Glass Studies*, 30, pp. 11-15.

Bimson, M. and Freestone, I.C. (1991) Glassmaking on the Komasterion site: The discovery of an Islamic Glass-making Site in Middle Egypt, in Bailey, D.M. (ed.), *Excavations at El-Ashmunein IV: Hermopolis Magna: Buildings of the Roman Period*. Londres, pp. 64-65.

Blaschke, T., Hay, G.J., Kelly, M., Lang, S., Hofmann, P., Addink, E., Queiroz Feitosa, R., Van Der Meer, F., Van Der Werff, H., Van Coillie, F. and Tiede, D. (2014) Geographic Object-Based Image Analysis - Towards a new paradigm. *ISPRS Journal of Photogrammetry and Remote Sensing*, 87, pp. 180-191.

Blaschke, T. and Strobl, J. (2001) What's wrong with pixels? Some recent developments interfacing remote sensing and GIS. *GIS-Zeitschrift für Geoinformationssysteme*, 14 (6), pp. 12-17.

Blomme, A., Elsen, J., Brems, D., Shortland. A.J., Dotsika, E. and Degryse P. (2015) Tracing the primary production location of core-formed glass vessels, Mediterranean Group I. *Journal of Archaeological Science: Reports*, 5, pp. 1-9.

Blomster, J.P., Neff, H. and Glascock, M.D. (2005) Olmec pottery production and export in ancient Mexico determined through elemental analysis. *Science*, 307, pp. 1068-1072.

Borgia, I., Brunetti, B., Mariani, I., Sgamellotti, A., Cariati, F., Fermo, P., Mellini, M., Viti, C. and Padaletti, G. (2002) Heterogeneous distribution of metal nanocrystals in glazes of historical pottery. *Applied Surface Science*, 185, pp. 206-216.

Boschetti, C., Henderson, J., Evans, J. and Leonelli, C. (2016) Mosaic tesserae from Italy and the production of Mediterranean coloured glasses (3rd century BC–4th century AD). Part I: chemical composition and technology. *Journal of Archaeological Science: Reports*, 7, pp. 303-308.

Boschetti, C. (2017) Beyond beauty. Glass inlays from Ptolemaic and Roman Egypt: technology and economy, *Abstract Book of the Conference "Glass of the Caesars @ 30"*, London November 2017, p. 1.

Breccia, E. (1932) *Le Musée Greco-Romain d'Alexandrie*, 1925-1931, Bergamo.

Brenningmeyer, T. and Begg, D.J.I. (2007) Reconstructing Tebtunis: Assembling a Site Model Using Archived Aerial Photography, *Digital Discovery. Exploring New Frontiers in Human Heritage. CAA2006. Computer Applications and Quantitative Methods in Archaeology*. Hagesmeister E.M., Budapest, pp. 338-343.

Bryan, B. M. (2008) A newly discovered statue of a queen from the reign of Amenhotep III. *Servant of Mut: Studies in honor of Richard A. Fazzini*, pp. 32-43. Leiden-Boston.

Brill, R. H. (1970) The chemical interpretation of the texts, in *Glass and glassmaking in ancient Mesopotamia*, Corning Museum of Glass, New York, pp. 105-128.

Brill, R.H. (1988) Scientific Investigations of the Jalame glass and related finds, in Weinberg, G.D. (ed.) *Excavations at Jalame: site of a glass factory in Late Roman Palestine*, University of Missouri Press, Columbia.

Brill, R.H. (1999) *Chemical analyses of early glasses, vol. 1 and 2*, Corning Museum of Glass, New York.

Brill, R.H. and Cahill, N.D. (1988) A red opaque glass from Sardis and some thoughts on red opaques in general. *Journal of Glass Studies*, 30, pp. 16-27.

Brill, R. H., and Moll, S. (1963) Electron Beam Probe Microanalysis of Ancient Glass. *Advances in Glass Technology, part 2*. New York: Plenum Press, pp. 293-302.

Brill, R.H., and Wampler, J.M. (1965) Isotope studies of ancient lead. *American Journal of Archaeology*, 71, pp. 63-77.

Brissau, P. and Zivie-Coche, C. (ed.) (1998) *Tanis: travaux récents sur le tell Sân el-Hagar. 1987-1997*, Éd. Noêsis: Paris.

Brugger, J., Gieré, R., Graeser, S. and Meisser N. (1997) The crystal chemistry of roméite. *Contributions to Mineralogy and Petrology*, 127(1-2), pp. 136-146.

Brun, N., Mazerolle, L. and Pernot, M. (1991) Microstructure of opaque red glass containing copper. *Journal of Materials Science Letters*, 10, pp. 1418-20.

Brun, N. and Pernot, M. (1992) The opaque red glass of Celtic enamels from continental Europe. *Archaeometry*, 34, pp. 235-52.

Brunton G., and Engelbach R. (1927) *Gurob*, London: Bernard Quartch.

Burigana, L. (2017) Elaborazione di immagini multispettrali: composizione e manipolazione di bande, *Proceedings of the workshop: Horus, visioni dall'alto dello spazio archeologico.* Padua: Padova University Press, pp. 39-46.

Burkhalter, F. (1985) Le mobilier des sanctuaires d'Egypte. *Zeitschrift fuer Papyrologie und Epigraphik*, vol. 59, pp. 123-134.

Cable, M. and Smedley, J.W. (1987) The replication of an opaque red glass from Nimrud. *Early vitreous materials, British Museum Occasional Paper*, 56, British Museum, London, pp. 151-164.

Caley, E.R. (1962) *Analyses of ancient glasses 1790-1957*. Corning Museum of Glass: New York.

Calvo del Castillo, H. and Strivay, D. (2012) X-Ray Methods, in Howell, G.M., Edwards and Vandenabeele P. (ed.), *Analytical Archaeometry: selected topic*. Croydon, RSC Publishing, pp. 59-102.

Capasso, M. and Davoli, P. (ed.), (2012) *Soknopaiou Nesos Project I (2003-2009)*, Pisa-Roma.

Cappozzo, M. (2006) La collezione egizia del Museo Nazionale Preistorico Etnografico "Luigi Pigorini". *Bullettino di Paletnologia Italiana*, 96, pp. 131-202.

Carpinelli, A., Azzalin, G., Bilotti, G., Cogo, M., Mason, G. and Peruzzo, F.E. (2017) Soknebtynis: planimetria digitale del tempio e del suo dromos, *Proceedings of the workshop: Horus, visioni dall'alto dello spazio archeologico.* Padua: Padova University Press, pp. 57-64.

Cauville, S. (1999) Dendera, *Encyclopedia of the Archaeology of Ancient Egypt*, edited by Bard, K.A., Routledge: Oxon, pp. 252-254.

Cervi, A. (2012) L'arredo ligneo del tempio di Soknopaios, in M. Capasso, P. Davoli (ed.) *Soknopaiou Nesos Project, I (2003-2009). Biblioteca di studi di egittologia e di papirologia 9*, Pisa-Roma: Fabrizio Serra editore, pp. 269-314.

Cesareo, R., Frazzoli, F. V., Mancini, C., Sciuti S., Marabelli, M., Mora, P., Rotondi, P., and Urbani, G. (1972) Non-Destructive Analysis of Chemical Elements in Paintings and Enamels. *Archaeometry*, 14, pp. 65-78.

Chikira, A. (1995) Glass Vessels. *Akoris. Report of the Excavations at Akoris in Middle Egypt 1981-1992*, Kyoto: Koyo Shobo, pp.234-245.

Clarysse, W. (2010) Egyptian Temples and Priests: Graeco-Roman. *Companion to Ancient Egypt*, pp. 274-290.

Codd, E.F. (1970) A relational model of data for large shared data banks. *Communications of the ACM*, 13 (6), pp. 377-387.

Collie, J.N. (1918) Notes on the "Sang de Boeuf" and the Copper-red Chinese Glazes. *Transactions of the Indian Ceramic Society*, 17, pp. 379-384.

Connolly, P., Rehren, T., Doulgeri-Intzesiloglou, A. and Arachoviti, P. (2012) The Hellenistic Glass of Pherai, Thessaly, *Annales du 18ème Congrès de l'Association Internationale pour l'Histoire du Verre*, Thessaloniki 2009, pp. 91-97.

Connor, A.J. (2014) *Temples as Economic Agents in Early Roman Egypt: the case of Tebtunis and Soknopaiou Nesos*. Unpublished PhD dissertation, University of Cincinnati.

Cooney, J.D. (1976) *Catalogue of Egyptian Antiquities in the British Museum, IV: Glass*. London: British Museum Publishing.

Cosyns, P., Janssens, K., Van der Linden, V. and Schalm, O. (2006) *Black glass in the Roman Empire: A work in progress*, pp. 30-41.

Cox, G. A. and Gillies, K. J. S. (1986) The X-ray fluorescence analysis of medieval durable blue soda glass from York Minster. *Archaeometry*, 28, pp. 57-68.

Crawford, D. (1971) *Kerkeosiris: An Egyptian Village in the Ptolemaic Period*, Cambridge .

Dal Sasso G., Maritan, L., Salvatori, S., Mazzoli, C., and Artioli, G. (2014) Discriminating pottery production by image analysis: a case study of Mesolithic and Neolithic pottery from Al Khiday (Khartoum, Sudan). *Journal of Archaeological Science*, 46, pp. 125-143. https://doi.org/10.1016/j.jas.2014.03.004.

Davoli, P. (2008) Papiri, archeologia e storia moderna. *Atene e Roma*, 1-2, pp. 100-124.

Dawson, W.R., and Uphill, E.P. (1995) *Who was who in Egyptology*, 3rd rev ed. by M.L. Bierbrier, London: Egypt Exploration Society,

De Carolis, E. (2006) *Vitrum. Il vetro fra arte e scienza nel mondo romano*. Firenze: Giunti, pp. 73-81.

De Cosson, A. (1935) *Marotis*. Morrison & Gibb Ltd: London And Edinburgh.

Deer, W.A., Howie, R.A. and Zussman, J. (1994) *Introduzione ai minerali che costituiscono le rocce*. Zanichelli: Bologna

Deer, W.A., Howie, R.A., and Zussman, J. (1978) *Rock forming minerals: 2A: Single-chain silicates*, 2nd edition, London: Longman.

Degryse, P. (ed.) (2014) *Glass Making in the Greco-Roman World: Results of the ARCHGLASS Project*. Leuven University Press: Leuven.

Degryse, P., Henderson, J. and Hodgins, G. (ed.) (2009) *Isotopes in vitreous materials*. Leuven University Press, Leuven.

Degryse, P. and Shortland, A. (2009) Trace elements in provenancing raw materials for Roman glass production. *Geologica Belgica,* 12(3-4), pp. 135-143.

Deotto, G. (2014) Il segno la forma l'uomo, *L'Egitto in Veneto, Atti del II Convegno Nazionale*, Padova 10 febbraio 2010, Padova: Cleup, pp. 68-71.

Deotto, G. (2015) *L'Università di Padova in Egitto. Analisi e ricostruzione dello scavo a Tebtynis attraverso la documentazione inedita*. Unpublished PhD dissertation, University of Padova.

Deotto, G., Bettineschi, C., Zanovello, P., Angelini, I. and Molin, G. (2017a) «Sempre nell'interno del santuario è stato trovato il materiale di un laboratorio di smalti colorati…»: localizzazione e studio di un'officina tolemaica per intarsi, *Proceedings of the workshop: Horus, visioni dall'alto dello spazio archeologico*. Padua: Padova University Press, pp. 83-90.

Deotto, G., Begg, I. and Toninello, L. (2017b) Tebtynis: a first view, *Proceedings of the workshop: Horus, visioni dall'alto dello spazio archeologico*. Padua: Padova University Press, pp. 49-46.

Deotto G., Bettineschi C., Bettanini C., Magnini L., Toninello L., Colombatti G., Aboudan A., Zanovello P., Menegazzi A., Benvenuti P., Debei S., De Guio A. and the

Horus Team, (forthcoming) Horus Project: aerospace technologies for archaeological research. *Archeologia Aerea* 10/ 16, Studi di Aerotopografia Archeologica.

Dik, J., Hermens, E., Peschar, R. and Schenk, H. (2005) Early production recipes for lead antimonate yellow in Italian art. *Archaeometry*, 47, pp. 593-607.

Downs R.T. (2006) The RRUFF Project: an integrated study of the chemistry, crystallography, Raman and infrared spectroscopy of minerals, *Program and Abstracts of the 19th General Meeting of the International Mineralogical Association in Kobe*, Japan, pp. 03-13.

Drennan, R.D. (2009) *Statistics for Archaeologists*, (2nd ed.). New York: Springer.

Duckworth, C.N. (2011) *The created stone: Chemical and archaeological perspectives on the colour and material properties of early Egyptian glass, 1500-1200 BC.* Unpublished Ph.D. thesis, University of Nottingham, England.

Duckworth, C.N. (2012) Imitation and creation: the color and perception of the earliest glasses in New Kingdom Egypt. *Cambridge Archaeological Journal*, 22 (3), pp. 309-327.

Duckworth, C.N. (2016) Addressing the invisible: experiment, data mining and the archaeometry of glass recycling in the I millennium AD, *Book of Abstracts of the 41st Symposium on Archaeometry*, Kalamata (Greece), May 15-21.2016.

Duckworth, C.N., Henderson, J., Rutten, F.J. and Nikita, K. (2012) Opacifiers in Late Bronze Age glasses: The use of ToF-SIMS to identify raw ingredients and production techniques. *Journal of Archaeological Science*, 39, pp. 143-152.

Dussart, O. and Velde, B. (1990) La composition du verre hellénistique en Jordanie et Syrie du Sud. *Syria*, 67(3-4), pp. 687-693.

El-Hinnawi, E.E. (1964) Mineralogical and Geochemical Studies on Egyptian (U.A.R.) Black Sands. *Beitrage zur Mineralogie und Petrographie*, 9, pp. 519-532.

Eramo, G., Aprile, A., Muntoni, I.M. and Zerboni, A., (2014) Textural and morphometric analysis applied to Holocene pottery from Takarkori rock shelter (SW Libya, Central Sahara): a quantitative sedimentological approach. *Archaeometry,* 56, pp. 36-57.

Étienne, M. (2009) *Les Portes du Ciel. Visions du monde dans l'Egypte ancienne*, co-published by Musée du Louvre Editions and Somogy.

Fabic, M. (2009) Advancing Confocal Laser Scanning Microscopy: the Advantage of Optical Metrology. *Optik & Photonik*, pp. 40-43.

Falk, D.A. (2015) *Ritual Processional Furniture: a Material and Religious Phenomenon in Egypt*. Unpublished PhD dissertation, University of Liverpool.

Farnsworth, M. and Ritchie, P.D. (1938) Spectrographic studies on ancient glass. *Technical Studies VI* (3).

Fazzini, R. (1999) Karnak, precinct of Mut. *Encyclopedia of the archaeology of ancient Egypt*, London: Routledge, pp. 397-400.

Fazzini, R. (2008) Report on the Brooklyn Museum's 2008 Season of Fieldwork at the Precinct of the Goddess Mut at South Karnak. Unpublished preliminary report. Available at: https://www.brooklynmuseum.org/features/mut/uploads/Preliminary_Report_2008.pdf (accessed last time in October 2017).

Fazzini, R. (2009) *Report on the Brooklyn Museum's 2009 Season of Fieldwork at the Precinct of the Goddess Mut at South Karnak*. Unpublished preliminary report.

Available at: https://www.brooklynmuseum.org/features/mut/uploads/Preliminary_Report_2009.pdf (accessed last time in October 2017).

Fiori, C. (2014) Production technology of Byzantine red mosaic glasses. *Ceramics International*, 41, pp. 3152-3157.

Fiori, C. and Vandini, M. (2004) Chemical composition of glass and its raw materials: chronological and geographical development in the first millennium AD. *When glass matters: Studies in the History of Science and Art from Graeco-Roman Antiquity to Early-Modern Era*, Leo S. Olschki: Firenze.

Fiori, C., Vandini, M. and Mazzotti, V. (2004) *I colori del vetro antico - Vetro musivo Bizantino*, Il prato (ed.), Saonara (Padova).

Fisher, A. (2008) *Hot Pursuit: integrating anthropology in search of ancient glass-blowers*. Plymouth: Lexington Books.

Fiori, C. (2015) Production technology of Byzantine red mosaic glasses. *Ceramics International*, 41, pp. 3152-3157.

Foster, H.E. and Jackson, C.M. (2009) The composition of 'naturally coloured' late Roman vessel glass from Britain and the implications for models of glass production and supply. *Journal of Archaeological Science*, 36, pp. 189-204.

Foster, H.E. and Jackson, C.M. (2010) The composition of late Romano-British colourless vessel glass: glass production and consumption. *Journal of Archaeological Science*, 37, pp. 3068-3080.

Foy, D. (2005) Une production de bols moulés à Beyrouth à la finde l'époque hellénistique et le commerce de ces verres en Méditerranée occidentale. *Journal of Glass Studies*, 47, pp. 11-36.

Foy, D. and Nenna, M.D. (2001) Tout Feu Tout Sable: mille ans de verre antique dans le Midi de la France. *Mille ans de verre antique dans le Midi de la France*. Marseille: Musées de Marseille.

Foy, D., Vichy, M. and Picon, M. (2000) Lingots de verre en Méditerrané occidentale, *Annales du 14th congrès de l'Association pour l'Histoire du Verre AIHV*, Amsterdam, pp. 51-57.

Foy, D., Picon, M., Vichy, M. and Thirion-Merle, V. (2003) Caractérisation des verres de la fin de l'Antiquité en Méditerranée occidentale: l'émergence de nouveaux courants commerciaux, Échanges et commerce du verre dans le monde antique, Actes du colloque de l'Association Française pour l'Archéologie du Verre, Aix-en-Provence et Marseille, 7-9 juin 2001, Editions Monique Mergoil, Montagnac, pp. 41-85.

Freestone, I. (1987) Composition and microstructure of early opaque red glass. *Early vitreous materials*, British Museum Occasional Paper, 56, British Museum, London, pp. 151-164.

Freestone, I.C., Bimson, M. and Buckton, D. (1990) Compositional categories of Byzantine glass tesserae, *Proceedings of the 11th Congress of the International Association for the History of Glass*, Basle, 1988, Amsterdam: AIHV, pp. 271-80.

Freestone I.C., Gorin-Rosen, Y. and Hughes, M.J. (2000) Primary glass from Israel and the production of glass in Late Antiquity and the Early Islamic period, in Nenna M.D. (ed.), La route du verre. Ateliers primaires et secondaires du second millénaire avant J.C. au Moyen Age. Travaux de la Maison de l'Orient Méditerranéen, 33. TMO, Lyon, pp. 65-82.

Freestone, I.C., Stapleton, C.P. and Rigby V. (2003) The production of red glass and enamel in the Late Iron Age, Roman and Byzantine periods. *Through a glass brightly:*

studies in Byzantine and Medieval art and archaeology, Oxbow Books, Oxford, pp. 142-154.

Freestone, I.C. and Stapleton, C.P. (2015) Composition, technology, and production of coloured glasses from mosaic vessels of the Early Roman Empire, in Bayley, J., Freestone, I. and Jackson, C. (ed.), *Glass of the Roman Empire.* Oxbow Books, Oxford, pp. 61-76.

Gallazzi, C. (1989) *Fouilles anciennes et fouilles nouvelles sur le site de Tebtynis*. BIFAO, LXXXIX, 179-191.

Gallazzi, C. (1992) Carlo Anti e Tebtynis: il lavoro svolto e le prospettive aperte. *Carlo Anti. Giornate di studio nel centenario della nascita*, Trieste, pp. 129-147.

Gallazzi, C. (1995) La ripresa degli scavi a Umm-el-Breigât (Tebtynis). *Acme*, XLVIII, pp. 3-24.

Gallazzi, C. (1997) Missione archeologica di Umm-el-Breigat (Tebtynis), in *Missioni Archeologiche Italiane: la ricerca archeologica, antropologica, etnologica*, Direzione generale delle relazioni culturali (ed.), Roma, pp. 37-40.

Gallazzi, C. (2001) La ricerca archeologica a Umm el-Breigat (Tebtynis), in Casini, M. (ed.), *Cento anni in Egitto: percorsi dell'archeologia italiana*. Milano: Electa, pp. 171-183.

Gallazzi, C. (2010) Umm-el-Breigât (Tebtynis) 2004-2008: gli scavi nel settore bizantino. *RIL*, 144, pp. 183-208.

Gallazzi, C. (2015) Umm-El-Breigât (Tebtynis): campagna di scavo dell'anno 2012. *Rendiconti Classe di Lettere e Scienze Morali Storiche,* 146, pp. 87-110.

Gallazzi, C. and Hadji-Minaglou, G. (2000) Tebtynis I. La reprise des fouilles et le quartier de la chapelle d'Isis-Thermouthis, *FIFAO* 42, Le Caire.

Gallo, F., Silvestri, A., Molin, G. and Marcante, A. (2014) Iron Age vessels from the Archaeological Museum of Adria (North-Eastern Italy): a textural, chemical and mineralogical study, *Proceedings of the 39th International Symposium on Archaeometry - ISA 2012*, pp. 198-207.

Gasperini, V., Paolucci, G. and Tocci, A. (2008) *Catalogo dei frammenti lignei e degli intarsi in pasta vitrea da Bakchias (1996-2002)*. Imola: Editrice La Mandragora.

Gauckler, P. (1915) *Nécropoles puniques de Carthage I*. 2 v. Paris: A. Picard.

Gedzevičiūtė, V. (2006) *Die Mosaikgläser des Martin von Wagner Museums-archäologische und materialkundliche Untersuchungen*. Magister Thesis, University Würzburg.

Gedzevičiūtė, V., Welter, N., Schussler, U. and Weiss, C. (2009) Chemical composition and colouring agents of Roman mosaic and millefiori glass, studied by electron microprobe analysis and Raman microspectrometry. *Archaeological and Anthropological Sciences*, 1, pp. 15-29.

Gimeno, D., Garcia-Valles, M., Fernandez-Turiel, J. L., Bazzocchi, F., Aulinas, M., Pugès, Tarozzi, C., Pia Riccardi, M., Basso, E., Fortina, C., Mendera, M. and Messiga, B. (2008) From Siena to Barcelona: deciphering colour recipes of Na-rich Mediterranean stained-glass windows at the XIII-XIV century transition. *Journal of Cultural Heritage*, 9, pp. 10-15.

Gliozzo, E. (2016) The composition of colourless glass: a review. *Journal of Archaeological and Anthropological Science*, DOI 10.1007/s12520-016-0388-y

Gliozzo, E., Lepri, B., Saguì, L. and TurbantiMemmi, I. (2015) Colourless glass from the Palatine and Esquiline hills in Rome (Italy). New data on antimony- and manganese-decoloured glass in the Roman period. *Archaeological and Anthropological Science*, DOI 10.1007/s12520-015-0264-1

Gliozzo, E., Santagostino Barbone, A., D'Acapito, F., Turchiano, M., Turbanti Memmi, I.G. and Volpe, G. (2010) The Sectilia Panels of Faragola (Ascoli Satriano, Southern Italy): A Multi-Analytical Study of the Green, Marbled (Green and Yellow), Blue and Blackish Glass Slabs. *Archeometry*, 52(3), pp. 389-415.

Goins, E. and Reedy, C.L. (2000) Digital image analysis in microscopy for objects and architectural conservation. *Objects Specialty Group Postprints, American Institut for Conservation of Historic and Artistic Works*, Vol. 7, pp. 122-137.

Goldstein, S.M. (1979) *Pre-Roman and Early Roman Glass in the Corning Museum of Glass*. Corning, New York: Corning Museum of Glass.

Gratuze, B. (2013) Glass Characterization Using Laser Ablation Inductively Coupled Plasma Mass Spectrometry Methods. *Modern Methods for Analyzing Archaeological and Historical Glass,* John Wiley & Sons, Ltd, pp. 201-234.

Gratuze, B. and Picon, M. (2005) Utilisation par l'industrie verrièrs des sels d'aluns des oasis égyptiennes au debut du premier millénaire avant notre ère, *Colloque International «L'alun de Méditerranée»*, 4-8 Juin 2003. Institut Français de Naples, Naples, pp. 269-276.

Gratuze, B., Soulier, I., Barradon, J.N. and Foy, D. (1992) De l'origine du cobalt dans le verres. *Revue d'Archéométrie*, 16, pp. 97-108.

Grenfell, B. and Hunt, A. (1901) *A Large Find of Ptolemaic Papyri*, APF1, pp. 376-378.

Grenfell, B. and Hunt, A. (1902) *The Tebtunis Papyri*, London.

Grenfell, B. and Hunt, A. (1907) *The Tebtunis Papyri*, part II, London.

Grieco, R. (2008) *Micromosaici romani - Roman Micromosaics*. Roma: Gangemi Editore.

Grose, D.F. (1977) Early Blown Glass: The Western Evidence. *Journal of Glass Studies*, 19, pp. 9-29.

Grose, D.F. (1989) *Early Ancient Glass: core-formed, rod-formed and cast vessels and objects from the late Bronze Age to the early Roman Empire, 1600 BC to AD 50*, Hudson Hills Press, New York.

Hadji-Minaglou, G. (2007) *Tebtynis IV. Les habitations à l'est du temple de Soknebtynis*, FIFAO 56.

Hadji-Minaglou, G. (2009) L'établissement thermal de Tebtynis (Fayoum). *Le bain collectif en Égypte*, EtudUr 7, Le Caire, pp. 181-190.

Haralick, R.M. and Shapiro, L.G. (1985) Image segmentation Techniques. *Computer Vision, Graphics and Image Processing*, 29, pp. 100-132.

Harden, D.B. (1936) *Roman Glass from Karanis*. Ann Arbor: University of Michigan Press.

Harden, D.B. (1940) The Glass. *Temples of Armant. A Preliminary Survey*, MEES 43, Londres, 2 vol.

Hay, G.J., Niemann, K.O. and Goodenough, D.G. (1997) Spatial thresholds, image-objects and upscaling: a multi-scale evaluation. *Remote Sensing of Environment,* 62(1), pp. 1-19.

Henderson, J. (1985) The Raw Materials of Early Glass Production. *Oxford Journal of Archaeology*, 4, pp. 267-291.

Henderson, J. (1988) Glass production and Bronze Age Europe. *Antiquity*, 62, pp. 435-451.

Henderson, J. (1991) Chemical and structural analysis of Roman enamels from Britain. *Archaeometry*, 90, pp. 285-294.

Henderson, J. (1996) Scientific analysis of selected Fishbourne vessel glass and its archaeological interpretation. *Excavations at Fishbourne 1969–1988, Chichester Excavations*, 9, Chichester, England: Chichester, District Council, pp. 189-92.

Henderson, J. (2000) *The science and archaeology of material*s, Routledge, London.

Henderson, J. (2002) Tradition and experiment in first millennium A.D. glass production - the emergence of early Islamic glass technology in late Antiquity. *Accounts of Chemical Research*, 35(8), pp. 594-602.

Henderson, J. (2013) *Ancient Glass: an interdisciplinary exploration*, Cambridge University Press.

Henderson, J., McLoughlin, S. and McPhail, D. (2004) Radical changes in Islamic glass technology: evidence for conservatism and experimentation with new glass recipes from early and middle Islamic Raqqa, Syria. *Archaeometry*, 46, pp. 439-68.

Himly, M.E. (1951) Beach Sands of the Mediterranean Coast of Egypt. *Journal of Sedimentary Petrology*, 21, pp. 109-120.

Hodgkinson, A.K. (2012) The excavation of the "industrial area", *Report to the Supreme Council of Antiquities on archaeological survey and excavation undertaken at Medinet el-Gurob*, 27 March-7 April 2012.

Insley Green, Chr. (1987) *The temple furniture from the sacred animal necropolis at north Saqqâra, 1964-1976*. London: EES.

Jackson, C.M. (2005) Making colourless glass in the Roman period. *Archaeometry*, 47, pp. 763-780.

Jackson, C.M., Booth, C.A. and Smedley, J.W. (2005) Glass by design? Raw materials, recipes and compositional data. *Archaeometry,* 47, pp. 781-95.

Jackson, C. M. and Nicholson, P.T. (2007) Compositional analysis of the vitreous materials found at Amarna, in Nicholson, P.T. (ed.), *Brilliant Things for Akhenaten: the production of glass. vitreous materials and pottery at Amarna site 045.1*. London: Egypt Exploration Society. pp. 101-116.

Jackson, C.M. and Paynter, S. (2015) A great big melting pot: exploring patterns of glass supply, consumption and recycling in Roman Coppergate, York. *Archaeometry*, 58 (1), pp. 68-95.

Jackson, C.M., Paynter, S., Nenna, M.D. and Degryse, P. (2016) Glassmaking using natron from el-Barnugi (Egypt); Pliny and the Roman glass industry. *Archaeological and Anthropological Science*. DOI: 10.1007/s12520-016-0447-4

Jackson, C.M. and Nicholson, P.T. (2010) The provenance of some glass ingots from the Uluburun shipwreck. *Journal of Archaeological Science*, 37, pp. 295-301.

Jouguet, P. (1932) Lettre de M. Carlo Anti sur les fouilles italiennes de Tebtynis (Égypte). *Comptes-rendus des séances de l'Académie des Inscriptions et Belles-Lettres*, 76e année, N. 4, pp. 359-361.

Kaczmarczyk, A. and Hedges, R.E.M., (1983) *Ancient Egyptian Faience: An Analytical Survey of Egyptian Faience from Predynastic to Roman Times*. Warminster, Aris and Phillips.

Kamrin, J. (2015) The Egyptian Museum Database, Digitizing, and Registrar Training Projects: Update 2012. *Bulletin of the Egyptological Seminar*, 19, pp. 413-440.

Kawanishi, H. and Miyamoto, J. (1995) Beads, Amulets And Miscellaneous Accessories, in *Akoris. Report of the Excavations at Akoris in Middle Egypt 1981-1992*, Kyoto: Koyo Shobo, pp. 228-234.

Keller, C.A. (1983) Problems of dating glass industries of the Egyptian New Kingdom: examples from Malkata and Lisht. *Journal of Glass Studies*, 25, pp. 19-28.

Killick, D. (2004) Social constructionist approaches to the study of technology. *World Archaeology*, 36, pp. 571-578.

Kucharczyk, R. (2005) Late Roman/ Early Byzantine Glass from the Auditoria on Kom el-Dikka in Alexandria. *Polish Archaeology in the Mediterranean*, 17, pp. 45-53.

Labrador, A.M. (1996) *Databases, in The Oxford Companion to Archaeology*, Oxford University press, pp. 379-382.

Lahlil, S., Biron, I., Galoisy, L. and Morin, G. (2006) Technological Processes to produce antimoniate opacified glass throught history, *Annales du 17e Congrès de l'Association Internationale pour l''Histoire du Verre*, Anvers, pp. 571-579.

Lahlil, S., Biron, I., Galoisy, L. and Morin, G. (2008) Rediscovering ancient glass technologies through the examination of opacifier crystals. *Applied Physics*, A 92, pp. 109-116.

Lahlil, S., Biron, I., Cotte, M., Susini, J. and Menguy, N. (2010a) Synthesis of calcium antimonate nano-crystals by the 18th dynasty Egyptian glassmakers. *Applied Physics*, A 98, pp. 1-8.

Lahlil, S., Biron, I., Cotte, M. and Susini, J. (2010b) New insight on the in situ crystallization of calcium antimonate opacified glass during the Roman period. *Applied Physics*, A 100, pp. 683-692.

Lahlil, S., Cotte, M., Biron, I., Szlachetko, J., Menguy, N. and Susini, J. (2011) Synthesizing lead antimonate in ancient and modern opaque glasses. *Journal of Analytical Atomic Spectrometry*, 26, pp. 1040-1050.

Larson, K.A. (2016) *From Luxury Product to Mass Commodity: Glass Production and Consumption in the Hellenistic World*. Unpublished PhD dissertation, University of Michigan.

Lazar, I. (2006) An Oil Lamp depicting a Roman Glass Furnace. *Journal of Dalmatian archaeology and history,* 99 (1), pp. 228-234.

Lilyquist, C. and Brill, R. H. (1993) *Studies in Early Egyptian Glass*. New York: The Metropolitan Museum of Art.

Livingood, P.C. and Cordell, A.S. (2008) Point/counter point: the accuracy and feasibility of digital image techniques in the analysis of ceramic thin sections. *Journal of Archaeological Science*, 36(3), pp. 867-872.

Litinas, N. (2008) *Tebtynis III. Vessels' Notations from Tebtynis*, FIFAO 55, Le Caire.

Lucas, A. and Harris, J. R. (1962) *Ancient Egyptian Materials and Industries*. 4th Edition. London.

Lunelli, A. (2014) La collezione papirologica dell'Università di Padova, *L'Egitto in Veneto, Atti del II Convegno Nazionale di Egittologia*, Padova 10 febbraio 2010, Padova, Cleup, pp. 43-50.

Magnini, L., Bettineschi, C. and De Guio, A. (2016) Object-based shell craters classification from Lidar-derived Sky-View Factor. *Archaeological Prospection*, DOI: 10.1002/arp.1565

Mahnke, C. (2008) Alexandrinische Mosaikglaseinlagen: die Typologie, Systematik und Herstellung von Gesichterdarstellungen in der ptolemäischen Glaskunst. *Philippika*, 22, Wiesbaden: Harrassowitz.

Majcherek, G. (1992) Excavations in Alexandria in 1990-91. *Polish Archaeology in the Mediterranean*, 3, pp. 5-14.

Majcherek, G. (1999) Kom el-Dikka. Excavations, 1997/98. *Polish Archaeology in the Mediterranean*, 10, pp. 29-39.

Majcherek, G. (2007). Kom el-Dikka. Excavation and preservation work. Preliminary report, 2004/2005. *Polish Archaeology in the Mediterranean*, 17, pp. 21-34.

Maltoni S. and Silvestri A. (2016) Innovation and tradition in the fourth century mosaic of the Casa delle Bestie Ferite in Aquileia, Italy: archaeometric characterisation of the glass *tesserae*. *Journal of Archaeological and Anthropological Science*, DOI 10.1007/s12520-016-0359-3.

Marini, P. (2014) Una scena di metallurgia e oreficeria dalla tomba M.I.D.A.N.05 a Dra Abu El-Naga. *EVO*, XXXVII, pp. 89-100.

Masquelier-Loorius, J. (2008) Les activités artisanales dans les annexes des temples: la production et le stockage dans les temples mémoriaux du Nouvel Empire, *Égypte, Afrique & Orient*, Centre Vauclusien d'égyptologie, pp. 57-64.

Mass, J.L., Stone, R.E. and Wypyski, M.T. (1998) The mineralogical and metallurgical origins of Roman opaque colored glasses, in McCray, P. and Kingery, W.D. (ed.), *The prehistory and history of glassmaking technology*, The American Ceramics Society, Columbus, Ohio, pp. 251-268.

Mass, J.L., Wypyski, M.T. and Stone, R.E. (2002) Malkata and Lisht glassmaking technologies: towards a specific link between second millennium BC metallurgists and glassmakers. *Archaeometry*, 44 (1), pp. 67-82.

Matson, F.R. (1951) The composition and working properties of ancient glass. *Journal of Chemical Education,* 28, pp. 69-82.

Melaerts, H. (2007) Petition concernant un procédure de recouvrement, in Sirks, A.B.J. and Worp, K.A. (ed.), *Papyri in Memory of P.J. Sijpesteijn*. The Americain Society of Papyrologists, 40, CPI Anthony Rowe ed., pp. 101-108.

Meleri, A. (2017a) Elaborazioni GIS per il sito di Tebtynis - georeferenziazione della mappa di Anti, *Proceedings of the workshop: Horus, visioni dall'alto dello spazio archeologico.* Padua: Padova University Press.

Meleri, A. (2017b) *Il Sito di Tebtynis In Egitto: Analisi Gis Di Cartografie E Foto degli Scavi Degli Anni Trenta*. Unpublished Dissertation, University of Padova.

Menegazzi, A. (2017) La mappa del tempio tra restauro e ricomposizione, *Proceedings of the workshop: Horus, visioni dall'alto dello spazio archeologico.* Padua: Padova University Press, pp. 65-68.

Menegazzi, A. and Urbani, C. (forthcoming) Gli archivi di Carlo Anti tra Padova e Venezia, *Proceedings of the Conference "Anti, Archeologia, Archivi"*, Venice (Italy), 14-16 June 2017.

Messiga, B. and Riccardi, M.P. (2001) A petrological approach to the study of ancient glass. *Periodico di Mineralogia*, 70 (1), pp. 50-70.

Messiga, B., Riccardi, M. P., Rebay, G., Basso, E. and Lerma, S. (2004) Microtextures recording melting-history of a medieval glass cake. *Journal of Non-Crystalline Solids*, 342, pp. 116-24.

von Minutoli, H.C. (1836) Über die Anfertigung und Nutzanwendung der farbigen gläser bei den Alten, Berlin.

Michalowski, K., Desroches, Ch., De Linage, J., Manteuffel J. and Zejmo-Zejamis M. (1950) *Tell Edfu 1939: rapport des fouilles franco-polonaises*, IFAO: Le Caire.

Molin, G., Bettineschi, C. and Angelini, I. (2013) Studi sulle *fayence* egizie del Veneto", *Catalogue of the Exhibition: "Egitto in Veneto"*, Padova april 19-june 30 2013, Cleup ed: Padova, pp. 105-120.

Molina, G., Odin, G.P., Pradell, T., Shortland, A.J. and Tite, M.S. (2014) Production technology and replication of lead antimonate yellow glass from New Kingdom Egypt and the Roman Empire. *Journal of Archaeological Science*, 41, pp. 171-184.

Monson, A., and Tait, J. (2001-2002) Putting papyri into archaeological context: new insights from Tebtunis, Egypt. *Archaeology International*, pp. 41-43.

Mostra d'arte antica (1932) *Mostra d'arte antica organizzata del Ministero dell'educazione nazionale e dall'Associazione internazionale per gli studi mediterranei*. Roma: Istituto Poligrafico dello Stato.

Moretti, C. and Hreglich, S. (2013) Raw Materials, Recipes and Procedures Used for Glass Making, in Janssens, K. (ed.), *Modern Methods for Analysing Archaeological and Historical Glass*. John Wiley & Sons, pp. 23-47.

Nenna, M.D. (1993) Eléments d'incrustation en verre des nécropoles alexandrines, *Annales du 12e Congrès de l'Association Internationale pour l'Histoire du Verre*, Vienna, 1991. Amsterdam: Association Internationale pour l'Histoire du Verre, pp. 45-52.

Nenna, M.D. (1995) Les éléments d'incrustation: une industrie égyptienne du verre. *Alessandria e il mondo Ellenistico-Romano*. Rome: L'Erma di Bretschneider, pp. 377-384.

Nenna, M.D. (1997) Le matériel en verre de Ayn Manawir. *BIFAO*, vol. 97, pp. 350-351.

Nenna, M.D. (1998) Les ateliers de verriers dans le monde grec aux époques classique et hellénistique. *Topoi*, pp. 693-701.

Nenna, M.D. (1999) Les Verres. *Exploration Archéologique de Délos*, Fascicule 37, Athens: École Française d'Athènes.

Nenna, M.D. (2000) Ateliers de production et sites de consommation en Égypte. Ve siècle av. J.-C. - VIIe siècle ap. J.-C. Premier bilan, *Annales du 14e Congrés de l'Association internationale pour l'Histoire du Verre*, Venice-Milan, 1998. Lochem: International Association for the History of Glass, pp. 20-24.

Nenna, M.D. (ed.) (2000) La route du verre: ateliers primaires et secondaires du second millénaire av. J.-C. au Moyen Age. *Travaux de la Maison de l'Orient Méditerranéen,* 33, Lyon: Maison de l'Orient Méditerranéen.

Nenna, M.D. (2006) Les artisanats du verre et de la faïence. Tradition et renouvellement dans l'Égypte gréco-romaine, in Meeks, D., Mathieu, B. and Wissa, M. (ed.), *L'Apport de l'Égypte à* l'*histoire des techniques.* Le Caire: IFAO, pp. 185-206.

Nenna, M.D., Picon, M. and Vichy, M. (2000) Ateliers primaries et secondaires en Égypte à l'époque gréco-romaine, in Nenna, M.D. (ed.), *La route du verre. Ateliers primaires et secondaires du second millénaire av. J.-C. au Moyen Âge*, Travaux de la Maison de l'Orient Mediterranéen no. 33, Lyon, pp. 97-112.

Nenna, M.D., Picon, M., Thirion-Merle, V., and Vichy, M. (2005) Ateliers primarie du Wadi Natrun: nouvelles decouvertes, *Annales du 16e Congres de l'Association Internationale pour l'Histoire du Verre*, pp. 59-63.

Nenna, M.D. (2015) Primary Glass Workshops in Graeco-Roman Egypt. Glass of the Roman World, in Bayley, J., Freestone, I. and Jackson, C. (ed.), Oxford: Oxbow Books, pp. 1-22.

Nenna, M.D. and Gratuze, B. (2009) Étude diachronique des compositions de verres employés dans les vases mosaïqués antiques: Résultats préliminaries, *Annales du 17e Congrès de l'Association Internationale pour l'Histoire du Verre.* Antwerp: Brussels, pp. 59-63.

Nenna, M.D., Picon, M., Thirion-Merle, V., and Vichy, M. (2005) Ateliers primaires du Wadi Natrun: Nouvelles Découvertes, *Annales du 16e Congrès de l'Association Internationale pour l'Histoire du Verre,* London, 2003. Nottingham, pp. 59-63.

Nenna, M.D., Picon, M. and Vichy, M. (2000) Ateliers primaires et secondaires en Égypte à l'époque Gréco-Romaine. *La Route du Verre. Ateliers primaires et secondaires du second millénaire av. J.-C. au Moyen Âge*, Travaux de la Maison de l'Orient Méditerranéen 33. Lyon: Maison de l'Orient, pp. 97-112.

Nenna M.D., (in collaboration with V. Arveiller-Dulong) (2011) *Verres antiques du Musée du Louvre III: Parure, instruments et éléments d'incrustation*, Paris.

Nenna, M.D. (2015a) Le mobilier religieux en bois incrusté de verre des temples égyptiens: nouvelles données (VIIIe av. J.-C. – Ier siècle apr. J.-C.), *Annales du 19e Congrès de l'Association International pour l'Histoire du Verre*, Piran, pp. 30-38.

Nenna, M.D. (2015b) Primary Glass Workshops in Graeco-Roman Egypt: Preliminary Report on the Excavations of the Site of Beni Salama, Wadi Natrun (2003, 2005-9), in *Glass of the Roman World*, Oxbow Books, pp. 1-22.

Nicholson, P.T. (1998) Materials and Technology, in Friedman, F.D. (ed.), *Gifts of the Nile: Ancient Egyptian Faience*, London, pp. 50-64.

Nicholson, P.T. (2013) Working in Memphis: The production of faience at Roman Period Kom Helul. *Excavation Memoir*, 105. London: Egypt Exploration Society.

Nicholson, P. T. (2007) Brilliant Things for Akhenaten: The production of glass, vitreous materials and pottery at Amarna Site O45.1. *Excavation Memoir*, 80. London: Egypt Exploration Society.

Nielsen, C.H. and Sigurdsson, H. (1981) Quantitative methods for electron microprobe analysis of sodium in natural and synthetic glasses. *American Mineralogist*, 66, pp. 1131-1138.

Nikita, K. and Henderson, J. (2006) Glass analyses from Mycenae, Thebes and Elateia: Compositional evidence for a Mycenaean glass industry. *Journal of Glass Studies*, 48, pp. 71–120.

O'Connel, E.R. (2007) Recontextualizing Berkeley's Tebtunis papyri, *Proceedings of the 24th International Congress of Papyrology*, Helsinki, 1-7 August, 2004, pp. 807-826.

Odgen, J. (2000) Metals, in Nicholson, P.T. and Shaw, I. (ed.), *Ancient Egyptian Productions and Technology*, Cambridge University Press.

Oikonomou, A., Henderson, J., Gnade, M., Chenery, S. and Zacharias, N. (2016) An archaeometric study of Hellenistic glass vessels: evidence for multiple sources. *Archaeological and Anthropological Sciences*. DOI: 10.1007/s12520-016-0336-x

Olcese, G., Cortese, C., Coletti, C., Giunta, S. and Manzini, I. (2013) Immensa Aequora. Una banca dei dati archeologici e archeometrici delle ceramiche prodotte in Italia centro-meridionale, *Proceedings of the workshop "Ricerche archeologiche, archeometriche e informatiche per la ricostruzione dell'economia e dei commerci nel bacino occidentale del Mediterraneo (metà IV sec. a.C. - I sec. d.C.)",* Rome, 24-26 January 2011, pp. 29-33.

Olmeda, G., Angelini, I., Molin, G., Boaro, S. and Leonardi, G. (2015) Archaeometric analysis of vitreous material ornaments from the Villa di Villa site (Treviso, Italy). *Rendiconti Lincei Scienze Fisiche E Naturali*. DOI 10.1007/s12210-015-0452-z

Olmi, F. and Sabelli, C. (1994) Brizziite, $NaSbO_3$, a new mineral from the Cetine mine (Tuscany, Italy): description and crystal structure. *European Journal of Mineralogy*, 6, pp. 667-672.

Oppenheim, A. L., Brill, R.H., von Saldern, A. and Barag, D. (1970) *Glass and Glass-Making in Ancient Mesopotamia*. New York: Corning Museum of Glass.

Paynter, S. (2006) Analyses of colourless Roman glass from Binchester, County Durham. *Journal Archaeological Science*, 33, pp. 1037-1057.

Paynter, S. (2008) Experiments in the reconstruction of Roman wood-fired glassworking furnaces: waste products and their formation processes. *Journal of Glass Studies*, 50, pp. 271-290.

Paleological Association of Japan, (1995) Akoris. Report of the Excavations at Akoris in Middle Egypt 1981-1992, Kyoto: Koyo Shobo.

Panich, L.M. (2016) Beyond the colonial curtain: Investigating indigenous use of obsidian in Spanish California through the pXRF analysis of artifacts from Mission Santa Clara. *Journal of Archaeological Science*, Reports 5, pp. 521-530.

Papi, E., Bigi, L., Camporeale, S., Carpentiero, G., D'Aco, D., Kenawi, M., Mariotti, E. and Passalacqua, L. (2010) La missione dell'Univeristà di Siena a Qasr Qarum - Dyonisias (2009-10), in Pirelli. R. (ed.), *Ricerche Italiane in Egitto*, IV Volume, Centro Archeologico Italiano: Il Cairo.

Parodi, H.D. (1908) *La verrerie in Egypte*. PhD Disseratationm, University of Grenoble, pp. 9.47.

Peltenburg E.J., (1987) Early faience: recent studies, origins and relations with glass, in Bimson, M. and Freestone, I.C. (ed.), *Early Vitreous Materials*, British Museum Occasional Paper 56, London, 5-29.

Pensabene, P. (1995) *Elementi architettonici di Alessandria e di altri siti egiziani*, Roma.

Per-neb, Coll. I (1992a) Ancient Egyptian glass and faience from the Per-neb collection. 1, Christie's London, 9 December. London: Christie's.

Per-neb, Coll. II (1992) Ancient Egyptian glass and faience from the Per-neb collection. 2, Catalogue of Christie's, Londres, 7 July. London: Christie's.

Per-Neb/ Groppi Coll. III (2012), Ancient Egyptian glass and faience from the Groppi Collection, Christie's London, 26 April. London: Christie's.

Petrie, W.F. (1890) *Kahun, Gurob, and Hawara*, London: K. Paul, Trench, Trübner.

Petrie, W.F. (1891) *Illhaun, Kahun and Gurob*. London: David Nutt.

Petrie, W.F. (1894) *Tell el-Amarna*. London: Methuen.

Petrie, W.M.F. (1909) *Memphis I*. British School of Archaeology in Egypt, London.

Petrie, W.M.F., (1910) *The arts and crafts of ancient Egypt*. London, T.N. Foulis ed.

Petrie, W.M.F. (1911) The pottery kilns at Memphis. *Historical Studies*, II, Quaritch, London, pp. 7-34.

Petrie, W.F. (1926) *Ancient weights and measures: illustrated by the Egyptian collection in University College, London*. London: Department of Egyptology, University College.

Petrie, W.F. and Griffith, F.L. (1888) *Tanis II*. London, Trubner & Co.

Pintaudi, R. (2008) *Antinoopolis I*. Firenze, Tipografia Latini.

Polikreti, K., Murphy, J.M.A., Vasilike Kantarelou, V. and Karydas, A.G. (2011) XRF analysis of glass beads from the Mycenaean palace of Nestor at Pylos, Peloponnesus, Greece: new insight into the LBA glass trade. *Journal of Archaeological Science*, 38, pp. 2889-2896.

Polla, A., Angelini I. and Artioli, G. (2006) Analisi d'immagine per la caratterizzazione strutturale dei materiali vetrosi. Materie prime e scambi nella

protostoria Italiana, *Atti della XXXIX Riunione Scientifica dell'Istituto Italiano di Preistoria e Protostoria*, Firenze, Italy, 25-27 November 2004, Vol III, pp. 1621-1626.

Preibisch, S., Saalfeld, S. and Tomancak P. (2009) Globally optimal stitching of tiled 3D microscopic image acquisitions. *Bioinformatics*, 25(11), pp. 1463-1465.

Push, E.B. and Rehren, T. (2007) *Hoctemperatur-Technologie in der Ramses-Stadt, Rubinglas für der Pharao*, Gerstenberg.

Ramadan, F.S. (2014) Characteristics of White Sand Deposits in Southern Sinai Region, Egypt. *Middle East Journal of Applied Sciences*, 4 (1), pp. 100-108.

Ramìrez-Meneses, E., Chavira, E., Domìguez-Crespo, M.A., Escamilla, R., Flores-Flores, J.O. and Soto-Guzman, A.B. (2007) Synthesis and characterization of $NaSbO_3$ compound. *Superficies y Vacìo*, 20, pp. 14-18.

Rapp, G. (2009) *Archaeomineralogy*. Springer.

Rasmussen, S.C. (2012) *How Glass Changed the World. The History and Chemistry of Glass from Antiquity to the 13th Century*, Springer.

Reade, W.D., Privat, L.K. (2016) Chemical characterization of archaeological glasses from the Hellenistic site of Jebel Khalid, Syria by electron probe microanalysis. *Heritage Science*, 4 (20), pp. 1-17. DOI 10.1186/s40494-016-0084-3

Reedy C.L. (2013) Review of Digital Image Analysis of Petrographic Thin Sections in Conservation Research. *Journal of the American Institute for Conservation*, pp. 127-146. DOI: http://dx.doi.org/10.1179/019713606806112531

Rehren, T. (2000) New Aspects of Ancient Egyptian Glassmaking. *Journal of Glass Studies*, 42, pp. 13-24.

Rehren, T. (2001) Aspects of the production of cobalt-blue glass in Egypt. *Archaeometry*, 43(4), pp. 483-89.

Rehren, T. (2008) A review of factors affecting the composition of early Egyptian glasses and faience: alkali and alkali earth oxides. *Journal of Archaeological Science*, 35, pp. 1345-1354.

Rehren, T., Connolly P., Schibille, N. and Schwarzer, H. (2015) Changes in glass consumption in Pergamon (Turkey) from Hellenistic to late Byzantine and Islamic times. *Journal of Archaeological Science*, 55, pp. 266-279.

Rehren, T. and Pusch, E. (2005) Late Bronze Age Egyptian glass production at Qantir-Piramesses. *Science*, 308, pp. 1756-1759.

Rehren, T., Spenser, L. and Triantafyllidis, P. (2005) The primary production of glass at Hellenistic Rhodes, *Annales du 16e Congrès de l'association Internationale pour l'Histoire du verre*, London, Nottingham: International Association for the History of Glass, pp. 39-43.

Ribechini, E., Orsini, S., Silvano, F. and Colombini, M.P. (2009) Py-GC/MS, GC/MS and FTIR investigations on LATE Roman-Egyptian adhesives from opus sectile: New insights into ancient recipes and technologies. *Analytica Chimica Acta*, 638, pp. 79-87.

Riefstahl, E. (1968) *Ancient Egyptian Glass and Glazes in the Brooklyn Museum*. Brooklyn: Brooklyn Museum.

Rodziewicz, M. (1984) *Alexandrie III: Les habitations romaines tardives d'Alexandrie: à la lumière des fouilles polonaises à Kôm el-Dikka*. Warsaw: Editions scientifiques de Pologne.

Rodziewicz, E. (1991) Remains of a Chryselephantine Statue in Alexandria. *Bulletin de la Société archéologique d'Alexandrie*, 44, pp. 119-130.

Rondot, V. (2004) *Tebtynis II. Le temple de Soknebtynis et son dromos*, FIFAO 50, Le Caire.

Rosenow, D. and Rehren, TH. (2014) Herding cats: Roman to Late Antique glass groups from Bubastis, northern Egypt. *Journal Archaeological Science*, 49, pp. 170-184

Rosi F., Manuali V., Miliani C., Brunetti B.G., Sgamellotti A., Grygarc T. and Hradilc D. (2009) Raman scattering features of lead pyroantimonate compounds. Part I: XRD and Raman characterization of $Pb_2Sb_2O_7$ doped with tin and zinc. *Journal of Raman Spectroscopy*, 40, pp. 107-111.

Sampsell, B.M. (2014) *The Geology of Egypt: a Traveler's Handbook*. AUC Press, The Cairo.

Samy, Y. and Abou El-Anwar, E. (2013) Textural and Mineralogical Characters of the Sand Fraction of Some Quaternary Sediments on Giza-Fayium District, Western side of the Nile Valley, Egypt. *Australian Journal of Basic and Applied Sciences*, 7(2), pp. 770-779.

Sanderson, D.C.W. and Hunter, J.R. (1981) Compositional variability in vegetable ash. *Science and Archaeology,* 23, pp. 27-30.

Santagostino Barbone, A., Gliozzo, E., d'Acapito, F., Memmi Turbanti, I., Turchiano, M. and Volpe, G. (2008) The Sectilia panels of Faragola (Ascoli-Satriono, southern Italy): A multi-analytical study of the red, orange and yellow glass slabs. *Archaeometry*, 50, pp. 451-73.

Sayre, E.V. and Smith, R.V. (1961) Compositional categories of ancient glass. *Science*, 133, pp. 1824-1826.

Sayre, E.V. (1963) The intentional use of antimony and manganese in ancient glasses, in Matson, F.R. and Rindone, G.E. (ed.), *Advances in Glass Technology*, Part 2. Plenum Press, New York, pp. 263-282

Schibille, N., Degryse, P., Corremans, M. and Specht, C.G. (2012) Chemical characterization of glass mosaic tesserae from sixth-century Sagalassos (south-west Turkey): chronology and production techniques. *Journal of Archaeological Science*, 39, pp. 1480-1492.

Schibille, N., Sterrett-Krause, A.E. and Freestone, I.C. (2016) Glass Groups, Glass Supply and Recycling in Late Roman Carthage. *Archaeological and Anthropological Science*, DOI:10.1007/s12520-016-0316-1

Schiering, W. (1991) *Die Werkstatt des Pheidias in Olympia*, 2: Werkstattfunde, Berlin

Schiering, W. (1999) Glas für eine Göttin: Zum Gewand einer klassischen Kolossalstatue (Nike?) in Olympia - Ein Beitrag zu experimentaller Archäologie. *Antike Welt*, 30, pp. 39-48.

Schreurs, J.W.H. and Brill, R.H. (1984) Iron and sulfur related colors in ancient glasses. *Archaeometry*, 26, pp. 199-209.

Seccaroni, C. and Haldi, J-P. (2016) *Cobalto, zaffera, smalto dall'antichità al XVIII secolo*. Enea.

Seefried, M. (1982) *Les pendentifs en verre sur noyau des pays de la méditerranée antique. Collection de l'École française de Rome*, 57. Rome: École française de Rome, Palais Farnèse.

Šelih, V.D. and van Elteren, J.T. (2011) Quantitative multi-element mapping of ancient glass using a simple and robust LA-ICP-MS rastering procedure in combination with image analysis. *Analytical and Bioanalytical Chemistry*, Volume 401, Issue 2, pp 745-755.

Schlick-Nolte, B. and Lierke, R. (2002) From silica to glass: on the track of the ancient glass artisans, in Bianchi, S. (ed.) *Reflections on Ancient Glass from the Borowski Collection*. Bible Lands Museum, Jerusalem. Mainz am Rhein: von Zabern. pp. 11 - 40.

Shaw, I. (2013) The Gurob Harem Palace Project, Spring 2012. *Journal of Egyptian Archaeology*, 98, pp. 43-54.

Shortland, A.J. (2000) Depictions of glass vessels in two Theban tombs and their role in the dating of early glass. *Journal of Egyptian Archaeology*, 86, pp.159-161.

Shortland, A.J. (2002) The use and origin of antimonate colorants in early Egyptian glass. *Archaeometry*, 44 (4), pp. 517-530.

Shortland, A.J. (2004) Evaporites of the Wadi Natrun: Seasonal and annual variation and its implication for ancient exploitation. *Archaeometry*, 46 (4), pp. 497-517.

Shortland, A.J. (2012) *Lapis Lazuli from the Kiln. Glass and Glassmaking in the Late Bronze Age*. Leuven University Press.

Shortland, A.J. and Eremin, K. (2006) The analysis of second millennium glass from Egypt and Mesopotamia, Part I: New WDS analyses. *Archaeometry*, 48, pp. 581-603.

Shortland, A.J., Schachner, T., Freestone, I.C. and Tite, M. (2006) Natron as a flux in the early vitreous materials industry-sources, beginnings and reasons for decline. *Journal of Archaeological Science*, 33(4), pp. 521-530.

Shortland, A. and Tite, M., 2000, Raw materials of glass from Amarna and implications for the origins of Egyptian glass. *Archaeometry*, 42, pp. 141-51.

Shortland, A.J., Tite, M.S. and Ewart, I. (2006) Ancient exploitation and use of cobalt alums from the western oases of Egypt. *Archaeometry*, 48, 1: 153-68.

Shortland, A.J., Rogers, N. and Eremin, K. (2007) Trace element discriminants between Egyptian and Mesopotamian late Bronze Age glasses. *Journal of Archaeological Science*, 34, pp. 781-789.

Shortland, A.J., Kirk, S., Eremin, K., Degryse, P. and Walton, M. (2017) The Analysis of Late Bronze Age Glass from Nuzi and the Question of the Origin of Glass-Making. *Archaeometry*, early view, DOI: 10.1111/arcm.12332.

Shugar, A.N. (2000) Byzantine opaque red glass tesserae from Beit Shean, Israel. *Archaeometry*, 42, pp. 375-384.

Shwartz, J. and Wild, H. (1950) *Qasr-Qarun/ Dionysias 1*. The Cairo: IFAO.

Shwartz, J. (1969) *Qasr-Qarun/ Dionysias 2*. The Cairo: IFAO.

Silvano, F. (2015) Glass Production in Antinoopolis, Egypt, *Annales du 19e Congrès de l'Association Internationale pour l'Histoire du Verre*, Piran, 2012, pp. 244-249.

Silvano, F. and Ribechini, E. (2014) Adesivi e collanti nell'Egitto tardo romano. *Egitto e Vicino Oriente*, XXXVII, pp. 123-192, DOI 10.12871/9788674150148

Silvestri, A., Molin, G. and Salviulo, G. (2008) The colourless glass of Julia Felix. *Journal of Archaeological Science*, 35, pp. 331-41.

Silvestri, A., Molin, G., Salviulo, G. and Schievenin, G. (2006) Sand for Roman glass production: an experimental and philological study on source of supply. *Archaeometry*, 48(3), pp. 415-32.

Silvestri, A., Tonietto, S. and Molin, G. (2011) The palaeo-Christian glass mosaic of St. Prosdocimus (Padova, Italy): archaeometric characterisation of "gold" tesserae. *Journal of Archaeological Science*, 38, pp. 3402-3414.

Silvestri, A., Tonietto, S., Molin, G. and Guerriero, P. (2014) The palaeo-Christian glassmosaic of St. Prosdocimus (Padova, Italy): archaeometric characterization of tesserae with copper- or tin-based opacifiers. *Journal of Archaeological Science*, 42, pp. 51-67.

Silvestri, A., Tonietto, S., Molin, G. and Guerriero, P. (2015) Multi-methodological study of palaeo-Christian glass mosaic tesserae of St. Maria Mater Domini (Vicenza, Italy). *European Journal of Mineralogy*, 27, pp. 225-245.

Smirniou, M. and Rehren, T. (2011) Direct evidence of primary glass production in late Bronze Age Amarna, Egypt. *Archaeometry*, 53, pp. 58-80.

Soldati, A. (2014) La collezione papirologica dell'Università di Padova, *L'Egitto in Veneto, Atti del II Convegno Nazionale*, Padova 10 febbraio 2010, Padova: Cleup, pp. 51-58.

Spaer, M. (2001) A*ncient Glass in the Israel Museum, Beads and Other Small Objects*. Jerusalem: Israel Museum.

Stern, E.M. (1989) Colored Glass Inlays in Architectural Ornament: Athens and Rhamous. *American Journal of Archaeology*, 93, pp. 254.

Stern, E. M. (1993) Glass working before glass blowing, *Annales du 12e Congrès de l'Association Internationale pour l'Histoire du Verre*. Amsterdam: AIHV, pp. 21-31.

Stern, E.M. (1993) The Glass from Heis. Sur les routes antiques de l'Azanie et de l'Inde: le fonds Révoil du Musée de l'homme (Heïs et Damo, en Somalie). *Mémoires de l'Académie des inscriptions et belles-lettres*, 13, Paris: F. Paillart, pp. 21-61.

Stern, E.M. (1999) Ancient Glass in Athenian Temple Treasuries. *Journal of Glass Studies*, 41, pp. 19-50.

Stern, E.M. (2002) The Ancient Glassblower's Tools, in *Hyalos, Vitrum, Gass: History, Technology and Conservation of Glass and Vitreous Materials in the Hellenic World*. Athens: Glasnet, pp. 159-165.

Stern, E.M. (2004) The Glass *Banausoi* of Sidon and Rome, in *When Glass Matters: Studies in the history of science and art from Graeco-Roman antiquity to early modern era*. Biblioteca di Nuncius. Studi e testi 53. Firenze: Leo S. Olschki, pp. 77-120.

Stern, E.M. (2007) Ancient Glass in a Philological Context. *Mnemosyne*, 60(3), pp. 341-406.

Stern, E.M. (2008) Glass Production. *The Oxford Handbook of Engineering and Technology in the Classical World*. Oxford: Oxford University Press, pp. 520-547.

Stern, E.M. (2012) Blowing Glass from Chunks Instead of Molten Glass: Archaeological and Literary Evidence. *Journal of Glass Studies*, 54, pp. 33-45.

Stern, E.M. and Schlick-Nolte, B. (1994) *Early Glass of the Ancient World 1600 BC - AD 50. Ernesto Wolfe Collection*, Verlag Hatje, Ostfildern, Germany.

Stevenson, A. (2014) Artefacts of excavation: the collection and distribution of Egyptian finds to museums, 1880-1915. *Journal of the History of Collections*, 26(1), pp. 89-102, DOI: 10.1093/jhc/fht017

Tait, H. (2012) *Five Thousand Years of Glass.* Revised ed. London. British Museum Press.

Takla, M.A. and Arafa, E.H. (1975) The Mineralogy of the Sand Dunes between Minya and Dairut, Egypt. *TMPM Tschermaks Min. Petr. Mitt.*, 22, pp. 164-173.

Tatton-Brown, V. and Andrews, C. (1991) Before the Invention of Glassblowing, in *Five Thousand Years of Glass*. London: British Museum Press, pp. 21-61.

Tite, M.S. (1987) Characterisation of early vitreous materials. *Archaeometry*, 29, pp. 21-34.

Tite, M.S., Shortland, A. and Bouquillon A. (2008) Glazed Steatite, in Tite, M.S. and Shortland A.J. (ed.) *Production Technology of faience and related early vitreous materials*. Oxford University School of Archaeology: Monograph 72, pp. 23-36.

Tite, M. S., Shortland, A. and Paynter, S. (2002) The beginnings of vitreous materials in the Near East and Egypt. *Accounts of Chemical Research*, 35 (8), pp. 585-593.

Tite, M.S. and Shortland, A. J. (2003) Production technology for copper- and cobalt-blue vitreous materials from the New Kingdom site of Amarna - a reappraisal. *Archaeometry,* 45 (2), pp. 285-312.

Tite, M. S., Shortland, A., Maniatis, Y., Kavoussanaki, D. and Harris, S. A. (2006) The composition of the soda-rich and mixed-alkali plant ashes used in the production of glass. *Journal of Archaeological Science*, 33, pp. 1284-1292.

Tite, M. S., Pradell, T. and Shortland, A. (2008) Discovery, production and use of tin-based opacifiers in glasses, enamels and glazes from the Late Iron Age onwards: a reassessment. *Archaeometry*, 50 (1), pp. 67-84.

Tite, M.S. and Shortland, A.J. (ed.) (2008) *Production Technology of Faience and Related Early Vitreous Materials*. Oxford: Oxford University School of Archaeology.

Thiers, C., Volokhine, Y. and Ermant, I. (2008) *Les cryptes du temple ptolémaïque. Étude épigraphique*. *MIFAO*, 124, Le Caire.

Thirion-Merle, V. (2005) Les verres de Beyrouth et les verres du Haut Empire dans le monde occidental: étude archéométrique. *Journal of Glass Studies,* 47, pp. 37-53.

Thompson, D.J. (1988) *Memphis under the Ptolemies*. Princeton: Princeton University Press.

Tonietto, S., Nestola, F., Redhammer, G.J., Silvestri, A., Molin, G. and Bruno, M. (2011) Pyroxene inclusions in paleo-Christian mosaic tesserae: a tool for constraining the glass manufacturing temperature. *Applied Physics A*, 103, pp. 207-212.

Triantafyllidis, P. (2000) New Evidence of the Glass Manufacture in Classical and Hellenistic Rhodes, *Annales du 14e Congrés de l'Association internationale pour l'Histoire du Verre,* Venice-Milan, 1998. Lochem: International Association for the History of Glass, pp. 30-34.

Triantafyllidis, P. (2003) Classical and Hellenistic workshop from Rhodes, *Echanges et commerce du verre dans le monde antique. Actes du colloque AHIV*, Aix-en-Provence et Marseille 2001. Mergoil Editor, Montagnac, pp. 131-138.

Turner, W. (1956) Studies in ancient glasses and glassmaking processes: part V. Raw materials and melting processes. *Trans Soc Glass Tech*, 40, pp. 277-300.

Turner–Walker, G. and Syversen, U. (2002) Quantifying histological changes in archaeological bones using BSE–SEM image analysis. *Archaeometry*, 44, pp. 461-468. Doi:10.1111/1475-4754.t01-1-00078

Valbelle, D. and Marchi, S. (2012) Un dépôt votif de la forteresse de Tell el-Herre, in *Parcourir l'éternité. Hommages à Jean Yoyotte*. Brepols, pp. 1009-1019.

Valz, E. (1992) Italian excavations at Tebtynis 1930-1935: the objects at Egyptian Museum, Torino, *Proceedings of the VI International Congress of Egyptology*, I, Torino, pp. 625-628.

Van der Werf, I., Mangone, A., Giannossa, L.C., Traini, A., Laviano, R., Coralini, A. and Sabbatini, L. (2009) Archaeometric investigation of Roman tesserae from Herculaneum (Italy) by the combined use of complementary micro-destructive analytical techniques. *Journal of Archaeological Science*, 36, pp. 2625-2634.

Vandier, J. (1970) Notice sur la vie et les travaux de M. Pierre Lacau, membre de l'Académie. *Comptes rendus des séances de l'Académie des Inscriptions et Belles-Lettres*, 114e année, N. 3. pp. 520-535.

Vandini, M., Fiori, C. and Cametti, R. (2006) Classification and Technology of Byzantine Mosaic Glass. *Annali di Chimica*, 96 pp. 587-599. doi:10.1002/adic.200690060

Varberg, J., Gratuze, B. and Kaul, F. (2015) Between Egypt, Mesopotamia and Scandinavia: Late Bronze Age glass beads found in Denmark. *Journal of Archaeological Science*, 54, pp. 168-181.

Verità, M., Maggetti, M., Saguì, L. and Santopadre, P. (2013) Colors of Roman glass: an investigation of the yellow sectilia in the Gorga collection. *Journal of Glass Studies*, 55, pp. 39-52.

Von Saldern, A., Nolte, B., La Baume, P. and Haevernick, T.H. (1974) *Gläser der Antike Sammlung Oppenländer*. Hamburg: Museum für Kunst und Gewerbe.

Wang, P. W. and Zhang, L. P. Structural role of lead in lead silicate glasses derived from XPS spectra. *J. Non-Cryst. Solids*, 194(1-2), pp. 129-134.

Welham, K., Jackson, C. and Smedley, J.W. (2000) Colour formation in sealing wax red glass, *Annales du Congrès de l'Association International pour l'Histoire du Verre*. Amsterdam: Association Internationale pour l'Histoire du Verre, pp. 11-15.

Weyl, W.A. (1959) Coloured Glasses. *The Society of Glass Technology*, Sheffield, 121-131, pp. 420-432.

Whitbread, I.K. (1991) Image and Data Processing in Ceramic Petrology, in Middleton, A. and Freestone, I. (ed.) *Recent Developments in Ceramic Petrology*. Occasional Paper, British Museum, no. 81, London, pp. 369-388.

Whitehouse, D. (1988) *Glass of the Roman Empire*. Corning Museum of Glass, Corning, NY.

Wold, S., Esbensen, K. and Geladi, P. (1987). Principal component analysis. *Chemometrics and Intelligent Laboratory Systems,* 2, pp. 37-52.

Wuttmann, M., Bousquet, B. Chauveau, Dils, M., Marchand, S., Schweitzer, A. and Volay, L. (1996) Premier rapport préliminaire des travaux sur le site de 'Ayn Manawir (oasis de Kharga), *BIFAO,* 96, pp. 385-451.

Yan, G., Mas, J.F., Maathuis, B.H.P., Zhang, X. and Van Dijk, P.M. (2006) Comparison of pixel-based and object-oriented image classification approaches - a case study in a coal fire area, Wuda, Inner Mongolia, China. *International Journal of Remote Sensing*, 27(18), pp. 4039-4055.

Yoyotte, J. (1972) Pétoubastis III. *Revue d'Egyptologie*, 24, pp. 216-223.

Zakrzewski, S., Shortland, A. and Rowland, J. (2016) *Science in the Study of Ancient Egypt*. New York/ London: Routledge.

Zanovello, P. and Ciampini, E.M. (2012) Progetto EgittoVeneto, *Frammenti d'Egitto. Atti del I convegno nazionale di Egittologia,* Padova, 15-16 novembre 2010, Cleup: Padova, pp. 5-8.

Zanovello, P. and Menegazzi, A. (2012) Gli archivi di Carlo Anti e Tebtynis: aspetti di valorizzazione, *Frammenti d'Egitto. Atti del I convegno nazionale di Egittologia,* Padova, 15-16 novembre 2010, Cleup: Padova, pp. 137-144.

Zanovello, P. and Menegazzi, A. (2014) Dalle ricerche di Carlo Anti al Progetto EgittoVeneto, *Antichità Egizie e Italia. Atti del III Convegno Nazionale Veneto di Egittologia*, Venezia, 14-16 settembre 2012, Ca' foscari University Press: Venice, pp. 95-99.

Zanovello, P., Menegazzi, A., Urbani, C., Begg, I. and Deotto, G. (2014-2015) Location of the Deposit of Papyri from the Temple Library at Tebtunis Identified. *Bollettino dell'Istituto Veneto di Scienze Lettere ed Arti*, Tomo CLXXIII, pp. 213-222.

Zanovello, P. and Deotto, G. (2013) Carlo Anti a Tebtynis, in Zanovello, P. and Ciampini, E.M. (ed.) *Catalogo della Mostra Egitto in Veneto*, Padova: Cleup, pp. 39-48.

APPENDIX

Table I - List of analyzed objects. The table summarizes the main data on the objects selected and sampled for in-depth archaeometric analyses, in particuar: image of the object (II column), name of the sample (III column), general typological determination (IV column), functional class (V column) and inlay type - cfr. § 9.1 (VI column). Also, the table indicates for each object the reference chromatic group (VII column), a brief description of the color/s and motif/s represented (VIII column), the dimensions in mm (IX culumn), Turin's inventory number (X column) and the area of the sampling (XI column).

N°	Image	Sample Name	Typology	Class	Inlay type	Group	Color/s and motifs	Dimensions (mm)	Inventory	Sampling area
1		Ty-I-B-616	T-shaped inlay	finished product	1	monochrome	blue	L1: 15.2; L2: 8.7; L3: 4.9	S. 18556/16	from broken edge
2		Ty-I-BBi-613	leg inlay	finished product	1	stratified	blue; white	L1: 21.9; L2: 20.3; L3: 3.8	S. 18556/13	from broken edge
3		Ty-I-RAu-605	leg inlay	finished product	1	monochrome	sealing-wax red + gold traces	L1: 32.1; L2: 18.4; L3: 5.2	S. 18556/05	from broken edge
4		Ty-I-RAu-622	inlay (fragment)	finished product	1	monochrome	sealing-wax red + gold traces	L1: 21.1; L2: 7.4; L3: 3.9	S. 18556/22	from broken edge
5		Ty-M-A-005	bar	waste	2	monochrome	light blue	L1: 30.2; L2: 3.8; L3: 1.4	S. 19200/05	from broken edge
6	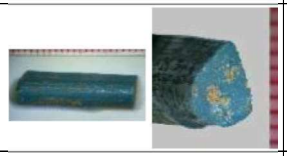	Ty-M-A-005a	drop-shaped bar	semifinished product	2	monochrome	light blue	L1: 19.3; Ømax: 4.3	S. 19200/05	from broken edge
7		Ty-M-A-006	fragment	finished product	1	monochrome	turquoise	L1: 18.1; L2: 4.7; L3: 4.2	S. 19200/06	from broken edge

Table I - List of analyzed objects

N°	Image	Sample Name	Typology	Class	Inlay type	Group	Color/s and motifs	Dimensions (mm)	Inventory	Sampling area
8		Ty-M-Ar-506	bar	finished product	2	monochrome	yellowish-orange	L1: 19.4; L2: 3.1; L3: 1.3	S. 18555/06	from broken edge
9		Ty-M-Ar-506a	bar	finished product	2	monochrome	yellowish-orange	L1: 25.7; L2: 4.0; L3: 1.0	S. 18555/06	from broken edge
10		Ty-M-B-002	inlay	finished product	1	monochrome	blue	L1: 14.8; L2: 11.7; L3: 2.4	S. 19200/02	from broken edge
11		Ty-M-B-004	bar	probably finished product	2	monochrome	transparent blue	L1: 22.8; L2: 8.1; L3: 3.6	S. 19200/04	from broken edge
12		Ty-M-BAu-002	bar (plumage)	finished product	2	monochrome	blue + gold traces	L1: 13.3; L2: 5.6; L3: 2.7	S. 19200/02	from broken edge
13		Ty-M-G-504	bar	finished product	2	monochrome	yellowish-orange	L1: 11.4; L2: 2.1; L3: 1.0	S. 18555/04	from broken edge
14		Ty-M-G-504a	bar	finished product	2	monochrome	yellowish-orange	L1: 43.2; L2: 2.5; L3: 0.8	S. 18555/04	from broken edge
15		Ty-M-G-504b	bar	finished product	2	monochrome	yellowish-orange	L1: 52.1; L2: 6.5; L3: 1.1	S. 18555/04	from broken edge

Table I - List of analyzed objects

N°	Image	Sample Name	Typology	Class	Inlay type	Group	Color/s and motifs	Dimensions (mm)	Inventory	Sampling area
16	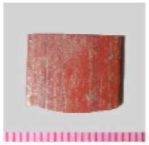	Ty-M-R-501	bar	finished product	1	monochrome	dull red	L1: 13.8; L2: 10.8; L3: 2.5	S. 18555/01	from broken edge
17		Ty-M-R-502d	bar (plumage?)	finished product	2	monochrome	sealing-wax red	L1: 14.1; L2: 5.0; L3: 2.0	S. 18555/02	from broken edge
18		Ty-M-R-505	bar	finished product	2	monochrome	dull red	L1: 71.4; L2: 2.6; L3: 1.5	S. 18555/05	from broken edge
19		Ty-M-R-507	inlay (knee?)	finished product	1	monochrome	sealing-wax red	L1: 10.8; L2: 6.1; L3: 6.6	S. 18555/07	from broken edge
20		Ty-M-RAu-502	bar/ plaque	finished product	1	monochrome	sealing-wax red + gold traces	L1: 22.3; L2: 14.4; L3: 2.3	S. 18555/02	from broken edge
21		Ty-M-RAu-502a	bar	finished product	2	monochrome	sealing-wax red + gold traces	L1: 11.7; L2: 4.1; L3: 2.4	S. 18555/02	from broken edge
22	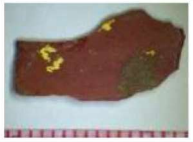	Ty-M-RAu-502b	bar	finished product	1	monochrome	sealing-wax red + gold traces	L1: 15.5; L2: 7.7; L3: 1.4	S. 18555/02	from broken edge
23		Ty-M-RAu-502c	bar	finished product	1	monochrome	sealing-wax red + gold traces	L1: 19.8; L2: 3.8; L3:1.9	S. 18555/02	from broken edge

Table I - List of analyzed objects

N°	Image	Sample Name	Typology	Class	Inlay type	Group	Color/s and motifs	Dimensions (mm)	Inventory	Sampling area
24		Ty-M-T-503	bar (plumage)	finished product	2	monochrome	transparent aqua	L1: 9.7; L2: 9.2; L3: 1.1	S. 18555/03	from broken edge
25	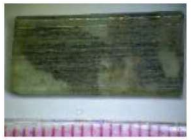	Ty-M-T-503a	bar (plumage)	finished product	2	monochrome	transparent aqua	L1: 17.5; L2: 8.3; L3: 1.5	S. 18555/03	from broken edge
26	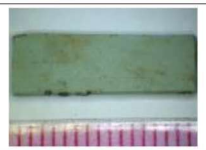	Ty-M-V-005	bar	finished product	2	monochrome	turquoise	L1: 17.1; L2: 6.0; L3: 1.5	S. 19200/05	from broken edge
27		Ty-M-V-005a	lump/ inlay	finished product	1	monochrome	turquoise	L1: 10.6; L2: 5.4; L3: 4.2	S. 19200/05	from broken edge
28		Ty-M-V-006	bar (plumage)	finished product	1	monochrome	turquoise	L1: 19.8; L2: 12.1; L3: 3.9	S. 19200/06	from broken edge
29		Ty-M-V-006a	bar/ plaque	finished product	2	monochrome	turquoise	L1: 18.5; L2: 11.7; L3: 2.9	S. 19200/06	from broken edge
30		Ty-P-A-402	cane slice	finished product	2	complex mosaic glass	blue and yellow arcs	L1: 10.6; L2: 3.5; L3: 2.9	S. 18554/02	from broken edge
31	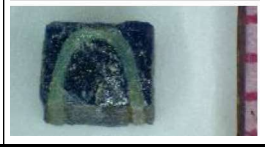	Ty-P-A-405	cane slice	finished product	2	complex mosaic glass	blue and turquoise arc	L1: 3.5; L2: 2.2; L3: 2.7	S. 18554/05	detached fragment

Table I - List of analyzed objects

N°	Image	Sample Name	Typology	Class	Inlay type	Group	Color/s and motifs	Dimensions (mm)	Inventory	Sampling area
32		Ty-P-A-408	cane slice	finished product	2	complex mosaic glass	blue and yellowish-orange arcs	L1: 4.4; L2: 3.7; L3: 0.6	S. 18554/08	from broken edge
33		Ty-P-A-418	mosaic bar	semifinished product	2	complex mosaic glass	blue, dull red and white arcs	L1: 32.8; L2: 13.8; L3: 11.9	S. 18554/18	from broken edge
34		Ty-P-A-419	mosaic bar	semifinished product	2	complex mosaic glass	blue, dull red and white arcs	L1: 15.8; L2: 14.9; L3: 4.9	S. 18554/19	from broken edge
35		Ty-P-CR-421	cane slice	finished product	2	complex mosaic glass	polychrome circles and lines	L1: 3.3; L2: 2.6; L3: 1.3	S. 18554/21	detached fragment
36		Ty-P-FL-004	mosaic bar	semifinished product	2	complex mosaic glass	polychrome lotus flowers	L1: 31.4; L2: 5.2; L3: 1.7	S. 19200/04	from broken edge
37		Ty-P-FL-404	mosaic bar	semifinished product	2	complex mosaic glass	polychrome lotus flower	L1: 17.1; L2: 4.1; L3: 3.7	S. 18554/04	from broken edge
38		Ty-P-FL-501	mosaic bar	semifinished product	2	complex mosaic glass	polychrome lotus flowers	L1: 19.6; L2: 10.5; L3: 2.3	S. 18555/01	from broken edge
39		Ty-P-FR-422	bar	finished product	2	complex mosaic glass	polychrome rosette	L1: 6.7; L2: 3.5; L3: 4.5	S. 18554/22	from broken edge

Table I - List of analyzed objects

N°	Image	Sample Name	Typology	Class	Inlay type	Group	Color/s and motifs	Dimensions (mm)	Inventory	Sampling area
40		Ty-Pn-B-001	lump	semifinished product	2	monochrome	blue, altered in violet	L1: 30.0; L2: 25.0; L3: 18.5	S. 19200/01	detached fragment
41		Ty-Pn-T-001	lump	waste	2	monochrome	transparent aqua	L1: 23.8; L2: 17.5; L3: 9.1	S. 19200/01	from broken edge
42		Ty-P-R-414	mosaic bar	semifinished product	2	complex mosaic glass	polychrome rosette	L1: 16.1; L2: 6.5; L3: 2.2	S. 18554/14	from broken edge
43		Ty-P-R-419	mosaic bar	semifinished product	2	complex mosaic glass	polychrome rosette	L1: 11.8; L2: 5.4; L3: 1.9	S. 18554/19	from broken edge
44		Ty-P-R-423	mosaic bar	semifinished product	2	complex mosaic glass	polychrome rosette	L1: 8.0; L2: 8.3; L3: 1.5	S. 18554/23	from broken edge
45		Ty-P-St-415	mosaic bar	semifinished product	2	complex mosaic glass	blue, white and yellow stars	L1: 6.6; L2: 5.3; L3: 1.7	S. 18554/15	from broken edge
46		Ty-P-StB-002	cold-assembled inlay	finished product	1	mosaic glass	blue; white; organic	L1: 18.2; L2: 12.3; L3: 3.6	S. 19200/02	from broken edge
47	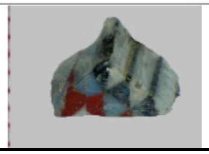	Ty-P-T-417	cane slice	finished product	2	complex mosaic glass	polychrome triangles	L1: 6.8; L2: 5.4; L3: 3.9	S. 18554/17	from broken edge

Table I - List of analyzed objects

N°	Image	Sample Name	Typology	Class	Inlay type	Group	Color/s and motifs	Dimensions (mm)	Inventory	Sampling area
48	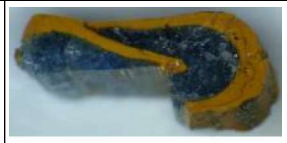	Ty-P-V-423	cane slice	finished product	2	complex mosaic glass	blue and yellowish-orange V-shaped	L1: 4.2; L2: 2.1; L3: 1.8	S. 18554/23	detached fragment
49		Ty-S-423a	cane slice	finished product	2	stratified	dull red; white; light blue; transparent	L1: 2.7; L2: 1.4; L3: 1.2	S. 18554/23	detached fragment
50		Ty-S-ARG-403	cane slice	finished product	2	stratified	light blue, red, yellow	L1: 9.1; L2: 6.5; L3: 4.3	S. 18554/03	from broken edge
51		Ty-S-ArG-506	rod	semifinished product?	2	stratified	yellowish-orange	L1: 15.6; L2: 7.3; L3: 1.5	S. 18555/06	from broken edge
52		Ty-Sb-B-003	rod	semifinished product	2	monochrome	transparent blue	L1: 43.3; Ømax: 9.5	S. 19200/03	from broken edge
53		Ty-S-BB-004	bar	waste	2	stratified	two shades of blue	L1: 18.8; L2: 6.1; L3: 2.1	S. 19200/04	from broken edge
54		Ty-S-BBi-004	bar	semifinished product	2	stratified	blue; white	L1: 25.1; L2: 5.5; L3: 1.3	S. 19200/04	from broken edge
55		Ty-S-BiBR-404	mosaic cane	semifinished product	2	stratified	white; blue; dull red	L1: 10.6; L2: 5.0; L3: 4.6	S. 18554/04	from broken edge

Table I - List of analyzed objects

N°	Image	Sample Name	Typology	Class	Inlay type	Group	Color/s and motifs	Dimensions (mm)	Inventory	Sampling area
56		Ty-S-BiBR-507	fragment	semifinished product?	2	stratified	white; blue?; red	L1: 9.4; L2: 6.6; L3: 2.7	S. 18555/07	from broken edge
57		Ty-S-BiR-507	bar	semifinished product?	2	stratified	white; red	L1: 10.1; L2: 4.8; L3: 1.1	S. 18555/07	from broken edge
58		Ty-S-BT-004	bar	semifinished product?	2	stratified	blue; transparent	L1: 8.8; L2: 7.6; L3: 1.8	S. 19200/04	from broken edge
59		Ty-S-BTW-004	bar	finished product	2	stratified	blue; white	L1: 16.1; L2: 5.5; L3: 1.5	S. 19200/04	from broken edge
60		Ty-S-GA-005	bar	semifinished product	2	stratified	light blue; yellowish-orange	L1: 14.8; L2: 6.1; L3: 2.2	S. 19200/05	from broken edge
61		Ty-S-GA-411	cane slice	finished product	2	stratified	yellow; blue	L1: 5.1; L2: 4.0; L3: 3.2	S. 18554/11	from broken edge
62		Ty-S-GB-413	cane slice	finished product	2	stratified	yellowish-orange; blue	L1: 5.8; L2: 5.4; L3: 1.1	S. 18554/13	from broken edge
63		Ty-S-GR-506	bar	semifinished product?	2	stratified	yellowish-orange; sealing-wax red	L1: 18.8; L2: 10.7; L3: 1.0	S. 18555/06	from broken edge

Table I - List of analyzed objects

N°	Image	Sample Name	Typology	Class	Inlay type	Group	Color/s and motifs	Dimensions (mm)	Inventory	Sampling area
64		Ty-S-GRT-501	bar	semifinished product?	2	stratified	yellowish-orange; dull red; transparent	L1: 15.6; L2: 1.4; L3: 0.9	S. 18555/01	from broken edge
65	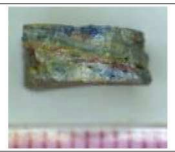	Ty-S-mix-006	bar	waste	2	stratified	mix of various colors	L1: 9.7; L2: 9.3; L3: 3.8	S. 19200/06	from broken edge
66		Ty-S-MR-502	bar	finished product	2	stratified	brown; sealing-wax red	L1: 27.1; L2: 8.3; L3: 2.0	S. 18555/02	from broken edge
67		Ty-S-RV-418	cold-assembled inlay	finished product	1	stratified	2 types of sealing-wax red; turquoise	L1: 16.4; L2: 11.5; L3: 5.3	S. 18554/18	from broken edge
68		Ty-S-TA-005	bar	semifinished product?	2	stratified	light blue; transparent	L1: 25.3; L2: 5.7; L3: 1.3	S. 19200/05	from broken edge
69		Ty-S-TR-501	bar	semifinished product?	2	stratified	dull red; transparent	L1: 9.4; L2: 5.4; L3: 2.4	S. 18555/01	from broken edge
70	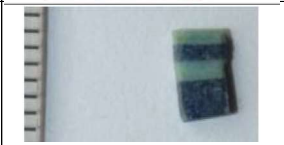	Ty-S-VA-405	cane slice	semifinished product?	2	stratified	turquoise; blue	L1: 5.7; L2: 2.9; L3: 1.1	S. 18554/05	from broken edge

Table II - Analytical protocol for each sample. This table lists all the analytical techniques (SM, OM, CLSM, SEM-EDS, EPMA and μ-Raman) employed to characterize each sample.

Nr.	Sample	Color	SM	OM	CLSM	SEM-EDS	EPMA	μ-Raman
1	Ty-I-B-616	opaque dark blue	X	X		X	X	
2	Ty-I-BBi-613-Bi	opaque white	X	X		X	X	
3	Ty-I-BBi-613-BT	transp. dark blue	X	X		X	X	
4	Ty-I-RAu-605	sealing-wax red	X	X		X	X	
5	Ty-I-RAu-622	sealing-wax red	X	X		X	X	X
6	Ty-M-A-005	opaque light blue	X	X		X	X	
7	Ty-M-A-005a	opaque light blue	X	X		X	X	X
8	Ty-M-A-006	opaque turquoise	X	X		X	X	X
9	Ty-M-Ar-506	yellowish-orange	X	X		X	X	
10	Ty-M-Ar-506a	yellowish-orange	X	X		X	X	
11	Ty-M-B-002	opaque dark blue	X	X		X	X	
12	Ty-M-B-004	transp. dark blue	X	X		X	X	
13	Ty-M-BAu-002	opaque dark blue	X	X		X	X	X
14	Ty-M-G-504	yellowish-orange	X	X		X	X	X
15	Ty-M-G-504a	yellowish-orange	X	X		X	X	X
16	Ty-M-G-504b	yellowish-orange	X	X		X	X	
17	Ty-M-R-501	dull red	X	X		X	X	
18	Ty-M-R-502d	sealing-wax red	X	X		X	X	
19	Ty-M-R-505	dull red	X	X		X	X	X
20	Ty-M-R-507	sealing-wax red	X	X		X	X	
21	Ty-M-RAu-502	sealing-wax red	X	X		X	X	X
22	Ty-M-RAu-502a	sealing-wax red	X	X		X	X	
23	Ty-M-RAu-502b	sealing-wax red	X	X		X	X	
24	Ty-M-RAu-502c	sealing-wax red	X	X		X	X	
25	Ty-M-T-503	aqua	X	X		X	X	
26	Ty-M-T-503a	aqua	X	X		X	X	
27	Ty-M-V-005	opaque turquoise	X	X		X	X	X
28	Ty-M-V-005a	opaque turquoise	X	X		X	X	
29	Ty-M-V-006	opaque turquoise	X	X		X	X	
30	Ty-M-V-006a	opaque turquoise	X	X		X	X	
31	Ty-P-A-402-B	opaque dark blue	X	X		X	X	X
32	Ty-P-A-402-G	yellow	X	X		X	X	X
33	Ty-P-A-408-Ar	yellowish-orange	X	X		X	X	
34	Ty-P-A-408-B	opaque dark blue	X	X		X	X	
35	Ty-P-A-415	polychrome	X		X			
36	Ty-P-A-418-B	opaque dark blue	X	X		X	X	
37	Ty-P-A-418-Bi	opaque white	X	X		X	X	
38	Ty-P-A-418-R1	dull red	X	X		X	X	
39	Ty-P-A-418-R2	dull red	X	X		X	X	
40	Ty-P-A-419-Bi	opaque white	X	X		X	X	
41	Ty-P-A-419-BT	transp. dark blue	X	X		X	X	
42	Ty-P-A-419-R	dull red	X	X		X	X	
43	Ty-P-CR-421-A	opaque light blue	X	X		X	X	X
44	Ty-P-CR-421-B	opaque dark blue	X	X		X	X	X
45	Ty-P-CR-421-Bi	opaque white	X	X		X	X	X
46	Ty-P-CR-421-BT	transp. dark blue	X	X		X	X	X
47	Ty-P-CR-421-G1	yellow	X	X		X	X	X
48	Ty-P-CR-421-G2	yellow	X	X		X	X	X

Table II - Analytical protocol for each sample

Nr.	Sample	Color	SM	OM	CLSM	SEM-EDS	EPMA	μ-Raman
49	Ty-P-CR-421-R	dull red	X	X		X	X	X
50	Ty-P-FL-004-B	opaque dark blue	X	X		X	X	X
51	Ty-P-FL-004-Bi	opaque white	X	X		X	X	X
52	Ty-P-FL-004-R	dull red	X	X		X	X	X
53	Ty-P-FL-404	polychrome	X		X			
54	Ty-P-FL-501-Bi	opaque white	X	X		X	X	X
55	Ty-P-FL-501-BT	transp. dark blue	X	X		X	X	X
56	Ty-P-FL-501-G	yellow	X	X		X	X	X
57	Ty-P-FL-501-R	dull red	X	X		X	X	X
58	Ty-P-FR-422-B	opaque dark blue	X	X		X	X	X
59	Ty-P-FR-422-Bi	opaque white	X	X		X	X	X
60	Ty-P-FR-422-G1	yellow	X	X		X	X	X
61	Ty-P-FR-422-G2	yellow	X	X		X	X	X
62	Ty-P-FR-422-R	dull red	X	X		X	X	X
63	Ty-P-FR-422-T1	true colorless	X	X		X	X	
64	Ty-P-FR-422-T2	true colorless	X	X		X		
65	Ty-Pn-B-001	transp. dark blue	X	X		X	X	
66	Ty-Pn-T-001	aqua	X	X		X	X	
67	Ty-P-R-414-B	opaque dark blue	X	X		X	X	
68	Ty-P-R-414-G	yellow	X	X		X	X	
69	Ty-P-R-414-T	true colorless	X	X		X	X	
70	Ty-P-R-419-A	opaque light blue	X	X		X	X	
71	Ty-P-R-419-Ar	yellowish-orange	X	X		X	X	
72	Ty-P-R-419-BO	opaque dark blue	X	X		X	X	
73	Ty-P-R-419-BT	transp. dark blue	X	X		X	X	
74	Ty-P-R-419-G	yellow	X	X		X	X	
75	Ty-P-R-419-R	sealing-wax red	X	X		X	X	
76	Ty-P-R-419-VT	transp. green	X	X		X	X	
77	Ty-P-R-423-Ar	yellowish-orange	X	X		X	X	X
78	Ty-P-R-423-B	opaque dark blue	X	X		X	X	X
79	Ty-P-R-423-BT	transp. dark blue	X	X		X	X	
80	Ty-P-R-423-G	yellow	X	X		X	X	X
81	Ty-P-R-423-R1	sealing-wax red	X	X		X	X	X
82	Ty-P-R-423-VT	transp. green	X	X		X	X	
83	Ty-P-St-415-B	opaque dark blue	X	X		X	X	
84	Ty-P-St-415-Bi	opaque white	X	X		X	X	
85	Ty-P-StB-002	opaque dark blue	X	X		X	X	
86	Ty-P-T-417-B	opaque dark blue	X	X		X	X	
87	Ty-P-T-417-Bi	opaque white	X	X		X	X	
88	Ty-P-T-417-R	dull red	X	X		X	X	
89	Ty-P-T-417-V	transp. green	X	X		X	X	
90	Ty-P-V-423-Ar	yellowish-orange	X	X		X		
91	Ty-P-V-423-B	opaque dark blue	X	X		X		
92	Ty-S-423a-A	opaque light blue	X	X		X	X	
93	Ty-S-423a-Bi	opaque white	X	X		X	X	
94	Ty-S-423a-R	dull red	X	X		X	X	
95	Ty-S-423a-T	true colorless	X	X		X	X	
96	Ty-S-ARG-403-A	opaque light blue	X	X		X	X	
97	Ty-S-ARG-403-G	yellow	X	X		X	X	
98	Ty-S-ArG-506-Ar	yellowish-orange	X	X		X	X	
99	Ty-S-ArG-506-G	yellowish-orange	X	X		X	X	

Table II - Analytical protocol for each sample

Nr.	Sample	Color	SM	OM	CLSM	SEM-EDS	EPMA	µ-Raman
100	Ty-Sb-B-003	transp. dark blue	X	X		X	X	
101	Ty-S-BB-004-BO	opaque dark blue	X	X		X	X	
102	Ty-S-BB-004-BT	transp. dark blue	X	X		X	X	
103	Ty-S-BBi-004-Bi	opaque white	X	X		X	X	
104	Ty-S-BBi-004-BT	transp. dark blue	X	X		X	X	
105	Ty-S-BiBR-404-Bi	opaque white	X	X		X	X	
106	Ty-S-BiBR-404-BO	opaque dark blue	X	X		X	X	
107	Ty-S-BiBR-404-R	dull red	X	X		X	X	
108	Ty-S-BiBR-507-Bi	opaque white	X	X		X	X	X
109	Ty-S-BiBR-507-R	dull red	X	X		X	X	X
110	Ty-S-BiBR-507-VT	transp. green	X	X		X	X	X
111	Ty-S-BiR-507-Bi	opaque white	X	X		X	X	X
112	Ty-S-BiR-507-R	dull red	X	X		X	X	X
113	Ty-S-BT-004-BO	opaque dark blue	X	X		X	X	
114	Ty-S-BT-004-BT	transp. dark blue	X	X		X	X	
115	Ty-S-BT-004-T	true colorless	X	X		X	X	
116	Ty-S-BTW-004-Bi	opaque white	X	X		X	X	
117	Ty-S-BTW-004-BT	transp. dark blue	X	X		X	X	
118	Ty-S-BTW-004-W	transp. dark blue	X	X		X	X	
119	Ty-S-GA-005-A	opaque light blue	X	X		X	X	
120	Ty-S-GA-005-Ar	yellowish-orange	X	X		X	X	
121	Ty-S-GA-411-A	opaque dark blue	X	X		X	X	
122	Ty-S-GA-411-G	yellow	X	X		X	X	
123	Ty-S-GB-413-Ar	yellowish-orange	X	X		X	X	
124	Ty-S-GB-413-BT	opaque dark blue	X	X		X	X	
125	Ty-S-GR-506-Ar	yellowish-orange	X	X		X	X	
126	Ty-S-GR-506-R	sealing-wax red	X	X		X	X	
127	Ty-S-GRT-501-Ar	yellowish-orange	X	X		X	X	X
128	Ty-S-GRT-501-Ar2	yellowish-orange	X	X		X		X
129	Ty-S-GRT-501-R	dull red	X	X		X	X	X
130	Ty-S-GRT-501-VT	transp. green	X	X		X		
131	Ty-S-mix-006-B	opaque dark blue	X	X		X		
132	Ty-S-mix-006-G	yellow	X	X		X		
133	Ty-S-mix-006-R	dull red	X	X		X		
134	Ty-S-MR-502-M	brown	X	X		X	X	X
135	Ty-S-MR-502-R	sealing-wax red	X	X		X	X	X
136	Ty-S-RV-418-R1	sealing-wax red	X	X		X	X	
137	Ty-S-RV-418-R2	sealing-wax red	X	X		X	X	
138	Ty-S-RV-418-V	opaque turquoise	X	X		X	X	
139	Ty-S-TA-005-A	opaque light blue	X	X		X	X	
140	Ty-S-TA-005-T	true colorless	X	X		X	X	
141	Ty-S-TR-501-R	dull red	X	X		X	X	
142	Ty-S-TR-501-T	true colorless	X	X		X	X	
143	Ty-S-VA-405-A	opaque turquoise	X	X		X	X	
144	Ty-S-VA-405-B	opaque dark blue	X	X		X	X	

Table III - EPMA results (glassy matrix). Chemical composition of the glassy matrix on the analyzed samples (EPMA data expressed as oxide weight percent), as a mean of 5-7 point analyses. Standard Deviations (SD) are also reported.

Sample Name		Na_2O	MgO	Al_2O_3	SiO_2	SO_3	P_2O_5	Cl	K_2O	CaO	TiO_2	MnO	FeO	CoO	CuO	As_2O_5	SnO_2	Sb_2O_5	PbO	Total
Ty-I-B-616	MEAN	18.29	0.85	2.26	66.84	0.40	0.06	1.13	0.48	5.57	0.28	0.01	1.15	0.56	0.48	0.01	0.03	1.83	0.08	100.34
	S.D.	0.20	0.02	0.03	0.29	0.05	0.01	0.04	0.01	0.03	0.03	0.01	0.11	0.06	0.08	0.01	0.03	0.05	0.13	
Ty-I-BBi-613-Bi	MEAN	13.20	1.48	2.15	59.65	0.80	0.43	0.38	1.29	5.49	0.12	1.46	0.81	0.00	0.06	0.01	0.13	6.65	7.28	101.40
	S.D.	0.08	0.04	0.08	0.06	0.02	0.04	0.04	0.03	0.17	0.03	0.08	0.06	0.00	0.05	0.01	0.02	0.50	0.06	
Ty-I-BBi-613-BT	MEAN	17.65	0.64	2.23	70.26	0.04	0.42	1.01	0.89	5.72	0.13	0.71	1.48	0.21	0.17	0.01	0.03	0.04	0.10	101.73
	S.D.	0.26	0.04	0.08	0.26	0.03	0.03	0.02	0.06	0.07	0.05	0.04	0.16	0.04	0.01	0.03	0.03	0.03	0.02	
Ty-I-RAu-605	MEAN	11.51	0.47	1.99	46.17	0.05	0.48	0.54	0.46	4.19	0.12	0.15	0.72	0.01	4.19	0.03	0.31	1.44	26.93	99.76
	S.D.	0.12	0.04	0.09	0.23	0.02	0.06	0.02	0.01	0.02	0.04	0.02	0.08	0.02	0.16	0.05	0.01	0.02	0.28	
Ty-I-RAu-622	MEAN	11.92	0.61	1.64	53.51	0.33	0.08	0.62	0.65	5.93	0.09	0.14	0.89	0.01	4.31	0.02	0.10	0.41	16.67	97.95
	S.D.	0.10	0.03	0.01	0.41	0.08	0.04	0.03	0.02	0.06	0.02	0.04	0.08	0.02	0.25	0.01	0.03	0.08	0.10	
Ty-M-A-005	MEAN	17.26	0.79	2.49	65.51	0.08	0.20	1.53	0.54	7.24	0.13	0.07	0.74	0.02	2.32	0.03	0.13	1.15	0.04	100.24
	S.D.	0.34	0.07	0.06	0.21	0.02	0.02	0.03	0.02	0.17	0.03	0.02	0.04	0.02	0.03	0.02	0.05	0.09	0.07	
Ty-M-A-005a	MEAN	17.11	1.10	2.30	65.00	0.18	0.47	1.27	0.69	5.39	0.18	0.24	1.28	0.04	2.65	0.22	0.20	1.26	1.17	100.75
	S.D.	0.33	0.05	0.02	0.59	0.06	0.05	0.03	0.03	0.03	0.01	0.02	0.04	0.02	0.08	0.09	0.03	0.07	0.16	
Ty-M-A-006	MEAN	13.47	0.52	0.91	67.20	0.05	0.31	0.98	0.32	2.03	0.07	0.74	0.56	0.01	1.66	0.00	0.04	2.62	8.35	99.86
	S.D.	0.17	0.04	0.04	0.54	0.04	0.10	0.03	0.02	0.06	0.03	0.04	0.29	0.02	0.04	0.01	0.03	0.16	0.12	
Ty-M-Ar-506	MEAN	8.41	0.37	1.58	46.84	0.14	0.42	0.41	0.62	4.70	0.07	0.06	1.25	0.00	9.36	0.03	0.02	1.90	25.01	101.18
	S.D.	0.20	0.05	0.04	0.13	0.04	0.04	0.05	0.01	0.04	0.05	0.03	0.06	0.00	0.43	0.02	0.01	0.09	0.58	
Ty-M-Ar-506a	MEAN	10.70	1.91	3.04	45.37	0.17	0.70	0.59	1.28	8.01	0.31	0.24	1.91	0.02	7.23	0.03	0.63	0.33	16.06	98.56
	S.D.	0.26	0.04	0.07	0.29	0.05	0.04	0.05	0.02	0.05	0.02	0.04	0.11	0.03	0.25	0.03	0.02	0.04	0.25	
Ty-M-B-002	MEAN	11.56	0.92	1.99	59.41	0.09	0.33	0.73	0.79	6.65	0.05	0.29	1.77	0.29	0.44	0.01	0.02	2.12	10.48	97.96
	S.D.	0.25	0.05	0.04	0.27	0.05	0.04	0.01	0.02	0.10	0.02	0.04	0.04	0.05	0.04	0.02	0.03	0.12	0.27	
Ty-M-B-004	MEAN	14.55	0.44	2.08	71.30	0.05	0.31	1.30	0.58	5.30	0.06	0.01	1.04	0.04	0.23	0.01	0.02	0.60	0.06	97.98
	S.D.	0.39	0.01	0.02	0.44	0.02	0.02	0.04	0.02	0.05	0.01	0.01	0.01	0.02	0.04	0.02	0.02	0.05	0.02	
Ty-M-BAu-002	MEAN	13.79	0.49	2.40	68.82	0.12	0.47	0.33	0.77	7.45	0.05	0.47	1.35	0.88	1.01	0.06	0.09	4.16	0.00	102.70
	S.D.	0.23	0.01	0.07	1.04	0.04	0.01	0.04	0.02	0.10	0.04	0.03	0.07	0.01	0.01	0.03	0.05	0.07	0.04	
Ty-M-G-504	MEAN	6.69	0.29	1.53	42.15	0.26	0.12	0.31	0.50	1.96	0.15	0.08	1.79	0.05	6.91	0.02	0.02	2.52	30.92	96.29
	S.D.	0.23	0.02	0.06	0.49	0.07	0.05	0.15	0.02	0.07	0.02	0.04	0.17	0.04	0.79	0.03	0.02	0.17	0.70	
Ty-M-G-504a	MEAN	11.02	1.61	2.74	45.15	0.67	0.39	0.71	1.06	6.93	0.25	0.20	2.20	0.02	8.03	0.03	0.94	0.45	18.18	100.58
	S.D.	0.16	0.04	0.03	0.35	0.03	0.07	0.03	0.03	0.08	0.02	0.04	0.05	0.02	0.27	0.03	0.05	0.04	0.50	
Ty-M-G-504b	MEAN	10.95	1.56	2.73	44.02	0.67	0.35	0.68	1.05	6.86	0.23	0.26	2.15	0.02	8.21	0.05	0.95	0.42	17.80	98.96
	S.D.	0.13	0.04	0.06	0.52	0.07	0.08	0.03	0.02	0.06	0.07	0.02	0.08	0.03	0.23	0.03	0.03	0.04	0.51	
Ty-M-R-501	MEAN	13.76	2.29	2.12	55.10	0.82	0.34	0.92	1.58	8.36	0.17	0.31	1.32	0.02	2.27	0.02	0.44	0.37	8.43	98.61
	S.D.	0.24	0.09	0.08	1.25	0.04	0.16	0.04	0.03	0.40	0.03	0.05	0.08	0.02	0.19	0.02	0.04	0.06	0.43	
Ty-M-R-502d	MEAN	10.47	0.84	2.85	41.29	0.05	0.29	0.52	0.50	1.49	0.52	0.23	1.54	0.05	4.11	0.03	0.00	0.00	35.08	99.85
	S.D.	0.26	0.02	0.05	0.44	0.01	0.05	0.01	0.02	0.02	0.06	0.05	0.04	0.06	0.09	0.02	0.00	0.00	0.80	
Ty-M-R-505	MEAN	14.01	2.29	2.26	56.29	0.27	0.76	0.94	1.60	8.55	0.19	0.07	1.02	0.01	1.69	0.03	0.41	0.36	7.96	98.72
	S.D.	0.16	0.03	0.05	0.35	0.02	0.04	0.06	0.02	0.12	0.03	0.02	0.04	0.02	0.07	0.02	0.06	0.01	0.08	
Ty-M-R-507	MEAN	11.78	0.60	1.69	53.99	0.13	0.35	0.68	0.64	5.69	0.07	0.48	1.13	0.03	5.85	0.03	0.10	0.40	16.51	100.13
	S.D.	0.13	0.02	0.03	0.40	0.01	0.03	0.03	0.03	0.11	0.03	0.02	0.07	0.02	0.12	0.03	0.03	0.05	0.71	
Ty-M-RAu-502	MEAN	10.06	0.84	1.87	38.87	0.24	0.34	0.73	0.63	4.65	0.15	0.13	1.18	0.02	4.04	0.00	1.12	0.51	34.25	99.63
	S.D.	0.06	0.03	0.11	0.51	0.02	0.03	0.01	0.01	0.07	0.01	0.05	0.05	0.03	0.11	0.00	0.02	0.04	0.47	

Table III - EPMA results (glassy matrix)

Sample Name		Na_2O	MgO	Al_2O_3	SiO_2	SO_3	P_2O_5	Cl	K_2O	CaO	TiO_2	MnO	FeO	CoO	CuO	As_2O_5	SnO_2	Sb_2O_5	PbO	Total
Ty-M-RAu-502a	MEAN	11.80	0.61	1.73	54.12	0.08	0.40	0.64	0.65	5.74	0.13	0.55	1.06	0.03	5.61	0.00	0.11	0.41	16.92	100.59
	S.D.	0.15	0.04	0.05	0.19	0.05	0.11	0.01	0.01	0.01	0.07	0.08	0.11	0.02	0.15	0.01	0.01	0.06	0.04	
Ty-M-RAu-502b	MEAN	11.57	0.47	1.48	54.22	0.40	0.09	0.69	0.66	4.21	0.08	0.43	0.46	0.01	4.47	0.01	0.11	1.61	15.50	96.53
	S.D.	0.11	0.03	0.03	0.36	0.02	0.02	0.02	0.03	0.05	0.02	0.12	0.08	0.02	0.39	0.02	0.02	0.07	0.52	
Ty-M-RAu-502c	MEAN	10.39	0.54	2.02	54.21	0.11	0.25	0.58	0.79	5.49	0.11	0.62	1.00	0.01	6.18	0.00	0.00	0.41	17.84	100.55
	S.D.	0.05	0.03	0.05	0.07	0.02	0.07	0.03	0.02	0.04	0.06	0.04	0.04	0.01	0.08	0.00	0.00	0.02	0.31	
Ty-M-T-503	MEAN	15.93	2.59	2.25	66.29	0.20	0.92	0.94	1.60	6.95	0.19	1.32	1.28	0.01	0.06	0.02	0.02	0.20	0.18	100.94
	S.D.	0.89	0.66	0.04	1.98	0.06	0.14	0.03	0.02	0.04	0.04	0.30	0.03	0.01	0.07	0.03	0.01	0.05	0.09	
Ty-M-T-503a	MEAN	15.23	1.70	2.12	67.75	0.24	0.71	0.97	1.64	6.51	0.14	0.83	1.04	0.03	0.18	0.01	0.01	0.11	0.01	99.23
	S.D.	0.01	0.09	0.05	0.11	0.04	0.03	0.04	0.01	0.09	0.00	0.03	0.04	0.05	0.05	0.01	0.02	0.05	0.02	
Ty-M-V-005	MEAN	10.59	0.51	1.95	59.88	0.08	0.42	0.38	0.68	7.04	0.05	0.39	0.48	0.01	2.57	0.04	0.20	5.22	11.20	101.69
	S.D.	0.11	0.02	0.07	1.42	0.03	0.02	0.03	0.03	0.35	0.04	0.03	0.01	0.01	0.05	0.04	0.05	1.48	0.31	
Ty-M-V-005a	MEAN	13.42	1.27	2.20	60.02	0.37	0.46	0.48	0.94	5.76	0.13	0.87	0.65	0.04	5.48	0.01	0.61	2.13	5.49	100.32
	S.D.	0.47	0.03	0.03	0.43	0.06	0.05	0.04	0.03	0.23	0.02	0.05	0.04	0.04	0.19	0.02	0.03	0.51	0.34	
Ty-M-V-006	MEAN	14.40	0.80	2.39	64.91	0.53	0.12	0.41	0.89	7.91	0.10	0.75	0.32	0.02	2.95	0.03	0.01	2.87	0.18	99.63
	S.D.	0.15	0.02	0.05	0.16	0.04	0.01	0.04	0.02	0.16	0.02	0.06	0.04	0.02	0.12	0.02	0.02	0.47	0.10	
Ty-M-V-006a	MEAN	13.89	0.53	0.92	67.08	0.03	0.31	0.95	0.33	2.01	0.07	0.75	0.47	0.02	1.73	0.00	0.03	2.65	7.03	98.81
	S.D.	0.15	0.03	0.02	0.62	0.03	0.10	0.03	0.03	0.05	0.05	0.04	0.04	0.02	0.02	0.01	0.02	0.29	0.43	
Ty-P-A-402-B	MEAN	13.76	0.48	2.59	67.10	0.39	0.07	0.32	0.85	7.29	0.05	0.48	1.40	0.79	1.02	0.03	0.05	4.01	0.10	100.79
	S.D.	0.19	0.01	0.04	0.22	0.01	0.03	0.10	0.06	0.15	0.02	0.01	0.06	0.04	0.15	0.03	0.03	0.06	0.06	
Ty-P-A-402-G	MEAN	5.93	0.21	1.14	46.90	0.20	0.07	0.38	0.34	3.01	0.07	0.03	1.10	0.02	0.06	0.00	0.00	1.48	36.53	97.52
	S.D.	0.10	0.04	0.03	0.63	0.01	0.02	0.04	0.02	0.13	0.02	0.03	0.34	0.03	0.02	0.00	0.00	0.20	0.91	
Ty-P-A-408-Ar	MEAN	11.20	1.53	2.59	45.56	0.30	0.62	0.57	1.05	7.09	0.27	0.31	2.13	0.10	6.89	0.03	0.85	0.43	17.60	99.15
	S.D.	0.32	0.08	0.12	0.61	0.01	0.05	0.02	0.05	0.13	0.03	0.00	0.02	0.05	0.18	0.06	0.03	0.02	0.52	
Ty-P-A-408-B	MEAN	16.34	0.63	1.94	67.74	0.39	0.08	1.22	0.70	4.80	0.14	0.65	1.33	0.31	0.42	0.01	0.02	1.73	1.52	99.99
	S.D.	0.28	0.04	0.04	0.82	0.07	0.03	0.07	0.02	0.14	0.04	0.01	0.02	0.03	0.05	0.01	0.02	0.12	0.22	
Ty-P-A-418-Bi	MEAN	16.37	2.61	2.69	65.37	0.06	0.30	0.99	0.71	7.98	0.12	0.03	0.61	0.01	0.00	0.02	0.02	4.32	0.11	102.32
	S.D.	0.30	0.05	0.05	0.80	0.02	0.02	0.02	0.02	0.07	0.03	0.03	0.02	0.01	0.01	0.03	0.02	0.30	0.05	
Ty-P-A-418-BO	MEAN	14.62	0.60	2.49	67.44	0.19	0.24	0.92	0.72	6.43	0.13	0.45	1.09	0.19	0.24	0.01	0.06	3.19	2.64	101.63
	S.D.	0.26	0.01	0.06	0.18	0.04	0.02	0.04	0.01	0.04	0.02	0.02	0.08	0.02	0.05	0.01	0.02	0.08	0.37	
Ty-P-A-418-R1	MEAN	13.59	2.85	2.48	56.47	1.36	0.17	1.05	1.90	7.96	0.17	0.54	1.67	0.01	2.02	0.01	0.44	0.41	7.66	100.76
	S.D.	0.27	0.02	0.06	0.48	0.03	0.04	0.03	0.02	0.07	0.01	0.05	0.09	0.02	0.19	0.01	0.03	0.05	0.31	
Ty-P-A-418-R2	MEAN	13.81	2.92	2.53	55.79	1.32	0.19	1.04	2.02	7.89	0.18	0.52	1.63	0.03	1.86	0.01	0.45	0.42	7.79	100.40
	S.D.	0.14	0.06	0.10	0.24	0.03	0.05	0.03	0.01	0.04	0.04	0.05	0.05	0.03	0.11	0.02	0.03	0.03	0.22	
Ty-P-A-419-Bi	MEAN	11.49	0.61	2.57	67.24	0.04	0.26	0.48	0.97	3.91	0.10	0.09	0.73	0.04	0.05	0.05	0.21	5.36	7.07	101.29
	S.D.	0.22	0.04	0.06	0.06	0.03	0.06	0.02	0.20	0.04	0.03	0.02	0.07	0.02	0.06	0.02	0.05	0.11	0.19	
Ty-P-A-419-BT	MEAN	14.27	0.68	2.01	69.85	0.18	0.19	1.11	1.07	4.83	0.15	0.44	1.53	0.11	0.43	0.02	0.02	2.77	1.03	100.69
	S.D.	0.19	0.05	0.04	0.13	0.03	0.04	0.03	0.03	0.05	0.05	0.03	0.06	0.04	0.06	0.02	0.02	0.07	0.10	
Ty-P-A-419-R	MEAN	12.42	3.38	1.89	60.55	1.60	0.16	0.82	3.00	7.42	0.12	0.62	2.70	0.03	1.46	0.13	0.72	0.27	3.67	100.97
	S.D.	0.16	0.03	0.04	0.18	0.08	0.02	0.02	0.04	0.04	0.07	0.03	0.02	0.05	0.08	0.04	0.03	0.04	0.10	
Ty-P-CR-421-A	MEAN	15.76	0.45	2.08	69.55	0.07	0.31	1.76	0.47	4.95	0.13	0.03	0.52	0.03	2.95	0.01	0.14	1.80	0.07	101.08
	S.D.	0.01	0.03	0.03	0.73	0.02	0.04	0.06	0.02	0.20	0.02	0.01	0.03	0.02	0.19	0.02	0.02	0.05	0.05	
Ty-P-CR-421-B	MEAN	15.30	0.69	2.68	69.07	0.12	0.23	1.06	0.70	6.31	0.13	0.37	1.24	0.19	0.35	0.04	0.02	3.15	0.99	102.63
	S.D.	0.12	0.03	0.04	0.30	0.03	0.05	0.03	0.01	0.06	0.02	0.06	0.03	0.04	0.05	0.05	0.01	0.06	0.19	

Table III - EPMA results (glassy matrix)

Sample Name		Na_2O	MgO	Al_2O_3	SiO_2	SO_3	P_2O_5	Cl	K_2O	CaO	TiO_2	MnO	FeO	CoO	CuO	As_2O_5	SnO_2	Sb_2O_5	PbO	Total
Ty-P-CR-421-Bi	MEAN	0.13	0.42	2.05	75.73	0.04	0.41	1.13	0.43	5.30	0.09	0.01	0.39	0.01	0.06	0.03	0.04	3.33	1.05	90.63
	S.D.	0.01	0.01	0.05	0.77	0.01	0.02	0.05	0.02	0.07	0.02	0.01	0.01	0.01	0.04	0.02	0.02	0.06	0.07	
Ty-P-CR-421-G1	MEAN	12.62	1.01	1.86	63.61	0.25	0.25	0.90	0.58	4.69	0.09	0.47	1.81	0.01	0.06	0.05	0.12	1.09	11.91	101.37
	S.D.	0.39	0.37	0.07	1.33	0.12	0.04	0.03	0.10	0.22	0.02	0.16	0.27	0.02	0.05	0.05	0.05	0.15	1.17	
Ty-P-CR-421-G2	MEAN	10.79	0.40	1.84	53.93	0.06	0.14	0.59	0.57	2.20	0.12	0.42	2.67	0.00	0.16	0.02	0.04	1.35	23.10	98.38
	S.D.	0.63	0.08	0.11	4.05	0.05	0.05	0.07	0.21	0.42	0.02	0.04	0.37	0.00	0.16	0.02	0.02	0.29	5.71	
Ty-P-CR-421-R	MEAN	13.89	2.77	2.45	56.77	1.09	0.24	0.99	1.95	8.24	0.17	0.45	1.45	0.01	1.66	0.04	0.42	0.34	7.38	100.29
	S.D.	0.22	0.08	0.03	0.24	0.06	0.04	0.02	0.09	0.07	0.04	0.03	0.05	0.02	0.22	0.03	0.04	0.05	0.24	
Ty-P-CR-421-T	MEAN	14.29	0.49	2.17	71.63	0.06	0.33	1.40	1.07	5.48	0.10	0.03	1.03	0.07	0.46	0.01	0.02	0.56	0.03	99.23
	S.D.	0.42	0.03	0.04	0.31	0.04	0.09	0.05	0.03	0.04	0.03	0.03	0.06	0.04	0.09	0.02	0.02	0.02	0.04	
Ty-P-FL-004-B	MEAN	16.27	0.71	2.77	68.77	0.10	0.19	1.21	0.85	5.22	0.20	0.09	2.36	0.20	0.41	0.01	0.01	2.71	0.19	102.27
	S.D.	0.17	0.03	0.03	0.13	0.02	0.04	0.06	0.01	0.03	0.03	0.03	0.01	0.05	0.04	0.02	0.02	0.05	0.04	
Ty-P-FL-004-Bi	MEAN	16.54	5.04	1.96	67.73	0.04	0.24	0.87	0.69	6.25	0.07	0.04	0.34	0.01	0.04	0.03	0.01	2.97	0.01	102.88
	S.D.	0.13	0.05	0.02	0.24	0.04	0.05	0.02	0.11	0.06	0.02	0.03	0.02	0.01	0.03	0.04	0.02	0.15	0.01	
Ty-P-FL-004-R	MEAN	14.72	2.37	2.29	57.19	0.84	0.22	0.94	1.49	8.50	0.20	0.32	1.30	0.00	2.03	0.00	0.46	0.33	8.40	101.61
	S.D.	0.19	0.02	0.02	0.36	0.05	0.08	0.06	0.09	0.09	0.05	0.02	0.04	0.01	0.19	0.00	0.04	0.04	0.15	
Ty-P-FL-501-Bi	MEAN	12.66	0.51	2.40	70.36	0.04	0.47	0.64	1.20	3.48	0.14	0.07	0.63	0.00	0.03	0.04	0.03	5.93	0.31	98.94
	S.D.	0.34	0.02	0.04	0.13	0.03	0.17	0.08	0.07	0.09	0.03	0.01	0.04	0.00	0.04	0.04	0.04	0.34	0.03	
Ty-P-FL-501-G	MEAN	13.00	0.77	2.14	64.79	0.22	0.38	0.69	0.96	3.52	0.13	0.27	1.26	0.02	0.13	0.01	0.14	4.15	7.12	99.68
	S.D.	0.28	0.02	0.07	1.13	0.02	0.00	0.05	0.04	0.06	0.03	0.03	0.03	0.03	0.11	0.02	0.03	0.09	0.21	
Ty-P-FL-501-R	MEAN	12.54	2.37	2.73	53.81	1.05	0.26	0.84	1.39	9.13	0.30	0.39	1.90	0.01	2.15	0.01	0.52	0.25	10.00	99.65
	S.D.	0.08	0.03	0.05	0.51	0.04	0.06	0.03	0.06	0.09	0.04	0.05	0.03	0.03	0.37	0.03	0.04	0.02	0.17	
Ty-P-FL-501-T	MEAN	14.36	2.53	1.90	67.64	1.24	0.16	1.01	1.96	6.32	0.20	0.95	1.46	0.05	0.18	0.02	0.00	0.16	0.05	100.17
	S.D.	0.19	0.13	0.05	0.57	0.01	0.06	0.03	0.03	0.06	0.03	0.04	0.05	0.01	0.06	0.02	0.00	0.02	0.05	
Ty-P-FR-422-B	MEAN	15.43	0.58	2.20	68.77	0.06	0.35	1.38	0.69	4.46	0.12	0.11	1.28	0.25	0.27	0.01	0.06	1.90	2.41	100.33
	S.D.	0.30	0.09	0.12	0.22	0.03	0.06	0.06	0.02	0.07	0.01	0.02	0.06	0.05	0.02	0.01	0.04	0.16	0.05	
Ty-P-FR-422-Bi	MEAN	16.73	5.16	2.00	67.23	0.05	0.28	0.86	0.59	6.19	0.06	0.01	0.34	0.01	0.03	0.06	0.02	2.88	0.03	102.53
	S.D.	0.23	0.10	0.02	0.27	0.04	0.01	0.02	0.01	0.03	0.02	0.02	0.04	0.01	0.02	0.05	0.02	0.19	0.03	
Ty-P-FR-422-G1	MEAN	15.04	0.53	2.16	65.90	0.09	0.23	1.14	0.56	5.58	0.10	0.13	1.35	0.01	0.03	0.00	0.01	0.93	6.56	100.35
	S.D.	0.15	0.06	0.04	0.96	0.03	0.04	0.12	0.06	0.34	0.01	0.04	0.63	0.02	0.02	0.00	0.02	0.05	0.57	
Ty-P-FR-422-G2	MEAN	12.96	0.59	2.11	58.33	0.09	0.21	0.98	0.60	3.88	0.13	0.53	1.78	0.00	0.05	0.03	0.05	0.86	16.04	99.21
	S.D.	0.14	0.05	0.02	0.34	0.03	0.06	0.05	0.07	0.13	0.02	0.01	0.10	0.00	0.03	0.04	0.02	0.10	0.32	
Ty-P-FR-422-R	MEAN	14.90	2.37	2.34	56.76	0.81	0.24	1.00	1.48	8.43	0.18	0.35	1.29	0.02	1.76	0.01	0.43	0.33	8.28	100.98
	S.D.	0.08	0.05	0.05	0.45	0.05	0.02	0.02	0.03	0.09	0.04	0.04	0.05	0.02	0.23	0.01	0.06	0.04	0.15	
Ty-P-FR-422-T1	MEAN	15.99	0.52	2.22	71.22	0.04	0.32	1.41	0.73	5.53	0.09	0.03	1.01	0.04	0.22	0.01	0.01	0.58	0.04	100.01
	S.D.	0.11	0.02	0.04	0.33	0.02	0.06	0.05	0.03	0.02	0.02	0.03	0.04	0.03	0.05	0.01	0.01	0.02	0.05	
Ty-Pn-B-001	MEAN	7.03	0.31	0.80	74.49	0.07	0.56	0.51	0.80	1.09	0.07	0.50	0.59	0.11	0.14	0.02	0.01	0.64	0.16	87.90
	S.D.	1.33	0.03	0.09	1.57	0.01	0.04	0.10	0.04	0.03	0.04	0.04	0.01	0.04	0.05	0.03	0.02	0.07	0.04	
Ty-Pn-T-001	MEAN	17.92	0.92	2.35	66.90	0.31	0.23	1.04	0.97	6.08	0.16	0.16	0.84	0.01	0.00	0.00	0.00	0.51	0.00	98.40
	S.D.	1.78	0.07	0.12	4.30	0.05	0.06	0.02	0.04	0.26	0.06	0.05	0.06	0.01	0.00	0.00	0.00	0.09	0.00	
Ty-P-R-414-B	MEAN	17.07	0.73	2.87	68.43	0.12	0.24	1.19	0.88	5.22	0.21	0.14	2.52	0.26	0.40	0.02	0.03	2.65	0.27	103.23
	S.D.	0.45	0.03	0.05	0.20	0.03	0.02	0.04	0.01	0.08	0.03	0.03	0.06	0.05	0.06	0.02	0.03	0.09	0.05	
Ty-P-R-414-G	MEAN	13.64	0.39	1.87	62.36	0.03	0.20	1.11	0.52	4.12	0.09	0.15	1.33	0.03	0.05	0.01	0.05	1.07	12.44	99.45
	S.D.	0.28	0.03	0.04	0.46	0.03	0.02	0.08	0.00	0.12	0.09	0.04	0.20	0.02	0.02	0.02	0.02	0.14	0.12	

Table III - EPMA results (glassy matrix)

Sample Name		Na_2O	MgO	Al_2O_3	SiO_2	SO_3	P_2O_5	Cl	K_2O	CaO	TiO_2	MnO	FeO	CoO	CuO	As_2O_5	SnO_2	Sb_2O_5	PbO	Total
Ty-P-R-414-T	MEAN	16.98	0.53	2.09	70.76	0.04	0.31	1.34	0.66	7.18	0.08	0.03	0.37	0.01	0.04	0.00	0.00	0.81	0.00	101.23
	S.D.	0.21	0.01	0.06	0.41	0.02	0.05	0.02	0.01	0.02	0.01	0.01	0.03	0.01	0.03	0.01	0.00	0.04	0.05	
Ty-P-R-419-Ar	MEAN	10.79	1.76	2.93	44.14	0.66	0.23	0.46	1.09	7.36	0.24	0.24	1.83	0.03	6.31	0.03	0.80	0.48	19.33	98.70
	S.D.	0.19	0.04	0.04	0.37	0.06	0.02	0.03	0.04	0.11	0.04	0.03	0.05	0.04	0.46	0.04	0.07	0.03	0.51	
Ty-P-R-419-BO	MEAN	16.42	0.68	2.74	64.28	0.09	0.24	1.19	0.90	5.18	0.18	0.13	2.47	0.21	0.45	0.04	0.01	2.72	0.16	98.07
	S.D.	0.28	0.03	0.08	0.87	0.03	0.03	0.05	0.03	0.03	0.02	0.03	0.07	0.03	0.08	0.03	0.02	0.20	0.02	
Ty-P-R-419-BT	MEAN	17.30	0.47	2.15	69.17	0.05	0.28	1.43	0.66	5.42	0.08	0.02	1.03	0.05	0.63	0.00	0.01	0.54	0.11	99.41
	S.D.	0.52	0.02	0.01	0.49	0.02	0.04	0.04	0.05	0.02	0.03	0.01	0.11	0.02	0.50	0.00	0.01	0.04	0.03	
Ty-P-R-419-G	MEAN	1.07	0.37	1.74	65.82	0.03	0.19	1.36	0.74	4.04	0.09	0.18	1.33	0.01	0.03	0.01	0.04	1.11	12.88	91.03
	S.D.	1.29	0.04	0.07	0.53	0.03	0.03	0.06	0.18	0.19	0.03	0.02	0.15	0.02	0.02	0.01	0.02	0.23	0.62	
Ty-P-R-419-R	MEAN	11.27	1.84	2.99	44.27	0.64	0.24	0.48	1.06	7.18	0.24	0.23	1.87	0.00	6.19	0.05	0.80	0.50	19.93	99.78
	S.D.	0.38	0.02	0.06	0.42	0.07	0.04	0.01	0.02	0.05	0.04	0.05	0.16	0.00	1.40	0.05	0.05	0.04	0.81	
Ty-P-R-419-VT	MEAN	12.31	1.78	2.95	44.90	0.62	0.25	0.45	0.76	7.34	0.25	0.19	1.79	0.02	4.85	0.02	0.86	0.51	19.35	99.22
	S.D.	0.11	0.03	0.08	0.15	0.04	0.04	0.04	0.03	0.05	0.05	0.04	0.05	0.03	0.10	0.03	0.06	0.03	0.52	
Ty-P-R-423-Ar	MEAN	11.55	1.61	2.80	45.93	0.67	0.58	0.71	1.10	7.02	0.25	0.28	2.26	0.00	6.87	0.02	0.91	0.46	16.67	99.68
	S.D.	0.15	0.03	0.03	0.42	0.04	0.17	0.02	0.02	0.07	0.03	0.04	0.01	0.00	0.74	0.04	0.06	0.06	0.65	
Ty-P-R-423-B	MEAN	16.49	0.67	2.63	67.88	0.12	0.23	1.18	1.15	5.15	0.19	0.14	2.41	0.21	0.45	0.04	0.03	2.58	0.23	101.79
	S.D.	0.32	0.03	0.07	0.43	0.03	0.06	0.06	0.07	0.06	0.06	0.03	0.01	0.06	0.05	0.03	0.03	0.03	0.07	
Ty-P-R-423-G	MEAN	13.12	0.35	1.76	64.60	0.05	0.25	1.26	0.52	4.13	0.07	0.15	1.21	0.00	0.08	0.02	0.06	1.05	11.59	100.25
	S.D.	0.24	0.03	0.08	0.63	0.03	0.11	0.10	0.01	0.10	0.02	0.03	0.23	0.00	0.06	0.01	0.03	0.12	0.29	
Ty-P-R-423-R1	MEAN	12.41	1.60	2.85	46.93	0.64	0.43	0.68	1.23	7.25	0.31	0.27	2.46	0.01	5.09	0.06	0.93	0.46	17.05	100.65
	S.D.	0.30	0.07	0.05	0.33	0.06	0.07	0.04	0.02	0.07	0.06	0.08	0.03	0.02	0.14	0.06	0.02	0.05	0.41	
Ty-P-R-423-BT	MEAN	16.92	0.94	2.60	65.19	0.11	0.18	1.53	0.56	9.16	0.15	0.07	1.27	0.07	0.19	0.00	0.02	0.46	1.74	101.16
	S.D.	0.18	0.03	0.04	0.65	0.03	0.02	0.01	0.01	0.06	0.04	0.01	0.06	0.02	0.03	0.00	0.02	0.05	0.40	
Ty-P-R-423-VT	MEAN	17.19	4.19	2.44	62.52	1.74	0.34	1.15	2.12	8.51	0.22	0.33	1.40	0.02	0.13	0.04	0.00	0.09	0.08	102.50
	S.D.	0.23	0.02	0.04	0.59	0.02	0.01	0.05	0.03	0.06	0.04	0.04	0.05	0.02	0.03	0.03	0.00	0.01	0.05	
Ty-P-St-415-B	MEAN	14.76	0.62	1.77	69.21	0.05	0.28	1.27	0.68	3.67	0.17	0.05	1.90	0.30	0.42	0.05	0.05	3.75	0.94	99.93
	S.D.	0.67	0.01	0.03	0.47	0.03	0.05	0.07	0.05	0.14	0.02	0.02	0.08	0.03	0.07	0.04	0.01	0.24	0.05	
Ty-P-St-415-Bi	MEAN	11.43	0.52	2.48	70.34	0.07	0.27	0.62	0.93	3.63	0.14	0.08	0.72	0.01	0.02	0.02	0.03	6.26	0.26	97.83
	S.D.	0.61	0.03	0.12	0.21	0.04	0.04	0.01	0.03	0.16	0.03	0.03	0.07	0.02	0.03	0.02	0.01	0.67	0.02	
Ty-P-StB-002	MEAN	13.22	0.89	2.51	66.46	0.19	0.43	0.46	0.90	7.37	0.08	0.94	2.22	0.36	0.50	0.03	0.04	3.62	0.83	101.06
	S.D.	0.17	0.01	0.03	0.42	0.04	0.02	0.02	0.02	0.09	0.02	0.02	0.08	0.05	0.08	0.03	0.03	0.03	0.04	
Ty-P-T-417-Bi	MEAN	14.90	0.62	2.47	69.93	0.07	0.26	0.82	1.77	4.46	0.11	0.11	0.56	0.00	0.01	0.02	0.04	4.80	0.81	101.77
	S.D.	0.63	0.09	0.16	0.42	0.02	0.01	0.05	0.01	0.12	0.01	0.01	0.05	0.00	0.02	0.03	0.03	1.45	0.21	
Ty-P-T-417-BO	MEAN	14.85	0.72	2.19	64.88	0.10	0.42	0.88	1.01	5.36	0.09	0.41	0.93	0.08	0.90	0.00	0.06	5.43	4.72	103.03
	S.D.	0.02	0.02	0.07	0.91	0.03	0.19	0.08	0.02	0.25	0.01	0.06	0.06	0.04	0.07	0.00	0.03	0.84	0.30	
Ty-P-T-417-R	MEAN	16.78	1.91	3.06	59.67	0.60	0.26	1.19	1.01	8.39	0.26	0.56	1.68	0.04	1.63	0.00	0.26	0.48	4.16	101.95
	S.D.	0.21	0.04	0.07	0.16	0.04	0.03	0.04	0.00	0.07	0.02	0.04	0.05	0.05	0.32	0.00	0.02	0.04	0.15	
Ty-P-T-417-VT	MEAN	16.89	4.61	1.02	60.67	1.73	0.24	0.97	1.81	9.99	0.05	0.95	1.37	0.01	0.02	0.00	0.00	0.11	0.02	100.45
	S.D.	0.35	0.02	0.03	0.40	0.05	0.05	0.01	0.06	0.01	0.03	0.05	0.02	0.00	0.03	0.01	0.00	0.03	0.04	
Ty-S-423a-A	MEAN	13.56	0.41	1.81	68.06	0.40	0.05	1.55	0.86	4.68	0.04	0.04	0.30	0.01	3.80	0.02	0.24	1.57	0.01	97.48
	S.D.	0.42	0.04	0.05	0.89	0.03	0.03	0.04	0.02	0.08	0.04	0.02	0.02	0.02	0.08	0.01	0.04	0.08	0.04	
Ty-S-423a-Bi	MEAN	16.26	4.98	1.85	66.98	0.33	0.03	0.80	0.60	6.23	0.07	0.06	0.32	0.02	0.08	0.04	0.02	2.87	0.01	101.60
	S.D.	0.24	0.03	0.01	0.51	0.05	0.02	0.01	0.09	0.02	0.02	0.01	0.02	0.02	0.00	0.04	0.02	0.07	0.05	

Table III - EPMA results (glassy matrix)

Sample Name		Na_2O	MgO	Al_2O_3	SiO_2	SO_3	P_2O_5	Cl	K_2O	CaO	TiO_2	MnO	FeO	CoO	CuO	As_2O_5	SnO_2	Sb_2O_5	PbO	Total
Ty-S-423a-R	MEAN	13.85	2.67	1.90	53.88	0.23	0.96	0.89	1.76	7.74	0.14	0.27	1.11	0.01	1.33	0.02	0.49	0.22	10.92	98.46
	S.D.	0.13	0.05	0.06	0.57	0.04	0.01	0.05	0.02	0.01	0.01	0.04	0.07	0.04	0.08	0.02	0.04	0.06	0.27	
Ty-S-423a-T	MEAN	15.06	0.47	2.07	69.97	0.38	0.04	1.35	0.82	5.24	0.09	0.02	0.84	0.05	0.44	0.02	0.00	0.57	0.12	97.53
	S.D.	0.19	0.01	0.05	0.19	0.03	0.01	0.01	0.02	0.06	0.04	0.02	0.04	0.03	0.07	0.03	0.01	0.01	0.01	
Ty-S-ARG-403-A	MEAN	15.55	0.48	2.20	69.00	0.07	0.30	1.56	0.49	4.72	0.07	0.03	0.52	0.00	3.36	0.02	0.14	1.84	0.20	100.56
	S.D.	0.18	0.02	0.05	0.34	0.01	0.04	0.01	0.01	0.07	0.01	0.03	0.03	0.00	0.12	0.02	0.03	0.34	0.08	
Ty-S-ARG-403-G	MEAN	11.82	0.53	2.12	69.85	0.05	0.30	1.19	0.49	5.80	0.08	0.14	1.24	0.01	0.05	0.01	0.01	0.92	5.34	99.94
	S.D.	0.36	0.02	0.02	1.71	0.01	0.01	0.09	0.01	0.32	0.03	0.03	0.18	0.01	0.04	0.01	0.02	0.06	1.86	
Ty-S-ArG-506-Ar	MEAN	10.97	1.39	1.99	40.47	0.52	0.32	1.10	0.91	5.22	0.23	0.16	1.65	0.01	7.93	0.03	0.91	0.38	27.73	101.92
	S.D.	0.11	0.03	0.04	0.31	0.05	0.08	0.07	0.02	0.03	0.02	0.05	0.03	0.01	0.68	0.03	0.08	0.06	0.24	
Ty-S-ArG-506-G	MEAN	11.12	1.81	1.97	40.93	0.76	0.40	0.76	1.08	5.53	0.19	0.42	1.52	0.01	9.25	0.03	1.24	0.57	22.69	100.26
	S.D.	0.20	0.05	0.01	0.24	0.05	0.03	0.08	0.01	0.03	0.04	0.05	0.06	0.01	0.18	0.03	0.02	0.23	0.66	
Ty-Sb-B-003	MEAN	13.18	0.66	2.11	71.55	0.23	0.09	0.80	0.66	8.40	0.08	0.58	0.32	0.15	0.04	0.01	0.04	0.03	0.13	99.03
	S.D.	0.17	0.05	0.06	0.20	0.01	0.01	0.02	0.00	0.01	0.04	0.03	0.08	0.05	0.03	0.01	0.05	0.02	0.02	
Ty-S-BB-004-BO	MEAN	15.54	0.69	2.60	67.89	0.09	0.19	1.19	0.87	5.21	0.19	0.13	2.33	0.20	0.41	0.05	0.03	2.55	0.32	100.49
	S.D.	0.17	0.02	0.08	0.48	0.04	0.05	0.03	0.02	0.03	0.05	0.03	0.11	0.03	0.03	0.04	0.01	0.02	0.02	
Ty-S-BB-004-BT	MEAN	13.65	0.53	2.13	69.98	0.06	0.35	1.68	0.66	6.09	0.08	0.04	0.99	0.15	0.23	0.01	0.01	0.82	0.10	97.55
	S.D.	0.38	0.03	0.05	0.29	0.05	0.04	0.01	0.03	0.05	0.03	0.04	0.04	0.03	0.04	0.02	0.01	0.02	0.10	
Ty-S-BBi-004-Bi	MEAN	14.34	0.60	1.65	71.57	0.07	0.31	0.89	0.71	3.82	0.19	0.44	0.60	0.03	0.03	0.00	0.03	4.16	0.72	100.17
	S.D.	0.73	0.03	0.06	3.19	0.03	0.06	0.05	0.07	0.48	0.05	0.02	0.07	0.05	0.03	0.00	0.03	3.78	0.03	
Ty-S-BBi-004-BT	MEAN	16.53	0.54	1.61	71.34	0.02	0.25	1.32	0.41	4.29	0.16	0.91	1.66	0.26	0.37	0.00	0.00	0.02	0.03	99.74
	S.D.	1.00	0.12	0.08	2.50	0.01	0.16	0.13	0.14	0.30	0.02	0.39	0.10	0.27	0.45	0.00	0.01	0.03	0.04	
Ty-S-BBi-004-BTc	MEAN	17.71	0.78	1.77	68.49	0.05	0.38	1.17	0.58	4.75	0.16	1.33	1.44	0.55	0.90	0.01	0.01	0.13	0.04	100.24
	S.D.	0.58	0.02	0.07	0.29	0.01	0.05	0.03	0.01	0.06	0.03	0.05	0.07	0.03	0.00	0.01	0.01	0.06	0.07	
Ty-S-BBi-004-BTs	MEAN	16.01	0.50	1.66	73.19	0.04	0.17	1.43	0.38	4.26	0.12	0.73	1.85	0.10	0.15	0.03	0.02	0.00	0.00	100.65
	S.D.	0.10	0.04	0.04	0.17	0.00	0.02	0.03	0.05	0.06	0.01	0.01	0.01	0.04	0.05	0.03	0.03	0.00	0.05	
Ty-S-BiBR-404-Bi	MEAN	16.98	5.05	1.99	66.77	0.04	0.28	0.85	0.56	6.25	0.09	0.02	0.39	0.01	0.01	0.05	0.01	3.00	0.01	102.34
	S.D.	0.21	0.03	0.03	0.27	0.03	0.06	0.03	0.04	0.03	0.05	0.03	0.02	0.01	0.02	0.01	0.02	0.21	0.04	
Ty-S-BiBR-404-BO	MEAN	17.31	0.71	2.75	67.24	0.11	0.23	1.21	0.87	5.16	0.21	0.13	2.47	0.25	0.46	0.01	0.01	2.67	0.20	102.02
	S.D.	0.11	0.02	0.06	0.47	0.01	0.06	0.07	0.04	0.01	0.05	0.03	0.10	0.04	0.05	0.01	0.01	0.12	0.09	
Ty-S-BiBR-404-R	MEAN	14.74	2.37	2.33	56.72	0.82	0.21	0.97	1.61	8.37	0.19	0.39	1.45	0.01	2.22	0.00	0.41	0.33	7.92	101.06
	S.D.	0.07	0.06	0.05	0.34	0.01	0.04	0.04	0.02	0.11	0.03	0.02	0.06	0.01	0.13	0.00	0.03	0.04	0.21	
Ty-S-BiBR-507-Bi	MEAN	16.53	5.01	1.95	67.19	0.04	0.27	0.85	0.52	6.23	0.05	0.01	0.39	0.01	0.04	0.03	0.01	2.86	0.04	102.04
	S.D.	0.20	0.06	0.06	0.38	0.04	0.05	0.04	0.01	0.03	0.01	0.03	0.03	0.02	0.05	0.03	0.01	0.12	0.04	
Ty-S-BiBR-507-R	MEAN	14.11	2.83	2.08	54.15	1.10	0.18	1.06	1.70	7.88	0.19	0.42	1.57	0.02	1.62	0.00	0.46	0.25	9.90	99.49
	S.D.	0.22	0.06	0.06	0.28	0.03	0.03	0.02	0.02	0.02	0.01	0.07	0.04	0.02	0.05	0.00	0.03	0.03	0.17	
Ty-S-BiBR-507-VT	MEAN	14.54	3.11	1.97	56.69	1.14	0.15	1.01	1.77	8.64	0.18	0.43	1.61	0.01	0.30	0.00	0.32	0.21	8.55	100.62
	S.D.	0.13	0.11	0.07	0.25	0.06	0.03	0.07	0.01	0.09	0.03	0.07	0.08	0.01	0.08	0.01	0.05	0.02	0.15	
Ty-S-BiR-507-Bi	MEAN	8.67	0.71	2.22	67.12	0.06	0.44	1.66	0.75	6.14	0.13	0.02	0.65	0.01	0.01	0.01	0.03	3.37	0.03	92.02
	S.D.	4.06	0.03	0.06	1.03	0.02	0.02	0.08	0.07	0.10	0.03	0.03	0.01	0.02	0.02	0.01	0.02	0.69	0.05	
Ty-S-BiR-507-R	MEAN	13.79	2.62	2.38	57.20	1.14	0.23	1.00	2.07	8.18	0.18	0.46	1.42	0.01	1.71	0.01	0.40	0.39	8.34	101.53
	S.D.	0.15	0.10	0.04	0.21	0.06	0.04	0.03	0.06	0.05	0.02	0.02	0.07	0.02	0.12	0.02	0.02	0.05	0.35	
Ty-S-BT-004-BO	MEAN	15.92	0.55	2.39	68.02	0.03	0.28	1.20	0.56	4.13	0.15	0.05	1.51	0.16	0.35	0.03	0.02	2.90	0.51	98.74
	S.D.	0.54	0.01	0.12	1.16	0.03	0.07	0.22	0.01	0.14	0.03	0.01	0.08	0.01	0.13	0.02	0.03	0.10	0.15	

Table III - EPMA results (glassy matrix)

Sample Name		Na_2O	MgO	Al_2O_3	SiO_2	SO_3	P_2O_5	Cl	K_2O	CaO	TiO_2	MnO	FeO	CoO	CuO	As_2O_5	SnO_2	Sb_2O_5	PbO	Total
Ty-S-BT-004-BT	MEAN	14.18	0.53	2.29	69.82	0.07	0.36	1.60	0.65	6.03	0.09	0.02	1.05	0.18	0.17	0.02	0.02	0.84	0.14	98.07
	S.D.	0.15	0.04	0.03	0.38	0.01	0.05	0.04	0.02	0.05	0.03	0.02	0.03	0.04	0.02	0.03	0.02	0.03	0.07	
Ty-S-BT-004-T	MEAN	8.79	0.36	1.99	71.92	0.05	0.28	1.80	1.19	4.87	0.06	0.01	0.24	0.01	0.01	0.02	0.01	0.75	0.06	92.43
	S.D.	0.37	0.01	0.08	0.54	0.02	0.03	0.02	0.05	0.09	0.05	0.01	0.05	0.02	0.01	0.03	0.01	0.02	0.05	
Ty-S-BTW-004-Bi	MEAN	11.67	0.74	2.00	60.07	0.19	0.29	0.68	0.64	4.03	0.19	0.70	0.83	0.04	0.06	0.03	0.18	5.24	12.55	100.12
	S.D.	0.29	0.03	0.03	0.69	0.05	0.06	0.02	0.02	0.08	0.07	0.05	0.03	0.04	0.05	0.03	0.05	0.23	0.46	
Ty-S-BTW-004-BT	MEAN	14.23	0.64	1.89	71.01	0.06	0.28	1.55	0.84	3.26	0.24	1.01	1.50	0.33	0.42	0.01	0.02	0.24	0.00	97.52
	S.D.	0.31	0.03	0.04	0.71	0.03	0.08	0.17	0.03	0.05	0.03	0.05	0.03	0.02	0.07	0.02	0.01	0.03	0.02	
Ty-S-BTW-004-W	MEAN	0.23	0.62	1.82	76.10	0.05	0.32	1.88	0.64	3.30	0.28	1.10	1.59	0.35	0.34	0.01	0.01	0.19	0.02	88.84
	S.D.	0.02	0.02	0.04	0.38	0.02	0.01	0.09	0.01	0.03	0.04	0.04	0.06	0.04	0.03	0.03	0.02	0.02	0.04	
Ty-S-GA-005-A	MEAN	16.05	0.42	1.83	70.51	0.04	0.18	1.25	0.36	4.50	0.07	0.04	0.86	0.02	2.64	0.27	0.20	1.99	0.39	101.62
	S.D.	0.24	0.04	0.01	0.48	0.02	0.04	0.05	0.01	0.06	0.04	0.01	0.02	0.02	0.10	0.04	0.02	0.06	0.08	
Ty-S-GA-005-Ar	MEAN	11.76	1.80	2.07	41.94	0.70	0.26	0.77	1.10	5.39	0.16	0.44	1.52	0.01	9.14	0.01	1.23	0.37	22.29	100.95
	S.D.	0.24	0.02	0.02	0.31	0.03	0.03	0.05	0.02	0.09	0.03	0.02	0.05	0.02	0.31	0.02	0.03	0.05	0.48	
Ty-S-GA-005-ArC	MEAN	11.31	1.39	2.10	41.00	0.49	0.25	1.18	0.90	5.25	0.22	0.16	1.68	0.03	7.02	0.02	0.93	0.38	27.72	102.02
	S.D.	0.20	0.07	0.05	0.35	0.05	0.02	0.04	0.01	0.07	0.03	0.02	0.07	0.04	0.53	0.02	0.01	0.04	0.36	
Ty-S-GA-005-ArS	MEAN	12.67	2.06	2.93	45.15	0.66	0.22	0.78	0.84	7.93	0.29	0.68	1.85	0.03	8.11	0.05	0.80	0.17	17.29	102.49
	S.D.	0.11	0.06	0.04	0.24	0.00	0.01	0.06	0.02	0.04	0.04	0.04	0.04	0.04	0.27	0.04	0.04	0.05	0.40	
Ty-S-GA-411-A	MEAN	14.78	0.60	2.52	69.45	0.20	0.23	0.85	0.64	8.02	0.07	0.33	0.79	0.06	0.06	0.01	0.01	2.26	0.07	100.94
	S.D.	0.29	0.01	0.02	0.24	0.02	0.03	0.01	0.01	0.07	0.07	0.03	0.04	0.04	0.04	0.01	0.01	0.03	0.09	
Ty-S-GA-411-G	MEAN	13.96	0.52	2.06	66.28	0.05	0.27	1.15	0.55	5.77	0.14	0.11	1.15	0.01	0.01	0.02	0.00	0.90	7.84	100.81
	S.D.	0.18	0.03	0.07	1.08	0.01	0.04	0.03	0.03	0.22	0.01	0.03	0.31	0.02	0.01	0.01	0.00	0.02	0.96	
Ty-S-GB-413-Ar	MEAN	11.83	1.64	2.95	44.98	0.66	0.32	0.71	1.07	7.06	0.21	0.26	2.40	0.01	6.86	0.06	0.92	0.42	18.18	100.54
	S.D.	0.33	0.04	0.06	0.30	0.06	0.04	0.03	0.03	0.06	0.03	0.03	0.12	0.01	0.66	0.01	0.03	0.03	0.50	
Ty-S-GB-413-BO	MEAN	15.23	0.78	2.89	68.32	0.03	0.17	1.45	0.65	3.37	0.25	0.17	1.92	0.32	0.44	0.06	0.03	3.06	0.25	99.39
	S.D.	0.45	0.03	0.02	0.36	0.04	0.01	0.03	0.05	0.03	0.01	0.03	0.04	0.04	0.05	0.02	0.04	0.12	0.05	
Ty-S-GB-413-BT	MEAN	0.49	0.24	0.73	73.25	0.05	0.41	2.30	0.29	6.34	0.06	0.07	0.98	0.30	0.32	0.01	0.01	0.00	0.04	85.90
	S.D.	0.04	0.03	0.07	0.38	0.02	0.04	0.08	0.03	0.07	0.03	0.01	0.02	0.08	0.03	0.01	0.01	0.00	0.08	
Ty-S-GR-506-Ar	MEAN	11.40	1.62	2.84	44.77	0.67	0.32	0.72	1.05	6.84	0.22	0.28	2.44	0.03	8.61	0.01	0.93	0.42	17.48	100.65
	S.D.	0.12	0.01	0.04	0.24	0.08	0.07	0.05	0.00	0.04	0.07	0.03	0.06	0.03	0.96	0.02	0.06	0.05	0.38	
Ty-S-GR-506-R	MEAN	10.35	0.97	1.74	39.00	0.41	0.34	0.78	0.92	4.63	0.15	0.17	1.20	0.00	4.83	0.04	0.88	0.52	32.68	99.63
	S.D.	0.17	0.05	0.05	0.39	0.03	0.07	0.02	0.01	0.03	0.01	0.01	0.09	0.01	0.17	0.03	0.01	0.04	0.07	
Ty-S-GRT-501-G	MEAN	11.48	1.74	2.01	42.63	0.75	0.38	0.77	1.10	5.47	0.20	0.41	1.41	0.03	8.04	0.01	1.25	0.39	21.67	99.75
	S.D.	0.30	0.04	0.04	0.97	0.05	0.07	0.04	0.03	0.14	0.04	0.03	0.02	0.04	1.02	0.02	0.05	0.15	0.19	
Ty-S-GRT-501-R	MEAN	13.84	2.56	2.28	56.28	1.15	0.26	0.99	2.07	8.05	0.18	0.43	1.37	0.01	1.72	0.01	0.39	0.34	7.87	99.81
	S.D.	0.32	0.07	0.08	0.26	0.05	0.04	0.02	0.02	0.09	0.03	0.02	0.05	0.01	0.31	0.03	0.05	0.03	0.27	
Ty-S-GRT-501-T	MEAN	9.14	1.78	1.93	43.81	0.74	0.34	0.79	1.26	5.73	0.20	0.43	1.48	0.04	5.35	0.04	1.27	0.42	24.19	98.92
	S.D.	0.18	0.03	0.03	0.23	0.03	0.07	0.02	0.02	0.08	0.02	0.06	0.07	0.05	0.20	0.05	0.06	0.03	0.52	
Ty-S-MR-502-M	MEAN	10.51	0.36	1.55	57.25	0.11	0.30	0.53	0.46	0.73	0.15	0.75	1.61	0.01	7.63	0.15	0.22	1.12	17.68	101.11
	S.D.	0.26	0.04	0.04	0.90	0.05	0.07	0.04	0.03	0.13	0.03	0.03	0.02	0.02	0.50	0.02	0.05	0.15	0.19	
Ty-S-MR-502-R	MEAN	11.98	0.28	1.01	56.31	0.04	0.41	0.66	0.42	2.07	0.12	0.74	0.79	0.04	7.53	0.05	0.00	0.81	17.24	100.50
	S.D.	0.13	0.01	0.03	0.41	0.01	0.02	0.03	0.03	0.13	0.03	0.02	0.07	0.02	0.10	0.03	0.03	0.05	0.70	
Ty-S-RV-418-R1	MEAN	9.97	0.78	2.76	41.52	0.07	0.17	0.53	0.42	1.48	0.48	0.22	1.59	0.04	3.64	0.03	0.01	0.01	36.20	99.92
	S.D.	0.11	0.04	0.07	0.52	0.03	0.04	0.03	0.01	0.03	0.06	0.01	0.03	0.06	0.12	0.02	0.01	0.02	0.60	

Table III - EPMA results (glassy matrix)

Sample Name		Na_2O	MgO	Al_2O_3	SiO_2	SO_3	P_2O_5	Cl	K_2O	CaO	TiO_2	MnO	FeO	CoO	CuO	As_2O_5	SnO_2	Sb_2O_5	PbO	Total
Ty-S-RV-418-R2	MEAN	9.04	0.72	2.83	39.36	0.07	0.18	0.38	0.42	1.36	0.50	0.19	1.60	0.01	3.21	0.05	0.02	0.02	40.11	100.04
	S.D.	0.15	0.05	0.03	0.49	0.03	0.05	0.02	0.02	0.03	0.05	0.04	0.05	0.01	0.28	0.06	0.03	0.02	0.71	
Ty-S-RV-418-R2s	MEAN	8.92	0.82	3.22	45.07	0.11	0.23	0.43	0.55	1.28	0.57	0.21	1.82	0.02	3.56	0.03	0.00	0.00	34.50	101.34
	S.D.	0.32	0.03	0.04	0.26	0.04	0.04	0.02	0.02	0.05	0.06	0.06	0.14	0.03	0.65	0.03	0.00	0.01	0.32	
Ty-S-RV-418-VO	MEAN	16.54	0.55	1.74	69.36	0.12	0.42	0.79	0.63	5.94	0.08	0.29	0.65	0.01	2.23	0.00	0.19	2.39	0.32	102.26
	S.D.	0.40	0.01	0.11	0.38	0.02	0.02	0.02	0.01	0.06	0.04	0.04	0.08	0.01	0.07	0.00	0.03	0.23	0.03	
Ty-S-TA-005-A	MEAN	17.75	0.75	2.44	67.18	0.09	0.27	1.42	0.51	6.96	0.13	0.05	0.71	0.02	2.24	0.03	0.09	1.21	0.05	101.89
	S.D.	0.16	0.03	0.04	0.41	0.03	0.04	0.09	0.02	0.03	0.04	0.01	0.05	0.02	0.03	0.02	0.02	0.09	0.04	
Ty-S-TA-005-T	MEAN	13.48	0.36	2.03	72.51	0.06	0.29	1.96	0.86	4.98	0.08	0.02	0.28	0.01	0.02	0.01	0.01	0.72	0.01	97.68
	S.D.	0.22	0.03	0.03	0.22	0.03	0.02	0.06	0.01	0.02	0.02	0.03	0.03	0.02	0.03	0.01	0.01	0.02	0.09	
Ty-S-TR-501-R	MEAN	13.86	2.30	2.37	56.97	0.84	0.23	0.96	1.58	8.40	0.15	0.35	1.31	0.02	2.45	0.01	0.42	0.36	8.06	100.63
	S.D.	0.11	0.03	0.03	0.16	0.01	0.04	0.05	0.04	0.02	0.02	0.04	0.01	0.02	0.02	0.01	0.06	0.02	0.31	
Ty-S-TR-501-T	MEAN	12.93	0.35	2.00	72.04	0.05	0.30	1.89	0.75	4.95	0.02	0.00	0.29	0.00	0.00	0.01	0.02	0.75	0.00	96.35
	S.D.	0.61	0.02	0.11	0.30	0.01	0.03	0.09	0.05	0.05	0.03	0.00	0.04	0.00	0.00	0.01	0.03	0.03	0.00	
Ty-S-VA-405-B	MEAN	14.45	0.53	1.97	65.02	0.52	0.12	0.74	0.99	5.34	0.24	0.28	1.46	0.15	0.49	0.01	0.04	6.07	0.15	98.56
	S.D.	0.56	0.03	0.05	0.50	0.03	0.00	0.05	0.01	0.11	0.03	0.02	0.04	0.03	0.05	0.00	0.02	0.38	0.13	
Ty-S-VA-405-V	MEAN	15.22	0.61	1.94	66.78	0.45	0.11	0.71	0.72	6.74	0.11	0.19	0.51	0.00	1.59	0.02	0.10	2.30	0.69	98.80
	S.D.	0.62	0.06	0.39	0.94	0.05	0.03	0.08	0.09	1.03	0.04	0.02	0.03	0.00	0.13	0.00	0.11	0.17	0.31	

Table VI - EPMA reduced compositions (glassy matrix). Reduced chemical compositions normalized at 100% of the glassy matrix in the samples from Tebtynis (excluding weathered samples) calculated from the EPMA analyses reported in table III.

Sample Name	Na_2O	MgO	Al_2O_3	SiO_2	SO_3	P_2O_5	Cl	K_2O	CaO	TiO_2	FeO
Ty-I-B-616	18.80	0.88	2.32	68.69	0.42	0.06	1.16	0.50	5.72	0.28	1.18
Ty-I-BBi-613-Bi	15.38	1.73	2.51	69.52	0.93	0.50	0.45	1.50	6.40	0.14	0.95
Ty-I-BBi-613-BT	17.57	0.64	2.22	69.93	0.04	0.42	1.01	0.88	5.69	0.13	1.48
Ty-I-RAu-605	17.26	0.71	2.98	69.22	0.07	0.71	0.81	0.69	6.29	0.18	1.09
Ty-I-RAu-622	15.63	0.79	2.15	70.16	0.43	0.11	0.82	0.85	7.78	0.12	1.17
Ty-M-A-005	17.89	0.82	2.58	67.89	0.08	0.20	1.58	0.56	7.50	0.14	0.76
Ty-M-A-005a	18.02	1.16	2.42	68.44	0.19	0.50	1.34	0.72	5.68	0.19	1.35
Ty-M-A-006	15.59	0.61	1.06	77.76	0.06	0.36	1.13	0.37	2.35	0.08	0.65
Ty-M-Ar-506	12.98	0.57	2.44	72.28	0.22	0.64	0.63	0.96	7.25	0.11	1.92
Ty-M-Ar-506a	14.47	2.58	4.10	61.32	0.24	0.94	0.80	1.72	10.83	0.42	2.58
Ty-M-B-002	13.71	1.09	2.36	70.47	0.11	0.40	0.87	0.94	7.89	0.06	2.10
Ty-M-B-004	15.00	0.46	2.15	73.50	0.05	0.32	1.34	0.60	5.46	0.06	1.07
Ty-M-BAu-002	14.36	0.51	2.50	71.67	0.12	0.49	0.34	0.80	7.75	0.05	1.41
Ty-M-G-504a	15.15	2.22	3.77	62.08	0.92	0.53	0.98	1.46	9.53	0.35	3.02
Ty-M-G-504b	15.37	2.19	3.83	61.77	0.94	0.49	0.95	1.48	9.63	0.33	3.02
Ty-M-R-501	15.86	2.63	2.45	63.50	0.94	0.39	1.06	1.82	9.64	0.19	1.52
Ty-M-R-502d	17.35	1.39	4.72	68.42	0.08	0.48	0.86	0.83	2.47	0.86	2.55
Ty-M-R-505	15.89	2.60	2.56	63.84	0.31	0.86	1.06	1.81	9.70	0.22	1.15
Ty-M-R-507	15.35	0.78	2.21	70.35	0.16	0.46	0.88	0.83	7.41	0.10	1.47
Ty-M-RAu-502	16.89	1.41	3.14	65.26	0.41	0.57	1.22	1.06	7.81	0.25	1.98
Ty-M-RAu-502a	15.34	0.80	2.25	70.34	0.10	0.52	0.83	0.84	7.46	0.17	1.38
Ty-M-RAu-502b	15.56	0.64	2.00	72.93	0.54	0.13	0.93	0.89	5.67	0.10	0.62
Ty-M-RAu-502c	13.76	0.71	2.67	71.82	0.15	0.33	0.77	1.05	7.27	0.14	1.33
Ty-M-T-503	16.07	2.62	2.27	66.86	0.20	0.92	0.95	1.61	7.01	0.19	1.30
Ty-M-T-503a	15.54	1.73	2.16	69.11	0.24	0.72	0.99	1.67	6.64	0.14	1.06
Ty-M-V-005	12.91	0.62	2.38	72.98	0.09	0.51	0.46	0.83	8.58	0.06	0.59
Ty-M-V-005a	15.66	1.48	2.57	70.05	0.43	0.54	0.56	1.10	6.72	0.15	0.76
Ty-M-V-006	15.52	0.86	2.58	69.97	0.57	0.13	0.45	0.95	8.52	0.11	0.34
Ty-M-V-006a	16.04	0.61	1.06	77.46	0.03	0.36	1.10	0.39	2.32	0.08	0.55
Ty-P-A-402-B	14.59	0.51	2.75	71.16	0.42	0.07	0.34	0.90	7.73	0.06	1.48
Ty-P-A-408-Ar	15.36	2.10	3.55	62.48	0.42	0.85	0.78	1.44	9.73	0.37	2.92
Ty-P-A-408-B	17.14	0.66	2.03	71.06	0.41	0.09	1.28	0.74	5.04	0.15	1.40
Ty-P-A-418-Bi	16.74	2.67	2.75	66.83	0.06	0.31	1.01	0.73	8.16	0.13	0.62
Ty-P-A-418-BO	15.41	0.63	2.62	71.10	0.20	0.25	0.97	0.76	6.77	0.13	1.15
Ty-P-A-418-R1	15.16	3.18	2.77	62.98	1.52	0.19	1.17	2.11	8.87	0.19	1.86
Ty-P-A-418-R2	15.46	3.27	2.83	62.46	1.48	0.22	1.16	2.26	8.84	0.20	1.83
Ty-P-A-419-Bi	13.00	0.69	2.91	76.05	0.05	0.30	0.54	1.10	4.42	0.12	0.82
Ty-P-A-419-BT	14.88	0.71	2.10	72.86	0.19	0.20	1.16	1.12	5.04	0.16	1.59
Ty-P-A-419-R	13.20	3.59	2.01	64.37	1.71	0.17	0.88	3.19	7.88	0.13	2.87
Ty-P-CR-421-A	16.41	0.47	2.17	72.40	0.08	0.33	1.83	0.49	5.15	0.14	0.55
Ty-P-CR-421-B	15.69	0.71	2.74	70.82	0.13	0.24	1.08	0.72	6.47	0.13	1.27
Ty-P-CR-421-BT	14.57	0.50	2.21	73.05	0.06	0.34	1.42	1.09	5.59	0.11	1.05
Ty-P-CR-421-G1	14.40	1.15	2.13	72.56	0.28	0.28	1.03	0.67	5.35	0.10	2.06
Ty-P-CR-421-G2	14.72	0.55	2.52	73.58	0.08	0.19	0.80	0.77	2.99	0.16	3.64
Ty-P-CR-421-R	15.43	3.08	2.72	63.08	1.22	0.26	1.10	2.17	9.15	0.19	1.61
Ty-P-FL-004-Bi	16.58	5.05	1.97	67.88	0.04	0.24	0.87	0.69	6.27	0.07	0.34

Table IV - EPMA reduced compositions (glassy matrix)

Sample Name	Na_2O	MgO	Al_2O_3	SiO_2	SO_3	P_2O_5	Cl	K_2O	CaO	TiO_2	FeO
Ty-P-FL-004-BO	16.49	0.72	2.81	69.71	0.10	0.19	1.22	0.86	5.29	0.20	2.39
Ty-P-FL-004-R	16.34	2.63	2.54	63.49	0.94	0.25	1.05	1.65	9.44	0.22	1.44
Ty-P-FL-501-Bi	13.68	0.55	2.59	76.04	0.04	0.51	0.69	1.30	3.76	0.15	0.68
Ty-P-FL-501-BT	14.54	2.56	1.92	68.49	1.25	0.16	1.02	1.99	6.40	0.20	1.48
Ty-P-FL-501-G	14.80	0.87	2.44	73.74	0.25	0.43	0.79	1.10	4.00	0.15	1.43
Ty-P-FL-501-R	14.53	2.75	3.17	62.34	1.22	0.30	0.98	1.61	10.57	0.35	2.20
Ty-P-FR-422-B	16.19	0.61	2.31	72.15	0.06	0.36	1.44	0.73	4.68	0.12	1.34
Ty-P-FR-422-Bi	16.82	5.18	2.01	67.58	0.05	0.28	0.87	0.59	6.22	0.06	0.34
Ty-P-FR-422-G1	16.23	0.58	2.33	71.11	0.09	0.25	1.23	0.60	6.02	0.11	1.46
Ty-P-FR-422-G2	15.87	0.73	2.58	71.44	0.11	0.25	1.20	0.73	4.75	0.15	2.18
Ty-P-FR-422-R	16.59	2.63	2.61	63.21	0.91	0.27	1.11	1.65	9.39	0.20	1.44
Ty-P-FR-422-T	16.14	0.52	2.24	71.88	0.04	0.32	1.42	0.74	5.58	0.09	1.02
Ty-Pn-T-001	18.34	0.94	2.40	68.46	0.32	0.23	1.07	1.00	6.22	0.16	0.86
Ty-P-R-414-B	17.16	0.74	2.88	68.79	0.12	0.24	1.19	0.88	5.25	0.22	2.53
Ty-P-R-414-G	15.93	0.46	2.18	72.81	0.03	0.23	1.29	0.61	4.80	0.10	1.55
Ty-P-R-414-T	16.92	0.52	2.08	70.53	0.04	0.31	1.33	0.66	7.15	0.08	0.37
Ty-P-R-419-Ar	15.09	2.47	4.10	61.75	0.92	0.32	0.64	1.53	10.30	0.33	2.56
Ty-P-R-419-BO	17.40	0.72	2.91	68.12	0.10	0.25	1.26	0.95	5.48	0.19	2.62
Ty-P-R-419-BT	17.64	0.48	2.20	70.55	0.06	0.29	1.46	0.67	5.52	0.09	1.05
Ty-P-R-419-R	15.63	2.55	4.14	61.42	0.89	0.33	0.67	1.47	9.96	0.34	2.59
Ty-P-R-419-VT	16.77	2.43	4.02	61.16	0.84	0.35	0.62	1.03	10.00	0.34	2.44
Ty-P-R-423-Ar	15.51	2.17	3.76	61.67	0.90	0.78	0.95	1.47	9.43	0.33	3.03
Ty-P-R-423-B	16.81	0.69	2.68	69.19	0.12	0.24	1.20	1.18	5.25	0.20	2.46
Ty-P-R-423-G	15.03	0.40	2.02	73.99	0.06	0.28	1.44	0.59	4.73	0.08	1.38
Ty-P-R-423-R	16.16	2.08	3.71	61.12	0.83	0.56	0.89	1.60	9.44	0.40	3.20
Ty-P-R-423-T	17.16	0.95	2.63	66.12	0.11	0.18	1.55	0.57	9.29	0.15	1.29
Ty-P-R-423-VT	16.88	4.11	2.40	61.41	1.71	0.33	1.13	2.08	8.36	0.21	1.37
Ty-P-St-415-B	15.64	0.66	1.87	73.33	0.05	0.30	1.35	0.72	3.89	0.18	2.01
Ty-P-St-415-Bi	12.54	0.57	2.72	77.17	0.08	0.30	0.68	1.02	3.98	0.16	0.79
Ty-P-StB-002	13.95	0.94	2.65	70.15	0.20	0.45	0.49	0.95	7.78	0.09	2.35
Ty-P-T-417-Bi	15.52	0.65	2.58	72.86	0.08	0.28	0.85	1.84	4.64	0.11	0.59
Ty-P-T-417-BO	16.24	0.79	2.40	70.96	0.11	0.46	0.97	1.10	5.86	0.10	1.02
Ty-P-T-417-R	17.70	2.02	3.23	62.94	0.63	0.27	1.26	1.07	8.85	0.27	1.77
Ty-P-T-417-VT	17.00	4.64	1.02	61.07	1.74	0.24	0.97	1.83	10.05	0.05	1.38
Ty-S-423a-A	14.78	0.45	1.97	74.20	0.43	0.06	1.69	0.93	5.11	0.05	0.33
Ty-S-423a-Bi	16.52	5.06	1.88	68.03	0.33	0.03	0.82	0.61	6.33	0.07	0.32
Ty-S-423a-R	16.27	3.14	2.24	63.28	0.27	1.13	1.05	2.06	9.09	0.17	1.31
Ty-S-423a-T	15.64	0.49	2.14	72.64	0.40	0.04	1.40	0.85	5.44	0.09	0.87
Ty-S-ARG-403-A	16.37	0.50	2.32	72.65	0.07	0.32	1.64	0.52	4.97	0.08	0.55
Ty-S-ARG-403-G	12.64	0.57	2.27	74.75	0.06	0.32	1.27	0.52	6.20	0.08	1.32
Ty-S-ArG-506-Ar	16.94	2.14	3.08	62.49	0.80	0.49	1.70	1.40	8.06	0.35	2.55
Ty-S-ArG-506-G	16.84	2.74	2.98	61.97	1.14	0.60	1.14	1.63	8.37	0.28	2.31
Ty-Sb-B-003	13.44	0.67	2.15	72.96	0.23	0.09	0.81	0.67	8.57	0.08	0.33
Ty-S-BB-004-BO	16.05	0.71	2.69	70.14	0.10	0.20	1.23	0.90	5.38	0.19	2.41
Ty-S-BB-004-BT	14.19	0.55	2.22	72.75	0.06	0.37	1.74	0.69	6.33	0.08	1.03
Ty-S-BBi-004-Bi	15.13	0.63	1.74	75.53	0.08	0.33	0.94	0.75	4.03	0.20	0.63
Ty-S-BBi-004-BT	16.84	0.55	1.64	72.70	0.02	0.26	1.35	0.42	4.37	0.16	1.69
Ty-S-BBi-004-BTc	18.21	0.80	1.82	70.41	0.05	0.39	1.20	0.60	4.88	0.16	1.48
Ty-S-BBi-004-BTs	16.07	0.50	1.67	73.47	0.04	0.17	1.43	0.39	4.28	0.12	1.86
Ty-S-BiBR-404-Bi	17.11	5.09	2.00	67.29	0.04	0.28	0.85	0.56	6.30	0.09	0.39

Table IV - EPMA reduced compositions (glassy matrix)

Sample Name	Na_2O	MgO	Al_2O_3	SiO_2	SO_3	P_2O_5	Cl	K_2O	CaO	TiO_2	FeO
Ty-S-BiBR-404-BO	17.61	0.72	2.80	68.42	0.11	0.24	1.23	0.89	5.25	0.22	2.51
Ty-S-BiBR-404-R	16.42	2.63	2.60	63.17	0.91	0.24	1.08	1.79	9.33	0.21	1.62
Ty-S-BiBR-507-Bi	16.69	5.06	1.97	67.85	0.04	0.27	0.86	0.53	6.29	0.05	0.39
Ty-S-BiBR-507-R	16.25	3.26	2.40	62.37	1.26	0.20	1.22	1.96	9.07	0.21	1.80
Ty-S-BiBR-507-VT	16.01	3.42	2.17	62.43	1.26	0.17	1.11	1.94	9.51	0.20	1.78
Ty-S-BiR-507-Bi	9.79	0.80	2.50	75.80	0.06	0.50	1.88	0.85	6.93	0.14	0.74
Ty-S-BiR-507-R	15.29	2.90	2.64	63.40	1.26	0.26	1.11	2.29	9.07	0.20	1.58
Ty-S-BT-004-BO	16.80	0.58	2.52	71.80	0.03	0.30	1.27	0.60	4.36	0.16	1.59
Ty-S-BT-004-BT	14.67	0.55	2.37	72.23	0.07	0.37	1.66	0.67	6.24	0.09	1.08
Ty-S-BT-004-T	9.60	0.40	2.18	78.56	0.05	0.31	1.96	1.30	5.32	0.06	0.26
Ty-S-BTW-004-Bi	14.35	0.91	2.46	73.86	0.23	0.36	0.84	0.79	4.95	0.23	1.02
Ty-S-BTW-004-BT	14.90	0.67	1.98	74.36	0.06	0.29	1.62	0.88	3.41	0.26	1.57
Ty-S-GA-005-A	16.71	0.44	1.91	73.39	0.04	0.19	1.30	0.38	4.69	0.07	0.89
Ty-S-GA-005-Ar	17.43	2.66	3.07	62.17	1.03	0.38	1.14	1.63	7.99	0.23	2.26
Ty-S-GA-005-ArC	17.20	2.11	3.19	62.35	0.74	0.37	1.80	1.37	7.98	0.34	2.55
Ty-S-GA-005-ArS	16.81	2.73	3.88	59.90	0.88	0.29	1.03	1.12	10.52	0.38	2.45
Ty-S-GA-411-A	15.06	0.61	2.56	70.76	0.21	0.23	0.86	0.66	8.17	0.07	0.81
Ty-S-GA-411-G	15.19	0.57	2.24	72.11	0.06	0.29	1.25	0.60	6.28	0.15	1.25
Ty-S-GB-413-Ar	16.02	2.22	3.99	60.92	0.90	0.44	0.97	1.45	9.56	0.29	3.25
Ty-S-GB-413-BO	16.02	0.82	3.04	71.87	0.03	0.17	1.52	0.69	3.55	0.26	2.02
Ty-S-GR-506-Ar	15.64	2.22	3.89	61.43	0.92	0.43	0.98	1.44	9.39	0.31	3.34
Ty-S-GR-506-R	17.11	1.60	2.88	64.46	0.68	0.57	1.28	1.52	7.66	0.25	1.99
Ty-S-GRT-501-Ar	16.89	2.56	2.96	62.74	1.11	0.56	1.14	1.61	8.05	0.29	2.08
Ty-S-GRT-501-R	15.54	2.88	2.56	63.21	1.30	0.30	1.11	2.32	9.04	0.20	1.54
Ty-S-GRT-501-T	13.60	2.65	2.88	65.20	1.10	0.50	1.18	1.87	8.53	0.29	2.20
Ty-S-MR-502-M	14.29	0.49	2.10	77.84	0.14	0.40	0.73	0.62	0.99	0.20	2.19
Ty-S-MR-502-R	16.17	0.37	1.36	75.99	0.06	0.56	0.90	0.56	2.79	0.17	1.07
Ty-S-RV-418-R1	16.68	1.31	4.62	69.46	0.11	0.29	0.89	0.71	2.47	0.81	2.66
Ty-S-RV-418-R2	16.02	1.28	5.01	69.73	0.12	0.31	0.68	0.74	2.40	0.88	2.83
Ty-S-RV-418-R2s	14.15	1.31	5.10	71.53	0.17	0.37	0.68	0.88	2.03	0.90	2.88
Ty-S-RV-418-VO	17.08	0.57	1.80	71.64	0.13	0.43	0.81	0.65	6.14	0.08	0.67
Ty-S-TA-005-A	18.07	0.76	2.49	68.40	0.10	0.27	1.44	0.52	7.09	0.13	0.73
Ty-S-TA-005-T	13.91	0.38	2.10	74.84	0.06	0.30	2.02	0.88	5.14	0.08	0.29
Ty-S-TR-501-R	15.58	2.58	2.66	64.04	0.94	0.26	1.08	1.78	9.44	0.17	1.47
Ty-S-TR-501-T	13.53	0.37	2.09	75.39	0.05	0.31	1.98	0.78	5.18	0.02	0.30
Ty-S-VA-405-B	15.82	0.58	2.15	71.17	0.57	0.13	0.81	1.08	5.84	0.26	1.60
Ty-S-VA-405-V	16.21	0.64	2.07	71.13	0.48	0.11	0.76	0.77	7.18	0.12	0.54

Table V - EPMA results (inclusions). Chemical composition determined by EPMA in oxide weight % on a selection of crystalline inclusions in the opaque samples from Tebtynis, divided per color-classes. Given the small dimensions of the considered crystals, only 1 point analysis was performed for each inclusion, using a spot size of 1 µm in order to minimizing the contamnation from the glassy matrix.

Sample name	Glass color	Na_2O	MgO	Al_2O_3	SiO_2	SO_3	P_2O_5	Cl	K_2O	CaO	TiO_2	MnO	FeO	CoO	CuO	As_2O_5	SnO_2	Sb_2O_5	PbO	Total
Ty-S-423a-Bi	white	0.11	0.00	0.00	0.41	0.02	0.00	0.02	0.00	13.59	0.04	0.03	0.06	0.00	0.00	0.24	0.37	82.50	0.00	97.42
Ty-P-St-415-Bi	white	0.13	0.00	0.04	0.96	0.00	0.03	0.02	0.08	14.01	0.00	0.04	0.01	0.01	0.00	0.31	0.43	83.59	0.00	99.65
Ty-P-FL-501-Bi	white	0.04	0.00	0.00	0.43	0.00	0.03	0.02	0.03	13.86	0.00	0.00	0.09	0.00	0.10	0.83	0.41	83.53	0.01	101.76
Ty-S-BiR-507-Bi	white	18.50	0.02	0.04	0.14	0.00	0.07	0.00	0.01	0.00	0.00	0.00	0.00	0.00	0.04	0.28	0.34	82.66	0.00	102.10
Ty-P-T-417-Bi	white	0.97	0.05	0.33	2.89	0.00	0.02	0.02	0.09	13.71	0.04	0.03	0.02	0.04	0.05	0.30	0.43	79.66	0.07	98.71
Ty-S-BBi-004-Bi	white	11.23	0.35	0.26	6.47	0.00	0.00	0.17	0.07	4.16	0.00	0.19	0.14	0.01	0.01	0.28	0.42	77.45	0.19	101.40
Ty-S-BiBR-507-Bi	white	0.79	0.67	0.06	2.19	0.00	0.00	0.06	0.01	23.53	0.01	0.03	0.07	0.01	0.00	0.03	0.19	71.23	0.00	98.87
Ty-P-FR-422-Bi	white	0.88	0.54	0.10	2.10	0.00	0.02	0.04	0.01	23.63	0.03	0.04	0.05	0.00	0.00	0.49	0.34	70.40	0.10	101.32
Ty-P-FL-004-Bi	white	0.95	0.26	0.07	2.59	0.00	0.04	0.02	0.00	23.96	0.00	0.00	0.10	0.00	0.06	0.43	0.34	69.94	0.00	100.52
Ty-I-BBi-613-Bi	white	0.88	0.05	0.00	1.72	0.00	0.00	0.02	0.05	23.15	0.25	0.40	0.02	0.05	0.00	0.36	0.73	69.35	2.82	99.85
Ty-S-BiBR-404-Bi	white	1.41	0.30	0.02	2.27	0.00	0.36	0.35	0.07	21.30	0.00	0.01	0.08	0.05	0.00	0.25	0.38	67.74	0.00	94.60
Ty-P-CR-421-Bi	white	5.88	0.15	0.55	18.94	0.00	0.18	0.22	0.13	9.24	0.08	0.04	0.15	0.05	0.15	0.32	0.40	59.83	0.25	100.18
Ty-P-A-418-Bi	white	1.29	1.27	0.64	18.82	0.00	0.14	0.30	0.18	18.32	0.08	0.03	0.27	0.00	0.00	0.18	0.26	48.79	0.16	90.72
Ty-P-FL-004-B	dark blue	6.57	0.09	0.19	1.33	0.00	0.08	0.17	0.03	7.00	0.00	0.08	3.17	0.00	0.06	0.62	0.40	80.39	0.00	94.26
Ty-M-B-002	dark blue	6.74	0.11	0.03	1.36	0.00	0.03	0.01	0.01	14.33	0.00	0.04	0.07	0.07	0.08	0.26	0.23	43.82	1.88	96.55
Ty-P-FR-422-B	dark blue	0.91	0.01	0.10	3.98	0.00	0.07	0.11	0.06	13.44	0.00	0.04	0.10	0.05	0.02	0.45	0.30	78.93	0.16	100.88
Ty-S-BB-004-BO	dark blue	9.16	0.19	0.24	0.62	0.00	0.06	0.05	0.02	4.38	0.00	0.08	0.49	0.00	0.58	0.49	0.37	85.26	0.04	99.74
Ty-P-CR-421-B	dark blue	0.06	0.03	0.00	0.21	0.00	0.00	0.02	0.00	14.23	0.04	0.10	0.00	0.00	0.03	0.43	0.40	83.79	0.00	92.22
Ty-M-B-002	dark blue	0.29	0.08	0.03	1.42	0.00	0.01	0.03	0.03	23.31	0.00	0.19	0.17	0.00	0.00	0.34	0.39	69.62	2.56	100.81
Ty-P-R-423-B	dark blue	0.36	0.00	0.02	0.42	0.00	0.00	0.03	0.03	14.04	0.17	0.03	0.22	0.03	0.00	0.41	0.33	84.17	0.00	100.26
Ty-S-VA-405-B	dark blue	0.40	0.03	0.00	1.41	0.06	0.00	0.05	0.04	24.23	0.00	0.02	0.20	0.00	0.10	0.33	0.35	69.44	0.00	96.67
Ty-I-B-616	dark blue	0.13	0.00	0.00	0.53	0.00	0.00	0.04	0.00	13.78	0.00	0.00	0.18	0.12	0.11	0.39	0.43	81.32	0.00	97.02
Ty-P-A-408-B	dark blue	0.25	0.01	0.00	0.22	0.02	0.00	0.00	0.03	14.05	0.06	0.12	0.07	0.02	0.00	0.35	0.40	84.12	0.00	99.74
Ty-P-A-418-BO	dark blue	0.22	0.15	0.00	0.74	0.00	0.01	0.01	0.00	22.14	0.12	0.72	1.49	1.30	0.20	0.29	0.29	70.96	0.07	98.70
Ty-S-GB-413-BO	dark blue	17.05	0.00	0.01	1.02	0.00	0.07	0.05	0.04	0.00	0.05	0.00	0.16	0.03	0.06	0.33	0.38	83.76	0.07	103.07
Ty-P-T-417-BO	dark blue	1.18	0.08	0.05	3.13	0.00	0.06	0.05	0.03	22.95	0.24	0.48	0.30	0.08	0.05	0.26	0.90	67.64	2.19	99.66
Ty-S-BT-004-BO	dark blue	7.93	0.14	0.33	8.26	0.00	0.16	0.18	0.10	8.25	0.06	0.04	0.47	0.03	0.06	0.26	0.39	72.20	0.15	99.00
Ty-P-R-419-BO	dark blue	0.13	0.04	0.00	0.46	0.00	0.03	0.04	0.04	14.01	0.00	0.03	0.24	0.00	0.14	0.28	0.40	83.94	0.10	99.88
Ty-P-StB-002	dark blue	0.22	0.07	0.00	0.41	0.00	0.08	0.01	0.02	24.44	0.05	0.58	0.28	0.01	0.10	0.22	0.33	72.55	0.36	99.75
Ty-P-R-414-B	dark blue	1.91	0.03	0.01	2.15	0.00	0.00	0.06	0.04	19.41	0.40	0.16	5.39	0.46	0.05	0.20	0.42	67.15	0.07	97.92
Ty-P-St-415-B	dark blue	9.53	0.33	0.59	19.06	0.00	0.14	0.40	0.47	0.44	0.05	0.06	0.44	0.17	0.00	0.17	0.31	63.78	0.21	96.14
Ty-M-BAu-002	dark blue	0.13	0.01	0.02	0.87	0.00	0.01	0.01	0.03	24.47	0.03	0.35	0.23	0.18	0.19	0.18	0.36	71.35	0.00	98.42
Ty-S-BiBR-404-BO	dark blue	0.07	0.02	0.01	0.56	0.00	0.05	0.04	0.01	13.90	0.00	0.02	0.27	0.02	0.08	0.18	0.39	83.31	0.00	98.94
Ty-P-CR-421	light blue	9.27	0.24	0.15	3.05	0.00	0.14	0.22	0.03	8.55	0.04	0.06	0.06	0.00	0.58	1.18	0.33	74.31	0.11	101.34
Ty-M-A-005	light blue	10.36	0.41	0.07	3.52	0.00	1.34	1.08	0.09	8.84	0.02	0.01	0.07	0.01	0.18	0.89	0.35	71.66	0.07	98.96
Ty-S-423a-A	light blue	8.25	0.19	0.10	2.74	0.09	0.00	0.09	0.03	5.85	0.00	0.00	0.02	0.00	0.78	0.44	0.36	80.64	0.04	99.67
Ty-S-GA-411-A	light blue	0.29	0.07	0.05	2.40	0.00	0.03	0.05	0.05	22.16	0.00	0.11	0.18	0.03	0.01	0.28	0.25	66.58	0.11	92.66
Ty-S-GA-005-A	light blue	0.31	0.00	0.05	1.23	0.00	0.03	0.06	0.02	13.67	0.00	0.00	0.05	0.04	0.58	0.33	0.42	81.78	0.00	98.57
Ty-M-A-005a	light blue	0.13	0.00	0.01	0.32	0.00	0.06	0.02	0.01	13.76	0.00	0.04	0.11	0.00	0.45	0.32	0.38	83.35	0.18	99.14
Ty-S-ARG-403	light blue	12.73	0.12	0.25	8.44	0.00	0.17	0.30	0.10	3.13	0.00	0.04	0.11	0.00	0.81	0.26	0.43	72.35	0.12	99.35

Table V - EPMA results (inclusions)

Sample name	Glass color	Na_2O	MgO	Al_2O_3	SiO_2	SO_3	P_2O_5	Cl	K_2O	CaO	TiO_2	MnO	FeO	CoO	CuO	As_2O_5	SnO_2	Sb_2O_5	PbO	Total
Ty-M-V-006	turquoise	0.41	0.01	0.00	0.62	0.23	0.00	0.01	0.00	14.16	0.01	0.00	0.00	0.05	0.33	0.40	0.36	83.74	0.00	100.36
Ty-S-VA-405-V	turquoise	1.07	0.00	0.04	0.60	0.05	0.00	0.03	0.04	12.59	0.00	0.07	0.02	0.00	0.17	0.48	0.39	84.12	0.05	99.76
Ty-S-RV-418-VO	turquoise	0.22	0.03	0.00	0.77	0.00	0.07	0.04	0.01	14.17	0.06	0.04	0.03	0.00	0.37	0.30	0.41	84.06	0.10	100.69
Ty-M-V-006a	turquoise	9.73	0.12	0.07	6.19	0.00	0.42	0.45	0.06	8.13	0.00	0.13	0.22	0.00	0.37	0.31	0.42	67.73	3.12	97.47
Ty-M-V-005	turquoise	0.93	0.16	0.17	4.74	0.00	0.10	0.03	0.03	21.20	0.06	0.39	0.10	0.00	0.52	0.32	0.48	66.96	3.60	99.79
Ty-M-V-005a	turquoise	1.11	0.28	0.19	6.94	0.00	0.06	0.05	0.12	21.06	0.07	0.86	0.16	0.00	1.97	0.29	1.12	63.73	1.77	99.77
Ty-M-A-006	turquoise	7.80	0.15	0.01	3.73	0.00	0.84	0.39	0.07	8.45	0.00	0.07	0.08	0.02	0.09	0.39	0.27	71.64	3.21	99.34
Ty-P-FL-501-G	yellow	1.79	0.00	0.00	0.35	0.00	0.00	0.03	0.04	12.28	0.02	0.08	0.16	0.00	0.14	0.53	0.34	83.51	0.09	101.35
Ty-P-FL-501-G	yellow	0.41	0.01	0.11	3.15	0.00	0.00	0.03	0.03	1.91	0.32	0.03	1.16	0.05	0.17	0.05	17.02	25.05	44.76	102.01
Ty-P-R-423-G	yellow	1.28	0.03	0.37	11.09	0.00	0.05	0.23	0.05	1.07	0.24	0.01	2.94	0.00	0.09	0.02	6.13	26.25	46.90	96.76
Ty-P-CR-421-G	yellow	0.81	0.03	0.17	3.24	0.00	0.00	0.06	0.01	2.08	0.31	0.18	3.46	0.00	0.37	0.18	3.11	33.82	45.81	98.46
Ty-P-R-414-G	yellow	1.22	0.00	0.12	4.39	0.00	0.05	0.11	0.04	1.63	0.31	0.00	3.55	0.06	0.00	0.09	2.51	32.41	49.18	95.67
Ty-P-R-419-G	yellow	0.68	0.00	0.15	4.04	0.00	0.10	0.11	0.06	0.84	0.29	0.04	4.44	0.00	0.00	0.05	2.16	31.86	52.87	97.69
Ty-P-FR-422-G1	yellow	0.65	0.00	0.03	1.31	0.00	0.00	0.04	0.01	2.91	0.60	0.10	3.74	0.06	0.00	0.16	1.71	37.25	44.77	102.42
Ty-P-FR-422-G2	yellow	0.72	0.00	0.06	2.45	0.00	0.02	0.03	0.02	0.88	0.39	0.03	4.68	0.09	0.00	0.18	0.22	33.87	48.56	100.62
Ty-P-A-402-G	yellow	0.63	0.00	0.06	3.00	0.29	0.00	0.03	0.01	0.85	0.54	0.00	4.34	0.08	0.00	0.14	0.13	31.30	53.97	95.44
Ty-S-GA-411-G	yellow	0.36	0.00	0.09	3.33	0.00	0.00	0.03	0.01	0.47	0.26	0.05	4.83	0.01	0.00	0.00	0.12	32.73	54.60	96.90
Ty-S-ARG-403	yellow	7.71	0.24	1.17	37.47	0.00	0.17	0.64	0.28	3.29	0.20	0.07	2.87	0.03	0.16	0.04	0.11	17.24	29.70	101.39
Ty-M-Ar-506	yellowish-orange	1.70	0.05	0.29	2.78	0.00	0.15	0.13	0.04	15.33	0.14	0.00	0.24	0.00	2.14	0.19	0.24	40.48	13.81	77.71
Ty-S-GA-005	yellowish-orange	0.01	0.00	0.00	0.12	0.00	0.01	0.00	0.00	0.19	0.00	0.00	0.06	0.00	0.67	0.00	99.24	0.00	0.12	100.42

Table VI - OBIA Tables. Summary of the results on the image analysis of the opaque white samples (a), dark blue samples (b), light blue samples (c), turquoise samples (d), yellow samples (e), one Ca-antimoniate opacified yellowish orange sample (f), sealing-wax red samples (g) and zoned sealing-wax red samples (h).

(a)

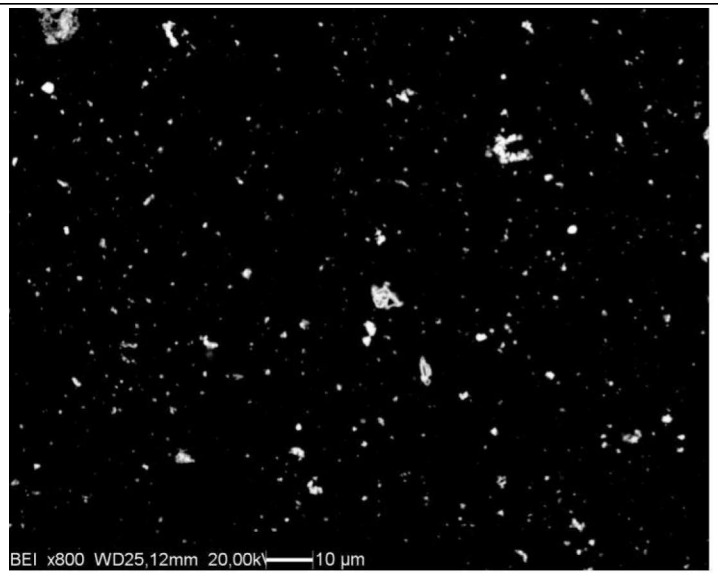

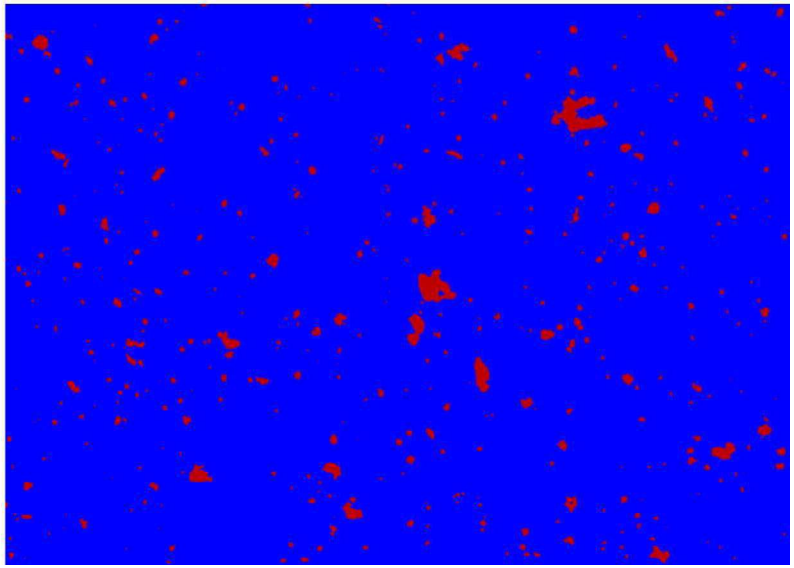

Sample name	Glassy matrix (area %)	Inclusions (area %)	Inclusions (nr. image-objects)	Average crystal area (µm^2)	Average crystal length (µm)
Ty-S-BiBR-404 (area 1)	95.22	4.78	975.00	0.87	1.01
Ty-S-BiBR-404 (area 2)	93.28	6.72	898.00	1.29	1.16
Ty-S-BiBR-404 (area 3)	95.91	4.09	1925.00	1.40	1.27
Ty-S-BiBR-404 (area 4)	97.01	2.99	486.00	0.95	1.09
MEAN	**95.36**	**4.64**	**1071.00**	**1.13**	**1.13**
S.D.	**1.57**	**1.57**	**608.46**	**0.26**	**0.11**
Ty-P-A-419 (area 1)	94.85	5.15	366.00	2.39	1.96
Ty-P-A-419 (area 2)	93.72	6.28	629.00	3.23	2.32
Ty-P-A-419 (area 3)	94.54	5.46	389.00	2.46	2.04
MEAN	**94.37**	**5.63**	**461.33**	**2.69**	**2.11**
S.D.	**0.58**	**0.58**	**145.66**	**0.47**	**0.19**
Ty-P-FL-501 (area 1)	95.60	4.40	268.00	0.67	1.04
Ty-P-FL-501 (area 2)	93.28	6.72	420.00	1.06	1.24
Ty-P-FL-501 (area 3)	95.32	4.68	258.00	0.80	1.11
MEAN	**94.73**	**5.27**	**315.33**	**0.84**	**1.13**
S.D.	**1.27**	**1.27**	**90.78**	**0.20**	**0.11**
white glasses MEAN	**94.82**	**5.18**	**615.89**	**1.55**	**1.46**

(b)

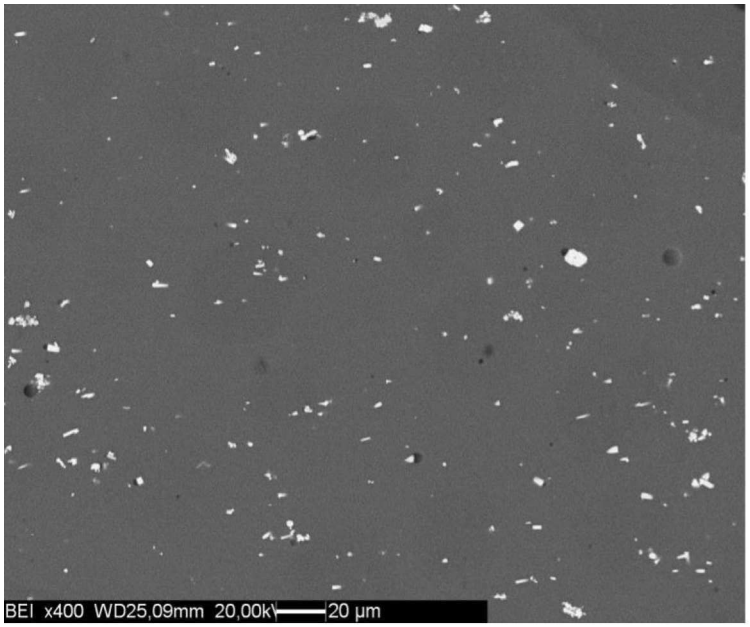

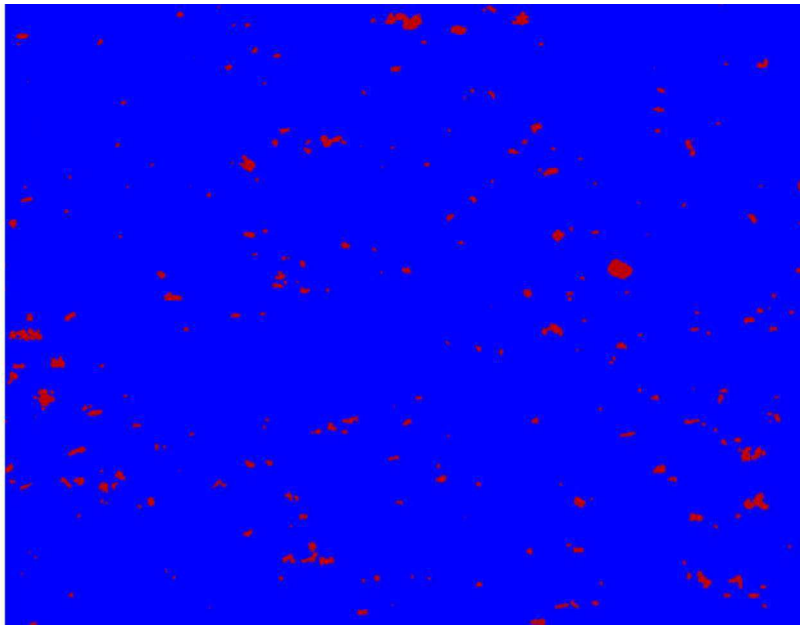

Sample name	Glassy matrix (area %)	Inclusions (area %)	Inclusions (nr. image-objects)	Average crystal area (µm^2)	Average crystal length (µm)
Ty-I-B-616 (area 1)	98.26	1.74	263.00	5.20	3.02
Ty-I-B-616 (area 2)	97.14	2.86	97.00	5.35	2.95
Ty-I-B-616 (area 3)	97.77	2.23	78.00	5.19	3.16
MEAN	**97.72**	**2.28**	**146.00**	**5.25**	**3.05**
S.D.	**0.56**	**0.56**	**101.77**	**0.09**	**0.10**
Ty-P-StB-002 (area 1)	97.64	2.36	2678.00	1.36	1.39
Ty-P-StB-002 (area 2)	97.80	2.20	187.00	1.25	1.16
Ty-P-StB-002 (area 3)	96.97	3.03	1815.00	1.18	1.28
MEAN	**97.47**	**2.53**	**1560.00**	**1.26**	**1.28**
S.D.	**0.44**	**0.44**	**1264.93**	**0.09**	**0.11**
Ty-P-R-419 (area 1)	97.91	2.09	217.00	2.72	1.96
Ty-P-R-419 (area 2)	98.09	1.91	362.00	2.89	2.02
Ty-P-R-419 (area 3)	96.96	3.04	85.00	4.51	1.87
MEAN	**97.65**	**2.35**	**221.33**	**3.38**	**1.95**
S.D.	**0.61**	**0.61**	**138.55**	**0.99**	**0.08**
dark blue glasses MEAN	**97.62**	**2.38**	**642.44**	**3.30**	**2.09**

(c)

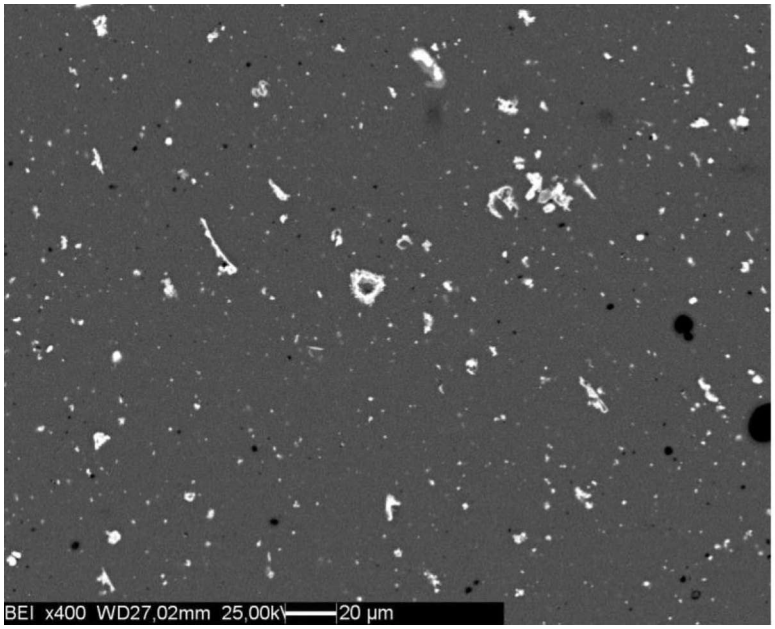

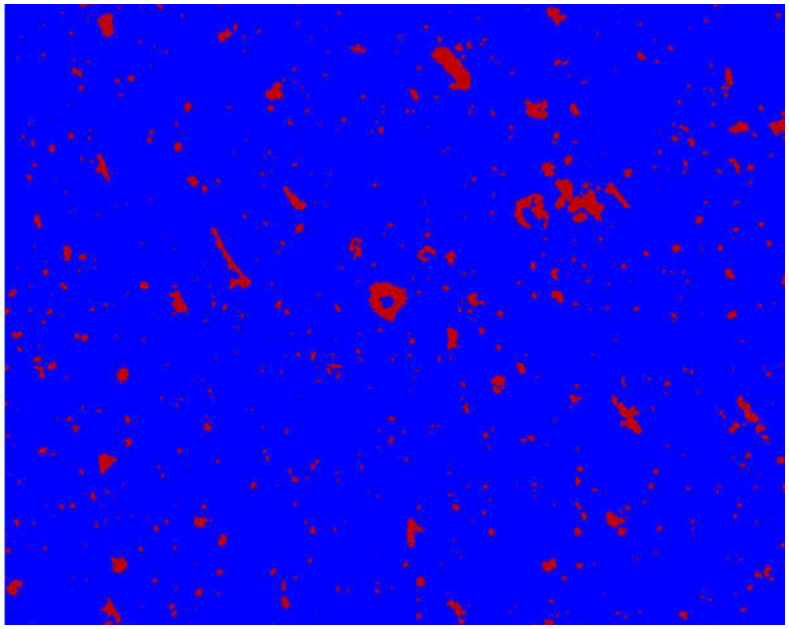

Sample name	Glassy matrix (area %)	Inclusions (area %)	Inclusions (nr. image-objects)	Average crystal area (µm^2)	Average crystal length (µm)
Ty-M-A-005 (area 1)	95.37	4.63	1462.00	7.36	3.16
Ty-M-A-005 (area 2)	95.83	4.17	1071.00	2.59	1.69
Ty-M-A-005 (area 3)	94.20	5.80	927.00	9.00	3.40
MEAN	**95.13**	**4.87**	**1153.33**	**6.32**	**2.75**
S.D.	**0.84**	**0.84**	**276.84**	**3.33**	**0.93**
Ty-S-TA-005 (area 1)	96.45	3.55	2337.00	8.66	3.51
Ty-S-TA-005 (area 2)	95.46	4.54	2463.00	5.81	2.49
Ty-S-TA-005 (area 3)	96.04	3.96	764.00	3.89	2.17
MEAN	**95.98**	**4.02**	**1854.67**	**6.12**	**2.72**
S.D.	**0.50**	**0.50**	**946.64**	**2.40**	**0.70**
Ty-M-A-005a (area 1)	96.59	3.41	206.00	2.76	2.02
Ty-M-A-005a (area 2)	96.92	3.08	216.00	1.83	1.70
Ty-M-A-005a (area 3)	96.43	3.57	609.00	2.23	1.79
MEAN	**96.65**	**3.35**	**343.67**	**2.27**	**1.84**
S.D.	**0.25**	**0.25**	**229.84**	**0.47**	**0.16**
light blue glasses MEAN	**95.92**	**4.08**	**1117.22**	**4.90**	**2.44**

(d)

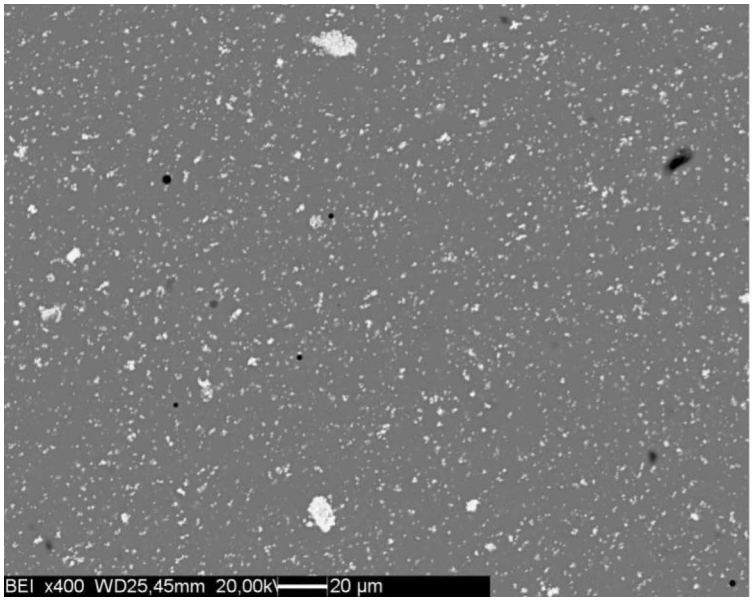

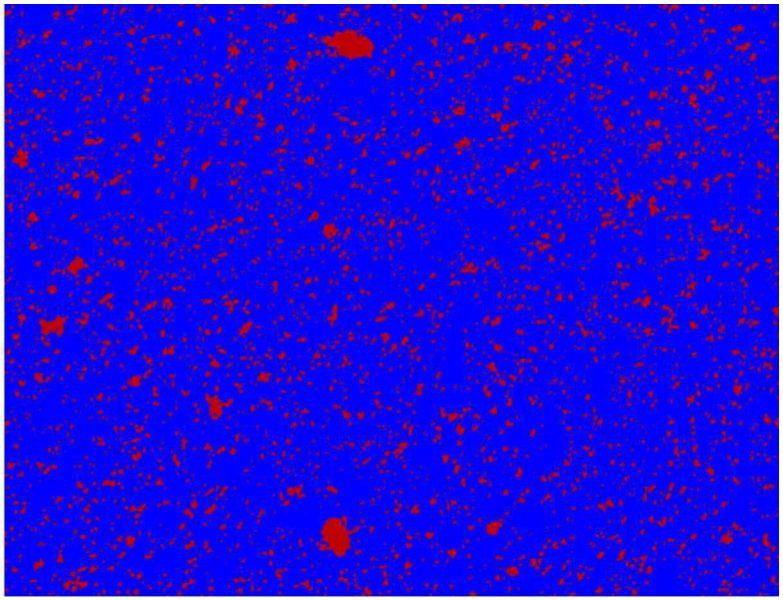

Sample name	Glassy matrix (area %)	Inclusions (area %)	Inclusions (nr. image-objects)	Average crystal area (µm^2)	Average crystal length (µm)
Ty-S-RV-418 (area 1)	96.46	3.54	1775.00	1.45	1.48
Ty-S-RV-418 (area 2)	95.95	4.05	433.00	1.23	1.34
Ty-S-RV-418 (area 3)	96.23	3.77	1322.00	1.46	1.48
MEAN	**96.21**	**3.79**	**1176.67**	**1.38**	**1.43**
S.D.	**0.26**	**0.26**	**682.70**	**0.13**	**0.08**
Ty-M-V-005a (area 1)	89.49	10.51	3509.00	2.33	1.80
Ty-M-V-005a (area 2)	89.87	10.13	3898.00	2.05	1.72
Ty-M-V-005a (area 3)	89.83	10.17	11631.00	2.23	1.84
MEAN	**89.73**	**10.27**	**6346.00**	**2.20**	**1.79**
S.D.	**0.21**	**0.21**	**4581.08**	**0.14**	**0.06**
Ty-M-V-005 (area 1)	94.73	5.27	5498.00	0.43	0.83
Ty-M-V-005 (area 2)	94.01	5.99	1047.00	0.26	0.68
Ty-M-V-005 (area 3)	93.48	6.52	1017.00	0.17	0.53
MEAN	**94.07**	**5.93**	**2520.67**	**0.29**	**0.68**
S.D.	**0.63**	**0.63**	**2578.49**	**0.13**	**0.15**
turquoise glasses MEAN	**93.34**	**6.66**	**3347.78**	**1.29**	**1.30**

(e)

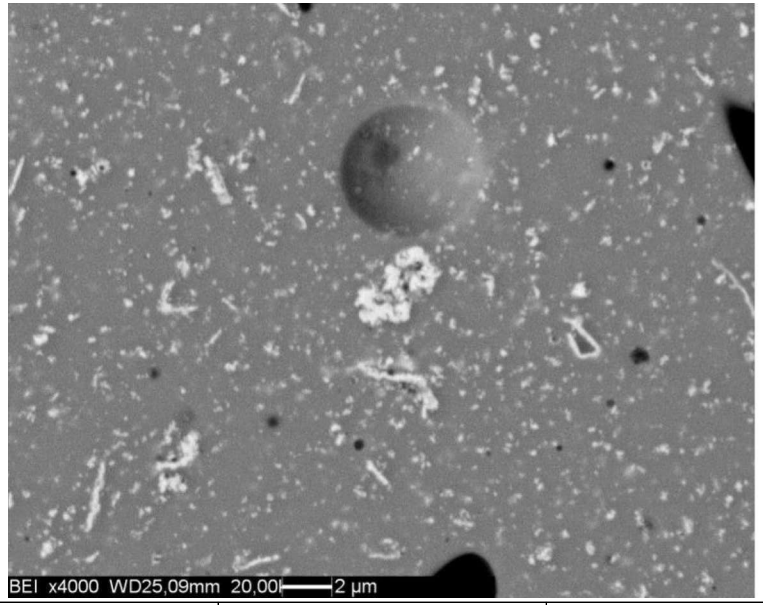

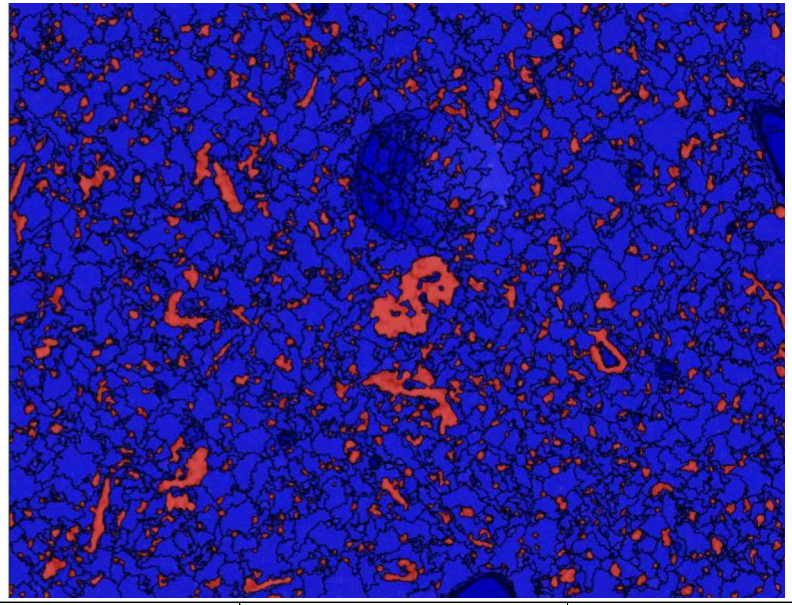

Sample name	Glassy matrix (area %)	Inclusions (area %)		Inclusions (nr. image-objects)		Average crystal area (µm^2)		Average crystal length (µm)	
		Antimoniates	*Quartz*	*Antimoniates*	*Quartz*	*Antimoniates*	*Quartz*	*Antimoniates*	*Quartz*
Ty-P-A-402 (area 1)	84.56	15.44		1435.00		26.06		5.85	
Ty-P-A-402 (area 2)	83.64	7.93	8.44	764.00	1.00	0.32	264.24	0.70	29.87
Ty-P-A-402 (area 3)	89.29	10.71		731.00		0.10		0.44	
MEAN	**85.83**	**11.36**		**976.67**		**8.83**		**2.33**	
S.D.	**3.03**	**3.80**		**397.27**		**14.93**		**3.05**	
Ty-P-R-423 (area 1)	95.63	4.37		303.00		0.67		0.92	
Ty-P-R-423 (area 2)	94.60	5.40		65.00		0.85		1.04	
Ty-P-R-423 (area 3)	93.30	6.70		93.00		3.45		1.87	
MEAN	**94.51**	**5.49**		**153.67**		**1.66**		**1.27**	
S.D.	**1.17**	**1.17**		**130.08**		**1.56**		**0.52**	
Ty-P-R-414 (area 1)	95.37	4.63		808.00		0.72		0.93	
Ty-P-R-414 (area 2)	94.51	5.49		85.00		0.84		1.16	
Ty-P-R-414 (area 3)	95.04	4.96		667.00		0.93		1.15	
MEAN	**94.98**	**5.02**		**520.00**		**0.83**		**1.08**	
S.D.	**0.43**	**0.43**		**383.26**		**0.10**		**0.13**	
yellow glasses MEAN	**91.77**	**5.26**		**336.83**		**1.24**		**1.18**	

(f)

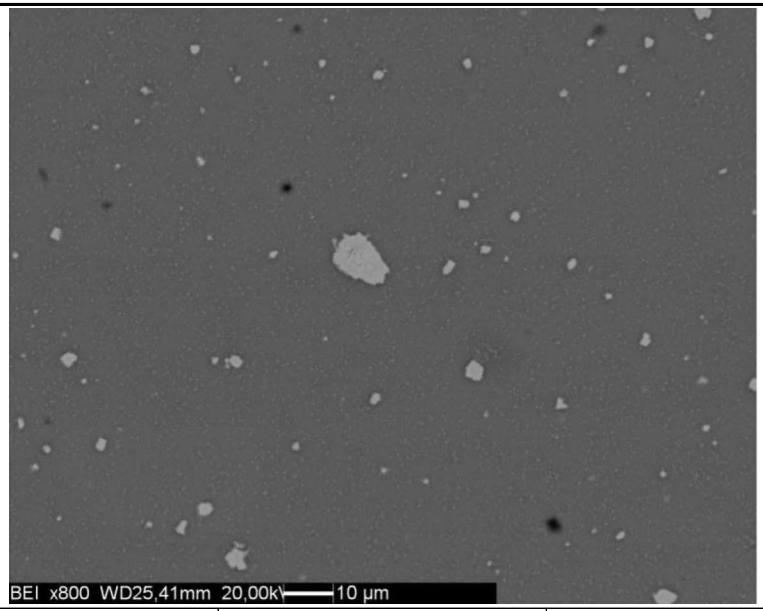

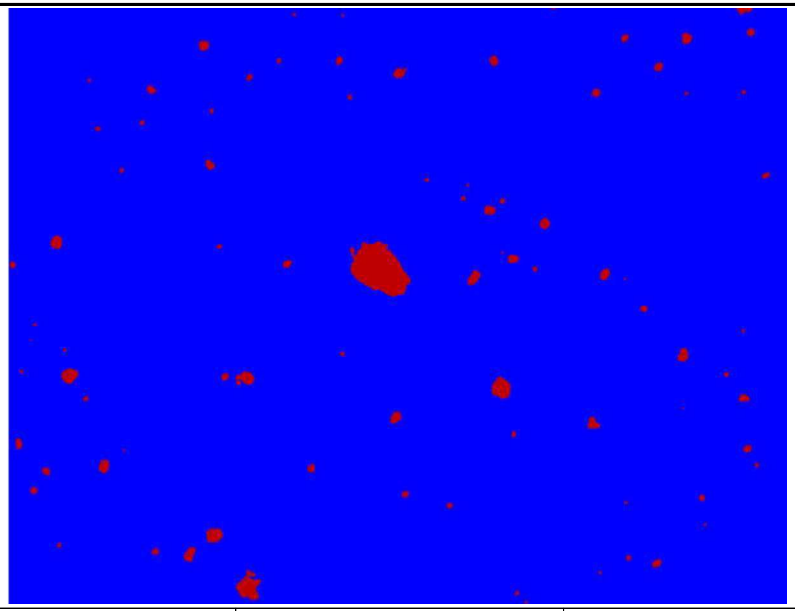

Sample name	Glassy matrix (area %)	Inclusions (area %)	Inclusions (nr. image-objects)	Average crystal area (µm^2)	Average crystal length (µm)
Ty-M-Ar-506 (area 1)	98.88	1.12	209.00	2.10	1.61
Ty-M-Ar-506 (area 2)	98.57	1.43	85.00	2.93	1.70
Ty-M-Ar-506 (area 3)	99.09	0.91	216.00	3.37	2.00
Ty-M-Ar-506 MEAN	**98.85**	**1.15**	**170.00**	**2.80**	**1.77**
S.D.	**0.26**	**0.26**	**73.70**	**0.65**	**0.21**

(g)

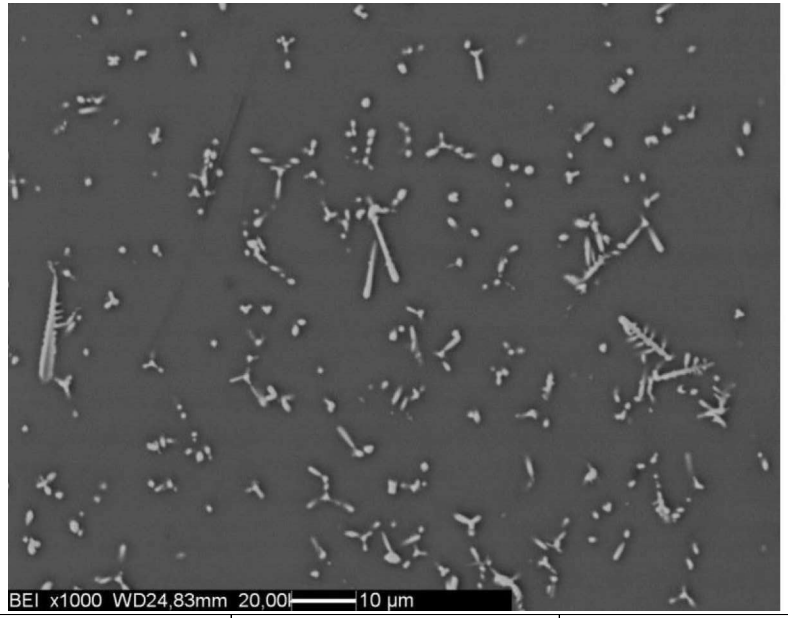

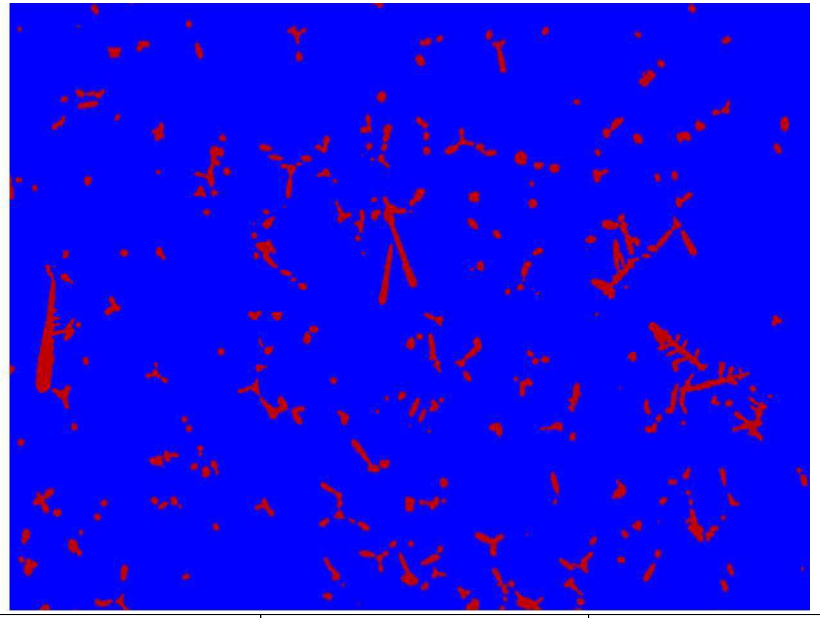

Sample name	Glassy matrix (area %)	Inclusions (area %)	Inclusions (nr. image-objects)	Average crystal area (µm^2)	Average crystal length (µm)
Ty-I-RAu-622 (area 1)	94.72	5.28	280.00	1.85	2.03
Ty-I-RAu-622 (area 2)	95.79	4.21	86.00	1.99	2.07
Ty-I-RAu-622 (area 3)	92.95	7.05	144.00	1.99	2.02
MEAN	**94.49**	**5.51**	**170.00**	**1.94**	**2.04**
S.D.	**1.43**	**1.43**	**99.58**	**0.08**	**0.03**
Ty-M-R-507 (area 1)	95.72	4.28	933.00	1.88	2.09
Ty-M-R-507 (area 2)	95.24	4.76	514.00	2.58	2.42
Ty-M-R-507 (area 3)	94.97	5.03	314.00	3.44	2.97
MEAN	**95.31**	**4.69**	**587.00**	**2.63**	**2.50**
S.D.	**0.38**	**0.38**	**315.89**	**0.78**	**0.44**
sealing-wax red glasses MEAN	**94.90**	**5.10**	**378.50**	**2.29**	**2.27**

(h)

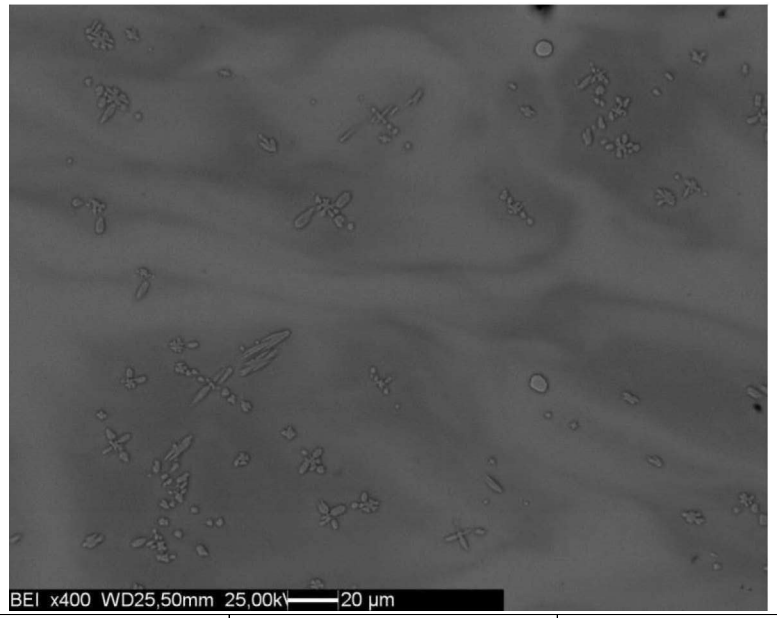

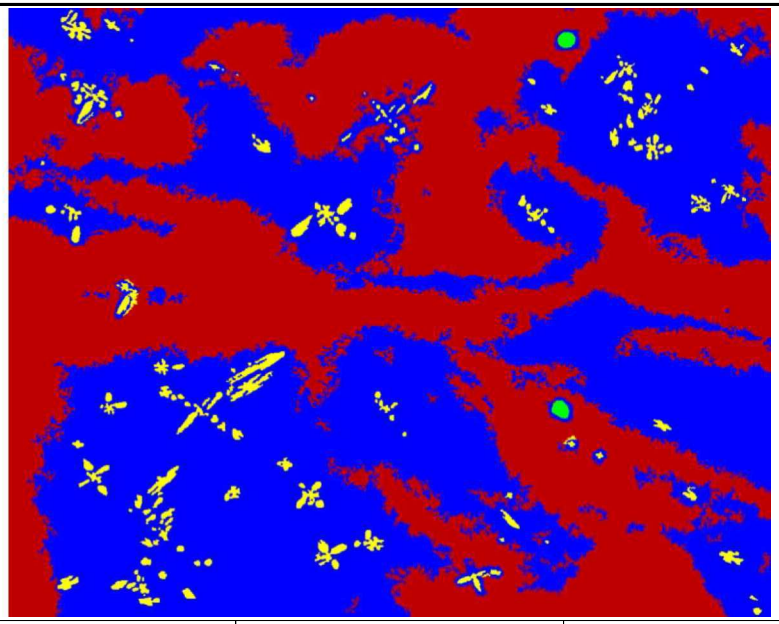

Sample name	Glassy matrix (area %)		Inclusions (area %)		Inclusions (nr. image-objects)		Average crystal area (µm^2)		Average crystal length (µm)	
	dark gray	*light gray*	*cuprite*	*metallic Cu*	*cuprite*	*metallic Cu*	*cuprite*	*metallic Cu*	*cuprite*	*metallic Cu*
Ty-S-RV-418 (area 1)	25.07	69.79	5.15	0.03	318.00	1.00	2.02	4.03	2.35	2.35
Ty-S-RV-418 (area 2)	38.73	54.92	6.34	0.07	151.00	1.00	2.08	3.51	2.42	2.15
Ty-S-RV-418 (area 3)	33.23	63.25	3.52	0.05	662.00	2.00	1.96	9.90	2.40	3.77
MEAN	**32.34**	**62.65**	**5.00**	**0.05**	**377.00**	**1.33**	**2.02**	**5.81**	**2.39**	**2.76**
S.D.	**6.88**	**7.45**	**1.42**	**0.02**	**260.56**	**0.58**	**0.06**	**3.55**	**0.03**	**0.89**
Ty-M-RAu-502 (area 1)	26.60	70.98	2.42	0.01	664.00	1.00	8.14	25.00	4.24	6.50
Ty-M-RAu-502 (area 2)	52.36	45.27	2.37	0.10	163.00	2.00	9.93	33.38	4.84	6.88
Ty-M-RAu-502 (area 3)	40.60	56.64	2.76	0.00	275.00	0.00	8.23	0.00	4.40	0.00
MEAN	**39.85**	**57.63**	**2.52**	**0.04**	**367.33**	**1.00**	**8.77**	**19.46**	**4.49**	**4.46**
S.D.	**12.89**	**12.88**	**0.21**	**0.05**	**262.95**	**1.00**	**1.01**	**17.36**	**0.31**	**3.87**
zoned sealing-wax red glasses MEAN	**36.10**	**60.14**	**3.76**	**0.04**	**372.17**	**1.17**	**5.39**	**12.64**	**3.44**	**3.61**

Table VII - Summary. This tabe summarizes the results obtained using the variuous analytical techniques employed during this work (SEM-EDS, EPMA, μ-Raman) in terms of chemical composition of the samples and identification of the mineral inclusions. In particular: an image of the object (column I), a SEM-BSE image exemplifying the texture of the sample (column II), the name of the sample (column III), its color-class (column IV), alkali type (column V), the main coloring/ opacifying inclusions (column VI), other types of inclusions such as sand-relics and newly formed phases (VII) and the results of the areal EDS and point spot EPMA analyses (VIII-XXVIII columns) as a mean of 5-7 analyses. In the case of chemical zonings (DG = dark gray glass; LG = light gray glass), EDS point spots data are also given as a mean of 3-6 point analyses according to the dimensions of the analyzed areas.

Sample image	SEM-BSE	Sample	Color	Alkali type	Main coloring/ opacifying inclusions	Other inclusions	Analysis Type	Na_2O	MgO	Al_2O_3	SiO_2	P_2O_5	SO_3	Cl	K_2O	CaO	TiO_2	MnO	FeO	CoO	CuO	As_2O_5	SnO_2	Sb_2O_5	PbO	Tot
	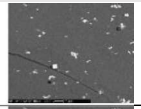	Ty-I-B-616	opaque dark blue	LMG	Ca antimoniates	no	EDS area	16.1	1.6	3.5	64.4	1.0	1.2	1.2	0.5	5.9			1.5		1.0			1.8		
	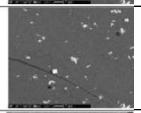	Ty-I-B-616	opaque dark blue	LMG	Ca antimoniates	no	EPMA	18.29	0.85	2.26	66.84	0.40	0.06	1.13	0.48	5.57	0.28	0.01	1.15	0.56	0.48	0.01	0.03	1.83	0.08	100.34
	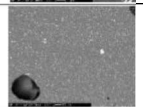	Ty-I-BBi-613-Bi	opaque white	LMG	Ca antimoniates	no	EDS area	8.2	2.0	3.3	54.0	1.5		0.5	1.2	6.3		1.8	1.1					0.5	11.93	
	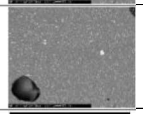	Ty-I-BBi-613-Bi	opaque white	LMG	Ca antimoniates	no	EPMA	13.20	1.48	2.15	59.65	0.80	0.43	0.38	1.29	5.49	0.12	1.46	0.81	0.00	0.06	0.01	0.13	0.17	7.28	101.40
	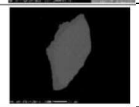	Ty-I-BBi-613-BT	transp. dark blue	LMG	no	1 small pyroxene	EDS area	13.1	1.5	3.4	70.3		0.7	1.0	0.6	5.7		1.1	2.1		0.5					
	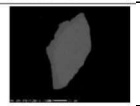	Ty-I-BBi-613-BT	transp. dark blue	LMG	no	1 small pyroxene	EPMA	17.65	0.64	2.23	70.26	0.04	0.42	1.01	0.89	5.72	0.13	0.71	1.48	0.21	0.17	0.01	0.03	0.04	0.10	101.73
	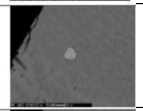	Ty-I-RAu-605	sealing-wax red	LMG	cuprite, metallic copper	wollastonite, plagioclase SiO_2	EDS area	8.2	1.8	4.1	48.5			1.0	0.5	4.3			0.8		5.9				22.98	
	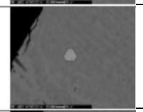	Ty-I-RAu-605	sealing-wax red	LMG	cuprite, metallic copper	wollastonite, plagioclase SiO_2	EDS points (DG)	6.5	1.9	4.2	49.8			1.1	0.9	4.2			0.8		6.7				25.77	
	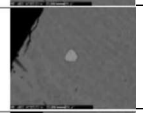	Ty-I-RAu-605	sealing-wax red	LMG	cuprite, metallic copper	wollastonite, plagioclase SiO_2	EDS points (LG)	4.6	2.0	3.9	46.4			1.2	0.4	3.6			0.7		3.8				26.33	
	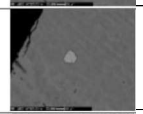	Ty-I-RAu-605	sealing-wax red	LMG	cuprite, metallic copper	wollastonite, plagioclase SiO_2	EPMA	11.51	0.47	1.99	46.17	0.05	0.48	0.54	0.46	4.19	0.12	0.15	0.72	0.01	4.19	0.03	0.31	1.44	26.93	99.76
	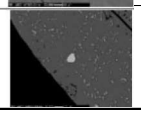	Ty-I-RAu-622	sealing-wax red	LMG	cuprite, metallic copper	corundum, SiO_2	EDS area	12.1	1.6	3.4	51.3			1.0	0.8	5.0		0.6	1.0		7.7				14.26	

Table VII - Summary

Sample image	SEM-BSE	Sample	Color	Alkali type	Main coloring/ opacifying inclusions	Other inclusions	Analysis Type	Na_2O	MgO	Al_2O_3	SiO_2	P_2O_5	SO_3	Cl	K_2O	CaO	TiO_2	MnO	FeO	CoO	CuO	As_2O_5	SnO_2	Sb_2O_5	PbO	Tot
	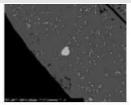	Ty-I-RAu-622	sealing-wax red	LMG	cuprite, metallic copper	corundum, SiO_2	EDS points (DG)	4.5	1.3	3.3	58.7			1.0	0.7	5.8		0.7	1.3		7.2				13.78	
	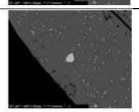	Ty-I-RAu-622	sealing-wax red	LMG	cuprite, metallic copper	corundum, SiO_2	EDS points (LG)	5.3	1.4	3.2	53.2			1.0	0.6	6.7		0.8	1.3		7.6				13.96	
	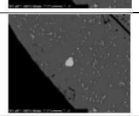	Ty-I-RAu-622	sealing-wax red	LMG	cuprite, metallic copper	corundum, SiO_2	EPMA	12	0.61	1.64	53.51	0.33	0.08	0.62	0.65	5.93	0.09	0.14	0.89	0.01	4.31	0.02	0.10	0.41	16.67	97.95
	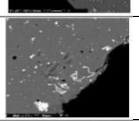	Ty-M-A-005	opaque light blue	LMG	Ca and Ca-Na antimoniates	wollastonite	EDS area	15.4	1.6	4.1	63.1		0.8	1.4	0.6	7.3			0.9		2.6			1.8		
	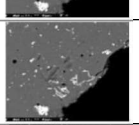	Ty-M-A-005	opaque light blue	LMG	Ca and Ca-Na antimoniates	wollastonite	EPMA	17.26	0.79	2.49	65.51	0.08	0.20	1.53	0.54	7.24	0.13	0.07	0.74	0.02	2.32	0.03	0.13	1.15	0.04	100.24
	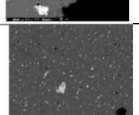	Ty-M-A-005a	opaque light blue	LMG	Ca, Na and Ca-Na antimoniates	no	EDS area	15.8	1.7	3.6	60.4	0.9	1.9	1.4	0.9	6.2			1.4		3.2			2.5		
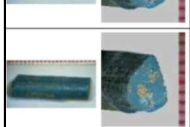	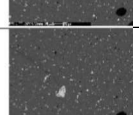	Ty-M-A-005a	opaque light blue	LMG	Ca, Na and Ca-Na antimoniates	no	EPMA	17.11	1.10	2.30	65.00	0.18	0.47	1.27	0.69	5.39	0.18	0.24	1.28	0.04	2.65	0.22	0.20	1.26	1.17	100.75
	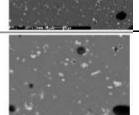	Ty-M-A-006	opaque turquoise	LMG	Ca antimoniates and Na antimoniates	SiO_2 (quartz)	EDS area	12.3		2.3	59.4			1.2	0.3	2.2		1.1	0.7		2.2			3.6	13.49	
	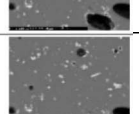	Ty-M-A-006	opaque turquoise	LMG	Ca antimoniates and Na antimoniates	SiO_2 (quartz)	EPMA	13.47	0.52	0.91	67.20	0.05	0.31	0.98	0.32	2.03	0.07	0.74	0.56	0.01	1.66	0.00	0.04	2.62	8.35	99.86
	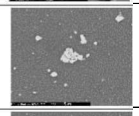	Ty-M-Ar-506	yellowish-orange	LMG	Ca-Pb antimoniates; cuprite	no	EDS area	9.9	1.7	3.7	47.5			0.7	0.6	4.7	0.1		1.0		7.6			1.2	19.90	
	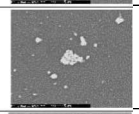	Ty-M-Ar-506	yellowish-orange	LMG	Ca-Pb antimoniates; cuprite	no	EPMA	8.41	0.37	1.58	46.84	0.14	0.42	0.41	0.62	4.70	0.07	0.06	1.25	0.00	9.36	0.03	0.02	1.90	25.01	101.18
	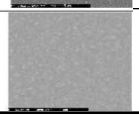	Ty-M-Ar-506a	yellowish-orange	LMG	cuprite, 1 small drop of metallic copper	wollastonite	EDS area	7.4	1.9	3.4	38.7			0.8	1.3	7.5			2.6		8.6				26.24	

Table VII - Summary

Sample image	SEM-BSE	Sample	Color	Alkali type	Main coloring/ opacifying inclusions	Other inclusions	Analysis Type	Na_2O	MgO	Al_2O_3	SiO_2	P_2O_5	SO_3	Cl	K_2O	CaO	TiO_2	MnO	FeO	CoO	CuO	As_2O_5	SnO_2	Sb_2O_5	PbO	Tot
	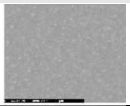	Ty-M-Ar-506a	yellowish-orange	LMG	cuprite, 1 small drop of metallic copper	wollastonite	EPMA	10.70	1.91	3.04	45.37	0.17	0.70	0.59	1.28	8.01	0.31	0.24	1.91	0.02	7.23	0.03	0.63	0.33	16.06	98.56
	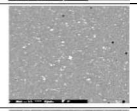	Ty-M-B-002	opaque dark blue	LMG	Ca and Ca-Pb antimoniates	no	EDS area	8.8	1.4	3.2	55.6			1.1	1.0	7.6	0.3	0.6	2.1		0.8			1.9	16.42	
	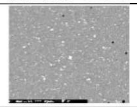	Ty-M-B-002	opaque dark blue	LMG	Ca and Ca-Pb antimoniates	no	EPMA	11.56	0.92	1.99	59.41	0.09	0.33	0.73	0.79	6.65	0.05	0.29	1.77	0.29	0.44	0.01	0.02	2.12	10.48	97.96
	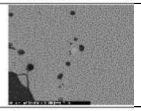	Ty-M-B-004	transp. dark blue	LMG	no	Fe oxide; ilmenite	EPMA	14.55	0.44	2.08	71.30	0.05	0.31	1.30	0.58	5.30	0.06	0.01	1.04	0.04	0.23	0.01	0.02	0.60	0.06	97.98
	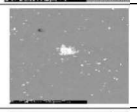	Ty-M-BAu-002	blue	LMG	Ca antimoniates	SiO_2	EDS area	10.7	1.0	3.3	67.2		0.8	0.5	0.9	8.4		0.7	1.6		1.2			3.7		
	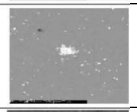	Ty-M-BAu-002	blue	LMG	Ca antimoniates	SiO_2	EPMA	13.79	0.49	2.40	68.82	0.12	0.47	0.33	0.77	7.45	0.05	0.47	1.35	0.88	1.01	0.06	0.09	4.16	0.00	102.70
	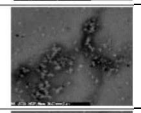	Ty-M-G-504	yellowish-orange	LMG	cuprite	no	EDS area	6.2	1.6	3.2	33.3			0.5	0.4	2.2			2.4		9.3		0.3		37.63	
	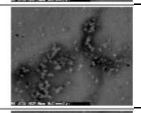	Ty-M-G-504	yellowish-orange	LMG	cuprite	no	EDS points (DG)	5.4	0.7	3.1	35.3			0.5	0.3	2.0		0.2	2.7		9.9				35.66	
	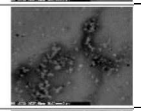	Ty-M-G-504	yellowish-orange	LMG	cuprite	no	EDS points (LG)	4.5	1.2	3.2	35.4			0.5	0.4	2.3		0.4	2.6		6.8				39.26	
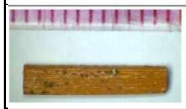	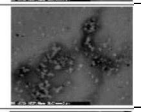	Ty-M-G-504	yellowish-orange	LMG	cuprite	no	EPMA	6.69	0.29	1.53	42.15	0.26	0.12	0.31	0.50	1.96	0.15	0.08	1.79	0.05	6.91	0.02	0.02	2.52	30.92	96.29
	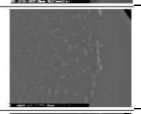	Ty-M-G-504a	yellowish-orange	LMG	cuprite	wollastonite	EDS area	7.7	1.6	3.5	36.1	1.7		0.9	1.2	6.7			2.7		9.1				26.61	
	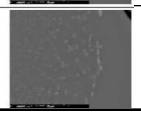	Ty-M-G-504a	yellowish-orange	LMG	cuprite	wollastonite	EPMA	11.02	1.61	2.74	45.15	0.67	0.39	0.71	1.06	6.93	0.25	0.20	2.20	0.02	8.03	0.03	0.94	0.45	18.18	100.58

Table VII - Summary

Sample image	SEM-BSE	Sample	Color	Alkali type	Main coloring/ opacifying inclusions	Other inclusions	Analysis Type	Na_2O	MgO	Al_2O_3	SiO_2	P_2O_5	SO_3	Cl	K_2O	CaO	TiO_2	MnO	FeO	CoO	CuO	As_2O_5	SnO_2	Sb_2O_5	PbO	Tot
	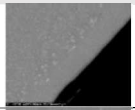	Ty-M-G-504b	yellowish-orange	LMG	cuprite	no	EDS area	8.5	1.9	3.7	37.4	1.7		1.0	1.3	6.6			2.5		8.7				24.82	
	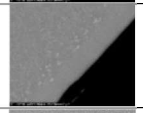	Ty-M-G-504b	yellowish-orange	LMG	cuprite	no	EPMA	10.95	1.56	2.73	44.02	0.67	0.35	0.68	1.05	6.86	0.23	0.26	2.15	0.02	8.21	0.05	0.95	0.42	17.80	98.96
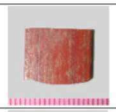	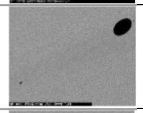	Ty-M-R-501	dull red	HMG	metallic copper, copper sulfides	no	EDS area	10.9	2.2	3.5	49.9	1.9		1.3	2.0	8.6	0.4	0.6	1.6		2.7				13.29	
	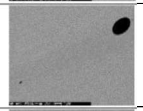	Ty-M-R-501	dull red	HMG	metallic copper, copper sulfides	no	EDS points (DG)	6.7	2.1	3.3	51.6	1.6		1.2	1.9	9.2	0.5	0.8	1.9		3.2				14.55	
	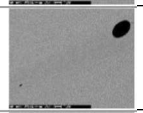	Ty-M-R-501	dull red	HMG	metallic copper, copper sulfides	no	EDS points (LG)	7.0	2.1	3.3	52.7	1.4		1.5	1.9	9.6	0.3	0.7	2.0		2.8				13.98	
	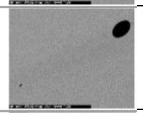	Ty-M-R-501	dull red	HMG	metallic copper, copper sulfides	no	EPMA	13.76	2.29	2.12	55.10	0.82	0.34	0.92	1.58	8.36	0.17	0.31	1.32	0.02	2.27	0.02	0.44	0.37	8.43	98.61
	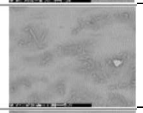	Ty-M-R-502d	sealin-wax red	LMG	cuprite, metallic copper	chloroxiphite	EDS area mix	10.5	2.4	5.1	43.9			0.9	0.5	1.3	0.4		1.3		4.9				25.24	
	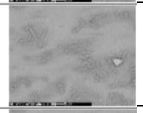	Ty-M-R-502d	sealin-wax red	LMG	cuprite, metallic copper	chloroxiphite	EDS points (DG)	6.3	2.1	5.0	47.0			0.8	0.5	1.2	0.5		1.6		8.1				24.87	
	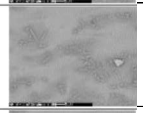	Ty-M-R-502d	sealin-wax red	LMG	cuprite, metallic copper	chloroxiphite	EDS points (LG)	4.5	2.2	5.0	47.4			1.0	0.5	1.5			1.7		3.4				30.01	
	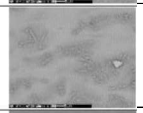	Ty-M-R-502d	sealin-wax red	LMG	cuprite, metallic copper	chloroxiphite	EPMA	10.47	0.84	2.85	41.29	0.05	0.29	0.52	0.50	1.49	0.52	0.23	1.54	0.05	4.11	0.03	0.00	0.00	35.08	99.85
		Ty-M-R-505	dull red	HMG	metallic copper, copper sulfides	wollastonite, Ca-Na silicates (devitrification phases)	EDS area	12.3	3.0	4.1	59.3			1.2	1.7	7.8		0.4	1.2		2.0				6.31	
		Ty-M-R-505	dull red	HMG	metallic copper, copper sulfides	wollastonite, Ca-Na silicates (devitrification phases)	EDS points (DG)	6.1	2.6	3.8	61.0			1.4	1.6	10.2		0.7	1.7		2.1				7.97	

Table VII - Summary

Sample image	SEM-BSE	Sample	Color	Alkali type	Main coloring/ opacifying inclusions	Other inclusions	Analysis Type	Na_2O	MgO	Al_2O_3	SiO_2	P_2O_5	SO_3	Cl	K_2O	CaO	TiO_2	MnO	FeO	CoO	CuO	As_2O_5	SnO_2	Sb_2O_5	PbO	Tot
		Ty-M-R-505	dull red	HMG	metallic copper, copper sulfides	wollastonite, Ca-Na silicates (devitrification phases)	EPMA	14.01	2.29	2.26	56.29	0.27	0.76	0.94	1.60	8.55	0.19	0.07	1.02	0.01	1.69	0.03	0.41	0.36	7.96	98.72
	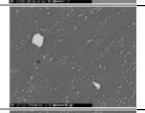	Ty-M-R-507	sealing-wax red	LMG	cuprite, metallic copper	no	EDS area mix	9.7	1.8	5.5	43.4			1.0	0.9	4.9		0.7	1.2		10.0				21.00	
	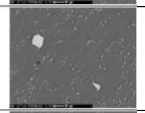	Ty-M-R-507	sealing-wax red	LMG	cuprite, metallic copper	no	EDS points (DG)	6.4	1.8	3.6	46.9			1.0	0.9	5.4		0.8	1.4		6.1				23.75	
	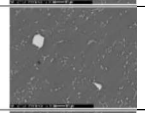	Ty-M-R-507	sealing-wax red	LMG	cuprite, metallic copper	no	EDS points (LG)	6.2	1.8	3.6	46.6			1.8	1.0	5.5		0.8	1.4		6.0				23.89	
	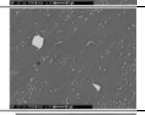	Ty-M-R-507	sealing-wax red	LMG	cuprite, metallic copper	no	EPMA	11.78	0.60	1.69	53.99	0.13	0.35	0.68	0.64	5.69	0.07	0.48	1.13	0.03	5.85	0.03	0.10	0.40	16.51	100.13
	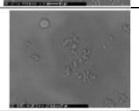	Ty-M-RAu-502	sealing-wax red	LMG	cuprite, metallic copper	wollastonite + Au foil	EDS area	7.8	1.7	3.3	29.8		0.4	0.6	0.6	3.8	0.2		1.4		6.8		1.3		39.39	
	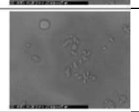	Ty-M-RAu-502	sealing-wax red	LMG	cuprite, metallic copper	wollastonite + Au foil	EDS points (DG)	5.6	1.7	3.3	32.5		0.5	1.0	0.8	4.0	0.2		1.6		4.1		1.9		39.82	
	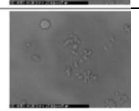	Ty-M-RAu-502	sealing-wax red	LMG	cuprite, metallic copper	wollastonite + Au foil	EDS points (LG)	5.6	1.7	3.1	29.5		0.5	0.9	0.5	4.0	0.0		1.4		4.1		1.8		43.48	
	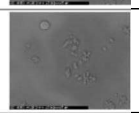	Ty-M-RAu-502	sealing-wax red	LMG	cuprite, metallic copper	wollastonite + Au foil	EPMA	10.06	0.84	1.87	38.87	0.24	0.34	0.73	0.63	4.65	0.15	0.13	1.18	0.02	4.04	0.00	1.12	0.51	34.25	99.63
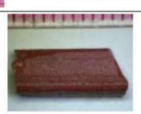	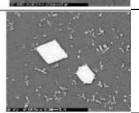	Ty-M-RAu-502a	sealing-wax red	LMG	cuprite, metallic copper	no	EDS area	11.3	1.5	3.3	52.8			0.9	0.7	5.1		0.5	1.1		7.9				13.75	
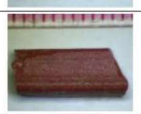	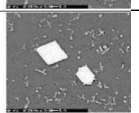	Ty-M-RAu-502a	sealing-wax red	LMG	cuprite, metallic copper	no	EPMA	11.80	0.61	1.73	54.12	0.08	0.40	0.64	0.65	5.74	0.13	0.55	1.06	0.03	5.61	0.00	0.11	0.41	16.92	100.59
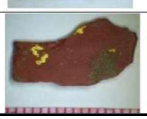	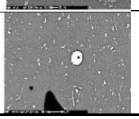	Ty-M-RAu-502b	sealing-wax red	LMG	cuprite, metallic copper	no	EDS area	9.7	1.4	3.0	45.3			0.9	0.8	4.1		1.0	0.8		10.2				21.07	

Table VII - Summary

Sample image	SEM-BSE	Sample	Color	Alkali type	Main coloring/ opacifying inclusions	Other inclusions	Analysis Type	Na_2O	MgO	Al_2O_3	SiO_2	P_2O_5	SO_3	Cl	K_2O	CaO	TiO_2	MnO	FeO	CoO	CuO	As_2O_5	SnO_2	Sb_2O_5	PbO	Tot
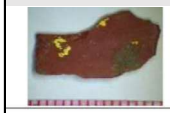	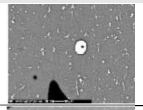	Ty-M-RAu-502b	sealing-wax red	LMG	cuprite, metallic copper	no	EPMA	11.57	0.47	1.48	54.22	0.40	0.09	0.69	0.66	4.21	0.08	0.43	0.46	0.01	4.47	0.01	0.11	1.61	15.50	96.53
	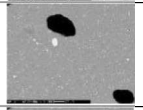	Ty-M-RAu-502c	sealing-wax red	LMG	cuprite, metallic copper	no	EDS area	8.7	1.8	3.7	43.2			0.9	1.0	4.6		0.8	1.1		10.1				22.19	
	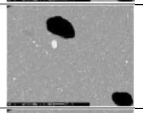	Ty-M-RAu-502c	sealing-wax red	LMG	cuprite, metallic copper	no	EDS points (DG)	7.7	1.5	2.9	33.0			1.1	1.2	5.1		0.9	1.3		15.9				27.24	
	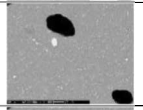	Ty-M-RAu-502c	sealing-wax red	LMG	cuprite, metallic copper	no	EDS points (LG)	5.7	1.7	3.6	43.6			1.2	1.2	5.4		1.0	1.4		6.7				26.48	
	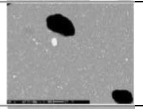	Ty-M-RAu-502c	sealing-wax red	LMG	cuprite, metallic copper	no	EPMA	10.39	0.54	2.02	54.21	0.11	0.25	0.58	0.79	5.49	0.11	0.62	1.00	0.01	6.18	0.00	0.00	0.41	17.84	100.55
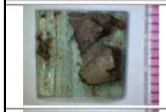		Ty-M-T-503	aqua	HMG	1 small Cu drop (EDS), 1 small Pb antimoniates (OM)	no	EDS area	11.4	2.0	3.5	67.4	1.2	0.7	1.7	1.7	7.6		1.7	1.7							
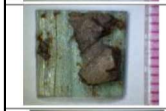		Ty-M-T-503	aqua	HMG	1 small Cu drop (EDS), 1 small Pb antimoniates (OM)	no	EPMA	15.93	2.59	2.25	66.29	0.20	0.92	0.94	1.60	6.95	0.19	1.32	1.28	0.01	0.06	0.02	0.02	0.20	0.18	100.94
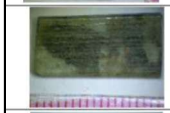	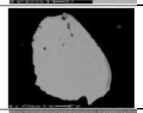	Ty-M-T-503a	aqua	HMG	no	no	EPMA	15.23	1.70	2.12	67.75	0.24	0.71	0.97	1.64	6.51	0.14	0.83	1.04	0.03	0.18	0.01	0.01	0.11	0.01	99.23
	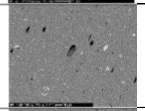	Ty-M-V-005	opaque turquoise	LMG	Ca and Ca-Pb antimoniates	no	EDS area	7.9	1.1	3.0	53.1				0.8	7.6		0.6	0.7		3.0			3.0	17.96	
	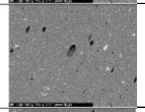	Ty-M-V-005	opaque turquoise	LMG	Ca and Ca-Pb antimoniates	no	EPMA	10.59	0.51	1.95	59.88	0.08	0.42	0.38	0.68	7.04	0.05	0.39	0.48	0.01	2.57	0.04	0.20	5.22	11.20	101.69
	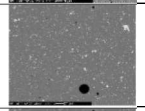	Ty-M-V-005a	opaque turquoise	LMG	Ca and Ca-Pb antimoniates	no	EDS area	13.5	2.0	3.8	56.2	1.4		0.7	0.9	5.7		0.8	0.5		3.7			1.7	8.26	
	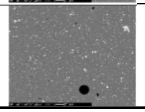	Ty-M-V-005a	opaque turquoise	LMG	Ca and Ca-Pb antimoniates	no	EPMA	13.42	1.27	2.20	60.02	0.37	0.46	0.48	0.94	5.76	0.13	0.87	0.65	0.04	5.48	0.01	0.61	2.13	5.49	100.32

Table VII - Summary

Sample image	SEM-BSE	Sample	Color	Alkali type	Main coloring/ opacifying inclusions	Other inclusions	Analysis Type	Na_2O	MgO	Al_2O_3	SiO_2	P_2O_5	SO_3	Cl	K_2O	CaO	TiO_2	MnO	FeO	CoO	CuO	As_2O_5	SnO_2	Sb_2O_5	PbO	Tot
	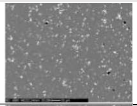	Ty-M-V-006	opaque turquoise	LMG	Ca antimoniates	no	EDS area	10.7	1.2	3.4	61.8	0.9		0.6	1.0	9.2		1.1	0.6		4.3			5.2		
	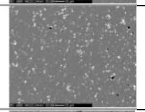	Ty-M-V-006	opaque turquoise	LMG	Ca antimoniates	no	EPMA	14.40	0.80	2.39	64.91	0.53	0.12	0.41	0.89	7.91	0.10	0.75	0.32	0.02	2.95	0.03	0.01	2.87	0.18	99.63
	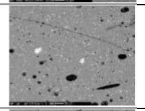	Ty-M-V-006a	opaque turquoise	LMG	Na and Ca antimoniates	corundum, anorthoclase, SiO_2	EDS area	11.2	1.1	2.2	60.9			1.1		2.1		1.1	0.8		2.3			3.4	12.60	
	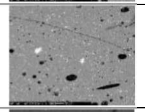	Ty-M-V-006a	opaque turquoise	LMG	Na and Ca antimoniates	corundum, anorthoclase, SiO_2	EPMA	13.89	0.53	0.92	67.08	0.03	0.31	0.95	0.33	2.01	0.07	0.75	0.47	0.02	1.73	0.00	0.03	2.65	7.03	98.81
	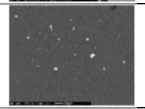	Ty-P-A-402-B	opaque dark blue	LMG	Ca antimoniates	no	EDS area	11.5	1.3	3.7	64.9	1.0		0.5	1.0	7.9		0.8	1.4	1.1	1.4			3.1		
	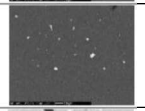	Ty-P-A-402-B	opaque dark blue	LMG	Ca antimoniates	no	EPMA	13.76	0.48	2.59	67.10	0.39	0.07	0.32	0.85	7.29	0.05	0.48	1.40	0.79	1.02	0.03	0.05	4.01	0.10	100.79
	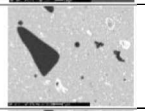	Ty-P-A-402-G	opaque yellow	LMG	Pb antimoniates, SiO_2 (quartz)	no	EDS area	3.8	1.5	2.4	34.9	1.7		0.7	0.3	2.2			1.6					1.4	45.98	
	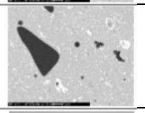	Ty-P-A-402-G	opaque yellow	LMG	Pb antimoniates, SiO_2 (quartz)	no	EPMA	5.93	0.21	1.14	46.90	0.20	0.07	0.38	0.34	3.01	0.07	0.03	1.10	0.02	0.06	0.00	0.00	1.48	36.53	97.52
		Ty-P-A-408-Ar	yellowish-orange	LMG	cuprite	wollastonite, malayaite	EDS area	9.0	1.9	3.8	37.8	1.7		1.2	1.2	6.7			2.4		8.5				24.04	
		Ty-P-A-408-Ar	yellowish-orange	LMG	cuprite	wollastonite, malayaite	EPMA	11.20	1.53	2.59	45.56	0.30	0.62	0.57	1.05	7.09	0.27	0.31	2.13	0.10	6.89	0.03	0.85	0.43	17.60	99.15
	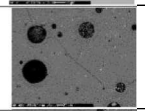	Ty-P-A-408-B	opaque dark blue	LMG	metallic copper with outer sulfide and chloride layers; Ca antimoniates	ilmenite	EDS area	13.2	1.3	3.5	63.0	0.9	2.2	1.3	0.9	1.3		1.0	1.5		0.8			5.1	3.50	
	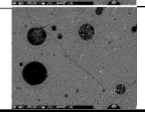	Ty-P-A-408-B	opaque dark blue	LMG	metallic copper with outer sulfide and chloride layers; Ca antimoniates	ilmenite	EPMA	16.34	0.63	1.94	67.74	0.39	0.08	1.22	0.70	4.80	0.14	0.65	1.33	0.31	0.42	0.01	0.02	1.73	1.52	99.99

Table VII - Summary

Sample image	SEM-BSE	Sample	Color	Alkali type	Main coloring/ opacifying inclusions	Other inclusions	Analysis Type	Na_2O	MgO	Al_2O_3	SiO_2	P_2O_5	SO_3	Cl	K_2O	CaO	TiO_2	MnO	FeO	CoO	CuO	As_2O_5	SnO_2	Sb_2O_5	PbO	Tot
	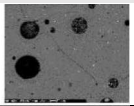	Ty-P-A-408-B-c	opaque dark blue	LMG	metallic copper with outer sulfide and chloride layers; Ca antimoniates	ilmenite	EDS points (LG)	8.8	1.4	3.5	63.8	0.7	2.4	1.2	0.7	3.3		1.0	1.9		0.6			6.0	4.29	
	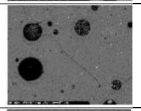	Ty-P-A-408-B-s	opaque dark blue	LMG	metallic copper with outer sulfide and chloride layers; Ca antimoniates	ilmenite	EDS points (DG)	9.1	1.3	3.4	66.4	0.9	2.1	1.6	0.9	0.6		1.2	1.8		0.5			5.9	3.57	
	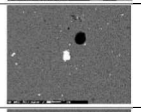	Ty-P-A-418-B	opaque dark blue	LMG	Ca antimoniates	no	EDS area	11.9	1.3	3.5	63.2	0.9	0.8	1.3	0.7	6.8		0.7	1.4		0.6			1.8	4.99	
	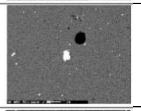	Ty-P-A-418-B	opaque dark blue	LMG	Ca antimoniates	no	EPMA	14.62	0.60	2.49	67.44	0.19	0.24	0.92	0.72	6.43	0.13	0.45	1.09	0.19	0.24	0.01	0.06	3.19	2.64	101.63
	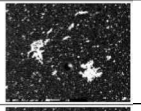	Ty-P-A-418-Bi	opaque white	LMG	Ca antimoniates	no	EDS area	13.8	2.4	3.6	64.0		1.0	1.8	0.8	9.1			0.8					3.1		
	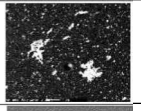	Ty-P-A-418-Bi	opaque white	LMG	Ca antimoniates	no	EPMA	16.37	2.61	2.69	65.37	0.06	0.30	0.99	0.71	7.98	0.12	0.03	0.61	0.01	0.00	0.02	0.02	4.32	0.11	102.32
	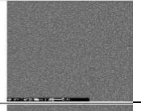	Ty-P-A-418-R	dull red	HMG	metallic copper, Cu sulfides	wollastonite	EDS area	10.5	2.7	3.5	52.0	2.3		1.4	2.2	8.0		0.8	1.7		2.7				10.96	
	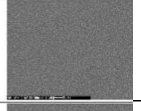	Ty-P-A-418-R	dull red	HMG	metallic copper, Cu sulfides	wollastonite	EDS points (DG)	5.9	2.2	3.2	55.1	1.7		1.9	2.3	9.6		1.0	2.4		2.4				12.04	
	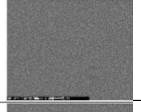	Ty-P-A-418-R	dull red	HMG	metallic copper, Cu sulfides	wollastonite	EDS points (LG)	7.5	2.7	3.3	52.7	2.0		1.3	2.1	8.1		0.9	2.0		2.4				13.62	
	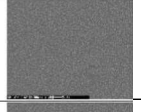	Ty-P-A-418-R1	dull red	HMG	metallic copper, Cu sulfides	wollastonite	EPMA	13.81	2.92	2.53	55.79	1.32	0.19	1.04	2.02	7.89	0.18	0.52	1.63	0.03	1.86	0.01	0.45	0.42	7.79	100.40
	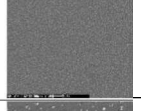	Ty-P-A-418-R2	dull red	HMG	metallic copper, Cu sulfides	wollastonite	EPMA	13.59	2.85	2.48	56.47	1.36	0.17	1.05	1.90	7.96	0.17	0.54	1.67	0.01	2.02	0.01	0.44	0.41	7.66	100.76
	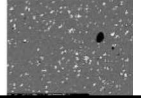	Ty-P-A-419-Bi	opaque white	LMG	Ca antimoniates	1 plagioclase	EDS area	8.9	1.6	4.0	61.1	1.0	0.7	0.7	4.2				0.9					6.6	9.53	

Table VII - Summary

Sample image	SEM-BSE	Sample	Color	Alkali type	Main coloring/ opacifying inclusions	Other inclusions	Analysis Type	Na_2O	MgO	Al_2O_3	SiO_2	P_2O_5	SO_3	Cl	K_2O	CaO	TiO_2	MnO	FeO	CoO	CuO	As_2O_5	SnO_2	Sb_2O_5	PbO	Tot
	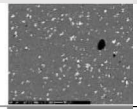	Ty-P-A-419-Bi	opaque white	LMG	Ca antimoniates	1 plagioclase	EPMA	11.49	0.61	2.57	67.24	0.04	0.26	0.48	0.97	3.91	0.10	0.09	0.73	0.04	0.05	0.05	0.21	5.36	7.07	101.29
		Ty-P-A-419-BT	transp. dark blue	LMG	few small Ca antimoniates	no	EDS area	11.8	1.9	4.0	70.5		1.9	1.5	1.0	5.1		0.6	1.8							
	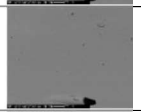	Ty-P-A-419-BT	transp. dark blue	LMG	few small Ca antimoniates	no	EPMA	14.27	0.68	2.01	69.85	0.18	0.19	1.11	1.07	4.83	0.15	0.44	1.53	0.11	0.43	0.02	0.02	2.77	1.03	100.69
	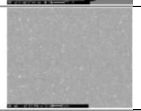	Ty-P-A-419-R	dull red	HMG	metallic copper, Cu sulfides	no	EDS area	8.7	3.6	3.5	57.9	2.3		0.9	3.0	7.2	0.2	0.7	3.1		1.9				6.22	
	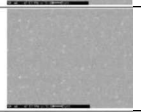	Ty-P-A-419-R	dull red	HMG	metallic copper, Cu sulfides	no	EPMA	14.27	0.68	2.01	69.85	0.18	0.19	1.11	1.07	4.83	0.15	0.44	1.53	0.11	0.43	0.02	0.02	2.77	1.03	100.69
	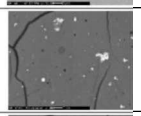	Ty-P-CR-421-A	opaque light blue	LMG	Ca and Ca-Na antimoniates	no	EDS area	16.5	1.3	3.5	64.0		1.0	1.6	0.4	4.2			0.8		3.9			2.5		
	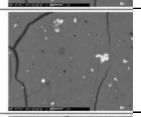	Ty-P-CR-421-A	opaque light blue	LMG	Ca and Ca-Na antimoniates	no	EPMA	15.76	0.45	2.08	69.55	0.07	0.31	1.76	0.47	4.95	0.13	0.03	0.52	0.03	2.95	0.01	0.14	1.80	0.07	101.08
	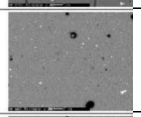	Ty-P-CR-421-B	opaque dark blue	LMG	Ca antimoniates	no	EDS area	13.2	1.6	3.9	64.6			1.2	0.8	2.2	6.4	0.7	1.6	0.4	0.8			1.4	0.89	
	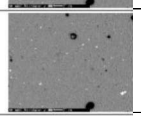	Ty-P-CR-421-B	opaque dark blue	LMG	Ca antimoniates	no	EPMA	15.30	0.69	2.68	69.07	0.12	0.23	1.06	0.70	6.31	0.13	0.37	1.24	0.19	0.35	0.04	0.02	3.15	0.99	102.63
	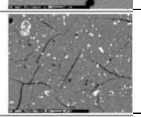	Ty-P-CR-421-Bi	opaque white	LMG	Ca and Ca-Na antimoniates	SiO_2 (quartz)	EDS area	2.0	1.8	4.2	76.3	0.9		1.1	0.3	5.7			0.8					4.7	1.70	
	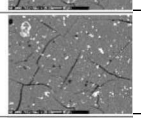	Ty-P-CR-421-Bi	opaque white	LMG	Ca and Ca-Na antimoniates	SiO_2 (quartz)	EPMA	0.13	0.42	2.05	75.73	0.04	0.41	1.13	0.43	5.30	0.09	0.01	0.39	0.01	0.06	0.03	0.04	3.33	1.05	90.63
	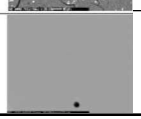	Ty-P-CR-421-BT	transp. dark blue	LMG	no	no	EDS area	12.9	1.8	3.9	67.6			1.7	1.4	5.3			1.4		1.0			1.3	1.25	

Table VII - Summary

Sample image	SEM-BSE	Sample	Color	Alkali type	Main coloring/ opacifying inclusions	Other inclusions	Analysis Type	Na_2O	MgO	Al_2O_3	SiO_2	P_2O_5	SO_3	Cl	K_2O	CaO	TiO_2	MnO	FeO	CoO	CuO	As_2O_5	SnO_2	Sb_2O_5	PbO	Tot
		Ty-P-CR-421-BT	transp. dark blue	LMG	no	no	EPMA	0.13	0.42	2.05	75.73	0.04	0.41	1.13	0.43	5.30	0.09	0.01	0.39	0.01	0.06	0.03	0.04	3.33	1.05	90.63
	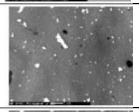	Ty-P-CR-421-G1	opaque yellow	LMG	Pb-Sn antimoniates	wollastonite, pyroxene, SiO_2 (quartz)	EDS area	9.4	1.4	3.1	45.5	1.1			0.3	2.2		0.8	2.6					0.9	30.31	
	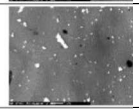	Ty-P-CR-421-G1	opaque yellow	LMG	Pb-Sn antimoniates	wollastonite, pyroxene, SiO_2 (quartz)	EPMA	12.62	1.01	1.86	63.61	0.25	0.25	0.90	0.58	4.69	0.09	0.47	1.81	0.01	0.06	0.05	0.12	1.09	11.91	101.37
	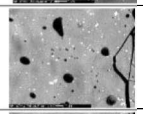	Ty-P-CR-421-G2	opaque yellow	LMG	Pb-Sn antimoniates	SiO_2 (quartz)	EDS area	11.0	1.6	3.0	53.9				0.7	4.3		0.8	2.1					1.2	19.86	
	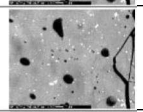	Ty-P-CR-421-G2	opaque yellow	LMG	Pb-Sn antimoniates	SiO_2 (quartz)	EPMA	10.79	0.40	1.84	53.93	0.06	0.14	0.59	0.57	2.20	0.12	0.42	2.67	0.00	0.16	0.02	0.04	1.35	23.10	98.38
	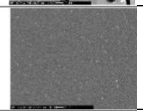	Ty-P-CR-421-R	dull red	HMG	metallic copper	wollastonite, plagiolase, albite, sanidine	EDS area	10.4	2.6	3.5	49.7	1.7		1.9	2.1	7.6	0.5	0.8	1.8		2.1				14.72	
	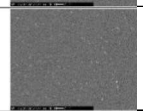	Ty-P-CR-421-R	dull red	HMG	metallic copper	wollastonite, plagiolase, albite, sanidine	EPMA	13.89	2.77	2.45	56.77	1.09	0.24	0.99	1.95	8.24	0.17	0.45	1.45	0.01	1.66	0.04	0.42	0.34	7.38	100.29
	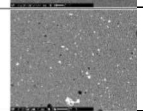	Ty-P-FL-004-B	opaque dark blue	LMG	Ca and Ca-Na antimoniates	K-feldspar (probably oligoclase)	EDS area	13.9	1.6	4.0	64.1	0.9	1.0	1.2	1.0	5.4			2.9		1.0			2.7		
	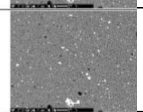	Ty-P-FL-004-B	opaque dark blue	LMG	Ca and Ca-Na antimoniates	K-feldspar (probably oligoclase)	EPMA	16.27	0.71	2.77	68.77	0.10	0.19	1.21	0.85	5.22	0.20	0.09	2.36	0.20	0.41	0.01	0.01	2.71	0.19	102.27
	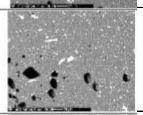	Ty-P-FL-004-Bi	opaque white	LMG	Ca antimoniates	ilmenite	EDS area	13.9	3.9	3.1	64.7	0.3	0.5	0.9	0.9	7.3								4.3		
	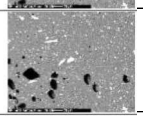	Ty-P-FL-004-Bi	opaque white	LMG	Ca antimoniates	ilmenite	EPMA	16.54	5.04	1.96	67.73	0.04	0.24	0.87	0.69	6.25	0.07	0.04	0.34	0.01	0.04	0.03	0.01	2.97	0.01	102.88
	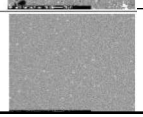	Ty-P-FL-004-R	dull red	HMG	metallic copper	wollastonite, SiO_2, anorthoclase, pyroxenes, epidote	EDS area	11.0	2.6	3.6	49.9	1.9		1.3	1.8	8.0		0.7	1.7		2.4				13.79	

Table VII - Summary

Sample image	SEM-BSE	Sample	Color	Alkali type	Main coloring/ opacifying inclusions	Other inclusions	Analysis Type	Na_2O	MgO	Al_2O_3	SiO_2	P_2O_5	SO_3	Cl	K_2O	CaO	TiO_2	MnO	FeO	CoO	CuO	As_2O_5	SnO_2	Sb_2O_5	PbO	Tot
	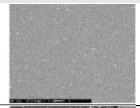	Ty-P-FL-004-R	dull red	HMG	metallic copper	wollastonite, SiO_2, anorthoclase, pyroxenes, epidote	EPMA	14.72	2.37	2.29	57.19	0.84	0.22	0.94	1.49	8.50	0.20	0.32	1.30	0.00	2.03	0.00	0.46	0.33	8.40	101.61
	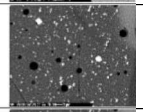	Ty-P-FL-501-Bi	opaque white	LMG	Ca antimoniates	no	EDS area	10.3	1.0	3.2	67.9		1.1	0.7	1.6	4.9			1.2					7.8		
	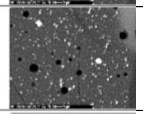	Ty-P-FL-501-Bi	opaque white	LMG	Ca antimoniates	no	EPMA	12.66	0.51	2.40	70.36	0.04	0.47	0.64	1.20	3.48	0.14	0.07	0.63	0.00	0.03	0.04	0.03	5.93	0.31	98.94
	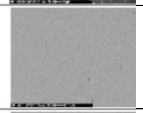	Ty-P-FL-501-BT	transp. dark blue	HMG	no	apatite	EDS area	10.9	2.5	3.1	65.7	2.0	1.1	1.3	2.3	6.8		1.5	2.2	0.3						
	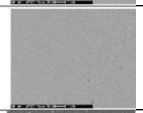	Ty-P-FL-501-BT	transp. dark blue	HMG	no	apatite	EPMA	14.36	2.53	1.90	67.64	1.24	0.16	1.01	1.96	6.32	0.20	0.95	1.46	0.05	0.18	0.02	0.00	0.16	0.05	100.17
	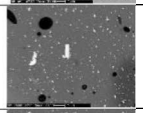	Ty-P-FL-501-G	opaque yellow	LMG	Ca antimoniates, Pb-Sn antimoniates	augite, Fe Ox, Ca-Pb silicate (devitrification phase)	EDS area	9.5	1.2	3.0	56.7	1.0	0.6	0.9	0.9	4.2		0.6	1.8					4.2	14.19	
	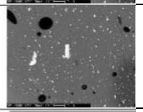	Ty-P-FL-501-G	opaque yellow	LMG	Ca antimoniates, Pb-Sn antimoniates	augite, Fe Ox, Ca-Pb silicate (devitrification phase)	EPMA	13.00	0.77	2.14	64.79	0.22	0.38	0.69	0.96	3.52	0.13	0.27	1.26	0.02	0.13	0.01	0.14	4.15	7.12	99.68
	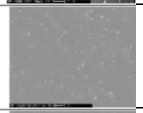	Ty-P-FL-501-R	dull red	HMG	metallic copper	wollastonite, augite	EDS area	8.5	2.0	3.3	46.2	1.5		1.0	1.5	9.0	0.4	0.8	2.6		3.1				18.34	
	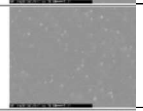	Ty-P-FL-501-R	dull red	HMG	metallic copper	wollastonite, augite	EPMA	12.54	2.37	2.73	53.81	1.05	0.26	0.84	1.39	9.13	0.30	0.39	1.90	0.01	2.15	0.01	0.52	0.25	10.00	99.65
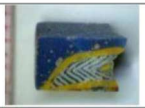	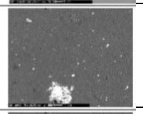	Ty-P-FR-422-B	opaque dark blue	LMG	Ca antimoniates	corundum, pyroxene, SiO_2	EDS area	17.2	1.5	3.6	63.7	0.8		2.6	1.4	4.2		0.3	1.5		0.7			2.2		
	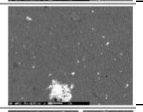	Ty-P-FR-422-B	opaque dark blue	LMG	Ca antimoniates	corundum, pyroxene, SiO_2	EPMA	15.43	0.58	2.20	68.77	0.06	0.35	1.38	0.69	4.46	0.12	0.11	1.28	0.25	0.27	0.01	0.06	1.90	2.41	100.33
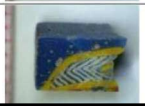	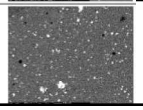	Ty-P-FR-422-Bi	opaque white	LMG	Ca antimoniates	no	EDS area	17.2	4.0	3.4	62.4		0.7	0.9	0.7	6.4			0.4					3.8		

Table VII - Summary

Sample image	SEM-BSE	Sample	Color	Alkali type	Main coloring/ opacifying inclusions	Other inclusions	Analysis Type	Na_2O	MgO	Al_2O_3	SiO_2	P_2O_5	SO_3	Cl	K_2O	CaO	TiO_2	MnO	FeO	CoO	CuO	As_2O_5	SnO_2	Sb_2O_5	PbO	Tot
	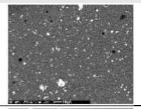	Ty-P-FR-422-Bi	opaque white	LMG	Ca antimoniates	no	EPMA	16.73	5.16	2.00	67.23	0.05	0.28	0.86	0.59	6.19	0.06	0.01	0.34	0.01	0.03	0.06	0.02	2.88	0.03	102.53
	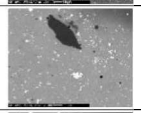	Ty-P-FR-422-G1	opaque yellow	LMG	Pb-Sn antimoniates	Pb-Ca-Na silicates (devitrification phases), SiO_2	EDS area	11.6	1.5	3.4	48.6				0.5	3.6		0.7	2.0					1.4	24.77	
	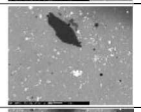	Ty-P-FR-422-G1	opaque yellow	LMG	Pb-Sn antimoniates	Pb-Ca-Na silicates (devitrification phases), SiO_2	EPMA	12.96	0.59	2.11	58.33	0.09	0.21	0.98	0.60	3.88	0.13	0.53	1.78	0.00	0.05	0.03	0.05	0.86	16.04	99.21
	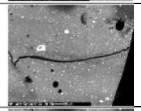	Ty-P-FR-422-G2	opaque yellow	LMG	Pb-Sn antimoniates	ilmenite, labradorite	EDS area	14.4	1.4	3.5	59.7	1.1		1.2	0.7	5.1			1.7					1.1	9.37	
	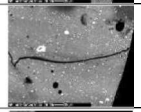	Ty-P-FR-422-G2	opaque yellow	LMG	Pb-Sn antimoniates	ilmenite, labradorite	EPMA	15.04	0.53	2.16	65.90	0.09	0.23	1.14	0.56	5.58	0.10	0.13	1.35	0.01	0.03	0.00	0.01	0.93	6.56	100.35
	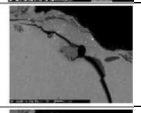	Ty-P-FR-422-R	dull red	HMG	metallic copper	Ca-Pb-Na silicates (devitrification phases), pyroxene, hematite, corundum, epidote	EDS area	13.9	2.4	3.6	51.5	1.6		1.9	1.5	7.6	0.4	0.5	1.6		2.5				10.83	
	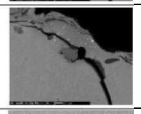	Ty-P-FR-422-R	dull red	HMG	metallic copper	Ca-Pb-Na silicates (devitrification phases), pyroxene, hematite, corundum, epidote	EPMA	14.90	2.37	2.34	56.76	0.81	0.24	1.00	1.48	8.43	0.18	0.35	1.29	0.02	1.76	0.01	0.43	0.33	8.28	100.98
	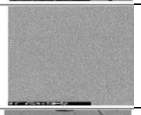	Ty-P-FR-422-T1	true colorless		no	apatite, SiO_2	EPMA	15.99	0.52	2.22	71.22	0.04	0.32	1.41	0.73	5.53	0.09	0.03	1.01	0.04	0.22	0.01	0.01	0.58	0.04	100.01
	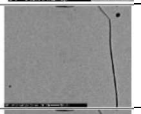	Ty-Pn-B-001	transp. dark blue	LMG	1 small Ca antimoniate	no	EDS area	5.0	1.1	2.6	84.5		1.4	0.8	0.9	1.5		0.6	0.8					0.7		
	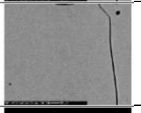	Ty-Pn-B-001	transp. dark blue	LMG	1 small Ca antimoniate	no	EPMA	7.03	0.31	0.80	74.49	0.07	0.56	0.51	0.80	1.09	0.07	0.50	0.59	0.11	0.14	0.02	0.01	0.64	0.16	87.90
		Ty-Pn-T-001	aqua	LMG	no	no	EPMA	17.92	0.92	2.35	66.90	0.31	0.23	1.04	0.97	6.08	0.16	0.16	0.84	0.01	0.00	0.00	0.00	0.51	0.00	98.40
	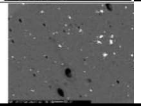	Ty-P-R-414-B	opaque dark blue	LMG	Ca antimoniates	no	EDS area	11.9	1.3	3.7	66.5	0.8	0.8	1.3	1.0	5.6	0.3	0.4	3.1		0.7			2.4		

Table VII - Summary

Sample image	SEM-BSE	Sample	Color	Alkali type	Main coloring/ opacifying inclusions	Other inclusions	Analysis Type	Na_2O	MgO	Al_2O_3	SiO_2	P_2O_5	SO_3	Cl	K_2O	CaO	TiO_2	MnO	FeO	CoO	CuO	As_2O_5	SnO_2	Sb_2O_5	PbO	Tot
	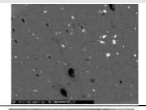	Ty-P-R-414-B	opaque dark blue	LMG	Ca antimoniates	no	EPMA	17.07	0.73	2.87	68.43	0.12	0.24	1.19	0.88	5.22	0.21	0.14	2.52	0.26	0.40	0.02	0.03	2.65	0.27	103.23
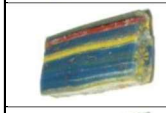	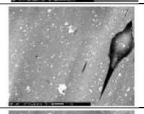	Ty-P-R-414-G	opaque yellow	LMG	Pb-Sn antimoniates	alkali feldspar (probably anorthoclase), Ca-Pb-Na silicates (devitrification phases)	EDS area	8.4	1.1	2.8	55.5			1.2	0.6	4.1			1.8					0.8	21.83	
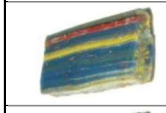	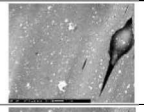	Ty-P-R-414-G	opaque yellow	LMG	Pb-Sn antimoniates	alkali feldspar (probably anorthoclase), Ca-Pb-Na silicates (devitrification phases)	EDS points (DG)	2.8	0.8	2.4	60.7			1.6	0.6	5.4			1.5					0.5	21.87	
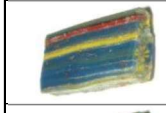	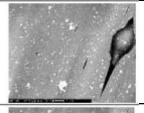	Ty-P-R-414-G	opaque yellow	LMG	Pb-Sn antimoniates	alkali feldspar (probably anorthoclase), Ca-Pb-Na silicates (devitrification phases)	EDS points (LG)	2.4	0.7	2.2	52.5			1.1	0.4	4.6			2.5					0.7	30.41	
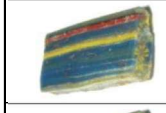	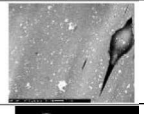	Ty-P-R-414-G	opaque yellow	LMG	Pb-Sn antimoniates	alkali feldspar (probably anorthoclase), Ca-Pb-Na silicates (devitrification phases)	EPMA	13.64	0.39	1.87	62.36	0.03	0.20	1.11	0.52	4.12	0.09	0.15	1.33	0.03	0.05	0.01	0.05	1.07	12.44	99.45
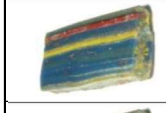	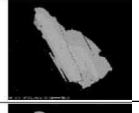	Ty-P-R-414-T	true colorless	LMG	no	no	EDS area	13.0	1.1	3.2	71.7		0.5	1.4	0.8	7.5			0.6							
		Ty-P-R-414-T	true colorless	LMG	no	no	EPMA	16.98	0.53	2.09	70.76	0.04	0.31	1.34	0.66	7.18	0.08	0.03	0.37	0.01	0.04	0.00	0.00	0.81	0.00	101.23
	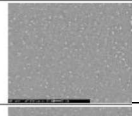	Ty-P-R-419-Ar	yellowish-orange	LMG	cuprite	wollastonite	EDS area	8.2	2.3	3.8	36.1	1.7		0.6	0.9	6.1	0.3	0.5	1.9		7.9		1.3		26.29	
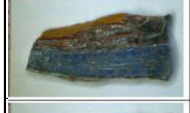	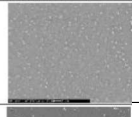	Ty-P-R-419-Ar	yellowish-orange	LMG	cuprite	wollastonite	EPMA	10.79	1.76	2.93	44.14	0.66	0.23	0.46	1.09	7.36	0.24	0.24	1.83	0.03	6.31	0.03	0.80	0.48	19.33	98.70
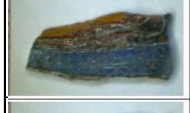	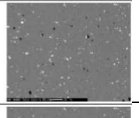	Ty-P-R-419-BO	opaque dark blue	LMG	Ca antimoniates	no	EDS area	15.4	1.9	4.3	64.4		1.1	1.3	0.9	5.0			2.6		0.6			2.3		
	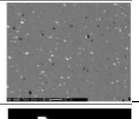	Ty-P-R-419-BO	blue	LMG	Ca antimoniates	no	EPMA	16.42	0.68	2.74	64.28	0.09	0.24	1.19	0.90	5.18	0.18	0.13	2.47	0.21	0.45	0.04	0.01	2.72	0.16	98.07
	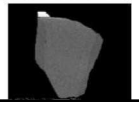	Ty-P-R-419-BT	transp. dark blue	LMG	no	no	EDS area	16.0	1.6	3.8	67.3		0.7	1.4	0.7	5.2			1.1	0.2	0.9			0.8		

Table VII - Summary

Sample image	SEM-BSE	Sample	Color	Alkali type	Main coloring/ opacifying inclusions	Other inclusions	Analysis Type	Na_2O	MgO	Al_2O_3	SiO_2	P_2O_5	SO_3	Cl	K_2O	CaO	TiO_2	MnO	FeO	CoO	CuO	As_2O_5	SnO_2	Sb_2O_5	PbO	Tot
	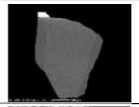	Ty-P-R-419-BT	transp. dark blue	LMG	no	no	EPMA	17.30	0.47	2.15	69.17	0.05	0.28	1.43	0.66	5.42	0.08	0.02	1.03	0.05	0.63	0.00	0.01	0.54	0.11	99.41
	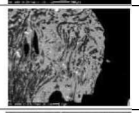	Ty-P-R-419-G	opaque yellow	LMG	Pb-Sn antimoniates	alkali feldspar, SiO_2	EPMA	1.07	0.37	1.74	65.82	0.03	0.19	1.36	0.74	4.04	0.09	0.18	1.33	0.01	0.03	0.01	0.04	1.11	12.88	91.03
	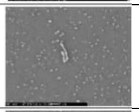	Ty-P-R-419-R	sealing-wax red	LMG	cuprite	wollastonite, corundum, Fe oxides	EDS area	8.7	2.2	3.7	36.6	1.8		0.6	0.7	6.1	0.3	0.4	1.9		6.2		1.3		27.35	
	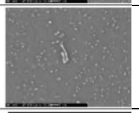	Ty-P-R-419-R	sealing-wax red	LMG	cuprite	wollastonite, corundum, Fe oxides	EPMA	11.27	1.84	2.99	44.27	0.64	0.24	0.48	1.06	7.18	0.24	0.23	1.87	0.00	6.19	0.05	0.80	0.50	19.93	99.78
	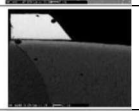	Ty-P-R-419-VT	transp. green	LMG	no	no	EPMA	12.31	1.78	2.95	44.90	0.62	0.25	0.45	0.76	7.34	0.25	0.19	1.79	0.02	4.85	0.02	0.86	0.51	19.35	99.22
		Ty-P-R-423-Ar	yellowish-orange	LMG	cuprite	wollastonite, SiO_2	EDS area	6.7	1.8	3.4	38.6	1.6		0.9	1.2	6.5		0.5	2.7		7.9				25.95	
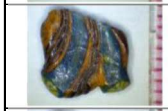	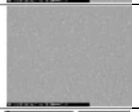	Ty-P-R-423-Ar	yellowish-orange	LMG	cuprite	wollastonite, SiO_2	EPMA	11.55	1.61	2.80	45.93	0.67	0.58	0.71	1.10	7.02	0.25	0.28	2.26	0.00	6.87	0.02	0.91	0.46	16.67	99.68
	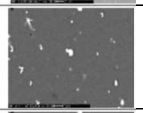	Ty-P-R-423-B	opaque dark blue	LMG	Ca antimoniates	no	EDS area	11.9	1.3	3.7	66.9	0.7	0.9	1.3	1.0	5.6			3.1		0.7			2.7		
	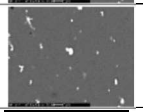	Ty-P-R-423-B	opaque dark blue	LMG	Ca antimoniates	no	EPMA	16.49	0.67	2.63	67.88	0.12	0.23	1.18	1.15	5.15	0.19	0.14	2.41	0.21	0.45	0.04	0.03	2.58	0.23	101.79
	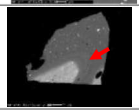	Ty-P-R-423-BT	transp. dark blue	LMG	no	no	EDS area	12.5	1.3	3.5	64.8			1.6	0.8	9.3	0.3		1.6		0.4				3.39	
	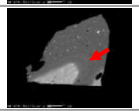	Ty-P-R-423-BT	transp. dark blue	LMG	no	no	EDS points (DG)	5.6	1.4	3.8	70.2			1.9	0.7	10.0	0.2		1.8		0.5				3.32	
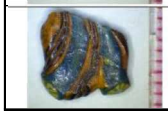	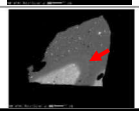	Ty-P-R-423-BT	transp. dark blue	LMG	no	no	EDS points (LG)	5.2	1.1	3.4	68.2			1.8	0.7	11.0	0.4		2.3		0.6				4.62	

Table VII - Summary

Sample image	SEM-BSE	Sample	Color	Alkali type	Main coloring/ opacifying inclusions	Other inclusions	Analysis Type	Na_2O	MgO	Al_2O_3	SiO_2	P_2O_5	SO_3	Cl	K_2O	CaO	TiO_2	MnO	FeO	CoO	CuO	As_2O_5	SnO_2	Sb_2O_5	PbO	Tot
	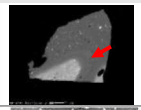	Ty-P-R-423-BT	transp. dark blue	LMG	no	no	EPMA	16.92	0.94	2.60	65.19	0.11	0.18	1.53	0.56	9.16	0.15	0.07	1.27	0.07	0.19	0.00	0.02	0.46	1.74	101.16
	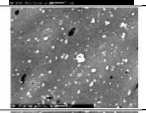	Ty-P-R-423-G	opaque yellow	LMG	Pb-Sn antimoniates	SiO_2	EDS area	8.3	1.2	2.9	56.7			1.3	0.5	3.9		0.3	1.7					0.9	20.46	
	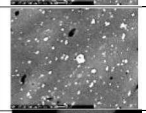	Ty-P-R-423-G	opaque yellow	LMG	Pb-Sn antimoniates	SiO_2	EPMA	13.12	0.35	1.76	64.60	0.05	0.25	1.26	0.52	4.13	0.07	0.15	1.21	0.00	0.08	0.02	0.06	1.05	11.59	100.25
	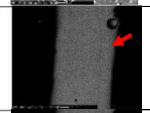	Ty-P-R-423-R	sealing-wax red	LMG	cuprite	no	EDS area	6.5	1.9	3.5	39.8	1.6		1.0	1.5	7.0		0.5	2.8		4.9				26.89	
	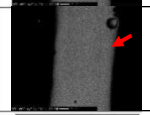	Ty-P-R-423-R	sealing-wax red	LMG	cuprite	no	EPMA	12.41	1.60	2.85	46.93	0.64	0.43	0.68	1.23	7.25	0.31	0.27	2.46	0.01	5.09	0.06	0.93	0.46	17.05	100.65
	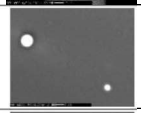	Ty-P-R-423-VT	transp. green	HMG	metallic copper, Cu and Pb sulfides	P-Ca-Na silicates (devitrification phases)	EDS area	12.0	3.7	3.6	61.6	2.5	0.9	1.3	2.3	8.8	0.3	0.5	1.9		0.5					
	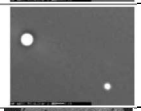	Ty-P-R-423-VT	transp. green	HMG	metallic copper, Cu and Pb sulfides	P-Ca-Na silicates (devitrification phases)	EPMA	17.19	4.19	2.44	62.52	1.74	0.34	1.15	2.12	8.51	0.22	0.33	1.40	0.02	0.13	0.04	0.00	0.09	0.08	102.50
	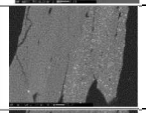	Ty-P-St-415-B	opque dark blue	LMG	few Ca antimoniates	no	EDS area	15.9	1.2	3.1	67.1			1.3	0.6	3.1			2.0	0.5	0.6			3.0	1.22	
	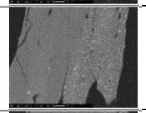	Ty-P-St-415-B	opque dark blue	LMG	few Ca antimoniates	no	EPMA	14.76	0.62	1.77	69.21	0.05	0.28	1.27	0.68	3.67	0.17	0.05	1.90	0.30	0.42	0.05	0.05	3.75	0.94	99.93
	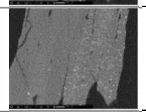	Ty-P-St-415-Bi	opaque white	LMG	Ca antimoniates	no	EDS area	4.2	1.5	4.0	73.1	0.8	1.2	0.7	2.0	4.3			1.0					7.0		
	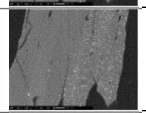	Ty-P-St-415-Bi	opaque white	LMG	Ca antimoniates	no	EPMA	11.43	0.52	2.48	70.34	0.07	0.27	0.62	0.93	3.63	0.14	0.08	0.72	0.01	0.02	0.02	0.03	6.26	0.26	97.83
	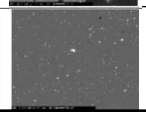	Ty-P-StB-002	opaque dark blue	LMG	Ca antimoniates	no	EDS area	11.1	1.4	3.7	65.0			0.6	0.9	8.4		1.2	2.4		0.9			2.6	1.52	

Table VII - Summary

Sample image	SEM-BSE	Sample	Color	Alkali type	Main coloring/ opacifying inclusions	Other inclusions	Analysis Type	Na_2O	MgO	Al_2O_3	SiO_2	P_2O_5	SO_3	Cl	K_2O	CaO	TiO_2	MnO	FeO	CoO	CuO	As_2O_5	SnO_2	Sb_2O_5	PbO	Tot
	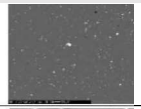	Ty-P-StB-002	opaque dark blue	LMG	Ca antimoniates	no	EPMA	13.22	0.89	2.51	66.46	0.19	0.43	0.46	0.90	7.37	0.08	0.94	2.22	0.36	0.50	0.03	0.04	3.62	0.83	101.06
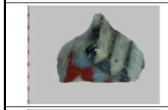	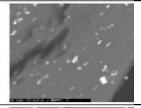	Ty-P-T-417-Bi	opaque white	LMG	Ca antimoniates	no	EDS area	11.7	1.2	3.6	67.7	0.8		0.9	1.7	4.8			0.8					5.2	1.43	
	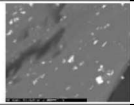	Ty-P-T-417-Bi	opaque white	LMG	Ca antimoniates	no	EPMA	14.90	0.62	2.47	69.93	0.07	0.26	0.82	1.77	4.46	0.11	0.11	0.56	0.00	0.01	0.02	0.04	4.80	0.81	101.77
	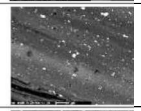	Ty-P-T-417-BO	opaque dark blue	LMG	Ca antimoniates	combeite	EDS area	12.2	1.4	3.5	61.3	1.0	1.1	0.9	0.7	5.3		0.7	1.1					4.2	5.92	
	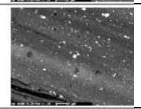	Ty-P-T-417-BO	opaque dark blue	LMG	Ca antimoniates	combeite	EDS points (DG)	5.3	1.0	2.7	64.0	0.7	0.4	1.4	1.3	7.3		1.1	1.7					4.8	7.43	
	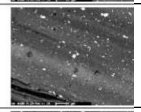	Ty-P-T-417-BO	opaque dark blue	LMG	Ca antimoniates	combeite	EDS points (LG)	4.6	0.8	2.7	56.7	0.5	1.1	0.9	0.6	5.8		1.1	1.8					3.3	18.54	
	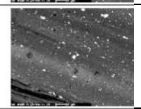	Ty-P-T-417-BO	opaque dark blue	LMG	Ca antimoniates	combeite	EPMA	14.85	0.72	2.19	64.88	0.10	0.42	0.88	1.01	5.36	0.09	0.41	0.93	0.08	0.90	0.00	0.06	5.43	4.72	103.03
	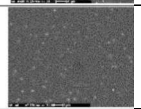	Ty-P-T-417-R	dull red	HMG	metallic copper, Cu sulfides	no	EDS area	13.0	2.1	3.9	55.2	1.4	0.9	1.3	1.1	8.3		0.6	1.8		2.4				7.21	
	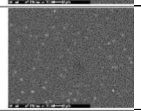	Ty-P-T-417-R	dull red	HMG	metallic copper, Cu sulfides	no	EPMA	16.78	1.91	3.06	59.67	0.60	0.26	1.19	1.01	8.39	0.26	0.56	1.68	0.04	1.63	0.00	0.26	0.48	4.16	101.95
	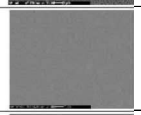	Ty-P-T-417-VT	transp. green	LMG	no	no	EDS area	13.2	4.1	2.3	60.5	2.3	0.8	1.1	2.0	10.4		1.3	1.7							
	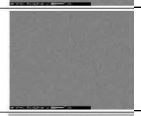	Ty-P-T-417-VT	transp. green	LMG	no	no	EPMA	16.89	4.61	1.02	60.67	1.73	0.24	0.97	1.81	9.99	0.05	0.95	1.37	0.01	0.02	0.00	0.00	0.11	0.02	100.45
		Ty-P-V-423-Ar	yellowish-orange	LMG	cuprite	wollastonite	EDS area	9.8	2.0	3.1	34.8	2.0		0.9	1.6	4.9			1.9		8.6			30.3		

Table VII - Summary

Sample image	SEM-BSE	Sample	Color	Alkali type	Main coloring/ opacifying inclusions	Other inclusions	Analysis Type	Na_2O	MgO	Al_2O_3	SiO_2	P_2O_5	SO_3	Cl	K_2O	CaO	TiO_2	MnO	FeO	CoO	CuO	As_2O_5	SnO_2	Sb_2O_5	PbO	Tot
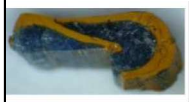		Ty-P-V-423-Ar	yellowish-orange	LMG	cuprite	wollastonite	EPMA																				
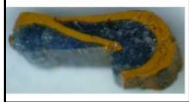	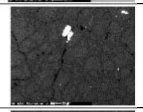	Ty-P-V-423-B	blue	LMG	Ca and Ca-Na antimoniates	no	EDS area	12.4	1.6	3.9	68.7	0.9	1.1	1.4	1.5	3.9			1.9					2.2		
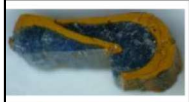	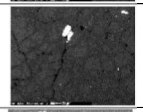	Ty-P-V-423-B	blue	LMG	Ca and Ca-Na antimoniates	no	EPMA																				
	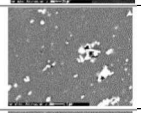	Ty-S-423a-A	opaque light blue	LMG	Ca and Ca-Na antimoniates	no	EDS area	15.0	1.3	3.7	62.5	0.6	0.9	1.5	0.5	4.8			0.6		4.3			4.0		
	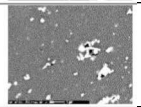	Ty-S-423a-A	opaque light blue	LMG	Ca and Ca-Na antimoniates	no	EPMA	13.56	0.41	1.81	68.06	0.40	0.05	1.55	0.86	4.68	0.04	0.04	0.30	0.01	3.80	0.02	0.24	1.57	0.01	97.48
	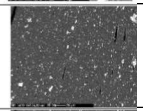	Ty-S-423a-Bi	opaque white	LMG	Ca antimoniates	no	EDS area	14.5	3.8	3.1	65.3	0.7		0.9	0.6	7.9			0.2					2.7		
	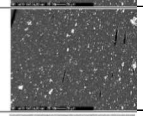	Ty-S-423a-Bi	opaque white	LMG	Ca antimoniates	no	EPMA	16.26	4.98	1.85	66.98	0.33	0.03	0.80	0.60	6.23	0.07	0.06	0.32	0.02	0.08	0.04	0.02	2.87	0.01	101.60
	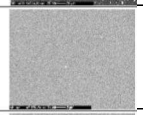	Ty-S-423a-R	dull red	HMG	metallic copper	Na-feldspar (probably albite), Fe oxides, SiO_2	EDS area	11.5	2.8	3.7	49.7			1.2	2.0	7.7			1.7		2.1				16.07	
		Ty-S-423a-R	dull red	HMG	metallic copper	Na-feldspar (probably albite), Fe oxides, SiO_2	EPMA	13.85	2.67	1.90	53.88	0.23	0.96	0.89	1.76	7.74	0.14	0.27	1.11	0.01	1.33	0.02	0.49	0.22	10.92	98.46
	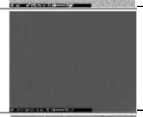	Ty-S-423a-T	true colorless	LMG	no	no	EPMA	15.06	0.47	2.07	69.97	0.38	0.04	1.35	0.82	5.24	0.09	0.02	0.84	0.05	0.44	0.02	0.00	0.57	0.12	97.53
	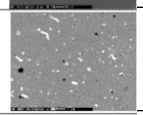	Ty-S-ARG-403-A	opaque light blue	LMG	Ca antimoniates	no	EDS area	16.1	1.3	3.9	61.6	1.0	1.4	1.7	0.7	2.7			0.7		3.5			5.0		
	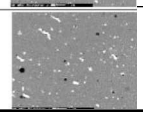	Ty-S-ARG-403-A	opaque light blue	LMG	Ca antimoniates	no	EPMA	15.55	0.48	2.20	69.00	0.07	0.30	1.56	0.49	4.72	0.07	0.03	0.52	0.00	3.36	0.02	0.14	1.84	0.20	100.56

Table VII - Summary

Sample image	SEM-BSE	Sample	Color	Alkali type	Main coloring/ opacifying inclusions	Other inclusions	Analysis Type	Na_2O	MgO	Al_2O_3	SiO_2	P_2O_5	SO_3	Cl	K_2O	CaO	TiO_2	MnO	FeO	CoO	CuO	As_2O_5	SnO_2	Sb_2O_5	PbO	Tot
	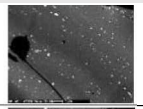	Ty-S-ARG-403-G	opaque yellow	LMG	Pb antimoniates	SiO_2	EDS area mix	12.8	1.6	4.0	60.0			1.3	0.7	5.8			1.7					0.2	9.97	
	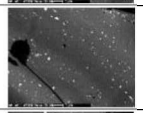	Ty-S-ARG-403-G	opaque yellow	LMG	Pb antimoniates and Pb silicates	SiO_2	EDS points (DG)	9.2	1.6	4.1	67.0			1.5	0.8	6.6			1.5		0.4			0.1	6.39	
	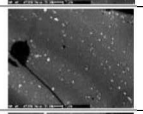	Ty-S-ARG-403-G	opaque yellow	LMG	Pb antimoniates and Pb silicates	SiO_2	EDS points (LG)	7.4	1.6	4.0	62.0			1.4	0.8	5.6			2.2		0.6			0.2	12.83	
	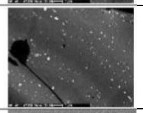	Ty-S-ARG-403-G	opaque yellow	LMG	Pb antimoniates and Pb silicates	no	EPMA	11.82	0.53	2.12	69.85	0.05	0.30	1.19	0.49	5.80	0.08	0.14	1.24	0.01	0.05	0.01	0.01	0.92	5.34	99.94
	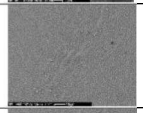	Ty-S-ArG-506-Ar	yellowish-orange	LMG	cuprite, 1 small Pb antimoniate	no	EDS area	10.1	2.6	4.2	42.8	2.6		1.6	0.9	4.9	0.3	0.4	1.5		6.3				20.21	
	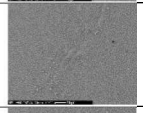	Ty-S-ArG-506-Ar	yellowish-orange	LMG	cuprite, 1 small Pb antimoniate	no	EDS points (DG)	6.0	2.7	4.3	45.4	2.5		1.6	1.0	5.4	0.3	0.3	1.7		4.7				22.20	
	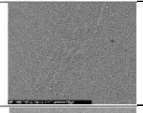	Ty-S-ArG-506-Ar	yellowish-orange	LMG	cuprite, 1 small Pb antimoniate	no	EDS points (LG)	6.2	2.7	4.2	44.3	2.7		1.7	0.9	5.2	0.3	0.4	1.6		5.3				22.49	
	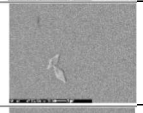	Ty-S-ArG-506-Ar	yellowish-orange	LMG	cuprite	malayaite	EPMA	10.97	1.39	1.99	40.47	0.52	0.32	1.10	0.91	5.22	0.23	0.16	1.65	0.01	7.93	0.03	0.91	0.38	27.73	101.92
	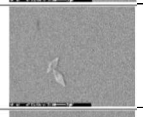	Ty-S-ArG-506-G	yellowish-orange	LMG	cuprite	malayaite	EDS area	10.7	2.9	4.1	44.3	2.5		1.2	1.1	5.3		0.6	1.3		7.1				17.27	
	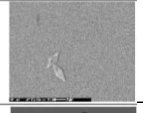	Ty-S-ArG-506-G	yellowish-orange	LMG	cuprite	malayaite	EPMA	11.12	1.81	1.97	40.93	0.76	0.40	0.76	1.08	5.53	0.19	0.42	1.52	0.01	9.25	0.03	1.24	0.57	22.69	100.26
	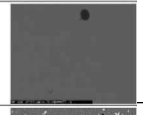	Ty-Sb-B-003	transp. dark blue	LMG	no	no	EPMA	13.18	0.66	2.11	71.55	0.23	0.09	0.80	0.66	8.40	0.08	0.58	0.32	0.15	0.04	0.01	0.04	0.03	0.13	99.03
	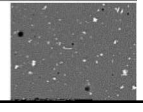	Ty-S-BB-004-BO	opaque dark blue	LMG	Ca and Ca-Na antimoniates	no	EDS area	14.1	1.3	4.0	62.9	1.1	1.3	1.4	1.3	4.1	1.0		2.7	0.5	0.7			3.5		

Table VII - Summary

Sample image	SEM-BSE	Sample	Color	Alkali type	Main coloring/ opacifying inclusions	Other inclusions	Analysis Type	Na_2O	MgO	Al_2O_3	SiO_2	P_2O_5	SO_3	Cl	K_2O	CaO	TiO_2	MnO	FeO	CoO	CuO	As_2O_5	SnO_2	Sb_2O_5	PbO	Tot
	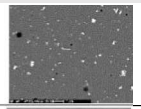	Ty-S-BB-004-BO	opaque dark blue	LMG	Ca and Ca-Na antimoniates	no	EPMA	15.54	0.69	2.60	67.89	0.09	0.19	1.19	0.87	5.21	0.19	0.13	2.33	0.20	0.41	0.05	0.03	2.55	0.32	100.49
		Ty-S-BB-004-BT	transp. dark blue	LMG	no	no	EPMA	13.65	0.53	2.13	69.98	0.06	0.35	1.68	0.66	6.09	0.08	0.04	0.99	0.15	0.23	0.01	0.01	0.82	0.10	97.55
	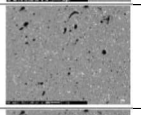	Ty-S-BBi-004-Bi	opaque white	LMG	Ca and Ca-Na antimoniates	no	EDS area	13.8	1.5	3.6	66.2		1.7	1.0	0.6	4.2		0.7	0.8					4.3	1.40	
	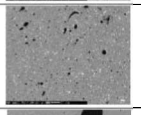	Ty-S-BBi-004-Bi	opaque white	LMG	Ca and Ca-Na antimoniates	no	EPMA	14.34	0.60	1.65	71.57	0.07	0.31	0.89	0.71	3.82	0.19	0.44	0.60	0.03	0.03	0.00	0.03	4.16	0.72	100.17
	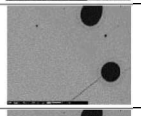	Ty-S-BBi-004-BT	transp. dark blue	LMG	no	no	EDS area	15.4	1.7	3.7	66.0		1.0	1.3	0.7	4.2		1.6	2.0	0.7	1.0					
	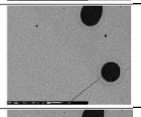	Ty-S-BBi-004-BT	transp. dark blue	LMG	no	no	EDS points (DG)	9.5	1.5	3.6	73.1		0.6	1.5	0.5	4.6	0.2	1.3	2.4		0.6				0.15	
	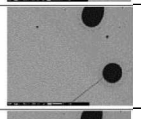	Ty-S-BBi-004-BT	transp. dark blue	LMG	no	no	EDS points (LG)	10.9	1.7	3.9	69.3		1.0	1.4	0.8	5.3	0.4	1.8	1.8	0.3	1.2					
	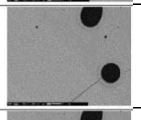	Ty-S-BBi-004-BT	transp. dark blue	LMG	no	no	EPMA	16.53	0.54	1.61	71.34	0.02	0.25	1.32	0.41	4.29	0.16	0.91	1.66	0.26	0.37	0.00	0.00	0.02	0.03	99.74
	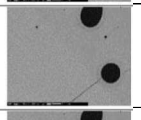	Ty-S-BBi-004-BTc	transp. dark blue	LMG	no	no	EPMA (LG)	16.01	0.50	1.66	73.19	0.04	0.17	1.43	0.38	4.26	0.12	0.73	1.85	0.10	0.15	0.03	0.02	0.00	0.00	100.65
	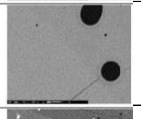	Ty-S-BBi-004-BTs	transp. dark blue	LMG	no	no	EPMA (DG)	17.71	0.78	1.77	68.49	0.05	0.38	1.17	0.58	4.75	0.16	1.33	1.44	0.55	0.90	0.01	0.01	0.13	0.04	100.24
	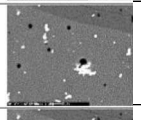	Ty-S-BiBR-404-B	opaque dark blue	LMG	Ca antimoniates	no	EDS area	13.8	1.2	3.7	65.5	0.8	1.0	1.3	0.8	5.4			2.9		0.8			2.6		
	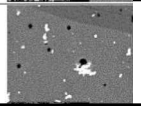	Ty-S-BiBR-404-B	opaque dark blue	LMG	Ca antimoniates	no	EPMA	17.31	0.71	2.75	67.24	0.11	0.23	1.21	0.87	5.16	0.21	0.13	2.47	0.25	0.46	0.01	0.01	2.67	0.20	102.02

Table VII - Summary

Sample image	SEM-BSE	Sample	Color	Alkali type	Main coloring/ opacifying inclusions	Other inclusions	Analysis Type	Na_2O	MgO	Al_2O_3	SiO_2	P_2O_5	SO_3	Cl	K_2O	CaO	TiO_2	MnO	FeO	CoO	CuO	As_2O_5	SnO_2	Sb_2O_5	PbO	Tot
	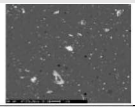	Ty-S-BiBR-404-Bi	opaque white	LMG	Ca antimoniates	no	EDS area	12.1	4.3	3.3	66.3		0.8	0.9	0.6	7.1			0.6					3.8		
	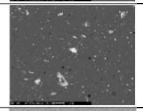	Ty-S-BiBR-404-Bi	opaque white	LMG	Ca antimoniates	no	EPMA	16.98	5.05	1.99	66.77	0.04	0.28	0.85	0.56	6.25	0.09	0.02	0.39	0.01	0.01	0.05	0.01	3.00	0.01	102.34
	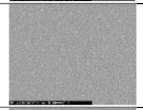	Ty-S-BiBR-404-R	dull red	HMG	metallic copper	pyroxene	EDS area	9.1	2.6	3.5	52.5	2.0		1.3	1.9	8.2		0.6	1.8		2.8				12.51	
	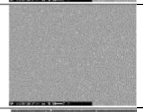	Ty-S-BiBR-404-R	dull red	HMG	metallic copper	pyroxene	EPMA	14.74	2.37	2.33	56.72	0.82	0.21	0.97	1.61	8.37	0.19	0.39	1.45	0.01	2.22	0.00	0.41	0.33	7.92	101.06
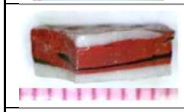	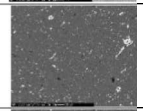	Ty-S-BiBR-507-Bi	opaque white	LMG	Ca antimoniates	no	EDS area	16.6	3.5	3.0	63.4		0.8	0.9	0.6	6.7			0.5					4.0		
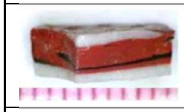	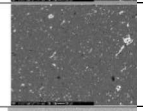	Ty-S-BiBR-507-Bi	opaque white	LMG	Ca antimoniates	no	EPMA	16.53	5.01	1.95	67.19	0.04	0.27	0.85	0.52	6.23	0.05	0.01	0.39	0.01	0.04	0.03	0.01	2.86	0.04	102.04
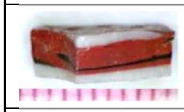	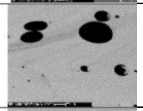	Ty-S-BiBR-507-R	dull red	HMG	metallic copper, Cu sulfides	wollastonite	EDS area	9.4	2.9	3.4	48.8	2.2		1.4	2.0	7.3		0.7	2.0		2.2				16.25	
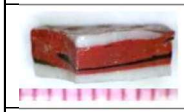	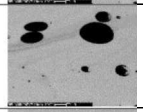	Ty-S-BiBR-507-R	dull red	HMG	metallic copper, Cu sulfides	wollastonite	EDS points (DG)	4.1	2.2	2.8	48.5	1.4		1.2	1.7	9.0		0.8	2.8		1.8				21.92	
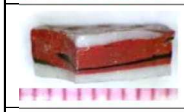	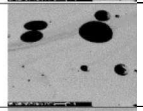	Ty-S-BiBR-507-R	dull red	HMG	metallic copper, Cu sulfides	wollastonite	EDS points (LG)	4.4	2.5	3.1	48.6	1.7		1.3	1.8	8.2		0.8	2.4		2.6				20.76	
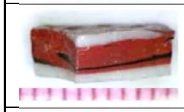	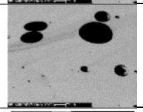	Ty-S-BiBR-507-R	dull red	HMG	metallic copper, Cu sulfides	wollastonite	EPMA	14.11	2.83	2.08	54.15	1.10	0.18	1.06	1.70	7.88	0.19	0.42	1.57	0.02	1.62	0.00	0.46	0.25	9.90	99.49
	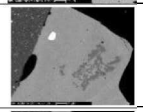	Ty-S-BiBR-507-VT	transp. green	HMG	metallic copper, Cu sulfides	wollastonite	EDS area	13.0	2.8	3.4	50.1	2.1		1.4	2.0	8.0		0.7	1.8		0.6				12.90	
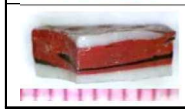	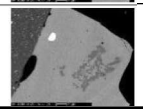	Ty-S-BiBR-507-VT	transp. green	HMG	metallic copper, Cu sulfides	wollastonite	EDS points (LG)	6.2	1.9	2.7	48.0	1.4		1.2	1.9	9.6		1.0	2.8		1.2				20.26	

Table VII - Summary

Sample image	SEM-BSE	Sample	Color	Alkali type	Main coloring/ opacifying inclusions	Other inclusions	Analysis Type	Na_2O	MgO	Al_2O_3	SiO_2	P_2O_5	SO_3	Cl	K_2O	CaO	TiO_2	MnO	FeO	CoO	CuO	As_2O_5	SnO_2	Sb_2O_5	PbO	Tot
	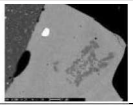	Ty-S-BiBR-507-VT	transp. green	HMG	metallic copper, Cu sulfides	wollastonite	EPMA	14.54	3.11	1.97	56.69	1.14	0.15	1.01	1.77	8.64	0.18	0.43	1.61	0.01	0.30	0.00	0.32	0.21	8.55	100.62
	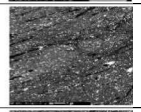	Ty-S-BiR-507-Bi	opaque white	LMG	Na and Na-Ca antimoniates	no	EDS area	11.6	1.5	3.6	67.5		1.3	1.8	0.8	6.2			1.0					4.8		
	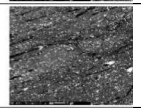	Ty-S-BiR-507-Bi	opaque white	LMG	Na and Na-Ca antimoniates	no	EPMA	8.67	0.71	2.22	67.12	0.06	0.44	1.66	0.75	6.14	0.13	0.02	0.65	0.01	0.01	0.01	0.03	3.37	0.03	92.02
		Ty-S-BiR-507-R	dull red	HMG	metallic copper	no	EDS area	9.5	2.7	3.5	55.1	1.9		1.2	2.2	8.1		0.7	2.0		2.2				9.92	
		Ty-S-BiR-507-R	dull red	HMG	metallic copper	no	EPMA	13.79	2.62	2.38	57.20	1.14	0.23	1.00	2.07	8.18	0.18	0.46	1.42	0.01	1.71	0.01	0.40	0.39	8.34	101.53
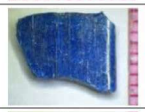	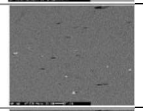	Ty-S-BT-004-BO	opaque dark blue	LMG	Ca and Ca-Na antimoniates	plagioclase (probably albite), Fe oxide	EDS area	13.9	1.1	3.5	68.5		1.2	1.5	0.7	4.8			2.0					2.4		
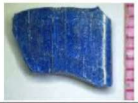	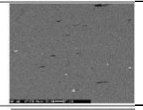	Ty-S-BT-004-BO	opaque dark blue	LMG	Ca and Ca-Na antimoniates	plagioclase (probably albite), Fe oxide	EPMA	15.92	0.55	2.39	68.02	0.03	0.28	1.20	0.56	4.13	0.15	0.05	1.51	0.16	0.35	0.03	0.02	2.90	0.51	98.74
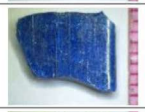	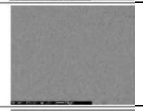	Ty-S-BT-004-BT	trans. dark blue	LMG	no	no	EDS area	13.8	0.9	3.1	69.8		0.8	1.8	0.9	6.6			1.2		0.7					
	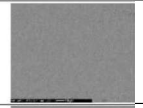	Ty-S-BT-004-BT	trans. dark blue	LMG	no	no	EPMA	14.18	0.53	2.29	69.82	0.07	0.36	1.60	0.65	6.03	0.09	0.02	1.05	0.18	0.17	0.02	0.02	0.84	0.14	98.07
		Ty-S-BT-004-T	true colorless	LMG	no	no	EDS area	10.3	1.1	3.3	75.2		1.0	2.0	1.0	5.8										
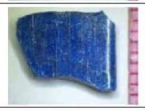	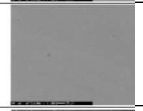	Ty-S-BT-004-T	true colorless	LMG	no	no	EPMA	8.79	0.36	1.99	71.92	0.05	0.28	1.80	1.19	4.87	0.06	0.01	0.24	0.01	0.01	0.02	0.01	0.75	0.06	92.43
	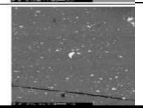	Ty-S-BTW-004-Bi	opaque white	LMG	Ca and Ca-Pb antimoniates	no	EDS area	8.1	1.4	3.1	53.7	1.1		1.0	0.3	4.2		0.9	1.1					4.4	19.12	

Table VII - Summary

Sample image	SEM-BSE	Sample	Color	Alkali type	Main coloring/ opacifying inclusions	Other inclusions	Analysis Type	Na_2O	MgO	Al_2O_3	SiO_2	P_2O_5	SO_3	Cl	K_2O	CaO	TiO_2	MnO	FeO	CoO	CuO	As_2O_5	SnO_2	Sb_2O_5	PbO	Tot
	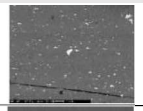	Ty-S-BTW-004-Bi	opaque white	LMG	Ca and Ca-Pb antimoniates	no	EPMA	11.67	0.74	2.00	60.07	0.19	0.29	0.68	0.64	4.03	0.19	0.70	0.83	0.04	0.06	0.03	0.18	5.24	12.55	100.12
		Ty-S-BTW-004-BT	transp. dark blue	LMG	no	no	EDS area	12.1	1.4	3.3	71.7		0.9	1.7	0.8	3.3		1.3	1.9	0.5	0.7					
		Ty-S-BTW-004-BT	transp. dark blue	LMG	no	no	EPMA	14.23	0.64	1.89	71.01	0.06	0.28	1.55	0.84	3.26	0.24	1.01	1.50	0.33	0.42	0.01	0.02	0.24	0.00	97.52
		Ty-S-BTW-004-W	transp. dark blue (altered)	LMG	no	no	EPMA	0.23	0.62	1.82	76.10	0.05	0.32	1.88	0.64	3.30	0.28	1.10	1.59	0.35	0.34	0.01	0.01	0.19	0.02	88.84
	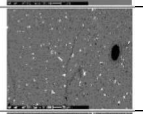	Ty-S-GA-005-A	opaque light blue	LMG	Ca antimoniates	no	EDS area	16.3	1.5	3.4	64.1		1.2	0.9	0.6	5.4			0.8		2.5			3.2		
	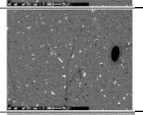	Ty-S-GA-005-A	opaque light blue	LMG	Ca antimoniates	no	EPMA	16.05	0.42	1.83	70.51	0.04	0.18	1.25	0.36	4.50	0.07	0.04	0.86	0.02	2.64	0.27	0.20	1.99	0.39	101.62
	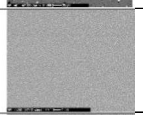	Ty-S-GA-005-Ar	yellowish-orange	LMG	cuprite	malayaite, cassiterite, wollastonite, SiO_2	EDS area	8.2	2.0	2.9	34.7	1.3		0.8	1.8	4.6		0.6	1.7		8.7				30.23	
		Ty-S-GA-005-Ar	yellowish-orange	LMG	cuprite	malayaite, cassiterite, wollastonite, SiO_2	EDS points (DG)	5.3	2.2	3.5	39.4	1.1		0.7	1.3	7.0		0.7	2.1		8.5				26.11	
	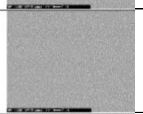	Ty-S-GA-005-Ar	yellowish-orange	LMG	cuprite	malayaite, cassiterite, wollastonite, SiO_2	EDS points (LG)	4.1	1.9	2.9	34.1	1.5		0.6	1.3	4.4		0.3	1.8		6.8				37.40	
		Ty-S-GA-005-Ar	yellowish-orange	LMG	cuprite	malayaite, cassiterite, wollastonite, SiO_2	EPMA	11.76	1.80	2.07	41.94	0.70	0.26	0.77	1.10	5.39	0.16	0.44	1.52	0.01	9.14	0.01	1.23	0.37	22.29	100.95
		Ty-S-GA-005-ArC	yellowish-orange	LMG	cuprite	malayaite, cassiterite, wollastonite, SiO_2	EPMA (LG)	12.67	2.06	2.93	45.15	0.66	0.22	0.78	0.84	7.93	0.29	0.68	1.85	0.03	8.11	0.05	0.80	0.17	17.29	102.49
		Ty-S-GA-005-ArS	yellowish-orange	LMG	cuprite	malayaite, cassiterite, wollastonite, SiO_2	EPMA (DG)	11.31	1.39	2.10	41.00	0.49	0.25	1.18	0.90	5.25	0.22	0.16	1.68	0.03	7.02	0.02	0.93	0.38	27.72	102.02

Table VII - Summary

Sample image	SEM-BSE	Sample	Color	Alkali type	Main coloring/ opacifying inclusions	Other inclusions	Analysis Type	Na_2O	MgO	Al_2O_3	SiO_2	P_2O_5	SO_3	Cl	K_2O	CaO	TiO_2	MnO	FeO	CoO	CuO	As_2O_5	SnO_2	Sb_2O_5	PbO	Tot
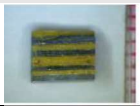	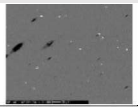	Ty-S-GA-411-A	opaque dark blue	LMG	Ca antimoniates	no	EDS area	10.8	1.5	4.0	70.0	0.9	0.8	0.9		8.1		0.4	0.4		0.1			1.3		
	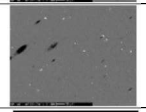	Ty-S-GA-411-A	opaque dark blue	LMG	Ca antimoniates	no	EPMA	14.78	0.60	2.52	69.45	0.20	0.23	0.85	0.64	8.02	0.07	0.33	0.79	0.06	0.06	0.01	0.01	2.26	0.07	100.94
	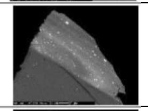	Ty-S-GA-411-G	opaque yellow	LMG	Pb antimoniates	no	EDS area	10.9	1.6	3.6	63.3			1.2	0.6	5.3			2.1					0.7	9.62	
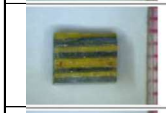	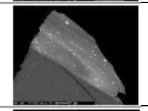	Ty-S-GA-411-G	opaque yellow	LMG	Pb antimoniates	no	EDS points (DG)	5.0	1.4	3.5	71.8			1.4	0.5	6.9			0.8					0.2	7.67	
	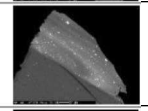	Ty-S-GA-411-G	opaque yellow	LMG	Pb antimoniates	no	EDS points (LG)	4.0	1.2	3.1	63.7			1.2	0.6	6.1			2.8					0.6	15.28	
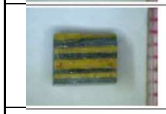	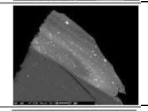	Ty-S-GA-411-G	opaque yellow	LMG	Pb antimoniates	no	EPMA	13.96	0.52	2.06	66.28	0.05	0.27	1.15	0.55	5.77	0.14	0.11	1.15	0.01	0.01	0.02	0.00	0.90	7.84	100.81
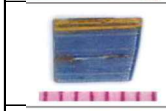	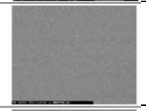	Ty-S-GB-413-Ar	yellowish-orange	LMG	cuprite	no	EDS area	7.1	2.1	3.7	39.4	1.9		1.4	1.3	6.3		0.2	2.5		8.0				24.36	
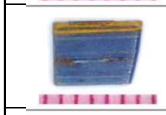		Ty-S-GB-413-Ar	yellowish-orange	LMG	cuprite	no	EPMA	11.83	1.64	2.95	44.98	0.66	0.32	0.71	1.07	7.06	0.21	0.26	2.40	0.01	6.86	0.06	0.92	0.42	18.18	100.54
	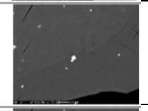	Ty-S-GB-413-B	opaque dark blue	LMG	Na and Na-Ca antimoniates	no	EDS area	13.7	1.5	4.0	68.3		1.0	1.5	0.6	3.2			2.3		0.8			2.8		
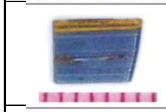	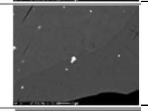	Ty-S-GB-413-B	opaque dark blue	LMG	Na and Na-Ca antimoniates	no	EPMA	15.23	0.78	2.89	68.32	0.03	0.17	1.45	0.65	3.37	0.25	0.17	1.92	0.32	0.44	0.06	0.03	3.06	0.25	99.39
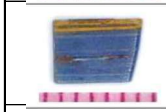		Ty-S-GB-413-T	transp. dark blue	LMG	no	no	EDS area	1.4	1.3	2.7	81.1		1.3	2.4	0.5	6.7		0.1	1.3		0.6					
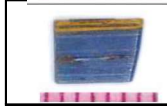	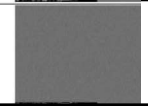	Ty-S-GB-413-T	transp. dark blue	LMG	no	no	EPMA	0.49	0.24	0.73	73.25	0.05	0.41	2.30	0.29	6.34	0.06	0.07	0.98	0.30	0.32	0.01	0.01	0.00	0.04	85.90

Table VII - Summary

Sample image	SEM-BSE	Sample	Color	Alkali type	Main coloring/ opacifying inclusions	Other inclusions	Analysis Type	Na_2O	MgO	Al_2O_3	SiO_2	P_2O_5	SO_3	Cl	K_2O	CaO	TiO_2	MnO	FeO	CoO	CuO	As_2O_5	SnO_2	Sb_2O_5	PbO	Tot
	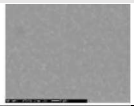	Ty-S-GR-506-Ar	yellowish-orange	LMG	cuprite	no	EDS area	11.7	2.5	4.6	46.7	2.2		1.0	1.1	6.5			2.0		6.7				13.74	
	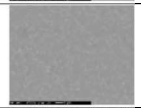	Ty-S-GR-506-Ar	yellowish-orange	LMG	cuprite	no	EPMA	11.40	1.62	2.84	44.77	0.67	0.32	0.72	1.05	6.84	0.22	0.28	2.44	0.03	8.61	0.01	0.93	0.42	17.48	100.65
	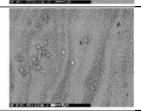	Ty-S-GR-506-R	sealing-wax red	LMG	cuprite, metallic copper	wollastonite	EDS area	11.0	2.2	3.9	41.7	2.5		1.1	1.0	4.2			1.1		6.4				23.14	
	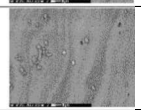	Ty-S-GR-506-R	sealing-wax red	LMG	cuprite, metallic copper	wollastonite	EDS points (DG)	5.2	1.9	3.8	46.1	2.3		1.2	1.0	4.6			1.3		4.5				25.89	
	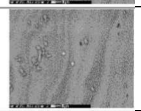	Ty-S-GR-506-R	sealing-wax red	LMG	cuprite, metallic copper	wollastonite	EDS points (LG)	5.7	2.1	3.7	42.9	2.6		1.3	1.0	4.8			1.4		4.5				27.73	
	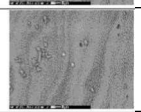	Ty-S-GR-506-R	sealing-wax red	LMG	cuprite, metallic copper	wollastonite	EPMA	10.35	0.97	1.74	39.00	0.41	0.34	0.78	0.92	4.63	0.15	0.17	1.20	0.00	4.83	0.04	0.88	0.52	32.68	99.63
	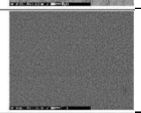	Ty-S-GRT-501-Ar	yellowish-orange	LMG	cuprite	SiO_2, malayaite, K-feldspar (probably microcline), wollastonite, perowskite, corundum, hematite	EDS area	11.5	2.7	4.0	42.4	3.0		1.4	1.3	3.9		0.6	1.4		7.1		3.0		16.40	
	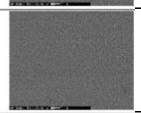	Ty-S-GRT-501-Ar	yellowish-orange	LMG	cuprite	SiO_2, malayaite, K-feldspar (probably microcline), wollastonite, perowskite, corundum, hematite	EPMA	11.48	1.74	2.01	42.63	0.75	0.38	0.77	1.10	5.47	0.20	0.41	1.41	0.03	8.04	0.01	1.25	0.39	21.67	99.75
	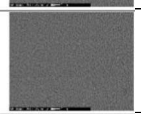	Ty-S-GRT-501-Ar2	yellowish-orange	LMG	cuprite	no	EDS points f.20-1	6.0	2.6	4.2	43.6	2.6		1.7	1.2	5.0			1.7		5.7				23.71	
	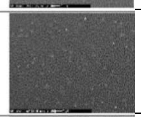	Ty-S-GRT-501-R	red	HMG	metallic copper	no	EDS area	13.8	3.0	4.1	58.2	2.2		1.1	2.0	7.7		0.5	1.3		1.5				4.50	
	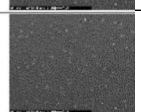	Ty-S-GRT-501-R	red	HMG	metallic copper	no	EPMA	13.84	2.56	2.28	56.28	1.15	0.26	0.99	2.07	8.05	0.18	0.43	1.37	0.01	1.72	0.01	0.39	0.34	7.87	99.81
	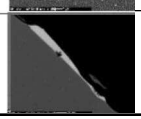	Ty-S-GRT-501-VT	red transp.	HMG	metallic copper	no	EDS area	5.9	2.9	4.2	47.9	2.6		1.1	1.4	6.1		0.6	1.5		5.0				19.09	

Table VII - Summary

Sample image	SEM-BSE	Sample	Color	Alkali type	Main coloring/ opacifying inclusions	Other inclusions	Analysis Type	Na_2O	MgO	Al_2O_3	SiO_2	P_2O_5	SO_3	Cl	K_2O	CaO	TiO_2	MnO	FeO	CoO	CuO	As_2O_5	SnO_2	Sb_2O_5	PbO	Tot
	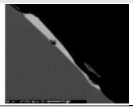	Ty-S-GRT-501-VT	red transp.	HMG	metallic copper	no	EPMA	9.14	1.78	1.93	43.81	0.74	0.34	0.79	1.26	5.73	0.20	0.43	1.48	0.04	5.35	0.04	1.27	0.42	24.19	98.92
	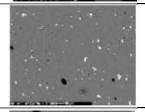	Ty-S-mix-006-B	opaque dark blue	LMG	Ca antimoniates	Fe oxide	EDS area	15.9	1.6	4.1	62.2	1.1	1.1	1.3	1.1	5.1			2.6		0.8			2.7		
	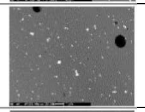	Ty-S-mix-006-G	opaque yellow	LMG	Pb antimoniates	SiO_2	EDS area	14.2	1.6	3.7	59.9	1.2			1.0	5.2			1.7					0.9	10.05	
	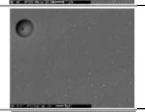	Ty-S-mix-006-R	dull red	HMG	metallic copper	no	EDS area	11.3	2.1	3.2	52.1	1.6			1.5	8.2	0.4	0.6	1.8		2.2				13.95	
	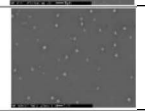	Ty-S-MR-502-M	brown	LMG	cuprite	zircon	EDS area	11.7	1.4	3.4	56.7			0.8	0.5	0.9		0.9	1.4		7.3				13.90	
	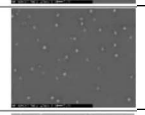	Ty-S-MR-502-M	brown	LMG	cuprite	zircon	EPMA	10.51	0.36	1.55	57.25	0.11	0.30	0.53	0.46	0.73	0.15	0.75	1.61	0.01	7.63	0.15	0.22	1.12	17.68	101.11
	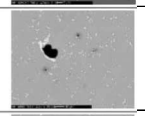	Ty-S-MR-502-R	sealing-wax red	LMG	cuprite	no	EDS area	12.5	1.3	2.9	55.5			0.9	0.4	2.0		0.8	0.8		9.1				12.76	
	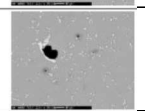	Ty-S-MR-502-R	sealing-wax red	LMG	cuprite	no	EPMA	11.98	0.28	1.01	56.31	0.04	0.41	0.66	0.42	2.07	0.12	0.74	0.79	0.04	7.53	0.05	0.00	0.81	17.24	100.50
	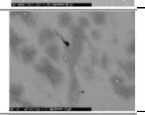	Ty-S-RV-418-R1	sealing-wax red	LMG	cuprite, metallic copper	no	EDS area	8.1	1.7	3.6	31.9			0.3	1.1	0.6		0.4	1.5		5.9				41.52	
	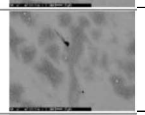	Ty-S-RV-418-R1	sealing-wax red	LMG	cuprite, metallic copper	no	EDS points (DG)	6.2	1.7	3.9	36.5			0.4	1.1	0.6		0.4	2.0		4.6				39.44	
	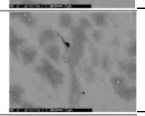	Ty-S-RV-418-R1	sealing-wax red	LMG	cuprite, metallic copper	no	EDS points (LG)	5.7	1.8	3.7	32.7			0.3	1.1	0.6		0.5	1.7		3.6				44.91	
	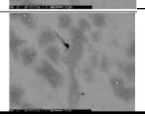	Ty-S-RV-418-R1	sealing-wax red	LMG	cuprite, metallic copper	no	EPMA	9.97	0.78	2.76	41.52	0.07	0.17	0.53	0.42	1.48	0.48	0.22	1.59	0.04	3.64	0.03	0.01	0.01	36.20	99.92

Table VII - Summary

Sample image	SEM-BSE	Sample	Color	Alkali type	Main coloring/ opacifying inclusions	Other inclusions	Analysis Type	Na_2O	MgO	Al_2O_3	SiO_2	P_2O_5	SO_3	Cl	K_2O	CaO	TiO_2	MnO	FeO	CoO	CuO	As_2O_5	SnO_2	Sb_2O_5	PbO	Tot
	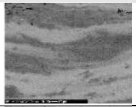	Ty-S-RV-418-R2	sealing-wax red	LMG	cuprite, metallic copper	no	EDS area	7.2	1.7	3.7	30.4			0.5	1.1	0.5		0.3	1.5		6.6				43.20	
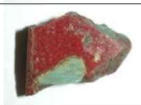	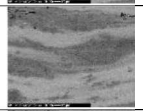	Ty-S-RV-418-R2	sealing-wax red	LMG	cuprite, metallic copper	no	EDS points (DG)	5.3	1.5	3.7	36.6			0.3	1.0	0.8		0.4	1.9		4.7				40.78	
	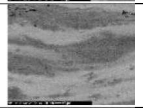	Ty-S-RV-418-R2	sealing-wax red	LMG	cuprite, metallic copper	no	EDS points (LG)	4.6	1.6	3.5	31.7			0.4	1.1	0.5		0.4	1.7		3.7				47.10	
	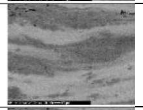	Ty-S-RV-418-R2	sealing-wax red	LMG	cuprite, metallic copper	no	EPMA	9.04	0.72	2.83	39.36	0.07	0.18	0.38	0.42	1.36	0.50	0.19	1.60	0.01	3.21	0.05	0.02	0.02	40.11	100.04
	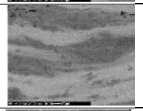	Ty-S-RV-418-R2s	sealing-wax red	LMG	cuprite, metallic copper	no	EPMA	8.92	0.82	3.22	45.07	0.11	0.23	0.43	0.55	1.28	0.57	0.21	1.82	0.02	3.56	0.03	0.00	0.00	34.50	101.34
	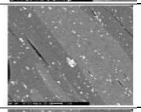	Ty-S-RV-418-V	opaque turquoise	LMG	Ca antimoniates	no	EDS area	12.9	1.7	3.6	68.1			1.4	1.0	5.6			0.8		2.4			2.3		
	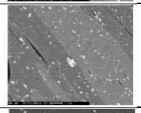	Ty-S-RV-418-V	opaque turquoise	LMG	Ca antimoniates	no	EPMA	16.54	0.55	1.74	69.36	0.12	0.42	0.79	0.63	5.94	0.08	0.29	0.65	0.01	2.23	0.00	0.19	2.39	0.32	102.26
	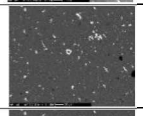	Ty-S-TA-005-A	opaque light blue	LMG	Ca and Ca-Na antimoniates	wollastonite, ilmenite, Fe oxide, corundum	EDS area	15.5	1.7	4.2	62.4		1.2	1.5	0.7	7.1			0.9		2.6			1.8		
	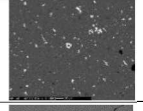	Ty-S-TA-005-A	opaque light blue	LMG	Ca and Ca-Na antimoniates	wollastonite, ilmenite, Fe oxide, corundum	EPMA	17.75	0.75	2.44	67.18	0.09	0.27	1.42	0.51	6.96	0.13	0.05	0.71	0.02	2.24	0.03	0.09	1.21	0.05	101.89
	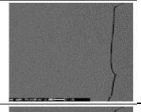	Ty-S-TA-005-T	true colorless	LMG	no	no	EDS area	12.5	1.7	4.4	68.6		1.6	2.2	1.5	5.3			0.5					1.4		
	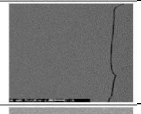	Ty-S-TA-005-T	true colorless	LMG	no	no	EPMA	13.48	0.36	2.03	72.51	0.06	0.29	1.96	0.86	4.98	0.08	0.02	0.28	0.01	0.02	0.01	0.01	0.72	0.01	97.68
	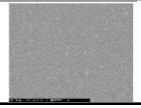	Ty-S-TR-501-R	dull red	HMG	metallic copper	SiO_2, ilmenite, K-feldspar	EDS area	14.8	3.0	4.1	59.1			1.8	1.6	7.6	0.2		1.2		1.8				5.04	

Table VII - Summary

Sample image	SEM-BSE	Sample	Color	Alkali type	Main coloring/ opacifying inclusions	Other inclusions	Analysis Type	Na_2O	MgO	Al_2O_3	SiO_2	P_2O_5	SO_3	Cl	K_2O	CaO	TiO_2	MnO	FeO	CoO	CuO	As_2O_5	SnO_2	Sb_2O_5	PbO	Tot
	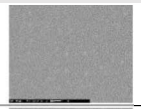	Ty-S-TR-501-R	dull red	HMG	metallic copper	SiO_2, ilmenite, K-feldspar	EDS points (DG)	4.8	2.3	3.7	60.5			1.0	1.5	9.7	0.2	0.6	2.0		2.8				10.01	
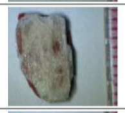	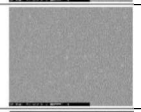	Ty-S-TR-501-R	dull red	HMG	metallic copper	SiO_2, ilmenite, K-feldspar	EPMA	13.86	2.30	2.37	56.97	0.84	0.23	0.96	1.58	8.40	0.15	0.35	1.31	0.02	2.45	0.01	0.42	0.36	8.06	100.63
	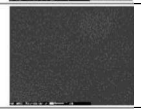	Ty-S-TR-501-T	true colorless	LMG	no	no	EDS area	16.9	1.0	3.5	70.7		0.8	1.8	0.6	4.3										
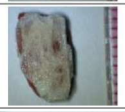	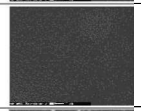	Ty-S-TR-501-T	true colorless	LMG	no	no	EPMA	12.93	0.35	2.00	72.04	0.05	0.30	1.89	0.75	4.95	0.02	0.00	0.29	0.00	0.00	0.01	0.02	0.75	0.00	96.35
	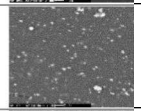	Ty-S-VA-405-A	opaque turquoise	LMG	Ca antimoniates	ilmenite	EDS area	13.5		3.2	66.8	0.5	1.4	1.0	0.9	8.1			0.8		2.3			1.6		
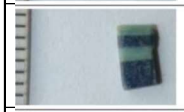	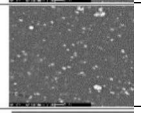	Ty-S-VA-405-A	opaque turquoise	LMG	Ca antimoniates	ilmenite	EPMA	14.45	0.53	1.97	65.02	0.52	0.12	0.74	0.99	5.34	0.24	0.28	1.46	0.15	0.49	0.01	0.04	6.07	0.15	98.56
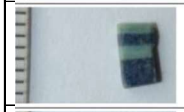	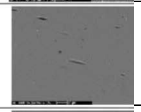	Ty-S-VA-405-B	opaque dark blue	LMG	very few Ca antimoniates	no	EDS area	14.6	0.9	3.2	64.5	0.8		0.9	1.0	6.3		0.7	2.3		1.0			3.9		
	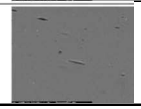	Ty-S-VA-405-B	opaque dark blue	LMG	very few Ca antimoniates	no	EPMA	15.22	0.61	1.94	66.78	0.45	0.11	0.71	0.72	6.74	0.11	0.19	0.51	0.00	1.59	0.02	0.10	2.30	0.69	98.80